

AD-A247 596



①

DTIC
ELECTE
MAR 5 1992
S C D

DISTRIBUTION STATEMENT A

Approved for public release;
Distribution Unlimited

REPORT DOCUMENTATION PAGE			Form Approved OMB No. 0704-0188	
<small>Public reporting burden for this collection of information is estimated to average 1 hour per response, including the time for reviewing instructions, searching existing data sources, gathering and maintaining the data needed, and completing and reviewing the collection of information. Send comments regarding this burden estimate or any other aspect of this collection of information, including suggestions for reducing this burden, to Washington Headquarters Services, Directorate for Information Operations and Reports, 1215 Jefferson Davis Highway, Suite 1204, Arlington, VA 22202-4302, and to the Office of Management and Budget, Paperwork Reduction Project (0704-0188), Washington, DC 20503.</small>				
1. AGENCY USE ONLY (Leave blank)	2. REPORT DATE 1/30/92	3. REPORT TYPE AND DATES COVERED Final TO 31 MAY 92		
4. TITLE AND SUBTITLE Chamber Testing		5. FUNDING NUMBERS AFOSR-91-0264 PE: 61102F PR: 2302 TA: C1		
6. AUTHOR(S) An-Bin Huang (Editor)		7. PERFORMING ORGANIZATION NAME(S) AND ADDRESS(ES) Clarkson University Potsdam, NY 13699		
9. SPONSORING/MONITORING AGENCY NAME(S) AND ADDRESS(ES) Air Force Office of Scientific Research (AFOSR/NA) Bolling AFB DC 20332-6448		8. PERFORMING ORGANIZATION REPORT NUMBER		
11. SUPPLEMENTARY NOTES ISBN-)-44-01652-X, ELSEVIER SCIENCE PUBLISHING CO.		10. SPONSORING/MONITORING AGENCY REPORT NUMBER AFOSR-91-0264		
12a. DISTRIBUTION/AVAILABILITY STATEMENT Unlimited		12b. DISTRIBUTION CODE		
13. ABSTRACT (Maximum 200 words) The First International Symposium on Calibration Chamber Testing has provided a forum for the exchange of concepts, information, and experiences related to the use of the calibration chamber. It was the first time such a conference was held on an international basis. The two-day Symposium brought together more than fifty researchers from Australia, Brazil, Canada, France, Italy, Japan, Norway, U.K., and the U.S.. In addition to the traditional use of the chamber for calibrating in situ soil testing, topics related to pile testing in chambers and other forms of physical and numerical simulations of field testing techniques were also included.				
14. SUBJECT TERMS SOILS TESTING, SOILS, CALIBRATION CHAMBER TESTING		15. NUMBER OF PAGES 405		
17. SECURITY CLASSIFICATION OF REPORT Unclassified		16. PRICE CODE		
18. SECURITY CLASSIFICATION OF THIS PAGE Unclassified		19. SECURITY CLASSIFICATION OF ABSTRACT Unclassified		
20. LIMITATION OF ABSTRACT None				

NSN 7540-01-280-5500

Standard Form 298 (Rev. 2-89)
Prescribed by ANSI Std. Z39-18
298-102

92-05505



Calibration Chamber Testing

Proceedings of the First International Symposium on Calibration
Chamber Testing/ISOCCT1, Potsdam, New York / 28-29 June 1991.
Sponsored in part by The National Science Foundation
Grant No. MSS-9104055

Editor

An-Bin Huang

Clarkson University
Potsdam, New York

Organizing Committee

An-Bin Huang, Chairman

Clarkson University

Roy H. Borden

North Carolina State University

Richard W. Peterson

Waterways Experiment Station

Mehmet T. Tumay

National Science Foundation

Elsevier Science Publishing Co
655 Avenue of the Americas Inc
New York NY 10010

\$145.00

NWW 3/9/92



Elsevier

New York • Amsterdam • London • Tokyo



Accession For	
NTIS GRA&I	<input checked="" type="checkbox"/>
DTIC Tab	<input type="checkbox"/>
Unannounced	<input type="checkbox"/>
Justification	
By ANUS.	
Distribution/	
Availability Codes	
Dist	Avail and/or Special
A-1	

92 3 02 157

No responsibility is assumed by the Publisher for any injury and/or damage to persons or property as a matter of products liability, negligence or otherwise, or from any use or operation of any methods, products, instructions or ideas contained in the material herein.

Elsevier Science Publishing Company, Inc.
655 Avenue of the Americas, New York, New York 10010

Sole distributors outside the United States and Canada:
Elsevier Science Publishers B.V.
P.O. Box 211, 1000 AE Amsterdam, The Netherlands

© 1991 by Elsevier Science Publishing Company, Inc.

This book has been registered with the Copyright Clearance Center, Inc. For further information, please contact the Copyright Clearance Center, Inc., Salem, Massachusetts.

All inquiries regarding copyrighted material from this publication, other than reproduction through the Copyright Clearance Center, Inc., should be directed to: Rights and Permissions Department, Elsevier Science Publishing Company, Inc., 655 Avenue of the Americas, New York, NY 10010. FAX 212-633-3977.

This book is printed on acid-free paper.

ISBN 0-444-01652-X

Current printing (last digit):

10 9 8 7 6 5 4 3 2 1

Manufactured in the United States of America

TABLE OF CONTENTS

Preface	vii
Acknowledgments	ix
 Keynote lectures	
History of the first six CRB calibration chambers J.C. Holden (presented by J.H. Schmertmann)	1
A critical appraisal of calibration chamber testing of sands V.N. Ghionna & M. Jamiolkowski	13
 Technical papers	
Preliminary results of CPT tests in calcareous Quiou sand M.S.S. Almeida, M. Jamiolkowski & R.W. Peterson	41
Pressuremeter testing in a clay calibration chamber W.F. Anderson & I.C. Pyrah	55
Hydraulic fracture simulations in a calibration chamber K. Been & K.M. Kosar	67
Compressibility and crushability of sands at high stresses R. Bellotti, C. Fretti, V.N. Ghionna & S. Pedroni	79
Design and development of a small calibration chamber for compressible sands R. Bellotti & S. Pedroni	91
Boundary displacement induced by DMT penetration R.H. Borden	101
Methods of sample fabrication in the Virginia Tech calibration chamber T.L. Brandon & G.W. Clough	119
Results of CPT's in Toyoura quartz sand V. Fioravante, M. Jamiolkowski, F. Tanizawa & F. Tatsuoka	135
Scale and boundary effects on calibration chamber pile tests P. Foray	147
Piezoblade tests in a clay calibration chamber A.-B. Huang, R.D. Bunting & T.C. Carney	161
Numerical simulation of a calibration chamber A.-B. Huang, M.Y. Ma & J.S. Lee	175
Fifteen+ years of model foundation testing in large chambers F.H. Kulhawy	185

Relative density, SPT and CPT interrelationships F.H. Kulhawy & P.W. Mayne	197
Laboratory investigation of small strain modulus anisotropy in sand D. LoPresti & D.A. O'Neill	213
Practical use of CPT correlations in sand based on calibration chamber tests T. Lunne	225
Calibration chamber correlations for horizontal in situ stress assessment using self-boring pressuremeter and cone penetration tests M. Manassero	237
Tentative method for estimating σ_{ho}' from q_c data in sands P.W. Mayne	249
Calibration chamber database and boundary effects correction for CPT data P.W. Mayne & F.H. Kulhawy	257
Calibration tests on the cone pressuremeter in carbonate sand N.R.F. Nutt & G.T. Houlsby	265
Houston's calibration chamber: case histories M.W. O'Neill	277
Chamber testing of piles in calcareous sand and silt A.K. Parkin	289
Model pressuremeter testing in an automated flexible wall calibration chamber D. Penumadu, A. Skandarajah & J.-L. Chameau	303
Penetration resistance of fine cohesionless materials R.W. Peterson	315
Overview of a large stress chamber system R.W. Peterson & K. Arulmoli	329
Miniature CPT tests in dense Monterey No.0/30 sand in a flexible double-walled calibration chamber A.J. Puppala, Y.B. Acar & M.T. Tumay	339
Correlation of initial tangent modulus and cone penetration resistance G.J. Rix & K.H. Stokoe	351
Characterization of soil in calibration chambers with seismic waves K.H. Stokoe, J.N.-K. Lee & S.H.-H. Lee	363
Miniature piezocone penetration tests on soft soils in a calibration chamber system G.Z. Voyiadjis, M.T. Tumay & P.U. Kurup	377
Principles and examples of centrifuge modeling D. Znidarcic	393
List of Authors	405

Preface

The First International Symposium on Calibration Chamber Testing has provided a forum for the exchange of concepts, information, and experiences related to the use of the calibration chamber. It was the first time such a conference was held on an international basis. The two-day Symposium brought together more than fifty researchers from Australia, Brazil, Canada, France, Italy, Japan, Norway, U.K., and the U.S.. In addition to the traditional use of the chamber for calibrating in situ soil testing, topics related to pile testing in chambers and other forms of physical and numerical simulations of field testing techniques were also included. The Proceedings contain the papers presented at the Symposium and additional papers contributed by individuals who did not have the opportunity to present them.

Major funding for the Symposium was provided by the National Science Foundation. Additional support was contributed by the U.S. Air Force Office of Scientific Research and Clarkson University. I would like to thank the sponsors and members of the organizing committee for their support. My graduate students, M.Y. Ma, T.C. Carney, A.A. Taney and M.A. Ciance played a vital role in the event and their efforts are gratefully acknowledged.

An-Bin Huang
Chairman, Organizing Committee

HISTORY OF THE FIRST SIX CRB CALIBRATION CHAMBERS

J. C. HOLDEN, VIC ROADS, MELBOURNE, AUSTRALIA

PREFACE

As the reader of this paper will see, I got to know Dr. Jim Holden very well when he came to the Univ. of Florida and built the second CRB-type chamber. Knowing of his intimate involvement with the beginnings of these chambers, I asked him to help me with reconstructing an accurate history. He at once agreed and jumped to the task with his usual enthusiasm and thoroughness and produced a report which I used as part of a verbal presentation to ISOCCT1. With only minor editing, this report has become the present paper. It tells his story -- he lived most of it and I only a relatively small part. I therefore suggested, and he agreed, that ISOCCT1 publish this paper under his name.

John H. Schmertmann,
18 Jul 91

ORIGINAL CRB CALIBRATION CHAMBER

The history of large calibration chambers started in 1969 at the Materials Research Division, Country Roads Board (CRB) (now called VIC ROADS), Melbourne, Victoria, Australia. Since 1953 the CRB had been performing foundation investigations using a 10 cm² mechanical cone penetrometer (based on the Dutch Cone), which was superseded in 1958 by an electrical cone penetrometer with a cone base diameter of 1.96 in. (50 mm), giving an area of 3 in.² (19.4 cm²) (Gawith and Bartlett, 1963). In 1967, the writer conceived the idea of the original CRB electrical friction-cone penetrometer, having a 3 in.² cone and a 72 in.² (465 cm²) friction sleeve (Barlett and Holden, 1968). To calibrate this friction-cone penetrometer in the laboratory under simulated field conditions, the writer also conceived the idea of the CRB calibration chamber.

Ron Lilley and the writer designed, built and commissioned this chamber in 1969. Gary Chapman (1975) described the features of the design and operation of the chamber. The original CRB chamber houses a sample 2 ft 6 in. (0.76 m) diam. by 3 ft (0.91 m).

The idea of the calibration chamber followed from the belief that there existed a great need to rigorously study the performance of the full-size penetrometer in the laboratory. Here the investigator could accurately measure and/or control the soil properties, stresses, and strains.

Other investigators had previously performed laboratory calibration testing in rigid-wall test pits (for example, Melzer, 1967; Tcheng, 1966). The decision to build a flexible-boundary chamber instead of a rigid-wall chamber resulted from the following argument (Holden, 1971).

For a given specimen size, one can demonstrate that a rigid lateral boundary has a larger influence on the cone penetration and frictional resistances of a penetrometer than a flexible boundary subjected to a constant pressure. Thus, one can make a flexible-boundary chamber relatively much smaller yet still large enough to keep the penetration resistances close to the field values. Apart from a greater testing output and less cost per test, the flexible-boundary chamber has the major advantage that the investigator can measure and/or control the vertical and lateral stresses and deformations. Table 1 summarizes the new ideas.

TABLE 1

KEY NEW (1969) IDEAS	
<hr/>	
O	FLEX. BOUNDARIES, BUT K_0 , NC & OC
O	STRESS CONTROL
O	SIZE & ACCESS FOR FULL-SCALE CPT
O	REPRODUCIBLE & UNIFORM SPECIMENS ("Pluvial" Deposition)

Because of greater practical benefits and simplicity in producing a reproducible, uniform soil "specimen", the research began with air-dry sands. Gus Veismanis (1975) performed the calibration tests using two local quartz sands (Earlston and South Oakleigh). The specimen preparation simulated as closely as possible a naturally-occurring aeolian deposition. The writer achieved this by a technique he named "pluvial deposition", using a traversing sand spreader they developed at the University of Melbourne (Holden, 1967; Gerrard, 1968) and based on the concept of Kolbuszewski and Jones (1961). To simulate the K_0 field conditions of zero lateral strain during consolidation, the writer utilized an ingenious cavity wall design (see Figure 1). By maintaining the cavity water pressure equal to the developing lateral sand pressure, the inner wall of the double-walled barrel does not move, thus giving an average K_0 condition.

The chamber testing research had the aim of correlating cone resistance and/or friction resistance directly with such engineering properties of the sand as shear strength angle and modulus of deformation. This would permit by-passing other variables such as density, sand grading, angularity, grain size, etc. From measurements made during the confined compression of the sample, one can determine the values of K_0 , the constrained modulus, M_0 , and the equivalent elastic parameters - Young's modulus, E^* and Poisson's ratio, μ^* (Holden, 1971; Veismanis, 1975). Veismanis separately determined the shear strength parameters from triaxial tests

on 20 cm by 10 cm diameter samples of sand also prepared by pluvial deposition.

The initial calibration tests concentrated on the 50 mm diam (3 in.²) CRB electrical friction-cone penetrometer. Later tests involved two designs of 10 cm² Fugro electrical friction-cone penetrometers (Veismanis, 1975). However, they discovered from their tests that they needed a larger chamber to accurately calibrate the penetrometers in dense sands, especially the large size CRB penetrometer.

UNIVERSITY OF FLORIDA CHAMBER

Under the guidance of Professor John Schmertmann, and as a Winston Churchill Fellow, the writer supervised the construction and installation at the University of Florida of a larger size calibration chamber (Figure 1), as redesigned by Ron Lilley (CRB). Practical considerations limited the maximum size of the specimen to 4 ft (1.22 m) diameter by 4 ft (1.22 m) high (Holden, 1971). A traversing sand spreader (University of Melbourne design) placed the sand into the mold that formed the sand specimen.

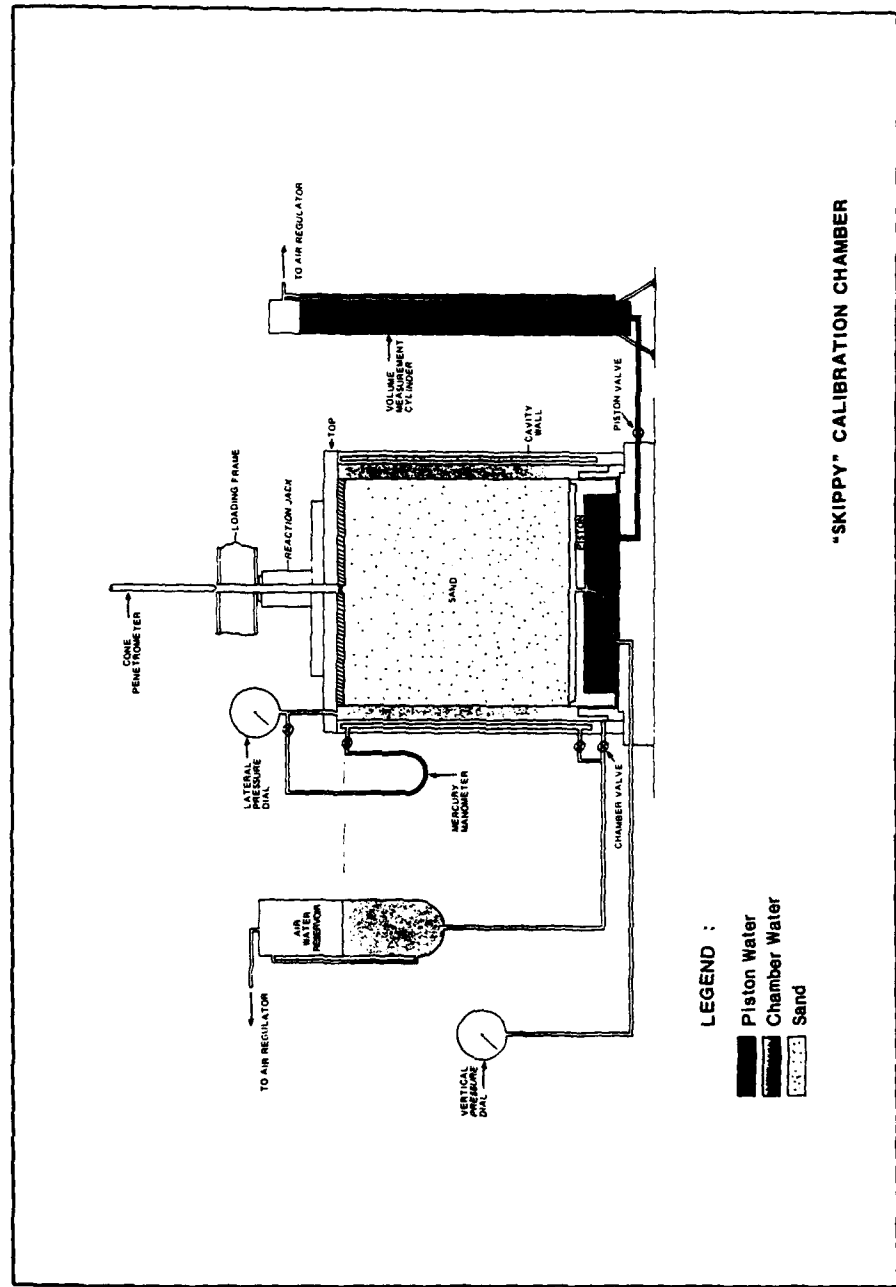
The writer supervised a series of exploratory tests to study (i) the effect of sample boundary conditions on the penetration resistances, (ii) the behavior of penetrometers of different designs, (iii) the effect of rod friction, (iv) the effect of discontinuous operation, and (v) sensing an interface between two sand layers. Other test results on two designs of 10 cm² Fugro penetrometers, each with a different position of friction sleeve, assisted in the selection of a design for the ASTM Standard D3441 (Holden 1971, 1975a).

To answer questions about the effect of rod friction on the cone resistance of continuously penetrating electrical penetrometers, the writer designed a reference cone penetrometer to measure a static value of cone resistance unaffected by rod friction (Holden, 1971). With this penetrometer, we also started to utilize stage testing - ie. using progressively higher overburden pressures at different stages in the penetration of a specimen.

The calibration tests had the prime purpose of establishing correlations between the penetration resistances of two penetrometers - a Fugro electrical friction-cone penetrometer (de Ruiter, 1971) and the Dutch mechanical friction-cone penetrometer (Begemann, 1969) - and various engineering properties of two sands - a local (Edgar) subangular quartz sand and the well-known, rounded, Ottawa sand.

The writer, working with John Schmertmann and his University of Florida colleagues, discovered that the constrained modulus, M_c , did not correlate uniquely with cone resistance, q_c , for all sands, as assumed by some previous workers. He then proposed methods for estimating the constrained modulus and the angle of internal friction for normally consolidated sands from field cone penetration tests (CPTs), based on calibration test results (Holden, 1975b). We also investigated the effect of overconsolidation in sands and

FIGURE 1



"SKIPPY" CALIBRATION CHAMBER

demonstrated that for a given sand the existing horizontal stress virtually controls the cone resistance, irrespective of its overconsolidation ratio. We also observed for the first time (Holden, 1971) the effect of sand crushing on the linear relationship between cone resistance and vertical stress in a uniform normally consolidated sand.

Commencing in 1971, post-graduate students also used the calibration chamber for research on the performance of pressuremeters in sands (Laier et al., 1975). Later, in 1974-5, Caillemer (1975) and Reese (1975) performed the first calibration tests using penetrometers in saturated sands.

MONASH UNIVERSITY CHAMBER

In 1973, Gary Chapman, a member of the writer's staff, took leave from the CRB and undertook post-graduate research at Monash University (Melbourne, Australia) on the laboratory calibration of penetrometers in air-dry sands. He supervised the design, construction and installation of a modified CRB chamber (for details, see Chapman, 1979). The main differences from the previous chambers, summarised by Chapman (1975), were as follows:

- (a) He increased the sample height to 6 ft (1.82 m) to (i) obtain a plateau in the friction resistance/depth graph under all conditions, and (ii) enable stage testing of standard 10 cm² electrical penetrometers.
- (b) He included the automatic recording of all pressures as well as the movement of the piston by using a displacement transducer.

The chamber testing began mid-1975 with calibration tests in a local (Frankston) quartz sand. These employed a standard type 10 cm² CRB electrical friction-cone penetrometer (Holden, 1974), with the friction sleeve load cell incorporating silicon beam transducers. Chapman prepared specimens by also using a traversing sand spreader (University of Melbourne design). Chapman and Donald (1981) published the results.

Later investigators used this chamber to study certain aspects of the internal design of the electrical penetrometer (Vuong, Donald and Parkin, 1988). In recent years, the university has used the chamber for tests on model piles in calcareous sands (Parkin et. al., 1990).

NGI CHAMBER

The involvement of the Norwegian Geotechnical Institute (NGI) in calibration chamber testing arose from their desire to correlate cone penetration resistances with in-situ strength and deformation properties of sands from the North Sea, where they used the electrical friction-cone penetrometer extensively in offshore site investigations for oil drilling platforms. In mid-1974, supported by a Norwegian post-doctoral research fellowship, the writer initiated a calibration chamber testing program at the NGI in Oslo.

An earlier research program had proposed calibration tests mainly on a 5 cm² friction-cone penetrometer under development by the NGI for offshore investigations. The CRB shipped their original chamber and traversing sand spreader to the NGI for these tests. The writer argued successfully that the calibration tests should concentrate on the standard 10 cm² penetrometer (Holden, 1976). The NGI decided to build another chamber based on the CRB design, but larger -- housing a sand specimen 1.22 m diameter by 1.5 m high. They chose the specimen height after considering the practical difficulties experienced by Gary Chapman while operating his chamber (1.82 m high specimen). The writer supervised the design, performed by Ragnar Johnsrud, and the construction of the NGI chamber. Nigel Last (1979a), who supervised the chamber's installation in 1976, also described the details of its design and operation.

In 1975, the NGI began a series of preliminary tests using the CRB chamber, and later the NGI chamber, to investigate the effect of the relative size of specimen and its boundary conditions on the performance of the penetrometers. The investigators intended to gain more evidence for an expected scale effect for penetrometers in sands. After discarding its original design, the NGI adopted the CRB design of electrical friction-cone penetrometer (Holden, 1974), for both the 5 cm² and 10 cm² sizes. The results of these preliminary tests were reported in a number of NGI Internal Reports (Series No. 52108-1,2,3,5,6,9,10) and summarised by Parkin and Lunne (1982).

Originally, the investigators acquired a large quantity of sand from the Frigg field in the North Sea. However, they eventually performed all testing on a local (Hokksund) angular, predominantly quartz, glacial sand. They initially considered the Frigg sand unsuitable, mainly because of the problems with pluvial deposition in air associated with its significant silt content. This led to the development of vacuo-pluviators for pluvially depositing silty sand in a vacuum (Holden, 1976), first on a small-scale for the NGI laboratory testing apparatus (Kildalen and Stenhamar, 1977) and later for the ISMES calibration chamber (see below).

Earlier, the writer (Holden, 1971) had become aware of the significant effect of sand structure on cone resistance. He initiated a subsidiary research project to investigate this effect for Hokksund sand using a small-scale laboratory pluviator (Kildalen and Stenhamar, 1977).

Previous experience (Holden, 1967) and previous calibration tests in the CRB chamber indicated that specimens

prepared by the traversing sand curtain of the CRB spreader could produce a layered, non-uniform specimen, and not very repeatable. This eventually led to the development of a mass sand spreader or static pluviator. To overcome the problems caused by the swirling, rising air currents produced by the sand raining in a confined space, the writer conceived the idea of allowing the sand jets to fall freely through a large drop onto two diffusers maintained at a small constant height above the sand surface. A cooperative research project with Moust Jacobsen (1976) at Aalborg University, Denmark verified the feasibility of the concept. Ragnar Johnsrud and the writer, who overcame a major problem associated with operating a large shutter plate under a hopper of sand, subsequently designed the NGI pluviator. Last (1979a) describes the details of the design and operation.

After each penetration test, the investigators removed the central column of sand, containing any crushed sand, using a suction technique. They took a standard size sample from a depth of 20 to 30 cm and subjected it to a sieve analysis. By plotting the silt content against the cone resistance, the writer (Holden, 1976) demonstrated the controlling influence of crushing on the cone resistance/depth profile obtained in the field.

In 1976, the writer persuaded his friend Alan Parkin from Monash University to continue the calibration tests in the NGI chamber. On Alan's return to Monash University, he constructed an NGI pluviator to replace their traversing sand spreader. He has written several reports and papers containing analyses of data from the calibration chambers, culminating in a state-of-the-art paper presented to ISOPT-1 (Parkin 1988). In 1977, Nigel Last (1979b) carried out calibration tests on saturated samples of Hokksund sand.

In 1980, the NGI shipped their chamber and pluviator, together with a quantity of Hokksund sand, to the University of Southampton, U.K., where they have remained until now. Here researchers conducted calibration tests from 1983 to 1986, on both 5 cm² and 10 cm² penetrometers, to fill a gap in the NGI data (Last et. al., 1987).

ENEL CHAMBER

The involvement of the Italian Electricity Board (ENEL) and Prof. Mike Jamolkowski, University of Turin, in calibration chamber testing arose from their desire to correlate cone penetration resistances with the liquefaction potential of sand deposits at proposed sites for nuclear power plants. In 1975, upon the recommendation of John Schmertmann, ENEL employed the writer to advise Gianni Bizzi of the ENEL Hydraulic and Structural Research Centre, Milan, on the design and operation of a calibration chamber.

ENEL designed a modified version of the CRB chamber in 1975 with the same dimensions as the NGI chamber - viz 1.22 m diam by 1.5 m high specimen. The improvements included a precision servo-controlled mechanical drive for the penetrometer, a sensitive device for volume change measurement,

and advanced methods for saturating samples (Bellotti et. al., 1982; Parkin, 1982).

ENEL began to use their chamber and NGI-design pluviator in 1978, with calibration tests performed using a 10 cm² Fugro electrical friction-cone penetrometer in a dry local (Ticino) quartz sand. They reported test results in several papers (eg. Baldi et. al., 1982). Their calibration tests also included using the Marchetti dilatometer (Bellotti et. al., 1979) and the Cambridge self-boring pressuremeter (Bellotti et. al., 1989).

ISMES CHAMBER

Beginning in 1981, the Italian investigators built the sixth calibration chamber of CRB design at the ISMES laboratories, Bergamo, Italy, under the direction of Gualtieri Baldi. The improvements to the ENEL chamber included (i) modifications to the NGI-design pluviator to permit raining sand in a high vacuum to produce very loose samples, (ii) a base piston guidance system to prevent it from sticking, and (iii) displacement transducers to directly measure the mid-height specimen deformations (Parkin, 1986). ISMES performed calibration tests using a standard 10 cm² electrical friction-cone penetrometer in Ticino and Hokksund sands. Baldi et. al., (1986) have reported these test results.

Table 2 summarizes the above-described initial six CRB-type calibration chambers. Since then other researchers around the world have built at least ten other chambers for calibration testing. Most of these have incorporated one or more of the concepts originated in the design and use of these initial six chambers.

TABLE 2 - SUMMARY OF CRB (VIC ROADS) TYPE CHAMBERS

WHEN	WHERE	SIZE
1969	ORIGINAL CRB Melbourne	H = 0.91 m D = 0.76 m
1971	UF Gainesville	H = 1.22 m D = 1.22 m
1973	MONASH UNIV. Melbourne	H = 1.82 m D = 1.22 m
1976	N.G.I. OSLO (U. Southampton 1980)	H = 1.5 m D = 1.22 m
1978	ENEL-CRIS Milan	H = 1.5 m D = 1.22 m
1981	ISMES Bergamo	H = 1.5 m D = 1.22 m

REFERENCES

1. Baldi, G., Bellotti, R., Ghionna, V., Jamiolkowski, M., and Pasqualini, E. (1982). Design parameters for sands from CPT. Proceedings, 2nd European Symp. on Penetration Testing, Amsterdam, 2:425-432.
2. Baldi, G., Bellotti, R., Ghionna, V., Jamiolkowski, M., and Pasqualini, E. (1986). Interpretation of CPT's and CPTU's. Part 2: Drained penetration of sands. 4th Int. Geotech. Seminar, Singapore.
3. Barlett, A.H. and Holden, J.C. (1968). Sampling and in-situ testing equipment used by the Country Roads Board of Victoria for evaluating the foundations of bridges and embankments. Proc. Fourth Aust. Road Res. Board Conf., Vol. 4, Part 2, p. 1723.
4. Begemann, H.K.S. (1969). The Dutch static penetration test with the adhesion jacket cone. LGM mededelingen, Vol. XII, No. 4.
5. Bellotti, R., Bizzi, G. and Ghionna, V. (1982). Design, construction and use of a calibration chamber. Proceedings, 2nd European Symp. Penetration Testing, Amsterdam, 2:439-446.
6. Bellotti, R., Bizzi, G., Ghionna, V., Jamiolkowski, M., Marchetti, S. and Pasqualini, E. (1979). Preliminary calibration tests of electrical cone and flat dilatometer in sand. Proceedings, 7th European Conference on Soil Mechanics and Foundation Engineering, Brighton, England, 1979, Vol. 2, p. 195.
7. Bellotti, R., Ghionna, V., Jamiolkowski, M., Robertson, P.K., and Peterson, R.W. (1989). Interpretation of moduli from self-boring pressuremeter tests in sand. Geotechnique,

- Vol. 39, No. 2, p. 269.
8. Caillemer, B. (1975). An experimental study in the UF static cone test calibration chamber, Part 1-Density distribution of pluvially placed sand, Part 2-Pore pressure distribution around Fugro tip. Master's Thesis, University of Florida, August 1975.
 9. Chapman, G.A. (1975). A calibration chamber for field test equipment. Proceedings, European Symp. Penetration Testing, Stockholm 1974, Vol. 2.2, pp. 59-65.
 10. Chapman, G.A. (1979). The interpretation of friction cone penetrometer tests in sand. Ph.D. Thesis, Department of Civil Engineering, Monash University, Melbourne.
 11. Chapman, G.A. and Donald, I.B. (1981). Interpretation of static penetration tests in sand. Proceedings, 10th Int. Conf. Soil Mech. and Found. Eng., Stockholm, 2:455-458.
 12. de Ruiter, J. (1971). Electric penetrometer for site investigations. Proc. A.S.C.E., Vol. 97, No. SM2, p. 457.
 13. Gawaith, A.H. and Barlett, A.H. (1963). Deep sounding cone penetrometer. Proc. Fourth Aust.-N.Z. Conf. on Soil Mech. and Found. Eng., p. 8.
 14. Gerrard, C.M. (1968). A theoretical and experimental investigation of some model pavements. Ph.D. thesis, University of Melbourne.
 15. Holden, J.C. (1967). Stresses and strains in a sand mass subjected to a uniform circular load. Report No. 13, Civil Engineering Department, University of Melbourne.
 16. Holden, J.C. (1971). Laboratory research on static cone penetrometers. Report No. CE-SM-71-1, Dept. of Civil Eng., Univ. of Florida.
 17. Holden, J.C. (1974). Penetration testing in Australia. State-of-the-art report, European Symposium on Penetration Testing, Stockholm, 1974. Proceedings, Vol. 1, p. 155.
 18. Holden, J.C. (1975a). The shape of the electrical penetrometer tip. European Symposium on Penetration Testing, Stockholm 1974. Proceedings, Vol. 2, Pt. 1, p. 100.
 19. Holden, J.C. (1975b). The determination of deformation and shear strength parameters for sands using the electrical friction-cone penetrometer. Proc. Nordisk Geoteknikermøde, Copenhagen, May 1975, p. 627. Reprinted in N.G.I. Publication No. 110, p. 55.
 20. Holden, J.C. (1976). The calibration of electrical penetrometers in sand. Final Report, NTNF Research Fellowship, Royal Norwegian Council for Scientific and Industrial Research (NTNF). Reprinted in Norwegian Geotechnical Institute Internal Report 52108-2., Jan. 1977.
 21. Jacobsen, M. (1976). On pluvial compaction of sand. Rapport 9, Laboratoriet for Fundering, Aalborg Universitetscenter, Denmark.
 22. Kildalen, S. and Stenhamar, P. (1977). NGI laboratory sand rainer. Norwegian Geotechnical Institute, Internal Report 51505-15.
 23. Kolbuszewski, J. and Jones, R.H. (1961). Preparation of sand samples for laboratory testing. Proceedings, Midland Soc. for Soil Mech. and Found. Eng., 4:107.
 24. Laier, J.E., Schmertmann, J.H., and Schaub, J.H. (1975). Effect of finite pressuremeter length in dry sand. Proceedings, ASCE Spec. Conf. on In-Situ Measurement of

- Soil Props., Rayleigh, N.C., 1:241-259.
25. Last, N.C. (1979a). The use of calibration chambers to study cone penetration behaviour in dry samples of Hokksund sand. Norwegian Geotechnical Institute, Internal Report 52108-6.
 26. Last, N.C. (1979b). The introduction of cone penetration tests on saturated samples of Hokksund sand in the NGI calibration chamber. Norwegian Geotechnical Institute, Internal Report 52108-7.
 27. Last, N.C., Butterfield, R., and Harkness, R.M. (1987). An investigation of full-scale penetrometers in a large triaxial calibration chamber - March 1983 to February 1986. Final Report to S.E.R.C., Civil Engineering Department, University of Southampton.
 28. Melzer, K.J. (1968). Sondenuntersuchungen in sand. Dissertation D82, Technischen Hochschule Aachen.
 29. Parkin, A.K. (1982). Visit to ENEL laboratories, Milano, Italy. Norwegian Geotechnical Institute, Internal Report 52108-14.
 30. Parkin, A.K. (1986). Calibration chamber testing: visit to ENEL and ISMES laboratories, Italy. Norwegian Geotech. Inst., Int. Rep. 52108-19.
 31. Parkin, A.K. (1988). The calibration of cone penetrometers. Proceedings, First Int. Symposium on Penetration Testing (ISOPT-1), Orlando, Florida, March 1988, Vol. 1, p. 221.
 32. Parkin, A.K., Yee, Y.W., Tan, C.P., and Wiloughby, D.R. (1990). Driven model piles in calcareous sand in a large calibration chamber. Proceedings, 22nd Annual Offshore Technology Conference, Houston, Texas, May 1990, p. 389.
 33. Parkin, A.K. and Lunne, T. (1982). Boundary effects in the laboratory calibration of a cone penetrometer for sand. Proceedings, 2nd European Symp. Penetration Testing, Amsterdam, 2:761-768.
 34. Reese, J. (1975). An experimental study of the effects of saturation on the q_c and f values from the cone penetration tests in the UF calibration chamber. Master's Thesis, University of Florida, August 1975.
 35. Tcheng, Y. (1966). Fondations profonds en milieu pulverulent a diverses compacities. Annales de l'Institut Technique du Batiment et des Travaux Publics, Sols et Fondations 54, Nos. 219-220, March-April 1966.
 36. Veismanis, A. (1975). Laboratory investigation of electrical friction cone penetrometers in sands. Proceedings, European Symp. Penetration Testing, Stockholm, June 1974, Vol. 2.2, pp. 407-419.
 37. Vuong, B., Donald, I.B., and Parkin, A.K. (1988). Some aspects of the design of a friction cone penetrometer. Proceedings, Fifth Aust.-New Zealand Conf. on Geomechanics, Sydney, August 1988, p. 198.

A CRITICAL APPRAISAL OF CALIBRATION CHAMBER TESTING OF SANDS

V.N. GHIONNA,* M. JAMIOLKOWSKI,**

*University of Pavia, Italy

**Technical University of Torino, Italy

ABSTRACT

The present status of CC testing of sands is summarized and areas in which new developments could be achieved through CC research are pointed out.

A number of important aspects which make use of the results of the CC tests controversial in engineering practice, are critically examined and their relative importance evaluated. Special attention is devoted to the following problems:

- the influence of geological time on structure and mechanical behaviour of sands;
- the need to extend CC research to more realistic soils such as silty, crushable and lightly cemented sands instead of the clean, uniform silica sands that have been used so far;
- the importance of the limited dimensions of the CC and of imposed boundary conditions on the results of in situ tests.

Finally, the possibility is pointed out of combining CC testing with a properly structured programme of centrifuge tests aimed at a more cost-effective research.

1. INTRODUCTION

The paper summarizes the experience of the writers in the validation of different in situ techniques in sands using large calibration chambers (CC) and presents their point of view on the future possibilities and developments of this specific area of the geotechnical research.

Since the development of the first two CC's, one at the Country Roads Bureau of Victoria in Australia in 1969 [Holden (1971)] and the other at the University of Florida in 1970 [Reese (1975) and Caillemer (1975)], various apparatuses, increasingly sophisticated and automated, have been developed around the world, making way for a research field which has experienced increasingly growth and whose most eloquent expression is the present Symposium.

An extensive list of the CC's most actively used in the validation of in situ techniques in sand is reported in Table I.

CC research in Italy, which was started with the valuable help and encouragement of prof. John Schmertmann and Dr. Jim Holden, has brought a deeper insight into the use of in situ test results in geotechnical design and has stimulated the development of new equipments and the improvement of existing ones.

CC testing [Been et al. (1988)] has the unquestionable merit of allowing the execution of in situ tests in a specimen of sand of large dimensions. During the experiment the state of the sand specimen, its stress and strain history, and boundary conditions (BC) are well controlled.

TABLE I. Principal Calibration Chambers used in geotechnical investigations
Adapted from Peterson (1986). Large-diameter stress cells used for
geotechnical investigations.

Test Cell Owner/Location	Specimen Diameter (m)	Specimen Height (m)	Boundary Conditions		
			Radial	Bottom	Top
Country Roads Bureau, Australia	0.76	0.91	Flexible	Cushion	Rigid
University of Florida, USA	1.2	1.2	Flexible	Cushion	Rigid
Monash University, Australia	1.2	1.8	Flexible	Cushion	Rigid
Norwegian Geotechnical Institute	1.20	1.50	Flexible	Cushion	Rigid
ENEL-CRIS, Milano, Italy	1.20	1.50	Flexible	Cushion	Rigid
ISMES, Bergamo, Italy	1.20	1.50	Flexible	Cushion	Rigid
University of California, Berkeley, USA	0.76	0.80	Flexible	Rigid	Rigid
University of Texas at Austin, USA	cube 2.1x2.1x2.1 m		All flexible		
University of Houston, USA	0.76	2.54	Flexible	Cushion	Cushion
North Carolina State University, USA	0.94	1.00	Flexible	Rigid	Rigid
Luisiana State University, USA	0.55	0.80	Flexible	Flexible	Rigid
Golder Associates, Calgary, Canada	1.40	1.00	Flexible	Rigid	Cushion
Virginia Polytechnic Institute and State University, USA	1.5	1.5	Flexible	Rigid	Rigid
University of Grenoble, France	1.2	1.5	Flexible	Cushion	Cushion
Oxford University, UK	0.90	1.10	Flexible	Cushion	Rigid
University of Tokyo, Japan	0.90	1.10	Flexible	Rigid	Rigid
University of Clarkson, USA	0.51	0.76	Flexible	Rigid	Rigid
University of Sheffield, UK	0.79	1.00	Flexible	Rigid	Flexible
Cornell University, USA	2.1	2.9	Flexible	Rigid	Rigid

In addition, the sand specimens, generally prepared by means of pluvial deposition in air or vacuum, using gravity mass or travelling sand spreaders [Jacobsen (1976), Battaglio et al. (1979), Rad and Tumay (1987)].

results highly repeatable and of good, or at least acceptable, uniformity.

The most recent CC's offer also the possibility of saturating the specimens without difficulties. The process, which employs deaired water and CO_2 or vacuum inside the samples, results in a very high degree of saturation which is reflected in Skempton's (1956) pore pressure coefficient B, with values ranging between 0.94 and 0.98 [see Bellotti et al. (1982)].

Up to now CC research has been limited to the uniform, predominantly silica sands, to a limited number of experiments on uncemented carbonate sands [Evans (1987), Almeida et al.] and to a few tests on a Belgium glauconitic sand [Bellotti and Jamiolkowski (1990)].

An attempt to use a more realistic material, like silty sand, in a calibration chamber test has been made at the Virginia Polytechnic Institute [Brandon et al. (1990)], requiring consolidation of the material starting from slurry. Despite this cumbersome and time-consuming specimen preparation procedure, results are promising.

At the present state of the art and despite unquestionable achievements of CC research, this area of experimental soil mechanics deserves to be closely re-examined in order to ascertain whether, after more than two decades of development, it will progress into a stage of innovation or face stagnation.

The answer to this crucial question mainly depends on the possibility of better understanding and quantifying the importance of a number of issues that are relevant to the reliability of CC experiments, and of extending the range of tested soils to include more realistic materials, such as silty, highly cemented, and aged sands.

2. PROBLEMS OF CC RESEARCH

In the following a number of problems are listed which are linked to the engineering interpretation and use of CC tests whose complete understanding and qualitative appreciation becomes of paramount importance for the future of this type of research.

- a. CC tests are performed on specimens of freshly reconstituted sands whose fabric may very well be different from that of natural soils deposits which have a highly developed structure, built up in geological time by phenomena such as drained creep, early diagenesis, cementation, etc., see for example; Dusseault and Morgenstern (1979), Mesri (1987), Mitchell and Solymar (1984), Palmer and Barton (1987), Hryciw (1986), Mitchell (1986, 1988), Barton and Palmer (1989), Schmertmann (1989), Mesri et al. (1990). As the main aim of the CC tests is to develop engineering correlations it is important to understand and quantify the influence of differences in structure as discussed above not only on the results of the specific test, but also on the geotechnical parameter to which the in situ test is to be correlated. As a typical example one can mention the correlation between drained Young's modulus E' and static cone resistance q_c .
- b. As mentioned before, most CC tests have so far been performed on uniform, clean, predominantly silica sands. Natural deposits of sands are rarely as uniform, and almost always contain a non negligible percentage of

finer, which confers the so far tested materials features of "academic" soils.

Moreover, many relevant engineering problems are linked to more crushable and compressible materials, such as carbonate and glauconitic sands which are usually slightly cemented.

It appears imperative to extend CC research in the future to soils which are different from the "academic" sands tested up to now.

In order to achieve this objective the following is required:

- methods allowing that uniform and repeatable specimens of silty sands be obtained at the desired densities;
- procedures allowing that a desired degree of cementation be uniformly distributed through the sample after specimen deposition;
- a way for continuously checking whether the conditions during a test on a saturated specimen are drained, undrained or partially drained. This last point is an essential prerequisite for a rational interpretation of CC tests run in saturated samples.

c. Since the early eighties, the problem of the influence of the finite dimensions of the CC on tests results has been recognized as one of the most important in this type of research. The problem first addressed by Holden (1967) has been analyzed by Veismanis (1974), Parkin and Lunne (1982), Jamiolkowski et al. (1985), Bellotti et al. (1985), Eid (1987), Schnaid and Houlsby (1990), without reaching any definitive conclusion. With specific reference to the Cone Penetration Test (CPT) for which the importance of the finite dimensions of the CC has been more thoroughly investigated, the chamber size effect can be inferred from the following:

- The experimental data show that in silica sand q_c normalized with respect to the current horizontal effective stress increases with increasing ratio of the chamber (D_c) to cone (d_c) diameter. This phenomenon is especially evident with boundary condition B-1 (see Fig.1) corresponding to the cone penetration under constant boundary stresses.
- As a logical consequence, q_c is influenced by the boundary conditions set-up during the penetration stage. Their influence on q_c increases with increasing D_R and decreases when mean effective stress σ'_0 and D_c/d_c ratio decrease.

Such effects are intimately linked to the sign and the amount of volumetric strain which CC specimen tends to exhibit during penetration of the cone.

Although the above observations were made for CPT, they also hold for other in situ techniques such as pressuremeter, dilatometer and plate loading tests when performed in CC.

Recently, Schnaid and Houlsby (1990) have documented experimentally the importance of chamber size effects on the ultimate cavity stress p_u obtained from pressuremeter tests. According to these authors the finite chamber dimensions influences to approximately the same extent, both p_u and q_c .

d. Another important question related to CC research involves the so-called scale effects. These effects refer basically to a number of phenomena which are pertinent also to the field situations, such as:

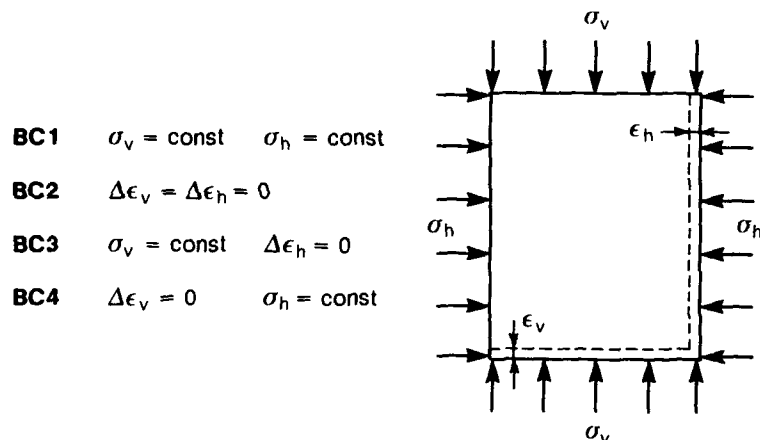


FIG. 1. Boundary conditions available in Italian CC's.

- Curvilinear strength envelope which is responsible for the fact that mobilized peak angle of friction ϕ'_p decreases with increasing normal effective stress σ'_{ff} acting on failure plane at failure. For more details and engineering relevance of this phenomenon to the bearing capacity problem in cohesionless soils, see De Beer (1967), Kerisel (1967), Vesic (1967), Baligh (1975), Steenfelt (1977), Meyerhof (1983) Bolton (1986), Bolton and Lau (1989).
- Progressive failure and formation of shear bands which are responsible for important scale effects in bearing capacity problems in sands, see for example; De Beer (1965), Yamaguchi et al. (1977), Tatsuoka et al. (1989, 1991).
- Influence of soil particle size on the results of in situ tests involving the development of large strains in the surrounding soil, especially such as the different types of penetration tests. The writers are not aware of any comprehensive studies covering this aspect of the problem. On the basis of limited information available [Steenfelt (1977), De Beer (1965), Peterson (1988)] one can postulate that in uniformly graded sands a ratio of d_c to the mean particle size D_{50} exceeding 20 to 40 might render uninfluential this factor on the results of CPT.

Length constraint of this paper, as well as the lack of a comprehensive knowledge and information, do not allow the writers to present exhaustive comments on the problems mentioned in this section. However, in the following part of the paper a series of preliminary data will be shown and some consideration will be devoted to the following problems:

- influence of geological time on the stress-strain behaviour of cohesionless soils and on the results of penetration tests;
- influence of chamber size and of applied boundary conditions on the q_c of the predominantly silica sands tested in the CC's.

3. INFLUENCE OF TIME

It is well known that geological time influences the mechanical behaviour of soils. This fact, widely accepted for cohesive soils in the last decade, has been also recognized to be relevant to cohesionless soils.

In the broad term "geological time", many physical-chemical phenomena are included, as already mentioned in section 2) of the paper. The importance of some of these phenomena on the penetration resistance and on the strength and stiffness of cohesionless soils are here below briefly examined in the light of the experimental data which have become available in the last few years.

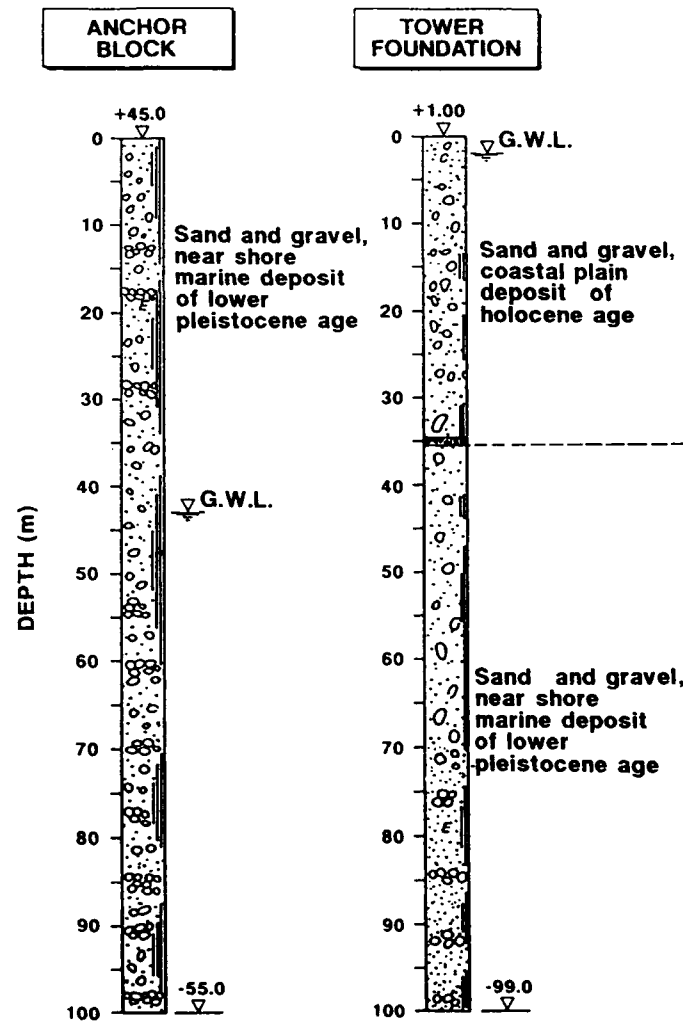


FIG. 2. Messina Strait Crossing - Sicilian shore.

a. Field evidences

Two examples of field evidences are reported showing that geological time can play an important role in the interpretation of penetration tests in granular soils.

The first case refers to the geotechnical studies conducted on gravelly sand deposits covering the shore north east from the town of Messina in relation to the design of the one span suspended bridge over the Messina Strait. The soil at the proposed site for the bridge tower foundation consists in the first 30 to 35 meters of sands and gravels belonging to the so called Holocene Coastal Plain formation which age has been estimated by geologists to range between 10 and 30 thousands years. Below this depth, a medium Pleistocene deposits of sands and gravels locally known as Messina Gravels formation are encountered. This formation can be estimated at least 500,000 years old.

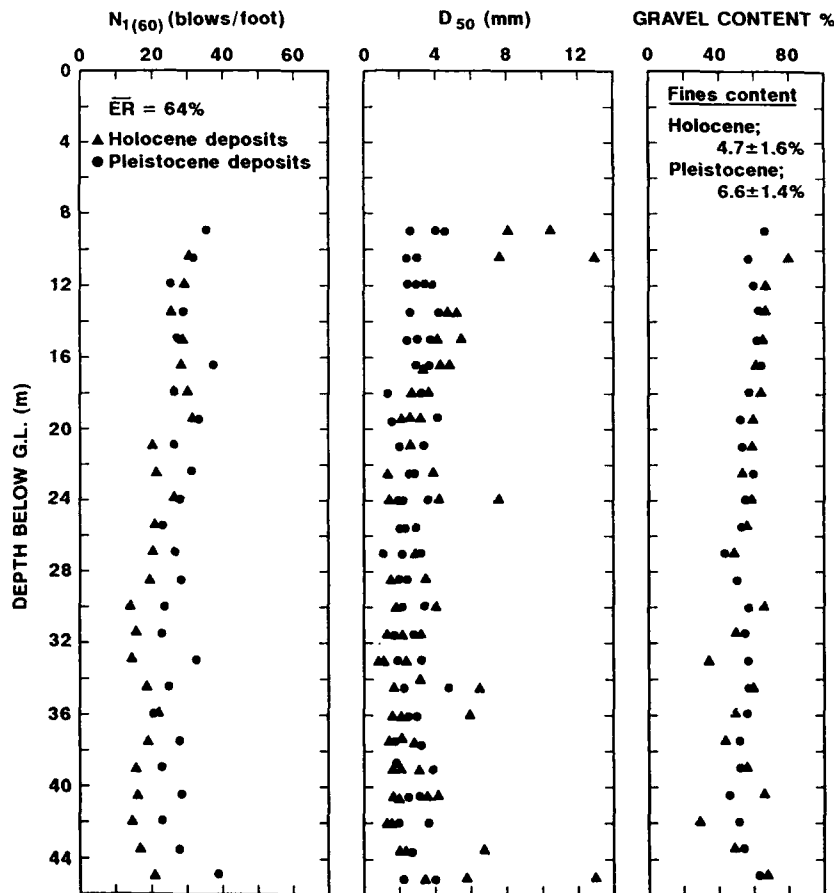


FIG. 3. Messina Strait Crossing - Sicilian shore normalized SPT resistance.

At the anchor block site, the top of the Pleistocene Messina Gravel formation is encountered at the depth of few meters below the G.L.. The soil profiles representative for the two sites are shown in Fig.2.

Both formations are composed of materials which are very similar in grading and mineralogical compositions, see Fig.3. Moreover, they have been deposited in similar deltaic and shallow sea environment. Fig.3 reports the normalized Standard Penetration resistance ($N_1(60)$) reduced to the rod energy equal to 60%, the mean particle size D_{50} and content of particles larger than 2 mm collected at the two locations. The data in Fig.3 show that the penetration resistance within the Pleistocene deposit is at best 10 to 15 percent higher than those of the Holocene Coastal Plain deposits. This is, at least partially, in disagreement with the conclusions by Skempton (1986) concerning the influence of geological age on Standard Penetration resistance. At the same two sites shear wave velocities V_s have been measured using the cross-hole technique. Fig.4 reports the modulus number K_2 of the maximum shear modulus G_o as obtained from the measured shear wave

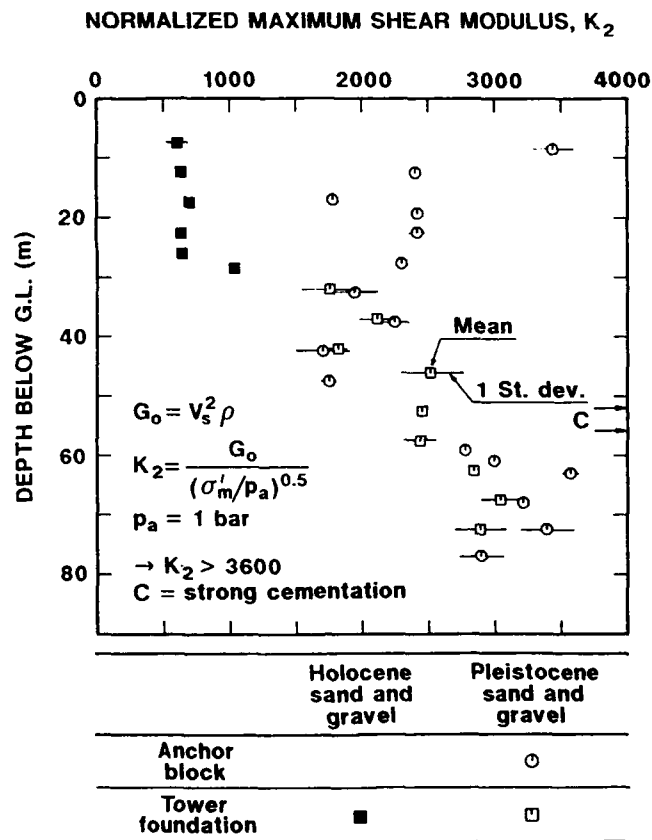


FIG. 4. Messina Strait Crossing - Sicilian shore normalized shear modulus from seismic tests.

velocities (K_2 = maximum shear modulus normalized with respect to σ'_0). It can be seen that at the tower foundation location the value of K_2 within the Holocene deposit is approximately 3 to 4 times lower than those encountered in the underlying Pleistocene formation. Furthermore, the values of K_2 within this latter formation at both locations coincide. The different sensitivity of SPT and shear modulus to the age of deposits appears evident for the examined case. Detailed geological investigations have been undertaken with the aim of explaining the reasons for the difference in K_2 in these two sand-gravel deposits having similar index properties and penetration resistance. The results of these studies showed that besides of the different amount of accumulated secondary compression, the Pleistocene deposit is very lightly cemented by calcium carbonate of biochemical origin and by oxides of iron and manganese. For further details see Ghionna and Jamiolkowski (1991).

Another interesting field case is represented by the University of Pavia testing site, see Ghionna et al. (1991), where a deposit of natural Ticino river sand having an age ranging between 15,000 years (top) and 30,000 years (bottom) is encountered at the depth ≈ 12 m below C.L.. The grading of this natural Ticino sand and of that used extensively in the Italian CC research are compared in Fig.5. Fig.6 reports the values of G_0 as inferred from in situ seismic tests, self-boring pressuremeter tests (Bellotti et al. 1989), engineering correlations with results of SPT's and CPT's and laboratory tests performed on the specimens reconstituted and reconsolidated to the state (e , σ'_0) supposed to exist in the field.

The data reported in Fig.6 clearly show that both laboratory tests and engineering correlations based on in situ tests results, underestimate the value of G_0 .

More specifically, the underprediction of G_0 is observed in the following:

- the correlation of q_c vs G_0 based on CC test results, see Bellotti et al. (1989), Baldi et al. (1989);

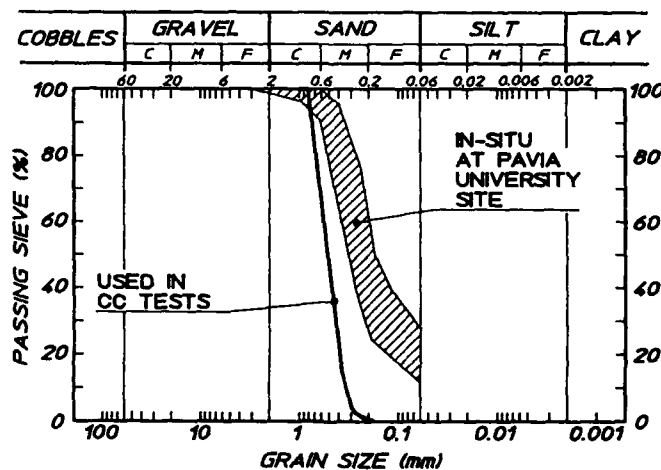


FIG. 5. Grading of Ticino Sand.

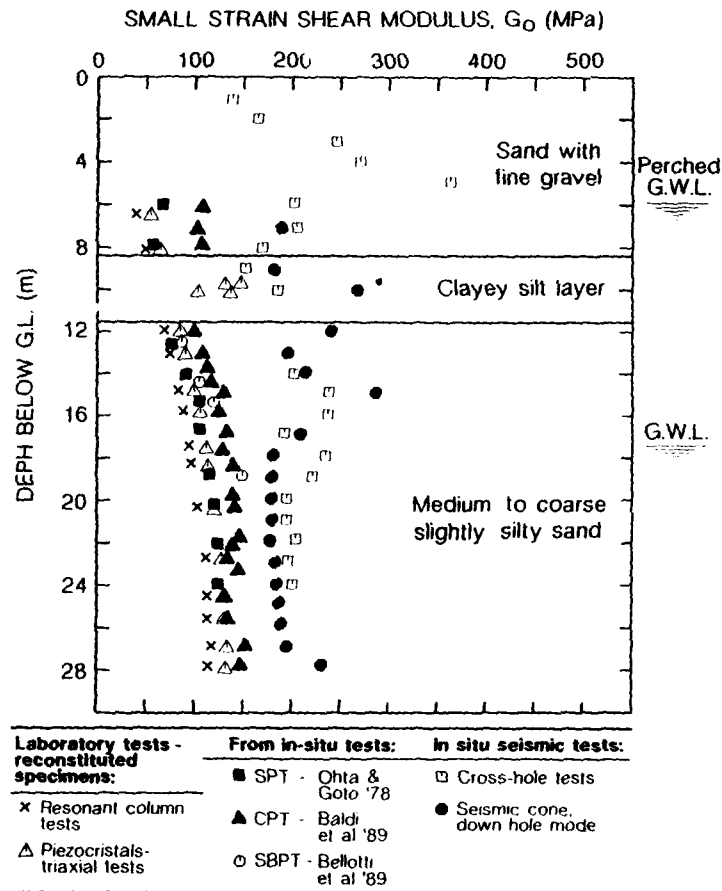


FIG. 6. Small strain shear modulus of Ticino sand at Pavia University Site Ghionna et al. (1991).

- the correlation of N_{SPT} vs G_0 established for very recent alluvial deposits in Japan, see Ohta and Goto (1978);
- the values of G_0 inferred from the SBPT's using the approach suggested by Bellotti et al. (1989) also established on the basis of the CC test results.

This underprediction ranges between 25 and 40% below the G.W.L. and it results even higher above G.W.L., suggesting that some kind of oxidation and/or cementation might be present.

Again, as for sands and gravels deposits at the location of Messina Strait Crossing the G_0 appears to be much more sensitive to the effects of the geological time than the results of SPT's and CPT's.

b. Drained Creep

Recent works by Mesri and his co-workers [Mesri and Castro (1987); Mesri (1989); Mesri et al. (1990)] have shown that secondary compression influences the mechanical properties of granular soils. Without going into details, in works mentioned above it is suggested that G_o increases with time due to secondary compression. This increase can be estimated from the following empirical relationship [Mesri et al. (1990)] based on the assumption that at given e , G_o is proportional to the square root of consolidation stress:

$$N_G = \frac{\Delta G}{G_p} = \exp \left[1.15 \frac{C_\alpha/C_c}{1 - C_r/C_\alpha} \right] - 1 \quad (1)$$

where:

ΔG = increase of G_o per log time of secondary compression [at least in principle, this value of ΔG should be also for stiffness evaluated at higher strain level]

$G_p = G_o$ at end of primary compression

C_α = coefficient of secondary compression $de/d \log t$

C_c = compression index beyond vertical yield stress = $de/d \log \sigma'_v$

C_r = recompression index up to the critical vertical yield stress $de/d \log \sigma'_v$.

With typical value of $0.015 \leq C_\alpha/C_c \leq 0.03$ [Mesri et al. (1990)] and $0.1 \leq C_r/C_c \leq 0.17$ one gets for granular soils $0.017 \leq N_G \leq 0.037$. The resonant column tests performed at the Technical University of Torino [Lo Presti (1990)] led to the values of N_G for granular material tested by the writers shown in Table II:

TABLE II. Values of N_G for four granular soils.

Soil	N_G
Ticino sand	0.012
Hokksund sand	0.011
Belgium Glauconitic sand	0.039
Messina sands and gravels	0.022 to 0.035

These values of N_G appear to be in good agreement with those predicted by means of the empirical formula suggested by Mesri et al. (1990). However, they probably slightly overestimate the increase of G_o per log time of secondary compression, incorporating also a small reduction of e which in turn determines an increase in stiffness.

As far as in situ tests and particularly, penetration tests are concerned, the influence of drained creep on their results is not yet well understood. From the work by Skempton (1986) one can infer that the SPT resistance in aged sands should be 25 to 50% higher than those in recent Holocene deposits.

Mesri et al. (1990), referring mainly to sands which had been previously subjected to densification processes, postulated the following empirical relationship expressing the increase of cone resistance with secondary compression:

$$\frac{q_c(t)}{q_c(t_R)} = \left[\frac{t}{t_R} \right]^{\frac{C_d C_\alpha}{C_c}} \quad (2)$$

$q_c(t)$ - cone resistance at time $t > t_R$

$q_c(t_R)$ - cone resistance at an arbitrary selected reference time t_R equal or higher than t_p necessary to achieve the primary consolidation

C_d - parameter reflecting any non-static mechanism leading to the reduction of e .

The above empirical expression leads to the conclusion that drained creep influences to a similar extent the increase of q_c and G_o with time. To be confirmed this postulate requires further research and field evidences. Its validity might be limited only to granular soils which have been subjected to vibratory and impact densification. For further details regarding the field cases on which Mesri et al. (1990) proposal is based, see Mitchell (1986), Hryciw (1986), Mitchell and Solymar (1984) and Mitchell (1988).

At present, the problem should be framed between two extreme limits: an upper bound postulated by Mesri et al. (1990) and a lower bound, resulting from the assumption that the large straining caused by penetration destructures the surrounding soil, at least within the limit of plastic zone. In this case, the influence of geological time, hence of drained creep on q_c , should be ideally linked to the increase of the stiffness in the outer elastic less strained zone where soil probably has not been destructured. This kind of scenario is implicitly connected to the idea that the mechanism of the cone penetration in sand can be in first approximation modelled by the theories of expanding cavities, hypothesis supported by recent work by Schnaid and Houlsby (1990).

In order to understand what could be the contribution of the increase in stiffness in the elastic zone towards an increase in q_c , simple calculations have been performed using the theory of expanding cylindrical cavity incorporating stress-strain non linearity modelled by a hyperbola, see Tseng (1989).

The calculations have been performed using stress-strain and strength characteristics of clean Ticino sand assuming no volumetric strain in the plastic zone [$\Delta = 0$, referring to Vesic (1972) theory] and the obtained results are shown in Table III.

From what is shown in this table one can argue that when the initial tangent stiffness E'_1 increases 100%, the q_c increases from 26% in loose sands to only 12% in very dense sands.

c. Cementation

Another structure-forming process frequently present in many natural deposits of granular soils is cementation. Reference is here made to a very light cementation which can seldom be detected by conventional site investigation techniques. As far as classification of cemented granular soils is

Table III. Influence of non-linear stiffness on q_c .

Tseng (1989) cylindrical cavity expansion model with hyperbolic stress-strain relationship in elastic zone and with $\Delta = 0$.

MEDIUM DENSE SAND, $\phi_p' = 36^\circ$, $\alpha = 0^\circ$ (*)

E_i' (MPa)	20	24	30	40
q_c (MPa)	4.2	4.5	4.8	5.3

DENSE SAND, $\phi_p' = 40^\circ$, $\alpha = 7^\circ$

E_i' (MPa)	45	54	68	90
q_c (MPa)	7.0	7.3	7.9	8.5

VERY DENSE SAND, $\phi_p' = 44^\circ$, $\alpha = 10^\circ$

E_i' (MPa)	110	132	165	220
q_c (MPa)	13.0	13.5	14.0	14.5

All values of q_c computed for $\sigma_o' = 100$ kPa.

(*) Angle expressing non linearity of shear strength envelope (Baligh, 1975)

concerned see Rad (1983).

The influence of such light cementation on stress-strain and strength behaviour of granular soils has been quite intensively investigated in the last decade [Rad (1983); Sitar (1983); Avramidis (1985); Al-Ghanem (1989), Poulos (1989)] through testing both artificially and naturally cemented soils.

Based on the results of these studies the following can be inferred:

- Cementation confers soils some value of cohesion intercept c' , with an almost negligible influence on the peak angle of shearing resistance (ϕ_p').
- For very lightly and lightly cemented soils [Rad (1983)] the magnitude of c' is relatively small, and generally does not exceed 20 to 40 kPa.

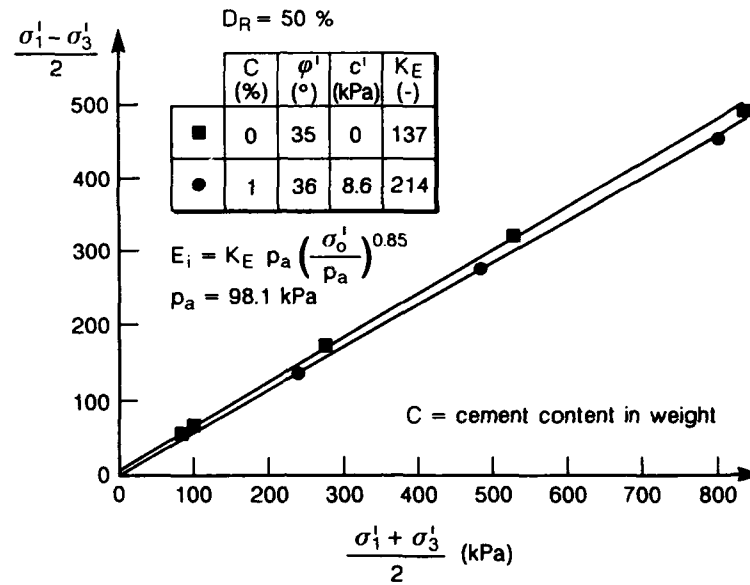
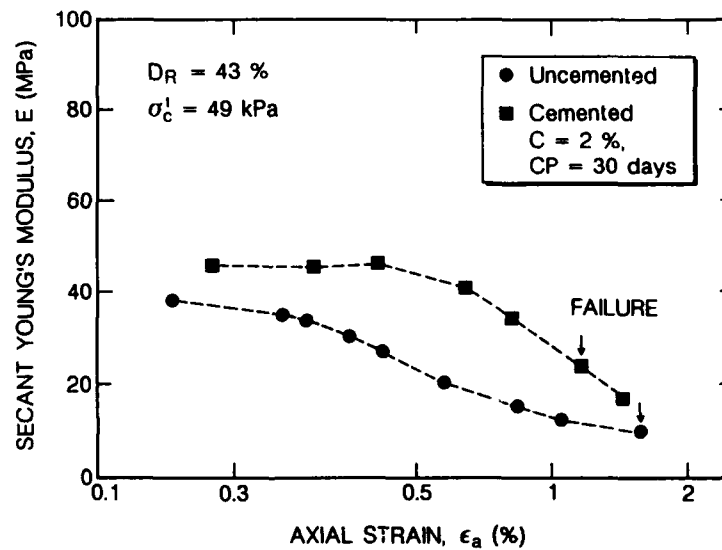


FIG. 7. Influence of slight cementation on strength and stiffness of Monterey sand. Adapted from Rad (1983).



C = cement content , CP = curing period

FIG. 8. Influence of cementation on stiffness of Monterey sand. Adapted from Avramidis (1985).

As an example, the strength envelopes of both uncemented and artificially cemented with 1% of portland cement Monterey 0/30 sand is shown in Fig.7.

- In contrast, even very light cementation has an important influence on the stiffness, especially at small and intermediate strain levels, see Fig.8.
- The stiffness of artificially cemented sands increases with the amount of cement, see Fig.9. In the case of CaCO_3 cementation, the whole problem becomes more complex, Al-Ghanem (1989) found that in the artificially CaCO_3 -cemented Monterey sand there is a kind of threshold content of cemented agent at which one achieves a maximum gain in the mechanical properties. Beyond such a threshold value of CaCO_3 both stiffness and strength tend to decrease.

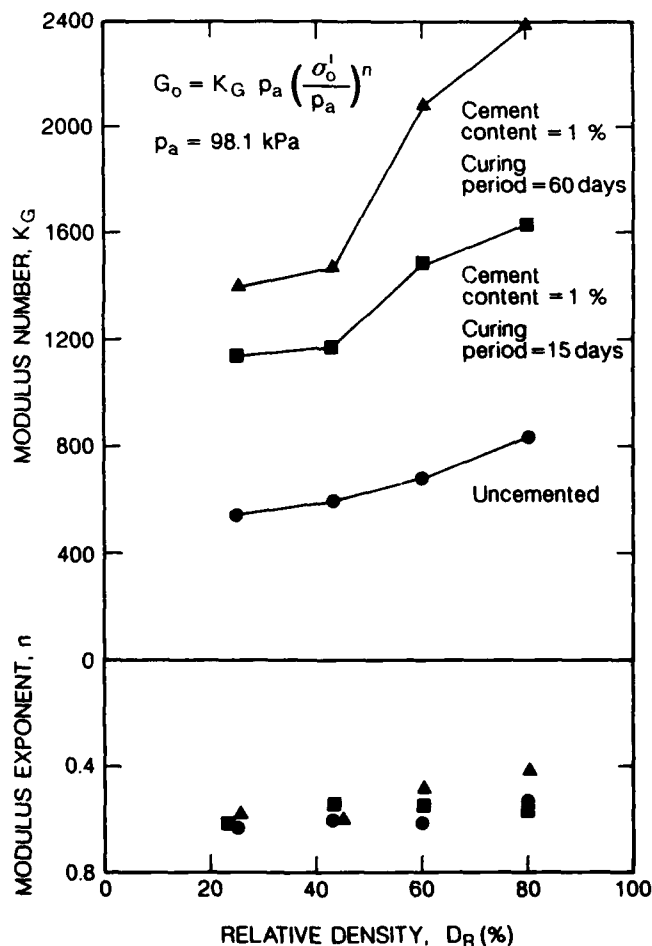


FIG. 9. Influence of cementation on maximum shear modulus of Monterey sand
 Adapted from Avramidis (1985).

- Works by Sitar (1983), Rad (1983) and Al-Ghanem (1989) indicated that the mechanical behaviour of artificially cemented sands is not substantially different from that which has been naturally cemented.
- The structure of lightly cemented granular soils is very brittle and extremely sensitive to sample disturbance.

Unfortunately, very little is known as far as influence of cementation on in situ tests and especially penetration tests results is concerned. The information available in literature [Rad and Tumay (1986) and Evans (1987), Poulos (1989)] is not conclusive in that respect.

In order to get a preliminary information on the possible influence of light cementation, the values of q_c have been computed with reference to a loose silica sand using classical bearing capacity formula valid for axis-symmetrical case [Berezantzev (1970)] and by means of Vesic (1972, 1977) approach making reference to the expanding cylindrical cavity theory.

The values of q_c computed for $\phi' = 36^\circ$ and c' equal respectively to 0, 20 and 40 kPa are reported in Table IV. Both simplified calculation approaches tend to suggest that a moderate cohesion intercept leads to an increase of q_c of the order of 22 to 45%. This might suggest that also cohesion

Table IV. Influence of c' on q_c in loose cemented sand.

Vesic (1972) cylindrical cavity expansion model with $\Delta = 0$:

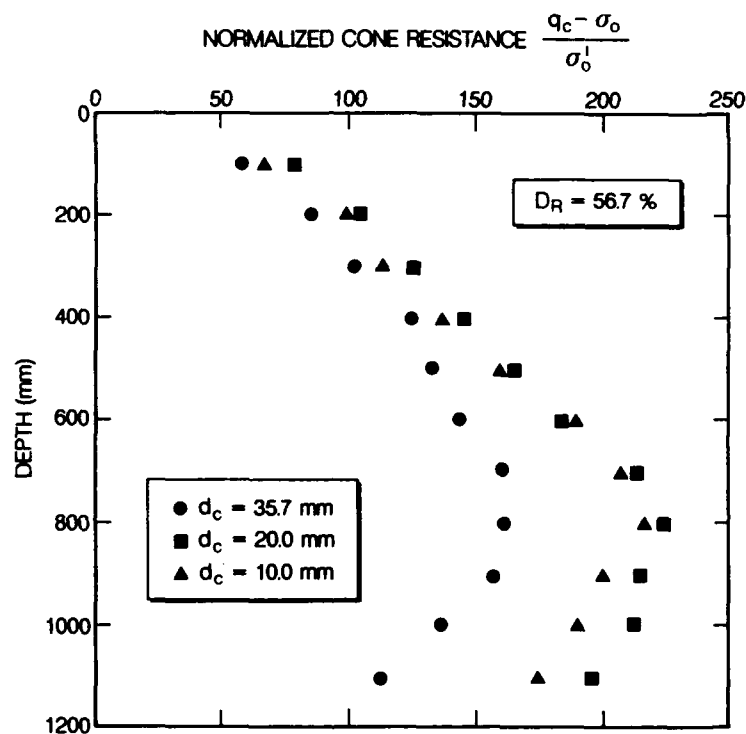
$\begin{matrix} c' \\ \text{(kPa)} \\ \text{G} \end{matrix}$	0	20	40
20	8.9	11.3	12.5
40	-	15.2	16.3
60	-	-	19.1

Berezantzev (1970) bearing capacity theory:

$\begin{matrix} c' \\ \text{(kPa)} \end{matrix}$	0	20	40
$\begin{matrix} q_c \\ \text{(MPa)} \end{matrix}$	8.5	10.4	12.3

All values of q_c computed $\phi'_p = 36^\circ$ and $\sigma'_o = 100$ kPa

intercept has a moderate impact on penetration resistance. Probably, also in this case as in that of the drained creep, the influence of light cementation on the penetration resistance should be linked to the contribute from increased stiffness in the outer less strained zone.



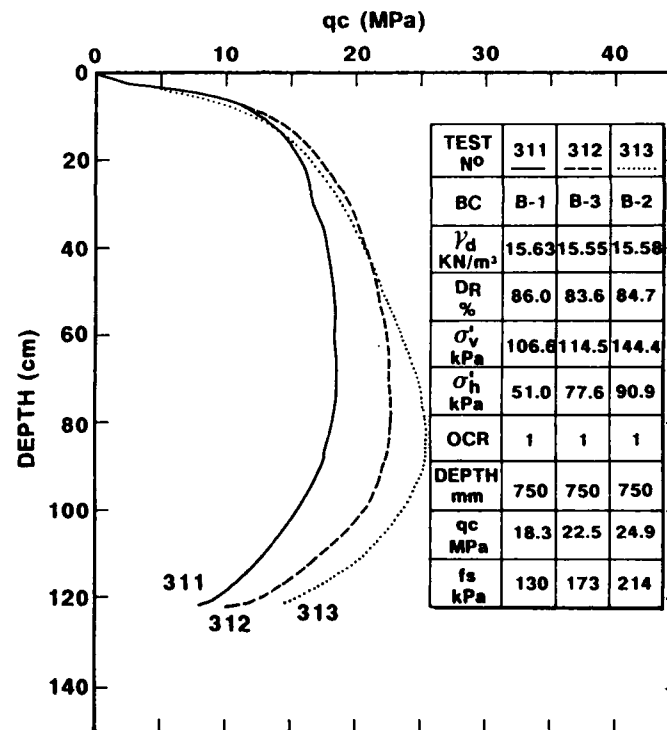
Test n.	363	366	364
BC (-)	1	1	1
D_R (%)	56.7	56.5	57.0
σ_{vp}^1 (kPa)	60.0	61.0	61.0
σ_{hp}^1 (kPa)	27.8	28.2	30.0
OCR (-)	1	1	1
d_c (mm)	35.7	20.0	10.0

FIG. 10. Influence of cone size on cone resistance of Toyoura sand.

4. CHAMBER SIZE AND BOUNDARY CONDITIONS EFFECTS

As previously noted, the limited size of the CC raises the important question of the validity of the obtained experimental results. This is mainly linked to the possible influence of the presence of the lateral boundary of the CC specimen. Chamber size effects are very difficult to be examined from a theoretical point of view, especially for penetration tests, for which the numerical analysis results to be very complex. In the case of CPT the existence of the chamber size and boundary conditions effects can be recognized in the following experimental facts typically encountered in dense silica sands when using a CC which is not sufficiently large:

- penetrating a specimen under constant boundary stresses a larger cone will give a smaller q_c than a smaller cone, see Fig.10;
- for a given D_c/d_c ratio, the measured q_c depends on the applied boundary conditions, see Fig.11;



CALIBRATION CHAMBER
SPECIMEN :

$H_c=1500\text{mm}$; $D_c=1200\text{mm}$

CONE DIAMETER :

$d_c=35.7\text{mm}$

FIG. 11. Influence of boundary conditions on cone resistance of very dense Toyoura sand.

- especially in CC's having both top and bottom rigid, the stress distribution within the specimen might not be uniform as evidenced by the FEM analysis performed by Sweeney (1987), see Fig.12.

The experimental data suggest that for a given sand and D_c/d_c ratio, chamber size effects are more pronounced in dense than in loose state and their importance decreases with increasing compressibility of tested material. Even if the examined phenomena are difficult to be quantified, the data reported in Figs 13 through 15 and Table IV document the above mentioned trends. The experimental results:

- clear the importance of D_c/d_c ratio on CPT results, Fig.10;
- suggest that in silica materials of low and moderate compressibility like Toyoura and Monterey sands, even in loose state, D_c/d_c higher than 30 to 35 is required in order to avoid chamber size effects, Figs.13 and 14 and Table IV;
- confirm that for the same types of sand in dense and very dense state, $D_c/d_c \geq 60$ is necessary in order to minimize the influence of the proximity of the lateral boundaries, Figs 13 and 14;

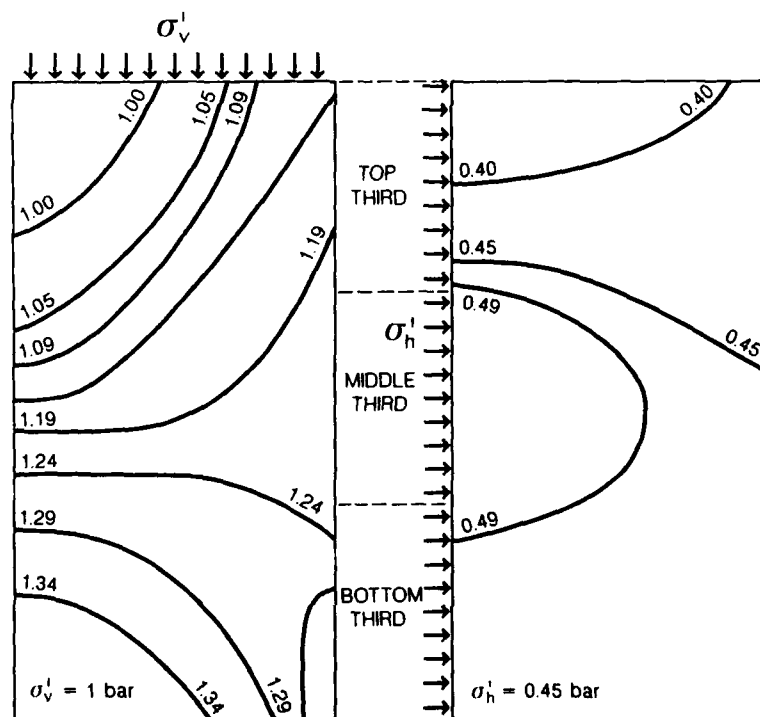


FIG. 12. Stress distribution in CC specimen from FEM analysis
Monterey 0/30 sand, $D_R = 24\%$. Sweeney (1987).

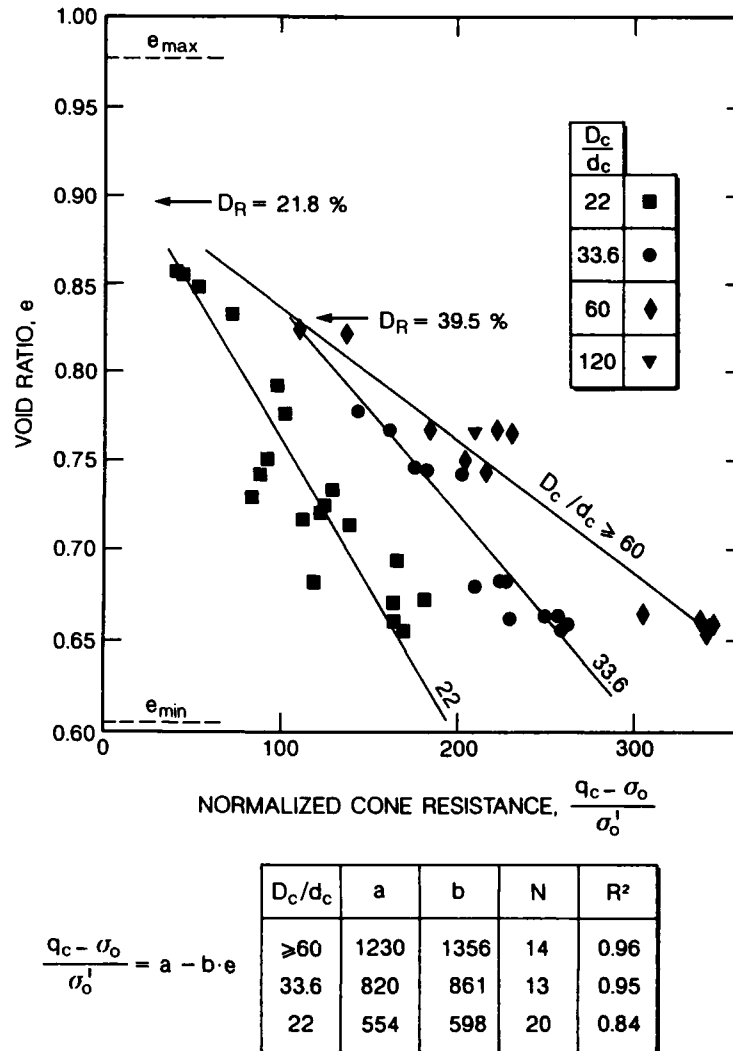


FIG. 13. Chamber size effect in Toyoura sand.

- emphasize the paramount importance of the compressibility of tested sand on the manifestation of the chamber size effects, Fig.15.

From the above statements it appears that in sands of low and moderate compressibility the use of CC's having dimensions sufficiently large to avoid the chamber size effects for dense specimens, might meet limitation in the cost-effectiveness of the research.

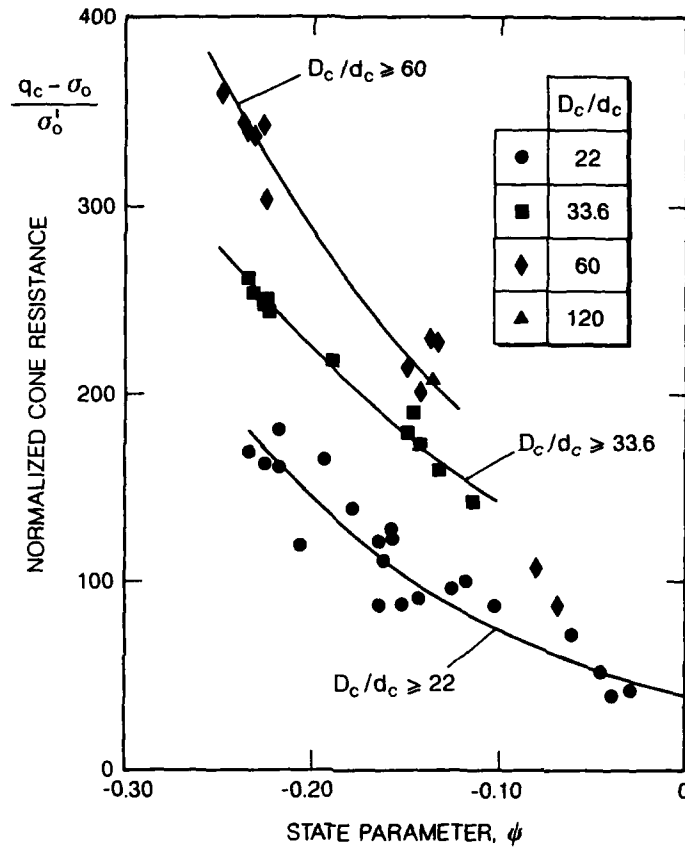


FIG. 14. Normalized cone resistance of Toyoura sand vs state parameter.

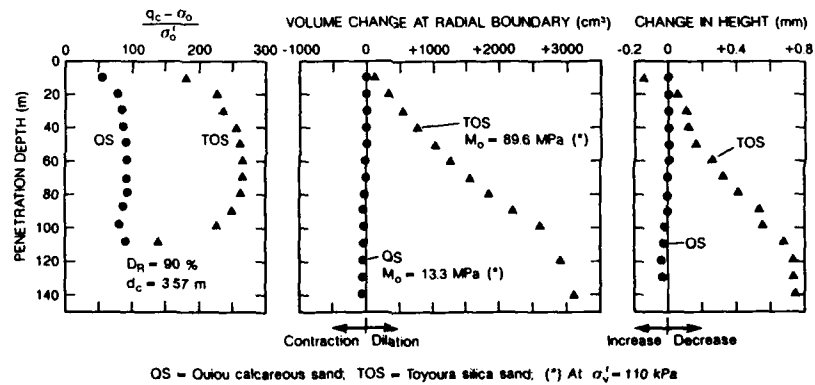


FIG. 15. CPT's performed in two very dense NC sands of different compressibility (Constant boundary stresses during penetration).

The problem can be at least partially overcome, implementing a computer controlled feed-back, at the radial boundary of the specimen to simulate the stress which will occur at the same radial distance in case of a cylinder having infinite radius. This solution has been adopted during the SBPT's performed in the ISMES CC following the concept illustrated in Fig.16. The expansion curves obtained in dense Ticino sand when using this type of radial boundary control yielded the ultimate cavity stress only slightly lower than those corresponding to $\sigma'_v = \text{const.}$ and $\Delta\epsilon_r = 0$ boundary conditions. Unfortunately, the use of this type of control is less straightforward for more complex boundary value problems than it is for pressuremeter tests. To attempt the same in case of penetration, dilatometer or plate loading tests, preliminary numerical simulations of each specific CC test with a help of an adequate constitutive equation, will be necessary.

Finally, considering the costs of each CC test, it is suggested that some of the unsolved problems mentioned in this paper, including that of the chamber size effects, can probably be solved in a more cost-effective manner

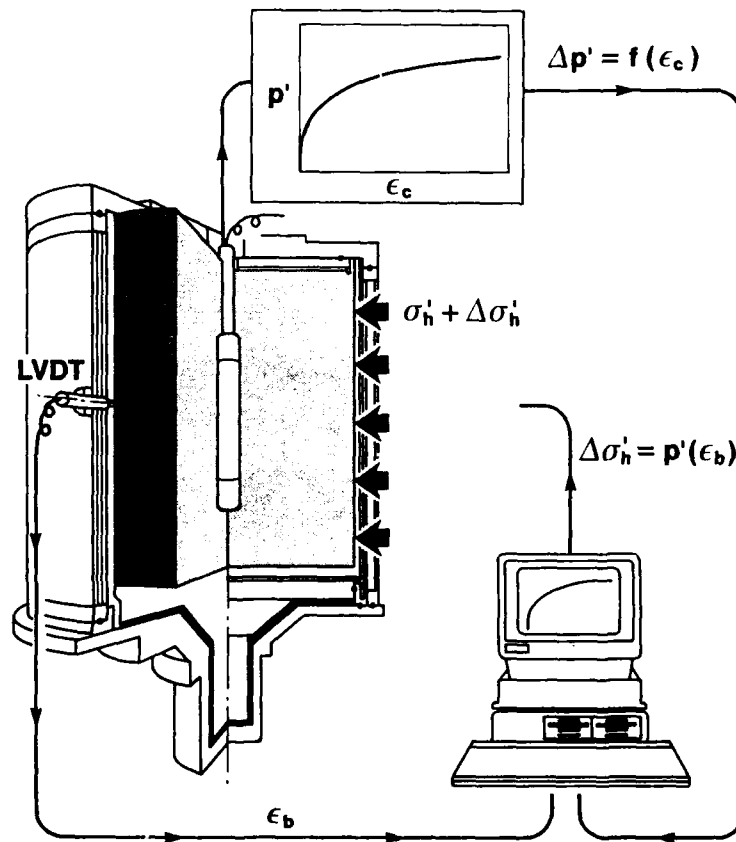


FIG. 16. SBPT in Calibration Chamber simulating infinite boundary.

by combining centrifuge and large size calibration tests. As an example Fig.17 shows a comparison of results of CPT's performed in Ticino sand using both CC and centrifuge.

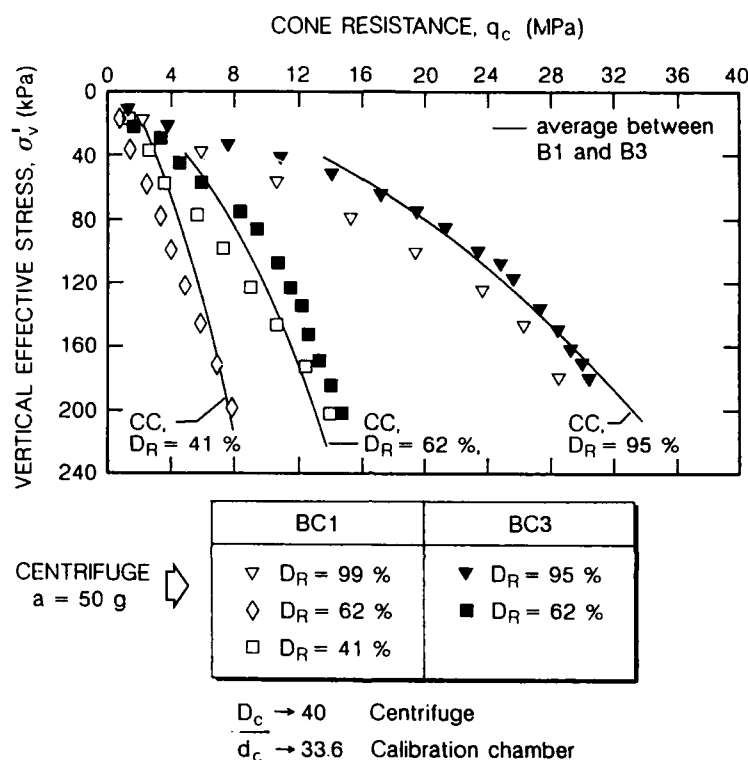


FIG. 17. q_c centrifuge vs q_c - CC in Ticino sand.

5. FINAL REMARKS

The paper presents a brief review of the present status of the CC testing and the related problems which need to be solved for a new impulse to be given to this area of geotechnical research.

From what previously reported the following final remarks can be formulated:

1. With few exceptions the present experience is limited to the tests on clean uniform sands, almost always predominantly silica materials of low to moderate compressibility. Therefore, the need to extend the CC experiments to more realistic types of granular deposits such as: silty, crushable, slightly cemented, etc., granular materials, is urgent.

2. In the last decade it has been demonstrated that geological time and related fabric and structure-forming processes play an important role in the mechanical behaviour of granular soils. In this circumstance, keeping in mind that CC tests are run in freshly deposited sands, it becomes imperative to understand better, and possibly quantify, the influence of this factor on the reliability of the engineering correlations worked out on the basis of this type of research.
3. Due to practical reasons the CC in use have finite dimensions. This fact, together with a lack of knowledge of the real conditions in terms of stresses or strains which one has to impose at the specimen boundaries are responsible for the so called chamber size effects which poses some question-marks regarding the use of the engineering correlations established from the CC tests in the field situation.
This problem which has not yet completely understood from a theoretical point of view and which has been only partially documented by experiments as far as cone and pressuremeter tests are concerned, deserves further research efforts.
Incidentally, the extension of CC research to the use of more realistic types of soil which are usually more compressible, will attenuate the impact of the chamber size and boundary conditions on test results.
4. Also, the techniques used to prepare the large dimension specimens for CC tests even with clean uniform sand is not fully satisfactory, especially at intermediate densities. The problem becomes more acute when moving into the preparation of CC specimens of non uniformly graded and silty sands. For such materials, new techniques assuring preparation of uniform and repeatable large size specimens, are needed.
5. Because testing in large size CC's is time-consuming and expensive, it might be convenient and cost-effective to combine it with centrifuge testing.

REFERENCES

- Al-Ghanem, A.M. (1989). "Factors Affecting the Strength Characteristics of Calcium-Carbonate-Cemented Soils". Ph.D. Thesis, The Univ. of Arizona.
- Avramidis, A. (1985). "Dynamic and Static Behaviour of Cemented Sands". Ph.D. Thesis, Illinois Institute of Technology, Chicago.
- Baldi, G. et al. (1989). "Modulus of Sands from CPT's and DMT's", 12th ICSMFE, Rio de Janeiro.
- Baligh, M.M. (1975). "Theory of Deep Site Static Cone Penetration Resistance". Res. Report R75-56, No.517, Dept. of Civil Eng., MIT, Cambridge, Mass.
- Barton, M.E. and Palmer, S.N. (1989). "The Relative Density of Geologically Aged, British Fine and Fine-Medium Sands". Quarterly Journ. of Engineering Geology, Vol.22, pp.49-58.
- Battaglio, M., Bellotti, R. and Pasqualini, R. (1979). "La deposizione pluviale come mezzo per la preparazione di provini di sabbia". Rivista Italiana di Geotecnica Anno XIII, N.2.

- Bellotti, R., Bizzi, G. and Ghionna, V. (1982). "Design, Construction and Use of a Calibration Chamber". Proc. ESOPT II, Amsterdam, Vol.2, pp.439-446.
- Bellotti, R. et al. (1985). "Laboratory Validation of In-Situ Tests". Geotechnical Engineering in Italy - An Overview, 1985, ISSMFE Golden Jubilee Volume, Associazione Geotecnica Italiana, Roma.
- Bellotti, R. Ghionna, V.N., Jamiolkowski, M., Robertson, P.K. and Peterson, R.W. (1989). "Interpretation of Moduli from Self-Boring Pressuremeter Tests in Sand". Géotechnique 39, No.2, 269-292.
- Bellotti, R. and Jamiolkowski, M. (1990). "Evaluation of CPT and DMT in Crushable and Silty Sands". Second Interim Report to US Army Corps of Engineers, Waterways Experimental Station, Vicksburg.
- Been, K. and Jefferies, M.G. (1985). "A State Parameter for Sand". Géotechnique n.2.
- Been, K., Crooks, J.H.A. and Rothenburg, L. (1988). "A Critical Appraisal of CPT Calibration Chamber Tests". Proc. ISOPT I, Orlando, Fla.
- Berezantsev, W.G. (1970). "Calculation of Foundations Basis". edit. Literature for Contructions, Leningrad (in russian).
- Bolton, M.C. (1986). "The Strength and Dilatancy of Sands". Geotechnique n.1
- Bolton, M.D. and Lau, C.K. (1989). "Scale Effects in the Bearing Capacity of Granular Soils". Proc. XII ICSMFE, Rio de Janeiro.
- Brandon, T.L., Clough, W.G. and Rahardjo, P.P. (1990). "Evaluation of Liquefaction Potential of Silty Sands Based on Cone Penetration Resistance". Final Report to the WSF Virginia Tech., Blacksburg.
- Caillemer, B.M. (1975). "An Experimental Study in the U.F. Static Cone Calibration Chamber", M.Sc. Thesis, Univ. of Florida, Gainesville.
- De Beer, E.E. (1965). "The Scale Effect on the Phenomenon of Progressive Rupture in Cohesionless Soils", Proc. VI ICSMFE, Toronto.
- De Beer, E.E. (1967). "Bearing Capacity and Settlement of Shallow Foundations on Sand", Proc. of Symposium on Bearing Capacity and Settlement of Foundations, Duke Univ., Durham.
- Dusseault, M.B. and Morgenstern, N.R. (1979). "Locked Sands". Quarterly Journ. of Engineering Geology, Vol.12, pp.117-131.
- Eid, W.K. (1987). "Scaling Effect on Cone Penetration Testing in Sand". Ph.D. Thesis Virginia Tech., Blacksburg.
- Evans, K.M. (1987). "A Model Study of the End Bearing Capacity of Piles in Layered Calcareous Soils", Ph.D. Thesis University of Oxford.
- Ghionna, V.N., Jamiolkowski, M. (1991). "Influence of Time on the Behaviour of Granular Soils". Panel discussion - Session 1b, Proc.X ECSMFE, Florence.
- Ghionna, V.N., Braga, G. and Macchi, G. (1991). "Studies for the Assessment of the Stability of Pavia's Medieval Towers" draft of a paper, personal communication.
- Holden, J.C. (1967). "Stresses and Strains in a Sand Mass Subjected to a Uniform Circular Load". Ph.D. Thesis, University of Melbourne.
- Holden, J.C. (1971). "Research on Performance of Soil Penetrometers". Country Roads Board of Victoria Internal Report CE-SM-71-1.

- Hryciw, R.D. (1986). "A Study of the Physical and Chemical Aspects of Blast Densification of Sand". Ph.D. Thesis, Northwestern Univ. Evanston, Illinois.
- Jacobsen, N. (1976). "On Pluvial Compaction of Sand". Reporter n.9, Laboratoriet for fundering. University of Aalborg. Denmark.
- Jamolkowski, M., Ladd, C.C., Germaine, J.T. and Lancellotta, R. (1985). "New Developments in Field and Laboratory Testing of Soils", Theme Lecture, Proc. XI ICSMFE, San Francisco.
- Kerisel, J. (1967). "Scaling Laws in Soil Mechanics", Proc. 3rd Panamerican Conf. on SMFE, Caracas.
- Lo Presti, D.C.F. (1990). Personal communication.
- Mesri, G. (1987). "The Fourth Law in Soil Mechanics: The Law of Compressibility" Proc. Int. Symp., Mexico City, I Vol.
- Mesri, G. and Castro, A. (1987). "The C_a/C_c concept and K_0 During Secondary Compression". JGED, ASCE, n°3.
- Mesri, G., Feng, T.W. and J.M. Benak (1990). "Postdensification Penetration Resistance of Clean Sands". JGED, ASCE, n°7.
- Meyerhof, G.G. (1983). "Scale Effect of Ultimate Pile Capacity", JGED, ASCE GT6.
- Mitchell, J.K. (1988). "Densification and Improvement of Hydraulic Fills", Hydraulic Fill Structures, Geotechnical Special Pub. n°21, ASCE.
- Mitchell, J.K. and Solymar, Z.V. (1984). "Time-Dependent Gain in Freshly Deposited and Densified Sand". JGED, ASCE, N°11.
- Mitchell, J.K. (1986). "Practical Problems from Surprising Soil Behaviour". JGED, ASCE, N°3.
- Ohta Y. and Goto, N. (1978). "Empirical Shear Wave Velocity Equations in Terms of Characteristic Soil Indexes", Earthquake Engineering and Structural Dynamics, Vol.6.
- Palmer, S.N. and Barton, M.E. (1987). "Porosity Reduction, Microfabric and Resultant Lithification in UK Uncemented Sands", British Geological Society, Special Publication N°36.
- Parkin, A.K. and Lunne, T. (1982). "Boundary Effects in the Laboratory Calibration of a Cone Penetrometer in Sand". Proc. ESOPT II, Amsterdam.
- Peterson, R.W. (1986). Personal communication.
- Peterson, R.W. (1988). "Laboratory Investigation of the Penetration Resistance of Fine Cohesionless Materials". Proc. ISOPT I, Orlando.
- Poulos, H.G. (1989). "The Mechanics of Calcareous Sediments". Research Report N.595, The Univ. of Sydney, School of Civil and Mining Engineering, Sydney.
- Rad, N.S. (1983). "Static and Dynamic Behaviour of Cemented Sands". Ph.D. Thesis, Stanford Univ.
- Rad, N.S. and Tumay, M.T. (1986). "Effect of Cementation on the Cone Penetration Resistance of Sand: A Model Study". GTJ, ASTM, n°3.
- Rad, N.S. and Tumay, M.T. (1987). "Factors Affecting Sand Specimen Preparation by Raining", ASTM Geotechnical Testing Journal, N°1.
- Reese, J.D. (1975). "An Experimental Study on the Effects of Saturation on

- the q_c and f_s Values from Cone Penetration Tests in the U.F. Calibration Chamber". M.Sc. Thesis, Univ. of Florida, Gainesville.
- Schmertmann, J.H. (1989). "The Mechanical Aging of Soils", 25th Terzaghi Lecture, to be published in JGED, ASCE.
- Schnaid, F. and Houlsby, G.T. (1990). "An Assessment of Chamber Size Effects in the Calibration Chamber of In Situ Tests in Sand". Soil Mechanic Report N°110/90, University of Oxford, Department of Engineering Science.
- Sitar, N. (1983). "Behaviour of Slopes in Weakly Cemented Soils Under Static and Dynamic Loading". Ph.D. Thesis, Stanford Univ., Stanford.
- Skempton, A.W. and McDonald, D.H. (1956). "Allowable Settlement of Buildings", Proc. Instn. Civ. Engrs, Part 3, V.5, pp.727-768.
- Skempton, A.W. (1986). "Standard Penetration Test Procedures and the Effects in Sands of Overburden Pressure, Relative Density, Particle Size, Ageing and Overconsolidation", Geotechnique, No.3.
- Steenfelt, J.S. (1977). "Scale Effect on Bearing Capacity Factor N_γ ". Proc. IX ICSMFE, Tokyo.
- Sweeney, B. (1987). "Liquefaction Evaluation Using a Miniature Cone Penetrometer and a Large Scale Calibration Chamber". Ph.D. Thesis, Stanford Univ.
- Tatsuoka, F., Nakamura, S., Huang, C.C. and Tani, K. (1989). "Strength Anisotropy and Shear Bond Direction in Plane Strain Tests on Sand". Soils and Foundations N°1.
- Tatsuoka, F., Okahara, M., Tanaka, T., Tani, K., Morimoto, T. and Sidiqee, M.S.A. (1991). "Progressive Failure and Particle Size Effect in Bearing Capacity of a Footing on Sand". Personal communication.
- Tseng, D.J. (1989). "Prediction of Cone Penetration Resistance and its Application to Liquefaction Assessment", Dissertation submitted in partial satisfaction for the requirements for the degree of Doctor of Philosophy. University of California, Berkeley.
- Veismanis, A. (1974). "Laboratory Investigation on Electrical Friction Penetrometers in Sand". Proc. ESOP 1, Stockholm.
- Vesic, A.S. (1967). "A Study of Bearing Capacity of Deep Foundations", Report B-189, Georgia Inst. of Technology, Atlanta.
- Vesic, A.S. (1972). "Expansion of Cavities in Infinite Soil Mass". JSMFD, ASCE, SM3, March.
- Vesic, A.S. (1977). "Design of Pile Foundation. National Cooperative Highway Research Program". Report 42, Transportation Research Board, Washington, D.C.
- Yamaguchi, H., Kimura, T. and Fujii, N. (1977). "On Scale Effect of Footings in Dense Sand". Proc. IX ICSMFE, Tokyo.

PRELIMINARY RESULT OF CPT TESTS IN CALCAREOUS QUIOU SAND

M.S.S ALMEIDA,* M. JAMIOLKOWSKI,** and R.W. PETERSON***

*COPPE - Fed. Univ. of Rio de Janeiro, Brazil

**Technical University of Torino, Italy

***U.S. Army Corps of Engineers, Waterways Experimental Station, Vicksburg, USA

ABSTRACT

This paper reports the results of 8 CPT's performed in calibration chamber tests on biogenic, carbonatic Quiou sand.

The compressibility and cone resistance of this highly crushable sand are compared against those of silica Ticino sand which has been subject to a comprehensive series of calibration chamber tests. This comparison reveals the importance that the compressibility and crushability exerts on both cone resistance and stiffness.

Furtherly, the high compressibility of the Quiou sand is documented via the results of oedometer tests that have reached the range of vertical stress of 12 to 13 MPa.

1. INTRODUCTION

The recent interest [Demars and Chaney (1982), Jewell and Andrews (1988), Jewell and Korshid (1988)] in the study of calcareous sediments has been stimulated by the extremely low measured load capacity of offshore piles installed in these materials [Angemeer et al. (1973)] compared with the values predicted by conventional methods. Calcareous offshore sands are originated primarily from biological processes that involve the sedimentation of skeletal remains of marine organisms from the upper waters of the ocean. After deposition various processes take place, the most important of which is the cementation due to the precipitation of bonds.

The main geotechnical features of the calcareous sediments are [Semple (1988)] angularity and structural weakness of their particles, variable cementation and the occurrence of calcareous sediments at higher voids ratio than silicate sediments. Hence, unlike silica sands, calcareous sediments tend to exhibit a volume reduction upon shearing, even at low stresses. It is now believed [Poulos (1989)] that while the crushability of the grains and the variable cementation are important features [Datta et al. (1982)] of these soils, the initial voids ratio [Semple (1988)] plays a key role in determining the behaviour of calcareous sediments and if duly considered some of the differences in behaviour between calcareous and non calcareous sediments become less significant. It has also been shown [Coop (1990)] that despite particle breakage, the behaviour of calcareous sands is consistent with the mean features of critical state soil mechanics.

Due to the characteristics outlined above, good quality sampling of calcareous sands is hampered by crushing of grains and damage of cementation bonds, thus laboratory testing should be complemented by means of in situ testing. Classification procedures developed for terrigenous materials

based on CPT tests [Robertson and Campanella (1984)] have been applied to calcareous sediments with relative degree of success [Ebelhar et al. (1988)], though at present the CPT is unable to distinguish between cementation and relative density [Rad and Tumay (1986)].

This paper presents preliminary results of CPT tests of an uncemented calcareous sand in a calibration chamber. This study is part of a wider research project on the evaluation of in situ tests performed in sands [Baldi et al. (1985), Jamiolkowski et al. (1988)]. The final aim of this study is to provide design parameters for soils most commonly found in nature, such as silty sands and crushable sands, and which are different from the accademic uniform quartz sands usually tested in calibration chambers.

2. TESTED SAND

The test sand was dug-out from the borrow area close to the village of Plousne, about 20 km from the town of Dinane Bretagne (France). The mineralogical composition of the Quiou sand is reported in Table I, which also gives information about the shape of the sand grains. As it can be seen it is essentially a biogenic carbonate sand having subangular to subrounded grains.

Table I. Mineralogical and morphological analyses of Quiou sand.

MINERALOGICAL COMPOSITION	{	SHELL FRAGMENTS _____	73.5 %
		CALCIUM CARBONATE AGGREGATES _____	14.5 %
		QUARTZ _____	11.8 %
		ROCK FRAGMENTS _____	0.2 %
GRAIN SHAPE	{	VERY ANGULAR _____	1.5 %
		ANGULAR _____	18.2 %
		SUBANGULAR _____	50.0 %
		SUBROUNDED _____	28.8 %
		ROUNDED _____	1.5 %

The sand, treated with a solution of HCL at 5%, revealed the CaCO_3 content equal to about 77% in weight. This value is in good agreement with the result of a stereo-microscope analysis which indicated that about 80% of the examined grains are composed of calcium carbonate. Levacher (1988) obtained 79% of calcium carbonate for a coarser Quiou sand. The predominance of calcium carbonate in these soils is the reason why they are called "calcareous sands".

Figure 1 shows the gradation curve of Quiou sand, which contains about 20% of grains passing through sieve n°200 ASTM. Because of problems arisen in the preparation of the Calibration Chamber (CC) specimens, it was decided to use in the first series of CC tests QS having only 3 to 4% of fines. The grading curve of this material is also shown in Fig.1. On the above material the maximum (γ_{\max}) and minimum (γ_{\min}) density have been determined following the ASTM Standard D-4253-83 procedure and the related results are shown in Fig.1.

$$\begin{aligned} \gamma_{\max} &= 11.67 \text{ kN/m}^3 & e_{\max} &= 1.281 & \gamma_s &= 26.62 \text{ kN/m}^3 \\ \gamma_{\min} &= 14.54 \text{ kN/m}^3 & e_{\min} &= 0.831 \end{aligned}$$

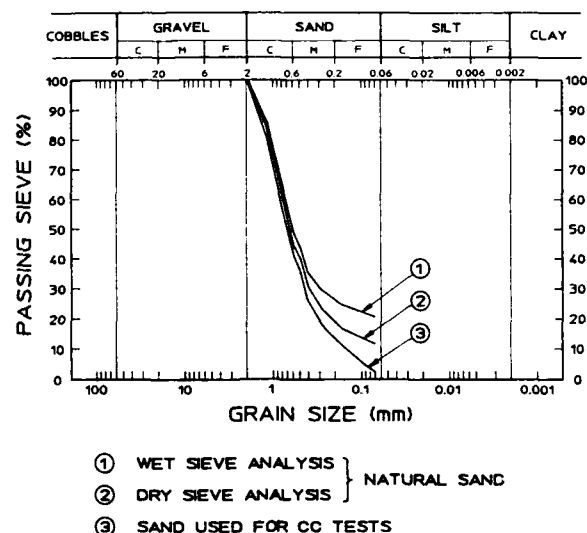


FIG. 1. Calcareous sand of Quiou.

3. OEDOMETER TESTS

A series of four oedometer tests at high stress levels has been performed at relative densities varying from 35% to 95%. The specimens have been prepared by means of dry pluviation as for calibration chamber specimens. It is well known that calcareous sands undergo considerable creep deformations [Semple (1988); Coop (1990)] and for this reason each loading step was limited to 30 seconds.

Voids ratio versus effective stress data of three tests are shown in Fig. 2. It is seen that the three specimens reach the virgin consolidation line at much lower stress levels than those necessary for the silicate sands to reach it. It also appears that particle crushing is gradual and this point is furtherly discussed in the following. Hence there is no clear definition of the yield stress. As the relative density increases the virgin consolidation line is reached at higher stress levels.

The average virgin compression index C_c of Quiou sand is 0.33. This value is close to $C_c = 0.34$ of an uncemented calcareous silty sand [Fahey (1988)] but is lower than $C_c = 0.50$ of the North Rankin soil [Semple (1988)] and even much lower than the $C_c = 0.76$ of the Dog's Bay sand [Coop (1990)]. Again a direct proportionality appears to exist between C_c and initial voids ratio, as suggested by Poulos (1989), i.e., the greater the voids ratio the greater the value of C_c .

The swelling lines of the three specimens indicate extremely low values of C_s , i.e., and almost irreversible plastic behaviour resulting from the soil crushing. Therefore, unlike terrigenous materials, calcareous soil present very high values of C_c/C_s , which feature is also observed by Coop (1990).

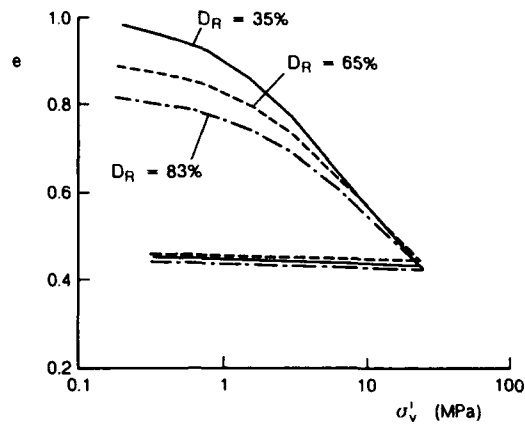
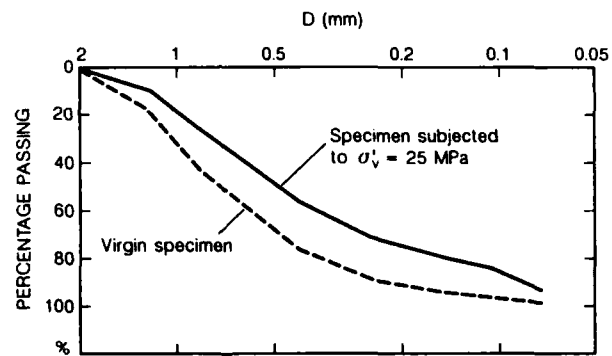
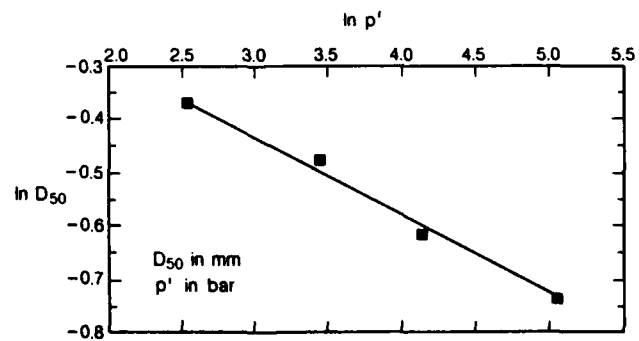


FIG. 2. Oedometer tests in Quiou sand.



a. Grading curves.



b. Mean grain size versus consolidation stress.

FIG. 3. Crushing of Quiou sand during oedometer tests.

A study of soil crushing has been performed for Quiou sand in which saturated specimens have been subject to different high vertical stresses and subsequent grading tests made in each of them. Results of grading tests at the two extreme soil conditions, i.e., the unstressed specimen and the specimen stressed at 25 MPa are shown in Fig.3a. For each tested sample D_{50} has been chosen as the parameter to represent particle size and it is plotted, similarly to Coop (1990), against the maximum stress attained during the test, as shown in Fig.3b. It is seen that particle breakage initiates at low stress levels, i.e., before stress levels corresponding to yield are reached. The same study has been performed in a series of dry specimens but, as expected, grain crushing was less severe than for saturated specimens.

4. EQUIPMENTS AND PROCEDURES

The tests presented hereunder have been performed in the ENEL-CRIS calibration chamber [Bellotti et al. (1982)] which can test a cylindrical sample of sand 1.2 m in diameter and 1.5 m in height. The equipment consist in a double wall chamber, a loading frame, a mass sand spreader for sand deposition and a saturation system. Boundary stresses or strains can be strictly controlled in the calibration chamber during both specimen preparation and penetration test.

All specimens have been prepared by pluvial deposition of dry sand in air using a gravity mass sand spreader. Sample formation has been performed in one operation using a sand container which holds enough sand for the specimen preparation. Values of relative density (D_R) ranged between 49 and 97%. These values of D_R should be considered as approximate because of the difficulties in assessing γ_{max} and γ_{min} in highly crushable sands and because of the small changes these values undergo with the repeated use of the same stock of sand for the tests. These differences exist even with the precaution of disregarding the 80 mm in diameter central core of the specimens after each CC test. The uniformity of the specimens was generally good, although somewhat erratic for medium-dense specimens $49\% \leq D_R \leq 62\%$. A series of eight CPT tests have been performed and these have been assigned numbers 356 to 363.

All penetration tests have been conducted in normal consolidated specimens, i.e., under the same stress conditions in which the specimens have been prepared. Five tests have been subjected to one-dimensional consolidation, i.e., under conditions of zero lateral strain. The remaining three tests have been consolidated along stress paths with the stress ratio $\sigma'_{hc}/\sigma'_{vc}$ equal to 1 and 2. Therefore, all specimens have been penetrated under conditions corresponding to constant boundary stresses (B-1).

Out of eight specimens, three were tested in dry conditions and five in fully saturated conditions. The technique used to saturate CC specimens has been described by Bellotti et al. (1988) and allows achievement of a very good degree of saturation reflected in the values of B ranging between 0.93 and 0.99.

All tests were performed using a standard 10 cm^2 ISMES electrical cone penetrometer. For tests in saturated specimens the penetrometer tip was furnished with a special hardened steel porous stone allowing measurement of the pore pressure during penetration. In the case of test n°358 the porous stone was located just behind the cone base, while the remaining four tests (359 through 362) were performed with a tip having the porous stone at the

cone apex. The pore pressure during cone penetration was simultaneously measured by means of the miniature piezometers embedded in the sand mass during pluvial deposition.

5. CPT TEST RESULTS

The results of the eight CC tests performed are summarized in Table II. It is seen that values of sleeve friction are extremely low, giving values of friction ratio FR always less than 0.1%. This suggests that there is little relevance in measuring friction loads in calcareous sands, though FR values as high as 4% have been obtained for some calcareous silty sands [Beringen et al. (1982), Ebelhar et al. (1988)].

Pore pressure measurements Δu by means of both the piezocone and piezometers embedded in the CC specimens, Fig.4 indicated that the cone penetration has occurred under virtually drained conditions. Indeed, associated pore pressure parameters B_q [Senneset and Janbu (1984)] to measured values of q_c and Δu are virtually zero, as the former are much greater than the latter.

Typical results of point resistance versus depth are given in Fig.5a for tests 360 and 362 performed under very close stress conditions, but different relative densities. It is seen the greater uniformity of the denser specimen, yielding, as expected, greater values of the point resistance. Tests 356 and 358, performed under very close relative densities and mean effective stresses are shown in Fig.5b and it is seen that the marginally greater relative density of the second test is offset by its saturated condition and very close point resistances are obtained. It is known [Baldi et al. (1985)] that the saturated condition decreases the point resistance by about 10% when compared with the dry condition.

It has been a recommended procedure [Been et al. (1986, 1987), Wroth (1988)] to analyse results of CPT tests in sands using the normalized cone resistance defined as:

$$\bar{q}_c = \frac{q_c - p_o}{p'_o}$$

where:

p_o = mean total stress acting on the CC specimen during cone penetration
 p'_o = mean effective stress acting on the CC specimen during cone penetration.

Figure 6 shows \bar{q}_c versus voids ratio e of two well studied silica sands and Quiou sand. It can be observed that \bar{q}_c for both silica and calcareous sands exhibit a well defined trend versus e [Semple (1988)].

Evans (1987) performed calibration chamber tests using a blunt penetrometer (virtually no change in q_c was noticed when a 60° cone was used) in Dog's Bay sand at a voids ratio of 1.70. Computed values of \bar{q}_c using Evans (1987) data for the present stress range ($50 < p'_o < 130$ kPa) varied between 34 and 53 [for the whole stress range ($33 < p'_o < 417$ kPa) \bar{q}_c varied between 21 and 61], hence lower than those of Quiou sand. Therefore an increase in voids ratio further decrease values of \bar{q}_c , thus supporting the findings reported in Fig.8 and the key role of the voids ratio [Semple (1988)] in calcareous sand behaviour.

Table II. CPT's performed in CC on Quiou calcareous sand.

$\gamma_s = 26.62 \text{ kN/m}^3$; $\gamma_{\text{max}} = 14.54 \text{ kN/m}^3$; $\gamma_{\text{min}} = 11.67 \text{ kN/m}^3$; $e_{\text{min}} = 0.831$; $e_{\text{max}} = 1.281$; $e_{\text{max}} - e_{\text{min}} = 0.450$

Test n°	γ_d [kN/m ³]	e	D_R [%]	σ'_{vc} [kPa]	σ'_{hc} [kPa]	p'_o [kPa]	M [MPa]	q_c [MPa]	BP [kPa]	f_s [kPa]	$\frac{q_c - p_o}{p'_o}$	Notes
356	14.05	0.894	86.0	113.9	46.6	68.3	14.2	7.97	0	18	115.7	Dry, $K_c = K_o$
357	12.92	1.060	49.1	112.1	46.7	68.8	8.3	5.18	0	16	74.3	Dry, $K_c = K_o$
358	14.13	0.884	88.2	102.3	50.5	67.8	11.9	7.88	33.6	1	113.7	Saturated ($B = 0.97$), $K_c = K_o$
359	12.98	1.051	51.1	105.8	50.5	68.9	7.2	3.97	59.5	1	54.8	Saturated ($B = 0.93$), $K_c = K_o$
360	13.00	1.048	51.8	107.5	102.2	103.9	* 5.8	5.00	214.5	0	44.0	Saturated ($B = 0.93$), $K_c = 1$
361	13.30	1.002	62.0	113.4	206.6	175.3	* 10.2	6.25	29.5	1	33.5	Saturated ($B = 0.99$), $K_c = 2$
362	14.43	0.845	96.9	101.6	100.9	101.1	* 12.4	11.37	28.0	4	110.2	Saturated ($B = 0.99$), $K_c = 1$
363	13.51	0.970	69.8	114.5	45.8	68.7	11.8	8.24	0	26	118.9	Dry, $K_c = K_o$

* bulk modulus

 γ_s - specific gravity γ_d - dry density

e - void ratio

σ'_{vc} - vertical
 σ'_{hc} - horizontal
 } consolidation stresses
 at mid-height of CC specimen

M - tangent constrained modulus during last load
 increment

 q_c - cone resistance at mid-height of CC specimen

B - tangent bulk modulus

BP - back pressure during cone penetration

 f_s - sleeve friction p_o - mean total stress p'_o - mean effective stress

K - consolidation stress ratio $\left[\frac{\sigma'_{hc}}{\sigma'_{vc}} \right]$

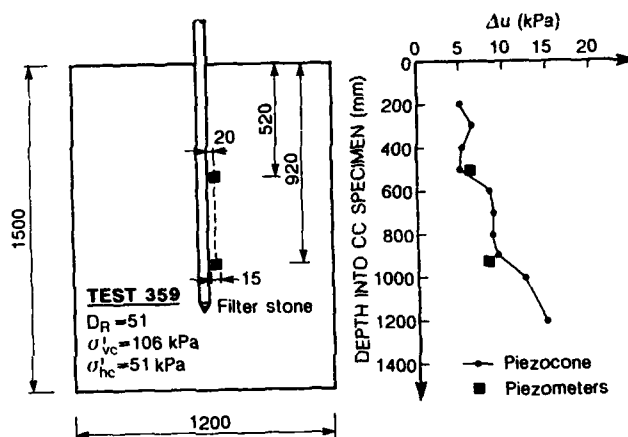


FIG. 4. Excess pore pressure during penetration into Qiou sand.

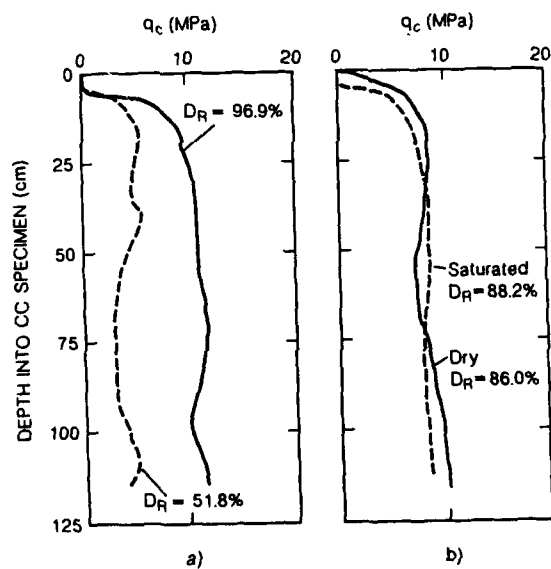


FIG. 5. Typical examples of CPT tests in Qiou sand.

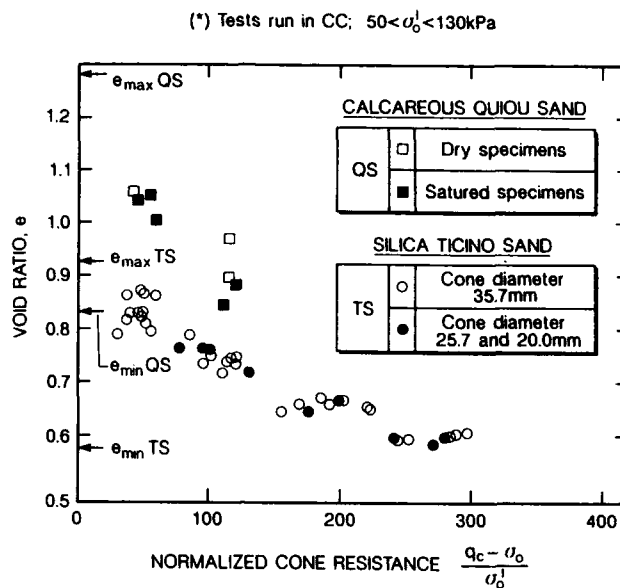


FIG. 6. Normalized cone resistance versus void ratio in NC Ticino and Quiou sands.

Test n.	356 (D)	357 (D)	358 (S)	359 (S)	360 (S)	361 (S)	362 (S)	363 (D)
D_R (%)	86.0	49.1	88.2	51.1	51.8	62.0	96.9	69.8
q_c (OS) MPa	7.97	5.18	7.88	3.97	5.00	6.25	11.37	8.00
q_c (TS) MPa	17.06	6.90	16.96	6.64	6.82	9.15	21.17	11.25

(D) = dry specimen, (S) = saturated specimen

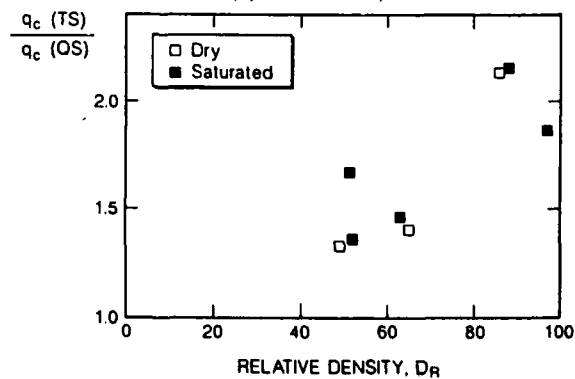


FIG. 7. Comparison of cone resistance of calcareous QS and silica TS at equal relative densities.

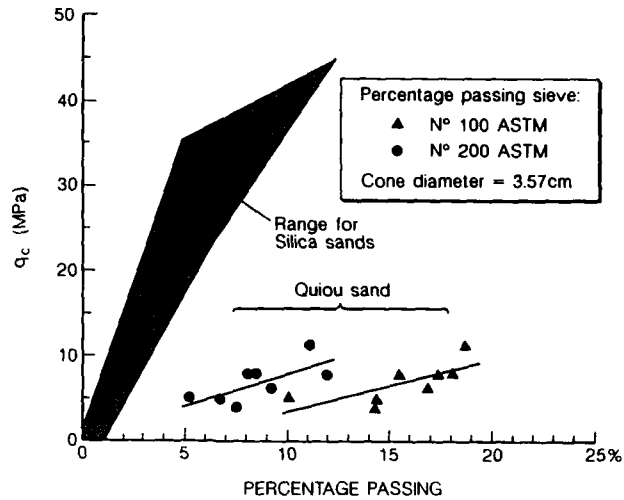


FIG. 8. Crushing of Quiou sand during cone penetration tests.

Point resistance of Quiou sand and of Ticino sand are compared in Fig. 7 at equal values of relative densities. As expected it appears that at equal D_R the cone resistance of the latter is appreciably higher than that of former, this difference being greater with increasing D_R . The results shown in Fig. 7 suggest that the use of q_c vs D_R established for silica sands [e.g. Schmertmann (1976); Jamiolkowski et al. (1988)] for calcareous sand can lead to a too conservative estimate of D_R .

Following each penetration test some amount of soil was taken from the mid height of the specimen and this was subject to grading analyses in which the percentage passing in ASTM sieves numbers 100 and 200 were recorded. In Fig. 8 the percentages passing are related with the point resistance for Quiou sand and two well studied silica sands. It is seen that a given increase of point resistance induces a much greater increase in the percentage of soil passing in the Quiou sand than for the two silica sands. In other words the lines q_c versus percentage passing are much steeper for silica sands. This feature is observed for both the 100 sieve and the 200 sieve. Therefore, it is seen that the cone penetration causes particle breakage in general, which however, is much greater for calcareous sands, as expected. A detailed study of crushability of sands in general has been presented by Bellotti et al. (1991).

Measurements taken during cone penetration evidenced that all eight tests, including the densest one (test 362), had exhibited a contractive behaviour, in evident contrast with what observed for specimens of silica sand, thus confirming the pronounced compressibility of the tested sand.

Referring to five tests (356 to 359 and 363) during which the CC specimens were subject to one-dimensional consolidation, the values of the tangent constrained modulus M_t evaluated at the same vertical stress at which the CPT was performed, results between 7.2 and 14.2 MPa, as shown in Table II. This is almost one order of magnitude lower than those typical for silica sand at the same D_R . However, the obtained M values normalized with

respect to the vertical effective stress (σ'_v) lead to a non-dimensional modulus number K_E which, if plotted versus e , exhibits a trend similar to that observed for two silica sands tested in the CC, as shown in Fig.9.

In the tests number 360, 361 and 363, the specimens were consolidated along stress paths using the stress ratio σ'_h/σ'_v , respectively equal to 1 and 2. For these specimens the bulk modulus (B) was evaluated instead of M. The relative results are also reported in Table II.

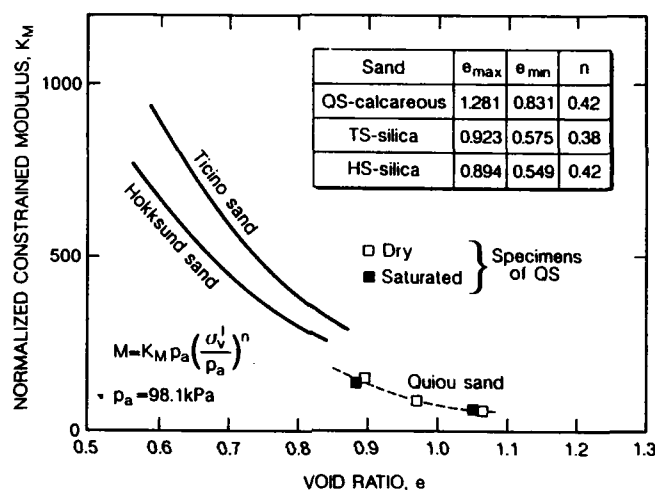


FIG. 9. Normalized constrained modulus of two silica and Quiou NC sands versus void ratio.

6. CONCLUSIONS

Preliminary results of CPT tests in an uncemented calcareous Quiou sand have been here presented against the background of oedometer tests and particle crushing studies. Limited data of grain crushing have confirmed the previous findings according to which a relationship exists between the applied stress and the D_{50} of the stressed specimen. The great compressibility of the calcareous sand was evidenced in both oedometer and calibration chamber tests.

Results of point resistance q_c measured in the Quiou sand are, for the same relative density, well up to half the value of q_c measured in the silica Ticino sand. However, voids ratio seems to be a better reference for comparing the behaviour of calcareous and silica sands. When normalized values of constrained modulus and point resistance are plotted against void ratio, the results of the two types of sands present the same trend, although smaller values are obtained for calcareous sands.

Grain crushing studies after cone penetration in both Quiou and Ticino sand have shown a correlation between the percentage of fines and point resistance and have also evidenced the greater particle breakage of the Quiou sand.

ACKNOWLEDGEMENTS

The work presented here has been made possible by a grant of the U.S. Government through the European Research Office of the U.S. Army (contract number DAJA45-88-C-0036). The first author was in sabbatical studies at ISMES, Italy when this paper is prepared.

REFERENCES

- Angemeer, J., Carlson, E. and Klick, J.H. (1973). "Techniques and Results of Offshore Pile Load Testing in Calcareous Soil". Proc., 5th Offshore Tech. Conf., Houston, Vol.2, pp.677-692.
- Baldi, G., Bellotti, R., Crippa, V., Fretti, C., Ghionna, V.N., Jamiolkowski, M., Ostricati, D., Pasqualini, E. and Pedroni, S. (1985). "Laboratory Validation of In-Situ Tests", AGI Golden Jubilee Vol. Geotech. Eng. in Italy, 11th ICSMFE, San Francisco, pp.251-270.
- Been, K., Crooks, J.H.A., Becker, D.A. and Jefferies, M.G. (1986). "The Cone Penetration Test in Sands: Part I, State Parameter and Interpretation". Géotechnique, No.2.
- Been, K., Jefferies, M.G., Crooks, J.H.A. and Rothenburg, L. (1987). "The Cone Penetration Test in Sands: Part II, General Inference of State". Geotechnique 37, pp.285-299.
- Bellotti, R., Bizzi, G. and Ghionna, V.N. (1982). "Design, Construction and Use of a Calibration Chamber". Proc. 2nd European Symposium on Penetration Testing Amsterdam, Vol.2, pp.439-446.
- Bellotti, R., Crippa, V., Pedroni, S. and Ghionna, V.N. (1988). "Saturation of Sand Specimen for Calibration Chamber Tests". Proc. ISOPT-1, Orlando, Fla.
- Bellotti, R., Fretti, C., Ghionna, V.N. and Pedroni, S. (1991). "Crushability of Sands in CPT Performed in Calibration Chamber". 9th Asian Regional Conference, Bangkok, December 1991.
- Beringen, F.L., Kolk, H.J. and Windle, D. (1982). "Cone Penetration and Laboratory Testing in Marine Calcareous Sediments". ASTM SPT 777, pp.179-209.
- Coop, M.R. (1990). "The Mechanisms of Uncemented Carbonate Sands", Geotechnique, 40, 4, pp.607-626.
- Datta, M., Gulhati, S.K. and Rao, G.V. (1982). "Engineering Behaviour of Carbonate Soils of India and Some Observations on Classification of Such Soils, SPT 777, ASTM, pp.113-140.
- Demars, K.R. and Chaney, R.C. (1982). "Geotechnical Properties, Behaviour and Performance of Calcareous Soils", ASTM STP 777 Presented at the ASTM Symposium, Fort Lauderdale, January 1981.
- Ebelhar, R.J., Young, A.G., Stieben, G.P. (1988). "Cone Penetrometer and Conductor Pullout Tests in Carbonate Soils Offshore Africa". Int. Conf. on Calcareous Sediments, Vol.1, pp.155-164, Perth, Australia.
- Evans, K.M. (1987). "A Model Study of the End Bearing Capacity of Piles in Layered Carbonate Soils". D.Phil. Thesis, Oxford University.
- Fahey, M. (1988). "The Response of Calcareous Soil in Static and Cyclic Triaxial Tests". Proc., Int. Conf. Calcareous Sediments, Perth, Australia,

- Vol.1, pp.61-68.
- Jamolkowski, M., Ghionna, V.N., Lancellotta, R. and Pasqualini, E. (1988). "New Correlations of Penetration Tests in Design Practice", Proc. 1st Int. Symp. Penetration Test, Orlando, pp.263-296.
- Jewell, R.J. and Andrews, D.C. (1988), Proc. Int. Conf. on Calcareous Sediments, Perth, Australia, March. 1988, 1.
- Jewell, R.J. and Khorshid, M.S. (1988). Proc. Int. Conf. on Calcareous Sediments, Perth, Australia, March, 1988, 2.
- Levacher, D. (1988). "Static, Tension or Cyclic Testing of Model Piles Driven in Calcareous Formations". Int. Conf. on Calcareous Sediments, Vol.1, pp.223-230, Perth, Australia.
- Poulos, H.G. (1989). "The Mechanics of Calcareous Sediments", Research Report n.595, School of Civil and Mining Engineering - University of Sydney - Australia.
- Rad, N.S. and Tumay, T. (1986). "Effect of Cementation on Cone Penetration Resistance in Sand". Proceedings Symposium on Use of In-Situ Testing in Geotechnical Engineering, ASCE, pp.926-948.
- Robertson, P.K. and Campanella, R.G. (1984). "Guidelines for Use and Interpretation of the Electric Cone Penetration Test". University of British Columbia.
- Schmertmann, J.H. (1976). "An Updated Correlation Between Relative Density, D_R and Fugro-type Electrical Cone Bearing q_c ". US-Army Corps of Engineers, Waterways Experimental Station, Vicksburg Miss.
- Senneset, K. and Janbu, N. (1984). "Shear Strength Parameters obtained from Static Cone Penetration Tests". ASTM STP 883, Symposium San Diego, pp.41-54.
- Semple, R. (1988). "State of the Art Report on Engineering Properties of Carbonate Soils". Proc. Int. Conf. on Calcareous Sediments, Perth, Australia, 2, 807-836.
- Wroth, C.P. (1988). "Penetration Testing - A more Rigorous Approach to Interpretation", I Int. Symp. on Penetration Testing, Vol.1, pp.303-311, Orlando.

PRESSUREMETER TESTING IN A CLAY CALIBRATION CHAMBER

William F Anderson and Ian C Pyrah
Department of Civil and Structural Engineering
University of Sheffield, UK

ABSTRACT

Limitations of laboratory scale simulations of the pressuremeter test in clay have led to a clay calibration chamber being developed in which full size field devices may be tested. Instrumented clay beds are produced in a repeatable manner by slurry consolidation and tests may be carried in the beds which are subjected to known vertical and horizontal stresses through flexible boundaries. Some aspects of the performance of the self boring pressuremeter have been examined.

INTRODUCTION

The pressuremeter is one of the most versatile field testing devices in that it may be used in a wide range of soil types and that there is a sound theoretical basis for the analysis of the results to obtain values for the engineering properties of the soil. It is also, particularly the self boring version, considered to be one of the best tools for estimating horizontal 'at rest' earth pressure in a soil deposit. In clays it is usually assumed that pressuremeter expansion occurs under undrained conditions and values are obtained for the shear modulus, G , and the undrained shear strength, c_u . However, comparative field studies [1, 2] have suggested that varying the pressuremeter expansion technique affects the results. A major problem in carrying out comparative field studies to examine the effects of using different test techniques is that the influence of natural soil variation is unknown. This problem is overcome by carrying out comparative studies in the laboratory in beds of clay prepared with known stress history and subjected to known boundary conditions. Instrumentation in the laboratory prepared clay beds allows certain aspects of the test to be examined in more detail than would be possible in the field.

During the pressuremeter test a cylindrical cavity in the soil is expanded. If it is assumed that radial expansion is occurring under plane strain conditions and, in the case of undrained testing of a saturated clay that the soil is incompressible, then radial strains of decreasing magnitude will occur with increasing radial distance from the cavity boundary. This situation may be simulated at small scale in the laboratory either by using a rigid body container whose diameter is so large that the strains at the outer boundary are negligible, or by using a hollow cylinder specimen with a flexible stress controlled outer boundary in a modified triaxial cell.

SMALL SCALE STUDIES

Initial comparative laboratory studies were carried out using both of the above methods. A 25mm diameter cavity was expanded in instrumented clay specimens produced by vertical (anisotropic) consolidation of a clay slurry, prepared at twice the liquid limit, around a 25mm diameter cavity former in a 1.03m diameter rigid body chamber as shown in Fig.1. The hollow cylinder specimens were produced by consolidating beds of clay slurry either isotropically or anisotropically, taking 150mm diameter specimens and then drilling a 25mm diameter central hole in them. They were then transferred to the modified triaxial cell shown in Fig.2 and

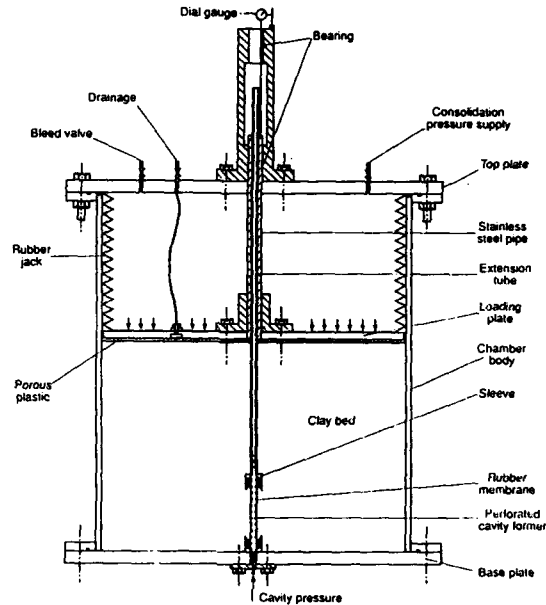


FIG.1. Rigid body chamber (1.03mm diameter) for 25mm diameter cavity expansion tests (instrumentation not shown)

reconsolidated either isotropically or anisotropically before being tested by cavity expansion. Details of the equipment, specimen preparation methods and expansion test techniques have been reported by Eid [3].

Because of the preparation time involved in consolidating the specimens in the rigid body container only a limited number of tests were carried out. Similar expansion techniques were used to test hollow specimens prepared with the same stress history in the modified triaxial cell. The expansion curves from both sets of tests were analysed to obtain soil parameters, and it was found that the modulus values from the rigid container tests were slightly lower than those from the hollow cylinder tests, probably due to slight differences in the manner in which the clay was consolidated around the cavity former. Undrained strength values derived from the test data were found to be higher from the rigid container tests than those from the hollow cylinder tests. When the complete stress-strain curves were derived using the subtangent method, it was found that those for the rigid container tests showed the stress rising to a peak at about 3% strain before falling off, and then rising again at around 4% (Fig.3). It is clear that the rigid boundary is having an effect, even with a container diameter more than 40 times the initial diameter of the expanding cavity.

Further small scale studies of the effects of using different cavity expansion techniques have therefore been confined to hollow cylinder tests on a number of different clays in the modified triaxial cell. These tests have confirmed that altering the test technique, either using stress control by applying the pressure in increments for fixed periods or strain control by expanding at a constant rate, does affect the expansion curve and the derived data [4,5]

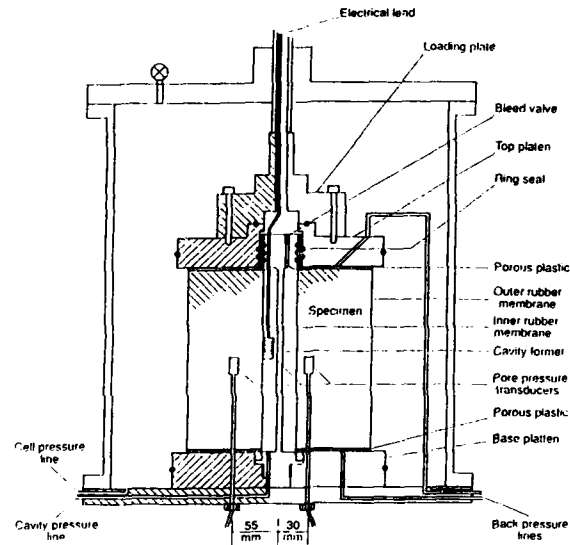


FIG.2. Modified triaxial cell for cavity expansion tests on 150mm dia. x 150mm high specimens

Measurements of pore water pressure within the clay mass during the tests have indicated that local consolidation occurs, and complementary numerical simulations of the small scale tests have shown that the trends found in the laboratory may be reproduced by considering not only local consolidation but also deviatoric creep during the cavity expansion. The simulations suggest that creep has the predominant effect in stress control tests and consolidation has the major influence in strain control tests [6]

In the small scale laboratory tests the influence of consolidation may be exaggerated because of the relatively short drainage path. However, numerical simulations of full size pressuremeter tests in San Francisco Bay Mud indicated that altering the expansion technique would lead to significant variations in derived parameters [7]. A flexible boundary clay

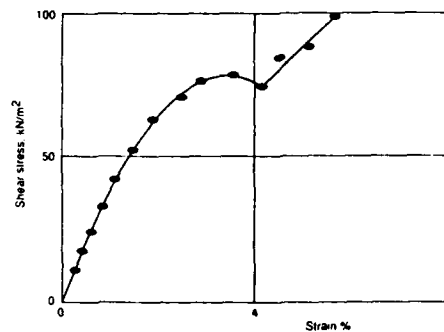


FIG.3. Derived shear stress-strain curve for cavity expansion test in rigid body container

calibration chamber, in which full size field test devices may be inserted, has therefore been developed. In this chamber not only may the effects of varying test technique be examined, but the performance of the field test equipment may also be studied in detail.

CLAY CALIBRATION CHAMBER

The preparation of repeatable clay beds with known stress history entails consolidating clay from a slurry and this causes problems due to the large volume changes which occur and the considerable time it takes for full consolidation. The calibration chamber was designed, and test procedures developed, so as to minimise these problems.

The calibration chamber, shown in Figure 4, consists of a single thick wall cylindrical body, 1.12 m high x 1.03 m diameter with stiffened flanges to which 45mm thick end plates are bolted. The chamber is designed for a maximum working pressure of 1500 kPa under which maximum radial deflection of the cylindrical body is 0.45 mm. The clay bed has an outside diameter of 785 mm and a height of approximately 1.0 metre. Around the clay there is a 1 mm thick rubber membrane. At the base the boundary is rigid, but the chamber design is such that it may, at a future date, be converted to a flexible boundary without too much difficulty. The top boundary is flexible, uniform pressure being applied through an annular rubber membrane and central piston cutter, through which in-situ testing devices up to 85 mm diameter may be introduced. The flexible top and outside boundaries allow either equal or different vertical and horizontal stresses to be applied to the clay bed. Preparation of clay beds from slurry takes place in two stages. Initially the calibration chamber is fitted with a 1.7 m high rigid body consolidometer (maximum working pressure 700 kPa) as shown in Fig.5. The inside of the consolidometer is lightly smeared with silicon grease to minimise side friction during consolidation. Prior to filling the consolidometer Druck pore pressure transducers and Kulite earth pressure cells are fixed in the desired

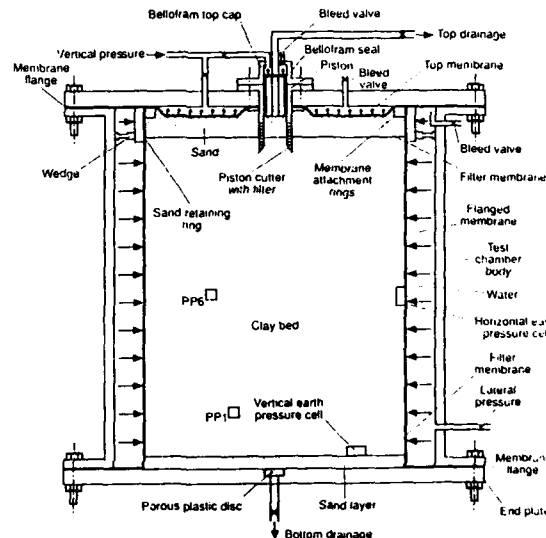


FIG.4. Calibration chamber with clay bed approximately 1m high x 0.785m diameter

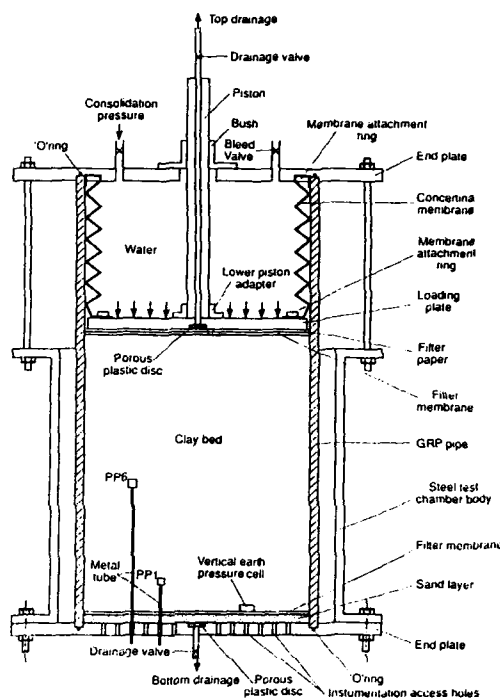


FIG.5. Calibration chamber consolidometer (1.7m high x 0.785m diameter)

positions on top of thin metal tubes which take the wires through instrumentation access holes in the base plate of the chamber.

Testing has so far been confined to Speswhite kaolin (LL = 72%, PL = 36%, 82% finer than 2μ). Sheeran and Krizek [8] recommend finding the most appropriate water content for slurry preparation and placement by trial and error with about 1.5 to 2 times the liquid limit being a good starting point. Preliminary tests showed that a consistent slurry of the high plasticity kaolin could be produced by mixing dry clay with water at 1.5 times the liquid limit. The slurry was slowly placed under water in the consolidometer to try to ensure full saturation. On completion of filling the slurry had a height of approximately 1.4 metres and a rigid loading plate and concertina rubber membrane, through which a vertical pressure can be applied, were fitted as shown in Fig 5.

After preliminary tests a consistent pressurising technique was adopted. A 70 kPa vertical pressure was applied for 3 days before being increased to 280 kPa. One dimensional consolidation took place with vertical drainage to the top and bottom. During consolidation the volume of water expelled from both ends of the clay bed, the settlement and clay bed pore water pressures were logged. Time for 90% consolidation of the slurry under one-dimensional conditions was some 6-7 weeks, but it was found that sufficient consolidation had occurred in 3-4 weeks for the clay bed to be self supporting and for the rigid boundary to be removed prior to the application of triaxial stresses. The criteria adopted for termination of the one-dimensional consolidation stage were:

- i) clay bed height reduced to 1.00 metre,
- ii) average degree of consolidation as indicated by clay bed pore

- pressure transducers was greater than 40%,
 iii) mid-height excess pore water pressures were less than 200 kPa.

When these criteria had been satisfied the consolidation pressure was reduced, the loading plate and concertina membrane removed and the consolidometer body slid off the clay bed. The outside rubber membrane was slid around the clay bed and at the top a sand retaining ring was wedged in position. This allowed the top drainage layer to be made up with sand to the thickness required to give the full height of bed to fill the calibration chamber. It also prevented interaction of the top flexible membrane and the outside flexible membrane when different horizontal and vertical pressures were applied to the bed.

The top plate, with flexible membrane and piston cutter attached, was fitted (Fig.4). At this stage the tubes supporting the pore pressure transducers were removed leaving the transducers free in the clay bed. Pressures were applied simultaneously to the top and outside of the clay. During consolidation under the triaxial stresses double vertical drainage was allowed, and top and bottom volume changes and clay bed pore water pressures were monitored. It took 12 days for the average degree of consolidation, as indicated by clay bed pore pressure transducers, to reach 90%, and at this stage it was considered that the clay bed was ready for testing. Further details of the equipment and testing procedures have been reported by Anderson et al. [9].

SELF BORING PRESSUREMETER TESTS

To allow detailed comparisons of the data from the small scale tests described earlier and full size pressuremeter tests to be made, conditions in the full scale tests have so far been kept as similar as possible to those at small scale.

In the majority of the small scale tests on kaolin the one-dimensionally consolidated specimen was reconsolidated under an isotropic stress of 280 kPa around a cavity former. This was replicated at full scale by inserting a Cambridge In-Situ Mark IX Self Boring Pressuremeter (80 mm dia) into the clay bed at the end of 1-D consolidation prior to the application of equal vertical and horizontal stresses for triaxial consolidation around the SBP (Fig.6). One clay bed has also been successfully subjected to different vertical and horizontal stresses to simulate K_0 conditions for normally consolidated kaolin.

Using the above procedures the time taken for clay slurry preparation, one-dimensional consolidation, triaxial consolidation, SBP testing and dismantling was 7-8 weeks. By accepting a slight reduction in the number of 'virgin' clay beds tested, and using a two stage technique, it was possible to plan for an increased number of tests within a given period.

This two stage technique involved allowing up to 24 hours for the excess pore water pressures set up during the first SBP expansion test to equalise throughout the clay bed while it remained under pressure with the chamber drainage valves closed. The chamber pressure was then raised to 560 kPa and the clay bed allowed to reconsolidate. The reconsolidation was considered complete when the clay bed pore pressure transducers indicated an average degree of consolidation in excess of 90%. This took about 10 days. The effective stresses in the clay bed after this reconsolidation were higher than those imposed earlier in the clay bed's history. It was assumed that the state of the clay bed was now such that it lay on the virgin compression line. However, because of differing stress paths imposed during the SBP expansion test at 280 kPa, it is recognised that the beds were unlikely to be perfectly uniform or repeatable. Nevertheless, the clay beds reused in this way allowed a lot more data to be obtained and individual aspects of the pressuremeter test to be examined.

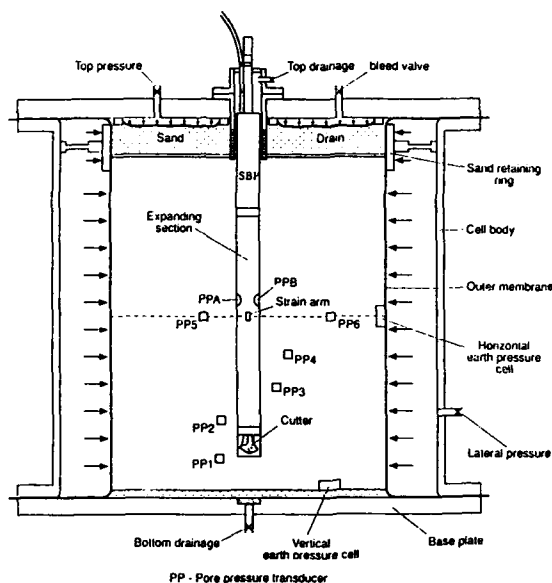


FIG.6. Calibration chamber with SBP inserted

On completion of each SBP test under the 560 kPa pressure, the calibration chamber was dismantled. During dismantling shear strengths were measured using a hand vane, and moisture content samples were taken at different heights and radial positions. The final positions of all clay bed instruments were recorded and all instruments plus the SBP were recalibrated.

RESULTS

Clay bed uniformity

During both one-dimensional and triaxial consolidation excess pore water pressures were monitored on a number of transducers situated 500mm above the base of the chamber i.e. at the mid-height of the consolidated bed. The maximum variation in the readings of these at any stage of consolidation was 7 kPa, with values generally within 2 - 3 kPa of each other indicating a fairly uniform consolidation on any horizontal plane in the clay bed.

Whilst post test measurements of water content and vane strength do not necessarily give a reliable guide to initial bed uniformity (as excess pore pressures will have been set up in the clay during SBP expansion leading to a variation in effective stress throughout the bed) it is worth noting that in any bed the post test water contents at mid-height at a distance of 300mm away from the SBP (i.e. at a position least likely to be affected by moisture migration) varied by less than 0.5%, with the exception of one bed where the variation was 1.3%.

One clay bed was prepared using the normal procedure under 280 kPa consolidation pressure, and then dismantled without any SBP insertion or testing so as to check uniformity. Laboratory vane tests were carried out at 30 locations during dismantling and these gave a mean value of undrained strength of 23.8 kPa with a standard deviation of 3.0 kPa. Undrained

triaxial tests were carried out on sixteen 38mm diameter specimens from different positions in the clay bed and these gave an average undrained strength of 26.9 kPa with a standard deviation of 3.5 kPa. Thirty samples of cuttings, each about 50 to 60 gm mass, were taken for water content determinations. The average value was 45.3% with a standard deviation of 1.0%. A slightly higher average water content of 46.5%, with a standard deviation of 0.9%, was obtained from the larger triaxial test samples. This higher value may be a consequence of better sealing in the triaxial tubes than in the moisture content tins.

When the effective stress changes which occur during the couple of days which it takes to dismantle the chamber and clay bed are considered, the undrained strength and water content variations reported above suggest a fairly uniform clay bed is being produced in the calibration chamber.

Instrument and membrane calibrations

Prior to clay bed preparation all pore pressure, earth pressure and calibration chamber pressure transducers were calibrated. Immediately before insertion, the SBP strain arms, total pressure cell and pore pressure cells were calibrated. A membrane correction calibration was also carried out. Recalibration was carried out when the test bed was dismantled. It was found that some drift occurred in all instruments, so prior to detailed analysis of the results all data were recalculated using calibration factors interpolated from pre-test and post-test calibrations assuming a uniform drift with time.

During calibration of the standard SBP Adiprene membranes it was found that the pressure at which the membrane started to lift off varied little for each strain arm, but the slopes of the pressure-strain membrane correction curves varied considerably, giving differences up to 45 kPa at 10% radial strain for the different strain arms. In analysing the SBP expansion test results it is essential to apply the appropriate correction to each strain arm and analyse the expansion curve for each arm individually, rather than using average values for all three arms.

SBP Expansion curves

The expansion curves for individual strain arms for a typical test are plotted in Fig.7. It can be seen that although the test is being carried out in a uniform clay bed the expansion is not symmetrical.

An estimate of the 'at rest' earth pressure in a soil mass may be obtained from the pressuremeter results by examining the early portion of the expansion curve and detecting the pressure at which membrane 'lift off' occurs. The early parts of the curves shown in Fig.7 are reproduced at larger scale in Fig.8. It can be seen that it is difficult to assess the lift off points. However, a best estimate was made for each strain arm in all of the tests carried out, and the results are compared with the calibration chamber outside pressure in Table 1.

DISCUSSION

Calibration chambers may be either rigid bodied or have a flexible stress controlled outside boundary. Numerical studies [10, 11] have indicated that for undrained cavity expansion in clays the expansion curve for a test carried out in a thick hollow cylinder may be significantly different to that performed in a material of infinite extent. Analyses have been carried out for hollow cylinders of different geometry, viz outside to inside diameter ratios ranging from 6 to 73, the latter representing the infinite case. For a particular geometry, the differences become more pronounced as the cavity strain increases and, based on

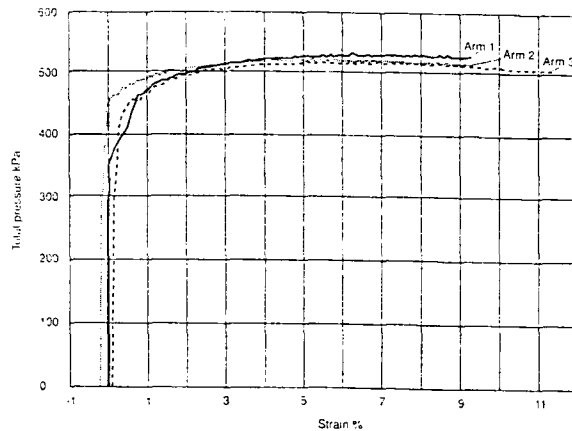


FIG.7. Expansion curves for individual strain arms (Bed 5 - 280kPa)

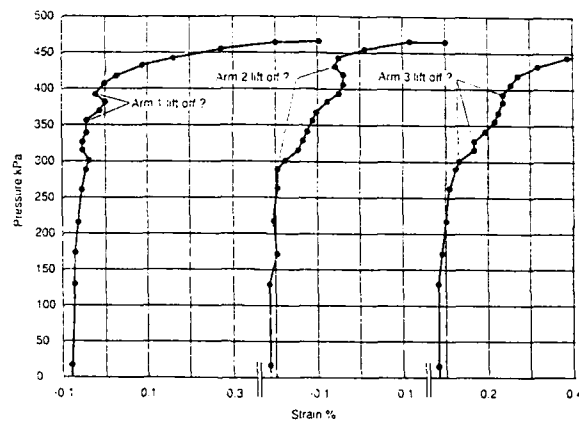


FIG.8. Assessment of lift off pressure for individual strain arms (Bed 5 - 280kPa)

outside to inside diameter ratios ranging from 6 to 73, the latter representing the infinite case. For a particular geometry, the differences become more pronounced as the cavity strain increases and, based on analyses using modified Cam clay, the effect on the derived strength is more significant than was predicted earlier using an elastic-perfectly plastic soil model. However, there are obvious practical difficulties in using a high ratio of outside to inside diameter especially when testing at full-scale. The small scale tests carried out in the rigid bodied chamber clearly demonstrate that even with a rigid chamber whose diameter is 40 times the initial diameter of the expanding cavity the boundary effects are significant above a cavity strain of a few percent. It is therefore essential to use flexible boundary chambers for pressuremeter studies or other tests in clay in which lateral straining is likely to occur.

Table I Estimated lift off Pressures

Test No.	Chamber Pressure (kPa)	Lift off Pressures (kPa)		
		Arm 1	Arm 2	Arm 3
4H	565	520	400	620
5L	282	395	290	300
5H	572	605	770	665
6L	283	395	265	250
6H	569	470	470	470
7L	287	280	280	280
7H	566	390	545	605
8H	566	640	610	530
9L	281	350	350	360
9H	558	660	660	660
10L	285	320	290	320
11L	283	290	365	310
11H	561	500	560	540

Huang et al [12] have reported on the design and performance of a small flexible boundary clay calibration chamber in which they carried out model pressuremeter tests with a chamber specimen diameter 18 times that of the pressuremeter. However the diameter of the pressuremeter is only 11.1mm diameter and scale effects during local consolidation will be even more marked than they were using the 25mm cavity in the modified triaxial cell described earlier. Numerical simulations [7,11], have confirmed this and highlighted the importance of testing at full-scale. Further studies [10] have indicated that for a test specimen with an outside to inside diameter ratio of approximately 9, i.e. the ratio for the full size chamber, the errors due to the hollow cylinder effect referred to above are approximately half of those when using a ratio of 6.

A major problem in preparing large clay specimens from slurry in a calibration chamber is the time that it takes for consolidation. Even for small scale laboratory simulations test specimen preparation can take of the order of a month. The techniques adopted for clay bed preparation with the full size calibration chamber allowed a turn round of tests every 2 to 2½ months. The clay bed behaviour during consolidation has been discussed elsewhere [9] but indications from end of test water contents and undrained strength are that reasonably uniform and repeatable beds were produced.

A major advantage of testing field devices in a well instrumented calibration chamber is that the instrument performance under real conditions may be examined in detail. Two aspects of pressuremeter testing, estimation of 'at rest' pressure and effects of membrane stiffness will be considered here.

There has been considerable discussion about the determination of 'at rest' pressure from pressuremeter tests and various methods of analysing results have been prepared. For the 'perfect' insertion achieved by consolidating the clay around the SBP it may be expected that the strain arms, having made a correction for system compliance and membrane stiffness, would all lift off at a pressure equal to the applied boundary pressure. However, as shown in Table 1, the lift off pressures for each arm generally varied and were rarely similar to the applied outside pressure. Variations of -35 kPa to +110 kPa (average +35 kPa) were found in the nominal 280 kPa tests and -275 kPa to +200 kPa (average +45 kPa) were found in the 560 kPa tests. The method or rate of testing did not seem to influence the accuracy of the 'at rest' pressure determination. This would suggest that the effects of varying membrane stiffness and compliance of the strain arm measurement system of the Cambridge In-Situ

Mark IX Self Boring Pressuremeter are such that lift off pressure in soft clay cannot be regarded as an accurate assessment of horizontal earth pressure.

In field pressuremeter tests in clay the individual arms rarely strain at the same rate or to the same displacement, and this is usually attributed to natural soil variability. In a uniform clay bed in the calibration chamber this would not be expected. However, as shown in Fig 7 uniform straining did not occur and this was found in all SBP tests carried out in the calibration chamber.

It is probable that this non-uniform expansion is a consequence of membrane stiffness. When calibration for membrane stiffness was carried out it was found that individual strain arm corrections varied. During a test a uniform internal pressure is applied to the membrane in contact with the soil. The greater the membrane stiffness at a particular arm the less the pressure actually applied to the soil at that location. This suggestion was confirmed when the individual arm expansion curves for each test were examined and it was found that generally the lowest strain at failure was associated with the arm with the greatest membrane stiffness correction. For the tests carried out in virgin beds consolidated at a nominal 280 kPa pressure it was found that derived shear modulus values and undrained shear strength values for individual arms varied by up to 18% and 13.5% respectively from the average values. These variations are probably due to varying membrane corrections.

For soft clay the membrane corrections for standard Adiprene membranes are significant when compared to the pressure levels applied to the soil. In one test it was found that if the pre-insertion membrane correction was used the derived undrained strength was 29 kPa. If, however, the post test membrane correction carried out after the SBP had been in the clay bed for a few weeks was used the derived strength was 41 kPa. It is suggested that in soft clays the standard Adiprene membrane is replaced by a softer membrane.

In addition to examining individual aspects of the SBP test in the calibration chamber, the instrumentation in the clay bed gives a greater insight into the soil behaviour than would be possible from field tests. In particular the pore pressure transducers in the clay bed have indicated that results from the SBP pore pressure transducers must be suspect and the assumption that local consolidation occurs due to radial drainage only may not be valid [6].

CONCLUSIONS

A flexible boundary clay calibration chamber has been constructed and specimen preparation techniques developed so that uniform clay beds may be prepared from slurry. The beds may be subjected to either equal or unequal vertical and horizontal stresses through flexible membranes. Full size in-situ test devices may be inserted into the beds and tests carried out with known boundary conditions. SBP tests carried out in the calibration chamber have highlighted limitations of using the SBP in soft clays.

REFERENCES

1. S. Amar, F. Baguelin, J.F. Jezequel and A. Le Mehaute, In-situ shear resistance of clays. Proc. ASCE Speciality Conf. on In-situ Measurement of Soil Properties, Raleigh, North Carolina, 1, pp.22-45 (1975).

2. D. Windle and C.P. Wroth, The use of a self boring pressuremeter to determine undrained properties of clay. *Ground Engineering*, 10, 6, pp.37-46 (1977).
3. M.M. Eid, Expansion of cylindrical cavities in clay. Ph.D Thesis, University of Sheffield (1978).
4. W.F. Anderson, I.C. Pyrah and F. Haji Ali, Pressuremeter testing of normally consolidated clays - the effects of varying test technique. In *Site Investigation Practice: Assessing BS5930*. Geol. Soc. Engng Group Spec. Pub. No.2, pp.125-132 (1986).
5. W.F. Anderson, I.C. Pyrah and L.S. Pang, Strain rate effects in the pressuremeter test. *Proc. Int.Symp on Geotechnical Engineering of Soft Soils*, Mexico City, 1, pp.11-16 (1987).
6. W.F. Anderson and I.C. Pyrah, Consolidation and creep effects in the PMT in clay. *Proc. 12th Int. Conf. on Soil Mechanics and Foundation Engng*, Rio de Janeiro, 1, pp.153-156 (1989).
7. W.F. Anderson and I.C. Pyrah, Undrained strength and deformation parameters from pressuremeter test results. *Proc. 2nd Int.Symp on Pressuremeters*, ASTM, STP 950, 324-338 (1986).
8. D.E. Sheeran and R.J. Krizak, Preparation of homogeneous soil samples by slurry consolidation. *J. of Materials*, 6, 2, pp.356-373 (1971).
9. W.F. Anderson, I.C. Pyrah and S.J. Fryer, A clay calibration chamber for testing field devices. *ASTM Geotechnical Testing Journal*, 14, 4, (1991).
10. I.C. Pyrah and W.F. Anderson, Numerical assessment of self-boring pressuremeters in a clay calibration chamber. *Proc. 3rd Int. Symposium on Pressuremeters*, Oxford, pp. 179-188 (1990).
11. R. Fukagawa, M. Fahey and H. Ohta, Effect of partial drainage on pressuremeter test in clay. *Soils and Foundations*, 30, 4, pp. 134-146 (1990).
12. A.B. Huang, R.D. Holtz and J.L. Chameau, A calibration chamber for cohesive soils. *ASTM Geotechnical Testing Journal*, 11, 1, pp. 30-35 (1988).

HYDRAULIC FRACTURE SIMULATIONS IN A CALIBRATION CHAMBER

K. BEEN AND K.M. KOSAR

Golder Associates Ltd
7017 Farrell Road S.E.
Calgary, Alberta
T2H 0T3, Canada.

INTRODUCTION

Large calibration chambers are mainly used for calibration of geotechnical in situ test instruments. The data are used to develop empirical correlations and also provide insight into the fundamental behaviour of the test instrument and soil sample in the chamber. Golder Associates developed a commercial version of a calibration chamber [1] specifically to develop empirical correlations between CPT penetration resistance, density and stress level for sands of particular engineering importance in Western Canada. This proved to be invaluable, as general empirical correlations developed for other sands were found not to be applicable in some cases [2].

There is a limited use for a calibration chamber for site specific CPT correlations in sands. The project has to be very large and important to warrant the costs for a chamber testing program. However, there are other applications for calibration chambers such as research into the basic mechanisms of hydraulic fracturing which is described in this paper.

The oil sands in Alberta represent a major resource of hydrocarbon fuels. This resource is currently being exploited by surface mining techniques by Syncrude Canada Ltd and by Suncor Inc near Fort McMurray. Where the oil sands are too deep for economical surface mining, recovery is likely to be by "in situ" methods. Several pilot projects have been initiated to develop this technology. In most cases, the recovery depends on hydraulic fracturing and thermal stimulation. Thus steam is injected into the formation under high pressures, resulting in hydraulic fractures and heating of the reservoir. The fractures increase the permeability of the formation and the viscosity of the bitumen is reduced by the temperature increase. The overall pressure in the formation is also increased by the injection process. After a period of steam injection, bitumen production commences.

A good understanding of the hydraulic fracturing process is essential to optimise the oil recovery process by steam stimulation. For example, fractures that extend into the caprock or basal formations may be detrimental and well spacing will also depend on fracture propagation distances. However, little is known about fractures as they are extremely difficult to trace in situ. The mechanisms of fracturing and fracture propagation in oil sands, which are uncemented and generally highly dilatant, is not immediately obvious.

Golder Associates calibration chamber is currently being used to study the mechanics of hydraulic fracturing in uncemented sands [3]. Following a brief introduction to the problem, this paper provides a description of some of the experimental apparatus and procedures being used, followed by presentation of some preliminary results which illustrate the complexity of the problem.

HYDRAULIC FRACTURING IN UNCEMENTED SAND FORMATIONS

In cemented materials hydraulic fracturing can be treated as a parting mechanism. Typically, the stress strain behaviour of the material is as shown on Figure 1a, with a distinct post peak strain softening response. The fracture is formed and propagated because the tensile strength of the material is exceeded. The material surrounding the fracture is essentially within the elastic range of behaviour. Fracture mechanics and bifurcation theory apply to the problem.

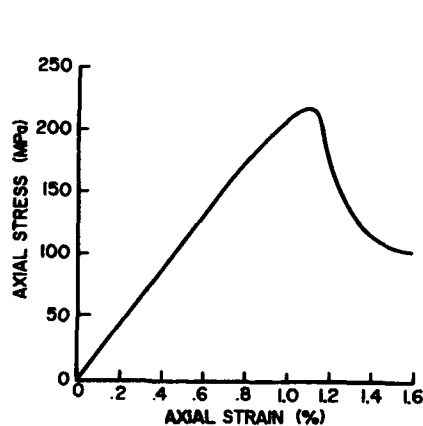


Figure 1a. Typical stress-strain behaviour of cemented sandstone reservoirs rock

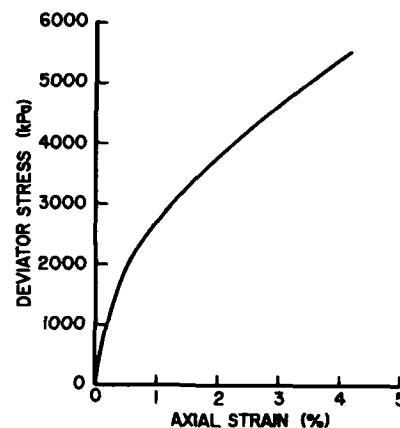


Figure 1b. Typical stress-strain behaviour of uncemented oil sands.

In oil sands, which are uncemented, behaviour is dominated by shear dilation. In general, dilatancy is associated with strain softening of sands. However, sand behaviour also depends on the boundary conditions such as drainage and displacement constraints. The stress-strain behaviour which may occur in situ is typically that shown on Figure 1b. The deviator stress response is strongly strain hardening, because the net effect of the dilatancy is to increase the effective confining stresses. This increase in confining stress may be due to negative pore pressures if the material is undrained, or due to a total stress increase in the surrounding confining material as the dilatant material expands. This change in stresses around the fracture (or sheared zone) will have an influence on the fracture propagation that is different from cemented, strain softening materials.

An additional difference between the behaviour of oil sands and cemented materials during hydraulic fracturing is that oil sands are, comparatively, more permeable. During injection of fluids into the formation, some of the fluid fills and propagates the fracture while some of the fluid flows into the surrounding material. (This is known as "leak-off" in the oil industry.) Fracturing in oil sands is characterized by much greater leakoff than in cemented materials because of the oil sands greater permeability.

APPARATUS, MATERIALS AND PROCEDURES

Calibration Chamber Configuration

The basic configuration of the calibration chamber currently being used to study the hydraulic fracturing phenomenon in oil sands is shown on Figure 2. This is the same chamber described by [1] for calibration of the CPT in sands.

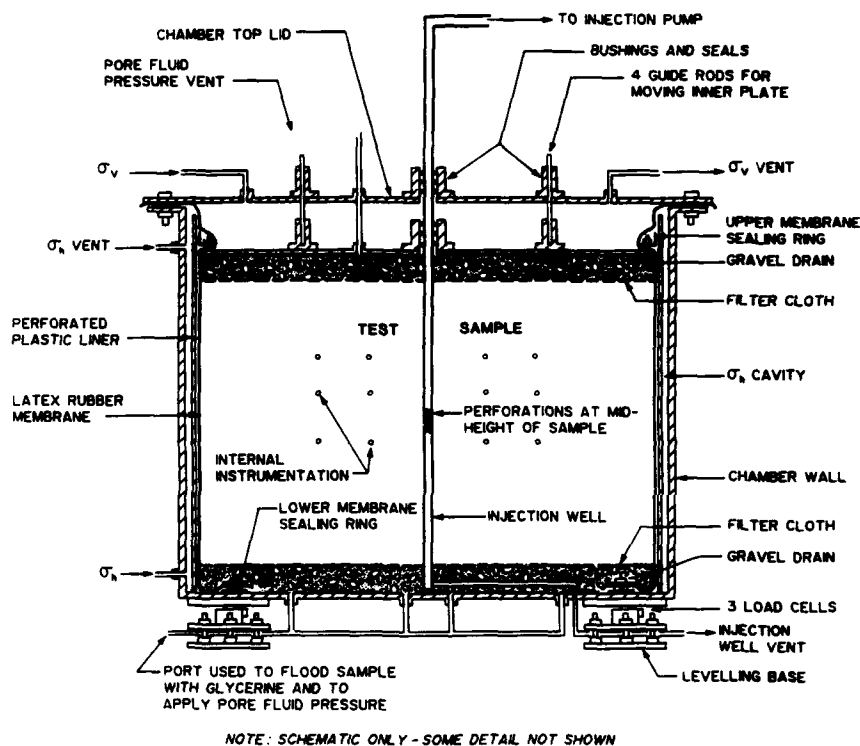


Figure 2. Schematic diagram of the Golder Associates calibration chamber used for hydraulic fracture tests.

Horizontal stresses are applied by hydraulic pressure through a latex rubber membrane. Vertical stresses are applied through a moving inner lid, also by hydraulic pressure. The sample can be back pressure saturated like a conventional small triaxial sample. It is possible to apply horizontal stresses which are greater than the vertical stresses with this chamber, and in fact most of the hydraulic fracture tests carried out to date have been with $K_0 > 1$.

A 34 mm outside diameter steel tube can be installed vertically in the centre of the sample. Hydraulic connectors lead from this tube through the base and lid of the chamber so that the tube can be deaired and flushed, or so that fluid can be injected. The central 50 mm of the tube is perforated with 50 holes, approximately 3.5 mm in diameter, to form the injection well for hydraulic fracturing.

In order to monitor the sample response to hydraulic fracturing, a number of instruments are installed in the sample. These consist of LVDT extensometers to measure displacements and pore pressure transducers. The number of instruments was minimised as there is a potential for the instruments to influence the local stresses and fracture propagation. A compromise must therefore be made between the amount of information (more instruments) and the quality of the information (fewer instruments to interfere with the test). Figure 2 shows the approximate locations of the instruments in the chamber.

The hydraulic fracture injection pump is a specially designed and constructed hydraulic system that can provide constant flow rates at pressures up to 3.5 MPa. It has a capacity of about 1000 ml. Figure 3 shows the design of this pump schematically.

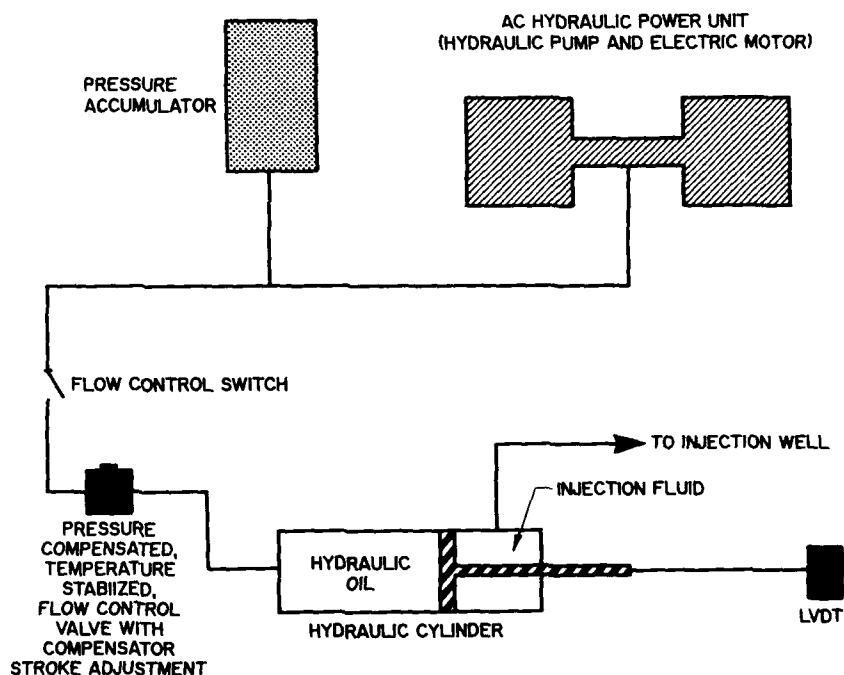


Figure 3. Schematic of constant flow rate hydraulic injection pump.

The data acquisition system for the chamber is a IBM PC based system, capable of scanning and recording 32 channels of data at a rate of 50 readings per second. This is achieved in burst mode (lasting 20 seconds) during an injection test, which lasts less than 5 seconds. At other times the system can be set to record data every few seconds, or minutes.

Materials

The sand used in this study was a very fine, uniformly graded, silica sand, Lane

Mountain 125 from Washington, USA. The pore fluid was glycerine, a highly viscous fluid which is also miscible with water. This combination of sand and fluid has a low permeability so that a fracture could be formed at relatively low injection rates and there would still be a significant volume of leakoff. Figure 4 shows the grain size distribution of the sand. The permeability of the glycerine in this sand was measured to be 4.4×10^{-6} cm/s.

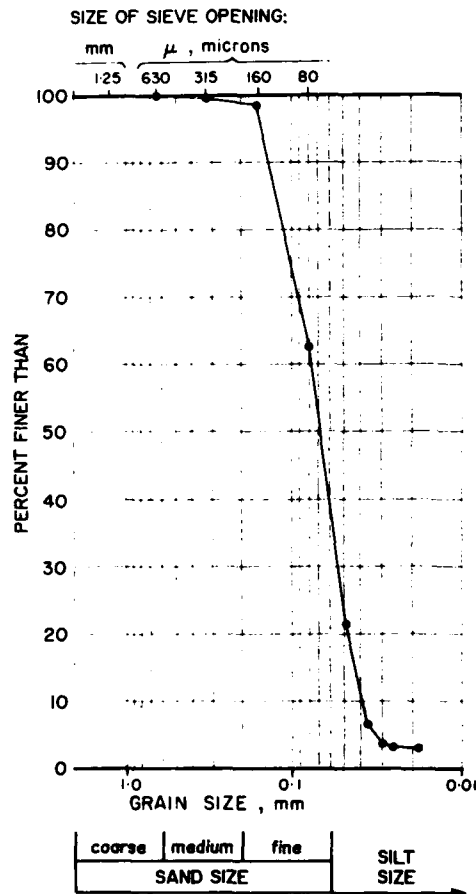


Figure 4.
Grain size distribution
of Lane Mountain sand.

The injection fluid for hydraulic fracturing was also glycerine, so that it was entirely compatible with the pore fluid. The injection glycerine was coloured with a fluorescent dye so that it could be distinguished from the pore fluid when the sample was examined after the test.

The purpose of the tests was to examine the mechanics of hydraulic fracturing of oil sands. This is usually carried out by steam injection into a sand matrix containing both

bitumen and water. The real problem is thus extremely complex and involves both thermal and multiphase flow. However, at this stage the intention is to obtain a better understanding of some of the basic mechanisms of fracturing and therefore a much simplified system has been modelled to date.

Procedures

The test procedure involved the following major steps:

- Internal instrumentation was suspended in the correct location in the chamber by fishing line. At this time the instruments were checked and preliminary zero readings taken.
- Dry sand was pluviated into the chamber from an overhead hopper in a single lift.
- The chamber lid was installed, the horizontal and vertical stress chambers filled and a nominal isotropic stress (about 5 kPa) applied to the sample.
- The glycerine pore fluid was then heated to about 70° C. At this temperature, the viscosity of glycerine is substantially reduced. The heated glycerine was then allowed to flow into the sample under a gravity head of about 2m. This stage of the saturation process typically lasted 24 hours. In some cases, where the flow rate was found to be low, the chamber and sand were also heated by means of heating coils and tape wrapped around the chamber. Hot glycerine was allowed to flow through the sample until no more air bubbles were observed in the outflow line.
- After the sample had cooled down to room temperature, the pressure lines were vented to atmosphere and all instrument zero readings were taken.
- The injection well was deaired by flowing glycerine through it from bottom to top under a gravity head of less than 1 m.
- The confining and back pressures were gradually increased to 200 kPa. It appeared that adequate saturation was generally obtained at this stress level. The sample was then isotropically consolidated under the desired minimum principal effective stress (generally 200 kPa in this test program), followed by the application of the deviatoric component and further consolidation. Consolidation was monitored by the internal pressure transducers.
- A series of baseline tests were then carried out on the sample before the main fracture test. These include a B test, a "triaxial" permeability test and a sub-fracture pressure injectivity test (radial permeability).
- Once the baseline data has been obtained and it is has been confirmed that there are no leaks in the system, the sample is unloaded to atmospheric pressure to allow the injection well to be primed with the dyed injection glycerine. The well is then connected to the injection pump and the fracturing can be carried out.
- The fracture test typically lasts 4 seconds, with up to 80 ml of fluid injected at a constant rate. During this time the data acquisition system is set on "burst" with readings of each channel taken 50 times per second.

- At the end of the injection phase, the well is sealed off and the pressures are monitored as they dissipate.
- When all the excess pressures have dissipated, the sample is unloaded back to atmospheric pressures, the chamber lid is removed and sample excavation commences.
- The sample is excavated in lifts of approximately 30 mm. This is done by hand with a small scoop or spatula. Because the glycerine is viscous and the sand fine, drainage is extremely slow and the material is removed in lumps, held together by negative pore pressures in the dilatant sand. Undisturbed shelly tube samples of the material are also taken at this stage for later laboratory triaxial and permeability testing.
- After each lift has been excavated, the surface of the sample is examined under ultra violet light for traces of the dye. Even extremely small amounts of the dye are visible under these conditions. The dye on the surface is marked with coloured string and the surface photographed under normal light. The dye locations are then digitised from the photograph. This provides a three dimensional map of where dye was observed.

During the course of the first few tests, a number of difficulties were encountered with the apparatus. The latex membrane tended to deteriorate at points of stress concentration when it was heated for a long period. Thus there were occasional problems with the seals at the ends of the membrane. In particular, if the O-rings were tightened down too hard they could extrude the membrane around them resulting in a leak.

Very small leaks were found to be critical to these tests. It was found that almost no consolidation (as measured by the pore pressure transducers near the centre of the sample) would occur if a very small leak existed. In normal CPT testing in the calibration chamber, pore pressure transducers in the sample are not used and the effect of a small leak near the ends of the sample is unknown.

The steel ring at the bottom of the chamber for fastening the membrane was originally fixed by a high strength, high temperature adhesive. The thermally induced stresses between this ring and the chamber base, however, were sufficiently large that the adhesive cracked. The ring was subsequently welded in place.

TYPICAL TEST RESULT

The primary information obtained from a typical hydraulic fracture test in the calibration chamber consists of the injection pressure versus time curve and a map of where dye was observed. The internal extensometers and the internal pore pressure transducers only occasionally showed a small response. This lack of response from the internal transducers is not surprising, given that approximately 50 ml of fluid was injected into a sample volume of 1.3 m³, which is only 0.004% by volume.

An injection curve is shown on Figure 5. Both the pressure and volume injected are shown as functions of time. For this test, the initial horizontal effective stress was 400 kPa, the vertical effective stress was 200 kPa (i.e. $K_0 = 2$) and the back pressure was 200 kPa. A total of 80 ml of glycerine was injected into the sample over the time period of

111 to 115 seconds (injection rate of 20 ml/s.)

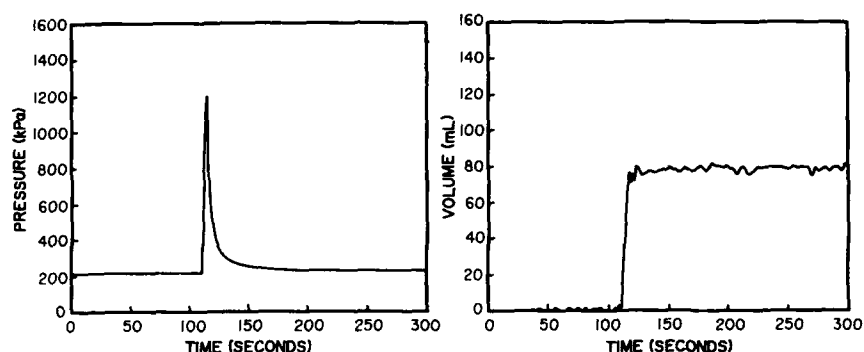


Figure 5. Pressure/volume injection curve for hydraulic fracture test.

The peak injection pressure in the well, measured at the perforated zone, was 1200 kPa. This peak pressure occurs at the end of the injection period at 115 seconds. The pressure in the well then decays rapidly and reaches equilibrium with the applied pore fluid pressure in about 35 seconds.

After the injection test, the sample was excavated from the chamber in 30 mm lifts as discussed previously. Each lift was then observed for traces of dye under ultra-violet light. Figure 6 is a photograph which shows how readily the dye can be detected in this way.



Figure 6. Photograph of fluorescent dye during excavation of the sample.

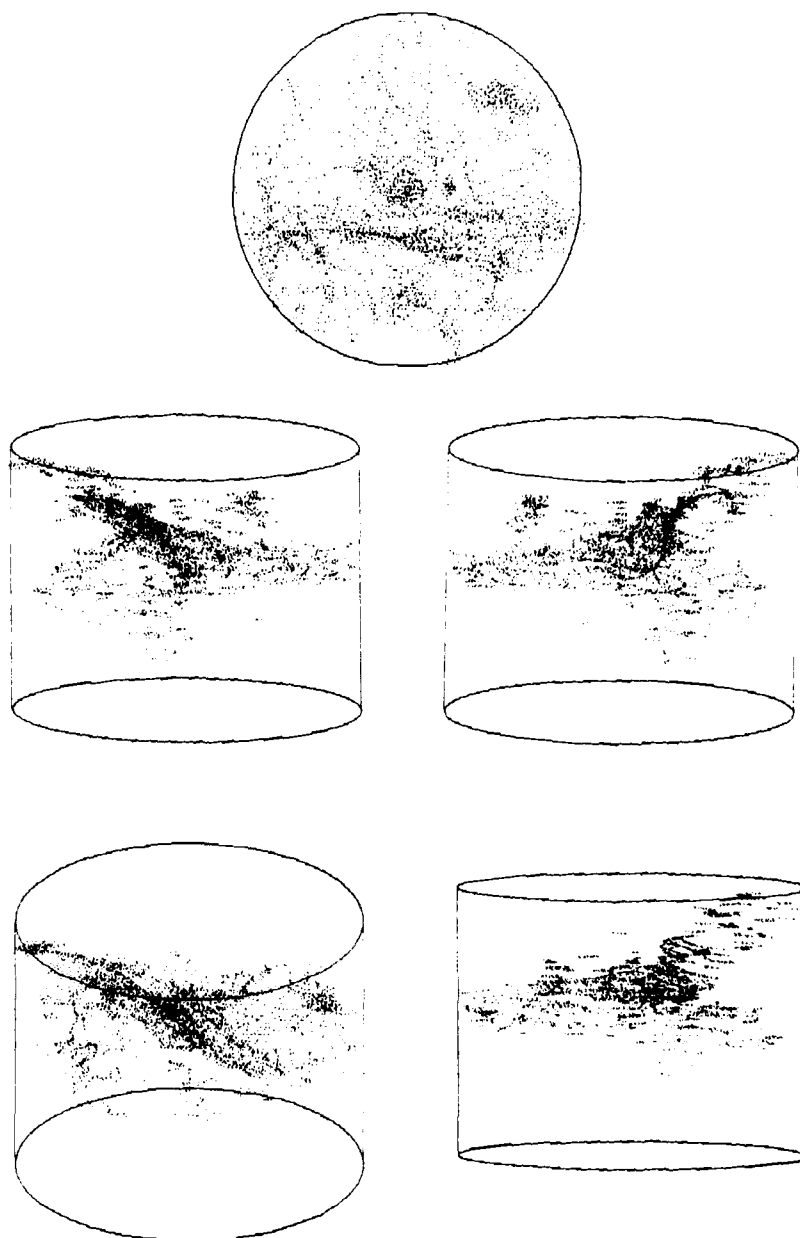


Figure 7. 3-D map of dye observations viewed from several directions.

Figure 7 shows several perspectives of the map of dye penetration into the sample. The dye in each 30 mm lift was detected, marked, photographed and then digitised. Each of the dots on Figure 7 represents a digitised dye location. In general a band or a plane of dye was observed, rather than discrete points. In this case several points in the plane or band were digitised, each point representing approximately the same area of detected dye. The density of dots on Figure 7 is therefore representative of the density of the dye detected.

It is clear from the photograph and maps that the injection fluid does not only fill a thin crack through the sand, but that there has been substantial penetration of the injection fluid into most of the sample. This is attributed to "leakoff". In fact it is not at all clear from the available information that a fracture was even formed.

The permeability of the sand to the glycerine is such that, at an injection pressure of 1200 kPa, i.e. the maximum observed in this test, the volume of glycerine that would flow into the sample is only 4 ml. In fact 80 ml were injected and the injection pressure was greater than the minor principal stress, so that it must be assumed that the sand was locally in a failure stress state during injection. The nature of this failure, or fracture, and its propagation is not yet well understood.

CONCLUSION

This paper has described a novel application of calibration chamber testing to examine the hydraulic fracturing phenomenon in oil sands.

There were several technical difficulties which had to be overcome for this application. The pore fluid and sand sample had to be selected carefully to be compatible with the membranes and other equipment, to provide the appropriate permeability and to be easily disposable after the test. In order to achieve saturation, the sample and the pore fluid had to be heated to reduce the viscosity. It was found that the membrane was prone to some deterioration at stress concentration points under high temperatures. Even small holes or leaks at the membrane seals could not be tolerated in these tests, because of the very low permeability of the material.

Few hydraulic fracture tests have been carried out to date, and the mechanics of the fracture process is still poorly understood. The typical test data presented in this paper illustrates this quite clearly. The extensive penetration of a very small amount of the dye into a large sample is surprising. In addition, there is no clear horizontal plane of "fracture" coincident with the plane of the minor principal effective stress. Further calibration chamber tests and more extensive numerical modelling are being undertaken to investigate the problem further.

ACKNOWLEDGEMENTS

The sponsors of this project to examine hydraulic fracturing in oil sands include Golder Associates, Esso Resources Canada, Shell Canada Resources, Mobil Oil Canada, Alberta Oil Sands Technical Research Authority (AOSTRA) and Canada Centre for Minerals and Energy Technology (CANMET). In addition, the patience and hard work of the technical staff who carried out the tests is acknowledged.

REFERENCES

1. Been, K., Lingnau, B.E., Crooks, J.H.A. and Leach, B. (1987). Cone penetration test calibration for Erksak (Beaufort Sea) sand. Canadian Geotechnical Journal, 24, 4, 601-610.
2. Sobkowicz, J. and Handford, G. (1990) The application of state-of-the-art static liquefaction concepts at Syncrude Canada Ltd. 43rd Canadian Geotechnical Conference, Quebec City.
3. Kosar, K.M. and Been, K. (1989). Large scale laboratory fracture test in Oil sands. Proc. 40th Annual Technical Meeting, Petroleum Society of the CIM, Banff, Canada, Paper 89-40-83. Vol II, p. 83-1.

COMPRESSIBILITY AND CRUSHABILITY OF SANDS AT HIGH STRESSES

R. BELLOTTI,* C. FRETTI,** V.N. GHIONNA,*** S. PEDRONI,*
* ENEL CRIS, 90/14 Ornato Street, 20162 Milan; ** ISMES, Levata
Street, 24068 Seriate, Bergamo; *** University of Pavia, 27100
Pavia;

ABSTRACT

The paper is concerned with the crushing measurements performed on four sands of very different origin and mineralogic composition; namely : two silica, one calcareous and one glauconitic sands. Sands crushability was studied both in an high capacity oedometer apparatus and in cone penetration tests (CPT) carried out in calibration chamber (CC).

Several crushability indexes were evaluated and their reliability checked correlating crushability threshold pressures to yield pressures observed in one-dimensional compression tests. Crushing amount in CPT's was correlated to cone resistance obtaining a well defined trend.

INTRODUCTION

The importance of sand crushability at high stresses has been pointed out since long time by several authors [1] [2] [3] [4] [5] [6] [7] [8] [9] [10] [11] [12].

The existence of a significant amount of crushing has systematically been observed and detected in cone penetration tests (CPT's) performed in the large calibration chambers (CC) for sand in use at ENEL CRIS and ISMES [13].

Evidences on crushability effects on CPT's results have also been reported by [14] [15] [16] [17] [18].

In some circumstances the crushed material can determine the formation of "cemented" zones around the cone. Fig. 1 shows the material below and around the cone in CPT's carried out on glauconitic sand. Fig. 2 shows the conical "plug" under the cone in a CPT's performed on calcareous sand. Fig. 3 shows the conical "plugs" detected under a rigid plate, with the same diameter of the standard cone, in a plate loading test (PLT) performed on silica sand.



Fig. 1



fig. 2

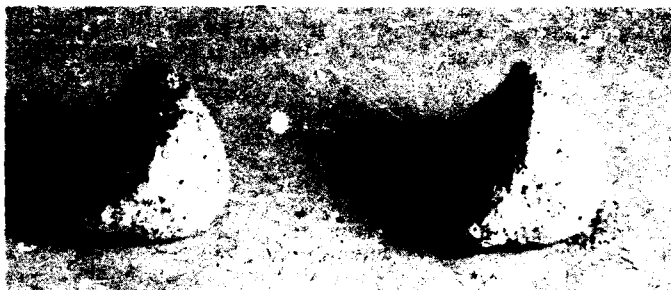


fig. 3

As generally agreed [9] [10] [11] [12] the most important effect of particle crushing is an increase of sand compressibility in the broadest sense including not only shear and bulk moduli but also dilatancy. Another important effect is a more pronounced curvature of the failure envelope up to an ultimate value of the friction angle which seems to be quite unaffected by crushing.

The combined effect of these factors in CPT's causes a reduction of both cone resistance (q_c) and lateral friction (f_s) [11] [12] [19].

The above evidences posed once again the need of a careful investigation on the influence of the sand crushability on sand compressibility and on CPT's results.

To this purpose a research program was started at ENEL CRIS geotechnical laboratory aimed at quantifying the crushability of the tested sands and at correlating it to compressibility and to CPT's results.

CRUSHING ASSESSMENT

A complete assessment of crushability effects should take into account that grain crushing is a very complex problem which is influenced by several factors like [20]:

- mineralogy
- particle angularity and roughness
- particle weakness
- grain size distribution
- void ratio
- cementation
- presence of water
- stress state and stress path
- time.

The paper reports the preliminary results obtained from 4 sands of very different formation and mineralogical composition; namely: two silica, one calcareous and one glauconitic sands. Results refer to the crushability behaviour displayed both in oedometer tests and CPT's performed in CC. Crushability in one-dimensional compression has been assessed using the crushing indexes proposed in literature [7] [9] [20] [21] [22] [23]. Such indexes fall into two classes:

- 1) indexes using the modification of the overall grain size distribution curve [20]

- 2) indexes using the differences observed on one or more specific sieve fractions: such differences are considered either in terms of percentage passing [7] [22] [23] or in term of grain diameter [21].

In the present paper, the reliability of the above indexes was evaluated checking their representativity with respect to the compressibility behaviour of sands in one-dimensional compression tests. The results shown in the following evidenciate that almost all the investigated indexes can be considered appropriate to the same extent.

Crushing evaluation in CPT's is much more complex because the crushed material is unevenly distributed around the cone tending to vanish at some radial distance from it. The extension of the "crushed" region is unknown; furthermore both the width of this region and the radial distribution of the crushed particles inside it are modified by the withdrawal of the cone from the CC.

Consequently crushing measurements concerning CPT's in CC must be considered purely conventional and only usefull for relative assessments. Due to the above aspects, previous studies on crushing in CPT's in CC [15] [16] [13] adopted qualitative crushing indexes like:

- percentage passing sieve ASTM No. 200 (P_{200})
- percentage passing sieve ASTM No. 100 (P_{100}).

Such parameters were chosen because of the very limited amount of fine particles characterizing the original grain size distribution of the tested silica sands. The results of the above studies [15] showed that crushing amount around the cone was directly related to the magnitude of the cone resistance (q_c). This was an obvious consequence of the fact that cone resistance (q_c) is directly related to the average normal and shear stress level existing around the cone.

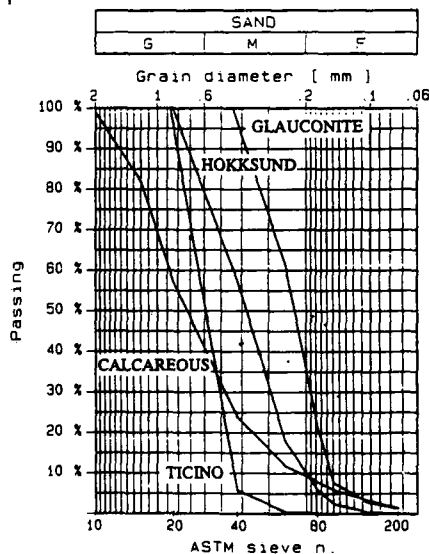


Fig. 4

TESTED SANDS

The following sands were tested in the present research:

- an italian silica sand from a fluvial deposit [Ticino sand (TS)]
- a norwegian silica sand from a glacial-marine origin [Hokksund sand (HS)]
- a calcareous bioclastic sand from a marine french deposit [Quiou sand (QS)]
- a glauconitic sand from a marine belgium deposit (GS).

Figure 4 shows the grain size distribution of the four tested sands; more information

about them can be found in [24] [25] [26].

OEDOMETER TESTS RESULTS

All sands were subjected to one-dimensional compression tests in a specially designed oedometer apparatus capable of applying vertical pressures up to 50 MPa.

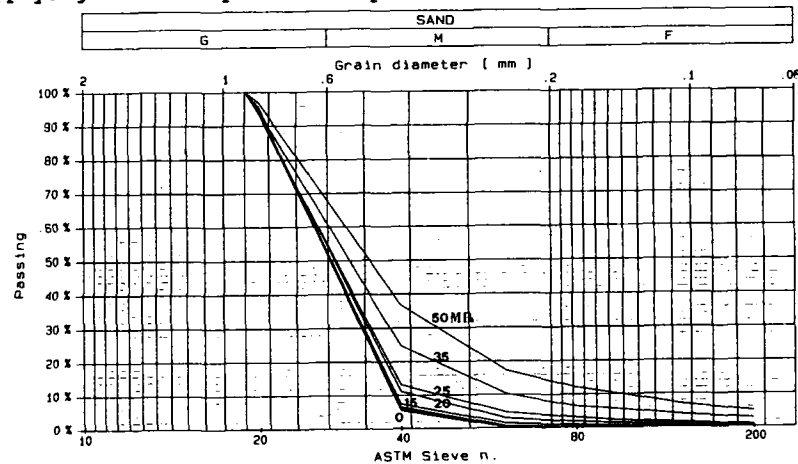


Fig. 5 - Ticino sand

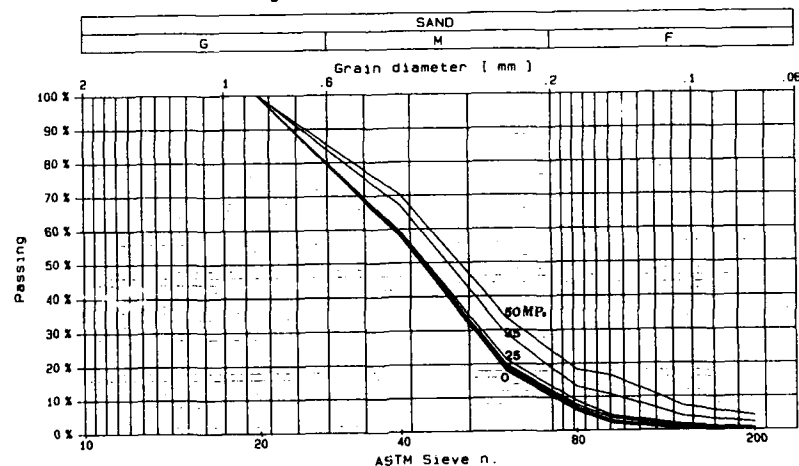


Fig. 6 - Høksund sand

The oedometer cell, made of stainless steel, houses sand samples having diameter of 50 mm and height of 25 mm. The thickness of the oedometer ring is 20 mm, to be sure of negligible lateral strains occur during the tests.

The vertical deformation of the sand sample is measured by two electrical vertical transducers, applied on the top cap and supported by two rigid bars connected to the base of the cell.

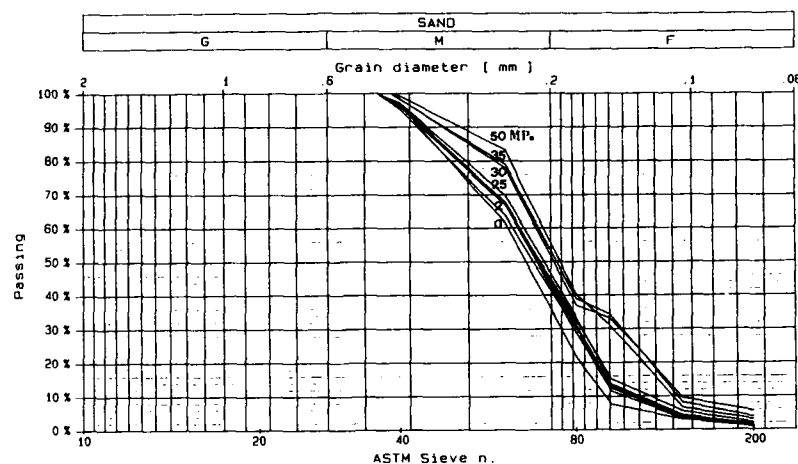


Fig. 7 - Glauconitic sand

In this way it is possible to avoid compliance effects of the apparatus on the vertical displacements of the sand samples. Compression tests carried out on the top cap and the steel porous stones allowed to verify that the deformability of these parts can be considered negligible with respect to the vertical strains of the sand samples.

Sand samples were formed by pluvial deposition method. Only dry samples of high relative density ($Dr = 90\%$) have been tested. The tests were performed in loading steps, each sample being subjected to one loading step only. At the end of each test the sample was removed and subjected to sieve analysis.

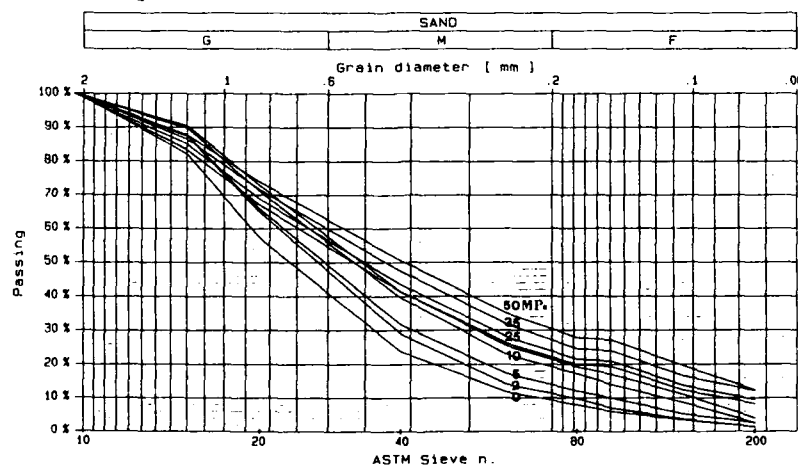


Fig. 8 - Calcareous sand

Figures 5-8 report the results of such sieve analyses concerning all four tested sands subjected to consolidation pressures ranging from 1 MPa to 50 MPa.

The modification of the grain size distribution curves was used to evaluate the following crushing indexes:

Crushing coefficient C_c [7]

$$C_c = (P_{10})_a / (P_{10})_i$$

$(P_{10})_a$ = % of sand, after stressing, finer than D10 of the original unstressed sand

$(P_{10})_i$ = % of original sand finer than D10

Breakage potential B_p [20]

$$B_p = \int b_p \cdot dp$$

b_p = breakage potential for the particles of size D

p = sieve fraction of particles of size D

dp = differential sieve fraction

Total breakage potential B_t [20]

$$B_t = B_p - B_{po}$$

B_p = breakage potential after stressing

B_{po} = breakage potential before stressing

Fineness modulus F_m [22],[27]

$$F_m = \sum r_i$$

r_i = % retained on a specified sieve i divided by 100

Besides the sieve siezes adopted by ACI (1986) (ASTM No. 100, No. 50, No. 30, No. 16, No. 8) the sieve No. 200 was also considered in this study.

Relative crushing index C_r [21]

$$C_r = (D_{15})_a / (D_{15})_i$$

$(D_{15})_a$ = grain size corresponding to 15% passing of sand after stressing

$(D_{15})_i$ = grain size corresponding to 15% passing of sand before stressing

Coefficients C_{60} , C_{80} [23]

$$C_{60} = (P_{60})_a / (P_{60})_i$$

$$C_{80} = (P_{80})_a / (P_{80})_i$$

$(P_{60})_a, (P_{80})_a$ = % of sand, after stressing, finer than D_{60} and D_{80} of the original unstressed sand respectively

$(P_{60})_i, (P_{80})_i$ = % of original sand finer than D_{60} and D_{80} respectively

The variation of the above crushability indexes with the vertical stress are plotted in figures 9 to 15.

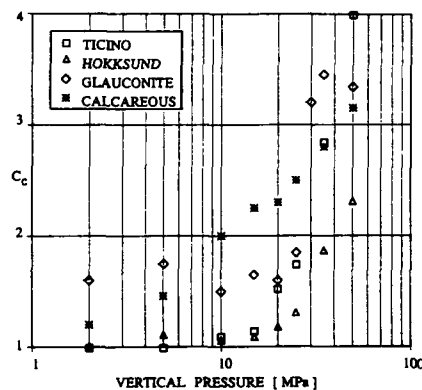


Fig. 9

The deviation from the initial trend indicates the existence of a threshold pressure at which a massive grain crushing starts to occur. All the above plots allow comparable values of the threshold pressures to be determined with the only exception of C_{60} and C_{80} which are, therefore, of poorer significance.

However the trend of B_t, B_p, F_m is more regular due to the integral nature of their definition; while C_c and C_r have a more evident change in trend.

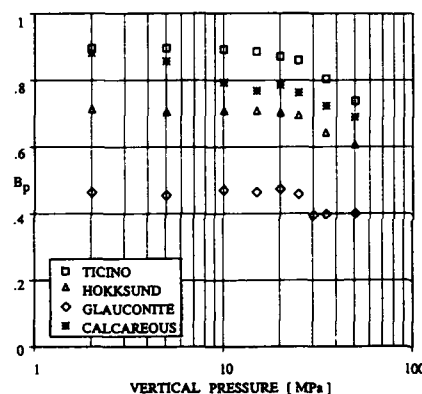


Fig. 10

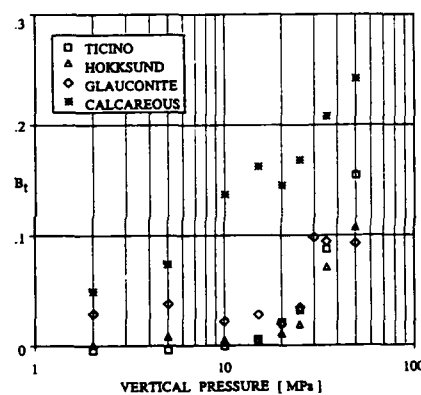


Fig. 11

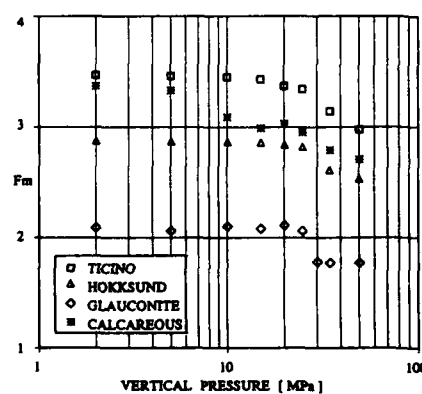


Fig. 12

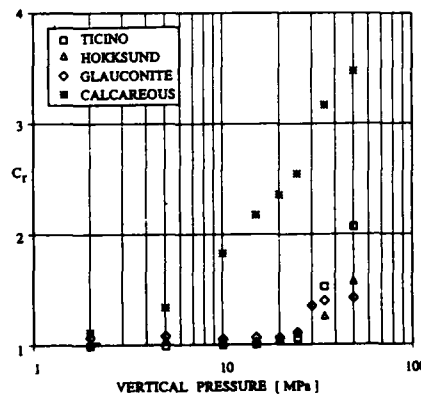


Fig. 13

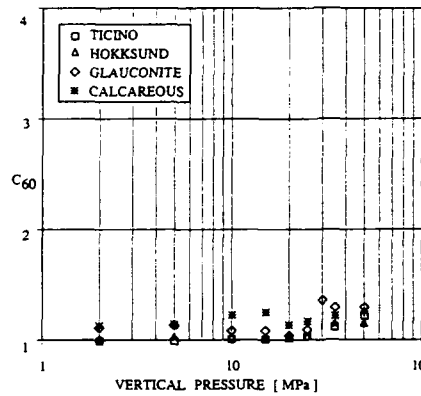


Fig. 14

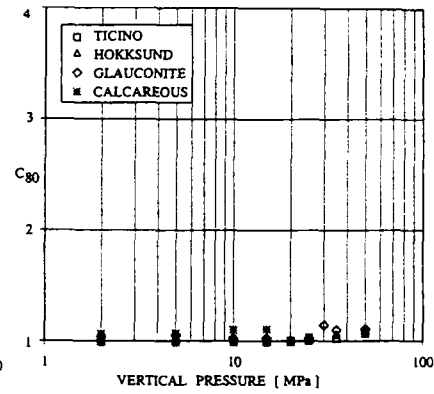


Fig. 15

In addition to the above crushability tests, traditional one-dimensional compression tests were also performed on all the tested sands. Dry samples at the same relative density of the previous ones were adopted. Typical one-dimensional compression curves are shown in figure 16

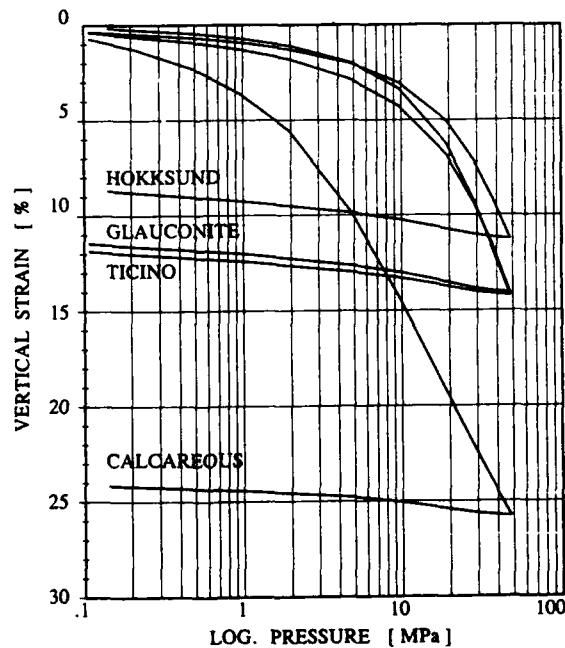


Fig. 16

Figure 17 reports the variation of the tangent constrained moduli (M_t) with the vertical effective consolidation pressure plotted in double logarithmic scale.

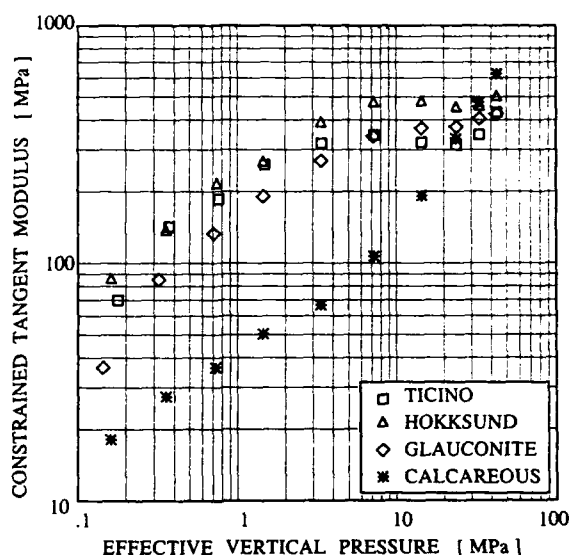


Fig. 17

A compressibility threshold is observed for all sands where the plots deviates from the linear trend.

Such threshold corresponds to a yield point for both silica and glauconite sands while it is indicative of a more rigid behaviour for the calcareous sand.

This behaviour is typical of a progressively densified material and can be associated with the crushability onset of QS with respect to the other sands. In fact, as shown by figures 9 to 15, crushing appears to be a progressive process for QS.

This results in a continuous production of fine particles whose rearrangement causes an increasing densification of the structure. At some elevated pressure a diagenetic recrystallization is likely to occur; this extreme behaviour has been observed for the all sands in the utmost part of the compression curves.

Comparison between figures 9 to 15 with figure 17 shows that threshold pressures evidenced by constrained moduli are in quite good agreement with those assessed from crushability indexes. Such agreement can be considered a further and more conclusive validation of the crushability indexes.

For all sands, observed values of yield pressures range between 10 MPa and 15 MPa while crushability threshold pressures are somewhat higher (15 MPa to 20 MPa).

CRUSHING RESULTS IN CONE PENETRATION TESTS IN CC

Crushing measurements in CPT's were performed during the emptying phase of the CC test. A cylindrical sampler, 120 mm in height and 100 mm in diameter, was used to recover sand samples at different depths along the central axis of the CC.

Crushing was expressed as increase in percentage passing sieves No.200 and No.100 with respect to the original untested sand. An average value of three measured at different depth around the mid-height of the CC was assumed and it was related to the cone resistance detected at mid-height of the sample.

Figure 18 shows the results concerning Ticino sand (TS). Single points refer to samples with different relative density, vertical consolidation stress and overconsolidation ratio.

As it can be seen there is a good evidence of a direct correlation between crushing amount and cone resistance. The wide scatter of data obliterates the possible existence of a crushability threshold of cone resistance. Furthermore, for a given sand, the correlation is quite independent of relative density, vertical consolidation stress and stress history.

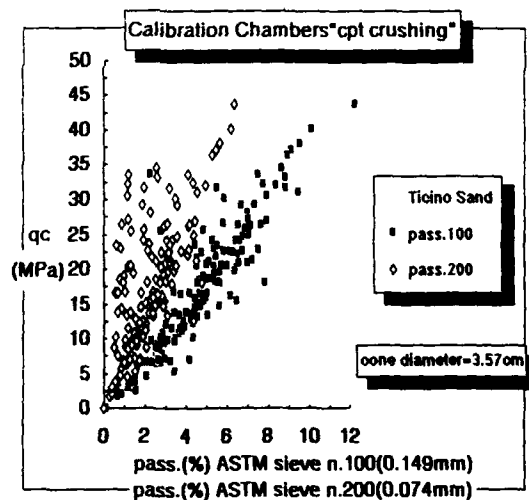


Fig. 18

CONCLUSION

The paper reports the results of crushing measurements performed on four sands of very different origin and mineralogical composition; namely: two silica sands (Ticino and Hoksund), one calcareous sand (Quiou) and one glauconitic sands. The crushability behaviour of the sands was studied both in an oedometer apparatus capable of applying consolidation pressures up to 50 MPa and in CPT's carried out in CC.

Several crushability indexes were evaluated [21] [7] [20] [9] [22] [23] and their trends with the applied pressures were used to evaluate their reliability.

Crushability threshold pressures were evidenced by such trends ranging for all tested sands in the interval 15 MPa to 20 MPa.

These threshold pressures were in quite good agreement with the yield pressures observed in one-dimensional compression curves.

Crushing measurements in CPT's exhibited a well defined trend vs. cone resistance which seems to be independent of consolidation stress, relative density and overconsolidation ratio.

REFERENCES

1. E.B. Hall and B.B. Gordon, Triaxial testing with large-scale high pressure equipment, A.S.T.M. Special Technical Publication on Laboratory shear testing of soils, STP 361, pp 315-328, (1963)
2. R.C. Hirschfeld and S.J. Poulos, High-pressure triaxial tests on a compacted sand and an undisturbed silt, A.S.T.M. Special Technical Publication on Laboratory shear testing of soils, STP 361, pp 329-339, (1963)
3. A.W. Bishop, D.L. Webb and A.E. Skinner, Triaxial tests on soils at elevated cell pressures, Proc. of the Roscoe memorial symposium, Cambridge, pp. 170-174, (1965)
4. A.S. Vesic and G.W. Clough, Behavior of granular materials under high stresses, Journal of Geotechnical Engineering, ASCE 94, No. SM3 - may 1968
5. J. Billam, Some aspects of the behaviour of granular materials at high pressures, Proc. of the Roscoe memorial symposium, Cambridge, pp. 170-174, (1965)
6. K.Y. Lo and M. Roy, Response of particulate materials at high pressures, Soils and Foundation, Vol. 13, No. 1, pp. 61-76, (1973)
7. M. Datta, S.K. Gulhati and G.V. Rao, Crushing of calcareous sands during shear, Proceedings of the 11th annual offshore technology conference, Houston, OTC No. 3525, pp 1459-1467 (1979)
8. M. Datta, S.K. Gulhati and G.V. Rao, Engineering behavior of carbonate soils of India and some observations on classification of such soils, A.S.T.M. Special Technical Publication on "Geotechnical properties, behavior and performance of calcareous soils", STP 777, pp 113-140 (1982)
9. J.L. Colliat-Dangus, Comportement des matériaux granulaires sous fortes contraintes, influence de la nature minéralogique du matériau étudié, Thèse de Doctorat-Ingénieur présentée à Grenoble (1986)
10. C..R. Golightly and A.F.L. Hyde, Some fundamental properties of carbonate sands, Proceedings of the international conference on calcareous sediments, Perth, march 1988
11. R.M. Semple, The mechanical properties of carbonate soils, State-of-the-art report, Proceedings of the international conference on calcareous sediments, Perth, march 1988

12. H.G. Poulos, The mechanics of calcareous sediments, Research report n.595, School of Civil and Mining Engineering, University of Sidney, Australia (1989)
13. R. Bellotti, G. Bizzi and V. Ghionna, Design, construction and use of a calibration chamber, Proceedings of the Second European Symposium on Penetration Testing, Amsterdam, vol.2, pp 439-446 (1982)
14. A. Veismanis, Laboratory investigation of electrical friction cone penetrometers in sand, Proceedings of the European Symposium on Penetration Testing, Stockholm, Vol. 2, Part 2, pp. 407-419 (1974)
15. J.C. Holden, The determination of deformation and shear strength parameters for sands using the electrical friction-cone penetrometer, N.G.I. Publication No. 110, pp. 55-66 (1976)
16. G.A. Chapman, The interpretation of friction cone penetrometer tests in sand, Ph.D.thesis, Department of Civil Engineering - Monash University (1979)
17. K. Joustra and J.G. De Gijt, Results and interpretation of cone penetration tests in soils of different mineralogic composition, Proceedings of the Second European Symposium on Penetration Testing, Amsterdam, vol.2, pp 615-626 (1982)
18. Rad and Tumay, Effect of cementation on the cone penetration resistance of sand: A model study, Geotechnical Testing Journal, Vol.2, No. 3, pp.117-125, (1986)
19. M.F. Randolph, The axial capacity of deep foundations in calcareous soil, Proceedings of the international conference on calcareous sediments, Perth, (1988)
20. B.O. Hardin, Crushing of soil particles, Journal of Geotechnical Engineering ASCE, Vol. 111, No. 10 (1985)
21. K.L. Lee and I. Farhoomand, Compressibility and crushing of granular soils in anisotropic triaxial compression, Canadian Geotechnical Journal, Vol. 4, No. 1, pp.68-100 (1967)
22. T.S. Hull, H.G. Poulos and H. Alehossein, The static behaviour of various calcareous sediments, Proceedings of the international conference on calcareous sediments, Perth, (1988)
23. M.J. Morrison, P.D. McIntyre, D.P. Sauls and M. Oosthuizen, Laboratory test results for carbonate soils from offshore Africa, Proceedings of the international conference on calcareous sediments, Perth, (1988)
24. S.G. Mc Rae, Glauconite, Earth Science Reviews, No. 4, Vol. 8, Elsevier, Amsterdam (1972)
25. R. Bellotti, V. Crippa, S. Pedroni, G. Baldi, C. Fretti, D. Ostricati, V. Ghionna, M. Jamiolkowski and E. Pasqualini, Laboratory validation of in situ tests, Italian Geotechnical Society Jubilee Volume, XI ICSMFE, San Francisco, pp. 251-270 (1985)
26. R. Bellotti and M. Jamiolkowski, Evaluation of CPT and DMT in crushable and silty sands, Waterways Expet. Stn., Contract No. DAJA45 - 88 - C -0036, (1991)
27. A.C.I. American Concrete Institut, Manual of concrete practice, Part I, Material and general properties of concrete, 211.3-15

DESIGN AND DEVELOPMENT OF A SMALL CALIBRATION CHAMBER FOR COMPRESSIBLE SANDS

R. BELLOTTI,* S. PEDRONI,*

* ENEL CRIS, 90/14 Ornato Street, 20162 Milan, Italy;

ABSTRACT

The paper describes the main features of the new calibration chamber (CC) for calcareous and silty sands developed at ENEL CRIS. It is based on the same operating principles than the existing one but it has smaller dimensions in order to reduce sand consumption originated by the high crushability of calcareous sand.

However, due to the high compressibility of calcareous and silty sands, chamber size and boundary conditions effects will be less pronounced.

INTRODUCTION

The need to design a calibration chamber, smaller than the one currently used at ENEL CRIS in Niguarda (Milan) [1], has arisen in relation to experiments on calcareous sand, namely on Quiou (France) and Dog Bay (Northern Ireland) sands.

Both sands show a high crushability that starts to occur at relatively low pressures.

Fig. 1 shows the changes in the grain size distribution undergone by Quiou sand (QS) during an oedometer test.

It can be noted that these changes occur even at usual consolidation pressures adopted in calibration chambers.

The higher crushability of QS is also demonstrated by the crushing measurements performed in the central part of the CC along the path of a cone penetration test (CPT).

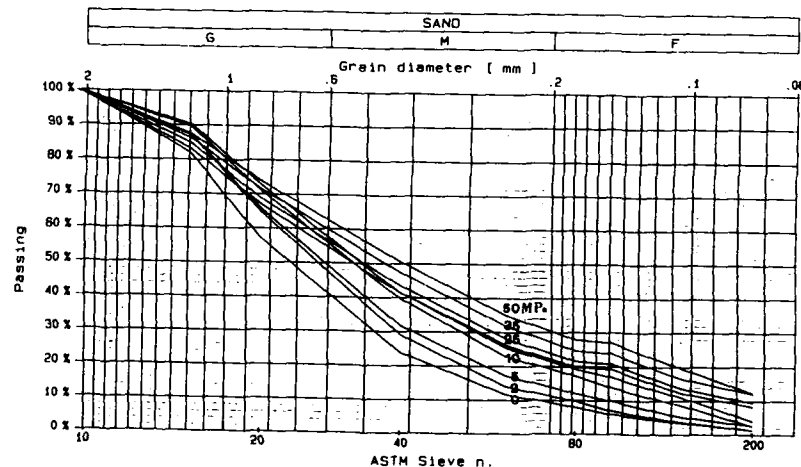


Fig. 1

Although these measurements are purely qualitative [2], nevertheless they can be used for relative assessments.

Tables 1 and 2 show that the amount of crushing measured in QS are 2 to 3 times higher than those measured in a silica sand like the Ticino sand (TS).

QUIOU SAND

Test N°	Passing sieve 200 ASTM	Passing sieve 100 ASTM
356	6.7%	9.6%
357	3.9%	4.2%
358	10.6%	11.5%
359	6.2%	8.4%
360	5.4%	8.5%
361	7.9%	11.0%
362	9.8%	12.8%
363	7.2%	12.2%

Table 1

TICINO SAND

Test n°	Passing sieve 200 ASTM	Passing sieve 100 ASTM	D _R
113	3.2%	6.0%	92%
114	1.2%	2.5%	52%
115	2.7%	4.9%	79%

Table 2

Due to the very pronounced tendency to crush, the use of calcareous sand in the large calibration chamber is problematic since it involves continuous renewal of sand samples and their replacement with fresh material. It can be estimated that the amount of sand corresponding to the load of a truck and trailer is consumed every 10 tests.

In order to find an optimum compromise between the demand to meet the significant financial aspects and the need to get small quantities of sand to ensure the homogeneity of the various samples, a smaller calibration chamber has been designed.

Its dimensions will combine a reduced sample volume avoiding, in the meantime, the imposition of the chamber size and boundary conditions (BC) effects on the test result.

As far as the CPT are concerned, previous studies [3] [4] [5] [6] [7] [8] [9] [10] have shown that the effect of the finite dimensions of the sample may correspond to an increase or a reduction in cone resistance (q_c) according to the type of boundary conditions adopted and to the overconsolidation ratio of the samples.

Furthermore it tends to decrease with decreasing the relative density and increasing the vertical pressure thus showing a strict dependance on the dilatancy behaviour of tested samples.

In the most unfavourable case of CPT's performed on silica samples tested at high relative density and low confining pressures (Fig.2), the chamber size and boundary conditions effects can be completely neglected from a practical point of

different rate of deposition in air. Consequently to avoid segregation pluvial deposition must be performed in vacuum.

Preliminary research on pluvial deposition in vacuum with TS to which small quantities of non-plastic silt have been added, has demonstrated a tendency of silt to be insensitive to the spreading effect of the meshes, remaining concentrated in the areas immediately surrounding the holes of the plate.

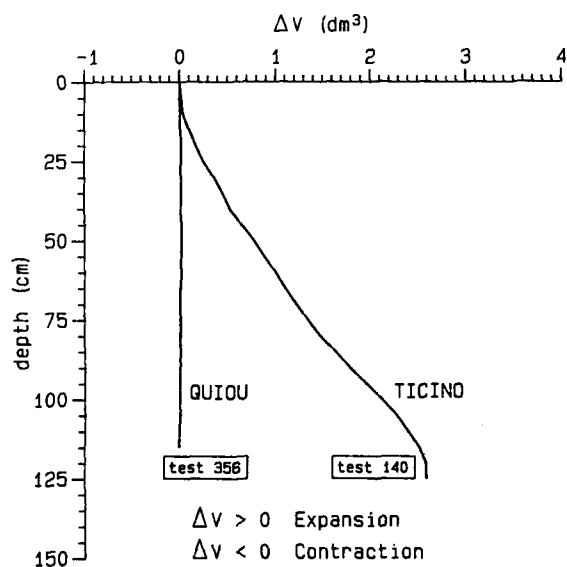


Fig. 3

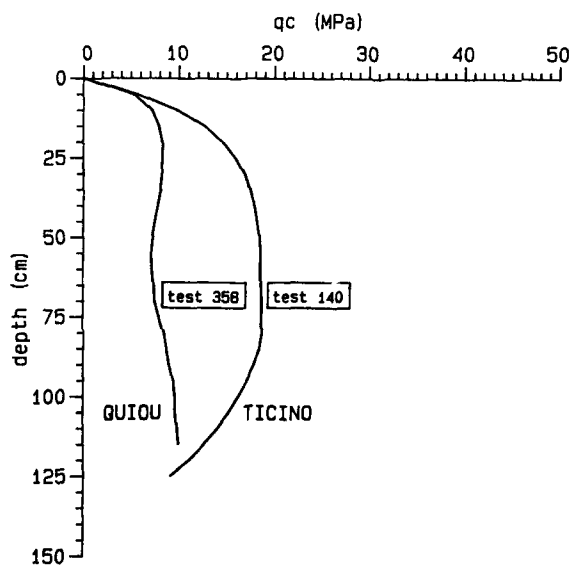


Fig. 4

An attempt to overcome this problem with the same deposition technique was made by adopting a device able to provide a slow rotating motion to the sample during deposition.

However, this system has the disadvantage of causing a non uniform distribution of the sand along the radius of the sample.

This is the result of the higher circumferential velocities existing at the edges of the rotating sample with respect to the center.

The problem can be solved by adopting specially designed shutter plates so that deposition occurs through triangular slots whose width is established according to the rotation speed of the sample (Fig. 5).

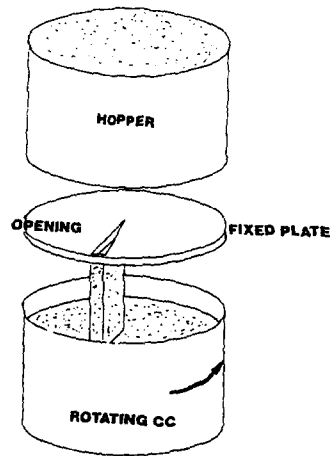


Fig. 5

DESCRIPTION OF THE CALIBRATION CHAMBER

Fig. 6 shows a schematic section of the new calibration chamber for calcareous and silty sands which will soon be operating at ENEL CRIS.

It is based on the same operating principles of the one currently in use.

Going into more details, the following characteristics have been preserved [1]:

- loading piston located at the base of the chamber;
- use of flexible membranes on the lateral boundary and on the base piston;
- rigid boundary at the top of the sample;
- undeformed vertical boundary of the sample ensured by the double wall system;

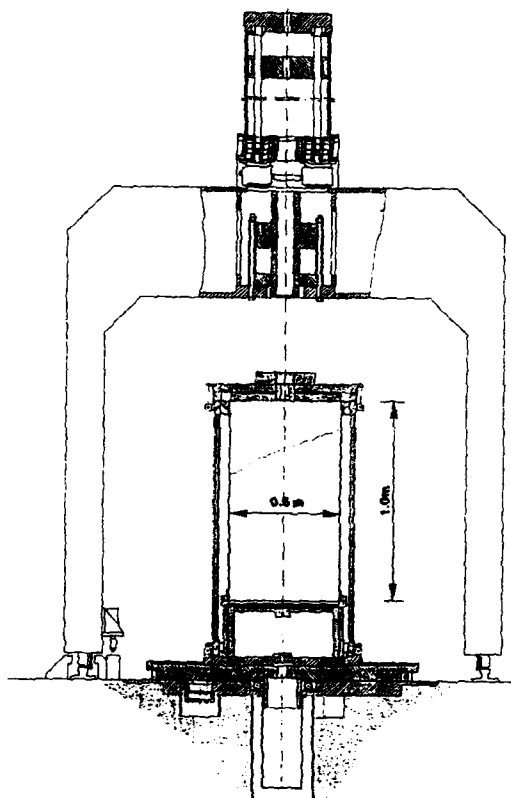


Fig. 6

- uniformity of the vertical pressures applied to the sample obtained by interposing a cushion of water between the piston and the samples;
- measurement of the horizontal pressures and of the average lateral boundary displacements of the sample by adopting an annular cell filled with water surrounding the perimeter of the sample;
- measurement of the vertical deformations of the sample by means of a displacement transducer mounted on the loading piston;
- possibility of creating the 4 boundary conditions defined in Fig. 7;
- field of application defined by the following maximum pressures $\sigma_v = 15 \text{ Kg/cm}^2$, $\sigma_h = 10 \text{ Kg/cm}^2$;

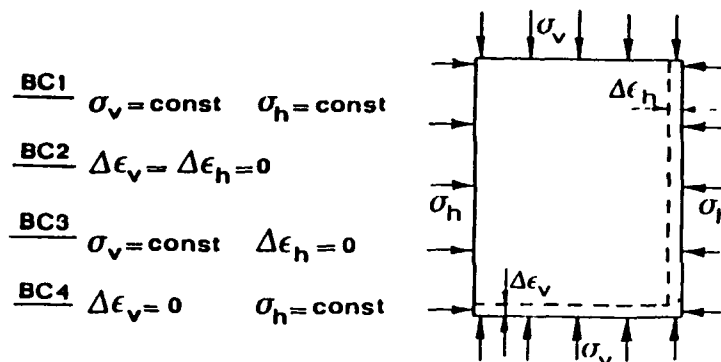


Fig. 7

- samples reconstituted by pluvial deposition method carried out by means of a sand-spreader with interchangeable perforated plates;
- possibility to raise the diffuser automatically during deposition, maintaining a constant falling height of the sand with respect to the deposition surface;
- possibility of performing deposition under vacuum;
- possibility of saturating the sand samples by adopting three different techniques [11]:
saturation with simple vacuum, saturation with double vacuum, saturation with CO_2 ;
- manual emptying of the chamber.

The new calibration chamber differs from the existing one in the following main aspects:

a) Smaller dimensions of the samples:

The calibration chamber houses cylindrical sand samples having the following dimensions:

height $h = 1.0$ m
diameter $\phi = 0.6$ m

b) Possibility of rotating the cell during formation with fixed sand-spreader.

The sample formation is carried out using the same sand-spreader of the larger calibration chamber actually in use. As a result, during deposition, the chamber is housed inside the sand-spreader resting on a circular plate rotated by means of step-by-step electric motor (see Fig. 7).

- c) Direct measurement of the radial displacement, at the lateral boundary through "proximity" transducer:

The measurements refer to specific points rather than being an overall average as in the previous chamber.

They are performed by means of a set of "proximity" transducers mounted on two diametrically opposite vertical rods.

The transducers are positioned next to metal plates glued into the membrane (see Fig. 8).

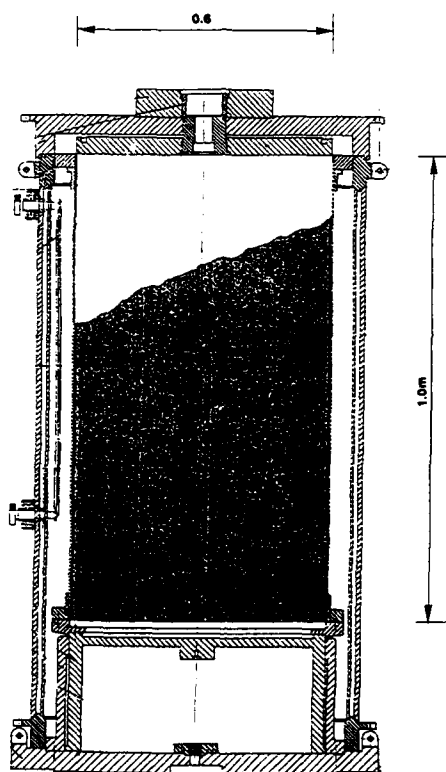


Fig. 8

- d) Allowance for higher vertical displacement of the piston :

A longer piston stroke was necessary to take into account the higher deformability of both calcareous and silty sands. The maximum displacement of the piston allowed by the new chamber is 200 mm, against the 100 mm of the previous one.

e) Loading frame translating on rail-beams (see Fig. 7):

This system has the following advantages compared with the previous one:

- an easier activity around the chamber;
- the possibility that the loading frame is used as a support for driving samplers into the specimen in order to check the uniformity of the samples in different locations [12] [13].

REFERENCES

1. R. Bellotti, G. Bizzi and V. Ghionna, Design, construction and use of a calibration chamber, Proceedings of the Second European Symposium on Penetration Testing, Amsterdam, vol.2, pp 439-446 (1982)
2. R. Bellotti and M. Jamiolkowski, Evaluation of CPT and DMT in crushable and silty sands, Waterways Expt. Stn., Contract No. DAJA45 - 88 - C -0036, (1991)
3. A.K. Parkin and T. Lunne, Boundary effects in the laboratory calibration of a cone penetrometer for sand, Proceedings of the Second European Symposium on Penetration Testing, Amsterdam, vol.2, pp 761-768 (1982)
4. V. Ghionna, Chamber size effects and boundary conditions effects, Seminar on cone penetration testing in the laboratory, Southampton University, (1984)
5. R. Bellotti, V. Crippa, S. Pedroni, G. Baldi, C. Fretti, D. Ostricati, V. Ghionna, M. Jamiolkowski and E. Pasqualini, Laboratory validation of in situ tests, Italian Geotechnical Society Jubilee Volume, XI ICSMFE, San Francisco, pp. 251-270 (1985)
6. K. Been, J.H.A. Crooks, D.E. Becker and M.G. Jefferies, The cone penetration test in sands: part I, state parameter interpretation, Geotechnique 36, No. 2, pp. 239-249, (1986)
7. W.K. Eid, Scaling effect in cone penetration testing in sand, Ph.D.thesis, Virginia Polytechnic Institute and State University, Blacksburg (1987)
8. G.T. Houlsby and H.S. Yu, Finite element analysis of the cone-pressuremeter test, Proceedings of the Third International Symposium on Pressuremeters, Oxford University (1990)
9. K. Been, D. Horsfield and M.G. Jefferies, discussion on Calibration chamber tests of a cone penetrometer in sand, Geotechnique 39, No. 4, pp. 728-729, (1989)
10. G.T. Houlsby and R. Hitchman, discussion on Calibration chamber test of a cone penetrometer in sand, Geotechnique 39, No. 4, pp. 729-731, (1988)
11. R. Bellotti, V. Crippa, S. Pedroni and V. Ghionna, Saturation of sand specimen for calibration chamber test, First International Symposium on Penetration Testing - ISOPT-1, Orlando, Florida (1988)
12. R. Bellotti and P. Morabito, Checks of the uniformity of the calibration chamber specimens, International Seminar on Calibration Chamber, Milano, (1986)
13. R. Bellotti, V. Ghionna and P. Morabito, Uniformity tests in calibration chamber samples by the thermal probe method, Geotechnical Testing Journal, Vol. 14, No. 2, pp.195-205 (1991)

Boundary Displacement Induced by DMT Penetration

Roy H. Borden

Department of Civil Engineering, North Carolina State University,
Raleigh, North Carolina, 27695-7908

ABSTRACT

This paper presents the results of dilatometer tests (DMT) performed in calibration chamber samples of Cape Fear sand. Measured and DMT-inferred constrained modulus values are compared, as well as the relationship between DMT E_D and stress state. Lateral stress measurements are also presented, with the results interpreted with respect to both relative density and state parameter and compared with those from calibration chamber tests on normally consolidated Hokksund and Ticino sands. The addition of the Cape Fear sand to the existing trend lines for the K_o^{DMT}/K_o -relative density relationship developed from data on Hokksund and Ticino sands suggests a limiting value of K_o^{DMT}/K_o between 0.5 and 1.0 at low relative densities. At higher relative densities, a significant difference exists between the current data and that obtained previously on the Hokksund and Ticino sands; suggesting the potential influence of calibration chamber sample diameter on the measured DMT results. On the other hand, measured radial-boundary displacements during DMT penetration of low density samples suggest no detrimental boundary effects.

INTRODUCTION

Penetration testing was developed as a method of obtaining soil characteristic information from soils in which undisturbed sampling was difficult or impossible. The flat dilatometer developed in the 1970s (1) is a penetration device which has been shown to provide reliable soil characteristic information. As with all penetration tests, the determination of the change in the in situ stress state created by the insertion of the dilatometer device is a complicated boundary value problem. Therefore, the index parameters obtained from the dilatometer test have been empirically correlated to the actual

soil properties. Recent development of large calibration chambers in which penetration testing can be conducted has lead to improved correlations, due to the capability of more strictly controlling the stress state of the soil.

In addition to the comparison of measured and DMT-inferred soil stiffness, the results of a study of existing correlations of horizontal stress index parameters obtained from the DMT with the actual horizontal stress applied to normally consolidated Cape Fear sand in calibration chamber tests is presented. The results are interpreted in terms of relative density and the state parameter, introduced by Been and Jefferies (2), which incorporates both the void ratio and stress level. Additional data incorporated into this study was obtained from similar calibration chamber tests performed on Hokksund and Ticino sands (3,4). This paper also describes the components of the NCSU calibration chamber: chamber, pressure systems, displacement measuring systems, computer control system, and the process of specimen preparation used. The results obtained from two series of tests on dense and loose sand specimens, consolidated under K_0 conditions and then subjected to lateral compression stress path loading are presented.

EXPERIMENTAL PROGRAM

Calibration Chamber

The NCSU calibration chamber (CC) system is shown in Figure 1. The chamber was designed with a fiberglass chamber wall to enable the use of a non-contacting radial displacement measuring system. The chamber is capable of accommodating a soil specimen of 37 inches in diameter and 37 inches high. Vertical stresses are applied to the specimen via the chamber piston ($D = 37$ inches), which is raised by pressurized air, supplied and controlled using Fairchild voltage to pressure regulators which are operated using a computer control system. The lateral stresses are also applied by of air pressure to the annulus surrounding between the sample and chamber wall.

The sample is enclosed by a rubber membrane which is clamped to the chamber base; the rubber membrane is sealed around a fiberglass top platen, which forms the top boundary of the sample, Figure 2. The thrust of the chamber piston is transferred from the sand to the top platen, into the concrete top cap and through four steel tie rods, which are screwed into nuts embedded into the concrete base.

The design concept for the NCSU CC aimed at the construction of a lateral displacement measuring system, for large sand specimens, with adequate accuracy. Among many available options, inductance coils, developed by Selig (5, 6) appeared to offer significant potential; studies by Markiewicz (7) endorsed their usage. In the system adopted, four pairs of inductance coils are used; three pairs to measure lateral displacements at the midheight of the specimen, and one pair at the center of the bottom piston, to measure the

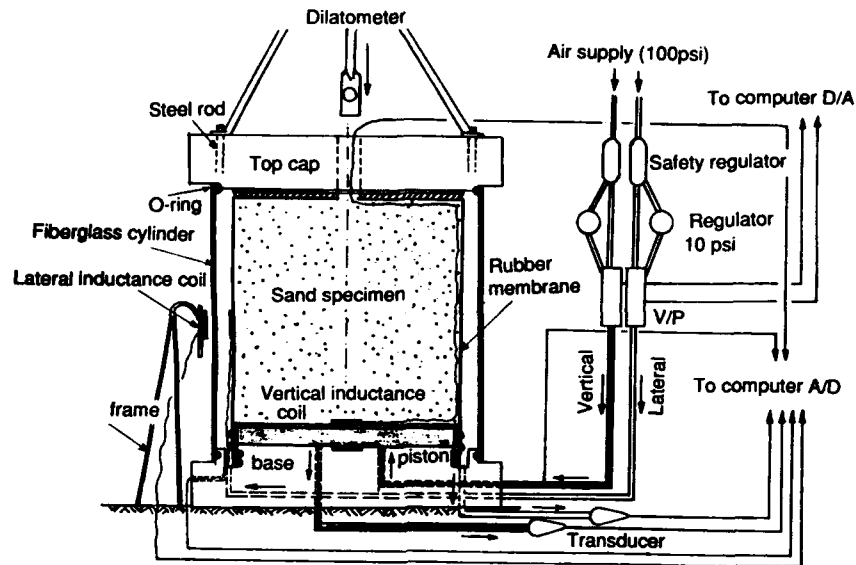


Figure 1. NCSU calibration chamber.

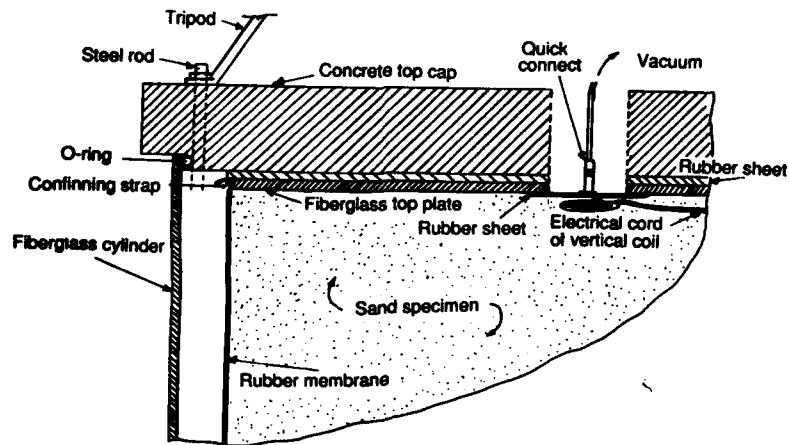


Figure 2. Calibration chamber detail.

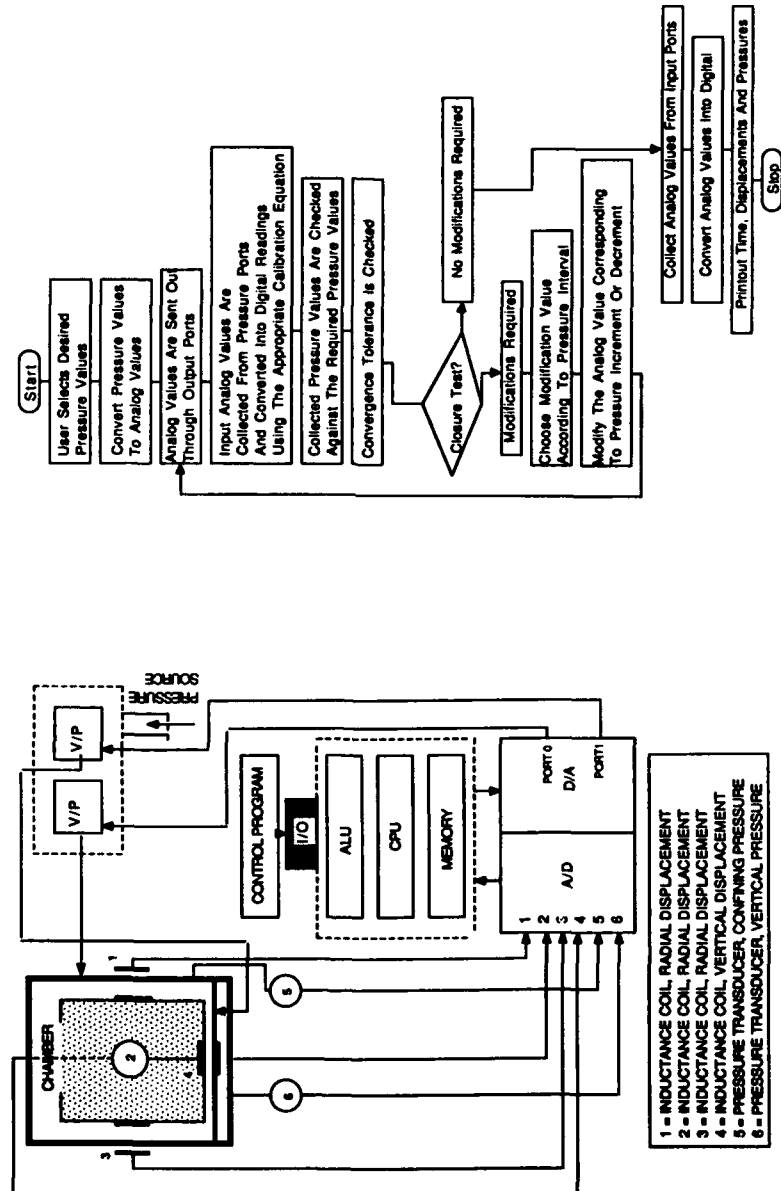


Figure 4. "CONTROL" flow chart.

Figure 3. Computer control system.

vertical displacement. For the three lateral measurement coil pairs, one coil of each pair is mounted on the rubber membrane, while the other coil is attached to a free-standing aluminum frame outside the chamber, as shown in Figure 1. The radial coils are positioned at 120 degrees around the circumference of the sample.

The computer control system, represented in Figure 3, consists of a Zenith 150 microcomputer with a hard drive outfitted with the Data Translation (DT) 2801 board. A DT 707 connector board was used for interfacing with the pressure transducers and the inductance coils. The DT 2801 board is a high performance analog and digital Input/Output board which is compatible with the IBM/compatible PC's. The board is equipped with 16 single ended Analog/Digital channels and two Digital/Analog ports. All functions on the board are controlled by writing and reading commands, command parameters and data, to registers installed on the board. The board is instrumented with 12 bit registers which have a resolution of 1 part in 4096.

A computer program "CONTROL", supported by the Data Translation real time PCLAB macro-routine libraries was written for the test control. In addition to monitoring the pressures, the computer program is also used for the collection of the displacement data, after achieving each required pressure increment. Eight single ended channels are used in the control process; four Analog/Digital channels for the collection of displacement data; two Digital/Analog channels for pressure application; and two Analog/ Digital channels for pressure monitoring. In order to account for noise effects, each collecting port is scanned 100 times each second, with the 100 readings then averaged to produce one reading per second. A flow chart of the program logic is given in Figure 4.

Specimen Preparation

The method of preparing sand specimens by pluvial deposition has been discussed in detail by many investigators (8,9). It was concluded that it is possible to form a uniform sand specimens in the laboratory with a relative density (D_R) varying as a function of the sand-raining intensity (mass/time). Different relative densities are achieved by changing the size of the openings on a perforated shutter plate. Figure 5 shows a schematic diagram of the sand-rain device developed at NCSU. The motorized device has a speed controller to enable the fall height between the diffuser and the rising sand surface to be maintained constant.

The sand-raining process begins when the shutter plate is opened. The sand contained in the upper cylinder begins to fall in jets and is dispersed by a series of three metal screens, referred to as the diffuser. The three metal screens, forming the diffuser are oriented at 45 degrees with respect to each other to better diffuse the sand into a uniform rain, as suggested by Jacobson (9). During the sand fall, the air in the chamber is replaced by the sand. Unless this

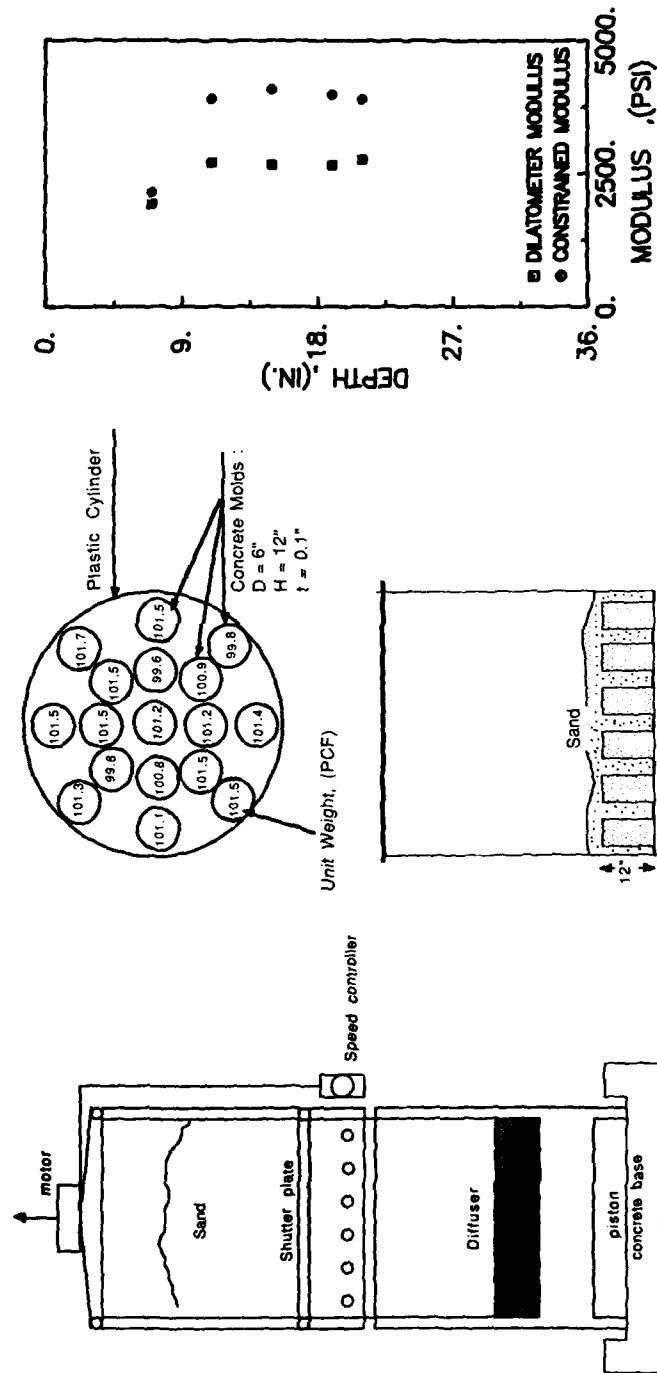


Figure 5. Sand-rain device.

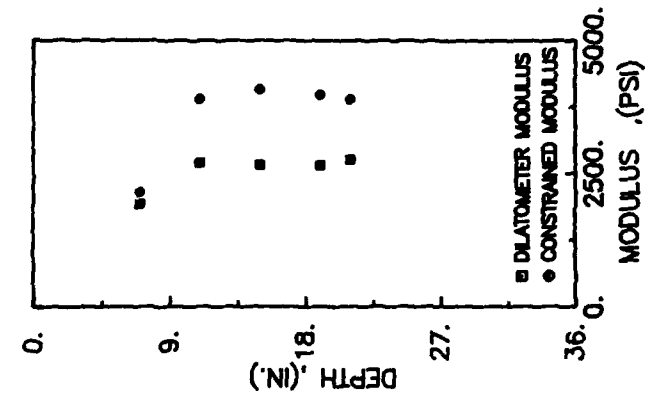


Figure 6. Sample uniformity in horizontal plane.

Figure 7. DMT-modulus profile.

air is vented out of the chamber, it will run up through the holes in the shutter plate creating air turbulence which will alter the uniformity of the sand jets, and lead to the formation of non-uniform specimens. During the formation of dense samples, the raining intensity is low, and this problem is insignificant. However, as a precautionary measure in the formation of low density samples, 24 "1-inch" diameter holes were drilled around the circumference of the plastic cylinder of the sand-rain device as air vents.

The following tests were performed in order to evaluate sample uniformity:

1. Horizontal direction variation: In order to evaluate the uniformity of the prepared specimen in the horizontal direction, 6 inch diameter, 12 inch high plastic concrete molds were placed on the ground inside the membrane stretcher, as shown in Figure 6. The diffuser was positioned as is normally done during the actual test, and the sand was rained through the diffuser into the molds. The results shown in Figure 6 are comparable to similar determinations made by Bellotti et al (10). In their experiments on dense sands they found that the average value of the specimen relative density is about 59% with a standard deviation of 10%. In this study, the average relative density, at the bottom of the specimen, was about 47% with 7% standard deviation. The standard deviations, for both studies, are relatively close, confirming the consistency of this method of specimen preparation.

2. Vertical direction variation: The uniformity of the dilatometer modulus with depth served as an indication of density uniformity in the vertical direction. Figure 7 shows the results of one such test in dense sand. It is clear that once a penetration is made to a depth below the influence zone of the top cap opening (10 inches and below), the soil response does indeed appear to be uniform.

The sand used in these tests is sub-angular to angular naturally occurring material obtained from the Cape Fear River in North Carolina. A summary of its properties and a grain size distribution curve are presented in Table 1 and Figure 8, respectively. A series of strain controlled isotropically consolidated undrained triaxial tests were performed to determine the steady state line (SSL) (11). Figure 9 presents the SSL for the Cape Fear sand in conjunction with those for the Hokksund and Ticino sands, as well as the Kogyuk sand with 0% silt used by Been and Jefferies (2) in their development of the state parameter. Table 1 also contains a summary of soil properties for the Hokksund and Ticino sands.

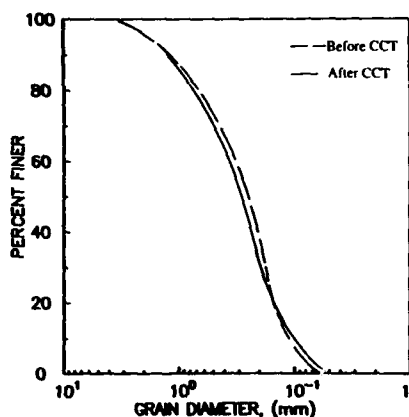


Figure 8. Grain size distribution of Cape Fear sand.

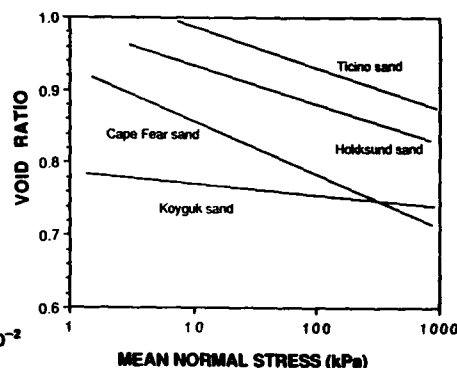


Figure 9. Steady state line for calibration chamber sands.

Table 1. Index properties of sands used in various calibration chambers.

Property	Cape Fear Sand	Hokksund Sand	Ticino Sand
d_{50} (mm)	0.69	0.39	0.53
d_{10} (mm)	0.29	0.21	0.36
C_U	2.76	2.10	1.60
G_s	2.67	2.70	2.69
e_{max}	0.802	0.894	0.931
e_{min}	0.527	0.549	0.579
e_{ss}	0.858	0.934	0.986
λ_{ss}	0.074	0.054	0.056

Modulus Correlations

In the tests described herein, a K_0 consolidation stress path was followed, as shown in Figure 10a. The desired state was obtained by incrementally increasing the vertical stress and in response to measured lateral stress changes incrementing the lateral stress accordingly. Figure 10b shows that each of the three radial displacement coils measured slightly different responses ($\pm 0.1\%$ strain), with one of the coils suggesting slight expansion while another suggests contraction. For control purposes, the output from the three coils was averaged to produce an average radial strain, with the absolute value minimized. The vertical strain corresponding to incremental increases, figure 10b, was used to determine the tangent constrained modulus (M) for each increment of loading, with the final value normalized by the DMT-inferred value obtained

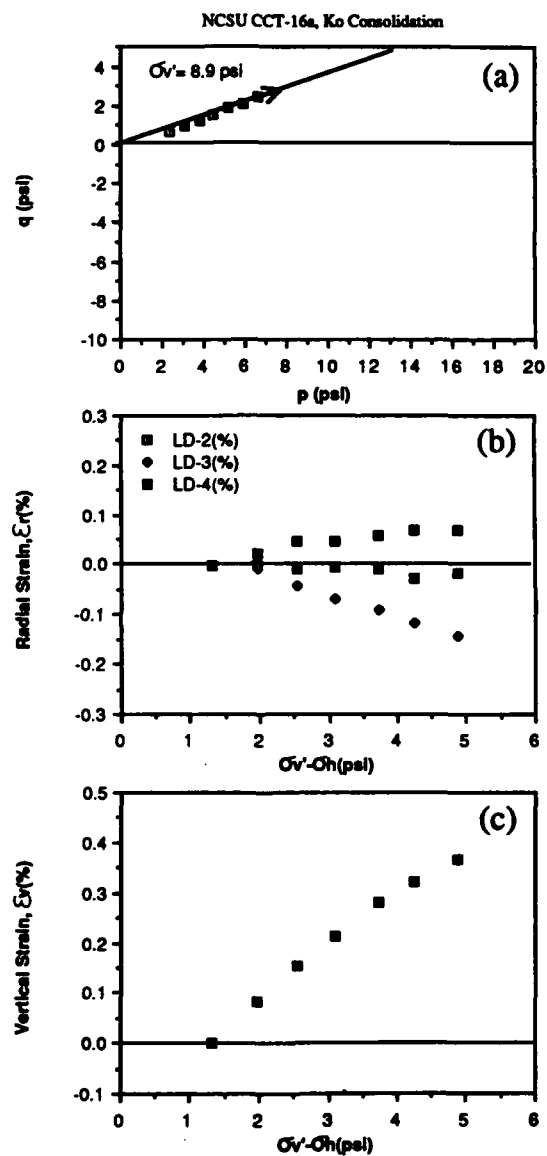


Figure 10. K_0 consolidation of sample CCT-16.

using the Marchetti correlation (12). These values, for the various density samples, are plotted in Figure 11 versus the DMT- P_o value normalized by the square root (SQRT) of the vertical effective stress, as suggested by Baldi et al (13). The data from this study are seen to plot somewhat lower than the range reported for normally consolidated Ticino sand, with an average value of approximately unity.

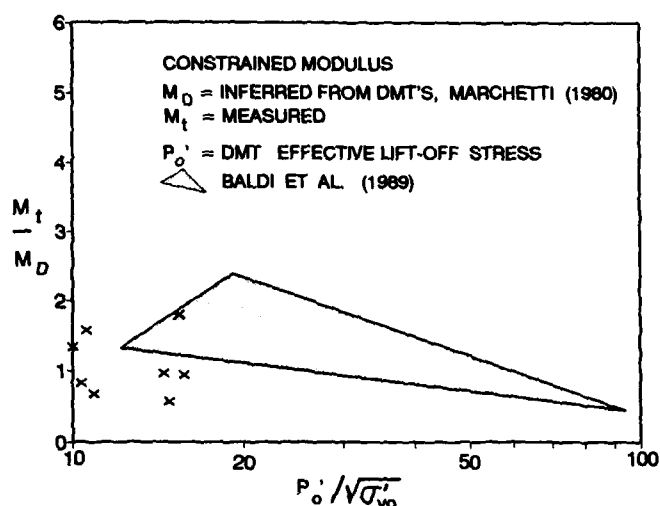


Figure 11. Constrained modulus of Cape Fear sand from DMT's performed in calibration chamber.

After consolidation to the desired stress level, DMT tests were conducted at depths of 6, 10 and 14 inches. Based on preliminary tests, such as those shown in Figure 7, this last test was considered representative of the sample. The normalized E_D values are plotted as a function of the SQRT of the normalized effective stress in Figure 12. The data obtained from tests on low and high relative density samples, respectively, fit linear functions with the modulus number for the dense samples approximately twice that for the loose.

Holding the DMT stationary, the specimens were then subjected to incremental lateral compression stress path loading, as shown in Figure 13d.

The measured vertical and average radial strains observed during this loading is shown in Figures 13e and 13f, respectively, for sample 16. After successive increments of increasing lateral stress, the DMT was pushed another 4 inches into the sample and a test conducted. In response to the observation that DMT data, and all other penetration test results for that matter, are relatively insensitive to strain and stress history (13), the E_D values obtained were plotted in Figure 14 in conjunction with the best-fit lines shown on Figure 12. The data obtained from each of the individual samples are noted by the connecting lines. For several of the samples, the E_D values fit the appropriate

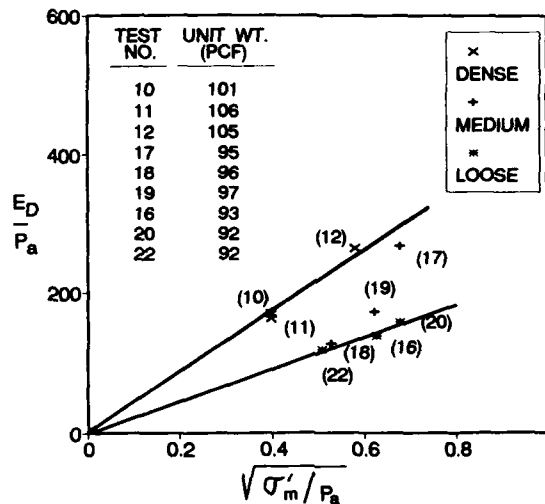


Figure 12. DMT modulus as a function of mean effective stress.

function from the normally consolidated samples remarkably well, suggesting that the DMT E_D is indeed predominately dependent on the current stress state and density.

Lateral Stress Correlations

Correlation of the K_D/K_0 ratio, called the amplification factor, to the state parameter has been suggested by Jamiolkowski et al (14) to be a rational approach for interpreting the calibration chamber data, based on the results of 57 calibration chamber tests on normally and overconsolidated Hokksund and Ticino sands. A similar correlation was investigated for normally consolidated Cape Fear sand. Although other functions were investigated, none provided a significantly better fit. The relationship between the state parameter and the amplification factor for these tests are shown in Figure 15 in conjunction with the data obtained from normally consolidated Hokksund and Ticino sand samples. This figure suggests that the slope of the amplification factor versus state parameter relationship for the Hokksund and Ticino sands is steeper than that of the Cape Fear sand.

Figure 16 presents the K_0^{DMT}/K_0 -relative density relationship presented by Jamiolkowski et al (14). The addition of the Cape Fear sand to the existing trend lines for the suggests that the trend line may approach a limiting value of K_0^{DMT}/K_0 between 0.5 and 1.0 at low relative densities. At the higher relative densities, corresponding to lower state parameter values, the K_0^{DMT}/K_0 values are significantly lower for the Cape Fear Sand than for either the Hokksund or

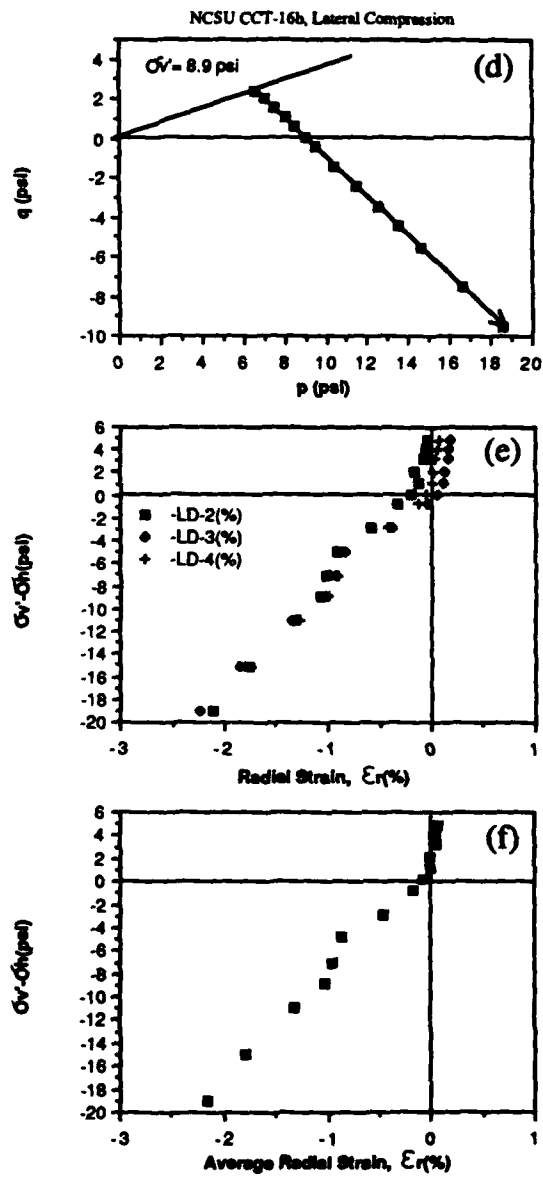


Figure 13. Lateral compression of sample CCT-16.

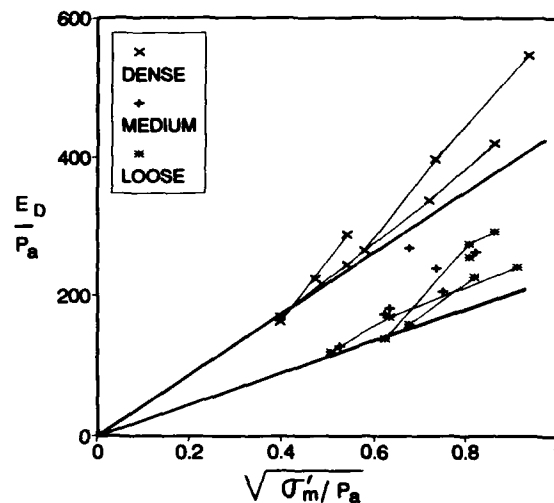


Figure 14. DMT modulus versus mean effective stress for lateral compression stress paths.

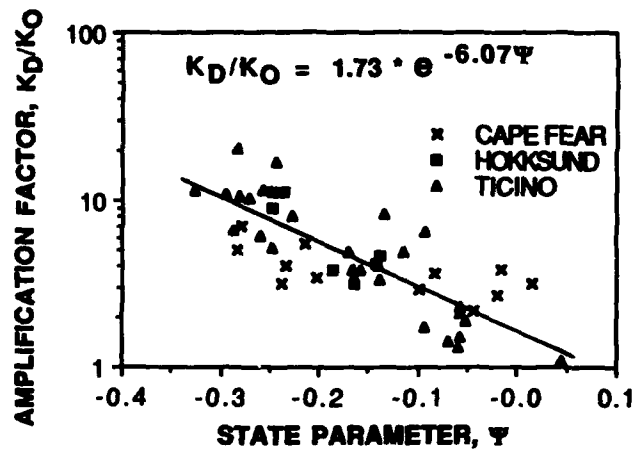


Figure 15. DMT amplification factor for normally consolidated sands [11].

Ticino sands. It should be noted that the latter tests were performed in a 1.5-m (59 inch) diameter chamber while the NCSU chamber is 0.97 m (37 inches) in diameter. It is possible that the difference in results in the more dilatant soils is related to the development of a plastic zone during penetration into the smaller chamber that extends to the boundary. In the more contractive materials, one would expect the plastic zone to be considerably smaller, thus minimizing the influence of chamber diameter. This concept would support the good agreement observed between the data obtained on medium density samples for

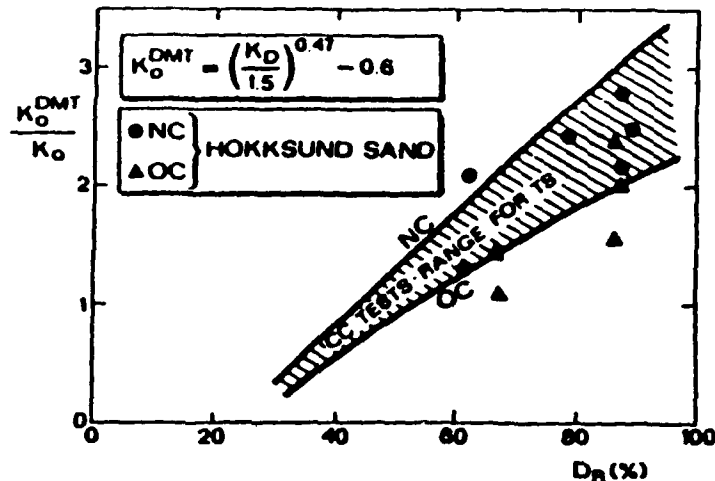


Figure 16. K_o^{DMT}/K_o for Hokksund and Ticino sands using Marchetti correlation [14].

all three soils, but would not explain the larger amplification factor observed on lower density samples of Cape Fear sand.

Jamiolkowski et al (14) have suggested that the empirical formula for K_o^{DMT} overestimates K_o in dense to very dense sands and underestimates it in loose sands. The results of the calibration chamber tests on Hokksund and Ticino sands, shown in Figure 16, show this trend. Examination of the results from the tests on Cape Fear sand, shown in Figure 17 in conjunction with the above data, suggest that at lower relative densities the trend is toward a K_o^{DMT}/K_o ratio of 0.5 to 1.0. As previously suggested, Marchetti's correlation tends to overestimate K_o for dense sands and underestimate it for loose sands, but to a lesser degree than for the Hokksund and Ticino sands.

Boundary Displacements During DMT Penetration

Finally, a very interesting observation was made during the insertion of the DMT in the lateral compression phase of the CC tests previously described. Figure 18 shows the measured mid-sample displacement for each of the radial inductance coils as a function of the depth of DMT penetration. With the exception of the horizontal displacements at a depth of 14 inches, which represent the sample compression during lateral compression loading, all displacements are the result of DMT penetration. Figure 18a shows a second level of lateral compression as a result of a lateral stress increment when the DMT was at a depth of 18 inches. It appears that the boundary was not influenced by penetration into these low density samples as long as the confining stress remained constant. One explanation may be related to the

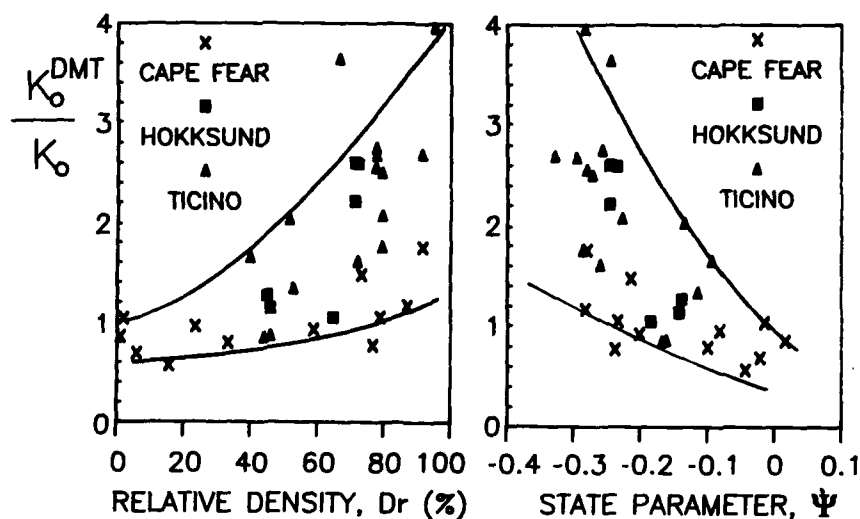


Figure 17. K_o^{DMT}/K_o for normally consolidated sands using Marchetti correlation [11].

shape of the DMT blade and the "groove" cut into the soil as the blade advances. Subsequent increases in lateral stress and distortions caused by further DMT penetration may result in the closing of this void and the resultant boundary displacement. It is not known whether this response might be observed in a larger chamber. Nevertheless, the relatively insignificant boundary displacements during penetration prior to the increase in lateral stress suggest that the chamber size was of no significance in the lower density tests. Similar data will need to be obtained for dense samples to allow a more complete explanation.

SUMMARY AND CONCLUSIONS

The relationships between DMT-inferred modulus and horizontal stress index parameter and the measured modulus and existing horizontal stress were evaluated for normally consolidated Cape Fear sand based on tests performed in calibration chamber samples. The M/M^{DMT} ratio was found to be somewhat lower than that reported for Ticino sand, with an average value of unity.

The test results were also interpreted in terms of the existing lateral stress index parameter, K_D , and the original Marchetti correlation of K_D and K_o , with respect to both relative density and state parameter. As previously suggested, Marchetti's correlation tends to overestimate K_o for dense sands and underestimate it for loose sands, but to a lesser degree than for the Hokksund and Ticino sands.

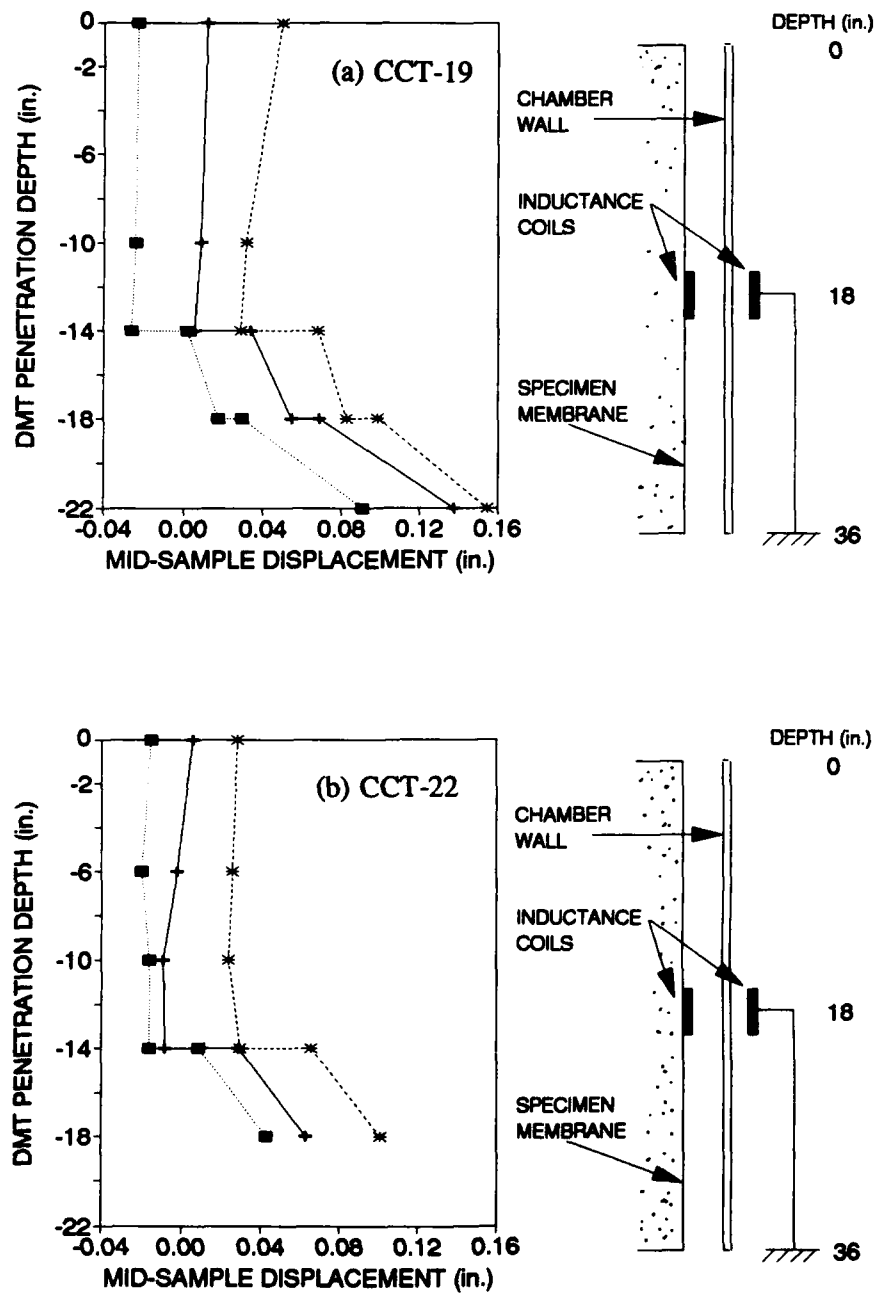


Figure 18. Mid-sample boundary displacements during DMT penetration.

The addition of the Cape Fear sand data to the existing trend lines for the K_o^{DMT}/K_o -relative density relationship presented by Jamiolkowski et al (16) suggests that the trend line approaches a limiting value of K_o^{DMT}/K_o between 0.5 and 1.0 at low relative densities. It is possible that the difference in results between the Cape Fear sand and the Hokksund and Ticino sands at higher relative densities could be related to calibration chamber size. Boundary displacement data showed the tests on low density samples to be unaffected by chamber dimensions, however this data is not available for denser samples.

ACKNOWLEDGMENTS

The calibration chamber tests reported were conducted under a research grant provided by the North Carolina Department of Transportation and FHWA. The significant contributions of Eduardo Suarez, Gene Hsu, Wei-Chen Lien and Dr. Mohammed Gabr in the fabrication of the calibration chamber and performance of the experimental studies is gratefully acknowledged. The assistance of Shuih-Liang Yan in the preparation of the figures for this paper is sincerely appreciated.

REFERENCES

1. Marchetti, S. (1975), "A New In Situ Test for the Measurement of Horizontal Soil Deformability," *Proceedings of Conference on In Situ Soil Properties*, Vol. 2, ASCE Specialty Conference, Raleigh. pp. 255-259.
2. Been, K. and Jefferies, M. G., "A State Parameter for Sands," *Geotechnique*, Vol. 35, No. 2, June, 1985, pp. 99-112.
3. Baldi, G., Bellotti, R., Ghionna, V., Jamiolkowski, M., Marchetti, S., and Pasqualini, E., (1986), "Flat Dilatometer Tests in Calibration Chambers," Use of in Situ Tests in Geotechnical Engineering, Proc. of In Situ '86, Virginia Tech, Blacksburg, VA. Geotech. Spec. Pub. No. 6, ASCE, pp. 431-446.
4. Jamiolkowski, M., personal communication.
5. Selig, E.T. and Grangaard, O.H. Jr., (1970), "A New Technique For Soil Strain Measurement," Materials Research and Standards, MTRSA, Vol. 10, No. 10, November, p.19.
6. Selig, E.T. (1975), "Soil Strain Measurement Using The Inductance Coil Method," Special Technical Publication 584, Performance Monitoring for Geotechnical Construction, ASTM, pp. 141-158.
7. Markiewicz, Thomas E., (1983), "Test Apparatus for The Investigation of Cavity Expansion by The Inductance Coil Measurement System." Civil Engineering Department Report, North Carolina State University.

8. Bieganousky, W., and Marcuson, W. (1976), "Uniform Placement of Sand," J. Soil. Mech. and Foundation Division, ASCE, Vol. 102.
9. Jacobson, M. (1976), "On Pluvial Compaction of Sands," Report No. 9, Laboratoriet for fundering. University of Aalborg-Danmark.
10. Bellotti, R., Bizzi, G., and Ghionna, V., (1982), "Design, Construction, and Use of a Calibration Chamber," Proc. ESOPT II, Amsterdam, Vol. 2.
11. Lawter, Robert S., Jr. and Borden, R. H. (1990), "Determination of Horizontal Stress in Normally Consolidated Sands by Using the Dilatometer Test: A Calibration Chamber Study," TRR 1278, Dynamic Testing of Aggregates and Soils and Lateral Stress Measurements, Transportation Research Board, pp. 135-140.
12. Marchetti, S., (1980), "In Situ Tests by Flat Dilatometer," Journal of the Geotechnical Engineering Division, ASCE, Vol. 106, No. GT3, Proc. Paper 15920, March, 1980, pp. 299-321.
13. Baldi, G., Bellotti, R., Ghionna, V.N., Jamiolkowski, M. and Lo Presti, D.C.F. (1989), "Modulus of Sands from CPT's and DMT's," ISSMFE, Rio.
14. Jamiolkowski, M., Ghionna, V. N., Lancellotta, R., Pasqualini, E., "New Correlations of Penetration Tests for Design Practice," Penetration Testing 1988, ISOPT-1, Vol. 1, 1988, pp. 263-296.

Methods of Sample Fabrication in the Virginia Tech Calibration Chamber

Thomas L. Brandon¹ and G. Wayne Clough²

ABSTRACT

Research at Virginia Tech on sample formation in a calibration chamber has involved both small and large-scale tests for clean and silty sands. Similar to previous investigations, pluviation was found to be the most efficient and reliable procedure for forming a sample of clean sand. The pluviation equipment was designed to allow control over key parameters so that a uniform specimen was obtained, while exercising control over densities achieved. Silty sands posed far more difficulty in sample fabrication than clean sands. After trials with different types of procedures, including pluviation through air and through a vacuum, it was determined that the best technique involved consolidation of the sample from a slurry. This allowed samples to be formed with a reasonable density and fabric. Tests within the sample mass showed that the samples were uniform, and that little segregation of particle sizes occurred.

INTRODUCTION

An important issue in calibration chamber research is the fabrication of the soil specimens for penetration testing. Ideally, the formation techniques should be able to create reproducible samples in terms of density and gradation. There should be an ability to obtain a range of density, and in some cases, a high degree of saturation is required. In addition, it is desirable to be able to use a similar sample fabrication technique for the creation of laboratory samples with similar fabrics.

Two different types of sands have been extensively tested in the Virginia Tech calibration chamber in the course of sponsored research. Prior to testing either sand, considerable effort was expended to obtain a proper sample fabrication technique to

¹ Associate Professor of Civil Engineering, Department of Civil Engineering, Virginia Polytechnic Institute and State University, Blacksburg, VA 24061

² Dean, College of Engineering, Virginia Polytechnic Institute and State University, Blacksburg, VA 24061

achieve the above goals. Each sand required a radically different method of sample fabrication.

THE VIRGINIA TECH CALIBRATION CHAMBER

The Virginia Tech calibration chamber is one of the largest in existence, and it affords a unique opportunity for controlled cone penetration testing. A soil specimen, approximately 1.5 m in diameter by 1.5 m tall, can be subjected to horizontal and vertical stresses up to 700 kPa. The vertical stresses are applied to the soil specimen via air pressure bags located below the bottom plate. Radial pressures are applied to the sample membrane by air pressure. The chamber allows up to seven cone penetration tests to be conducted in one test specimen where boundary effects do not cause interference between adjacent tests.

The chamber was designed with the primary intention of cone testing of dry sands. No provisions for pore pressure control or back-pressure saturation techniques were incorporated into the design. A detailed description of the design and construction of the calibration chamber is presented by Sweeney (1987) and Sweeney and Clough (1990). A cross-section of the calibration chamber equipped for cone penetration testing is shown in Figure 1.

Soils Tested in the Calibration Chamber

Two different sands have been extensively tested in the Virginia Tech calibration chamber. Monterey 0/30, a commercially available, washed, beach sand, was the first soil to be tested in the chamber. This sand is predominantly quartz, and classifies as an SP according to ASTM D-2487-85. This soil has been used in projects involving the development of a miniature cone penetrometer (Sweeney, 1987) and to study size effects in penetration testing (Eid, 1987).

In a separate study, approximately 82,000 kg of Yatesville silty sand were acquired to study the liquefaction potential of silty sands. This soil is found in Lawrence County, Kentucky, and was obtained from the site of the U. S. Army Corps of Engineers' Yatesville Lake Dam. Yatesville silty sand contains approximately 42% non-plastic fines, and has a specific gravity of 2.67. It classifies as an SM according to ASTM D-2487-85. The gradation curves for both soils are shown in Figure 2.

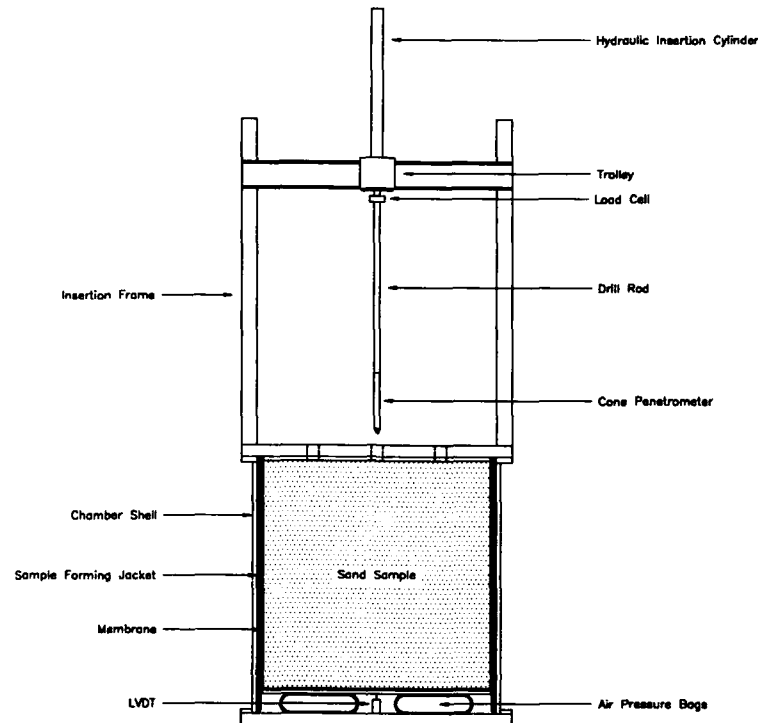


Figure 1 Cross-section of calibration chamber with insertion frame in place for cone penetration testing.

Investigation of Pluviation of Clean Sands

Deposition by pluviation involves the free fall of soil grains through air or water so that the particles come to rest in a repeatable configuration. The intensity of deposition, expressed as mass per unit area per unit time, is controlled by the diameter of the aperture through which the soil flows. The pluviation technique has advantages over other techniques of sample fabrication because of its simple operation and its approximation of a natural deposition process. It has been the major method of sample fabrication in calibration chamber testing.

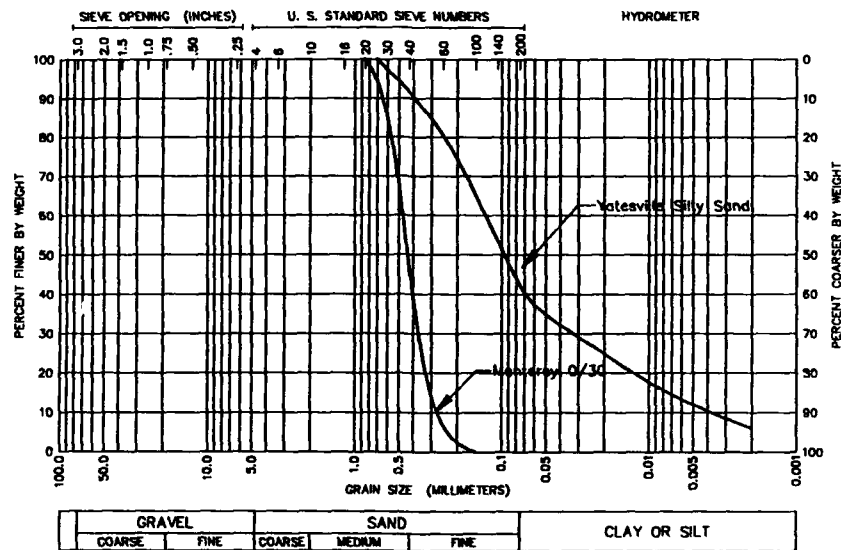


Figure 2 Gradation curves for Monterey 0/30 and Yatesville Silty Sands.

For clean sands, there are established laboratory methods for specimen preparation using pluviation. In an attempt to form saturated specimens of clean sands for triaxial testing, Bishop and Henkel (1957) devised an apparatus for depositing the sand in water through a funnel. ASTM D-4254-83 provides a method to determine the maximum void ratio of uniform cohesionless soil based on pluviation, which was modified by Castro (1969) and Mulilis et al. (1975) to form triaxial specimens.

Considerable research has been conducted to examine the variables influencing the densities and fabrics which can be achieved by pluviation, and the practical applications of the techniques to calibration chamber testing (Kolbuszewski, 1948; Walker and Whitaker, 1967; Chapman, 1974; Jacobsen, 1976; Bellotti et al., 1982; Miura and Toki, 1982; Vaid and Negussey, 1984; and Rad and Tumay, 1987).

Concurrent with the design of the Virginia Tech calibration chamber, Eid (1987) performed an extensive study to develop a pluviation system for laboratory and calibration chamber specimens. The research involved developing scale models of pluviators, examining the influence of the geometry of the system, and extending the design to the calibration chamber. The basic design of the pluviation apparatus is patterned after that presented by Jacobsen (1976), where the sand falls in "jets" through a perforated plate onto diffuser sieves. The diffuser sieves create a uniform rain of sand for the deposition of the sample. A schematic of the pluviator is shown in Figure 3.

The major variables studied by Eid were: (1) mean diameter of the sand grains, (2) the diameter and number of holes in the perforated plate, (3) the distance from the perforated plate to the diffuser sieves, F , (4) the distance between the diffuser sieves, S , (5) the sieve opening size, and (6) the distance from the diffuser sieves to the top of the deposited specimen. Of these parameters, the diameter and number of the holes in the plate, which can be expressed as the plate porosity, can greatly influence the achieved densities. Figure 4 shows the range in densities obtained in the model pluviator by varying the plate porosity. It should be noted that for the smallest plate porosity, a relative density greater than that obtained using ASTM D-4253-83 was obtained.

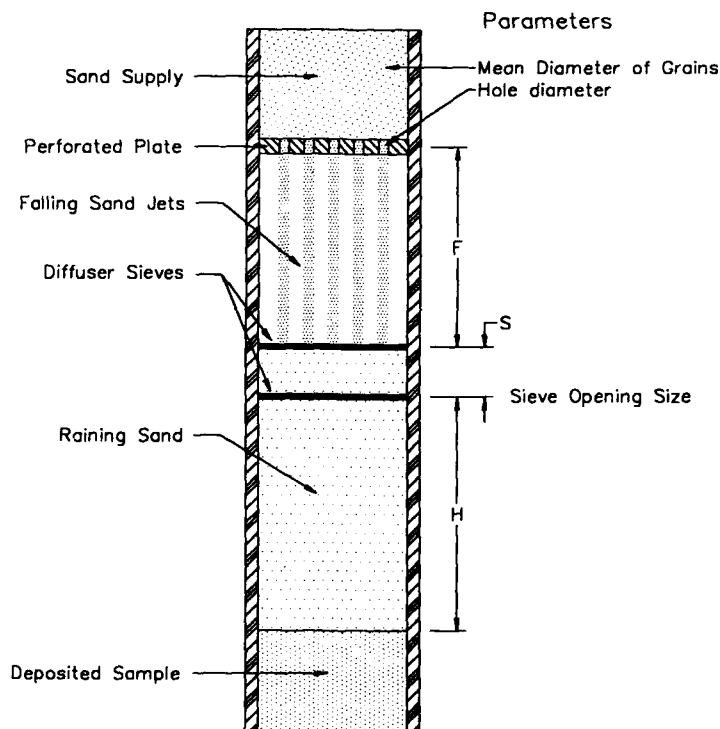


Figure 3 Schematic of small scale sand pluviation apparatus developed by Eid (1987).

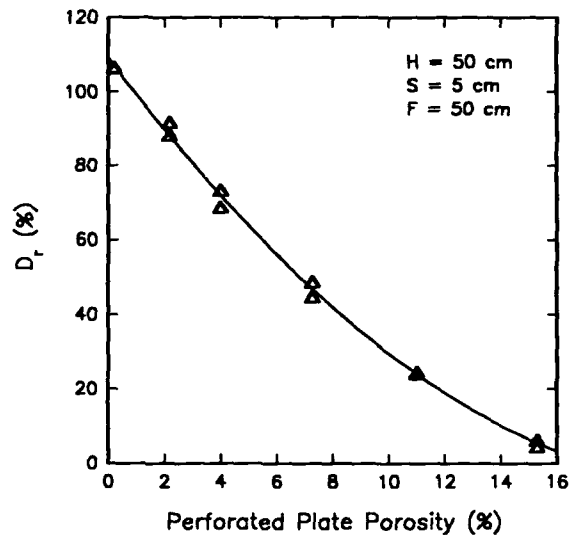


Figure 4 Relative densities obtained with model pluviator by varying the plate porosity (after Eid, 1987).

Fabrication of Monterey 0/30 Calibration Chamber Specimens

Based on the model tests, it was decided that the plate porosity should be used as the controlling parameter to be varied to obtain different densities for the full-scale pluviator in the calibration chamber. Shown in Figure 5 is the final design of the rainer for the calibration chamber.

The chamber rainer differs in design from the model rainer in two major aspects:

- 1.) A shutter plate was installed under the perforated plate to control the start of the raining procedure.
- 2.) The diffuser sieves are mobile. As a sample is being deposited, the diffuser sieves are continuously raised to maintain a constant distance from the diffuser sieves to the top of the sample.

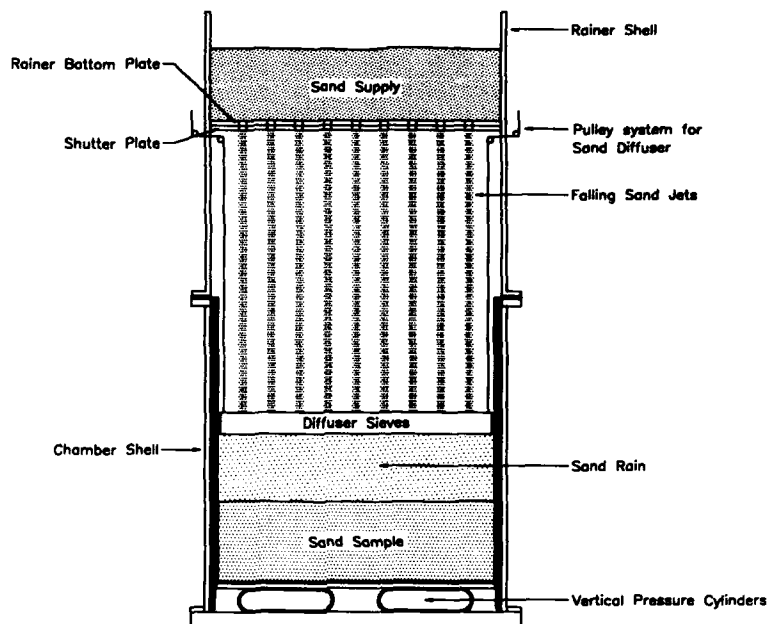


Figure 5 Calibration chamber sand rainer.

Two different perforated plates, with plate porosities of 2.8% and 9.1%, were made for the calibration chamber in order to achieve samples of different densities. A series of tests were conducted to examine the reproducibility of samples created with the full-scale rainer. The soil is first placed in a hopper, and the weight of the soil was recorded by a tension load cell. After a sample was deposited, a bulk relative density was calculated based on the volume of soil deposited. The tests showed that the perforated plate with a porosity of 2.8% produced samples with a bulk relative density of 74%, and the plate with a porosity of 9.1% produced a bulk relative density of 24%. In both cases, the variation in densities achieved for a number of trials was less than $\pm 4\%$.

Since it is difficult to perform conventional density tests in uniform clean sands, the density variation with depth was investigated via cone penetration tests. Shown in Figure 6 is a cone record measured for a sample of Monterey 0/30 deposited at a relative density of 74%. Except for the upper portion of the curve, where the tip resistance is influenced by the boundary effects of the top plate, the resistance is relatively constant with depth. This would indicate that a high degree of sample uniformity can be obtained by the calibration chamber rainer.

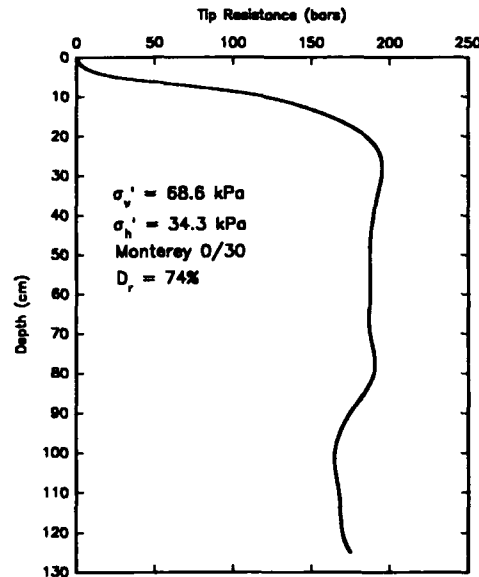


Figure 6 Cone record for calibration chamber specimen of Monterey 0/30 deposited at a relative density of 74%.

Fabrication of Yatesville Silty Sand Calibration Chamber Specimens

For a research project concerning cone penetration testing in silty sand, it was desired to create calibration chamber specimens of Yatesville silty sand at dry densities ranging from 16 to 19 kN/m³. A major concern in the fabrication of calibration chamber specimens was the minimization of segregation. Due to the uniformity of Monterey 0/30, this was not a problem in the earlier investigations of sample fabrication. As with Monterey 0/30, a laboratory study was performed prior to attempting full-scale tests in the chamber.

First, an attempt was made to pluviated the silty sand using the model pluviator developed by Eid (1987). It was apparent from the early trials that the Eid pluviator as designed for clean sands would not work for the silty sand. The soil simply would not pour in a regular fashion through the diffuser sieves. The fines would come to rest on the sieves and clog up the holes, causing the remaining soil to pile up on the sieves. Also, the silty sand did not pour in steady continuous jets through the perforated hopper plate.

Second, an attempt was made to create samples bypassing the hopper system and pouring the soil onto the diffuser sieves using an inverted flask. Unfortunately, problems

still arose with soil getting caught on the diffuser sieves and this disrupted the raining process leading to nonuniform specimen formation.

Third, the procedure used by Mulilis et al. (1975) was attempted, whereby the soil is dropped directly from the inverted flask, eliminating use of the diffuser sieves altogether. With this method, segregation was evident by the creation of a small cloud of fines during deposition. Also, the dry densities achieved ($< 15 \text{ kN/m}^3$) were lower than the desired range of densities.

In a final attempt to create samples by pluviation, a vacuum pluviator was constructed. The main reasoning in this attempt was that in the presence of a vacuum, the silt fraction would have the same falling velocity as the larger sand particles, perhaps preventing segregation. Under a vacuum, there is no air resistance to a falling object, so particles will fall freely without deceleration. Compared to pluviation in air, there is a substantial gain of velocity and energy at impact for particles dropped under vacuum. There is no terminal velocity, therefore the influence of the height of fall should be magnified.

Observation of the vacuum pluviation process showed that there was much less dust created compared to pluviation in air, and that the dust stayed close to the surface of the deposited material. There was a small increase in density of specimens pluviated through vacuum compared to those pluviated in air, but the increase in density was not proportional to the calculated increase in impact energy. Again, the densities achieved were low, and were relatively insensitive to the height of fall.

Due to the repeated difficulties encountered in forming samples by pluviation, an attempt was made to create samples by consolidation from a slurry. A batch consolidometer was used for the initial laboratory investigation. The consolidometer had been previously used by Fleming (1985) to prepare reconstituted specimens of silt. The device allows a 12.7 cm diameter by 12.7 cm high specimen of soil to be consolidated to K_0 conditions using top and bottom drainage.

Samples were consolidated from slurry at vertical pressures from about 90 to 160 kPa. The time necessary for consolidation in the laboratory batch consolidometer was typically 40 - 60 minutes in the range of the applied pressures, resulting in coefficients of consolidation, c_v , ranging from 0.08 and $0.14 \text{ m}^2/\text{day}$. Based on these data, the time to complete consolidation of a calibration chamber specimen (1.5 m high by 1.5 m diameter) for double drainage conditions would be about 1 to 2 weeks. The densities achieved were in the desired range of 16 to 19 kN/m^3 . Based on the laboratory study, consolidation from a slurry was found to be the best method to form specimens of silty sand, and it was accepted for the formation of calibration chamber specimens.

Consolidation of Silty Sand Slurry in the Calibration Chamber

The slurry consolidation process in the calibration chamber began by mixing the slurry approximately the same water content as used for the laboratory batch consolidometer specimens. However, due to the large volume of the sample and to speed up the preparation, only visual judgement was relied upon to maintain the uniformity of the water content throughout the slurry. The slurry was prepared by hand mixing and by using a concrete mixer. Typically, when using the concrete mixer with two laborers, the fabrication of 2.6 m^3 of slurry could be completed in about eight hours. Before it was consolidated, the slurry was allowed to compress for 24 to 48 hours under its own weight.

The calibration chamber specimens were drained only at the top and bottom during consolidation. Radial drainage was ruled out because the drains themselves could possibly increase the vertical stiffness of the sample. Also, radial drainage could cause a stiffer outer shell of soil to be formed which could withstand the imposed consolidation stress. This would result in a softer sample core, thereby giving a non-uniform specimen. Cylindrical mats of eight to ten layers of burlap cloth enclosed in a cotton fabric were used for both top and bottom drainage. Six flexible plastic lines were attached to the bottom drainage layer to allow water to be removed through the top drainage layer. Water exited the calibration chamber through the seven cone penetration holes located in the top plate of the chamber.

To ensure that the vertical compression of the specimen would not exceed the maximum travel of the bottom plate (15 cm), the specimen was first consolidated radially. After 24 hours of consolidation under a radial stress of 42 kPa, the sample was ready for full consolidation under the desired final pressures. In the calibration chamber test program, the samples were consolidated under vertical stresses of 70 kPa, 100 kPa, and 140 kPa for $K = 1.0$ and $K = 0.4$.

For some tests, the vertical compression of the sample was monitored over time using an LVDT, and a conventional consolidation curve was obtained. A typical consolidation curve is shown in Fig. 7. On average, 18 to 20 days were needed to complete the specimen fabrication process. For other tests, a plastic piezometer pipe was placed through one of the cone penetration holes to the bottom plate. The pipe served both as a conduit for the dissipation of the excess pore pressures at the base of the specimen during consolidation, and also as a tell-tale for monitoring the compression of the specimen.

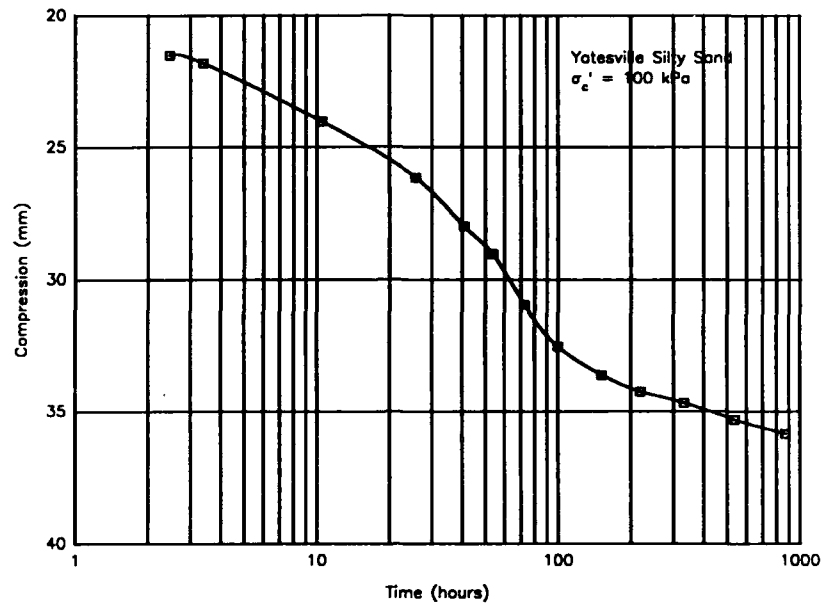


Figure 7 Time-settlement relationship measured for a calibration chamber specimen consolidated from a slurry.

After a cone penetration test was conducted, it was possible to obtain Shelby tube samples and block samples to measure the density profile of the calibration chamber specimen. Density profiles with depth for five calibration chamber tests are shown in Figure 8. Two of the test specimens had very uniform densities, with maximum variations of about 0.2 kN/m^3 . The other three specimens had density variations of up to 1.6 kN/m^3 . None of the specimens had a significant lateral variation of void ratio.

Sieve analyses were conducted on the specimens obtained for the density measurements. In Figure 9, the percentage of fines measured at different depths for a calibration chamber specimen is shown. The data suggest that there was no significant segregation during the fabrication procedure. Degrees of saturation obtained from the slurry consolidation technique averaged about 95%.

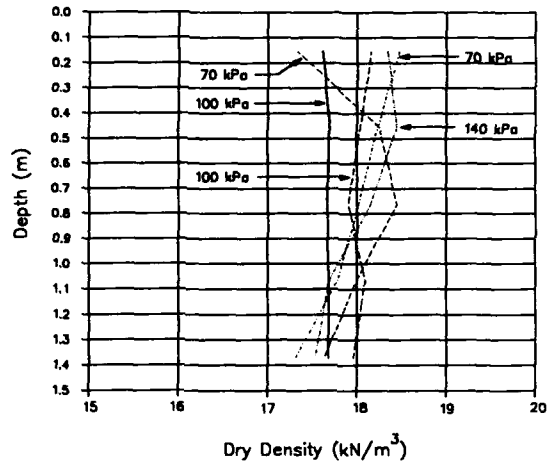


Figure 8 Density profile obtained in a calibration chamber specimen.

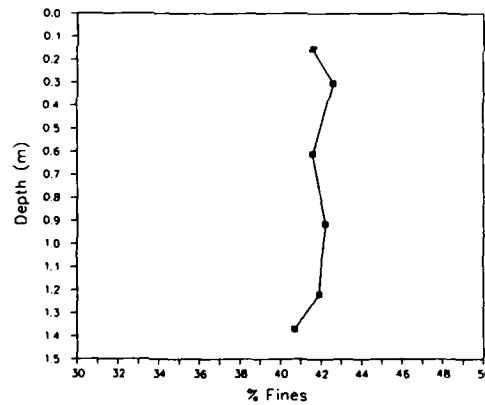


Figure 9 Percent fines versus depth for calibration chamber specimen of Yatesville Silty Sand.

Summary and Conclusions

Research at Virginia Tech on sample formation in a calibration chamber has involved both small and large-scale tests, as well as clean and silty sands. As with other investigations, pluviation was found to be the most efficient and reliable procedure for forming a sample of clean sand. The pluviation equipment was designed to allow control over key parameters so that a uniform specimen was obtained, while exercising control

over densities achieved. Silty sands posed far more difficulty in sample fabrication than clean sands. After trials with different types of procedures, including pluviation through air and through a vacuum, it was determined that the best technique involved consolidation of the sample from a slurry. This allowed samples to be formed with a reasonable density and fabric. Tests within the sample mass showed that the samples were uniform, and that little segregation of particle sizes occurred.

The key findings from the research include:

- (1) The density and uniformity of clean sand samples formed by pluviation was found to be affected by many parameters; the best results were obtained by controlling all parameters so that only the number and sizes of holes in the rainer plate affected the density.
- (2) Distance of fall of the sand in the Virginia Tech pluviation process was kept constant using a mobile sieve set which moved up as the sand mass formed below the sieves.
- (3) Using two different rainer plates, a dense and loose sample configuration was obtained. In both cases, the variation in densities over all trials was less than $\pm 4\%$.
- (4) Calibration chamber samples of silty sand formed from a slurry required about 18 to 20 days to consolidate. Drained was limited to the top and bottom of the sample to prevent a "soft" core from forming.
- (5) The uniformity of the silty sand samples was verified using multiple penetrations with a miniature cone, and after-test density and water content measurements and sieve analyses.
- (6) Silty sand chamber specimens were formed with density variation no larger than 1.6 kN/m^3 , and consistent grain sizes, indicating no significant segregation.

References

- Bellotti, R., Bizza, G., and Ghionna, V. (1982). "Design, Construction, and Use of a Calibration Chamber," *Proceedings of the 2nd European Symposium on Penetration Testing*, Amsterdam, Vol. 2, pp. 439-446.
- Bishop, A. W., and Henkel, D. J. (1957). *The Measurement of Soil Properties in the Triaxial Test*. Edward Arnold Publishers, Ltd..
- Castro, G. (1969). "Liquefaction of Sands." *Harvard Soil Mechanics Series 81*, Harvard University, Cambridge, Mass.

- Chapman, G. A. (1974). "A Calibration Chamber for Field Test Equipment." *Proceedings, First European Symposium on Penetration Testing, Stockholm*, Vol. 2, Part 2, pp. 59-65.
- Eid, W. K. (1987). "Scaling Effect in Cone Penetration Testing in Sand." thesis presented to Virginia Polytechnic Institute and State University in partial fulfillment of the requirements for the degree of Doctor of Philosophy.
- Fleming, L., "The Strength and Deformation Characteristics of Offshore California Silts", Thesis submitted to the University of California, Berkeley in partial fulfillment of the requirements for the degree of Doctor of Philosophy, 1985, 177 p.
- Jacobsen, M. (1976). "On Pluvial Compaction of Sand," Report No. 9, Laboratoriet for Fundering, University Aalborg, Denmark.
- Kolbuszewski, J. J. (1948). "An Experimental Study of the Maximum and Minimum Porosities of Sands," *Proc. of the 2nd International Conference on Soil Mechanics and Foundation Engineering, Rotterdam*, Vol. 7, pp. 158-165.
- Miura, S., and Toki, S. (1982). "A Sample Preparation Method and its Effect on Static and Cyclic Deformation - Strength Properties of Sand." *Soils and Foundation*, 22(1), 61-77.
- Mori, K., Seed, H. B., and Chan, C. K. (1978). "Influence of Sample Disturbance on Sand Response to Cyclic Loading." *J. Geotech. Engrg., ASCE*, 104(3), 323-340.
- Mulilis, J. P., Chan, C. K., and Seed, H. B. (1975). "The effects of Sample Preparation on the Cyclic Stress-Strain Behavior of Sands." *Earthquake Engineering Research Center, University of California, Berkeley*.
- Nemat-Nasser, S. and Takahashi, K. (1984). "Liquefaction and Fabric of Sand." *J. Geotech. Engrg., ASCE*, 110(9), 1291-1306.
- Oda, M.; Koishikawa, I.; and Higuchi, T. (1978). "Experimental Study of Anisotropic Shear Strength of Sand by Plane Strain Test, *Soils and Foundation*, 18(1).
- Rad, N. S., and Tumay, M. T. (1987). "Factors Affecting Sand Specimen Preparation by Raining." *Geotechnical Testing Journal, ASTM*, March, pp. 37.
- Sweeney, B. P., and Clough, G. W. (1990). "Design of a Large Calibration Chamber." *ASTM Geotechnical Testing Journal*, Vol. 13, No. 1, 36-44.
- Sweeney, B. P. (1987). "Liquefaction Evaluation Using a Miniature Cone Penetrometer." thesis presented to Virginia Polytechnic Institute and State University in partial fulfillment of the requirements for the degree of Doctor of Philosophy.

- Tatsuoka, et. al. (1980). "Standard Penetration Tests and Soil Liquefaction Potential Evaluation." *Soils and Foundation*, 20(4), 99-111.
- Vaid, Y. P. and Negussey, D. (1984). "Relative Density of Pluviated Sand Samples." *Soils and Foundations*, 24(2), 101-105.
- Walker, B. P. and Whitaker, T. (1967). "An Apparatus for Forming Beds of Sands for Model Foundation Tests," *Geotechnique*, Vol. 17, No. 2, pp. 161-167.

RESULTS OF CPT'S IN TOYOURA QUARTZ SAND

V. FIORAVANTE,* M. JAMIOLKOWSKI,** F. TANIZAWA,*** and F. TATSUOKA***
*ISMES, Bergamo (Italy); **Technical University of Torino (Italy);
***University of Tokyo (Japan)

ABSTRACT

The paper summarizes the results of CPT's performed in Calibration Chamber (CC) in dry Toyoura sand. Three different cones having diameter of 35.7, 20 and 10 mm respectively have been used. Measured cone resistance q_c has been normalized with respect to current effective stress, examining thereafter the influence on normalized resistance of the ratio between CC and cone diameter. Empirical correlations between q_c , maximum shear modulus and constrained modulus are also exposed.

1. SUMMARY

The paper analyses the results of 28 CC tests performed in dry Toyoura sand. After a brief description of the test sand and of the experimental facilities used, the following aspects of the problem are examined:

- normalization of the cone resistance with respect to the ambient effective stresses;
- influence of the CC size and applied boundary conditions on measured cone resistance;
- correlation between cone resistance and stiffnesses of the tested sand.

2. CALIBRATION CHAMBER

A detailed description of the calibration chamber (CC) especially developed for specimens of 1.2 m in diameter and 1.5 m in height can be found in Bellotti et al. (1982). The equipment consists in a flexible wall chamber, a loading frame, a mass sand spreader for the deposition of the sand and a saturation system.

The chamber consists in two cells which include the specimen. It allows to obtain a zero average lateral strain boundary condition by keeping the pressure in the outer cell equal to the one developed by the specimen in the inner cell. The specimen is bounded at the sides and base by flexible membranes; vertical stresses are applied to the specimen via the chamber piston while lateral stresses are applied by the pressure of water surrounding the specimen.

The resulting boundary conditions (BC) that can be imposed to the specimen, both vertical and horizontal are: constant stress and zero average strain. The maximum vertical and horizontal applicable stresses are 1.5 MPa and 0.75 MPa respectively.

The loading frame counteracts the vertical load transferred to the lid during the compression of the specimen and holds the mechanical press which pushes the in situ device into the chamber.

The specimen is prepared by the pluvial deposition technique using a travelling sand spreader which consists in a sand hopper, a basement and a sand diffuser.

3. TEST SAND

A series of 28 tests were performed using Toyoura sand, a uniform fine sand having sub-angular grains with a high content of quartz. In Table I the index properties are indicated, while Fig.1 shows a grain size distribution.

TABLE I. Index properties of Toyoura sand.

Grain shape	Sub-angular
Quartz	$\approx 90\%$
Chert	$\approx 3\%$
G_s	2.645
D_{50}	$\approx 0.16 \text{ mm}$
U_c	≈ 1.5
e_{\max}	0.977
e_{\min}	0.605

The maximum and minimum void ratios were determined by the method specified by the Japanese Society of Soil Mechanics and Foundation Engineering.

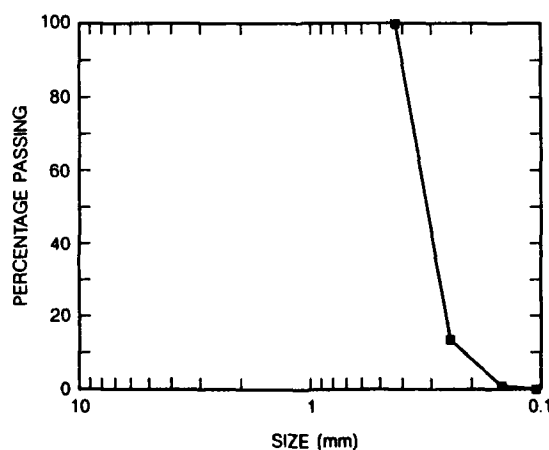


FIG. 1. Grading of Toyoura sand.

Since the differences between saturated and dry samples in the measured quantities were found to be very small by Tatsuoka et al. (1986) and Iwasaki et al. (1988), all tests were performed in dry samples.

4. SAMPLE PREPARATION

Each sample was prepared by pluviating air-dry sand accurately weighted, through air by travelling sand spreader to obtain a prefixed value of relative density (D_R); a rather wide range of D_R (varying from 41 to 91%) was investigated.

During the deposition the side membrane is sealed around the top edge of the chamber barrel and forced by a low vacuum applied to the inner cell, against an open ended cylinder (specimen former). Therefore, the top plate is gently lowered after accurate levelling of the top surface and the side membrane is sealed against it. The specimen former is removed after the chamber inner cell has been filled with water and the vacuum on the membrane has been released.

Four submergible displacement transducers have been placed at the midheight of the sample on the external chamber wall to monitor the lateral deformation of the sample.

Finally the inner and outer cells were deaired by flushing them with water for approximately 30 minutes under a small lateral pressure equal to about 2 kPa.

5. CONSOLIDATION STAGE

The consolidation was controlled by the operator and the final stress level was reached by subsequent steps, applied at time intervals of about 15 minutes, to allow a stabilization of the specimen settlements. All the samples were consolidated in K_0 condition (i.e. zero average lateral strain) either normalconsolidated (NC) or overconsolidated (OC).

Two sequences of vertical load were applied for NC samples (i.e. $\sigma_v = 20, 35, 50, 75, 100$ kPa used for 17 tests and $\sigma_v = 10, 20, 30, 40, 50$ kPa for 5 tests) while the sequence for 5 OC samples was the same (the vertical load was increased by steps of 50 kPa up to a maximum of 800 kPa, then decreased at the same rate, in order to get $OCR \approx 7.3$). The data, as far as the correspondent horizontal stress and the vertical settlement (deformation) of the sample are concerned, were recorded during this stage, as well as the imposed vertical stress.

6. PENETRATION TEST

After the consolidation stage, the specimens were left for 30 minutes at a constant stress, then the desired boundary conditions (BC) have been selected by closing the valves of the vertical hydraulic piston and of the outer annular chamber.

Three BC were used for these tests:

- BC1 ($\Delta\sigma_v = \Delta\sigma_h = 0$): the later inner cell is connected to the outer cell, after accurately adjusting the pressure in the outer one; both valves are open;

- BC2 ($\Delta\epsilon_v = \Delta\epsilon_v = 0$): the piston and the chamber valves are closed;
- BC3 ($\Delta\epsilon_h = \Delta\sigma_v = 0$): the piston valve is open while the chamber one is closed.

Thereafter, a cone penetration test was performed at a rate of penetration equal to 2 cm/s, while the cone resistance q_c and the friction f_s were recorded.

A typical result is shown in Fig.2 where the tip and the shaft resistance measured during penetration (in BC3 condition) are plotted against depth. The figure shows the initial build-up of the resistances, followed by a reasonably well defined plateau of q_c and finally a reduction in q_c as the flexible bottom boundary begins to influence the results. A slight increase of q_c and f_s between the depth of 25 and 95 cm reflects the increase of the horizontal boundary stress σ_h during cone penetration, consequence of the adopted boundary conditions.

In order to evaluate the CC size effect, three different diameter of the cone penetrometer were used ($d_c = 35.7$ mm, used for 13 tests, $d_c = 20.0$ mm, for 13 tests and $d_c = 10.0$ mm, used for two tests).

In this paper, the CC size effect is referred to the influence that the ratio D_c/d_c of the CC diameter to the cone diameter has on the cone resistance at the given applied boundary conditions.

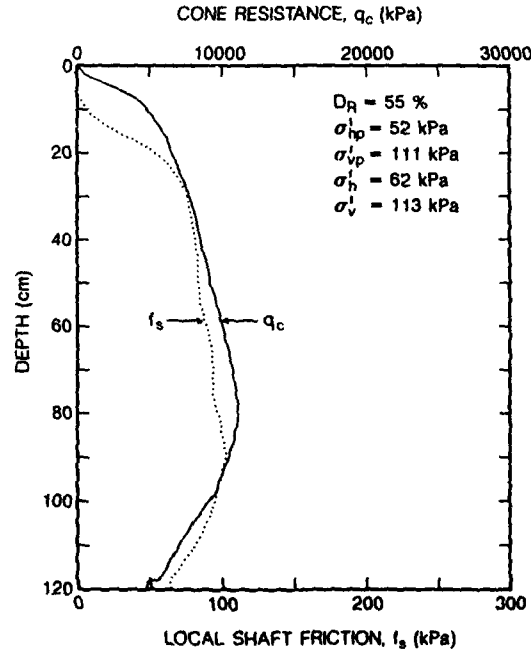


FIG. 2. An example of CC test in Toyoura sand.

8. NORMALIZED CONE RESISTANCE

In analysing the test results, the first step was to relate the q_c values obtained to the stress conditions acting on the sample during penetration and to the void ratio after consolidation, whose product reflects the state of the tested specimens.

In this respect q_c values were "normalized" as follows:

$$NCR_o = \frac{(q_c - \sigma_o)}{\sigma'_o} \quad \text{or} \quad NCR_h = \frac{(q_c - \sigma_h)}{\sigma'_h} \quad (1)$$

and then have been plotted against void ratio in Fig.3 and Fig.4 respectively. The results were grouped in three families related to the three cone diameters used; for two of them ($d_c = 35.7$ and $d_c = 20$ mm) a linear regression has been attempted.

From the above figures it can be noted:

- The scatter of the first correlation (NCR_o) is lower than the one of the second (NCR_h), suggesting that, for the examined CC tests, the tip resistance is substantially dependent on the density and on both horizontal and vertical stresses.

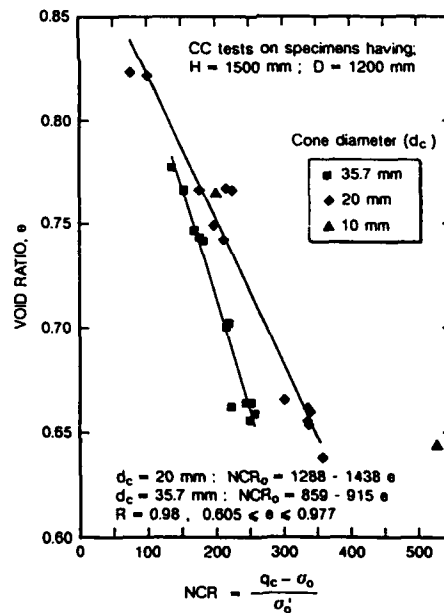


FIG. 3. Normalized cone resistance vs void ratio in Toyoura sand.

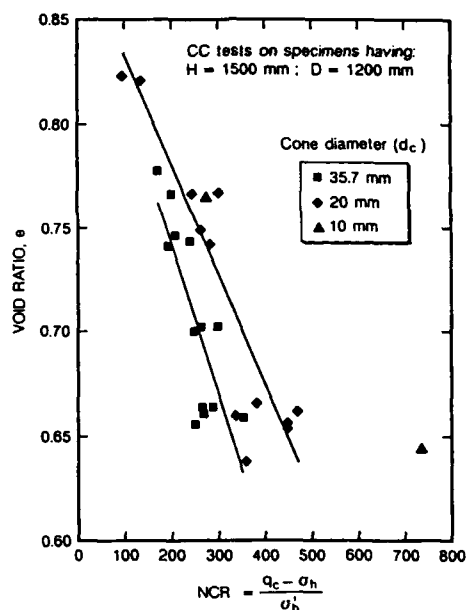


FIG. 4. Normalized cone resistance vs void ratio in Toyoura sand.

- The decrease of the cone diameter, as related to the constant CC diameter D_c , leads to a substantial increase of the cone resistance in very dense sand, while, for loose sand this effect tends to disappear. However, it is difficult to establish in q_c the difference between $d_c = 20$ and 10 mm since only two tests have been conducted so far with $d_c = 10$ mm.

- The Normalized Cone Resistance seems to be independent from OCR.

- The two linear correlations computed can be written as follows:

$$\begin{aligned} d_c = 20.0 \text{ mm} \quad NCR_0 &= 1288 - 1438 \cdot e & (R = 0.98) \\ d_c = 35.7 \text{ mm} \quad NCR_0 &= 859 - 915 \cdot e & (R = 0.98) \end{aligned} \quad (2)$$

(where R = coefficient of correlation).

9. CHAMBER SIZE AND BOUNDARY CONDITIONS EFFECTS

The influence of CC size on cone resistance is shown in Fig.5 where two tests of very dense Toyoura sand, 311 ($d_c = 35.7$ mm) and 314 ($d_c = 20$ mm) are compared. The tests have almost the same void ratio and the same hori-

zontal and vertical stresses. It can be noted that for the smaller value of d_c the cone resistance increases of about 30%.

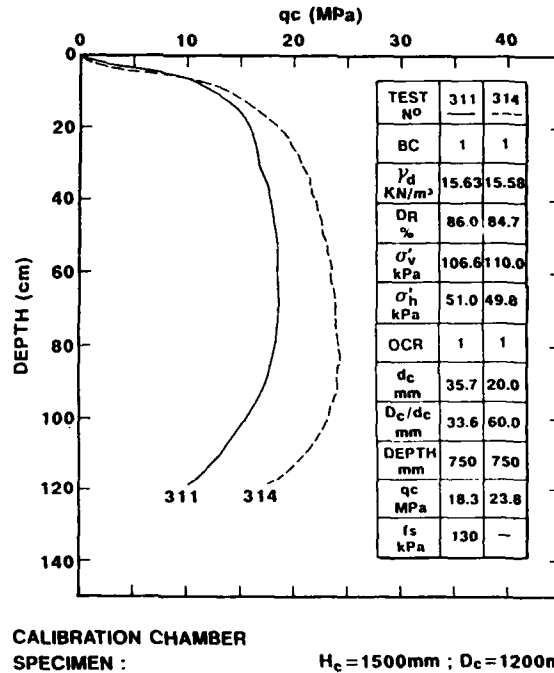


FIG. 5. Influence of Calibration Chamber size on cone resistance of very dense Toyoura sand.

By comparing three tests on medium dense sand, $D_R \approx 57\%$ (i.e. 363, 366 and 364 for $d_c = 35.7$, 20 and 10 mm respectively, see Table II) having a similar stress condition the following can be noted:

- the increment of q_c , moving from $d_c = 35.7$ to $d_c = 20$ mm, is about 15%;
- moving from $d_c = 20$ mm to $d_c = 10$ mm, no increment of q_c was recorded.

The above confirms that the influence of CC size increases as the density increases as previously pointed out (see Figs.3 and 4).

The influence of boundary conditions on cone resistance of very dense Toyoura sand is shown in Fig.6, when the q_c measured is plotted against depth for the three boundary conditions used.

It is important to note that for $\Delta\epsilon_h = 0$ condition (BC 2 and 3) the horizontal boundary stress increases substantially during penetration producing an increasing in q_c .

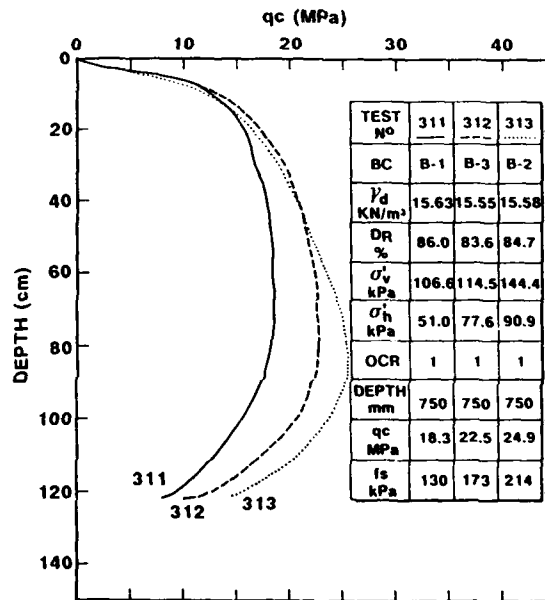
An empirical correlation which allows separation of the influence of σ'_h and σ'_v on the measured value of q_c is given by the equation:

$$q_c = C_0 \left[\sigma'_v \right]^{C_1} \left[\sigma'_h \right]^{C_2} \exp (C_3 D_R) \quad (3)$$

where C_0 , C_1 , C_2 and C_3 are empirical constant.

This equation fits very satisfactory the test data by the coefficients:

d_c (mm)	C_0	C_1	C_2	C_3
20.0	231	0.1177	0.417	2.97
35.7	116	0.272	0.593	1.678



CALIBRATION CHAMBER
SPECIMEN : $H_c=1500\text{mm}$; $D_c=1200\text{mm}$
CONE DIAMETER : $d_c=35.7\text{mm}$

FIG. 6. Influence of boundary conditions on cone resistance of very dense Toyoura sand.

It is important to note the greater influence of the horizontal effective stress with respect to the vertical one.

Figure 7 shows the relation between the q_c values evaluated by the eq.(3) and those measured, for the two cone diameters.

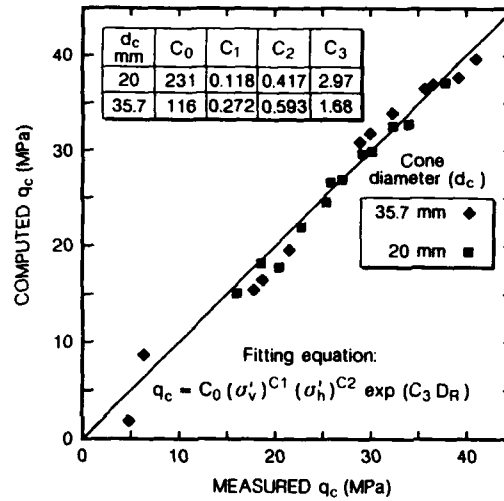


FIG. 7. Measured vs computed cone resistance of Toyoura sand.

10. CORRELATION BETWEEN q_c and M

A unique correlation between penetration resistance and a non-linear deformation modulus cannot exist [Jamiolkowski et al.(1988)]. Nevertheless, because the modulus is, in first approximation, a function of the same soil parameter as q_c (i.e. D_R , σ'_v and σ'_h) an empirical correlation can be attempted. In this respect all the q_c data corresponding to NC samples were plotted against the tangent constrained modulus measured at the last increment of σ'_v (see Fig. 8) during consolidation; the results are shown in Fig. 9.

All the available data fall within a narrow range that can be expressed by means of the following equation:

$$M = (13 + 15) (q_c)^{0.5} \quad (5)$$

11. CORRELATION BETWEEN q_c AND G_o

The problems involved with the non-linearity of the deformation moduli renders attractive the tentatives to correlate the tip resistance to the maximum shear modulus G_o measurable in situ by means of seismic methods and laboratory during resonant column tests at the shear strain level $\gamma < 10^{-5}$.

From resonant column tests on Toyoura sand [Iwasaki and Tatsuoka (1977)] the following correlation has been determined:

$$G_p = C_o p_a \left(\frac{\sigma'_o}{p_a} \right)^n \left(D_R \right)^m \quad (6)$$

where:

$C_o = 1238$, $n = 0.40$, $m = 0.39$ empirical coefficients

$p_a = 98.1$ kPa, atmospheric pressure.

From eq.(6) G_o was computed for the 28 CC tests and then plotted versus q_c in Fig.9.

The two linear correlations between G_o and q_c for the two cone diameters are:

$$\begin{aligned} d_c &= 20.0 \text{ mm} & G_o &= 1.76 q_c + 57.25 & (R &= 0.97) \\ d_c &= 35.7 \text{ mm} & G_o &= 2.26 q_c + 59.2 & (R &= 0.98) \end{aligned} \quad (7)$$

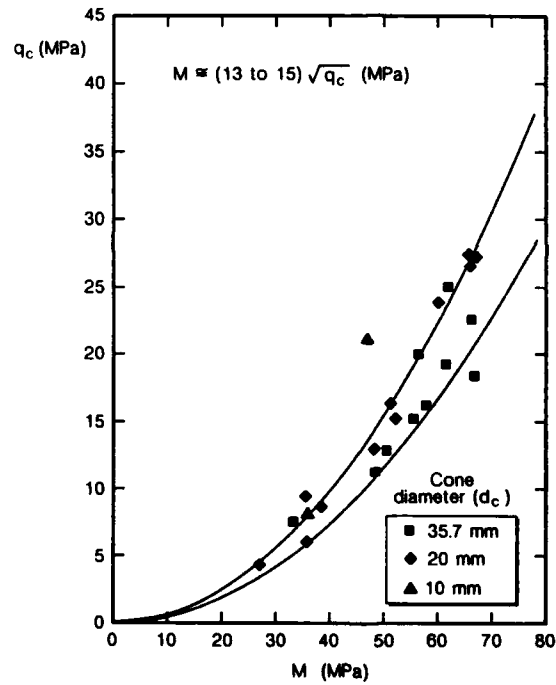


FIG. 8. Constrained modulus vs cone resistance calibration chamber tests in Toyoura sand.

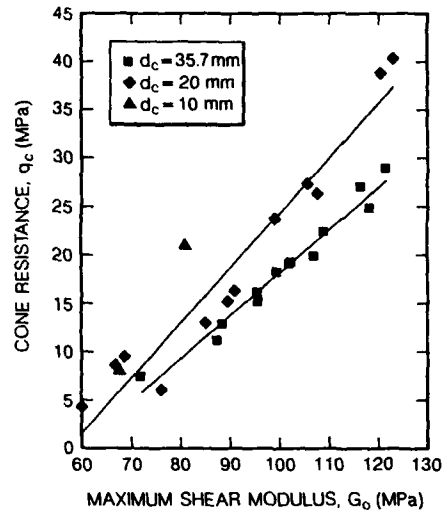


FIG. 9. Maximum shear modulus vs cone resistance. Calibration chamber tests in Toyoura sands.

REFERENCES

- Bellotti, R., Bizzi, G. and Ghionna, V. (1982). "Design Construction and Use of a Calibration Chamber". Proc. of the 2nd European Symposium on Penetration Testing, Amsterdam.
- Iwasaki, K., Tanizawa, F., Zhou, S. and Tatsuoka, F. (1988). "Cone Resistance and Liquefaction Strength of Sand. Penetration Testing". ISOPT-1 De Ruiter (ed.). Balkema, Rotterdam.
- Iwasaki, K. and Tatsuoka, F. (1977). "Dynamic Soil Properties with Emphasis on Comparison of Laboratory Tests and Field Measurements". Proc. 6th World Conference on Earthquake Engineering.
- Jamiolkowski, M., Ghionna, V.N., Lancellotta, R. and Pasqualini, E. (1988). "New Correlations of Penetration Tests for Design Practice". ISOPT-1 De Ruiter (ed.). Balkema, Rotterdam.
- Tatsuoka, F., Goto, S. and Sakamoto, M. (1986). "Effects of some Factors on Strength and Deformation Characteristics of Sand at Low Pressures". Soils and Foundations. No.1.

SCALE AND BOUNDARY EFFECTS ON CALIBRATION CHAMBER PILE TESTS

P. FORAY
Institut de Mécanique de Grenoble
Domaine Universitaire
B.P. 53 X, 38041 GRENOBLE CEDEX FRANCE

ABSTRACT

The I.M.G. Calibration Chamber is presented, with emphasis in its capability of applying regulated conditions to the lateral boundary of the Chamber in order to simulate the lateral stiffness of an infinite soil mass. Thus, the C.C. can also be used to realize a physical modeling of geotechnical axisymmetric problems involving a high stress level, such as long offshore piles, anchors, nailing etc.... The concept of interface behaviour between granular soil and structure has been used to define the best lateral boundary conditions to be applied, and to analyze the different scale effects which can occur in C.C. testing. Some experimental data from model pile tests are presented with some guidelines for the corrections to be made in order to extrapolate the laboratory results to in-situ piles.

INTRODUCTION

The original purpose of Calibration Chamber Testing is to study the response of in-situ devices like CPT, PMT or DMT in well-defined conditions of pressure, OCR and relative density. Very accurate correlations between the design parameters of the soil obtained from triaxial tests and data from the in-situ device have been proposed, among others, by Schmertmann (78), Villet and Mitchell (81), Baldi et al. (82), and Jamiolkowski et al. (88), Jamiolkowski and Tatsuoka (90).

In Calibration Testing, the penetration or pressuremeter device generally corresponds to the field apparatus, and no scaling effect due to the model size will occur. The main effect to be considered is that of the chamber boundary, which can be represented by the ratio R_d of the chamber diameter to the penetrometer diameter. For a given ratio, it is considered that the chamber size has no effect when no significant difference is observed when applying the two extreme lateral boundary conditions, so-called B1 (constant lateral pressure) and B3 (no lateral volume change). The second problem in Calibration Testing is the one of the representativity of the re-moulded soil with respect to the original soil. Aging or cementation effects are difficult to take into account.

If the Calibration Chamber is now considered as a physical modeling installation, scaling effect will occur due to the fact that the gravity is the same between the prototype and the model. Complete similitude conditions will only be satisfied in a Centrifuge, but it is interesting to analyze how a cheaper installation can give some good results and how some scale effects will appear in both C.C and Centrifuge Testing.

The I.M.G. Calibration Chamber has been designed to study both aspects : testing of in-situ devices and modelling of the behaviour of long offshore piles for which in-situ loading tests with instrumented piles are difficult to perform. The main feature of this chamber is the possibility of applying boundary conditions intermediate between B1 and B3 to reproduce the stiffness of an infinite surrounding soil mass.

In this paper, it is analyzed how a research on the specific behaviour

of interface between granular soil and structure developed in I.M.G. by Boulon (85), Boulon et al. (86) can be applied to both aspects of C.C testing :

- Defining intermediate lateral boundary conditions between B1 and B3 ;
- Analyzing the scaling effect in the C.C in model tests involving friction between soil and structure.

Examples of pile model tests are given to illustrate these aspects.

THE I.M.G. CALIBRATION CHAMBER

The I.M.G. C.C consists basically of three cylindrical elements of 50 cm height and 1,20 m internal diameter joined together by flanges with "O" rings. The total height is actually 1,50 m, but could be reduced, or extended to 2,00 m by adding another element. Each cylindrical element can be equipped by a lateral toroidal membrane fixed to the 50 cm high vertical wall (Fig. 1).

The bottom and the top of the chamber consist in two rigid plates with a thickness of 10 cm, with a central hole of 10 cm diameter. This allows the chamber to be used to study the lateral friction along an element of pile, as shown fig. 9 corresponding to a small prototype chamber developed by Eissautier (86). The bottom hole of the chamber is sealed when using the station as a normal C.C.

Two membranes fixed on the internal face of the upper and bottom plates and filled with water apply the vertical stress conditions. The lateral membranes are filled with water and can be controlled by an hydraulic servo-jack with a water/oil interface. A regulation loop between the data of a pore pressure transducer and a displacement sensor on the water jack allows the application of any kind of lateral boundary conditions : constant pressure B1, no volume change B2 or a prescribed relation between σ_h and ϵ_h . (Genevois (89), Mokrani (91)).

The soil sample is generally pluviated sand using the classical technique of controlled rate-of-fall with double diffuser mesh developed in the Italian chambers. To get very dense sand, vibration techniques are used. The sand can be saturated (for CPTU testing for example) with the following steps : vacuum, CO₂, de-aired water and backpressure.

Two penetration systems are fixed on a rigid frame which can be moved on two rails above the chamber. An hydraulic jack can apply the standard 2cm/s penetration rate, and a mechanical jack is used to perform any kind of monotonic or cyclic loading test with controlled displacements.

THE BOUNDARY CONDITIONS IN POINT RESISTANCE

- i) The effect of the boundary conditions in laboratory calibration of field CPT devices has been extensively studied by Lunne and Parkin (82), Jamiolkowski and Tatsuoka (90), Ghionna et al. (88). It is generally considered that no significant influence of a classical chamber size (1,20 m) occurs for loose to medium sands, but that in dense to very dense sands and overconsolidated sands the measured cone resistance is lower than the one which could be observed in an infinite soil mass. Thus, corrections factors for q_c have been proposed as a function of the chamber to cone diameter ratio.
- ii) It is now considered that the horizontal effective stress is a more

significant parameter than the vertical effective stress in governing the cone resistance or the dilatometer parameters. In calibrating the response of these devices, no significant difference will be observed between the results with B1 and B3 conditions if the maximum value of (σ_h)B3 is taken into account in place of the initial σ'_h , as shown by Jamiolkowski and Tatsuoka (90).

- iii) The Chamber size effect, for a given apparatus, depends on the relative density and the confining stress of the soil, i.e. its capacity to dilate radially. Thus, for a given relative density, the chamber effect should be higher at a low confining stress level, and lower at a high stress level or for a more compressive sand.

The combination of the effects of these two parameters for a given sand can be represented by the state parameter ψ as defined by Labanieh (84), Been and Jefferies (85) and extensively developed by Been et al. (86). The study of Been et al. (86) confirms that chamber size effects can be expressed as a function of ψ , and that the highest values of the correction factor corresponds to the lowest negative values of ψ , i.e. dense sand and low confining pressure. Penetration tests performed at I.M.G. at very low overburden pressure and reported by Foray and Puech (76) are in agreement with the general observation of a decrease in q_c when decreasing the chamber size (figure 2).

- iv) The penetration of the cone point or of a model-pile point at large depth simulated by a high confining stress level in the C.C induces very high stresses in the zone directly under the point, with as a consequence, a high crushing and compressibility of this zone and a modification of the mechanical properties of the sand in this area. This compressibility induces a "local failure" mechanism under the point, and the best approach is actually the cavity expansion model taking into account the curvilinear failure envelope and the compressibility of the plastic zone (Vesic 68, Baligh 82), as confirmed by Jamiolkowski (88). The analysis of the cone pressuremeter test as a cylindrical cavity expansion process developed by Houlsby and Yu (90) confirms also this approach.

The figure 3 indicates the modification of the grain-size distribution of the sand under a model pile tested in dense sand under a vertical stress of 200 kPa. Comparing this with triaxial tests under high stresses performed by Colliat (86), the crushing coefficient corresponds to a mean triaxial confining stress of 10 MPa which is in agreement with the order of magnitude of the measured point resistance. Total stress sensors measuring the radial stress in the soil around the pile during the penetration at a distance of 1,5 and 3,5 diameters of the pile axis indicate a decrease of radial stress with the distance to the pile corresponding to that indicated by the cavity expansion model (fig. 4). It has to be noted that the strong loading of the soil produced by the penetration of the point is followed by an unloading when the cell is in front of the shaft.

The figures 5a) and 5b) indicate the qualitative evolution of the three components σ_r , σ_θ and σ_z of the stress tensor measured during the driving process of the pile at a radial distance of 3.5 diameters from the model pile and at two depths $Z = 75$ cm in 5a) and $z = 100$ cm in 5b). Even if the quantitative values of these stresses are doubtful due to the difficulty of calibration and positioning total stress sensors, it is interesting to note that a strong peak in both σ_v and σ_r occurs when the point of the pile reaches a depth 15 to 20 cm above the level of the cells. The strongly compacted sand behind the tip behaves like an "enlarged" penetrating base and induces a lateral expansion, followed by an unloading.

Stress paths measured during the loading stage of the pile, at a distance of 3.5 diameters from the pile point also indicate a similarity with a pressuremeter stress path in its elastic stage, as shown fig. 6.

All these observations are in agreement with lateral stress measurements on the shaft of a penetrometer done by Robertson (84) and Huntsman et al. (86). It can be concluded that at a certain radial distance from the pile, the stresses induced in the soil by the penetration of the point can be modelled by a cavity expansion approach, with a loading - unloading step.

That means that the lateral boundary of the chamber is also submitted to a loading-unloading pressuremeter stress path during the cone penetration or the model pile installation. The loading stage of the pile corresponds, at least for driven piles, to a lateral reloading process.

Thus, the ideal lateral boundary conditions, intermediate between B1 and B3, should reproduce such a loading path. As the stress level transmitted to the lateral boundary corresponds to an elastic range, this can be done applying to the lateral boundary a pressuremeter stiffness representing the effect of an infinite lateral surrounding soil.

THE BOUNDARY CONDITIONS IN LATERAL FRICTION

Extensive research on the behaviour of interfaces between granular soil and structures has been developed at I.M.G. since the early 80's by Boulon (85, 86, 89) with a special emphasis in the application to the prediction of lateral friction along piles (Boulon and Foray (86)). It has been considered that Calibration Chamber tests could be used in the two aspects : i) as a boundary problem to check numerical simulation and ii) as a physical model to give practical design values.

Experimental visualisations performed by Robinsky and Morrisson (64), Plumelle (79) and Davidson et al (81) have shown that during the penetration or the loading stage of a pile in sand, large shear displacements are localized in a very thin zone of about ten times the grain diameter, close to the pile shaft. This suggests that the mechanism governing the pile-soil contact can be modelled by a direct shear test, between soil and a rough surface.

The large displacements in the thin interface layer induce strong dilative or contractive effects according to the initial confining stress, relative density, pile-soil roughness, grain-size and mineralogical nature of the sand. This explains the experimental observation that the lateral stress along the pile shaft depends not only of the installation procedure but changes also during the loading stage of a pile.

Thus, the soil mass beyond the interface layer will be submitted radially to a pressuremeter loading path depending on the dilative behaviour of the interface, and tangentially to a simple shear with shear stresses decreasing rapidly with the radial distance from the shaft.

An elemental study of the mechanisms of pile-soil interaction has been performed in laboratory by Plytas (85) Boulon et al (85), Valin (86) Hoteit (90) using a direct shear test with a controlled normal stiffness representing the effect of the surrounding soil. A simple calculation shows that this stiffness k is related to the pressuremeter-modulus E_p and to the pile radius R by :

$$k = \Delta\sigma'_h / \Delta u = 2E_p / R$$

u : radial displacement at the interface boundary

$k = 0$ represents the constant normal stress conditions i.e. B1 conditions.

$k = \infty$ represents the no-volume change conditions, i.e. B3 conditions.

Typical results of such tests are presented in figure 7, for a siliceous and a calcareous sand, showing the influence of density, stiffness and material compressibility. These stress paths are in complete agreement with stress-paths measured during model-pile tests figure 8. Similar results have been reported by Jardine (91).

It is interesting to note that, as for the point resistance, the soil at a certain distance from the pile shaft undergoes to a first approximation a pressuremeter loading path during the loading stage.

Again, the correct lateral boundary conditions to be applied to the chamber for all problems involving frictional contact should be a lateral pressuremeter stiffness. This is true for model compression / or tension piles, anchors ..., or any kind of reinforcing elements.

A small prototype C.C. (26 cm internal diameter, 50 cm high) has been designed and tested by Eissautier (88) to study the effects of the lateral boundary conditions on friction elements of 3.2 cm diameter ($R_d = 8$). The stiffness corresponding to the regulated lateral conditions had been determined from pressuremeter tests previously performed in the same sand at various confining pressures in a large diameter chamber (1,5 m). Figure 9 indicates the effect of the boundary conditions on the friction mobilization curves (9a), on the lateral pressure of the chamber (9b), and on the lateral displacement of the boundary (9c). Some comparison tests with the same sand and the same model-pile have been performed in a large chamber of 1,50 m diameter with rigid walls and an overburden pressure of 100 kPa. The corresponding R_d is 43. A good agreement can be observed figure 10 in the friction-mobilization curves between the regulated test in the small C.C. and the tension test in the large chamber. After the peak, a decrease in lateral friction is observed for the large C.C. test, but this is due to the drop in the lateral stress close to the point when pulling-out the pile. These results confirm that the lateral friction is governed by a mechanism of direct shear with a lateral pressuremeter stiffness.

As a conclusion, in a model-pile test in the C.C., point resistance and lateral friction will both induce pressuremeter stress paths in the far surrounding soil. A correct simulation of the problem can be obtained by applying regulated boundary conditions corresponding to the lateral stiffness of the soil.

Such tests have been performed at I.M.G. by Genevois (89) and Mokrani (91), with the purpose of obtaining the bearing capacity coefficients of long piles in sand. The influence of relative density, overburden pressure and pile installation has been studied (Foray et al. (89), (91)). An example of the results is given in figure 11.

The evolution of the lateral pressure at the boundary of the chamber during the driving process of a model pile and then during the static loading step, is indicated in figure 12 together with the data of the lateral volume change. It can be noted that in this test with a high overburden pressure of 400 kPa and a dense sand, the changes of lateral pressure are relatively small, of about 15 kPa. In the same test with an overburden pressure of 200 kPa, the boundary had a much more dilative behaviour, with changes in lateral pressure up to 80 kPa.

The stiffness to be applied to the boundary has been evaluated from the unloading-reloading pressuremeter modulus performed in the C.C. with the same conditions of density and overburden pressure (Mokrani et al. 90).

SCALE EFFECTS IN PILE TESTING

Various scale effects can occur in Pile Testing in the C.C. due in part to the non-satisfaction of the complete similitude conditions in lg testing, but also in scale effects which occur also in Centrifuge Testing, mainly due to the ratio between the size of the model and the average diameter of the grains.

Non-satisfaction of similitude conditions :

- i) A model-pile test in the C.C., including the study of both point resistance and lateral friction induces a distortion in the vertical scale. The C.C. reproduces what occurs around the pile at a given depth, simulated by the vertical overburden pressure. But as the pile length in the C.C. is relatively short, the measured lateral friction can be more influenced by the vicinity of the point than in the case of a current section of the real pile at a larger distance of the point. Friction tests like those presented above separate both effects, but cannot simulate the interaction between point and shaft. The combination of friction tests and complete model pile tests, or the use of small diameter instrumented piles can give an answer to this problem.
- ii) The distortion in vertical scale can give another induced effect : residual stresses due to pile installation are relatively lower for a short rigid pile than for a long compressible pile. This can affect the first stage of the load-transfer curves and the tension resistance of the pile.
- iii) The pile installation procedure should simulate the in-situ conditions. For driven piles, the driving energy applied to the model has to represent the true energy transmitted to the real pile. For jacked piles, the chamber depth may be not sufficient to take into account the effects of the large displacements of the real pile on the initial lateral stresses.

Scale effects due to the grain size

- i) The size of large calibration chambers is generally sufficient to allow us to use models with a diameter large enough to avoid scale effects for the point resistance, except for small penetrometers or piles in coarse sand or in gravel. In this case the assumption of a continuum medium around the point is not respected, as for a real penetrometer in gravel. This problem occurs also in Centrifuge testing if the prototype material is used. But generally in most of the C.C. tests, chamber size effects can occur, but not scale effects. The very large scale tests performed by Kérisel et al. (62) have shown that the diameter of the pile has no influence on the point resistance developed in a continuous penetration, beyond the famous "critical depth". But of course the point loading curve of an already-installed pile is a function of the pile diameter.
- ii) The most important scale effect in physical modeling appears when a localization of the deformation is produced, either within the soil mass by shear bands with a thickness corresponding to the diameter of the grains, or at the contact between pile and soil, with an interface

layer of about ten grain diameters. For a given material, the thickness of the shear bands or the interface layer will be the same in a model test or in the prototype test. That means that the relative influence of the localization is much greater in the model than in reality. This phenomena occurs both in C.C. or in Centrifuge testing.

In the first part of this paper it has been emphasized that the point resistance at large depth generally induces "local failure" due to the high compressibility and crushing of the sand under the point, and that this can be approximately represented by a cavity expansion mechanism. Thus, no significant localization within the soil mass is to be expected in penetration or pile modeling.

But the effect of the ratio of pile diameter to grain diameter on lateral friction has to be analyzed starting from the same concept of interface behaviour, as it has been developed in the boundary condition problem.

The mobilization of the shear friction stress at the pile-soil interface is governed by the lateral stiffness k given $k = 2 \frac{E_p}{R}$. As k is proportional to $1/R$, that means that a model pile of 2 cm diameter induces a lateral stiffness 50 times the one of a real pile with a diameter of 100 cm.

Thus, it is necessary to evaluate the change in mobilized friction with the lateral stiffness, in order to define correction factors. This can be done from direct interface shear tests with controlled stiffness. Figure 13 shows the values of the maximum friction obtained by Plytas (85), Valin (86) and Hoteit (90) with a Hostun medium sand ($d_{50} = 0.7$ mm), high density and a) rough surface, b), smooth surface. The lower values of k correspond to the tests with constant normal stresses and the highest values correspond to the tests with no-volume change. It can be verified that the interface properties depend highly from the stiffness, the initial normal stress and the roughness of the contact. In addition, other tests have shown the influence of relative density, sand mineralogy and the size of the grain. From these tests, Genevois (89) proposed scale correction factors τ^* where

$$\tau^* = \frac{\tau_{k \text{ model}}}{\tau_{k \text{ prototype}}}$$

$\tau_{k \text{ model}}$ represents the maximum friction with the stiffness corresponding to the model radius

$\tau_{k \text{ prototype}}$ represents the maximum friction with the stiffness corresponding to the prototype radius.

An upper bound of τ^* is given by the ratio of the frictions corresponding to the no-volume change test and the constant normal stress test. Figure 14 indicates the evolution of τ^* with the initial horizontal stress around the pile for Hostun medium sand, dense or loose and with a rough or a smooth surface. The curves are given for stiffnesses of 20000 kPa/mm (model) and 1000 kPa/mm (prototype) in dense sand, and 10000 kPa/mm (model) and 500 kPa/mm (prototype) in loose sand. With these data, the friction measured in the C.C. can be twice or three times the friction mobilized along the real pile at low overburden pressures. At very high overburden pressures, the scale effect becomes very small due to the contractive behaviour of the interface at high stresses. This corresponds to the decrease in the lateral pressure coefficient K when increasing the overburden pressure, as it is generally observed in in-situ tests and as it has been measured in C.C. tests.

The scale factors given figure 14 are rather high due to the relatively

great average grain-size. For the Hostun RF sand, with a d_{50} of only 0.38 mm the interface is less dilative and a scale factor τ^* of about 1.3 has been considered in most of the C.C. pile tests performed in this sand.

CONCLUSIONS

- i) The Calibration Chamber can be considered as a physical modeling installation for Pile Testing. This implies to study the effects of the lateral boundary conditions not only on the point resistance, but also on the lateral friction, first during the pile installation and then during the compression or tension test.
- ii) The analysis of point penetration by a cavity expansion mechanism seems to be confirmed by stress-paths measured in the soil mass at a certain distance of the point. In a first approximation, the lateral boundary of the chamber undergoes a pressuremeter stress-path.
- iii) The analysis of the lateral friction as a mechanism of interface direct shear test with a controlled normal stiffness indicates that, beyond the thin interface layer, the soil is also submitted to a pressuremeter expansion / or contraction.
- iv) The application of lateral boundary conditions to the chamber corresponding to the stiffness of an infinite soil-mass surrounding the model pile, intermediate between B1 and B3, represents a reasonable approach to avoid chamber size effects and to use model-piles with a diameter larger than that of the cone-penetrometer.
- v) Various scale effects occur when testing model piles in C.C. or in Centrifuge. The main one is due to the ratio of the pile diameter to the average grain diameter, inducing a higher lateral friction along the model pile than along the real pile. Scale effect coefficients are presented, determined from direct shear tests with different stiffnesses.
- vi) When taking into account all these effects, Pile testing in C.C. is a useful way to evaluate the design parameters, especially for the long offshore piles which are difficult to instrumentate in-situ. Correlations and design rules can also be defined with the data of in-situ tests performed in the same conditions. Pile tests in C.C. can also be used as boundary problems for numerical simulations.

ACKNOWLEDGEMENTS

The author gratefully acknowledges M. Boulon, J.M. Genevois, S. Labanieh and L. Mokrani for their contribution to various aspects of this research work, and Société Nationale Elf-Aquitaine and Institut Français du Pétrole for their financial support to C.C. testing at I.M.G.

REFERENCES

- Baldi, G., Bellotti, R., Ghionna, V., Jamiolkowski, M. & Pasqualini, E. (1982), Design parameters for sand from CPT. Proc. 2nd Eur. Symp. Penetration Testing, Amsterdam 2, 425-438.
- Baligh, M. M. (1976), Cavity expansion in sand with curved envelopes. J. Geotech. Engng. Div. Am. Soc. Civ. Engrs 102, GT11, 1131-1146.
- Been K. & Jefferies, M. G. (1985), A state parameter for sands. Géotechnique 35, No. 2, 99-112.
- Been, K., Crooks, J.H.A., Becker, D.A. and Jefferies, M.G. (1986), The cone penetration test in Sands : Part I, State parameter and interpretation, Géotechnique, n° 2.
- Boulon, M., Plytas, C., Foray P., Comportement d'interface et prévision du frottement latéral le long des pieux et tirants d'ancrage. Revue française de Géotechnique, n° 35, 1985.
- Boulon, M., Plytas C., Soil structure directionally dependent interface constitutive equation. Application to the prediction of shaft friction along piles. IIInd International Conference on numerical models in Geomechanics. Ghent, Belgium, March 1986, pp. 43-54.

- Boulon, M., Foray, P., Physical and numerical simulation of lateral shaft friction along offshore piles in sand, IIIrd International Conference on numerical methods in offshore piling, Nantes, 21-22 mai 1986.
- Boulon, M., Foray, P., A contribution to the prediction of piles behaviour by physical and numerical simulation, European Conference on numerical methods in Geomechanics (ECONMIG) Stuttgart, 16-18 september 1986.
- Boulon, M., A consistent model for soil-structure interface behaviour, third international conference on numerical models in Geomechanics (NUMOG III) Niagara Falls, Canada, May 1989.
- Colliat-Dangus, J.L., Desrues, J., Foray, P., "Triaxial testing of Granular soil under elevated cell pressure". Advanced triaxial testing soil and rock, ASTM STP 977. American society for testing and materials, Philadelphia 1988, pp.290-310.
- Eissautier M., Frottement lateral des pieux en milieu pulvérulent. Thèse de Doctorat Université Joseph Fourier, Grenoble 1988.
- Foray, P., Puech, A. (1976), Influence de la compressibilité sur la force portante des pieux en milieu pulvérulent. Annales de l'I.T.B.T.P., n° 131, mai 1976.
- Foray, P., Genevois, J.M., Labanieh, S., Goulois, A., (1989) "Effect of pile installation on the bearing capacity of piles in sand". Proc. XII ICSMFE, Rio (aug. 89).
- Foray, P., Labanieh, S., Mokrani, L., Colliat-Dangus, J.L., (1991) "Bearing capacity of piles from calibration chamber tests". International Conference on Deep Foundations. Paris, march 1991.
- Genevois, J.M. (1989) "Simulation Physique du Comportement des pieux en Chambre de Calibration". Thèse de Doctorat. Université Joseph Fourier, Grenoble, mars 89.
- Ghienna, V. (1988) "Chamber and boundary conditions : effects on qc". 3rd Seminar on Calibration of in-situ devices in Laboratory and field tests. Oslo, ja. 1988.
- Houlsby, G.T. and Yu, H.S. (1990) "Finite element analysis of the cone- pressuremeter test". Proc. of the Third Int. Symposium on Pressuremeters. Oxford, April 1990.
- Hoteit, N. (1990) "Interface shear tests with controlled normal stiffness. Thèse de Doctorat Université Joseph Fourier, Grenoble.
- Huntsman, S.R., Mitchell, J.K., Klejbuk, L.W., Shinde S.B. (1988) "Lateral stress measurement during Cone Penetration". Proc. ISOPT I, Orlando, Florida.
- Jamiolkowski, M. and Robertson, P.K. (1988) "Closing Address. Future Trends for Penetration Testing". Proc. Geotechnical Conference on Penetration Testing in U.K., Institution of Civil Engineers, University of Birmingham.
- Jamiolkowski, M., Ghienna, V.N., Lancellota, R. and Pasqualini, E. (1988) "New Correlations of Penetration Tests for Design Practice. Proc. ISOPT-I, Orlando, Fla.
- Jamiolkowski, M. and Tatsuka F. (1990) "Calibration of static cone and research dilatometer in fine Toyoura sand". Fourth Seminar on Research involving validation of in-situ devices in large C.C., Grenoble, 1990.
- Jardine, R. and Christolas, S. (1991) "Recent developments in defining and measuring static piling parameters". General Report in the International Conference on Deep Foundations, Paris 19-21 march 1991.
- Labanieh, S. (1984) "Modélisations non linéaires de la rhéologie des sables et applications". Thèse de Doctorat ès Sciences, University of Grenoble.
- Labanieh, S. (1991) "Critical state and constitutive Parameters identification". Third International Conference on constitutive laws. TUCSON (Janvier 1991).
- Kerisel, J. Adam (1962) "Fondations Profondes", Annales de l'ITBIP, série SF n° 39, nov. 1962.
- Lunne, T. and Christoffersen, H. P. (1983) "Interpretation of cone penetrometer data for offshore sands", Proc. 15th Offshore Technology Conf. Houston, pp. 181-188.
- Mokrani, L. (1991). Modélisation physique des fondations profondes en sables marins. Thèse de Doctorat Institut National Polytechnique de Grenoble, octobre 1991.
- Parkin, A. and Lunne T. (1982) "Boundary effects in the laboratory calibration of a cone penetrometer in sand" Proc. 2nd European Symposium on Penetration Testing Amsterdam 2, pp. 761-768.
- Plumelle C. (1979) "Experimental study of pull-out anchors" Thèse de Doctorat, Université Paris VI.
- Plytas, C. (1985) "Contribution à l'étude expérimentale et numérique des Interfaces sols granulaires/structures". Thèse de Doctorat Université Joseph Fourier Grenoble.
- Robertson, P. K. (1986) "In situ Testing and its application to Foundation Engineering", Canadian Geotechnical Journal n° 4.
- Robinsky and Morrison (1964) "Sand displacement and compaction around model friction piles" Canadian Geotechnical Journal Vol. 1, n° 2.

- Schmertmann J. H. (1975) "Measurement of in-situ shear strength" ASCE Spec. Conf. In-situ measurement of Soil Properties, Raleigh 2, pp. 57-138.
- Valin (1985) "Etude expérimentale des interfaces sol-pieu. Essais de cisaillement direct à rigidité imposée". Rapport de DEA, I. N. P. G. Grenoble.
- Vesic, A.S. (1972) "Expansion of cavities in infinite soil masses" J. Soil Mech. Found. Div. ASCE 98, SM3, pp. 265-290.
- Villet, W.C.B. and Mitchell J. K. (1981) "Cone resistance, relative density and friction angle". Proc. ASCE Spec. Conf. Session Cone Penetration Testing and Experience St Louis, pp. 178-208.

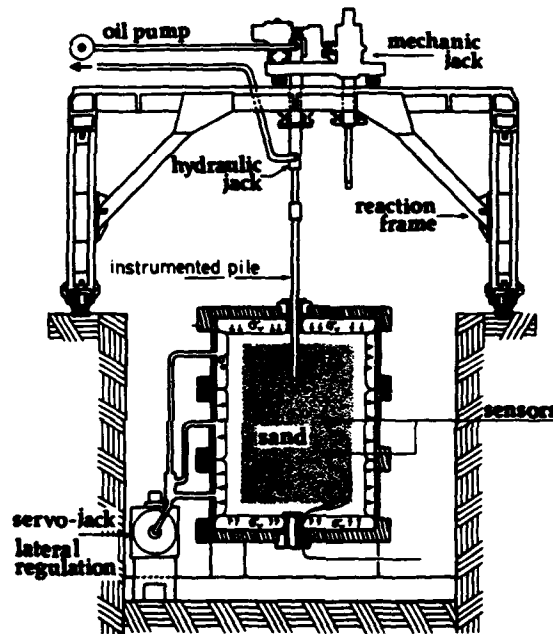


figure 1 : The I.M.G. Calibration Chamber.

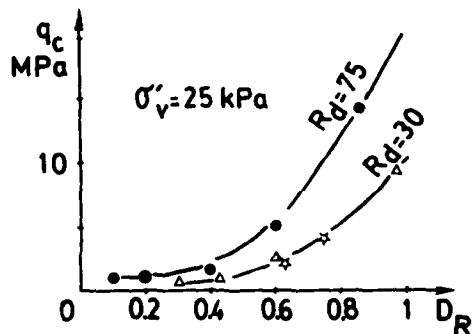


figure 2 : Chamber-Size effects with B3 conditions.

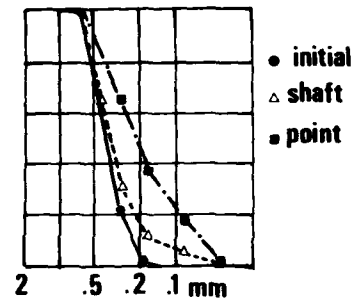


figure 3 : Grain-Size distribution of Hostun RF sand.

- (1) Initial distribution
- (2) After test, under the point
- (3) After test, along the shaft.

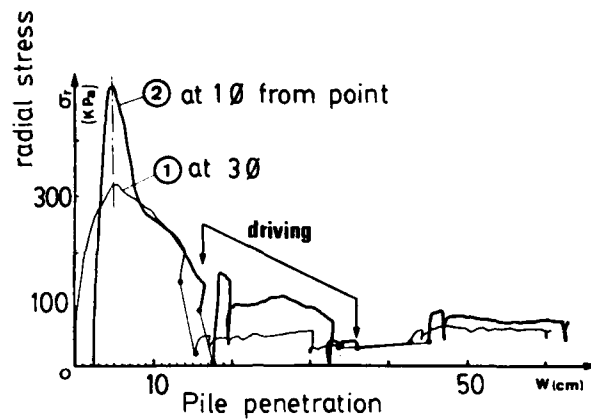


figure 4 : Increase in radial stress in the soil around the point during the loading stage, at a radial distance of 1 and 3 diameters from the model-pile.

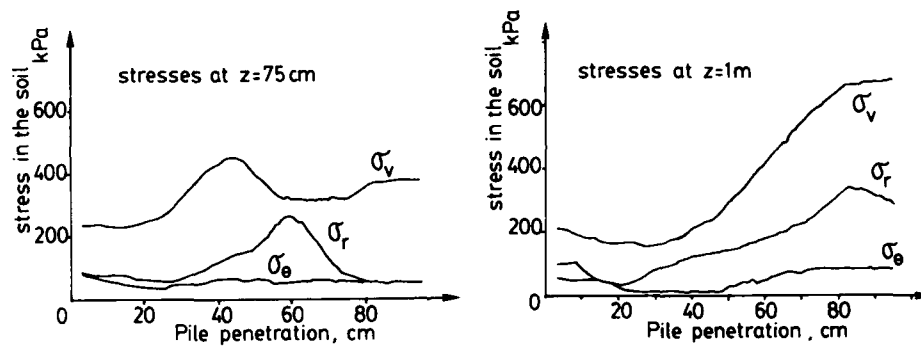


figure 5 : Evolution of the radial stress in the soil during the pile installation.

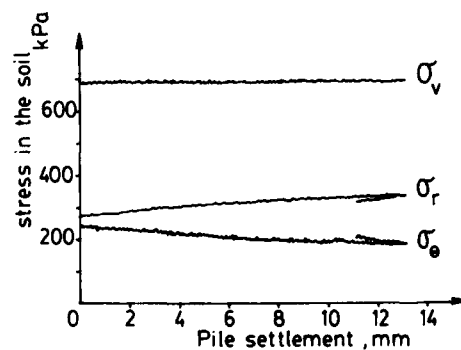


figure 6 : Stresses measured in the soil at 3,5 diameters of the point during compression test.

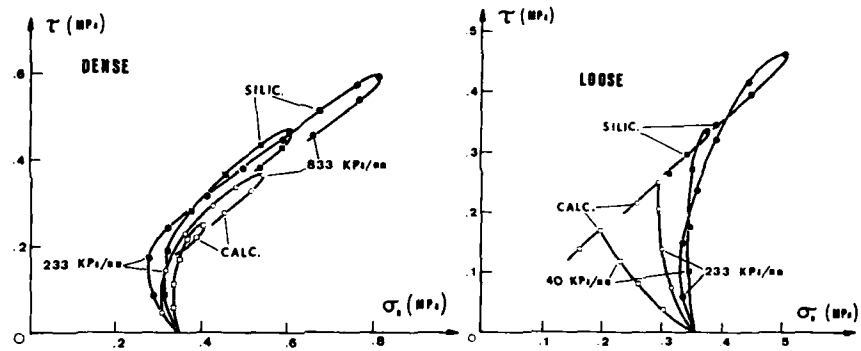


figure 7 : Interface direct shear tests with controlled lateral stiffness (after Boulon).

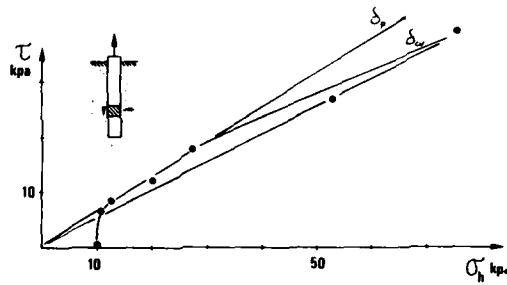


figure 8 : Stress-paths measured at the pile-soil interface.

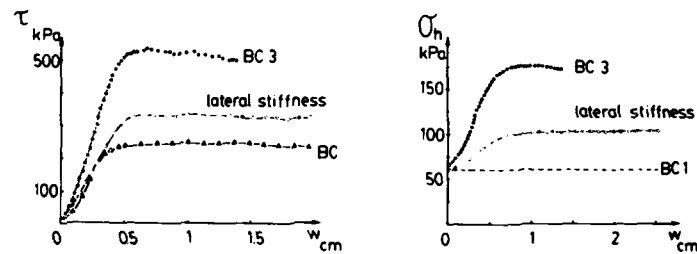
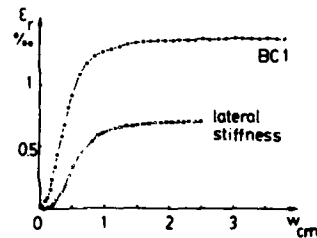


figure 9 : Influence of the boundary or lateral friction along a model-pile in a small C.C.

- a) Friction mobilisation
- b) Boundary lateral stress
- c) Lateral volume change.



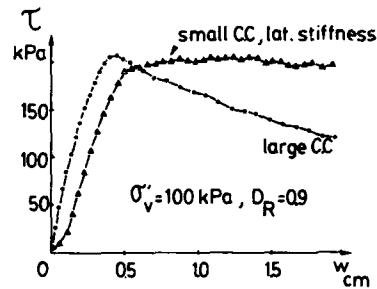


figure 10 : Comparison between a large C.C. pull-out test and a small C.C. test with controlled lateral stiffness.

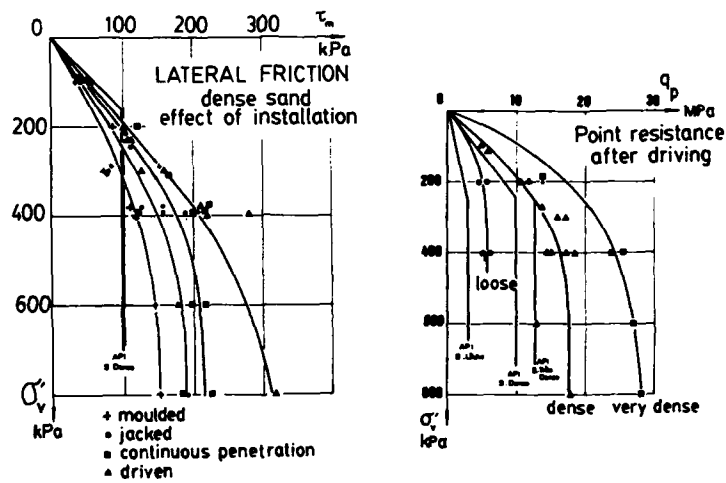


figure 11 : Example of C.C. pile tests results. Influence of density, overburden pressure and pile installation on point resistance and lateral friction.

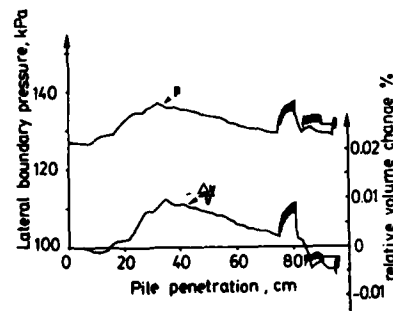


figure 12 : Evolution of the boundary lateral stress in a regulated pile test during the pile installation and the loading test.

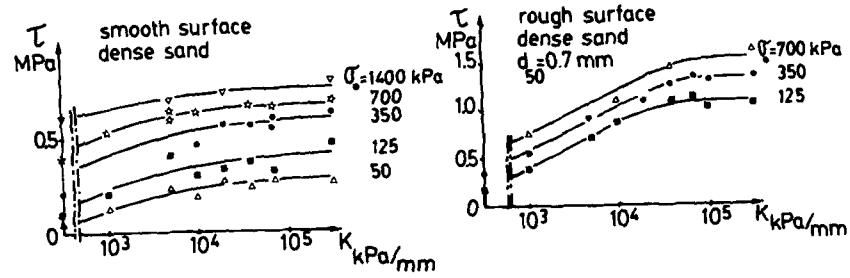


figure 13 : Maximum friction mobilized in an interface shear test with controlled normal stiffness.

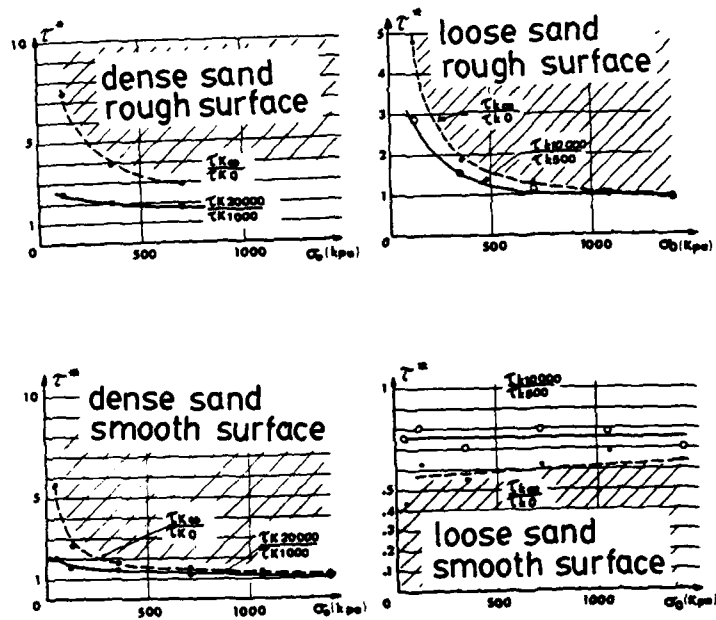


figure 14 : Scale effect as a function of initial normal stress for Hostun medium sand ($d_{50} = 0,7$ mm).

PIEZOBLADE TESTS IN A CLAY CALIBRATION CHAMBER

A.-B. Huang*, R.D. Bunting**, and T.C. Carney*

*Department of Civil and Environmental Engineering, Clarkson University, Potsdam, New York 13676; **Gannett Fleming, Inc., P.O. Box 1963, Harrisburg, PA 17105-1963, U.S.A.

ABSTRACT

A series of piezoblade penetration tests have been performed in a clay calibration chamber under a back pressure. The piezoblade was half the size of a flat Marchetti Dilatometer. The clay specimens were normally consolidated under isotropic as well as anisotropic conditions. Piezometers were installed on the piezoblade and within the clay specimen to monitor the penetration induced excess pore pressure and its dissipation. The results indicated that the penetration induced pore pressure is mainly controlled by the soil behavior in the horizontal direction. The pore pressure dissipation around the blade is more likely to be one-dimensional than axisymmetric.

INTRODUCTION

The Flat Dilatometer (DMT) developed by Marchetti [7,8] has become an important in situ testing tool in Geotechnical Engineering. Applications of DMT have included the determination of in situ lateral stress, soil compressibility, consolidation characteristics, stress history, design parameters for vertically and laterally loaded piles as well as soil classifications [6]. However, these applications have been mostly empirical; mainly due to the lack of understanding of the penetration mechanisms of a flat plate such as DMT. Studies by Campanella and Robertson [4] have indicated that the dilatometer expansion pressure is strongly influenced by the surrounding pore pressure for tests in normally consolidated clays. Hence, an improved understanding of flat-plate penetration induced pore pressure should lead to better interpretation of the test results.

As part of an effort to study the penetration mechanisms of flat plates in saturated clays, a series of piezoblade penetration tests were performed in a calibration chamber. All tests reported herein were conducted in a normally consolidated clay specimens. The results presented in this paper concentrate on the penetration induced excess pore pressure and its dissipation.

THE CHAMBER SYSTEM AND THE PIEZOBLADE

The calibration chamber system consists of a slurry consolidometer, a calibration chamber. The system set up and testing procedures followed those developed by Huang et al. [1]. Figure 1 depicts important features of the calibration chamber fabricated in this study. The system is capable of preparing a clay specimen of 508 mm diameter and with a height of between 600 and 762 mm. The clay specimen can be consolidated in the chamber isotropically, anisotropically under a given stress ratio or under K_0 conditions. The boundary conditions in the vertical and horizontal directions can be either stress controlled or rigid. A total of 13 open

ended piezometers were installed on the bottom plate of the chamber (see Figure 1). The piezometers were made of 1.65 mm O.D., 0.23 mm wall

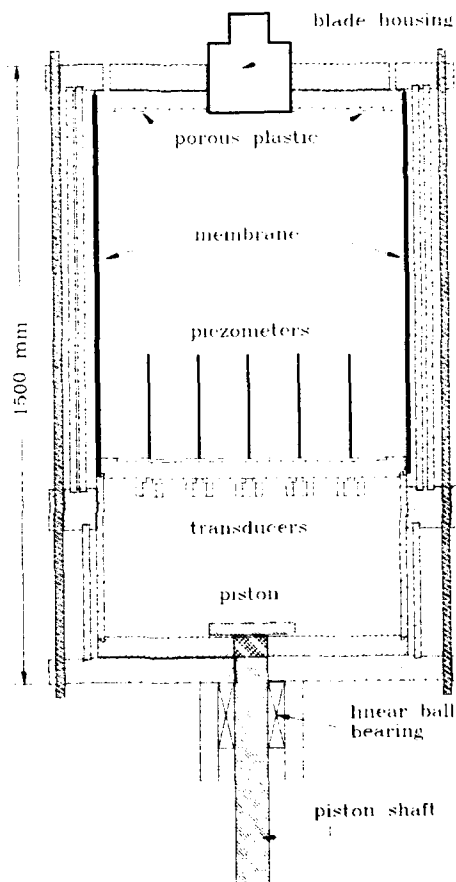


Figure 1. Schematic view of the calibration chamber.

stainless steel tubing filtered with porous plastic. The piezometer tips were at approximately 260 mm from the bottom of the specimen.

A piezoblade (Figure 2) which is approximately half the size of a Marchetti DMT was used in the study. It has an apex angle of 20 degrees. Four cavities were incorporated on the piezoblade to allow pore pressure measurements on its surface. The cavities, 6.4 mm diameter and 3.2 mm deep, were filled with porous plastic. These cavities were connected to pressure transducers outside the CC through 1.65 mm OD, 0.23 mm wall stainless steel tubing. The ratio of specimen radius over model flat-plate half thickness was 75. Studies using the strain path method [2] have indicated that significant soil disturbance around a flat-plate does not

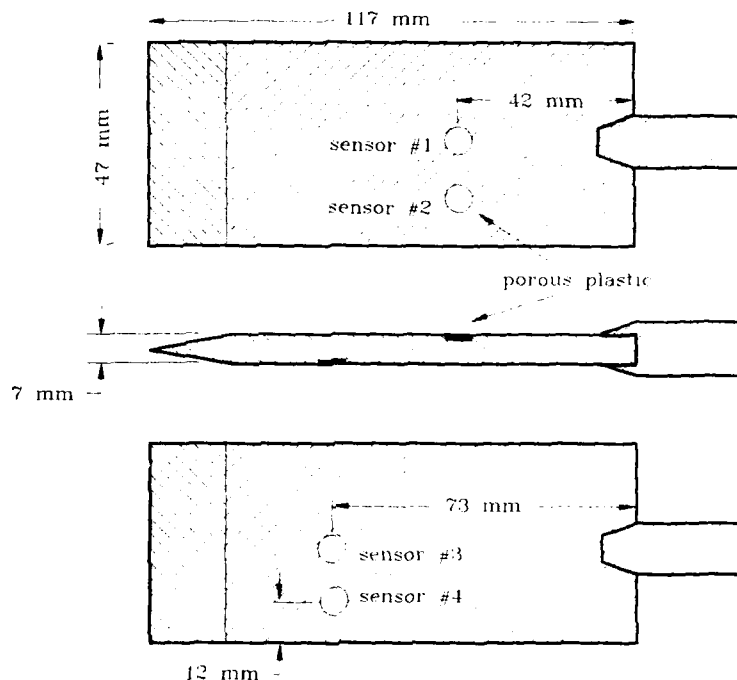


Figure 2. The piezoblade.

extend beyond a distance of 10 times the half thickness of the plate. Thus, the above ratio is adequate, especially when the lateral boundary was stress controlled.

PROPERTIES OF THE LABORATORY PREPARED CLAY

A mixture of 50% kaolinite and 50% Edgar sand was used to create the clay specimens in the CC tests. The Edgar sand is a uniform fine sand from Edgar, Florida. The mixture has a plasticity limit of 16% and a liquid limit of 30%. The kaolinite/sand slurry was mixed at an initial water content equal to 2.5 times the liquid limit using deionized and deaired water. The slurry was consolidated in a 63.5 mm inside diameter slurry consolidometer under a vertical stress of 138 kPa.

To establish the geotechnical properties, a series of controlled gradient consolidation (CGC) tests and consolidated undrained triaxial tests were performed on this laboratory prepared clay. An additional test was conducted in a rigid wall K_0 triaxial cell to establish the relationship between K_0 and stress history for the clay. The K_0 triaxial cell design and test procedure follow the concept by Campanella and Vaid [4].

Both isotropically (CIU) and anisotropically (CAU) consolidated undrained triaxial tests were performed. In CAU tests, the K_0 value shown

in Table 1 was used in the anisotropic consolidation of the clay specimen. Table 1 summarizes the basic engineering properties and key parameters derived from the consolidation and triaxial tests.

THE CALIBRATION CHAMBER TESTING PROCEDURE

A 524 mm diameter and 813 mm high chamber specimen was consolidated in a slurry consolidometer. Mixture of the slurry and consolidation stress are the same as those used in triaxial specimen preparations. All piezometers were flushed and saturated with deaired water before the slurry consolidation. At the end of slurry consolidation the clay specimen, with the chamber bottom plate attached, was completely encased in a 3.2 mm thick rubber membrane. All the piezometers were embedded in the specimen at this stage.

After the slurry consolidation, the clay specimen was installed in the calibration chamber for the second stage consolidation. A housing unit located on top of the chamber (see Figure 1) holds the model plate. This housing unit was connected to the chamber top drainage so that they can be flushed and back pressured simultaneously. The drainage system and the piezo-units on the piezoblade were flushed with deaired water.

Table 1. Properties of the kaolinite/sand mixture.

Triaxial Tests				
	CAU (206 kPa)		CIU (206 kPa)	
	Axial Compression	Axial Extension	Axial Compression	Axial Extension
A_f	0.59	1.17	1.10	1.54
s_u/σ'_{vc}	0.30	0.13	0.29	0.22
E_{50}/s_u	1700	666	800	1400
Control Gradient Consolidation Tests				
	$C_v, 10^{-3} \text{ cm}^2/\text{sec}$			
	Virgin Loading	Unload	Reload	
	2.0 to 7.0	10.0 to 50.0	5.0 to 40.0	

The second stage consolidation could be isotropic or anisotropic. In the isotropic consolidation, $\sigma'_h = \sigma'_v = 206 \text{ kPa}$. The consolidation stress was applied in one increment. In the anisotropic consolidation, $\sigma'_v = 206 \text{ kPa}$ and $\sigma'_h/\sigma'_v = 0.52$. The anisotropic consolidation was servo controlled by a computer. The piezometers in the specimen were used as part of a doubly drained controlled gradient consolidation procedure. Readings taken at the piezometer tips represent the pore pressure at 254 mm from the bottom of specimen. The σ'_h and σ'_v were individually adjusted to maintain an excess pore pressure of 69 kPa at the piezometer tip level. The adjustment also assures a constant σ'_h/σ'_v ratio of 0.52. The chamber consolidation took approximately 3 weeks.

A back pressure of 414 kPa was used in the first two weeks of all the consolidations. It was subsequently increased to 689 kPa for the remainder of the consolidation and the following penetration test. The increased

back pressure enhances the quality of pore pressure measurements. Penetration followed after the primary consolidation. A stepper motor driven linear actuator was used to push the model plate. The penetration had two stages; the depth of penetration in the first stage was 130 mm and the second was 440 mm. At the end of penetration, the center of the piezoblade was at the level of the piezometer tips in the clay specimen.

Table 2 furnishes a summary of the model piezoblade (PIEZ1 to PIEZ5) tests. The only difference between tests PIEZ3 and PIEZ5 are the locations of piezo units #1 and #2. Pore pressure readings taken at piezo units #3 and #4 serve as a check of repeatability of the chamber system and test procedure. The stabilized excess pore pressure readings taken from the corresponding piezo units agreed within 18%.

Table 2. Summary of piezoblade tests.

Test No.	Consolidation	Back Pres., kPa	Vertical Stress, kPa	Horizontal Stress, kPa	Penetration Rate, cm/s
PIEZ1	Isotropic	690	896	896	6.0
PIEZ2	Isotropic	690	896	896	2.0
PIEZ3	Anisotropic	690	896	797	2.0
PIEZ5	Anisotropic	690	896	797	2.0

FLAT-PLATE PENETRATION INDUCED PORE PRESSURE

To present the data, a coordinate system shown in Figure 3 is used. The half thickness of the blade ($R = 3.5 \text{ mm}$) was used to normalize linear dimensions. When appropriate, stresses and pore pressures are normalized with respect to vertical consolidation stress (σ'_{vc}).

The penetration induced excess pore pressure, Δu is defined as

$$\Delta u = u_T - u_o \quad (1)$$

where u_T = total recorded pore pressure and u_o = back pressure. Negative excess pore pressure exceeding the limit set for the instrumentations occurred during test PIEZ1. Although no readings could be taken, it is fair to conclude that negative pore pressure can be induced by high penetration rate as it was the case for test PIEZ1.

Figure 4 shows the profiles of $\Delta u/\sigma'_{vc}$ developed during the penetration in tests PIEZ2 and PIEZ3. Stable excess pore pressure was developed at 150 mm after the penetration was initiated. For both tests, the excess pore pressure at the mid height of the blade (sensors 3 and 4) was higher than that recorded toward the end of the blade (sensors 1 and 2). Sensor No. 2 of test PIEZ3 was accidentally disconnected during penetration and therefore results are not shown. The normalized excess pore pressure, $\Delta u/\sigma'_{vc}$ from all the sensors ranged from 1.5 to 2 during the steady penetration in test PIEZ2. The corresponding values in test PIEZ3 varied from 0.9 to 1.4. These values correspond to $\Delta u/s_u$ ranging from 5.4 to 7.1 for test PIEZ2 and from 3.2 to 5 for test PIEZ3. They are

either close or within the range of those predicted according to the cavity expansion theory [10] where

$$4 < \Delta u/s_u < 7 \quad (\text{spherical cavity}) \quad (2)$$

$$\text{and} \quad 3 < \Delta u/s_u < 5 \quad (\text{cylindrical cavity}) \quad (3)$$

The penetration induced pore pressure in the isotropically consolidated specimen (PIEZ2) was higher than that in an anisotropically

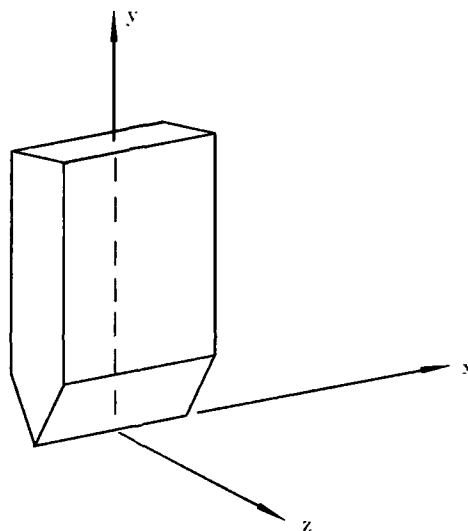


Figure 3. The coordination system.

consolidated specimen (PIEZ3) by as much as 43%. For cylindrical penetrometers [7],

$$\Delta u = s_u [\ln(G/s_u) - 2\ln(z/R)] \quad (4)$$

According to the s_u and G values from axial extension triaxial tests and Equation 4, the ratio of Δu at the penetrometer boundary ($z = R$) is

$$\frac{[s_u \ln(G/s_u)]_{CIU}}{[s_u \ln(G/s_u)]_{CAU}} = 2.5 \quad (5)$$

The same ratio from axial compression tests is 0.83. The data would indicate therefore that the rigidity index in the lateral direction is the predominant factor in the development of excess pore pressure.

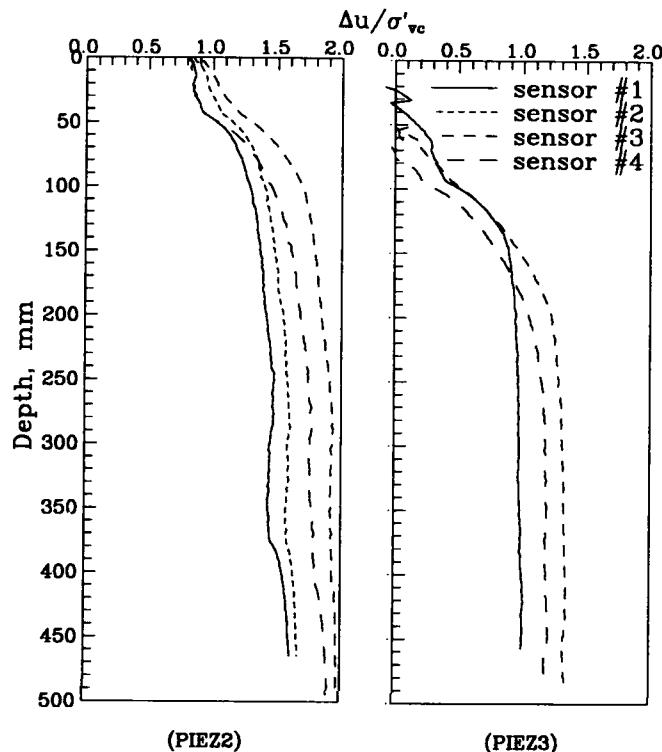


Figure 4. Profile of excess pore pressure from tests PIEZ2 and PIEZ3.

EXCESS PORE PRESSURE DISTRIBUTION AND DISSIPATION

The rate of excess pore pressure dissipation is governed mostly by the coefficient of consolidation of the surrounding soil. Attempts have been made to determine the coefficient of consolidation based on the pore pressure dissipation record from flat-plate penetration tests [5]. These methods used procedures primarily developed for cylindrical penetrometers. One important drawback of the current approach is the lack of knowledge regarding the distribution of excess pore pressure at the beginning of and during its dissipation.

Piezometers were located within the clay specimen to allow the pore pressure distribution to be monitored. To visualize the distribution of the excess pore pressure, contour lines were created by interpolating these piezometer readings using a commercial software called SURFER. Contours shown in Figure 5 resulted from these interpolations represent the distribution of excess pore pressure in the xz plane and at the same level as pore pressure sensors 3 and 4 ($y/R = 13$). The data show that the pore pressure was fairly uniform across the face of the piezoblade (in the x direction) during dissipation for test PIEZ2 (isotropically consolidated specimen). For test PIEZ3 (anisotropically consolidated specimen) the pore pressure dissipation follows an axisymmetric pattern. The penetration

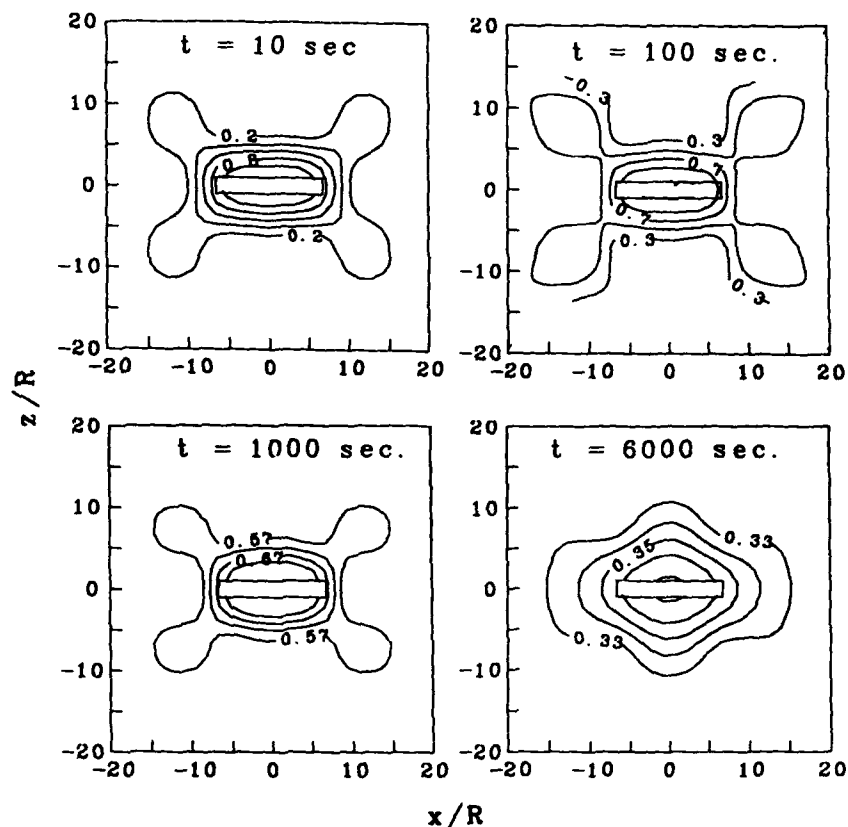


Figure 5a. Contours of pore pressure dissipation from test PIEZ2.

induced excess pore pressure diminishes within a distance of $20R$ (R = half thickness of the piezoblade). This is significantly less than that predicted for an axisymmetric penetrometer [7].

Ideally, a three-dimensional solution should be provided to properly interpret the pore pressure dissipation data and to determine the coefficient of consolidation. However, the coefficient of consolidation is influenced by the state of stress and could vary by as much as one order of magnitude as indicated in the reference consolidation tests. In addition, a three-dimensional distribution of initial excess pore pressure would be necessary for such a solution. It would be extremely difficult to obtain such information, even in a calibration chamber. Therefore, some simplifications are necessary and justified to determine the "approximate" coefficient of consolidation in a reasonable and practical fashion. The key is however, to provide the rational and implications for such simplifications, which are missing in our current interpretation procedures.

To provide a simplified analytical description of the initial excess

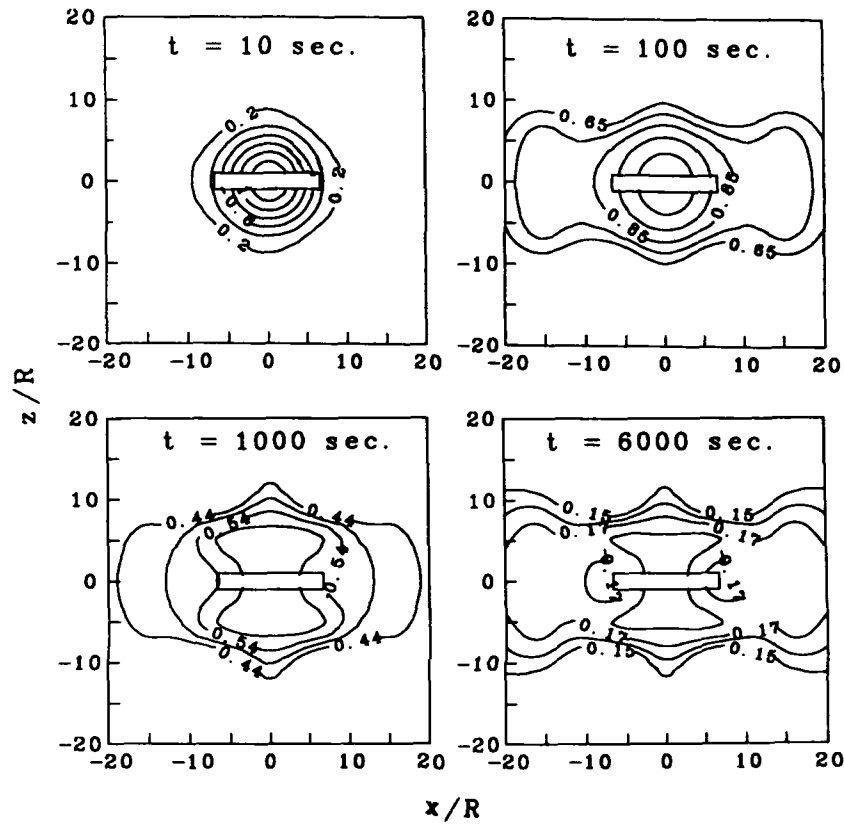


Figure 5b. Contours of pore pressure dissipation from test PIEZ3.

pore pressure distribution and its dissipation, the following assumptions are made:

- 1) Soil consolidation is linear (constant coefficient of consolidation, c_h) and uncoupled (the total stress remains constant during consolidation).
- 2) The initial excess pore pressure distribution at the end of a piezoblade penetration is uniform in y direction.
- 3) The consolidation is computed based on the initial excess pore pressure distribution on the $x=0$ plane (perpendicular to the piezoblade surface) and consider dissipation of the pore pressure in two extreme cases; one-dimensional (in z direction only) and axisymmetric.
- 4) The initial excess pore pressure distribution, normalized with respect to the excess pore pressure at the piezoblade surface, Δu_0 , on the $x=0$ plane is approximated as

$$\frac{\Delta u}{\Delta u_0} = \frac{(b^m + R^n)}{(b^m + z^n)} \quad (6)$$

where m and n are variables to be determined from curve fitting the chamber data. Results of the curve fitting show that for the isotropically consolidated specimen (PIEZ2) $m = 1.8$ and $n = 2.6$. For the anisotropically consolidated specimen (PIEZ3) $m = 2.7$ and $n = 3.0$. Curves based on Equation 6 are plotted in Figure 6. Equation 6 was used to determine the initial excess pore pressure distribution for tests PIEZ2 and PIEZ3 and facilitate the numerical computations.

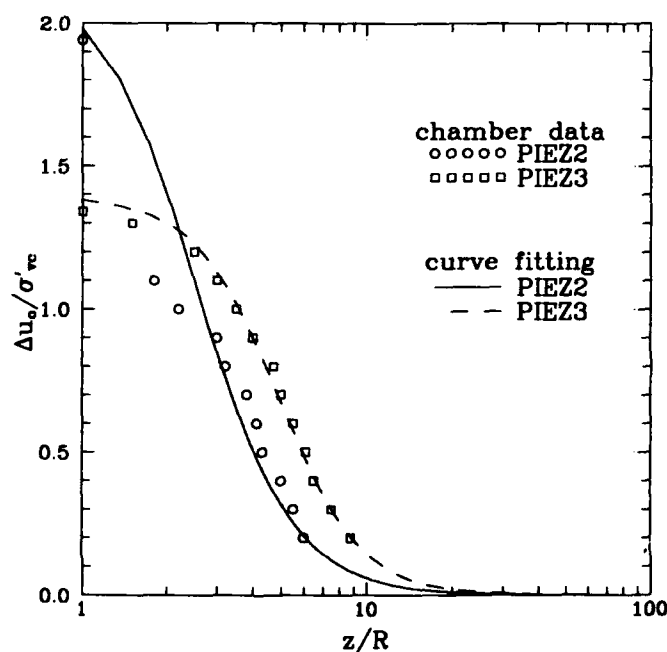


Figure 6. Initial pore pressure distribution.

A finite difference program was used to solve the one-dimensional and axisymmetric consolidation. Boundary conditions consider the penetrometer surface and the clay specimen outer boundary impermeable. Computational results in terms of $\Delta u/\sigma_{vc}'$ at the flat-plate surface ($x=0$, $z=R$) versus time factor Γ ($= c_h t/R^2$) are shown in Figure 7. Notice that Δu does not necessarily reach 0 at large Γ . This is because of the limited and impermeable outer boundary used in the analyses which is also the case in chamber testing.

The c_h value are determined by comparing the pore pressure dissipation data taken at sensor #3 (see Figure 8) and the analytical solution. The t_{50} is taken as the time elapsed when 50% of the excess pore pressure on the flat-plate surface has dissipated according to the dissipation data.

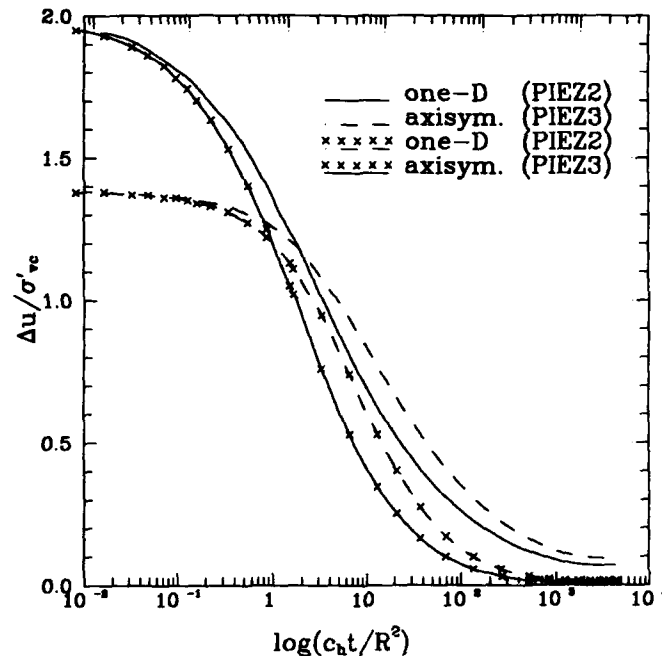


Figure 7. Computed pore pressure dissipation curves.

The corresponding Γ_{50} is selected from the analytical solution. c_h is then calculated as

$$c_h = \Gamma_{50} R^2 t_{50} \quad (9)$$

Table 3 shows the estimated c_h values following the aforementioned procedure. The results of CGC tests performed on samples taken from the chamber specimens are also included in Table 3. The c_h values based on one-dimensional solutions are higher than those from axisymmetric solutions. For the isotropically consolidated specimen, the estimated c_h is at least one order of magnitude smaller than those from CGC tests shown in Tables 3. For the anisotropically consolidated specimen, the estimated c_h based on one-dimensional solution is close to the lower bound of the corresponding CGC values.

From the aforementioned analysis, it appears that a one-dimensional solution is more desirable than the axisymmetric approach, which is the current approach. However, neglecting the fact that the blade has a finite width would result in an underestimation of c_h . Figure 4 shows that during dissipation, the pore pressure was relatively higher towards the corners of the blade. Thus, the pore pressure dissipation had two components. One away from the $z=0$ plane and the other towards the $x=0$ plane. These two components offset each other and thus resulted in a rather slow dissipation as recorded at the center of the blade (sensor #3). This was clearly the case for test PIEZ2 although less distinctive for PIEZ3 where the magnitude of excess pore pressure was significantly less.

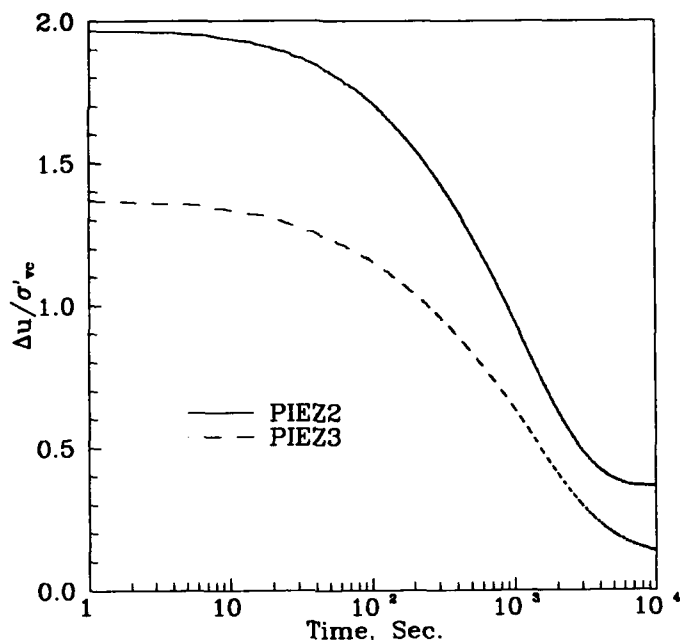


Figure 8. Pore pressure dissipation curves from chamber tests.

Table 3. The estimated and measured c_h values.

Consolidation Test	$C_h, 10^{-3} \text{ cm}^2/\text{sec}$			
	Estimated		Experimental	
	One-Dimensional	Axisymmetric	Reload	Virgin Loading
Isotropic	0.48	0.20	6.9 to 67.4	4.6 to 8.6
Anisotropic	2.80	1.50	11.1 to 72.5	4.5 to 9.7

CONCLUDING REMARKS

The flat plate is a three-dimensional penetrometer. The actual penetration mechanisms in clays are very complicated. A somewhat empirical approach is inevitable when interpreting the results of flat plate penetration tests such as the DMT. To establish empirical rules generally requires a large number of well documented data points. Unlike calibration chamber tests in sands, it is not practical to perform a large number of tests in a clay chamber. However, the tests presented in the paper did offer some important guidelines in establishing these empirical rules.

The chamber tests showed strong evidence that the flat plate penetration induced pore pressure is primarily determined by the soil behavior in the lateral direction. The mechanical properties of soils are

generally anisotropic. This study suggests that we should limit the soil properties in the horizontal direction when establishing empirical rules from dilatometer tests. A practical way to obtain a lower bound c_h would be to interpret the pore pressure dissipation around a flat plate as one dimensional.

ACKNOWLEDGEMENTS

Financial support for this research was provided by the National Science Foundation (Grant MSM-8717065) and the U.S. Air Force Office of Scientific Research (Grant AFOSR-88-0114).

REFERENCES

1. Huang, A.-B., Holtz, R.D., and Chameau, J.-L. (1988), "A Calibration Chamber for Cohesive Soils," *Geotechnical Testing Journal*, **11**, No.1, pp. 30-35.
2. Huang, A.-B. (1989), "Strain Path Analyses for Arbitrary Three-dimensional Penetrometers," *International Journal for Numerical and Analytical Methods in Geomechanics*, **13**, No.5, pp.551-564.
3. Campanella, R.G., and Robertson, P.K. (1991), "Use and Interpretation of a Research Dilatometer," *Canadian Geotechnical Journal*, Vol.28, **1**, pp.113-126.
4. Campanella, R.G., and Vaid, Y.P. (1972), "A Simple K_0 Triaxial Cell," *Canadian Geotechnical Journal*, **2**, pp.249-260.
5. Kabir, M.G., and Lutenegeger, A.J. (1990), "In Situ Estimate of The Coefficient of Consolidation in Clays," *Canadian Geotechnical Journal*, Vol.27, **1**, pp.58-67.
6. Lutenegeger, A.J. (1988), "Current Status of The Marchetti Dilatometer Test," *Proceedings, 1st International Symposium on Penetration Testing*, Orlando, Florida, pp.137-155.
7. Marchetti, S. (1975), "A New in Situ Test for Measurement of Horizontal Soil Deformability," *Proceedings, Conf. on In Situ Measurement of Soil Properties*, Raleigh, North Carolina, pp.255-259.
8. Marchetti, S. (1980), "In Situ Tests by Flat Dilatometer," *Journal of Geotechnical Engineering Division, ASCE*, **106**, GT3, pp.299-321.
9. Randolph, M.F., and Wroth, C.P., (1979) "An Analytical Solution for The Consolidation Around A Driven Pile," *International Journal for Numerical and Analytical Methods in Geomechanics*, **3**, pp.217-229.
10. Robertson, P.K., and Campanella, R.G., (1983) "Interpretation of Cone Penetration Tests. Part II: Clay," *Canadian Geotechnical Journal*, **20**, pp.734-745.

NUMERICAL SIMULATION OF A CALIBRATION CHAMBER

A.-B. Huang, M.Y. Ma, and J.S. Lee

Department of Civil and Environmental Engineering, Clarkson University,
Potsdam, New York 13676, U.S.A.

ABSTRACT

A two dimensional numerical technique which couples discrete element method with boundary element method was developed to simulate a calibration chamber for granular soils. Soil particles in the near field where strains are large are simulated as disks using the discrete element method. In the far field and extending to infinity, the soil is considered as a linear elastic continuum and simulated by the boundary element method. This numerical technique enabled the cone penetration tests be simulated in an infinite soil mass as well as boundary conditions typically applied in a physical calibration chamber. The simulation also allowed the cone penetration mechanisms be evaluated from micromechanical point of view. The paper describes the numerical techniques and demonstrates results of simulated penetration tests and discusses the boundary effects on test results.

INTRODUCTION

The cone penetration test has been used extensively in Geotechnical Engineering. Because of the difficulty in taking undisturbed granular soil samples, in situ testing is the only practical method to characterize granular soil deposits. However, as in many other penetration tests, interpretation of cone penetration test results is empirical due to the lack of fundamental understanding of the penetration mechanisms. Laboratory calibration chamber tests have been used by many researchers [e.g., 1 and 7] to establish correlations for design practice. A soil deposit with known stress history and boundary conditions can be created in a calibration chamber. The specimens can be uniform and repeatable. The chamber specimen, however, has a limited lateral dimension which deviates from the field condition where the soil extends laterally to a far greater distance. Some form of correction is thus in order when interpreting chamber cone penetration test data. Also, the type of measurements that can be conducted in a chamber is limited to those of boundary conditions. These measurements do not help in improving our understanding of penetration mechanisms.

As part of an effort to study the penetration mechanisms in granular soils, a series of numerically simulated cone penetration tests were performed. The granular medium is numerically simulated as a two dimensional particulate assembly using the discrete element method (DEM). Soil particles were simulated as two-dimensional disks in DEM. A constant stress or zero strain conditions can be applied on the particulate assembly boundary. By coupling with the boundary element method (BEM), the simulation was also capable of simulating an infinite soil mass. The paper describes the numerical simulation techniques, presents results of simulated penetration tests under different boundary conditions and discusses their implications in the interpretation of chamber cone penetration tests.

THE PARTICULATE CHAMBER

Penetration is a large strain problem which makes it extremely difficult to simulate using continuum mechanics techniques such as the Finite Element Method. The DEM [3] treats a granular soil deposit as an assembly of discrete particulates. It is capable of handling large strain problems and its advantage over FEM is obvious. The DEM simulation reported herein mimics the procedure of a physical calibration chamber testing. The DEM region contains 12000 disks using a constant contact stiffness. Figure 1 shows the size distribution of the disks and other physical properties assigned to the DEM simulation. As in a physical chamber testing, the disks were pluviated into the chamber from a hopper under a gravity of 1 g. Each of the four boundaries can be considered as either strain or stress controlled. A strain controlled boundary is flat, rigid and frictionless. The stress controlled boundary was simulated as a series of "boundary disks". The external stress is converted into forces and applied to the boundary disks by a linear distribution.

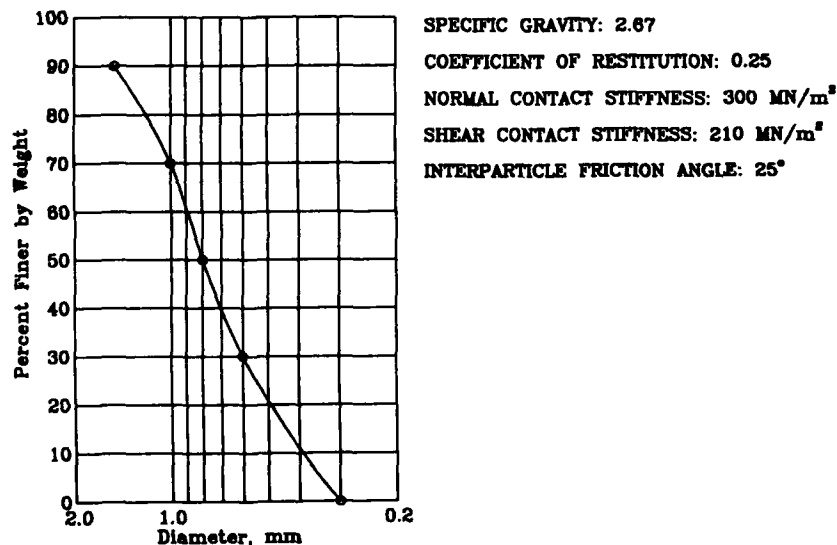


Figure 1. Size distribution and related properties of the DEM disks.

A realistic DEM simulation that mimics a field granular soil deposit demands a large number of disks which is beyond our current computational capability. Thus, a balance has to be reached between a realistic simulation and practicality in computation. Fortunately, large strains are expected only in close vicinity of the penetrometer [5]. Hence, it is reasonable to assume the material as linear elastic in the far field and be simulated using BEM. In addition to its simplicity, BEM is capable of simulating a soil mass extending outwards to infinity. A combined DEM/BEM simulation provides a realistic emulation of a field testing condition. Figure 2 shows the assembled DEM/BEM particulate chamber along with the penetrometer. DEM uses an explicit scheme where computations are based on time increments. BEM employs an implicit scheme which is time independent. A true coupling between DEM and BEM is therefore, difficult if not impossible. A simplified coupling which was based on linear distribution of contact forces between DEM disks and the BEM nodal points was developed. The

algorithm of DEM/BEM coupling is shown in Figure 3. Taking advantage of symmetry, only half of the penetrometer and soil mass was simulated. The center vertical wall was rigid and frictionless. The penetrometer has a 60° apex angle. The coordinate system shown in Figure 2 is used in presenting the data. All linear dimensions are normalized with respect to the half width ($R = 5 \text{ mm}$) of the penetrometer.

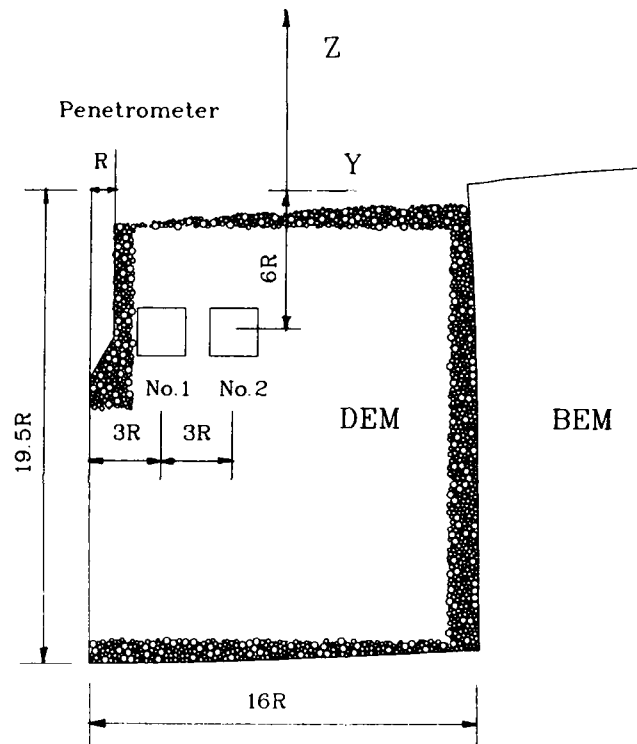


Figure 2. The particulate chamber.

When not coupled with BEM, the numerical technique requires that the bottom boundary of the DEM region be rigid. The capability of simulating an infinite soil mass is not available in physical CC testing. Thus, an expanded and slightly different convention are used in this paper (Table 1) to specify the boundary conditions.

Table 1. Boundary conditions in simulated CC.

BC1	σ_v, σ_h constant ($\epsilon_v = 0$ at bottom)
BC2	$\epsilon_v = \epsilon_h = 0$
BC3	σ_v constant, $\epsilon_h = 0$ ($\epsilon_v = 0$ at bottom)
BC4	σ_h constant, $\epsilon_v = 0$
BC5	field conditions

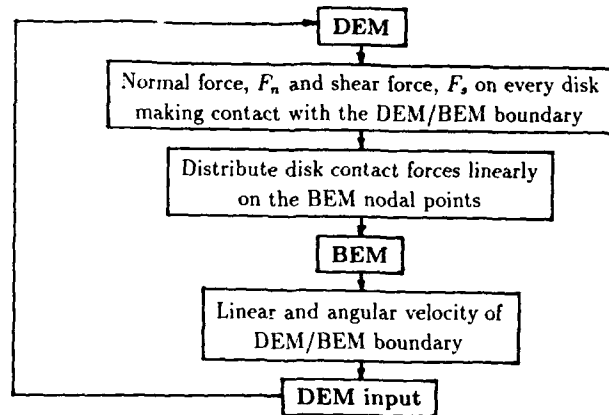


Figure 3. DEM/BEM coupling algorithm.

PROPERTIES OF THE PARTICULATE ASSEMBLY

Laboratory tests were simulated to provide reference properties and those required for the BEM simulation. Figure 4 shows the stress-strain curves from the simulated K_0 consolidations. Simulated biaxial tests were performed on the disk assembly under a shearing mode of axial compression and lateral compression. The disk assembly was normally consolidated under zero lateral strain (K_0) conditions with a vertical consolidation stress (σ_{vc}) of 1200 kPa. The results of axial compression and lateral compression tests are shown in Figure 5. The peak stress difference from axial compression test corresponds to a friction angle of 35° . The Young's modulus (44 MPa) needed in the BEM simulation was determined based on the simulated lateral compression test.

SIMULATED CC PENETRATION TESTS

Boundary conditions of BC1, BC3 and BC5 (see Table 1) were applied in a series of simulated penetration tests. For the case of BC1 and BC3, only the DEM simulated particulate assembly was used in the computations. As shown in Figure 2, the width of the simulated particulate assembly was 16R. Or, the simulated CC has an equivalent diameter ratio, R_p (diameter of the CC specimen over the diameter of the cone) of 16 for the cases of BC1 and BC3. The particulate assembly was normally consolidated under K_0 conditions to a maximum vertical stress (σ_{vc}) of 1200 kPa. In addition to tip resistance, q_c as typically recorded in a cone penetration test, DEM computes the position and contact forces for every disk. The result enables the micromechanical behavior of the particulate assembly be evaluated at any position and any stage of penetration. However, recording all the data throughout the penetration is impractical as it requires too much computer memory. Instead, responses of disks (i.e., displacement and contact forces) in two monitor zones denoted as No.1 and No.2 (Figure 2) were recorded.

Profiles of q_c from the simulated penetration tests are shown in Figure 6. In all three cases, a fairly stable q_c value was reached shortly after the penetration started. The effects of limited lateral dimension in

the case of BC1 are clearly demonstrated by the significantly lower q_c values versus those of BC5. The q_c 's between BC3 and BC5 were similar except that q_c values fluctuated more in the case of BC3. The q_c value from BC5 corresponds to a friction angle of approximately 30° using the interpretation method by Durgunoglu and Mitchell [4].

Figure 7 demonstrates the distribution of normal contact forces within the particulate mass for all three cases analyzed. The line thickness is proportional to the magnitude of contact force. The result shows that there is only a slight increase of contact forces in the vertical direction in the case of BC1. The contact forces are concentrated in the lateral direction for the case of BC3. The boundary condition of BC5 resulted in a distribution of contact forces somewhat in between the above two cases but closer to BC3.

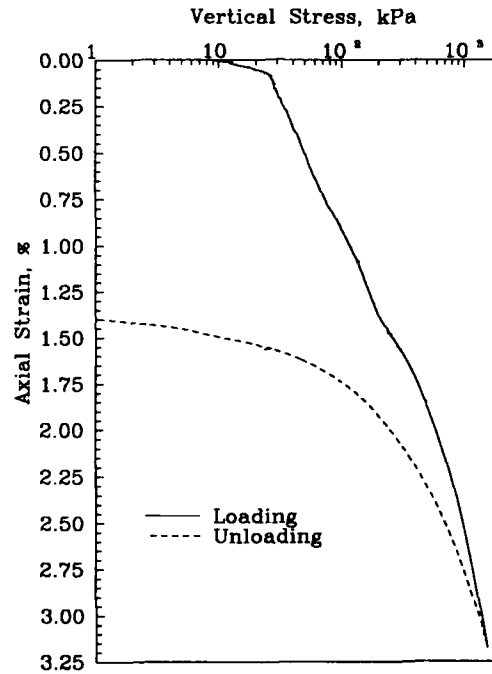


Figure 4. Simulated K_0 consolidation test result.

The theory by Christoffersen et al. [2] was used to compute stress tensor from the contact forces.

$$\sigma_{ij} = \frac{1}{V} \sum_{\alpha=1}^N \frac{1}{2} (f_i^\alpha d_j^\alpha + f_j^\alpha d_i^\alpha) \quad (1)$$

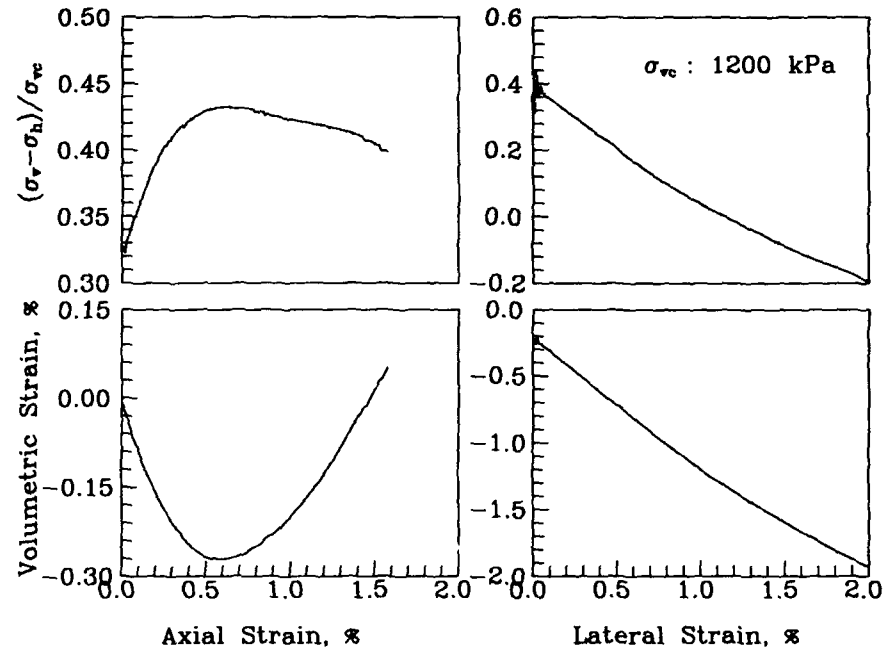


Figure 5. Results of axial compression and lateral compression tests.

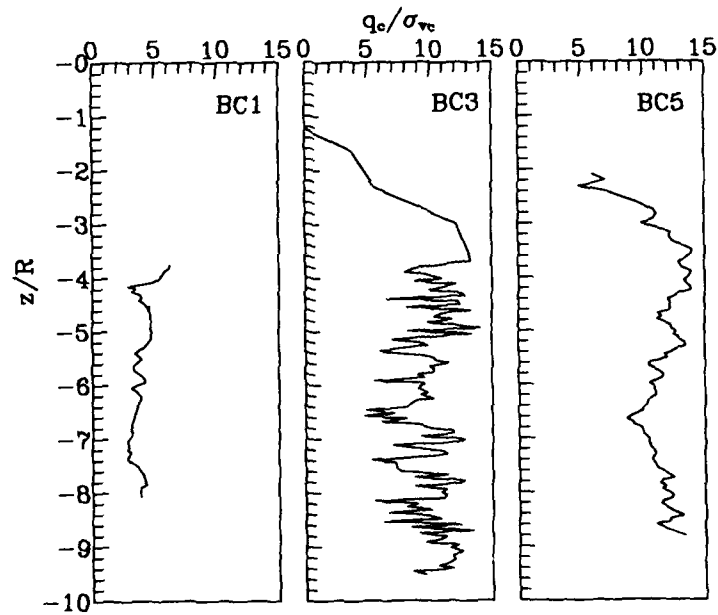


Figure 6. Computed q_c profiles.

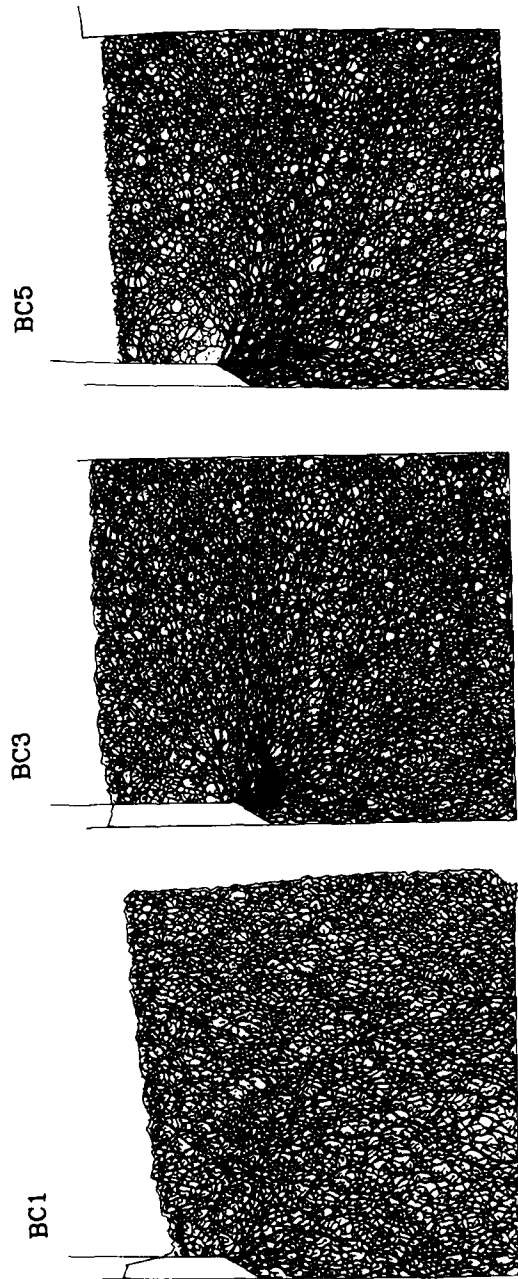


Figure 7. Distribution of normal contact forces.

where

f_i = contact force between disks

d_i = vector connecting the centers of disks in contact

V = total volume (area in two-dimension) of monitor zone

N = number of particulates

Stress paths can be computed based on Equation 1 using the recorded contact forces in monitor zones No.1 and No.2. Compressive stress is positive. The relative position of the penetrometer in reference to the level of the monitor zones is shown in Figure 8. As demonstrated in Figure 9, all stress components showed stress reversals as in the case of penetration tests in clays [1]. The magnitude of stresses in the case of BC1 was significantly lower than those of BC3 and BC5. However, the trend of stress paths were similar in all three cases.

Figure 10 depicts the penetration induced displacement paths in y (d_y) and z (d_z) directions. The displacement value represents the average among all the disks in the monitor zones. The pattern of displacement paths was similar between BC1 and BC5 which showed a monotonic increase of d_y and d_z . In the case of BC3, there was a reversal of d_z . The magnitude of displacements was different by four fold between the maximum (BC1) and the minimum (BC3).

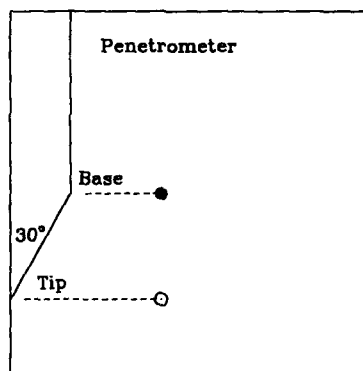


Figure 8. Relative position between the penetrometer and monitor zones.

CONCLUDING REMARKS

The boundary condition BC1 is commonly used in physical chamber testing. The simulated CC tests indicate that BC1 is not always more desirable than BC3. If the interest is in correlating q_c and stress related parameters, it appears that BC3 should result in data close to those in the field condition. However, if displacement or strain field is of interest then BC1 should provide at least a qualitatively correct emulation. It should be emphasized that the diameter ratio R_D used in the simulations was very low as a calibration chamber. The boundary effects are expected to be less distinctive as R_D increases.

It should be kept in mind that the soil element around the cone experiences stress reversals as in the case of penetration tests in clays. This would complicate the correlation between q_c value and soil stress-strain relationships.

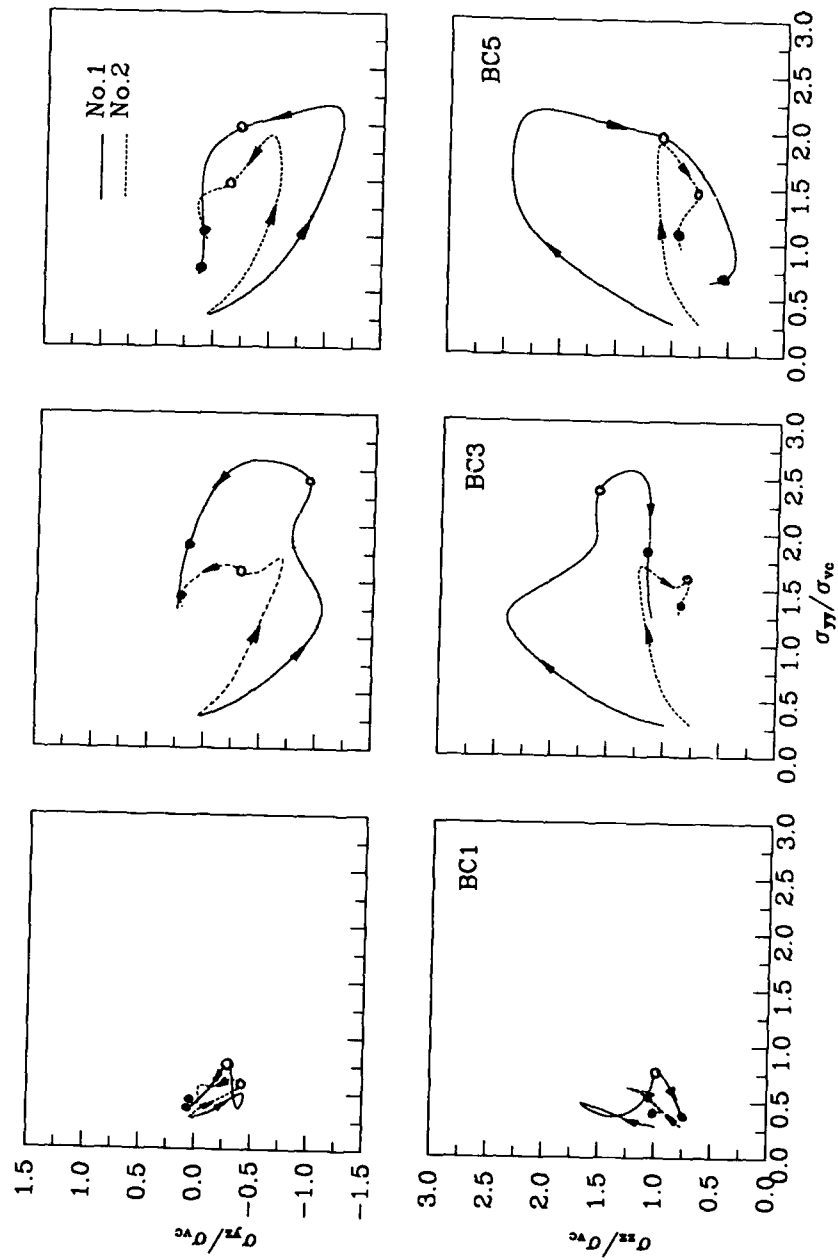


Figure 9. Computed stress paths.

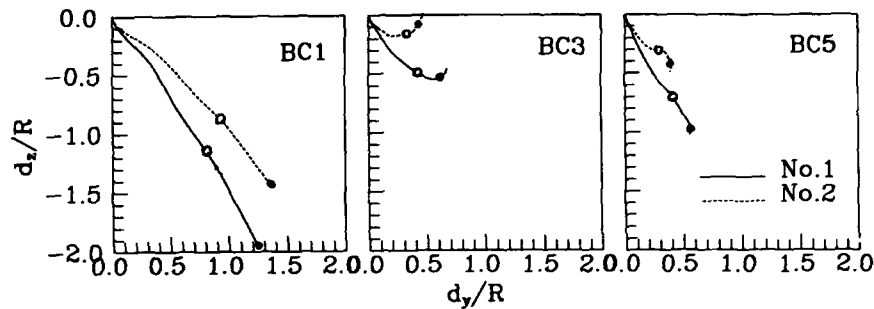


Figure 10. Computed displacement paths.

ACKNOWLEDGEMENTS

Funding for this research was provided by the New York State Science and Technology Foundation through the Center for Advanced Materials Processing at Clarkson University and the National Science Foundation (Grant No. MSS-9021973).

REFERENCES

1. M.M. Baligh, Undrained Deep Penetration, I: Shear Stresses, *Geotechnique* **36**, No.4, 471-485 (1986).
2. J. Christoffersen, M.M. Mehrabadi and S. Nemat-Nasser, A Micromechanical Description of Granular Material Behavior, *Journal of Applied Mechanics*, **48**, 339-344 (1981).
3. P.A. Cundall, and O.D.L. Strack, A Discrete Numerical Model for Granular Assemblies, *Geotechnique*, **29**, 47-65 (1979).
4. H.T. Durgunoglu and J.K. Mitchell, Influence of Penetrometer Characteristics on Static Penetration Resistance, *Proceedings, 1st European Symposium on Penetration Testing*, Stockholm, 133-139 (1974).
5. A.B. Huang, Strain Path Analyses for Arbitrary Three-Dimensional Penetrometers, *International Journal for Numerical and Analytical Methods in Geomechanics*, **13**, 551-564 (1989).
6. M. Jamiolkowski, V.N. Ghionna, R. Lancellotta and E. Pasqualini, New Correlations of Penetration Tests for Design Practice, *Proceedings, Penetration Testing 1988, ISOPT-1, Florida*, 263-296 (1988).
7. A.K. Parkin, The Calibration of Cone Penetrometers, *Proceedings, Penetration Testing 1988, ISOPT-1, Florida*, 221-243 (1988).

FIFTEEN+ YEARS OF MODEL FOUNDATION TESTING IN LARGE CHAMBERS

FRED H. KULHAWY

School of Civil and Environmental Engineering, Hollister Hall,
Cornell University, Ithaca, NY 14853-3501

ABSTRACT

A general overview is given of fifteen+ years of model foundation testing in large chambers. The emphasis has been on drilled shaft foundations. The overall testing program is surveyed, and some experimental lessons learned are noted.

INTRODUCTION

In 1974, I was fortunate to be able to initiate a research program on the behavior of foundations, with emphasis on drilled shafts and focus on foundations for transmission line structures. This research has been supported by the electric utility industry, initially on a modest basis by the Niagara Mohawk Power Corporation (NMPC) and subsequently (since 1980) on a broad basis by the Electric Power Research Institute (EPRI). One field testing phase also was co-sponsored by the Empire State Electric Energy Research Corporation (ESEERCO). Although the research has had a broad basis, a significant component has been the testing of larger-scale foundation models in large chambers. This paper focuses on this model testing and related issues.

SCOPE OF RESEARCH PROGRAM

The structure and current status of the EPRI research project is depicted in Figure 1. As shown, the project includes a variety of experiments, leading to design methods and design aids. Double solid boxes indicate completed phases, dotted outer and solid inner boxes indicate partially completed phases, and dotted boxes indicate phases yet to be initiated. A general overall description of this effort is given by Kulhawy and Trautmann [8].

The model foundation testing occupies the box entitled "Laboratory Load Tests", and it appears to be of relatively modest scope. However, this component actually represents a lion's share of the research expenditures on this \$5 million plus project.

Table I summarizes the model foundation testing efforts to date by foundation type, loading mode, and soil type. As can be seen, a wide variety of loading modes have been addressed in both sand and clay (to represent drained and undrained loading, respectively). The focus to date has been on drilled shafts, with only one modest study on grillages.

In addition to the references reporting foundation test results, there have been a number of other pertinent references that have focused on key experimental issues. Without these support studies, the main foundation results would be of lesser use. Included so far have been studies of stress measurement in soil [3, 20, 22] and reliable in-situ density measurement [15, 21], in addition to work on developing a clay that is very useful for large-scale laboratory testing [13]. Furthermore, there has been a major effort to develop a manual on estimating soil properties that addresses most test and in-situ conditions [6].

TESTING FACILITIES

Figure 2 gives an overall plan view of the laboratory layout, showing the

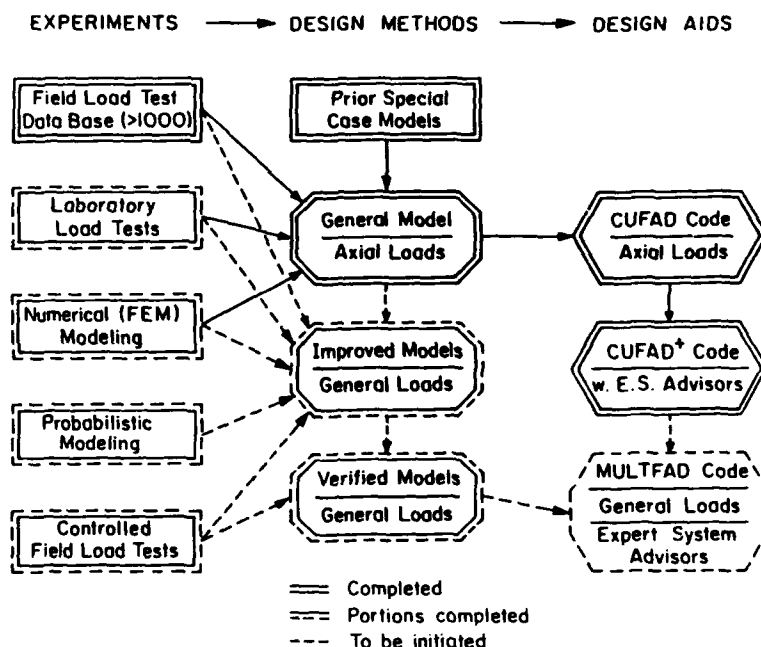


FIG. 1. Overview of EPRI research project

TABLE 1. Model foundation testing efforts to date (1991)

Model Foundation	Loading Mode	References on Testing	
		Sand	Clay
Drilled Shaft	Static Axial Uplift	4, 5, 14, 17	2
	Static Axial Compression	14, 17	2
	Repeated Axial	14, 16, 17, 18	12
	Static Lateral/Moment	1	10, 11
	Repeated Lateral/Moment	1	11
	Static Inclined	19	in progress
	Repeated Inclined	in progress	in progress
Grillage	Static Axial Uplift	7, 9	

location of the in-ground test pit for the sand tests and the above-ground clay chambers. The test pit is 2.1 m diameter by 2.9 m deep and is constructed of corrugated steel culvert sections. Augers allow for removal of sand from the pit into an adjacent storage chamber. Figure 3 gives details of the test pit, while Figure 4 gives a true perspective of the size of the test pit. Figure 5 illustrates one type of combined load test in this test pit.

Two basic sizes of clay chambers have been used to date. The medium-size chambers are 0.6 m diameter by 1.2 m high, and the large-size chamber is 1.37 m diameter by 2.13 m high. These chambers are split vertically into two sections to facilitate soil removal, in-situ sampling, and instrumentation recovery. Figure 6 gives a perspective of the large clay chamber.

All testing is done under computer control using a HP-1000 minicomputer

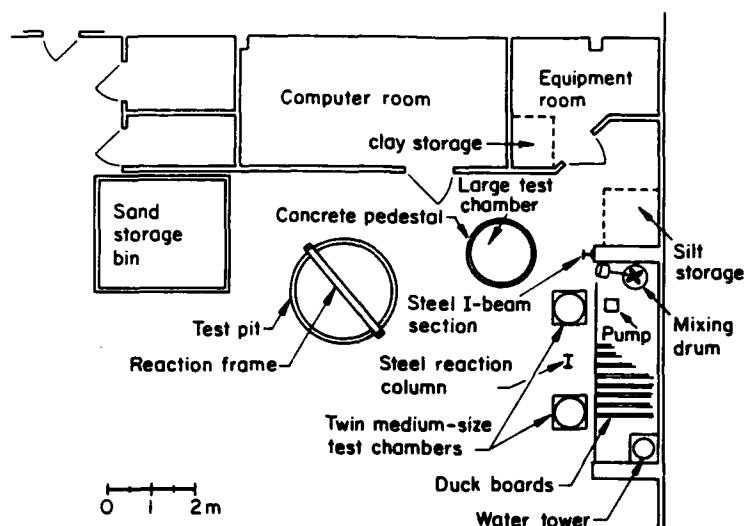


FIG. 2. Plan view of Cornell model testing laboratory

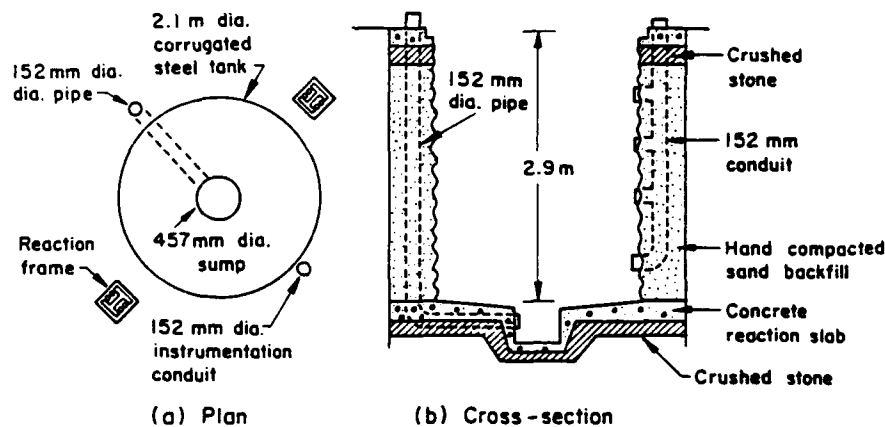


FIG. 3. Details of sand test pit

in conjunction with a dual-channel MTS closed-loop servo-controlled hydraulic testing system. Loading can be applied in a static mode or in repeated loading up to a rapid mode consistent with wind loading. Load also can be applied in axial, lateral, moment, or combined modes. As shown in Table I, we have only exploited several loading modes to date. Figure 7 shows the overall control center, which has been essentially the same since 1984.

For monitoring the test performance, a full suite of DCDTs, stress cells, and soil and pore water stress transducers are used. The data acquisition system operates in real time to compare all test results in a consistent manner.

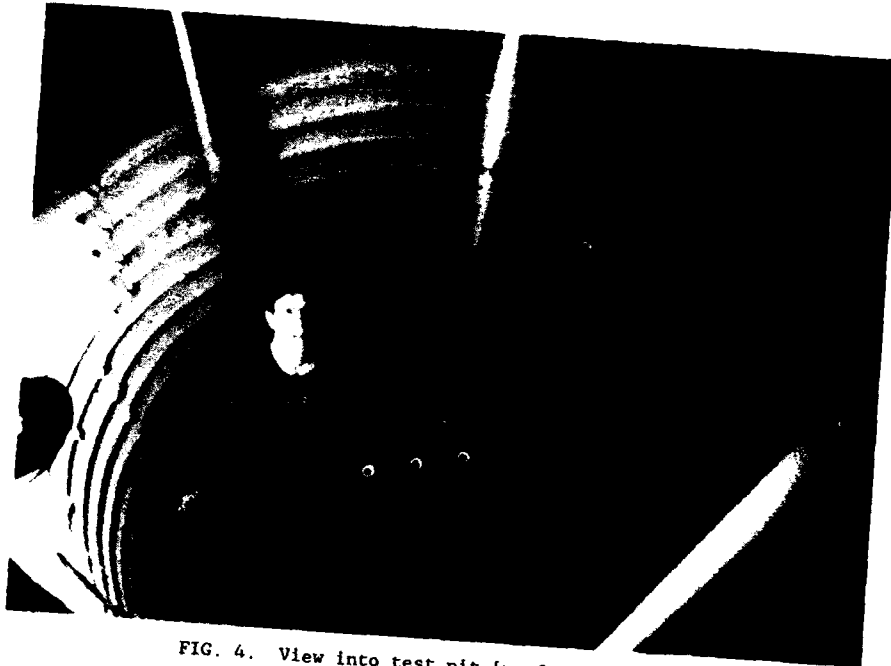


FIG. 4. View into test pit [w. J.P. Turner]

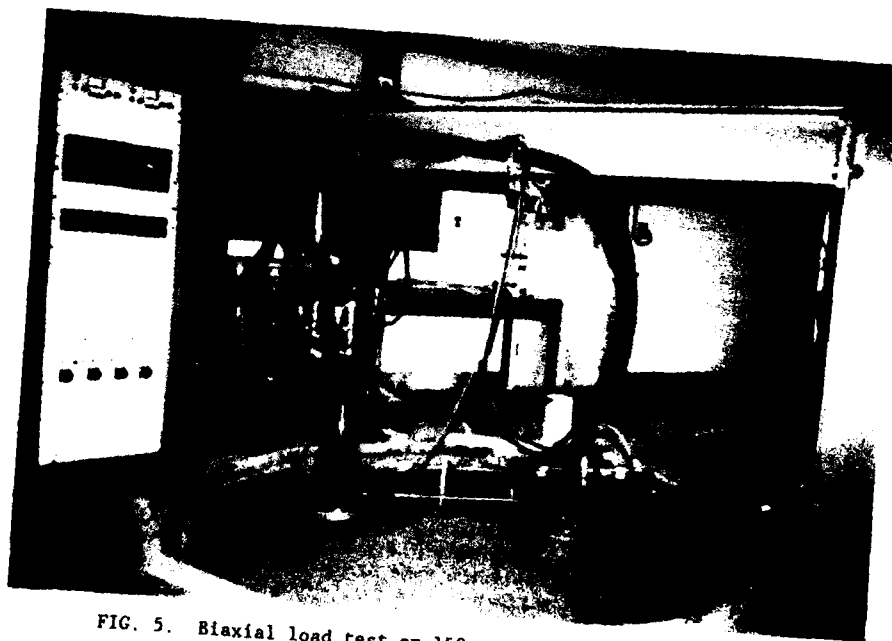


FIG. 5. Biaxial load test on 150 mm diameter drilled shaft



FIG. 6. Half of large chamber filled with clay deposit (w. l to r, P.W. Mayne, F.H. Kulhawy, S.W. Agaiby, K.J. McManus, J.N. Kay, S. Vidic (kneeling), T.C. Pumphrey (seated))

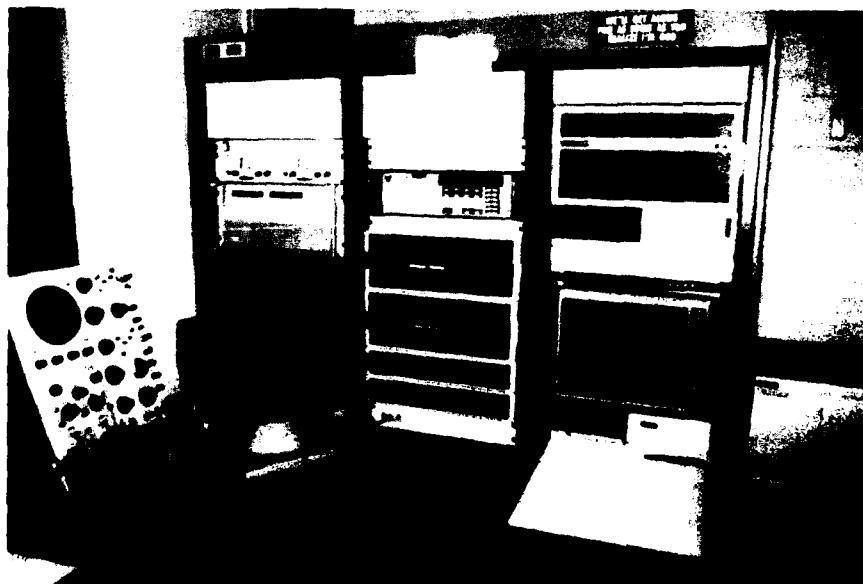


FIG. 7. Control center with HP-1000 minicomputer and MTS system

The only problem one has, especially for repeated load tests, is that too much data can be generated for very small sampling intervals.

To evaluate the soil characteristics, all of the desirable laboratory equipment are available, ranging from triaxial to direct simple shear tests. Furthermore, a variety of in-situ procedures are available. At present, we use miniature vane shear, small-scale electric cone, piezoprobe, and dilatometer tests, as appropriate in specific soil types.

SAMPLE PREPARATION AND TEST SET-UP

One of our overall goals has been to try to create a range of soil deposits that replicate prototype in-situ conditions with regard to strength, stress history, stress state, etc. For the sands, loose and medium dense normally consolidated deposits are created by air pluviation (raining) methods. Dense, overconsolidated deposits are prepared by raining, followed by vibration or static loading. These procedures can achieve most any desired ground condition.

For the clay deposits, slurry consolidation is used to prepare the deposits and give initial gravity responses. One-dimensional vertical surcharging then is used to achieve high overconsolidation ratios (OCR) and firm soils. In the laboratory environment, normally consolidated or low OCR clays are not desirable because they are just too soft to work with.

With both types of soils, every reasonable effort is made to simulate the actual field construction process. For shafts in clay, augers are used to excavate the shaft, followed by concrete placement. For shafts in sand, a casing must be used to hold the shaft open prior to concrete placement. For gril-lages in sand, open excavation and backfilling are used. Overall, we have had very good success with our soil preparation, quality or material property control, and test set-up. Details can be found in the references identified in Table I.

Figure 8 illustrates the range of drilled shafts tested in the sand deposits in axial loading, with diameters of 76 mm, 152 mm, and 305 mm. Within this size range, the overall shaft behavior was found to be consistent and predictable, and it was fundamentally the same as that of larger size shafts used in practice. For shafts in clay, and for either lateral/moment or inclined loading, smaller sizes were used, ranging from 59 to 174 mm in diameter. As with the sand, the overall shaft behavior within this range was consistent and predictable, and it was comparable with field behavior.

Figure 9 shows a large clay deposit with a 174 mm diameter shaft after testing and during excavation. The left side of the clay shows the overall consistency and homogeneity of the deposit. Although not clear in this figure, the failure surface essentially was a cylinder that was just outside the cast-in-place concrete shaft. On the right side of the figure is a 50 mm x 50 mm grid within which water content samples were taken to evaluate the clay consistency. Figure 10 shows these water contents, from which it can be seen that the clay is quite uniform.

Careful quality control has been and will continue to be maintained for all of the test deposits.

Most recently, we have been using control techniques during sample preparation and after model foundation testing. For the sand deposits, the unit weights are checked during preparation using density cups for loose and medium dense sand and the density scoop in dense sands. After foundation testing, dilatometer and cone soundings are made in relatively undisturbed areas away from the model foundations. Both have worked well, except for the dilatometer in loose sands. In this situation, the sand is loose and very compressible, and the overburden stress is very small. Because of these factors, no dilatometer A readings could be recorded.

For the clay deposits, careful control of mixture quantities is necessary to achieve repeatable deposits. During excavation for the model foundation shaft, water content samples were taken and vane shear tests were done using



FIG. 8. Range of drilled shafts tested (76 mm, 152 mm, 305 mm diameter)
[w. K.J. McManus]



FIG. 9. Large clay deposit illustrating drilled shaft and water content sample locations

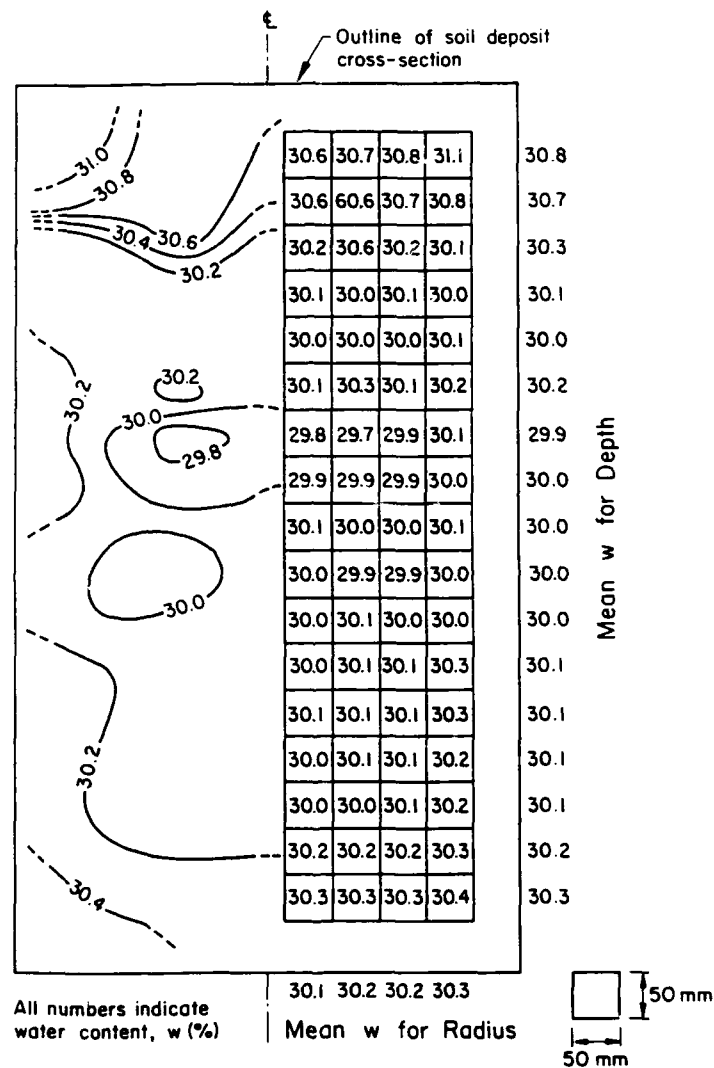


FIG. 10. Water contents in large clay deposit

a 12.7 mm diameter vane with a height to width ratio of two. Figure 11 illustrates the vane testing. After model foundation testing, water contents were taken (as noted in Figures 9 and 10) and, occasionally, torque tests were done. Most recently, cone and piezoprobe soundings also have been made. The miniature electric cone has a diameter of 23.3 mm, while the piezoprobe has a 19.0 mm diameter. Piezoprobes were made with transducers at the tip and behind the tip to provide proper information for interpreting the cone data.

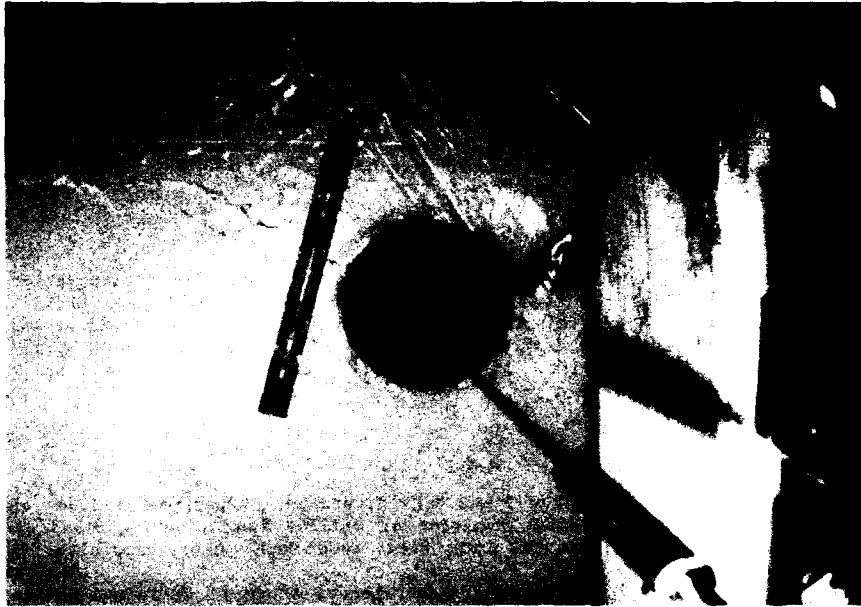


FIG. 11. Shaft excavation in clay with miniature vane shear test in progress

SOME MODELING LESSONS LEARNED

During the testing studies, we have learned much about soil deposit preparation and foundation modeling. All has been reported in detail in the references cited to date. However, it is appropriate to point out a few broad generalizations that are pervasive throughout the research.

First, prototype behavior can be replicated in test chambers if the models and the chambers are large enough. From our experience, models much less than 50 mm in diameter deviate from prototype behavior, particularly in sands. Models this small also pose major problems with instrumentation and construction modeling. For these reasons, we focus on larger models in chambers that are large enough to minimize any potential boundary effects.

Second, it is important to model the foundation construction process as well as possible in the laboratory. For example, model grillages that are embedded during soil deposit preparation have little ability to replicate prototype conditions.

Third, it is very important to represent correctly the soil strength and compressibility and the in-situ state of stress in the soil deposit. Under low overburden stresses, these parameters are highly nonlinear and vary dramatically over very small depths. Standard laboratory shear and compressibility tests must be conducted at comparable low stress levels to represent the soil properties realistically. The same is true for the in-situ stress measurements, where the calibrations must be done at very low stress. Within this same context, cautions must be applied in scaling observations directly. On occasion, at small scale and low stresses, local or punching shear type of mechanisms develop while, at prototype scale and higher stresses, general shear develops. One must be certain that the observations are consistent at all scales.

Lastly, and perhaps most importantly, is the need to pay attention to every possible detail of soil preparation, model construction, instrumentation,

scaling, and interpretation. One overlooked detail can impact all of these factors.

SUMMARY

A broad overview was given of the electric utility-sponsored foundations research that we have been conducting since 1974. The overall testing program was reviewed, and some lessons learned were noted.

ACKNOWLEDGMENTS

These studies have been supported by Niagara Mohawk Power Corporation (1974-80) and the Electric Power Research Institute (since 1980) under RPL493. Vito J. Longo is the EPRI project manager. A. Avcişoy drafted the figures, and K. J. Stewart prepared the text. And a great big thank you to all of my co-authors in the reference list. It would not have been possible without their outstanding efforts.

REFERENCES

1. S.W. Agaiby, F.H. Kulhawy, and C.H. Trautmann, "Experimental Study of Drained Lateral & Moment Behavior of Drilled Shafts During Static & Repeated Loading", Rpt. EL-xxxx, Elec. Power Res. Inst., Palo Alto, in press (1991).
2. J.F. Beech and F.H. Kulhawy, "Experimental Study of Undrained Uplift Behavior of Drilled Shaft Foundations", Rpt. EL-5323, Elec. Power Res. Inst., Palo Alto, 350 p. (1987).
3. S.C. Boyce and F.H. Kulhawy, "Laboratory Determination of Horizontal Stress in Cohesionless Soil", Geot. Eng. Rpt. 83-1, Cornell Univ., Ithaca, 324 p. (1983).
4. D.W. Kozera, F.H. Kulhawy, and J.L. Withiam, "Uplift Capacity of Model Shafts in Sand", Contract Rpt. B-49(2), Niagara Mohawk Power Corp., Syracuse, 110 p. (1977). (also Geot. Eng. Rpt. 77-1, Cornell Univ.)
5. F.H. Kulhawy, D.W. Kozera, and J.L. Withiam, "Uplift Testing of Model Drilled Shafts in Sand", J. Geot. Eng. Div. (ASCE), 105(GT1), 31-47 (1979).
6. F.H. Kulhawy and P.W. Mayne, "Manual on Estimating Soil Properties for Foundation Design", Rpt. EL-6800, Elec. Power Res. Inst., Palo Alto, 306 p. (1990).
7. F.H. Kulhawy, C.N. Nicolaides, and C.H. Trautmann, "Experimental Investigation of Uplift Behavior of Spread Foundations in Cohesionless Soil", Rpt. EL-xxxx, Elec. Power Res. Inst., Palo Alto, in press (1991).
8. F.H. Kulhawy and C.H. Trautmann, "Foundation Engineering Research at Cornell University", Geot. News, 8(4), 36-38 (1990).
9. F.H. Kulhawy, C.H. Trautmann, and C.N. Nicolaides, "Spread Foundations in Uplift: Experimental Study", Fndns. for Trans. Line Towers (GSP 8), Ed. J.L. Briaud, ASCE, New York, 96-109 (1987).
10. P.W. Mayne and F.H. Kulhawy, "Load-Displacement Behavior of Laterally Loaded Rigid Drilled Shafts in Clay", Proc. 4th Intl. Conf. Piling & Deep Fndns., Stresa (1991).
11. P.W. Mayne, F.H. Kulhawy, and C.H. Trautmann, "Experimental Study of Undrained Lateral & Moment Behavior of Drilled Shafts During Static and Repeated Loading", Rpt. EL-xxxx, Elec. Power Res. Inst., Palo Alto, in press (1991).
12. K.J. McManus and F.H. Kulhawy, "Cyclic Axial Loading of Drilled Shaft Foundations in Cohesive Soil for Transmission Line Structures", Rpt. EL-7161, Elec. Power Res. Inst., Palo Alto, 290 p. (1991).
13. K.J. McManus and F.H. Kulhawy, "A Cohesive Soil for Large-Size Laboratory

- Deposits", Geot. Test. J. (ASTM), 14(1), 26-34 (1991).
14. J.P. Stewart and F.H. Kulhawy, "Experimental Investigation of Uplift Capacity of Drilled Shaft Foundations in Cohesionless Soil", Contract Rpt. B-49(6), Niagara Mohawk Power Corp., Syracuse, 422 p. (1981). (also Geot. Eng. Rpt. 81-2, Cornell Univ.)
 15. C.H. Trautmann, F.H. Kulhawy, and T.D. O'Rourke, "Sand Density Measurements for Laboratory Studies", Geot. Test. J. (ASTM), 8(4), 159-165 (1985).
 16. J.P. Turner and F.H. Kulhawy, "Prediction of Drilled Shaft Displacements Under Repeated Axial Loads", Proc. Intl. Symp. Prediction & Performance Geot. Eng., Calgary, 105-112 (1987).
 17. J.P. Turner and F.H. Kulhawy, "Experimental Analysis of Drilled Shaft Foundations Subjected to Repeated Axial Loads Under Drained Conditions", Rpt. EL-5325, Elec. Power Res. Inst., Palo Alto, 350 p. (1987).
 18. J.P. Turner and F.H. Kulhawy, "Drained Uplift Capacity of Drilled Shafts Under Repeated Axial Loading", J. Geot. Eng. (ASCE), 116(3), 470-491 (1990).
 19. S. Vidic, F.H. Kulhawy, and C.H. Trautmann, "Drained Behavior of Drilled Shaft Foundations During Inclined Loading", Rpt. EL-xxxx, Elec. Power Res. Inst., Palo Alto, in press (1991).
 20. W.A. Weiler and F.H. Kulhawy, "Behavior of Stress Cells in Soil", Contract Rpt. B-49(4), Niagara Mohawk Power Corp., Syracuse, 312 p. (1978). (also Geot. Eng. Rpt. 78-2, Cornell Univ.)
 21. W.A. Weiler and F.H. Kulhawy, "Accuracy of Density Scoop for Unit Weight Determinations in Cohesionless Soil", Geot. Test. J. (ASTM), 1(4), 234-236 (1978).
 22. W.A. Weiler and F.H. Kulhawy, "Factors Affecting Stress Cell Measurements in Soil", J. Geot. Eng. Div. (ASCE), 108(GT12), 1529-1548 (1982).

RELATIVE DENSITY, SPT, AND CPT INTERRELATIONSHIPS

FRED H. KULHAWY* and PAUL W. MAYNE**

*School of Civil and Environmental Engineering, Hollister Hall, Cornell University, Ithaca, NY 14853-3501; **School of Civil Engineering, Georgia Institute of Technology, Atlanta, GA 30332

ABSTRACT

An overall evaluation is made of relative density, SPT, and CPT relationships. For the SPT, the relationships build upon guidelines given by Skempton in 1986. The CPT relationships are developed from calibration chamber studies. Consistent relationships are developed between the tests and the relative density as a function of field procedures, overburden stress, and soil variables. Extensions are made to most CPT types, and the direct relationships between SPT and CPT data are examined. The results are of direct use for most site investigation and evaluation studies.

INTRODUCTION

Relative density (D_r) is a general indexing term used to describe the degree of compactness of a cohesionless soil, such as "loose" or "dense" sand. Traditionally, D_r has been a useful guide for estimating the in-situ liquefaction potential of sands [45], as well as the soil strength [10] and settlement modulus [21]. The relative density is defined by:

$$D_r = (e_{\max} - e) / (e_{\max} - e_{\min}) \quad (1)$$

in which e = current void ratio and e_{\max} and e_{\min} are the maximum and minimum void ratios, respectively, as determined by specific laboratory test procedures. Since the determination of D_r depends on the accuracy of three distinct and separate measurements of void ratio, errors may occur in routine site investigations where sampling of sands is difficult, if not impossible, using conventional procedures. In addition, several different test procedures exist for defining e_{\max} and e_{\min} . Consequently, D_r often is assessed indirectly by means of empirical correlations with in-situ field tests, such as the standard penetration test (SPT) and cone penetration test (CPT).

For some time, the term and concept of "relative density" have been criticized by a number of researchers because D_r , by itself, is incapable of describing the differences between the contractive and dilative behavior of sands. Alternative procedures for defining the soil state, such as the state parameter [e.g., 6, 7] may be more fundamentally sound. However, they are much more difficult to use in practice as well. Although perhaps less than ideal, current practice still relies on D_r . In this paper, existing procedures for evaluating D_r from the SPT are revised, and a new approach is given for evaluating D_r from the CPT. Extensions are made to include most CPT types, and the direct relationships between SPT and CPT data are examined.

STANDARD PENETRATION TEST (SPT) RELATIONSHIP

The SPT has been the traditional penetration test used in much of U.S. practice. Accordingly, numerous correlations have been suggested between the SPT driving resistance (N value) and a number of soil properties or indices. Very early correlations attempted to link D_r with N directly. However, since

the classic 1957 research of Gibbs and Holtz [16], it has been known that the relationship between D_r and N is not that simple.

Recently, Skempton [47] analyzed available laboratory and field SPT data from Japan, China, the U.K., and the U.S. His study showed that two types of corrections are necessary to "standardize" the measured N value to a consistent point of reference, which then can be correlated directly with D_r as a function of the soil characteristics.

The first type of correction relates to the field procedures used to measure the N value. In theory, the free-fall energy for the SPT is 0.623 kN (140 lb) times the 0.76 m (30 in.) drop, which gives 0.475 kN-m (4200 lb-in.). However, the average energy ratio commonly developed is about 55 to 60% of the free-fall value in the U.S., although this ratio can vary from about 30 to 90% for particular drillers and SPT equipment in practice. Other factors influencing the N value are the borehole diameter, sampling method, and rod length. These factors are summarized in Table I and are used in the following equation:

$$N_{60} = C_{ER} C_B C_S C_R N \quad (2)$$

in which N_{60} = N value corrected for field procedures to an average energy ratio of 60%, N = measured SPT N value, and the C terms are correction factors for energy ratio (C_{ER}), borehole diameter (C_B), sampling method (C_S), and rod length (C_R).

The second type relates to the correction for the stress level influence on the N value. To provide for a consistent reference point, the N_{60} value is modified as follows:

$$(N_1)_{60} = C_N N_{60} \quad (3)$$

in which $(N_1)_{60}$ = N_{60} value corrected to a reference stress of one atmosphere and C_N = correction factor for overburden stress. A number of different relationships have been suggested for C_N , as shown in Figure 1. The correction factors proposed by Skempton are based largely on laboratory test data from calibration chambers, while the others have been derived from field data. Basically, all of the methods give similar corrections for $\bar{\sigma}_{vo} > 0.5 p_a$, within the expected accuracy of the SPT. Therefore, the simplest equation for C_N can be used for this depth range, as given below by Liao and Whitman [27]:

$$C_N = (p_a / \bar{\sigma}_{vo})^{0.5} \quad (4)$$

in which $\bar{\sigma}_{vo}$ = effective vertical overburden stress and p_a = atmospheric pressure (1.013 bars = 1.058 tsf = 1.033 kg/cm² = 101.3 kN/m²) to provide dimensionless units. However, for shallower depths where $\bar{\sigma}_{vo} < 0.5 p_a$, significant

TABLE I. SPT correction factors for field procedures (based on Skempton, 1986)

Factor	Equipment Variables	Correction	
		Term	Value
Energy ratio	Safety hammer	C_{ER}	0.9
	Donut hammer		0.75
Borehole diameter	65 to 115 mm (2.5 to 4.5 in.)	C_B	1.0
	150 mm (6 in.)		1.05
	200 mm (8 in.)		1.15
Sampling method	Standard sampler	C_S	1.0
	Sampler without liner		1.2
Rod length	> 10 m (> 30 ft)	C_R	1.0
	6 to 10 m (20 to 30 ft)		0.95
	4 to 6 m (13 to 20 ft)		0.85
	3 to 4 m (10 to 13 ft)		0.75

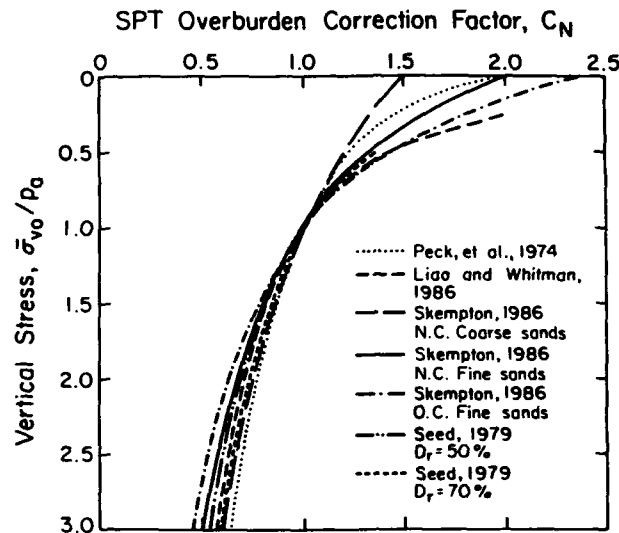


FIG. 1. Comparison of SPT overburden corrections

variations occur among the proposed C_N values. Within this range, it is prudent to evaluate the field data carefully because substantial uncertainties are present in evaluating C_N . For reference, Skempton's equation for C_N is:

$$C_N = (C_a C_b + 1) / (C_a C_b + \bar{\sigma}_{vo}/P_a) \quad (5)$$

in which $C_a = 1$ for fine and 2 for coarse sand, and $C_b = 1$ for normally consolidated and 0.7 for overconsolidated sand. Values of C_N greater than those given by Eq. 5 appear to be likely at shallow depths [e.g., 27, 39].

Once the measured N value has been corrected for both field procedures and overburden stress effects, it can be used to evaluate the relative density as a function of the soil characteristics. Commonly, these evaluations are done using the term $(N_1)_{60}/D_r^2$. Figure 2 shows the effect of particle size on $(N_1)_{60}/D_r^2$. The laboratory data in this figure were obtained from laboratory studies at the Waterways Experiment Station (WES) on Platte River Sand ($D_{50} = 2.10$ mm), Standard Concrete Sand ($D_{50} = 0.50$ mm), and Reid Bedford Model Sand ($D_{50} = 0.25$ mm) [8, 9, 29]. Most of the data were for unaged, normally consolidated (NC) sands (overconsolidation ratio OCR = 1), although a series of tests on the Reid Bedford Model Sand was conducted in an overconsolidated state with OCR = 3. Skempton's interpretation of these data is shown, but it is believed that the averaged curves he used led to an underestimation of $(N_1)_{60}/D_r^2$. Table II gives a re-evaluation of all of the WES data using both Skempton's C_N factor (Eq. 5) and Liao and Whitman's C_N factor (Eq. 4). Both regressions give higher values of $(N_1)_{60}/D_r^2$ than Skempton, with the Liao and Whitman C_N factor yielding higher coefficients of determination (r^2). These results can be approximated as follows:

$$(N_1)_{60}/D_r^2 = 60 + 25 \log D_{50} \quad (\text{with } D_{50} \text{ in mm}) \quad (6)$$

which is applicable for NC, unaged sands.

Figure 2 also shows that overconsolidation and aging increase the value of $(N_1)_{60}/D_r^2$. The WES data include OCR = 1 and OCR = 3. The Niigata data on NC, aged sand were tabulated by Skempton, but they were re-evaluated

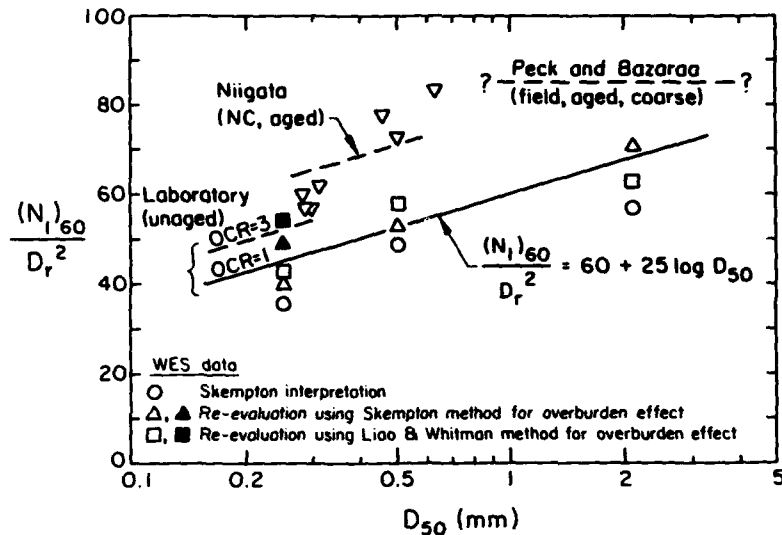


FIG. 2. Particle size effect on blow count for sands

TABLE II. Re-evaluation of WES data for $(N_1)_{60}/D_r^2$

Sand	Skempton $(N_1)_{60}/D_r^2$	Regression Re-evaluation Results			
		Eq. 5 for C_N		Eq. 4 for C_N	
		$(N_1)_{60}/D_r^2$	r^2	$(N_1)_{60}/D_r^2$	r^2
Platte River	57	20	0.54	63	0.88
Standard Concrete	49	20	0.70	58	0.95
Reid Bedford (OCR = 1)	36	113	0.44	43	0.76
Reid Bedford (OCR = 3)	47	12	0.79	55	0.76

individually. The Peck and Bazaraa [39] results are for coarser sands (no exact particle size given) from field test evaluations. These results would represent a range of "typical" aged and overconsolidated conditions.

Figure 3 illustrates the data as a function of age of the deposits. The WES laboratory data are plotted at an age of several days. The Niigata, Ogi-shima, and Kawagishi data summarized by Skempton represent NC recent fills that were assigned approximate ages of 30 to 40 years. The time is not known for the OC, aged results from Peck and Bazaraa, so it is estimated at 100 to 10,000 years. The other four sites (A, B, C, D) are given by Barton, et al. [5]. They represent OC, aged, fine and fine to medium sands of four geologic periods, as noted.

Based on Figures 2 and 3, it is clear that particle size, aging, and over-consolidation significantly influence the value of $(N_1)_{60}/D_r^2$. These effects can be quantified as follows:

$$D_r^2 = (N_1)_{60} / (C_P C_A C_{OCR}) \quad (7)$$

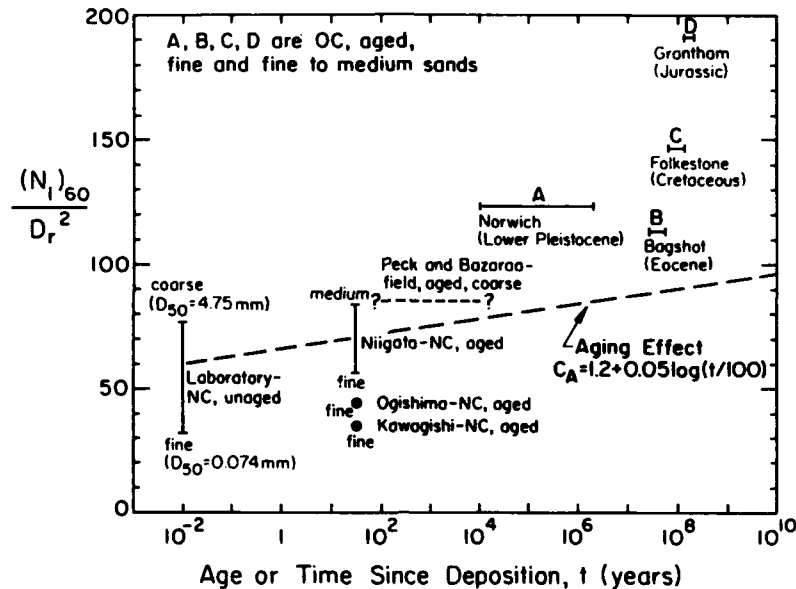


FIG. 3. Aging effect on blow count for sands

in which C_p , C_A , and C_{OCR} are the correction factors given in Table III. C_p is based on Figure 2. C_A is based on a conservative interpretation of the imprecise data in Figure 3. C_{OCR} is based on direct evaluation of the WES data and interpretation of the Peck and Bazaraa and Barton, et al. results. It also is consistent with the studies presented by Tokimatsu [49] on normalized N values.

Finally, the complete expression for relative density (D_r) in terms of the SPT N value, including all corrections and modifying terms, is:

$$D_r^2 = \frac{C_{ER} C_B C_S C_R C_N N}{C_p C_A C_{OCR}} \quad (\text{with } D_r \text{ in decimal form}) \quad (8)$$

in which N = measured N value and the corrections are as follows: energy ratio (C_{ER}), borehole diameter (C_B), sampling method (C_S), rod length (C_R), overburden stress (C_N), particle size (C_p), aging (C_A), and overconsolidation (C_{OCR}).

CONE PENETRATION TEST (CPT) RELATIONSHIP

The electric cone penetration test (CPT) has become perhaps the second

TABLE III. SPT correction factors for soil variables

Effect	Parameter	Correction	
		Term	Value
Particle Size	D_{50} of sand (in mm)	C_p	$60 + 25 \log D_{50}$
Aging	Time (t in years)	C_A	$1.2 + 0.05 \log (t/100)$
Overconsolidation	$OCR = \bar{\sigma}_p / \bar{\sigma}_{vo}$	C_{OCR}	$OCR^{0.18}$

most common penetration test in the U.S. In various parts of the world, it is the most common test. Numerous correlations also have been developed between the CPT test measurements (q_c = tip resistance, f_s = side resistance) and a number of soil properties or indices. As with the SPT, very early correlations attempted to link D_r with q_c directly. However, it was learned quickly that the relationship between D_r and q_c is not that simple.

In contrast with the SPT, where the relationships were developed primarily from studies on natural sands in the field, the CPT studies have been conducted largely on reconstituted sands in calibration chambers in the laboratory. Based on these studies, a number of D_r - q_c relationships have been proposed [e.g., 20], in which experimental constants are required that are particular to the specific sand being tested in the laboratory. Unfortunately, these constants have not been correlated directly with basic soil properties.

One of the main problems in using the calibration chamber studies has been the effect of boundary conditions on the resulting CPT measurements. These boundary effects have been noted for some time [e.g., 37], and an early form of correction factor was presented by Jamiolkowski, et al. [19], based on data obtained from tests on only two clean sands. However, these corrections are not unique. The approach given by Mayne and Kulhawy [32] is more general and is representative of a fairly wide range of sands. Therefore, it is used in this paper.

For many years, it has been demonstrated that there is generally a linear correspondence between q_c and N [e.g., 34, 41]. Therefore, it is reasonable to assume that D_r will vary with q_c in a comparable manner as D_r varies with N . As shown previously, D_r^2 varies linearly with N , taking into account the types of corrections for field procedures, reference stress level, and soil variables. The first type relates only to the SPT, where energy input at the top of the rods is correlated to the N value measured at the bottom of the borehole. In contrast, the q_c values are measured at the tip directly, so no corrections for field procedures are needed. However, corrections are necessary for the reference stress level and soil variables.

For the stress level, the normalized cone tip resistance (Q_{CD}) is given by:

$$Q_{CD} = C_q (q_c/p_a) = (q_c/p_a)/(\sigma_{vo}/p_a)^{0.5} \quad (9)$$

in which p_a = atmospheric pressure and $C_q = C_N$ as given by Eq. 4. This form of normalizing q_c is common in the literature. It may be possible to refine the exponent to 0.6 or 0.7, as suggested by Jamiolkowski, et al. [20]; however, Parkin [38] recommends that 0.5 be used since the differences are minimal. In addition, this power function is consistent with recommendations given by Liao and Whitman [27] for the SPT.

The corrected calibration chamber data summarized by Mayne and Kulhawy [32] for NC, unaged, uncemented sands are presented in Figure 4. In all cases, a linear relationship was obtained for D_r^2 versus Q_{CD} . Following conventional recommendations [e.g., 3, 41], the NC sands were separated into three categories represented by low, medium, and high compressibilities. Low compressibility (Figure 4a) generally corresponds to quartz sands with little, if any, fines. Medium compressibility (Figure 4b) includes quartz sands with some feldspar. High compressibility (Figure 4c) indicates sands with small percentages of fines, mica, and other compressible minerals. Most natural sands likely will be more toward the medium to high range of compressibility. As shown in these figures, the correlation is good below the limit of possible particle crushing. This limit was established by statistical analysis of the data, optimizing r^2 as a function of different limiting Q_{CD} values from 250 up to the entire data set. The limiting Q_{CD} values shown provide the maximum r^2 for the data and define the boundary of possible particle crushing. Similar limiting values of q_c for defining the grain crushing region were suggested by Veismanis [50] and Holden [18].

Figure 5 shows comparable calibration chamber data on OC sands of mixed compressibility. For these sands, the data have been separated into three

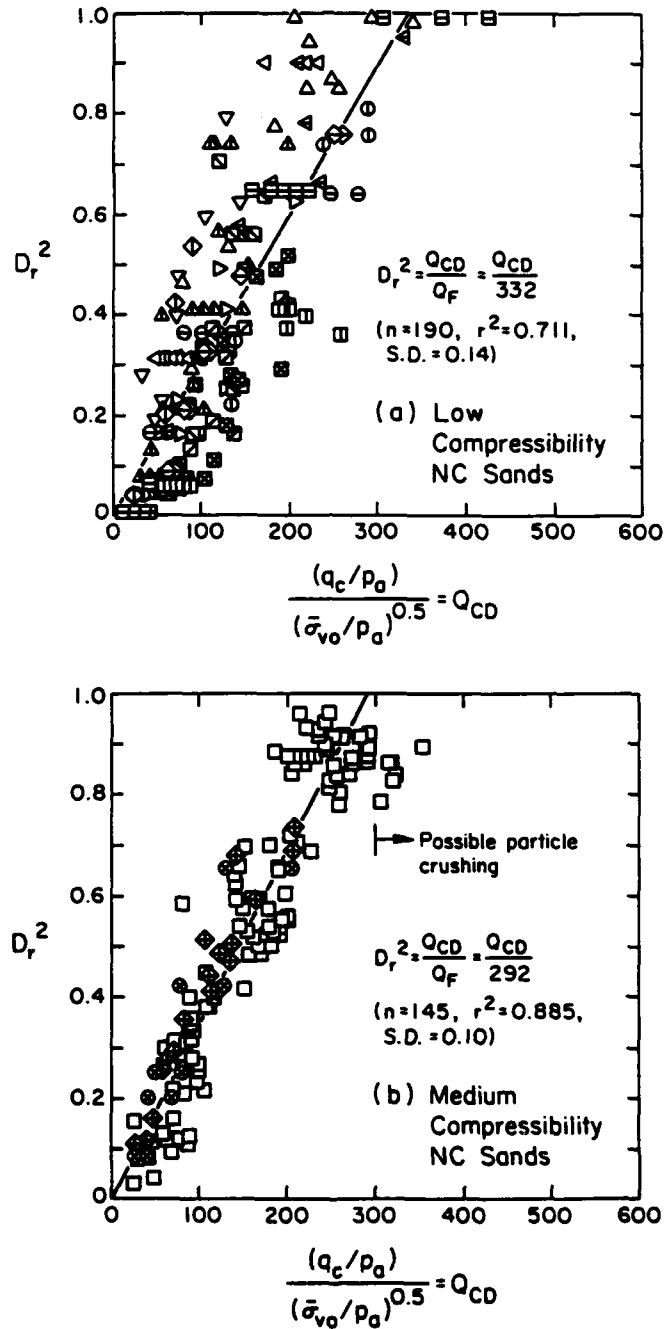


FIG. 4. Calibration chamber data on NC sands

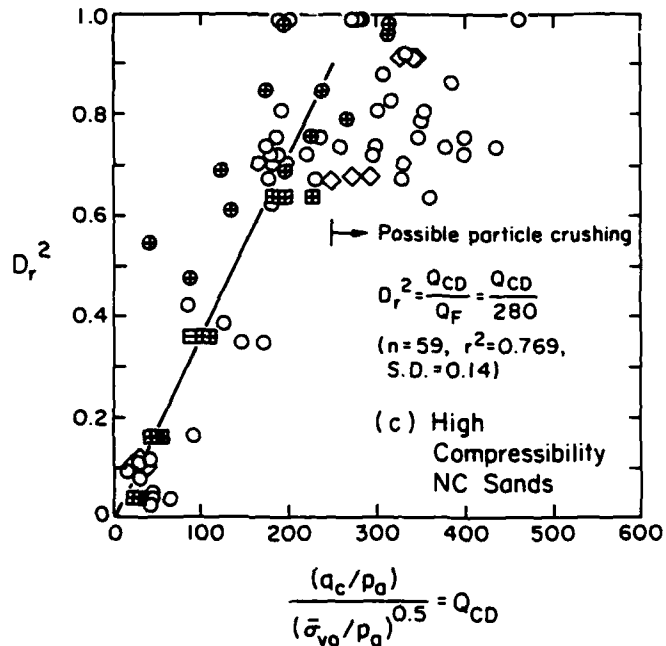


FIG. 4. Calibration chamber data on NC sands (continued)

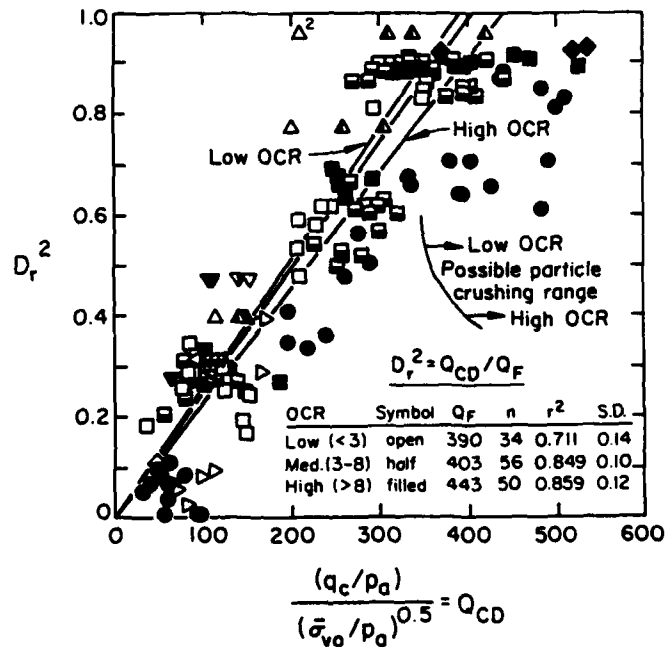


FIG. 5. Calibration chamber data on OC sands

categories based on distinct ranges of overconsolidation: low ($OCR < 3$), medium ($3 < OCR < 8$), and high ($8 < OCR < 15$). These data also were optimized using r^2 criteria for different Q_{CD} limiting values, resulting in the regression lines and possible particle crushing limits shown.

A summary of these relationships is given in Figure 6 for all of the corrected calibration chamber data. This figure clearly shows the influence of compressibility and OCR on the relationship between D_r^2 and dimensionless cone tip resistance. These relationships can be quantified approximately as follows:

$$D_r^2 = \frac{Q_{CD}}{Q_F} = \frac{C_q (q_c/p_a)}{305 Q_C Q_{OCR}} \quad (10)$$

in which Q_F = overall cone factor for all soil variables, Q_C = compressibility factor (0.91 for high, 1.0 for medium, and 1.09 for low), and Q_{OCR} = overconsolidation factor ($= OCR^{0.18}$), similar to C_{OCR} for the standard penetration test. (Note that Tokimatsu [49] suggested that both SPT and CPT resistances vary similarly with OCR.) The Q_{OCR} factor was evaluated using the mean OCR values for the low, medium, and high OCR data equal to 2.3, 5.1, and 10.1, respectively. The majority of natural sands are likely to be of medium to high compressibility and low to medium OCR.

Examination of Eq. 8 for the SPT N value and Eq. 10 for the CPT q_c value shows some important similarities. The overburden stress effect is the same, as is the influence of OCR. However, the N correlation includes variations from particle size while the q_c correlation includes variations from soil mass compressibility. It is likely that the different databases have influenced the relative importance of these parameters.

Perhaps the most important difference between the N and q_c relationships

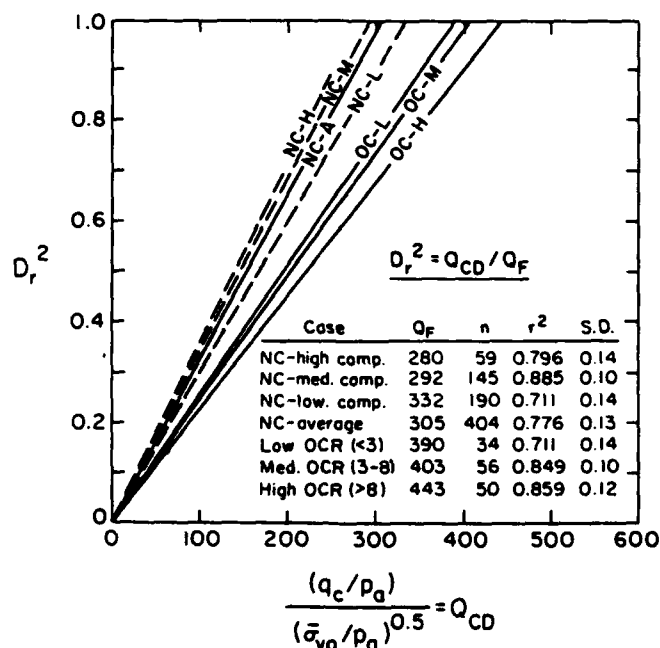


FIG. 6. Summary of calibration chamber studies

is the influence of aging. Eq. 8 includes aging directly, but Eq. 10 is applicable only for unaged sands. Presuming that the same functional relationship for aging holds for both N and q_c , as is probable considering all other similarities, then Eq. 10 would be modified as follows:

$$D_r^2 = \frac{C_q (q_c/P_a)}{305 C_A Q_c Q_{OCR}} \quad (11)$$

with C_A as given in Table III. This aging correction is somewhat speculative at this time in terms of precise magnitude. However, the general changes with aging are at least qualitatively explained by this correction [e.g., 21, 35, 44]. Clarification of this aging issue will be needed in the future.

GENERALIZATION TO OTHER CONE TYPES

Correlations developed for electric cones can not be used directly for mechanical cones since these cones do not give the same results, largely because of the different cone geometries. The traditional mechanical cones, such as the Delft, Begemann, and Gouda cones, all have a reduction in diameter behind the cone tip. In contrast, the Fugro electric cone (essentially the de facto standard) has the same tip and sleeve diameter. Several approximate relationships between these cone types have been suggested [e.g., 1, 4, 42, 43, 48]. In general, these proposals note that q_c (electric) $>$ q_c (mechanical) for sands, while the reverse is true in clays and silts. To generalize these observations, data were summarized from 14 sands and 10 clays and silts that were tested using both Fugro electric and several mechanical cones. The results are shown in Figure 7 and indicate a very good correlation.

It also should be noted that CPT results can vary as a function of electric cone type. A recent study by Lunne, et al. [28] compared the results of 14 different types of commercially-available electric cones in the same sand. The variations in q_c were relatively small, but values of the side resistance (f_s) varied dramatically, in some cases by a factor of 3. These results undoubtedly would influence all interpretations made from the test results, so it is prudent to conduct verification and local calibration tests with specific CPT equipment.

The introduction of the piezocone (CPTU) and the resulting comparative studies of the CPT and CPTU have shown that all cones require a correction for pore water stresses acting on any unequal areas of the cone. A further complication with the piezocone is that its design has not yet been standardized [e.g., 11]. Most commercially-available piezocones place the porous element either on the cone tip face or just behind the cone tip. Technically, the measurement of pore water stresses behind the tip (u_{bt}) is required to correct the cone tip resistance (q_c) for pore water stresses acting on unequal areas of the cone. On the other hand, pore water stress measurements on the cone tip or face provide the maximum reading, which may be best for delineation of stratigraphy. Appropriate corrections for piezocones are addressed by Mayne, et al. [33].

INTERRELATIONSHIP BETWEEN SPT N AND ELECTRIC CPT q_c VALUES

Because of the numerous correlations developed for either SPT or CPT data, it is advantageous to have a procedure to interrelate N and the reference q_c from the electric cone. Both are penetration resistances (although the SPT is dynamic and the CPT is quasi-static), and they are the most common forms of in-situ testing used worldwide today. A number of investigators have proposed single numerical values of q_c/N . However, studies by Robertson and Campanella [41] showed that q_c/N may be correlated with grain size. Newer data have been combined with the previous data from Robertson and Campanella to result in

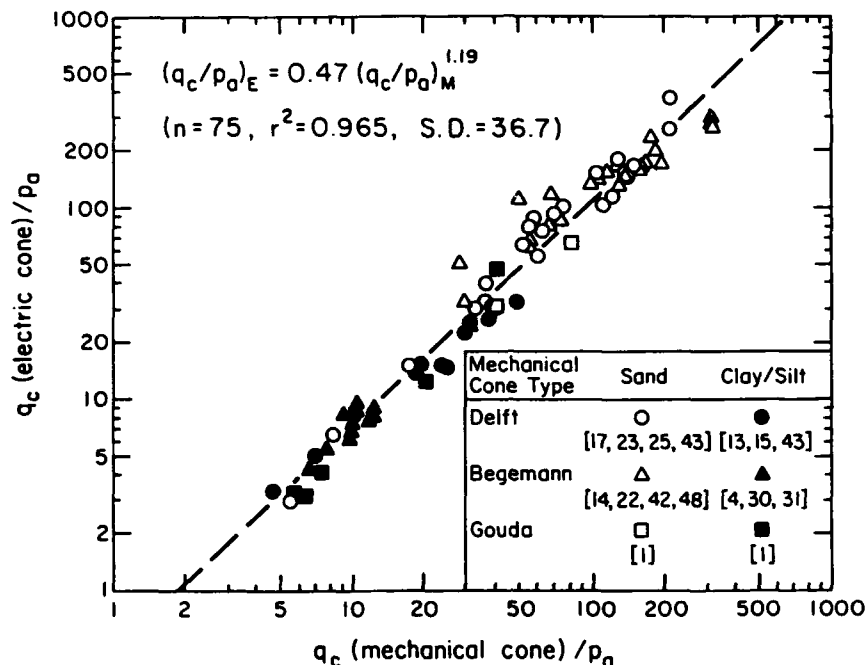


FIG. 7. Correlation of q_c between Fugro electric cone and three mechanical cone types

Figure 8. This new relationship generally confirms the trend of the data, and it extends the relationship to mean grain sizes up to 10 mm. The solid line represents the regression equation for the full data set.

In other studies, the ratio of q_c/N has been correlated to the percentage of fines (clay and silt sizes). For example, Jamiolkowski, et al. [20] indicate the trend presented in Figure 9 for Italian soils. In addition to these data, other available data were summarized to substantiate a general trend between q_c/N and fines content, as shown in Figure 10. Use of Figures 8 and 10 will provide the best estimate relationship between q_c and N , with the ratio decreasing with increasing fines content.

SUMMARY AND CONCLUSIONS

Relative density can be evaluated from the results of SPT and CPT tests, as long as corrections are made for field procedures, overburden stress, and soil variables. The soil variables include grain size, compressibility, overconsolidation, and aging. Extensions are made to include most CPT types, and a simple relationship is given to relate q_c for different cone types. Direct relationships between the SPT N value and the CPT q_c value are examined and are shown to be a function of several soil variables. Understanding the various interrelationships presented will lead to an improved appreciation of field tests and soil variables.

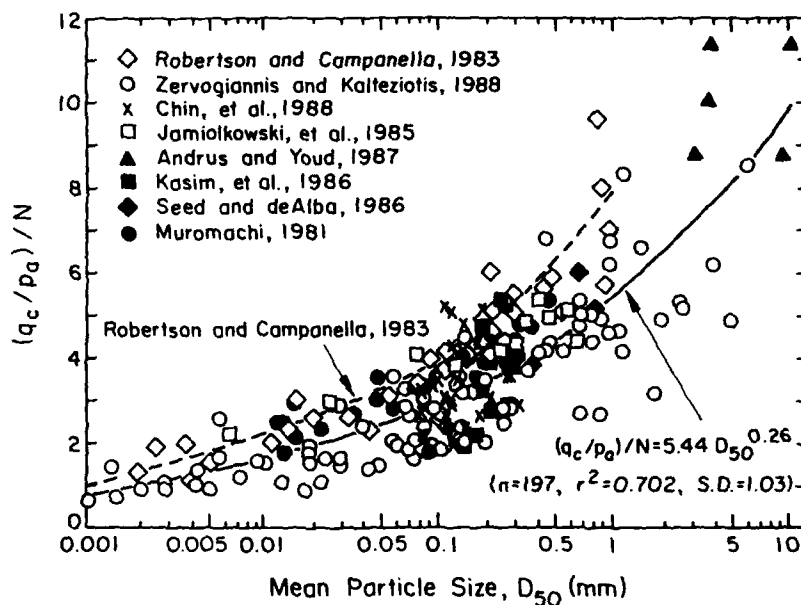


FIG. 8. Variation of q_c/N with grain size for Fugro electric cone

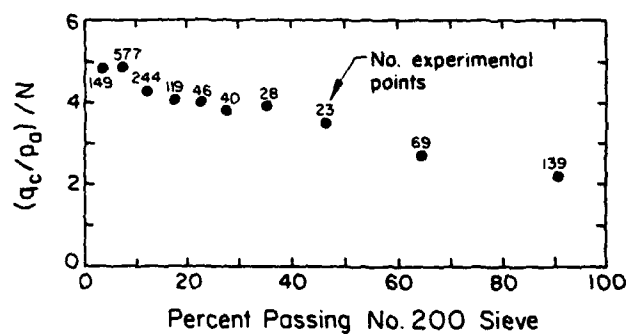


FIG. 9. Variation of q_c/N with fines content (Source: Jamiolkowski, et al. [20], p. 1895)

ACKNOWLEDGMENTS

This study was supported by the Electric Power Research Institute under RP1493-6, and it has been previously reported in EPRI Report EL-6800 [26]. Vito J. Longo was the EPRI project manager. A. Avcişoy prepared the figures, and L. Mayes and K. J. Stewart prepared the text.

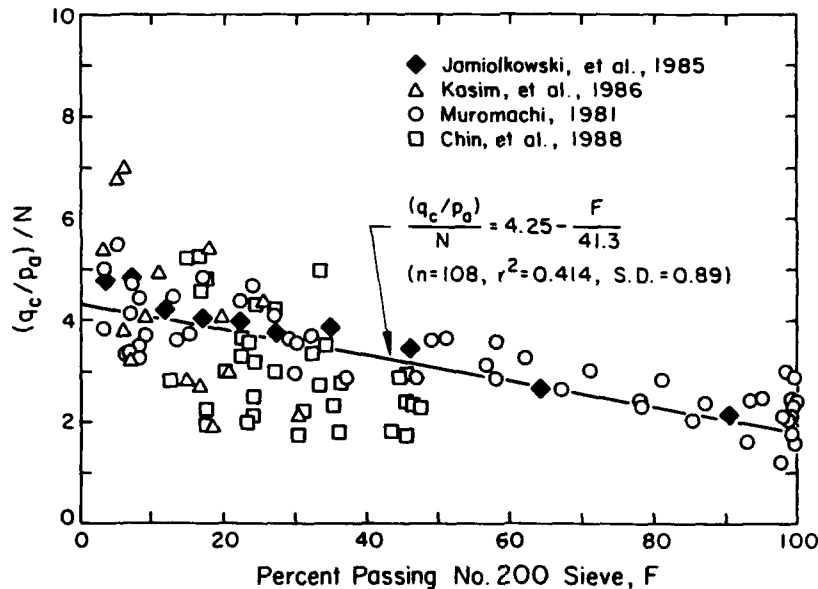


FIG. 10. Recommended variation of q_c/N with fines content

REFERENCES

1. S. Amar, "Use of Static Penetrometer in Laboratoires des Ponts et Chaussées", Proc. Eur. Symp. Pen. Test. (2.2), Stockholm, 7-12 (1974).
2. R.D. Andrus and T.L. Youd, "Subsurface Investigation of a Liquefaction-Induced Lateral Spread, Thousand Springs Valley, Idaho", Misc. Paper GL-87-8, U.S. Army Eng. Waterways Exp. Sta., Vicksburg, 131 p. (1987).
3. G. Baldi, R. Bellotti, V. Ghionna, M. Jamiolkowski, and E. Pasqualini, "Design Parameters for Sands from CPT", Proc. 2nd Eur. Symp. Pen. Test. (2), Amsterdam, 425-432 (1982).
4. M.M. Baligh, V. Vivatrat, and C.C. Ladd, "Exploration and Evaluation of Engineering Properties for Foundation Design of Offshore Structures", Civil Eng. Rpt. R78-40, M.I.T., Cambridge, 268 p. (1978).
5. M.E. Barton, M.R. Cooper, and S.N. Palmer, "Diagenetic Alteration and Micro-Structural Characteristics of Sands", Pen. Test. in U.K., Thomas Telford, London, 57-60 (1988).
6. K. Been, J.H.A. Crooks, D.E. Becker, and M.G. Jefferies, "Cone Penetration Test in Sands: Part I, State Parameter Interpretation", Geotechnique, 36 (2), 239-249 (1986).
7. K. Been, M.G. Jefferies, J.H.A. Crooks, and L. Rothenburg, "Cone Penetration Test in Sands: Part II, General Inference of State", Geotechnique, 37 (3), 285-299 (1987).
8. W.A. Bieganousky and W.F. Marcuson III, "Laboratory Standard Penetration Tests on Reid Bedford Model and Ottawa Sands", Res. Rpt. S-76-2 (1), U.S. Army Eng. Waterways Exp. Sta., Vicksburg, 156 p. (1976).
9. W.A. Bieganousky and W.F. Marcuson III, "Laboratory Standard Penetration Tests on Platte River Sand and Standard Concrete Sand", Res. Rpt. S-76-2 (2), U.S. Army Eng. Waterways Exp. Sta., Vicksburg, 87 p. (1977).
10. M.D. Bolton, "Strength and Dilatancy of Sands", Geotechnique, 36 (1), 65-78 (1986).

11. R.G. Campanella and P.K. Robertson, "Current Status of Piezocone Test", Proc. 1st Intl. Symp. Pen. Test. (1), Orlando, 93-116 (1988).
12. C.T. Chin, S.W. Duann, and T.C. Kao, "SPT-CPT Correlations for Granular Soils", Proc. 1st Intl. Symp. Pen. Test. (1), Orlando, 335-339 (1988).
13. E.E. De Beer, "Scale Effects in Results of Penetration Tests Performed in Stiff Clays", Proc. Eur. Symp. Pen. Test. (2.2), Stockholm, 105-115 (1974).
14. J. De Ruiter, "Electric Penetrometer for Site Investigations", J. Soil Mech. & Fndns. Div. (ASCE), 97 (SM2), 457-472 (1971).
15. M.J.D. Dobie, "Study of Cone Penetration Tests in Singapore Marine Clay", Proc. 1st Intl. Symp. Pen. Test. (2), Orlando, 737-744 (1988).
16. H.J. Gibbs and W.G. Holtz, "Research on Determining Density of Sands by Spoon Penetration Testing", Proc. 4th Intl. Conf. Soil Mech. & Fndn. Eng. (1), London, 35-39 (1957).
17. W.J. Heijnen, "Dutch Cone Test: Study of Shape of Electrical Cone", Proc. 8th Intl. Conf. Soil Mech. & Fndn. Eng. (1.1), Moscow, 79-83 (1973).
18. J.C. Holden, "Determination of Deformation and Shear Strength Parameters for Sands Using Electrical Friction Cone Penetrometer", Rpt. 110, Norwegian Geot. Inst., Oslo, 55-60 (1976).
19. M. Jamiolkowski, C.C. Ladd, J. Germaine, and R. Lancellotta, "New Developments in Field and Laboratory Testing of Soils", Proc. 11th Intl. Conf. Soil Mech. & Fndn. Eng. (1), San Francisco, 57-154 (1985).
20. M. Jamiolkowski, G. Baldi, R. Bellotti, V. Chionna, and E. Pasqualini, "Penetration Resistance and Liquefaction of Sands", Proc. 11th Intl. Conf. Soil Mech. & Fndn. Eng. (4), San Francisco, 1891-1896 (1985).
21. M. Jamiolkowski, V. Chionna, R. Lancellotta, and E. Pasqualini, "New Correlations of Penetration Tests for Design Practice", Proc. 1st Intl. Symp. Pen. Test. (1), Orlando, 263-296 (1988).
22. G. Jones and E. Rust, "Piezometer Penetration Testing", Proc. 2nd Eur. Symp. Pen. Test. (2), Amsterdam, 607-613 (1982).
23. K. Jousstra, "Comparative Measurements on Influence of Cone Shape on Results of Soundings", Proc. Eur. Symp. Pen. Test. (2.2), Stockholm, 199-200 (1974).
24. A.G. Kasim, M.Y. Chu, and C.N. Jensen, "Field Correlation of Cone and Standard Penetration Tests", J. Geot. Eng. (ASCE), 112 (3), 368-372 (1986).
25. L. Kok, "Effect of Penetration Speed and Cone Shape on CPT Results", Proc. Eur. Symp. Pen. Test. (2.2), Stockholm, 215-216 (1974).
26. F.H. Kulhawy and P.W. Mayne, "Manual on Estimating Soil Properties for Foundation Design", Rpt. EL-6800, Elec. Power Res. Inst., Palo Alto, 306 p. (1990).
27. S.S. Liao and R.V. Whitman, "Overburden Correction Factors for SPT in Sand", J. Geot. Eng. (ASCE), 112 (3), 373-377 (1986).
28. T. Lunne, D. Eidsmoen, D. Gillespie, and J. Howland, "Laboratory and Field Evaluation of Cone Penetrometers", Use of In-Situ Tests in Geot. Eng. (GSP 6), Ed. S.P. Clemence, ASCE, New York, 714-729 (1986).
29. W.F. Marcuson III and W.A. Bieganski, "SPT and Relative Density in Coarse Sands", J. Geot. Eng. Div. (ASCE), 103 (GT11), 1295-1309 (1977).
30. P.W. Mayne, D.D. Frost, and P.G. Swanson, "Geot. Rpt., CEBAF Project, Newport News, VA", Law Eng. NK5-1182 to DMJM, Washington, 580 p. (1986).
31. P.W. Mayne and J.B. Kemper, "Profiling OCR in Stiff Clays by CPT and SPT", Geot. Test. J. (ASTM), 11 (2), 139-147 (1988).
32. P.W. Mayne and F.H. Kulhawy, "Calibration Chamber Database and Boundary Effects Correction for CPT Data", This proc. vol. (1991).
33. P.W. Mayne, F.H. Kulhawy, and J.N. Kay, "Observations on the Development of Pore Water Stresses During Cone Penetration in Clays", Can. Geot. J., 27 (4), 418-428 (1990).
34. G.G. Meyerhof, "Penetration Tests and Bearing Capacity of Cohesionless Soils", J. Soil Mech. & Fndns. Div. (ASCE), 82 (SM1), 1-19 (1956).
35. J.K. Mitchell, "Practical Problems from Surprising Soil Behavior", J. Geot. Eng. (ASCE), 112 (3), 255-289 (1986).

36. T. Muromachi, "Cone Penetration Testing in Japan", *Cone Pen. Test. & Exp.*, Ed. G.M. Norris & R.D. Holtz, ASCE, New York, 49-75 (1981).
37. A.K. Parkin and T. Lunne, "Boundary Effects in Laboratory Calibration of Cone Penetrometer for Sand", *Proc. 2nd Eur. Symp. Pen. Test.* (2), Amsterdam, 761-768 (1982).
38. A.K. Parkin, "Calibration of Cone Penetrometers", *Proc. 1st Intl. Symp. Pen. Test.* (1), Orlando, 221-244 (1988).
39. R.B. Peck and A.R.S. Bazaraa, Discussion of "Settlement of Spread Footings on Sand", *J. Soil Mech. & Fndns. Div. (ASCE)*, 95 (SM3), 905-909 (1969).
40. R.B. Peck, W.E. Hanson, and T.H. Thornburn, *Foundation Engineering*, 2nd Ed., Wiley, New York, 311-314 (1974).
41. P.K. Robertson and R.G. Campanella, "Interpretation of Cone Penetration Tests: Sand", *Can. Geot. J.*, 20 (4), 718-733 (1983).
42. A.H. Rol, "Comparative Study on Cone Resistances Measured with Three Types of CPT Tips", *Proc. 2nd Eur. Symp. Pen. Test.* (2), Amsterdam, 813-819 (1982).
43. J.H. Schmertmann, "Guidelines for Cone Penetration Test Performance and Design", *Rpt. FHWA-TS-78-209*, Fed. Highway Admin., Washington, 145 p. (1978).
44. J.H. Schmertmann, "Mechanical Aging of Soils", 25th Terzaghi Lecture Presented at ASCE Annual Meeting, New Orleans, 10 Oct. 1989.
45. H.B. Seed, "Soil Liquefaction and Cyclic Mobility Evaluation for Level Ground During Earthquakes", *J. Geot. Eng. Div. (ASCE)*, 105 (GT2), 201-255 (1979).
46. H.B. Seed and P. de Alba, "Use of SPT and CPT Tests for Evaluating Liquefaction Resistance of Sands", *Use of In-Situ Tests in Geot. Eng. (GSP 6)*, Ed. S.P. Clemence, ASCE, New York, 281-302 (1986).
47. A.W. Skempton, "Standard Penetration Test Procedures and Effects in Sands of Overburden Pressure, Relative Density, Particle Size, Ageing, and Overconsolidation", *Geotechnique*, 36 (3), 425-447 (1986).
48. F.P. Smits, "Cone Penetration Tests in Dry Sand", *Proc. 2nd Eur. Symp. Pen. Test.* (2), Amsterdam, 887-881 (1982).
49. K. Tokimatsu, "Penetration Tests for Dynamic Problems", *Proc. 1st Intl. Symp. Pen. Test.* (1), Orlando, 117-136 (1988).
50. A. Veismanis, "Laboratory Investigation of Electrical Friction Cone Penetrometers in Sand", *Proc. Eur. Symp. Pen. Test.* (2.2), Stockholm, 407-419 (1974).
51. C.S. Zervogiannis and N.A. Kalteziotis, "Experiences and Relationships from Penetration Testing in Greece", *Proc. 1st Intl. Symp. Pen. Test.* (2), Orlando, 1063-1071 (1988).

LABORATORY INVESTIGATION OF SMALL STRAIN MODULUS ANISOTROPY IN SAND

D. LoPresti* and D. A. O'Neill**
with ENEL-CRIS, Via Ornato, 90/14, 20100 Milan, Italy; *Technical
University, Corso Duca degli Abruzzi, 24, 10129 Turin, Italy; **ISMES SpA,
Via Pastrengo, 9, 24068 Seriate (BG), Italy

INTRODUCTION

The testing technique and initial results obtained from seismic tests performed in the ISMES calibration chamber on dry specimens of Ticino Sand are presented in this paper. The experimental program was designed to investigate the anisotropy of the small strain elastic moduli in pluvially deposited, uniform sand specimens. Stress level effects on the small strain stiffness also come into consideration.

Many authors (e.g. [9]) have shown that the strains associated with typical working loads are relatively small, less than 0.05% to 0.1%. Consequently, adequate geotechnical analysis of deformations for situations far from failure require knowledge of stiffnesses characteristic of the soil at strains ranging from very small (less than 0.001%) up to approximately 1%. The dependence of sand stiffness on stress and strain levels over this strain interval is relatively well documented in the literature. The anisotropy of stress-strain behavior at small strains, on the other hand, has received far less attention notwithstanding the generally recognized anisotropic nature of sands.

Vibrations imparted to the soil during the seismic measurements result in shear strains less than 0.0003% and thus the moduli calculated refer to very small strain levels. Since these strain levels are less than 0.001%, it is the maximum, or initial, modulus which is determined, that which is truly linearly elastic, i.e. independent of strain level [7].

To fully describe the anisotropy of the specimen, the elastic modulus must be evaluated in various directions with respect to the deposition direction. Use of Love's simplified anisotropic (transversely isotropic) elastic model [12] requires experimental determination of five independent material parameters, all of which can be obtained by measuring seismic shear (S) and compression (P) wave propagation velocities in vertical and horizontal directions and in one oblique direction [10]. The internal, geophone-based technique for use in large calibration chamber, dry sand specimens described herein is particularly well-adapted to such an investigation as all moduli of interest can be studied in one specimen. Errors that typically accompany use of different specimens or, even worse, different test devices are thus eliminated. This technique can only be used, however, for the measurement of the maximum stiffness and thus the significant degradation of the modulus with increasing, but still small (less than 0.1%) strain cannot be investigated.

Seismic measurements in large sand specimens have previously been studied, both in cylindrical calibration chambers [14] and in cubical chambers [10] [16], the latter of which is capable of applying true triaxial principal stress conditions.

APPARATUS AND TEST PROCEDURE

The tests were performed in the ISMES calibration chamber, the physical characteristics of which are described by Bellotti et al. [4]. In this chamber, the 1.2 m diameter, 1.4 m tall cylindrical specimens can be

Published 1991 by Elsevier Science Publishing Company, Inc.
Calibration Chamber Testing
Editor: A.-B. Huang

consolidated along any desired stress path. Subsequent penetration of various in situ instruments can be effected controlling the applied stress or strain boundary conditions in accordance with B1, B2, B3 or B4 specifications. Of relevance to this study are the physical boundary conditions wherein the membrane-encased specimen is surrounded by water in the lateral direction, a rigid steel top cap and a water-filled rubber cushion as a bottom boundary. These boundaries result in reflected waves which must be minimized.

Each dry sand specimen was pluviated through air using the travelling sand spreader which deposits one layer of sand at a time through a thin rectangular aperture at the bottom of a hopper oriented perpendicular to the travel direction. This device produces homogeneous specimens of relative density, D_r , varying between approximately 20% and 100% depending on the aperture width. The height of drop between the aperture and the soil surface is maintained at a constant 160 cm.

To effect the seismic velocity determination, miniature cylindrical geophones employed as both sources and receivers were positioned within the sand specimen during the deposition process. These velocity transducers (model no. L40 A-1, natural frequency = 60 Hz, of Mark Products, Houston, Texas) are 3.5 cm in length with a diameter equal to 3.1 cm. S wave velocities were studied by considering an array of geophones oriented side-by-side such that their cylindrical axes were perpendicular to the propagation direction while for P waves the geophones were oriented end-to-end with the geophone axis parallel to the direction of propagation.

A function generator and a power amplifier were used to control the character of the 50 V peak-to-peak signal sent to the source geophone. The frequency of the source wave (3000 Hz and 2000 Hz for P and S waves, respectively) was chosen such that the wavelength of the propagating vibration was greater than three times the size of any obstruction (e.g., geophone) in its path, and less than half the travel distance so as to avoid near field effects [15]. Received signals were conditioned by operational amplifiers and bandpass filters, one of each devoted to each receptor, and then observed on a two-channel digital oscilloscope. Filters, often avoided due to the distortion suffered by the conditioned signal, were necessary since the calibration chamber is not isolated from ambient vibrations. The equipment configuration is as indicated in Fig. 1.

Seismic velocities were interpreted in the time domain using the visual true interval method, wherein the signals from two receivers in response to a single source impulse are considered on the oscilloscope screen in the evaluation of the interval travel time. Thus, the substantial time delay errors associated with the conditioning equipment and the method of activating the source were avoided as were difficulties associated with identifying the actual time of arrival. To evaluate the most opportune reference point on the received wave the configuration in Fig. 1 was carefully studied using a dynamic signal analyser (Hewlett-Packard 3562A). On the basis of interpretation of the impulse response, slightly distorted due to the filter, the point on each received wave $1/4$ wavelength after the "arrival time" was chosen as the point of comparison.

Use of the true interval method requires use of a linear array of three geophones in the direction of interest for each measurement, as indicated schematically in Fig. 2. The three shear wave velocities studied in this research: S_{vh} , S_{hv} and S_{hh} ; and the two compression waves: P_v and P_h are also indicated. The notation used herein is such that the direction of wave propagation and polarization for S waves are identified by the first and second subscripts, respectively, while for P waves, propagation and vibration are in the same direction.

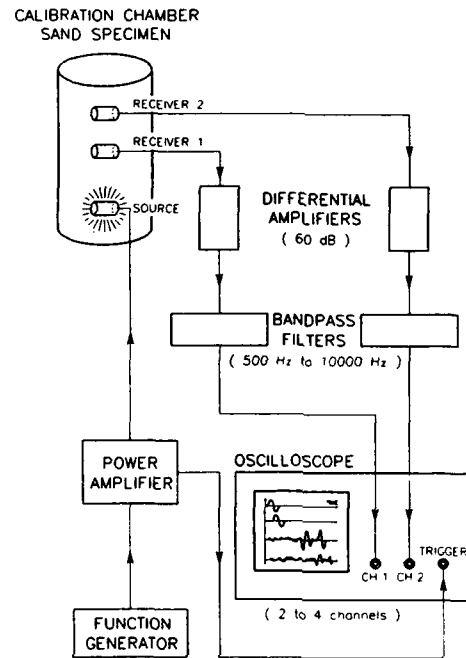


Figure 1. Seismic measurement equipment configuration.

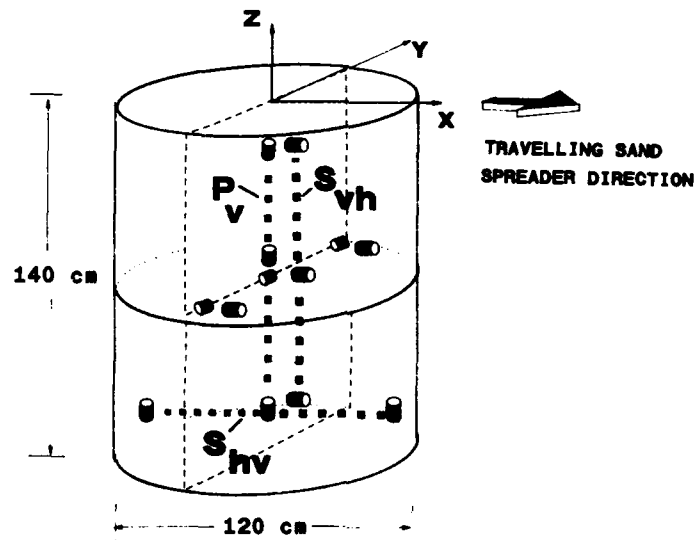


Figure 2. Distribution of geophones in the calibration chamber sand specimen.

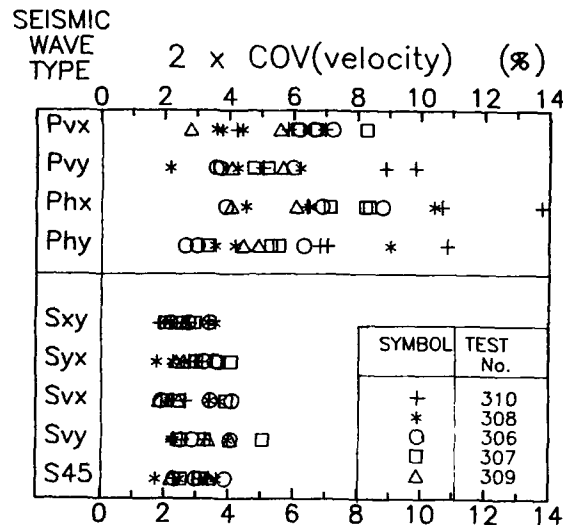


Figure 3. Coefficient of variation associated with the evaluation of seismic wave velocity in the calibration chamber.

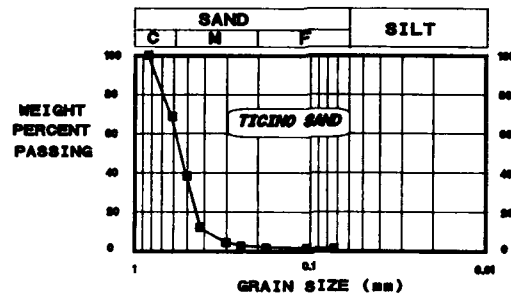
Interval travel time measurements were effected a minimum of 15 minutes after application of each consolidation stress increment. The stress state under which velocities are considered refers to the vertical and horizontal effective stress acting at the midpoint of the travel path (i.e., between the two receiving geophones). Separation distance was corrected for the strain incurred at a given stress level, assuming a linear strain distribution.

The error associated with this seismic technique has been interpreted in terms of repeatability of the measurement. Data presented in Fig. 3 represent the evaluation of six separate readings of the interval travel time using the same geophones at a given stress level. P and S wave travel time measurements from five different tests indicate standard deviations equal to ± 0.025 msec and 0.020 msec, respectively, resulting in 95% confidence level (two times the coefficient of variation) velocities equal to $\pm 6\%$ and $\pm 3\%$, respectively. The larger scatter associated with the P waves is largely due to their lower travel time.

TEST PROGRAM

The cohesionless soil investigated was medium to coarse Ticino sand, a soil of fluvial origin obtained from the Po river valley in northern Italy. The characteristics of Ticino sand are presented in Fig. 4. Over the past decade, this sand has received intensive attention in the laboratory, including numerous cone penetration, dilatometer and pressuremeter tests in the calibration chamber [3] [8], as well as exhaustive triaxial and resonant column test series [1] [2] [5] [17]. The seismic measurement test program comprised a total of 18 tests performed on 18 different dry sand, calibration chamber specimens. Two densities were considered: low medium ($D_r=35-45\%$) and very dense ($D_r=85-90\%$).

The program was designed to evaluate small strain modulus anisotropy in accordance with the cross anisotropic elastic model of Love [12], wherein



$$\gamma_{\text{MAX}} = 1700 \text{ kg/m}^3 \quad e_{\text{MIN}} = 0.582 \quad G_s = 2.65$$

$$\gamma_{\text{MIN}} = 1391 \text{ kg/m}^3 \quad e_{\text{MAX}} = 0.934 \quad C_u = 1.6$$

GEOMORPHOLOGY: angular (20 %), subangular (55 %),
subrounded (25 %).

SPHERICITY: 0.7 TO 0.8

MINERALOGY: QUARTZ (28%), FELDSPAR (30%)
MICA (5%), OPAQUES.

DESCRIPTION: UNIFORM COARSE TO MEDIUM SAND

Figure 4. Grain size characteristics of Ticino sand.

the horizontal plane is isotropic and strains are related to stresses as follows:

$$\begin{vmatrix} \sigma_x \\ \sigma_y \\ \sigma_z \\ \tau_{yz} \\ \tau_{zx} \\ \tau_{xy} \end{vmatrix} = \begin{vmatrix} C_{11} & C_{12} & C_{13} & 0 & 0 & 0 \\ C_{12} & C_{11} & C_{13} & 0 & 0 & 0 \\ C_{13} & C_{13} & C_{33} & 0 & 0 & 0 \\ 0 & 0 & 0 & C_{44} & 0 & 0 \\ 0 & 0 & 0 & 0 & C_{44} & 0 \\ 0 & 0 & 0 & 0 & 0 & C_{66} \end{vmatrix} \begin{vmatrix} \epsilon_x \\ \epsilon_y \\ \epsilon_z \\ \gamma_{yz} \\ \gamma_{zx} \\ \gamma_{xy} \end{vmatrix} \quad (1)$$

where: $\sigma_x, \sigma_y, \sigma_z$ = normal stresses
 $\tau_{yz}, \tau_{zx}, \tau_{xy}$ = shear stresses
 $\epsilon_x, \epsilon_y, \epsilon_z$ = normal strains
 $\gamma_{yz}, \gamma_{zx}, \gamma_{xy}$ = shear strains
 C_{11} = constrained modulus of the isotropic plane, M_h
 C_{33} = constrained modulus of the anisotropic plane, M_v
 C_{44} = shear modulus of the anisotropic plane, G_{vh}
 C_{66} = shear modulus of the isotropic plane, G_{hh}
 C_{13} = fifth independent parameter requiring oblique measurement
 $C_{12} = M_h - 2G_{hh}$ (dependent parameter)

According to elastic theory, the relationships between seismic velocities and the moduli are as follows:

$$G = \rho v_s^2 \quad (2)$$

$$M = \rho v_p^2 \quad (3)$$

where: G - elastic shear modulus
 M - elastic constrained modulus
 ρ - mass density of the soil
 V_s - shear wave velocity
 V_p - compression wave velocity

Specific moduli related to elements of the above stiffness matrix are associated with velocities of appropriate propagation and vibration directions. Measurements of C_{11} , C_{33} , C_{44} and C_{66} , simply related to vertical and horizontal measurements as indicated above were considered in the early stages of the test program. Additional measurements in an oblique direction are necessary for evaluation of C_{13} . Tests are currently underway in which travel times are being measured for P and S waves propagated 45 degrees from the horizontal.

Many definitions exist to describe the various types of anisotropy associated with various stages in the development of a soil deposit. Herein, definitions presented by Casagrande and Carillo [6] are considered in which inherent anisotropy refers to a "physical characteristic of the material and entirely independent of applied stresses" and induced (or evolving) anisotropy refers to that due to incurred strain associated with applied stresses. Inherent anisotropy was evaluated by subjecting the specimen to isotropic consolidation increments. Two such tests were performed, one each at D_r equal to 40% and 90%, up to stress levels of 600 kPa. Induced anisotropy was considered by subjecting the specimens to a constant consolidation stress ratio, K_c ($=\sigma'_h/\sigma'_v$) with tests employing K_c equal to 0.33, 0.5, 0.66 and 1.5 for $D_r=40\%$ and K_c equal to 0.5, 0.66 and 1.5 for the very dense specimens. The maximum stress levels varied with respect to the capacity of the calibration chamber, ranging from $\sigma'_v=600$ kPa for low K_c and dropping to 300 kPa for $K_c=1.5$.

The dependence of anisotropic elastic characteristics on stress level was accounted for within the framework proposed by Roesler [13] in which the principal effective stresses are considered in terms of their orientation with respect to the seismic wave propagation and vibration directions. The validity of these relationships as presented below has been confirmed by extensive studies at the University of Texas at Austin [16].

$$V_p = C_1 \sigma'_a{}^{2na} \sigma'_c{}^{nc} \quad (4)$$

$$V_s = C_2 \sigma'_a{}^{na} \sigma'_b{}^{nb} \sigma'_c{}^{nc} \quad (5)$$

where:

V_p - compression wave velocity
 V_s - shear wave velocity
 σ'_a - principal effective stress parallel to wave propagation direction
 σ'_b - principal effective stress parallel to wave polarization direction
 σ'_c - principal effective stress parallel to the out-of-plane direction
and C_1 , C_2 , na , nb and nc are experimentally determined parameters.

The exponents na , nb and nc for Ticino sand were evaluated by performing tests in which one of the two controllable applied principal stresses (axial or radial) was maintained constant while the other was increased in increments of 25 kPa or 50 kPa. After the application of each increment all wave interval travel times were measured. The biaxial nature of the calibration chamber limits the rigorous evaluation of this relationship in that the effect of σ'_c cannot be determined for S_{hv} or S_{vh} waves.

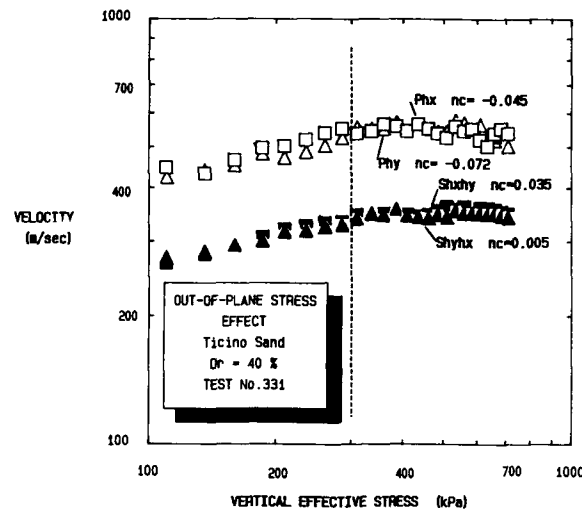


Figure 5. Effect of the out-of-plane principal effective stress, σ'_c , on wave velocity.

TEST RESULTS

Aspects associated with stress level effects on the seismic velocity which should be independent of the elastic anisotropy of the specimen [13], are discussed prior to anisotropic evaluations. As aforementioned, the principal effective stresses are studied within the Roesler [13] framework (Eqns. 4 and 5). The σ'_v -V relationship can be simplified since the effect of the out-of-plane stress, σ'_c , on wave propagation velocities has been found to be very small [10] [13]. This finding is supported by data presented in Fig. 5 in which the propagation velocity of horizontal P waves (P_{hx} and P_{hy}) and horizontally propagated and polarized S waves (S_{hxhy} and S_{hyhx}) are plotted versus σ'_v . The subscripts x and y associated with the wave types in Fig. 5 refer to the directions parallel and orthogonal to the travelling sand spreader (Fig. 2).

The specimen was consolidated isotropically to 300 kPa, during which all velocities increased. Then, σ'_h was maintained constant at 300 kPa while σ'_v was increased to 700 kPa, during which the horizontal wave velocities remained essentially constant. It is worth noting that only a small variation in one velocity measurement is sufficient to result in a non-zero exponent determined via linear regression. Of note also is that there is virtually no difference between the velocities of x and y oriented waves, thus confirming the isotropy of the horizontal plane.

The exponents n_a and n_b were evaluated assuming n_c equal to zero. Examples of these data are shown in Figs. 6 and 7 for n_a and n_b , respectively. Again, the specimens were isotropically consolidated to 300 kPa following which σ'_v was maintained constant. Bearing in mind the quality of the linear regressions (coefficients of regression varying between 0.8 and 0.9), these data demonstrate the effect of increasing σ'_h on waves propagating in the horizontal direction (S_{hv} ; $n_a=0.12$) and on waves vibrating in the horizontal direction (S_{vh} ; $n_b=0.15$). Considering all available data in this manner, n_a was found to be about equal to n_b with an average value of about 0.13. Note that when n_a is assumed equal to n_b , a

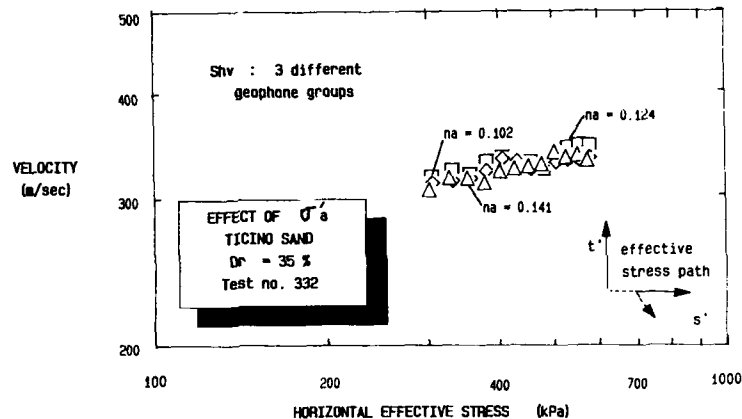


Figure 6. Effect of the principal effective stress in the direction of wave propagation, σ'_a , on wave velocity.

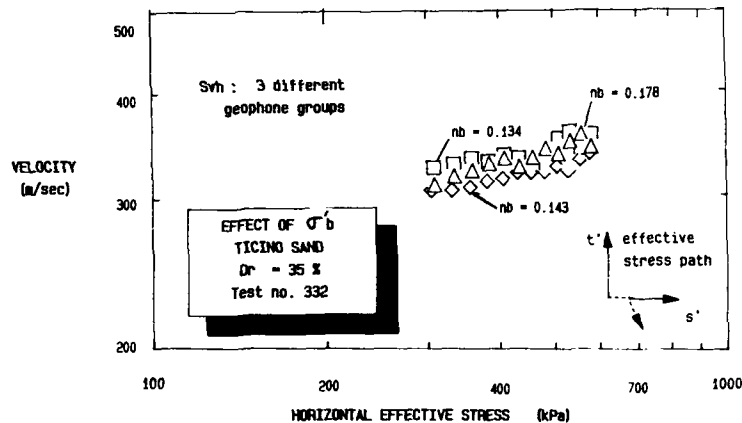


Figure 7. Effect of the principal effective stress in the direction of wave vibration, σ'_b , on wave velocity.

slightly lower value of the average exponent was determined ($n_a \approx n_b \approx 0.12$). This could be due to the fact that when individual exponents are studied, (e.g. Figs. 6 and 7), the "negligible" effects of the other two stresses serve to increase the wave velocity measured and thus are mistakenly interpreted as a slightly increased value of the exponent calculated.

Results presented for isotropically consolidated specimens (Figs. 8 and 9) allude to the inherent anisotropy of medium and very dense specimens of dry Ticino sand deposited using the travelling sand spreader. At both relative densities ($D_r = 40\%$ and 85%) and for both S and P waves, the propagation velocities in the horizontal direction were greater than those in the vertical direction. On the basis of these measurements, the inherent elastic anisotropy of this sand can be characterized by ratios between horizontal and vertical shear moduli (G_{hh}/G_{vh}) and constrained moduli (M_{hh}/M_{vh}) equal to approximately 1.2.

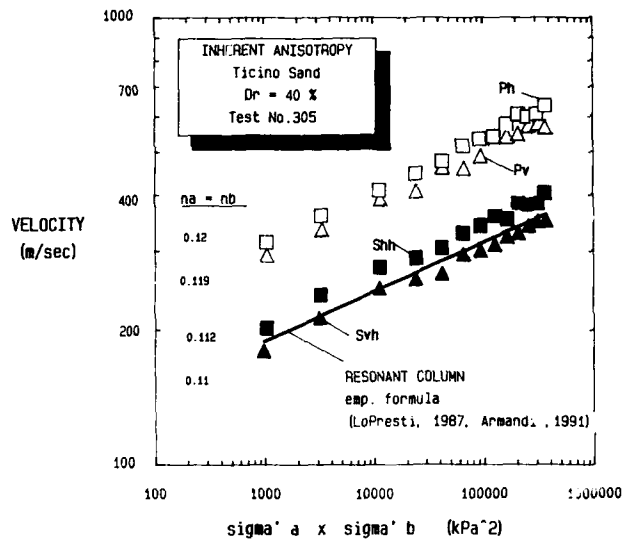


Figure 8. Seismic wave velocities measured in isotropically consolidated specimens prepared at relative density equal to 40%.

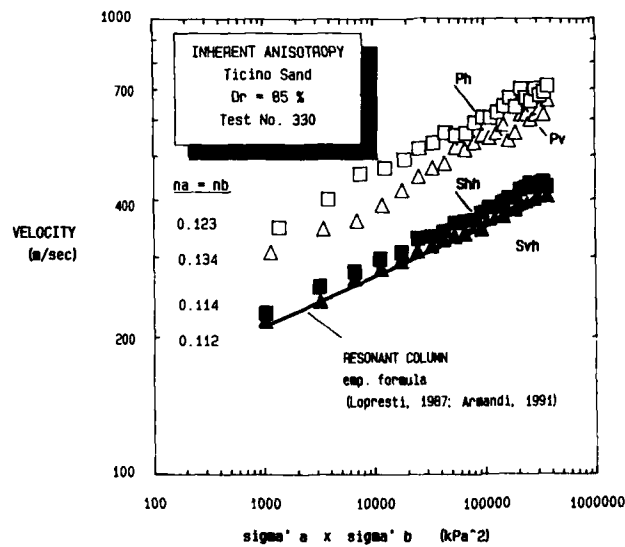


Figure 9. Seismic wave velocities measured in isotropically consolidated specimens prepared at relative density equal to 90%.

Also presented in Figs. 8 and 9 are estimates of shear modulus based on an empirical equation involving the octahedral effective stress and the void ratio derived from results from resonant column, RC, tests on isotropically consolidated medium ($D_r=40\%$) and very dense ($D_r=90\%$) specimens

of Ticino sand [1] [17]. The seismic wave monitored in the RC device is a vertically propagating, horizontally vibrating S wave (S_{vh}). The correlation with the measurements in the calibration chamber is notably good.

Evaluation of induced or evolving anisotropy is effected by consolidating different specimens along different paths at constant $\sigma'_{hc}/\sigma'_{vc}$. The anisotropy measured is thus a combination of inherent and that induced by strains incurred by the application of a nonisotropic consolidation stress ratio, $K_c \neq 1$. These data are presented in Figs. 10 and 11 for S and P waves from tests performed on medium dense specimens. Data obtained from very dense specimens, not shown here, exhibited far less scatter.

The data in these figures clearly manifest the inherent anisotropy (greater velocities for the horizontally propagating waves), regardless of K_c . On the other hand, neither S waves nor P waves immediately appear to be affected by the stress ratio. Note, however, for the S_{hh} waves the velocities for $K_c=0.3$ and 0.5 are approximately equal, while corresponding S_{vh} velocities are lower for the lower K_c , resulting in an increase in the ratio of the moduli, G_{hh}/G_{vh} . Studying this aspect closely, the data indicate that for K_c less than about 0.7 , the velocity of the S_{vh} waves decreases with decreasing K_c such that the ratio G_{hh}/G_{vh} increases to approximately 1.3 . Data for the dense specimens showed the same trend for the effect of K_c on S wave velocities. A trend of decreasing G_{max} with decreasing K_c was also noted by Yu and Richart [18] on the basis of resonant column test results. Additional research at stress ratios less than unity are necessary to better describe this phenomenon.

CONCLUSIONS

The seismic method presented wherein both S and P wave velocities are measured in large, dry sand specimens in the calibration chamber is well adapted to the investigation of small strain modulus anisotropy. Employing the visual true interval method using two receivers, the 95% confidence level scatter associated with the technique is equal to approximately $\pm 3\%$ and $\pm 6\%$ for S and P wave velocities, respectively. Appropriate disposition of approximately 25 to 30 geophones at three elevations within the sand specimen permits measurement of S_{vh} , S_{hv} , S_{hh} , P_v and P_h velocities. Implanting a minimum of six geophones at a tilt allows the evaluation of obliquely propagating S and P waves.

The dry, pluviated, Ticino sand specimens demonstrated a slight inherent anisotropy with elastic moduli in the horizontal plane approximately 20% greater than those measured in the vertical direction. The effect of different constant values of K_c , ranging from 0.3 to 1.5 , indicated limited induced anisotropy for this sand. Essentially, for K_c greater than about 0.7 , the anisotropy was essentially equal to that measured under isotropic conditions. As the stress ratio is further decreased, however, for both relative densities investigated there appears to be a measurable reduction in the S_{vh} wave, thus increasing the shear stiffness ratio. Additional research is needed to better quantify this effect. Additional investigation is also required to fully describe the elastic anisotropy of the specimen, particularly with regard to the evaluation of the C_{13} parameter of the stiffness matrix. Tests are currently underway to measure the velocities of S and P waves propagating at 45 degrees from the horizontal.

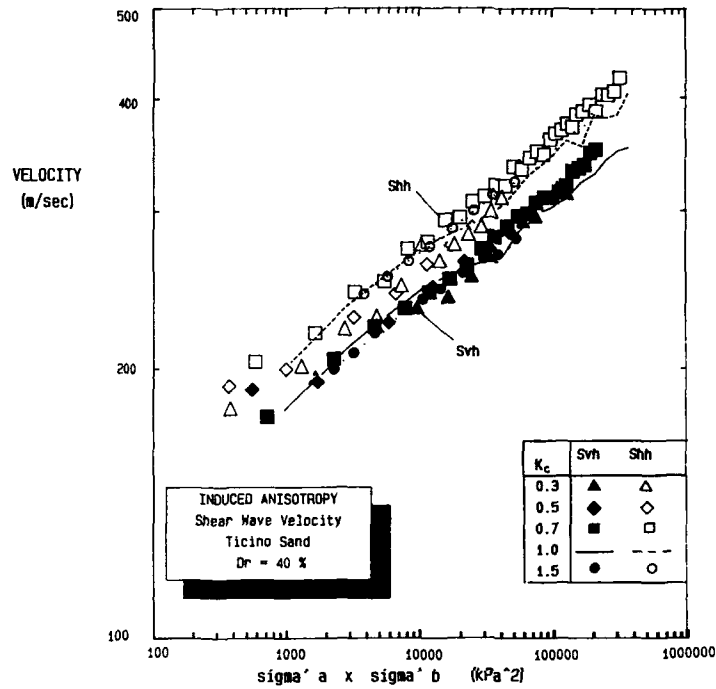


Figure 10. Shear wave velocity measured on specimens subjected to different consolidation stress ratios, K_c .

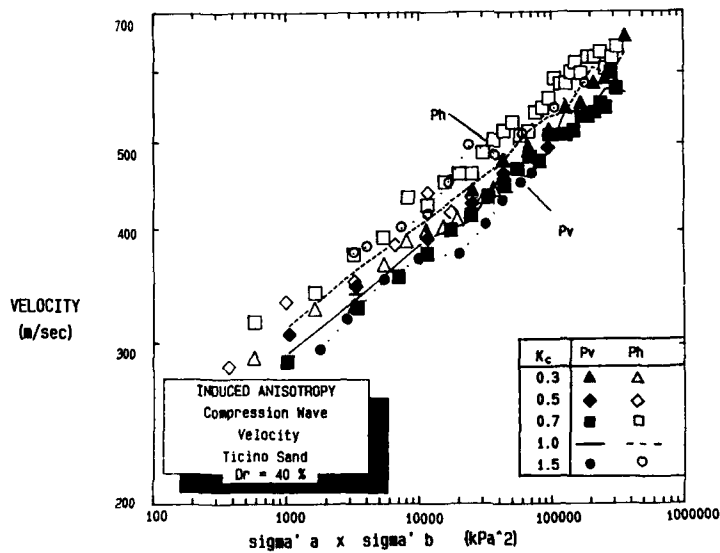


Figure 11. Compression wave velocities measured on specimens subjected to different consolidation stress ratios, K_c .

ACKNOWLEDGEMENTS

The contributions of Drs. K. Stokoe (Univ. Texas at Austin, Austin, Texas) and G. Rix (Georgia Inst. of Tech., Atlanta, Georgia) to the realization and execution of the experimental program are gratefully acknowledged.

REFERENCES

1. Armandi, M. (1991), Caratteristiche della deformabilit  delle sabbie del Ticino and di Toyoura da prove di colonna risonante e taglio torsionale, M.Sc. Thesis, Politecnico di Torino.
2. Baldi, G. et al. (1985), Laboratory validation of in situ tests, Associazione Geotecnica Italiana Jubilee Volume, XI Int. Conf. on Soil Mech. and Found. Eng., San Francisco.
3. Bellotti, R., V. Ghionna, M. Jamiolkowski, R. Lancellotta and G. Manfredini (1986), Deformation characteristics of cohesionless soils from in situ tests, Proc. In Situ 1986 GT div., Amer. Society of Civil Eng., Blacksburg, Virginia.
4. Bellotti, R., G. Bizzi and V. Ghionna (1982), Design, construction and use of a calibration chamber, Proc. ESOPT II, Amsterdam, Vol.2, pp439-446.
5. Carriglio, F. (1989), Caratteristiche sforzi-deformazioni-resistenza delle sabbie, Ph.D. Thesis, Politecnico di Torino, 292p.
6. Casagrande, A. and N. Carillo (1944), Shear failure of anisotropic materials, Proc. Boston Society of Civil Engineers, Vol.31, pp74-87.
7. Hardin, B. (1978), The nature of stress-strain behavior for soils, Proc. Earthquake Engineering and Soil Mechanics, Amer. Soc. of Civil Engineers, pp3-90.
8. Jamiolkowski, M., V. Ghionna, R. Lancellotta and E. Pasqualini (1988), New applications of penetration tests in design practice, ISOPT-I, Orlando, Florida.
9. Jardine, R., D. Potts, A. Fourie and J.B. Burland (1986), Studies of the influence of non-linear stress strain characteristics in soil-structure interaction, Geotechnique, Vol.36, No.3, pp377-396.
10. Lee, S. and K. Stokoe (1986), Investigation of low amplitude shear wave velocity in anisotropic material, Report GR86-6, Civil Eng. Dept., Univ. of Texas at Austin, 343p.
11. Lopresti, D.C.F. (1987), Comportamento della sabbia del Ticino in prove di colonna risonante, Ph.D. Thesis, Politecnico di Torino, 252p.
12. Love, A. (1892), A Treatise on the Mathematical Theory of Elasticity, 2 Vols. Cambridge University Press.
13. Roesler, S. (1979), Anisotropic shear modulus due to stress anisotropy, Journal of the Geotechnical Engineering Division, American Society of Engineers, Vol.105, GT7, pp871-880.
14. Schmertmann, J.H. (1978), Effect of shear stress on dynamic bulk modulus of sand, U.S. Army Engineering Waterways Experiment Station, Technical Report S-78-16, 92pp.
15. Stokoe, K., Y.S. Mok, N. Lee, R. Lopez (1989), In situ seismic methods: Recent advances in testing: Understanding and applications, XIV Conferenze di Geotecnica di Torino, Politecnico di Torino.
16. Stokoe, K., S. Lee and D. Knox (1985), Shear moduli measurements under true triaxial stresses, Advances in the Art of Testing Soils under Cyclic Conditions, October 1985, Detroit, Michigan, pp166-185.
17. Tatsuoka, F., T. Iwasaki, S. Fukushima and H. Sudo (1979), Stress conditions and stress histories affecting shear modulus and damping of sand under cyclic loading, Soils and Foundations, Vol.19, No.2, pp29-43.
18. Yu, P. and F. Richart (1984), Stress ratio effects on shear modulus of dry sand, Journal of Geotechnical Engineering, Amer. Society of Civil Eng., Vol.110, No.3, pp331-345.

PRACTICAL USE OF CPT CORRELATIONS IN SAND BASED ON CALIBRATION CHAMBER TESTS

TOM LUNNE

Norwegian Geotechnical Institute, P.O.Box 40 Taasen, 0801 Oslo 8, Norway

ABSTRACT

Over the last 20 years large (> 1 m diameter) flexible wall calibration chambers (CC) have been used to obtain correlations between results of CPTs and engineering soil parameters in sand. These correlations can now be used to estimate *in situ* sand density, shear strength and various moduli from field CPTs.

The correlations are used and compared to best estimate reference parameters at the NGI sand research site. Another case history of a very dense North Sea sand is included to demonstrate some of the problems related to using the correlations in practice. Finally some recommendations are given for future work to improve the applicability of CC based correlations.

INTRODUCTION

Due to the fact that it is difficult and frequently impossible to obtain undisturbed samples in sandy soils the engineer in practice has to rely on the interpretation of *in situ* test results.

Most interpretation methods that are currently in use are empirically based on calibration chamber (CC) testing results. Even theoretical interpretation methods for deriving shear strength parameters (i.e. bearing capacity and cavity expansion theories) are calibrated and adjusted with CC test results.

The calibration chamber work that has been performed over the last 20 years has therefore had a very important impact on the practical engineering use of CPT results in determining sand properties.

This paper gives a status of the present interpretation methods available that are based directly on CC testing. The Drammen and Slepner sands are used as case histories illustrating the use of the available interpretation methods. Finally some recommendations are made regarding the need for further CC testing to obtain more reliable and useful correlations.

ENGINEERING INTERPRETATION METHODS BASED ON CALIBRATION CHAMBER TESTS

General

The following is a review of the CC based correlations that are thought to be most commonly used today.

It is not space herein for a detailed discussion on the uncertainties and possible errors that may be involved in CC based CPT interpretation methods. However, a comprehensive review given by Been et al. (5). They discussed systematically the following factors:

- chamber size and boundary effects
- sand fabric (*in situ* vs field)
- effect of sand type
- potential errors in CC test procedures

The reader is also referred to Parkin (14) for discussion of the items listed above.

Relative density

Schmertmann (16, 17, 18) issued first unofficially and later officially relationship

between cone resistance, relative density and vertical stress. The latest Schmertmann recommendation (18) is included as dotted lines in Figure 1.

Schmertmann (18) pointed out that for overconsolidated (OC) sands Figure 1 will predict relative densities that are too high. Based on CC tests Schmertmann recommended computing an equivalent normally consolidated q_c , q_{cnc} from the following equations:

$$q_{coc}/q_{cnc} = 1 + 0.75(K_{0oc}/K_{0nc} - 1)$$

$$K_{0oc}/K_{0nc} = (OCR)^{0.42}$$

where: K_0 = coefficient of lateral earth pressure at rest
OCR = overconsolidation ratio

In order to use this approach K_{0oc} or OCR needs to be assessed. Later studies of available CC test data have led to updated q_c , D_r , σ_v' correlations by Lunne and Christophersen (11) as included in Figure 1. The above authors stressed that the correlations given are strictly valid only for normally consolidated ($K_0 = 0.45$), unaged clean fine to medium quartz sands.

For both normally consolidated and overconsolidated sands Baldi et al. (1) proposed

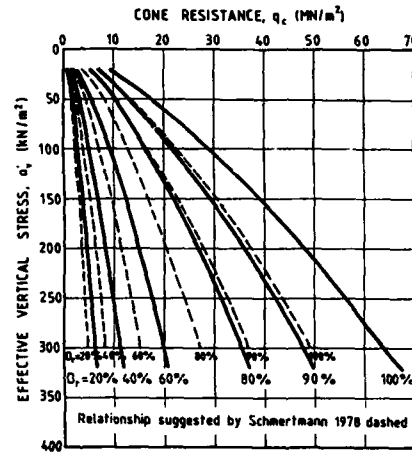


FIG. 1 Cone resistance, relative density, vertical stress plot for normally consolidated sands (from Lunne and Christophersen, 1983).

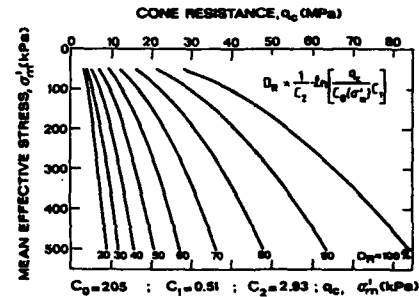


Fig. 2 Cone resistance, relative density, vertical stress plot for normally consolidated and overconsolidated Ticino sand (after Baldi et al., 1986).

the correlation shown in Figure 2 where effective stress σ'_{mean} is to be used instead of σ_v' . Again the correlations in Figure 2 are for clean fine to medium unaged quartz sand.

Shear strength

Schmertmann (18) proposed using the CC based q_c , σ_v' , D_r correlation (Figure 1) to find D_r and then the angle of internal friction ϕ' can be found from a D_r - ϕ' correlation. Both in Figure 3 and in the following discussion ϕ' corresponds to the measured peak friction angle from drained triaxial tests.

At the same time Robertson and Campanella (15) and Lunne and Christophersen (11) reviewed the CC data available on NC sands and recommended N_q ($=q_c/\sigma_{v0}'$) vs $\tan \phi'$ relationships that were almost identical as shown in the bearing capacity diagram given in Figure 4.

A recent trend is to interpret CPT test results in terms of a state parameter, ψ , instead of relative density. The state parameter combines the influence of void ratio and stress level

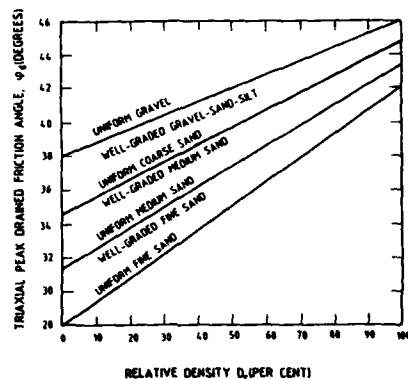


Fig. 3 Relationship between ϕ_D and D_r (suggested by Schmertmann, 1978).

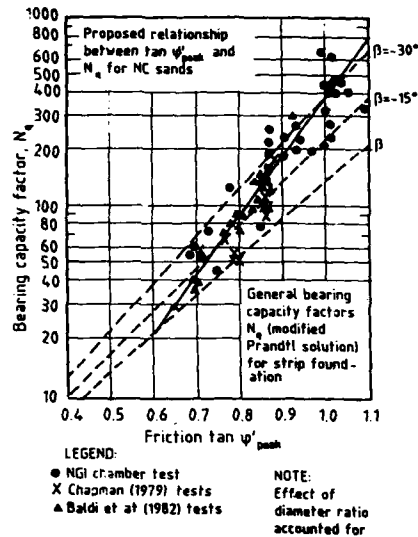


Fig. 4 Bearing capacity factor N_q vs. $\tan \phi_{peak}$ (NC sands) recommended by Lunne and Christophersen (1983).

with reference to an ultimate (steady) state, and can be used to describe sand behaviour, including shear strength.

The state parameter ψ represents the difference in the void ratio of a soil at a given mean effective stress, $\sigma'_{mean} = (\sigma'_{vo} + 2\sigma'_{ho})/3$, and the void ratio on the steady state line, at the same mean effective stress. The state parameter is used to describe whether the soil is contractive or dilative. Been and Jefferies (3) suggested that the state parameter correlates well with engineering parameters such as peak angle of shearing resistance determined in a triaxial test. The steady state line and its slope can be determined from a series of stress controlled triaxial tests.

Been et al. (4), based on a study of calibration chamber tests, developed a procedure for finding the state parameter in sand from cone penetration tests.

Two basic requirements for this method are to take samples and to run triaxial tests to determine the steady state line and to determine the horizontal stress.

Constrained modulus

From CC tests constrained modulus can be determined from the consolidation phase i.e. from one dimensional loading or unloading in the calibration chamber.

From a careful study of available CC data Robertson and Campanella (15) recommended the relationship between the tangent constrained modulus, M_o , σ'_v and q_c as shown in Figure 5.

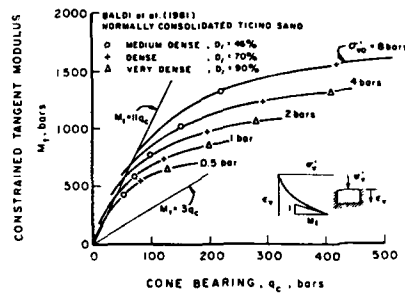
Lunne and Christophersen (11) recommended a more simple and somewhat more conservative approach for NC sands:

$$\begin{aligned} M_o &= 4 q_c \text{ for } q_c < 10 \text{ MPa} \\ M_o &= 2 q_c + 20 \text{ for } 10 \text{ MPa} < q_c < 50 \text{ MPa} \\ M_o &= 120 \text{ MPa for } q_c > 50 \text{ MPa} \end{aligned}$$

Lunne and Christophersen also included OC sands in their study and recommended as a rough guideline to use:

$$\begin{aligned} M_o &= 5 q_c \text{ for } q_c < 50 \text{ MPa} \\ M_o &= 250 \text{ MPa for } q_c > 50 \text{ MPa} \end{aligned}$$

Baldi et al. (1) proposed the correlations shown in Figure 6, which were derived from



From Robertson and Campanella (1983)

Fig. 5 Evaluation of constrained modulus of n.c. sand from q_c and σ'_{v0} (from Robertson and Campanella, 1983).

CC tests on NC and OC Ticino sand. Relative density needs to be determined as described earlier.

Small strain shear modulus, G_0

Baldi et al. (2) argue that correlations between G_0 and cone resistance show less uncertainties than correlations to M_0 and E . This is because a large amount of experimental data show that G_0 in cohesionless soils is influenced very little by the stress and strain history. Based on CC tests and extensive laboratory work by others Robertson and Campanella (15) proposed a correlation for normally consolidated, uncemented quartz sands where $G_0 = f(q_c, \sigma'_{v0})$ as shown in Figure 7.

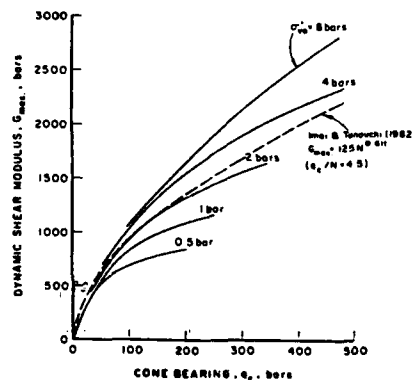


Fig. 7 Evaluation of small strain shear modulus from cone resistance of nc sands (from Robertson and Campanella, 1983).

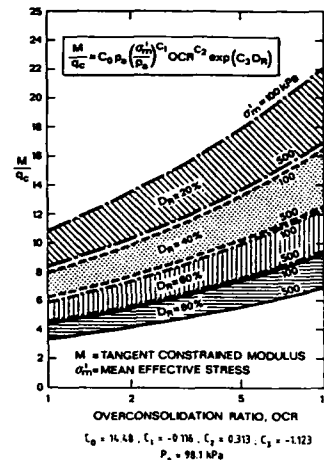


Fig. 6 Constrained modulus of sand from cone penetration resistance (Jamiolkowski et al., 1988).

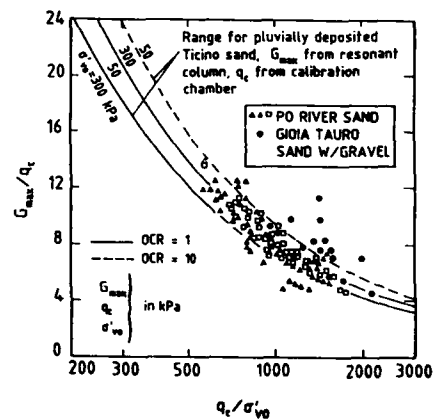


Fig. 8 Small strain shear modulus from cone resistance for uncemented quartz sands (from Baldi et al., 1989).

Based on further CC tests and resonant column tests Baldi et al. (2) gave the tentative correlation between G_0 and $q_c/\sqrt{\sigma'_{v0}}$ for uncemented predominantly silica sands as shown in Figure 8. Experience from field tests were also taken into account.

Further discussion on the use of these correlations are given by Baldi et al. (2).

General remarks on stiffness parameters

Carriglio et al. (8) have stressed that based on CC and in situ tests only "elastic" deformation moduli of sands (i.e. moduli evaluated at stress levels below the current yield surface) can be reliably correlated to cone penetration resistance. They presented correlations between normalized elastic moduli and normalized cone resistance via the state parameter ψ .

Baldi et al. (2) have also presented correlations between the drained Young's modulus and cone resistance for settlement analysis.

APPLICATION OF PRESENTLY USED INTERPRETATION METHODS TO TWO SANDS

General

In order to illustrate some of the problems encountered in practice when using the correlations described above two cases will be used in the following:

- The Drammen sand which has been used for research purposes by NGI for 30 years.
- The North Sea Sleipner sand where several important foundation studies for large gravity base structures have been conducted by NGI.

The difficulty of establishing good reference in situ values for engineering soil parameters will be illustrated through these cases.

Description of Drammen sand

The test site is located at Holmen in the Drammen River outlet into the Drammens fjord. Beneath an artificial fill of stones, gravel and sand, about 2 m thick is a uniform sand layer down to about 22 m which is known as the Drammen sand. The sand was deposited some 2-4000 years ago. In connection with foundation studies for some silos the first CPTs were carried out by NGI in 1952. Since then a number of studies with in situ testing have been performed at this site.

As documented by several studies this site is very uniform (e.g. 12). Figure 9 includes an average q_c -profile vs. depth.

The Drammen sand is varying from medium to medium to coarse. Other properties are listed in Table 1, which shows that the Drammen sand is very similar to sands used in calibration chamber research.

Dilatometer tests at the site indicate that $K = 0.4$ is a reasonable value in the depth interval 4-20 m.

The Drammen sand compares reasonably well with the calibration

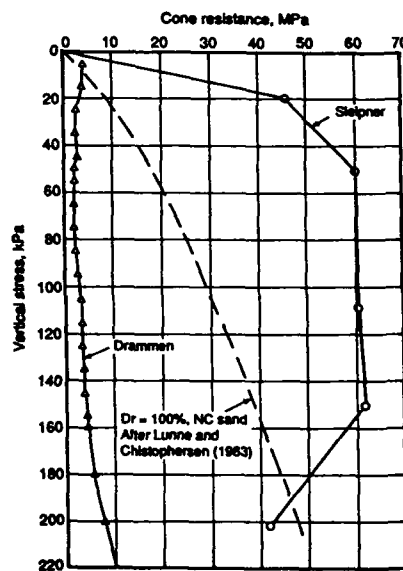


Fig. 9 Average q_c -profiles for Holmen and Sleipner sands.

TABLE 1. Classification properties of CC sands and Drammen and Sleipner sands

SAND PARAMETER	Hokksund	Ticino	Drammen	Sleipner
Mineralogy	35% quartz 45% feldspar 10% mica	Mainly quartz 5% mica	55% quartz 35% feldspar	92% quartz 8% feldspar
Angularity	Subrounded	Subrounded	Subrounded	Subrounded
$d_{60}/d_{10}=C_u$	0.50/0.27=1.85	0.65/0.40=1.13	0.63/0.23=2.7	0.14/0.09=1.56
e_{max}	0.92	0.89	0.89	1.00
e_{min}	0.56	(0.52)	0.43	0.54
Specific gravity of grains	2.70	2.67	2.68	2.62

chamber sands (see Table 1) and it is known that it is not geologically overconsolidated although it has had opportunity to age for 2-3000 years. In mineral composition the Hokksund sand is comparable with Drammen sand and in fact it has been taken only about 20 km away.

Description of Sleipner sand

The Sleipner Field is located in about 80 m water depth in the North Sea. The uppermost 22 m of very dense sand was deposited less than 100 000 years ago. The high density of the sand is postulated to be a result of compaction by wave activity when the sand was deposited at a much shallower water depth than at present in addition to the effect of aging which Schmertmann (19) has demonstrated to be very important. It is not believed that this sand has been preloaded by ice.

Figure 9 shows the average cone resistance in the upper sand layer which is very uniform. For comparison the highest values of q_c measured on NC Hokksund sand are included.

Table 1 includes classification data from the Sleipner sands. It is quite similar to several of the sands tested in the CC.

Prediction of in situ porosity or D_r

Drammen: In order to get a better understanding of the in situ density of the Holmen sand NGI subcontracted Delft Geotechnics to do tests with two of their special probes: the electrical resistivity test (ERT) and the nuclear density test (NDT).

Based on the measurements with each of these probes the relative density has been computed using laboratory values of maximum and minimum void ratios. As has been frequently pointed out there are problems with reliable measurement of these values, nevertheless NGI and Delft Geotechnic obtained reasonably similar values.

The resulting values are shown in Figure 10 together with results of 'undisturbed' 54 mm piston samples (worked out from water content measurements). As can be observed there is a large difference between the D_r values determined by the different methods.

Relative density values interpreted from the CPTs using methods outlined previously lie reasonably close together and between the results from the NDT and ERT determined values. Lunne (12) argued that the best estimate D_r -profile is likely to be closest to the CPT

determined values. Some of the arguments were:

- sample are very likely densified and hence laboratory values are too high
- NDT measurement was done with 15 cm² cone and close distance between radioactive source and detector (210 mm).
- some uncertainties related to ERT determinations due to the indirect way these results are used to compute in situ porosity and hence D_r .

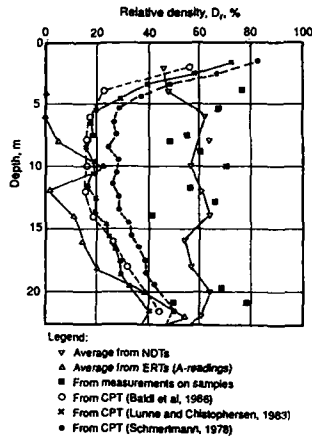


Fig. 10 Relative density assessed by different methods for Holmen sand.

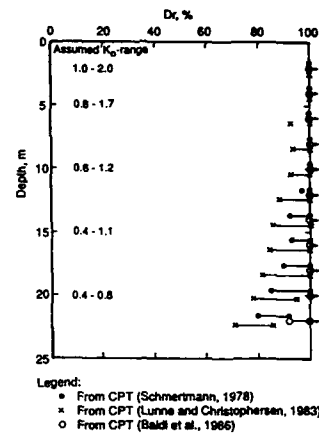


Fig. 11 Relative density assessed by different methods for Sleipner sand.

Sleipner: At Sleipner there is no measurement (besides CPT) which can be used to evaluate the in situ value of K_0 and this parameter is quite uncertain.

In order to apply the interpretation methods described earlier we have somewhat arbitrarily chosen a possible upper and lower limit of K_0 vs. depth as listed in Figure 11. Even the highest K_0 values results in $D_r \geq 100\%$ in the upper 6 m. The curves recommended by Schmertmann and Lunne and Christophersen yield D_r -values that can possibly decrease to around $D_r = 80\%$ at 20 m depth using the highest estimate of K_0 .

The Baldi et al. (1) curves yield $D_r \geq 100\%$ down to 20 m. NGI in the soil parameter report, which was the bases for engineering analysis, recommended that laboratory tests be run on samples compacted to $D_r = 100\%$ and that in the upper 10 m $D_r = 100\%$ was used reducing to 90% at 20 m depth.

Prediction of drained shear strength

Drammen: The in situ shear strength is not possible to uniquely define, however a likely range of values that would be measured in a CAU triaxial test (ϕ_p' = peak value) is found as follows:

CAU triaxial tests were run on both reconstituted and 'undisturbed' samples at various consolidation stresses equivalent to the actual depth interval.

From these tests relationships between D_r and ϕ_p' could be drawn with 'undisturbed' samples giving considerably higher ϕ_p' (2-3°) than reconstituted samples at a given D_r and consolidation stresses. The range shown in Figure 12 resulted. The ϕ_p' values computed from CPT profiles using the methods described above are also included in Figure 2. For the state parameter method previously published data (4) on Hokksund sand was used. Above 15 m depth the CPT ϕ_p' -values fall in the middle between the CPT/laboratory test values. Below 15 m the CPT/laboratory values are somewhat higher. The variation among the ϕ_p' -profiles interpreted from the CPT results does not exceed 1.5°.

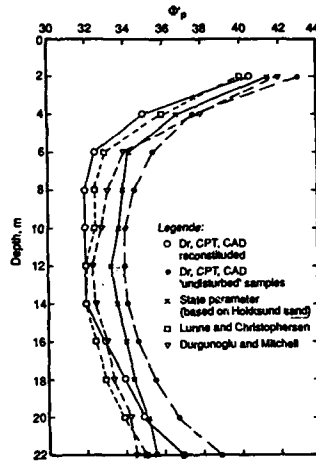


Fig. 12 Friction angle interpreted from different methods for Holmen sand.

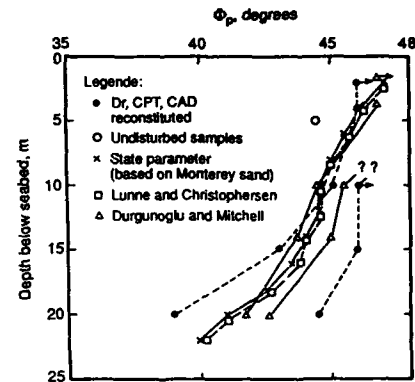


Fig. 13 Friction angle interpreted from different methods for Sleipner sand.

Sleipner: Using the range in D_r values shown in Figure 11, ϕ_p' from drained triaxial tests on reconstituted samples are given in Figure 13.

Figure 13 also includes CPT interpreted values. The lower range of ϕ_p' from Durgunoglu and Mitchell method compares well with values found using both Lunne and Christophersen's recommendation (Figure 4) and the state parameter approach. Due to lack of special laboratory tests at Sleipner (to define steady state line) the correlations given for Monterey sand (3, 4) have been used. Results of triaxial test on undisturbed sample are also included - the fact that ϕ_p' from this test is lower is very likely caused by the sample becoming less dense during sampling.

Mineralogical studies did not indicate any cementation of the Sleipner sand.

Prediction of constrained modulus, M_o

Figure 14 shows the range of best estimate constrained modulus, M_o , back figured from settlement observations of a large silo (base area 16 x 30 m) at the test site and also based on results of in situ screw plate tests and oedometer tests on recovered samples.

Most emphasis has been given to the settlement-backfigured values due to:

- The samples on which the oedometer tests were run may have been disturbed during sampling and sample handling and the structure of the sand may have been changed.
- The installation of the screw plate may cause some densification and/or preloading of the sand underneath the plate which would tend to give too high modulus values.

Figure 14 also includes the predicted

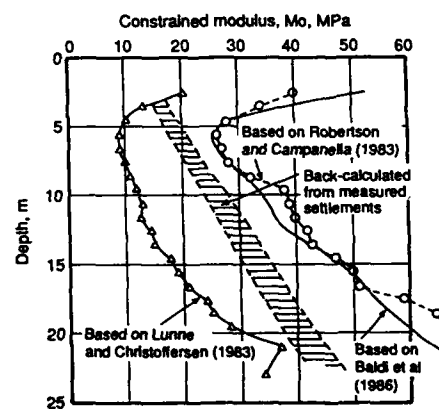


Fig. 14 Constrained modulus, M_o , interpreted by CPTs compared to best estimate values for Holmen sand.

M_o values from the CC based correlations by Robertson and Campanella (15), Lunne and Christophersen (11) and Baldi et al. (1).

The figure confirms that the Lunne and Christophersen recommendation is indeed very conservative and can be used to obtain a lower estimate of M_o . On the other hand for the Drammen sand the two other correlations give non-conservative estimates and should be used with caution.

Prediction of small strain shear modulus, G_o

The small strain shear modulus, G_o , is the only parameter for which it is relatively simple to obtain reliable in situ reference values through the measurement of shear wave velocity, v_s . G_o can then be computed from

$$G_o = \rho v_s^2$$

Reference G_o values were obtained using crosshole measurements and tests with the UBC seismic cone, as shown in Figure 15.

Recently, surface Rayleigh wave measurements were also made giving quite similar results (at least below 6 m depth).

Figure 15 also includes the predicted profile of G_o vs depth based on the Robertson and Campanella (15) recommendation which can be seen to fit remarkably well with the reference values. The correlation proposed by Jamiolkowski et al. (10) on the other hand yields a G_o vs depth profile that significantly overpredicts the reference profile. However, Jamiolkowski et al. (10) reports that their CC based correlation compares reasonably well with field correlations obtained at some Italian sites.

The reason for the differences in the Robertson and Campanella and Jamiolkowski et al. correlations should be examined further.

Discussion

When interpreting CPT results there are in practice two cases:

- a) Where only CPT results are available, no samples have been taken i.e. there are no classification data available for the penetrated sands.
- b) Samples have been taken and sand classification data are available.

On important projects samples should always be taken and b) applies. In this case it is relevant to compare the actual sand to CC sands and make a judgement as to applicability of the correlation discussed above and make any correction as suggested f.inst. by Schmertmann (18).

For case a) there is a need to establish criteria as to when CC correlations are relevant; this should be in terms of the CPT/plezocone parameters q_c , f_s , u , R_f .

The effects of sand aging and possible cementation effects has not been addressed

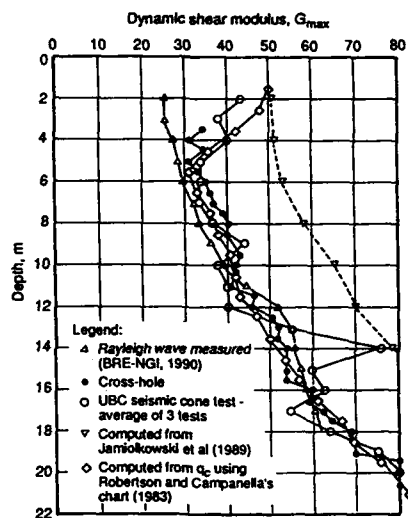


Fig. 15 Small strain modulus, G_o , assessed from CPT results compared to geophysically determined values.

above. Schmertmann (19) has demonstrated the importance of these effects. However, at this stage they are difficult to quantify and take into account in practical interpretation of CPT results.

RECOMMENDATIONS FOR SOME FUTURE WORK RELATED TO INTERPRETATION OF CPTs IN SAND

Based on CC research the last 20 years our ability to interpret CPT results in terms of soil engineering parameters has significantly improved. However, the reviews of available CC based correlations and uncertainties involved, as well as the two case histories, have stressed the importance of some further work to be done:

1. The effects of boundaries and sample size still seems to be introducing unknown uncertainties as regards to the applicability of CC results for field conditions. More tests that better model field behaviour, such as recent work at Southampton University (9) should be continued.
2. More field case histories are required to verify the validity of the CC based correlations. Better determination of reference field parameters should be attempted.
3. Important work has been done towards measuring/estimation in situ horizontal stress in the field, but the reliability of the present available methods (e.g. lateral stress cone and dilatometer) is still not satisfactory.
4. More clear and well defined criteria for the use of CC based correlations are applicable are needed. This should be in terms of PCPT results (fs, qc, u) and also classification data on obtained samples.

ACKNOWLEDGEMENT

The writer would like to acknowledge Dr. Joe Keaveny of NGI and Dr. Alan Parkin of Monash University, who carefully reviewed the manuscript and offered valuable comments.

REFERENCES

1. Baldi, G., Bellotti, R., Ghionna, V.N., Jamiolkowski, M. and Pasqualini, E. (1986). Interpretation of CPT's and CPTU's; 2nd part: drained penetration of sands. Fourth International Geotechnical Seminar, Singapore, proceedings; pp. 143-156.
2. Baldi, G., Bellotti, R., Ghionna, V.N., Jamiolkowski, M. and Lo Presti, D.C.F. (1989). Modulus of sands from CPT's and DMT's. Paper to 12th International Conference on Soil Mechanics and Foundation Engineering, Session 2, Rio de Janeiro, Brazil.
3. Been, K. and Jefferies, M.G. (1985). A state parameter for sands. *Géotechnique*, Vol. 35, No. 2, pp. 99-112.
4. Been, K., Crooks, J.H.A., Becker, D.E. and Jefferies, M.G. (1986). The cone penetration test in sands: part I, state parameter interpretation. *Géotechnique*, Vol. 36, No. 2, pp. 239-249.
5. Been, K., Crooks, J.H.A. and Rothenburg (1988). A critical appraisal of CPT calibration chamber tests. International Symposium on Penetration Testing. ISOPT-1. Orlando, USA. Proc. Vol. 2, pp. 651-660.
6. Bellotti, R., Ghionna, V., Jamiolkowski, M., Lancellotta R. and Manfredini, G. (1986). Deformation characteristics of cohesionless soils from in situ tests. ASCE spec. Conf. In Situ '86. Use of In Situ Tests in Geotechnical Engineering, Blacksburg, Virginia, USA, pp. 47-73.

7. Bellotti, R., Ghionna, V.N., Jamiolkowski, M., Lancellotta, R. and Robertson, P.K. (1989). Shear strength of sand from CPT. Paper to 12th International Conference on Soil Mechanics and Foundation Engineering, Session 2, Rio de Janeiro, Brazil.
8. Carriglio, F., V. Ghionna, M. Jamiolkowski and R. Lancellotta (1991). Cone resistance and stiffness of sands. Submitted to Geotechnique for possible publication.
9. Harkness, R. (1991). Boundary Control and Deformation Fields in a Penetrometer Calibration Chamber. Final Report to SERC, 1991 (in preparation).
10. Jamiolkowski, M., Ghionna, V.N. and Lancellotta, R. (1988). New correlations of penetration tests for design practice. International Symposium on Penetration Testing ISOPT-1. Orlando, USA. Proc., Vol. 1, pp. 263-296.
11. Lunne, T. and Christoffersen, H.P. (1983). Interpretation of cone penetrometer data for offshore sands. 15th Offshore Technology Conference, Houston, Texas, USA. Proceedings, Vol. 1, pp. 181-192.
12. Lunne, T. (1986). Interpretation of cone penetration tests in sand at Holmen, Drammen. NGI Report No. 40019-22, 3 September, 1986.
13. Mitchell, J. and T. Lunne (1978). Cone resistance as measure of sand strength. American Society of Civil Engineers. Proceedings, Vol. 104, No. G-77, pp. 995-1012. Also published in: Norwegian Geotechnical Institute. Publication, 123.
14. Parkin, A. (1988). The Calibration of Cone Penetrometers. International Symposium on Penetration Testing. ISOPT-1. Orlando, USA. Proc. Vol. 1., pp. 221-244.
15. Robertson, P.K. and Campanella, R.G. (1983). Interpretation of cone penetrometer test. Part I. Sand, Canadian Geotechnical Journal, Vol. 20, No. 4, pp. 718-733.
16. Schmertmann, J.H. (1971) "Letter to McClelland Engineers Inc. Dated 7 October 1971. Not published.
17. Schmertmann, J.H. (1976). Measurement of in situ shear strength. ASCE, Spec. Conference on In Situ Measurement of Soil Properties. Raleigh, North Carolina, USA. Proceedings, Vol. 2, pp. 57-138.
18. Schmertmann, J.H. (1978). Guidelines for cone penetration test, performance and design. U.S. Department of Transportation. Federal Highway Administration. Report, FHWA-TS-78-209. Washington D.C., USA. 145 p.
19. Schmertmann, J.J. (1989). The mechanical aging of soils. To be published in

CALIBRATION CHAMBER CORRELATIONS FOR HORIZONTAL IN SITU STRESS ASSESSMENT
USING SELF-BORING PRESSUREMETER AND CONE PENETRATION TESTS

M. MANASSERO
Technical University of Torino, Italy

ABSTRACT

A procedure for the assessment of initial horizontal in situ stress in cohesionless deposits (σ_{ho}) has been developed combining the results of Self Boring Pressuremeter Test (SBPT) and Static Cone Penetration Test (CPT). The reliability of the proposed approach has been evaluated using a large number of SBPT's and CPT's performed in the Calibration Chamber (CC) of the Italian National Electricity Board Research Center (ENEL CRIS) of Milan. Applications of the proposed procedure to natural sand deposits are also shown. The inferred σ_{ho} using the proposed procedure is hereby compared with σ_{ho} assessed from other in situ tests like Flat Dilatometer (DMT), and Lateral Stress Cone (LS-CPT).

1. INTRODUCTION

The knowledge of the initial stress state is broadly recognized to be of great importance for the geotechnical characterization of natural deposits.

On the other hand, at the time of writing with particular reference to cohesionless deposits, a fully reliable procedure for determining in situ stress σ_{ho} has not been established yet.

Assessment of σ_{ho} from in situ tests has been attempted via Self-Boring Pressuremeter Tests or using push-in devices like Marchetti Flat Dilatometer Test, Iowa Stepped Blade, Spade Like Total Stress Cell, Lateral Stress Cone and Cone Pressuremeter.

As far as the direct assessment of σ_{ho} from "lift-off pressure" (p_o) of SBPT is concerned, it is still questioned [1, 2, 3] whether existing self-boring devices, even after the best possible installation, are able to measure σ_{ho} correctly.

With regard to push-in devices, to account for the disturbance of surrounding soil caused by insertion of the probe, empirical correlations have to be developed like those tried by many researchers [1, 4, 5, 6, 7, 8, 9, 10, 11, 12], which however did not give too encouraging results.

A framework for assessing horizontal in situ stress and/or coefficient of earth pressure at rest (K_o) which combines the results of CPT's and SBPT's, is here presented and is compared against other existing methods.

2. BASIC ASSUMPTIONS

It is generally accepted [12, 13, 14, 15, 16, 17] that effective point resistance (q') from CPT and effective limit pressure of an expanding cylindrical cavity (p') in a purely frictional soil are functions of initial effective stress state, relative density (D_r) and stiffness (G).

Therefore the following two different functions of the same variables can be written:

$$q'_c = F_1 (D_R; \sigma'_{ho}; \sigma'_{vo}; G) \quad (1)$$

$$p'_u = F_2 (D_R; \sigma'_{ho}; \sigma'_{vo}; G) \quad (2)$$

where:

σ'_{vo} : initial vertical effective stress
 σ'_{ho} : initial horizontal effective stress

D_R is the soil parameter that more influences q'_c and p'_u magnitude; σ'_{ho} , σ'_{vo} and G follow in order of importance [18, 19].

Considering similar cohesionless deposits (e.g. prevalently silica sands), it is possible to assume, roughly, that for a given stress-path the stiffness parameter is a function of relative density, of initial stress state, and in the broadest sense, of deposition and stress history (SH):

$$G = F_3 [D_R; \sigma'_{ho}; \sigma'_{vo}; SH] \quad (3a)$$

Neglecting in first approximation, factors like anisotropy and aging and considering therefore SH directly related to $K = \sigma'_{ho} / \sigma'_{vo}$ it is possible to write the following simplified function for the stiffness parameter:

$$G = F_4 (D_R; \sigma'_{ho}; \sigma'_{vo}) \quad (3b)$$

Looking at eqs. (1), (2) and (3b) it is possible to express the functions for q'_c and p'_u as follows:

$$q'_c = F_5 (D_R; \sigma'_{ho}; \sigma'_{vo}) \quad (4)$$

$$p'_u = F_6 (D_R; \sigma'_{ho}; \sigma'_{vo}) \quad (5)$$

Solving the system of eqs. (4) and (5) D_R and σ'_{ho} can be inferred knowing q'_c , p'_u and σ'_{vo} .

3. INPUT DATA

Based on the previous considerations the input data necessary for the assessment of σ'_{ho} are σ'_{vo} , q'_c and p'_u . No significant or specific problems exist for the evaluation of σ'_{vo} and q'_c however, further considerations have to be done as far as p'_u is concerned.

Limit pressure in expansion of cylindrical cavity in sand can be obtained both performing cone pressuremeter tests [20] and/or using the procedure for p'_u assessment from SBPT recently proposed by Ghionna et al. [21].

In the framework of the SBPT interpretation method proposed by Manassero [22, 23], p'_u from SBPT can be inferred [21] extrapolating pressuremeter curve in a double logarithmic scale with a straight line having a slope only function of constant volume friction angle (ϕ_v) up to reach $(V - V_0) / V = 1$ therefore $V = \infty$, being V_0 initial volume and V current volume of the cavity during expansion.

All the values of p'_u that will be taken into account in the following have been inferred from SBPT's using this last procedure. Among the SBPT's carried out in CC and in situ, only those where enough large expansion of the probe has been reached to allow a correct application of extrapolation procedure [21], have been used for p'_u assessment.

4. TESTED SANDS

Ticino sand (TS) has been used in CC tests carried out in the laboratory of ENEL CRIS of Milan.

In situ tests have been carried out in a Po river sand deposit near Mantova town (site 1) and in a Ticino river sand deposit at Pavia town (site 2).

Fig. 1 shows the grain size distributions of the three tested sands, while the soil profile and CPT log for the two considered sites are shown in fig. 2.

Po river sand (site 1) is a clean or only slightly silty, low to medium density deposit ($D_r = 50 + 60\%$) of the quaternary age. Geological history of this deposit and laboratory tests on same silty lenses do not allow for significant mechanical overconsolidation.

Based on these studies and tests the best estimation for earth pressure coefficient at rest gives $K \approx 0.50 + 0.60$.

On the basis of the available geological evidence Ticino river sand located in the subsoil of the urban area of Pavia (site 2) is a normally consolidated material (NC) with age ranging between 15.000 and 30.000 years. The best estimation of K values given by Jaky [24] formula ($K = 1 - \sin \phi'$) ranges between $0.40 + 0.50$. The angle of shearing resistance ϕ' required by Jaky's formula has been derived from CPT interpretation.

The relative density of the deposit is about 60%.

For detailed descriptions of subsoil characteristics and parameters of the considered sands, see [25] for CC tests on Ticino sand, [3] for Po river sand (site 1) and [26] for Ticino river sand (site 2).

5. PROPOSED PROCEDURES FOR σ'_{ho} AND K_o ASSESSMENT

Three different approaches, within the same framework, have been attempted for the σ'_{ho} assessment using q'_c and p'_u .

The first hypothesizes the following relationships between q'_c , p'_u , D_r and σ'_{ho}

$$D_r = \frac{1}{B_2} \ln \left[\frac{p'_u}{B_o (\sigma'_{ho})^{B_1}} \right] \quad (6)$$

$$D_r = \frac{1}{C_2} \ln \left[\frac{q'_c}{C_o (\sigma'_{ho})^{C_1}} \right] \quad (7)$$

where:

$B_o = 23.7$; $B_1 = 0.72$; $B_2 = 1.46$: constants of the best fit of 17 SBPT's in CC shown in tab. I;

$C_o = 220$; $C_1 = 0.53$; $C_2 = 2.64$: constants of the best fit of 228 CPT's in CC [18].

Correlation coefficients for eqs. (6) and (7) are respectively: $R(6) = 0.93$ and $R(7) = 0.94$.

Simplifying D_r from eqs. (6) and (7) the following equation is obtained for σ'_{ho}

$$\sigma'_{ho} = \left[\left(\frac{p'_u}{B_o} \right)^{C_2} \left(\frac{C_o}{q'_c} \right)^{B_2} \right] \left(\frac{1}{C_2 B_1 - C_1 B_2} \right) \quad (8)$$

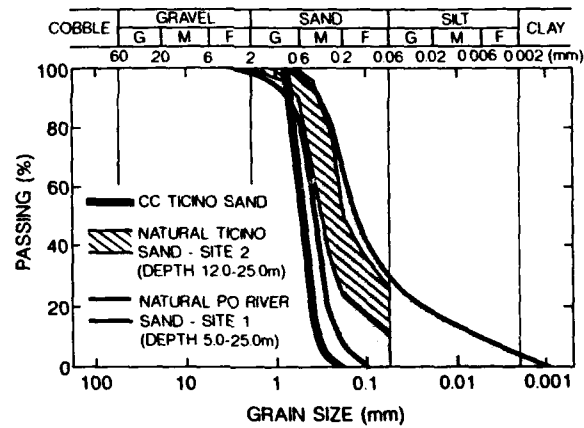


FIG. 1 . Grain size distribution of tested sands.

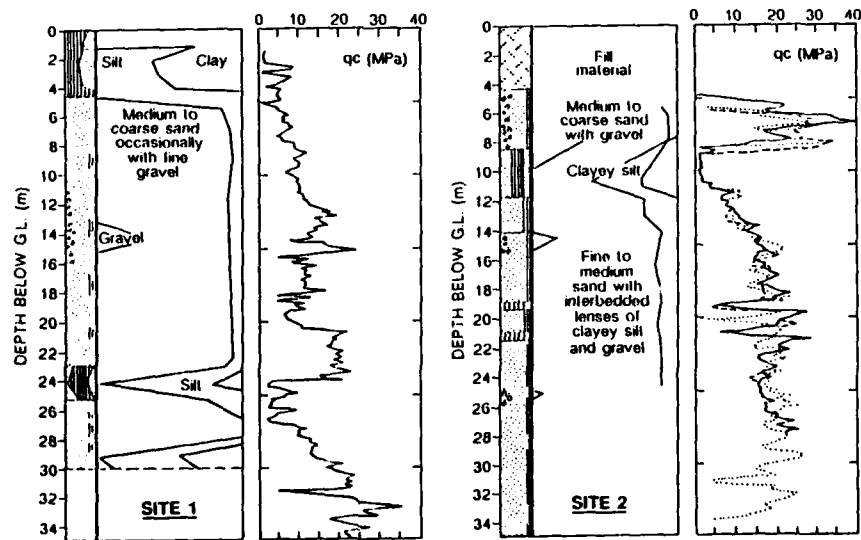


FIG. 2 . Soil profile, grading characteristics and cone resistance of Site 1 and Site 2.

The comparison between the coefficients B_1 and C_1 suggests a larger influence of σ'_{ho} on p'_u rather than on q'_c . This is to be expected considering the very different strain pattern existing around a penetrating cone and an expanding cylindrical cavity. The second procedure used in this paper refers to Schnaid and Houlsby [12] relationships summarized in the following:

$$D_R = D_0 \frac{(q'_c - \sigma'_{ho})}{\sigma'_{ho}} + D_1 \quad (9)$$

$$D_R = E_0 \frac{(q'_c - \sigma'_{ho})}{(p'_u - \sigma'_{ho})} + E_1 \quad (10)$$

TABLE I: Calibration Chamber tests on Ticino Sand and σ'_{ho} assessments

TEST N.	D_R %	ψ [°]	OCR [-]	σ'_{vo} [CC] [KPa]	σ'_{ho} [CC] [KPa]	p'_u [KPa]	q'_c [KPa]	p'_o [KPa]	σ'_{ho} [1] [KPa]	σ'_{ho} [2] [KPa]	σ'_{ho} [3] [KPa]
209	50	- 0.126	1.00	116.7	52.0	798.7	6840	45.0	44.9	42.2	51.5
212	65	- 0.176	2.86	110.9	82.4	1566.8	12262	104.3	102.4	90.8	90.8
216	46	- 0.122	7.57	60.8	56.9	872.8	5593	73.2	71.9	66.2	55.3
218	65	- 0.188	7.66	59.8	59.8	1153.9	10077	80.2	64.3	59.9	60.4
219	66	- 0.176	5.46	112.9	101.0	1871.1	13815	131.3	133.1	116.0	108.5
222	46	- 0.109	5.50	111.8	95.2	1393.4	8027	141.3	135.1	128.6	95.1
234	76	- 0.219	5.34	115.8	103.9	2033.7	18337	117.4	111.9	102.7	106.4
237	75	- 0.210	2.90	96.1	81.4	1762.0	15548	79.2	99.0	97.6	92.5
238	75	- 0.209	2.83	101.0	83.4	1530.8	15894	44.1	69.0	76.3	77.0
239	75	- 0.208	2.84	101.0	86.3	1695.2	16118	61.3	86.2	88.9	87.2
241	92	- 0.268	2.76	104.0	86.3	2228.1	25293	74.5	91.1	102.4	101.4
252	75	- 0.215	1.00	101.0	53.0	1188.2	13295	67.6	48.0	58.3	60.7
258	86	- 0.218	1.00	495.4	226.6	4191.5	40074	43.8	221.4	208.7	245.7
259	92	- 0.259	4.63	138.3	139.3	2456.2	32138	36.3	83.8	104.6	108.0
261	92	- 0.252	3.99	199.1	157.9	3695.7	35146	56.8	195.3	185.6	186.9
262	89	- 0.271	1.00	113.8	45.1	1336.6	18155	54.5	42.1	52.2	62.6
263	89	- 0.256	1.00	112.8	103.0	2410.5	25602	125.6	107.9	107.7	113.2

ψ : State parameter ; p'_o : lift-off effective pressure of SBPT

D_R : Relative Density ; q'_c : effective point resistance from CPT

p'_u : effective limit pressure from SBPT ; OCR: overconsolidation ratio

σ'_{vo} [CC]; σ'_{ho} [CC] : vertical and horizontal effective stress in CC before CPT and SBPT

σ'_{ho} [1]; σ'_{ho} [2]; σ'_{ho} [3] : horizontal effective stresses assessed respectively from eqs. (8), (9, 10) and (13).

where:

$q_c = q'_c + u_o$; $p_u = p'_u + u_o$; u_o = hydrostatic pore pressure;

$D_0 = 0.00161$; $D_1 = 0.422$; $E_0 = 0.0586$; $E_1 = 0.155$: constants of the best fit of the SBPT's and CPT's given in tab. I.

Correlation coefficients are: $R(9) = 0.79$; $R(10) = 0.80$.

The combination of eqs. (9) and (10) gives $\sigma'_{ho} = f(q_c, p_u)$ expressed as the root of a quadratic equation.

The third approach is based on the state parameter (ψ) concept [27] that combines D and σ' in a unique state index, being $\sigma'_o = (\sigma'_{vo} + 2\sigma'_{ho})/3$. The proposed relationships are:

$$\frac{p_u - u_o}{\sigma'_{vo} K_o} = H_o e^{(H_1 \psi)} \quad (11)$$

$$\frac{q_c - \sigma'_o}{\sigma'_o} = M_o e^{(M_1 \psi)} \quad (12)$$

where:

$H_o = 10.43$; $H_1 = 3.13$: constants of the best fit of 17 SBPT's in CC shown in tab. I;

$M_o = 30.8$; $M_1 = 8.75$: constants of the best fit of 228 CPT's in CC [17]

Correlation coefficients are: $R(11) = 0.84$; $R(12) = 0.90$.

A similar set of equations was already developed for the DMT and CPT in CC by Jamiolkowski et al. [17].

If the state parameter is eliminated equalizing eqs. (11) and (12) and considering:

$$\frac{q_c - \sigma'_o}{\sigma'_o} \approx \frac{q_c}{\sigma'_{vo}} \left[\frac{3}{1 + 2K_o} \right]$$

the following equation is obtained:

$$K_{SBP} = L_o K_o \left[\frac{3 q_c}{\sigma'_{vo} (1 + 2K_o)} \right]^{L_1} \quad (13)$$

where:

$$K_{SBP} = \frac{p'_u}{\sigma'_{vo}};$$

$L_o = 3.06$; $L_1 = 0.358$: constants.

7. RESULTS AND OBSERVATIONS

The eqs. (8), (9, 10) and (13) represent the set of best fitting curves for σ'_{ho} and/or K evaluation using CC tests (see fig. 3 and tab. I). Graphical descriptions of eqs. (8) and (13) are shown in figs. 4 and 5.

It is interesting to compare fig. 5 with figs. 6 and 7 where similar relationships, to infer K from LS-CPT and from combined information by DMT and CPT, have been reported by Jamiolkowski and Robertson [11].

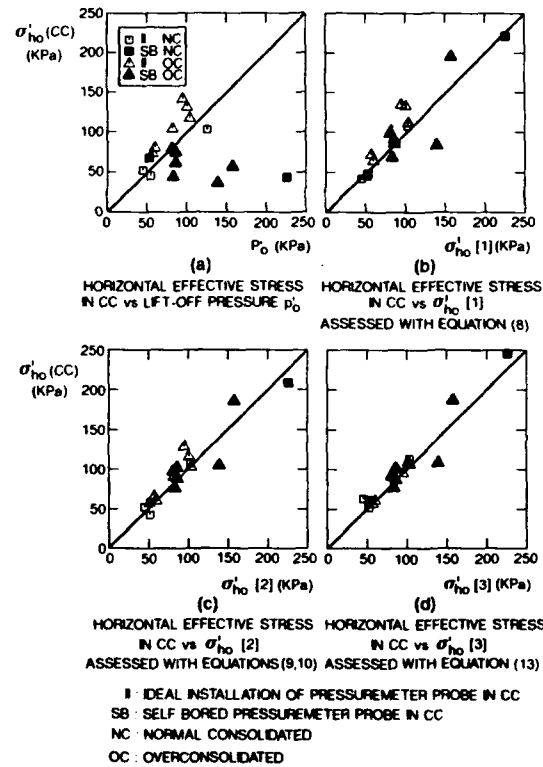
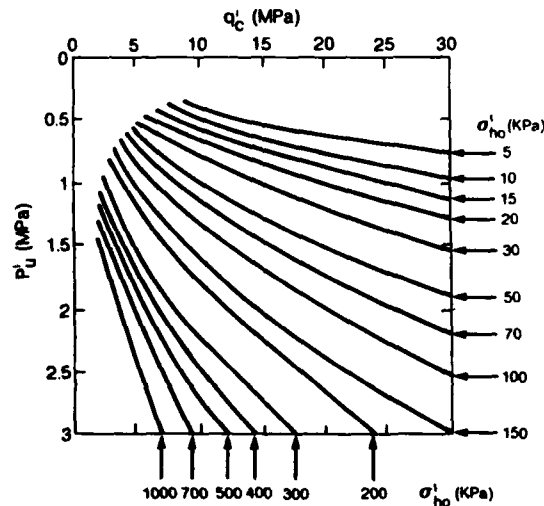


FIG. 3 . Estimated and applied horizontal stress values in CC.

FIG. 4 . Evaluation of σ'_{ho} from q'_c and p'_u using equation (8)

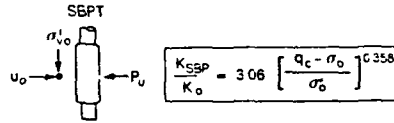
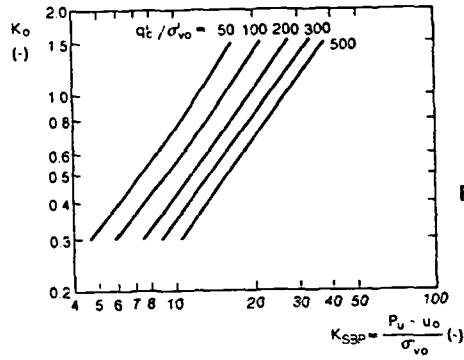


FIG. 5 . K_o from self boring pressuremeter and cone penetration tests for Ticino sand in CC.

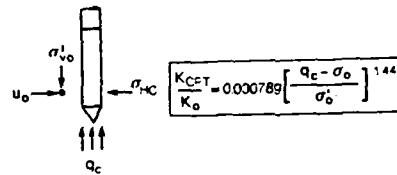
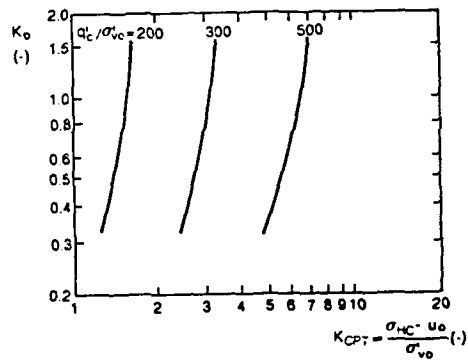


FIG. 6 . K_o from lateral stress cone for Monterey NO sand (data from Jeffries et al. [10])

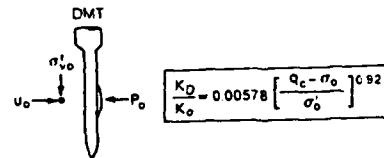
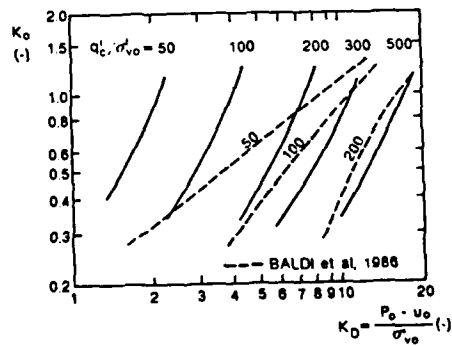


FIG. 7 . K_o from DMT's and CPT's performed on Ticino sand in CC (data from Jamiolkowski et al. [17])

Fig. 6 shows that K' assessment from LS-CPT is very sensitive and illconditioned to the measurement of K_{CPT} ; a better situation can be found in fig. 7 for DMT and CPT combined results with particular reference to corrected curves from in situ tests [9].

The assessment of K from curves of Fig. 5 seems to be the most reliable, because it is not particularly sensitive to both q'_c and p'_u measurements.

The eqs. (8), (9, 10) and (13) have been used to infer σ'_{ho} and K_o from tests carried out in sites 1 and 2.

Final results are summarized in Tab. II together with K_o from SBPT lift-off pressure.

The best estimations of K by geological and geotechnical characterizations of the considered sites and assessed K from proposed procedures and other available methods are synthetized in figs. (8a) and (8b) respectively for site 1 and site 2.

Looking at these figures the following observations can be done:

- excluding the tests in which the assessed values are clearly too high, the proposed approaches for K evaluation based on q'_c from CPT and p'_u from SBPT give encouraging results;
- the best estimation of K from CPT and SBPT has been obtained using eq. (13); in this case the average values for coefficient of earth pressure at rest are $K_o = 0.62$ for site 1 and $K_o = 0.50$ for site 2. These coefficients are in the range of the best estimations based on geological history and on laboratory tests in the cohesive layers of the considered deposits;

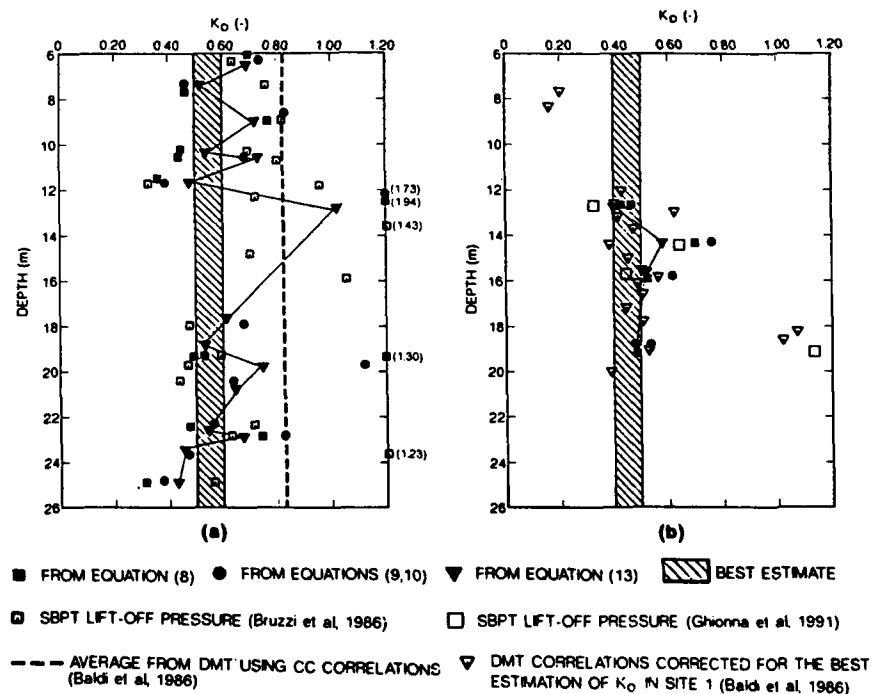


FIG. 8 . Comparison of K_o from different in situ tests. (a) Site 1 ; (b) Site 2.

TABLE II: In situ test results and K_o assessment

		Depth	σ'_{v_0}	u_0	p'_u	q'_c	$K_0 [LO]$	$K_0 [1]$	$K_0 [2]$	$K_0 [3]$	
		[m]	[KPa]	[KPa]	[KPa]	[KPa]	[-]	[-]	[-]	[-]	
SITE 1	Po River Sand	S4017	7.4	79.1	64.3	758.7	7560	0.75	0.44	0.44	0.53
		8.9	94.9	78.5	1379.8	12189	0.82	0.81	0.75	0.79	
		10.4	106.5	94.9	994.7	10148	0.69	0.42	0.43	0.52	
		17.9	176.5	170.3	1661.0	12194	0.47	0.67	0.60	0.60	
		19.4	190.4	185.6	1507.0	11386	0.49	0.54	0.49	0.52	
		20.9	204.2	200.9	2340.0	21412	0.42	0.62	0.58	0.64	
		22.8	221.6	220.3	2343.0	16492	0.63	0.81	0.71	0.68	
		24.9	237.8	244.9	1364.0	10389	0.57	0.39	0.35	0.40	
	S4003	6.2	88.9	60.2	984.0	7531	0.62	0.73	0.66	0.68	
		10.7	116.6	90.8	432.0	12679	0.79	0.68	0.63	0.69	
		12.2	128.7	106.1	1883.0	9423	0.69	1.73	1.94	1.03	
		19.7	201.3	180.5	2006.7	10187	0.45	1.16	1.30	0.75	
	S5051	22.3	249.5	182.5	2132.0	17096	0.71	0.55	0.49	0.54	
		23.8	263.1	197.8	1679.6	12320	1.23	0.46	0.41	0.45	
		11.8	153.1	75.2	1063.2	9657	0.32	0.37	0.35	0.44	
SITE 2	Ticino River Sand S1 and S2	12.7	259.3	~ 0	1311.0	7950	0.34	0.46	0.42	0.40	
		14.4	288.7	~ 0	2229.0	12900	0.65	0.76	0.70	0.57	
		15.8	323.9	~ 0	2483.0	16820	0.45	0.62	0.53	0.53	
		19.0	379.5	~ 10	2525.0	17270	1.12	0.53	0.48	0.48	
Best estimate of earth pressure coefficient at rest Site 1: $K_0 = 0.50 + 0.60$; Site 2: $K_0 = 0.4 + 0.5$											

σ'_{v0} : vertical effective pressure ; u_0 : hydrostatic pore pressure

q'_c : point resistance from CPT ; p'_u : limit pressure from SBPT

$K_o [LO]$: coefficient of earth pressure at rest from SBPT lift-off pressure

$K_o [1]$; $K_o [2]$; $K_o [3]$: coefficients of earth pressure at rest respectively from eqs. (8), (9, 10) and (13)

- the proposed procedures, using the best fit coefficients from CC tests, behave pretty well for in situ K evaluation without any correction. As far as CPT-DMT approach is concerned an in situ K overestimation of about 50% seems to occur without any correction of CC best fit coefficients [9];
- the averages of in situ coefficients K from lift-off pressure and from proposed approaches are rather similar, but less scatter is noted on the single values from the proposed procedures (in particular from eq. (13)). The approaches based on q'_c and p'_u seem to minimize disturbance due to SBPT probe installation;
- to make definite considerations on K assessment using q' and p' more CC and in situ experimental data are necessary also to get full significance from a statistical point of view considering in particular overconsolidated deposits;
- relationships to derive parameters, such as K , may be sensitive to environmental factors (aging, cementation, etc.) that exist for most natural sands. This topic needs to be investigated carefully in the future.

8. REFERENCES

1. Robertson P.K. (1982) "In-Situ Testing of Soil with Emphasis on Its Application to Liquefaction Assessment". Ph.D. Thesis, Univ. of British Columbia, Vancouver.
2. Fahey M. & Randolph M.F. (1985) "Effect of Disturbance on Parameters Derived from Self-Boring Pressuremeter Tests in Sand". Discussion Closure. *Geotechnique*, vol. 35, No. 2, 219-222.
3. Bruzzi D., Ghionna V.N., Jamiolkowski M., Lancellotta R., R. & Manfredini G. (1986) "Self-Boring Pressuremeter in Po River sand". Proc. 2nd Int. Symp. Pressuremeter and Its Marine Applications, Texas, STP 950. Austin, American Society for Testing and Materials, 57-73.
4. Windle D. (1976) "In-Situ Testing of Soils with a Self-Boring Pressuremeter". Ph.D Thesis, University of Cambridge, U.K.
5. Marchetti S. (1980) "In-Situ Tests by Flat Dilatometer". Journal of the Geotechnical Engineering Division, ASCE, vol. 106, No. GT3, Proc. Paper 15290, Mar., 299-321.
6. Handy R.L., Remmes B., Moldt S., Lutenegeger A.J. & Trott G. (1982) "In-Situ Stress Determination by Iowa Stepped Blade". Journal of the Geotech. Div., ASCE, GT11.
7. Schmertmann J.H. (1983) "Revised Procedure for Calculating K_o and OCR from DMT's with $I_p > 1.2$ and Which Incorporates the Penetration Force Measurements to Permit Calculating the Plain Strain Friction Angle". DMT Workshop 16-18 March 1983, Gainesville Florida.
8. Huntsman S.R. (1985) "Determination of In-Situ Lateral Pressure of Cohesionless Soils by Static Cone Penetrometer". Ph.D. Thesis, Univ. of California, Berkeley.
9. Baldi G., Bellotti R., Ghionna V.N., Jamiolkowski M., Marchetti S. & Pasqualini E. (1986) "Flat Dilatometer Test in Calibration Chamber". Proc. 2nd Int. Symp. on Pressuremeter and Its Marine Applications. Texas STP 950, Austin ASTM.
10. Jefferies N.G. & Jonsson L. (1987) "The Cone Penetration Test in Sands: Part 3 Horizontal Geostatic Stress Measurements During Cone Penetration". Draft, submitted to *Geotechnique* for publication.
11. Jamiolkowski M. & Robertson P.K. (1988) "Future Trends for Penetration Testing". Geotechnology Conference on Penetration Testing in the U.K., University of Birmingham, T. Telford.
12. Schnaid F. & Houlsby G.T. (1990) "Calibration Chamber Tests of the Cone-Pressuremeter in Sand". Proc. Int. Symposium on Pressuremeters. Oxford, April, T. Telford, London pp. 263-272.

13. Ladanyi B. (1963) "Evaluation of Pressuremeter Tests in Granular Soils". Proc. 2nd Pan-Am. Conf. Soil Mech., vol. 1, 3-30.
14. Vesic A. (1972) "Expansion of Cavities in Infinite Soil Mass". J. Soil Mech. Fans Div. Am. Soc. Civ. Engrs. vol. 98, SM 3, 265-290.
15. Carter J.P., Booker J.R. & Yeung S.K. (1986) "Cavity Expansion in Cohesive Frictional Soils". Geotechnique vol. 36, No. 3, pp. 349-358.
16. Wroth C.P. (1988) "Penetration Testing - a More Rigorous Approach to Interpretation". Proc. 1st Int. Symp. on Penetration Testing, ISOPT I, Orlando, Florida, vol. 1.
17. Jamiolkowski M., Ghionna V.T., Lancellotta R. & Pasqualini E. (1988) "New Correlations of Penetration Test for Design Practice". Proceedings of Penetration Testing 1988, ISOPT-I, Orlando, Florida, vol. 1.
18. Baldi G., Bellotti R., Ghionna V.N., Jamiolkowski M. & Pasqualini E. (1986) "Interpretation of CPT's and CPTU's. 2nd. Part: Drained Penetration of Sands". Proc. IV Int. Geotech. Seminar on Field Instrumentation and in Situ Measurements. Nanyang Tech. Inst. Singapore.
19. Yu, H.S. & Houlsby G.T. (1991) "Finite Cavity Expansion in Dilatant Soils: Loading Analysis". Geotechnique vol. 41, n° 2, 173-183.
20. Hughes J.M.O. & Robertson P.K. (1985) "Full Displacement Pressuremeters Testing in Sands". Canadian Geotechnical Journal, vol. 22, No. 3, 298-307.
21. Ghionna V.N., Jamiolkowski M. & Manassero M. (1990) "Limit Pressure in Expansion of Cylindrical Cavity in Sand". Proc. Int. Symposium on Pressuremeters, Oxford, April 1990, Thomas Telford, London, 149-158.
22. Manassero M. (1987) "Un Nuovo Approccio all'Interpretazione della Prova Pressiometrica in Sabbia". Tesi di Dottorato in Ingegneria Geotecnica, Politecnico di Torino, Dipartimento di Ingegneria Strutturale.
23. Manassero M. (1989) "Stress-Strain Relationships from Drained Self-Boring Pressuremeter Test in Sands". Géotechnique vol. 39, No. 2, 293-307.
24. Jaky J. (1944) "The Coefficient of Earth Pressure at Rest". Journal of the Society of Hungarian Architects and Engineers, 355-358.
25. Baldi G., Bellotti R., Crippa V., Fretti C., Ghionna V.N., Jamiolkowski M., Ostricati D., Paqualini E. & Pedroni S. (1985) "Laboratory Validation of In-Situ Tests". AGI Golden Jubilee Vol. Geotech. Eng. in Italy, 11th ICSMFE, San Francisco, 251-270.
26. Ghionna V.N., Braga G. & Macchi G. (1991) "Studies for the Assessment of the Stability of Pavia's Medieval Tower". Submitted to Ass. Geotec. Italiana for publication in the special volume "The Contribution of Geotechnical Engineering to the preservations of Italian Historic Sites", X ECSMFE Firenze - Italy.
27. Been K. & Jefferies M.G. (1985) "A State Parameter for Sands". Géotechnique, vol. 35, No. 2, 99-112.

TENTATIVE METHOD FOR ESTIMATING σ_{ho}' FROM q_c DATA IN SANDS

P.W. Mayne*

*Georgia Institute of Technology, School of Civil Engineering, Atlanta, GA 30332-0355

ABSTRACT

A tentative and preliminary procedure for estimating the in-situ effective horizontal stress (σ_{ho}') in unaged uncemented clean uniform sands from measurements of CPT cone tip resistance (q_c) is presented. The empirical methodology is derived from a statistical analysis of calibration chamber data compiled from 24 different sands. Since the procedure requires an *a priori* knowledge of stress history, the problem is solved by iteration and assuming a dependent relationship between K_o and OCR. Three well-documented field case studies involving natural sands are used to illustrate the procedure.

INTRODUCTION

Although the importance and difficulty of determining the in-situ horizontal stress coefficient $K_o = \sigma_{ho}'/\sigma_{vo}'$ in clean sands is well appreciated, few procedures have been developed for estimating its value in the field. Some limited success with attempts at direct measurement has been achieved with the self-boring pressuremeter [2, 3, 10, 23] and new developments with the lateral stress cone penetrometer have been promising [1, 8, 14, 17]. A number of indirect procedures have been developed for the dilatometer test [9, 13, 14]. One recent approach by Masood, et al. [14] involves the use of the measured CPT sleeve friction (f_s) to determine K_o .

Many researchers involved with calibration chamber testing of sands have noted for quite some time that the cone tip resistance is significantly influenced by the magnitude of horizontal stress (σ_{hc}') applied prior to cone penetration [4, 6, 7, 11, 19, 22]. Therefore, a database derived from 24 different series of CPT calibration chamber tests on relatively clean uniform unaged NC and OC sands was reviewed to investigate a σ_{hc}' - q_c relationship. Specific details concerning the database, sand properties, and chamber boundary corrections are given in a companion paper by Mayne and Kulhawy [15].

DERIVED CORRELATION

For dense Høksund sand, Parkin [19] showed a unique relationship between σ_{hc}' and q_c , regardless of prior stress history (OCRs = 1, 2, 4, and 8) or applied boundary condition (BC1 and BC3). The sand specimens were K_o -consolidated prior to cone penetration and suggested that $\sigma_{hc}' \propto q_c^{1.6}$ for the relatively dense condition of the sand. Houlby and Hitchman [7] also noted a similar power function expression relating σ_{hc}' and q_c for tests on Leighton-Buzzard sand; however, in these experiments, anisotropic stress states were applied to the specimens without K_o conditions being maintained during consolidation. For different initial relative densities (loose, medium, dense), different constants of proportionality were found for the sand, yet each level of D_r appeared to have the same exponent in the power function format.

The calibration chamber database supported a general σ_{hc}' - q_c - D_r relationship, as shown by Figure 1. For clarity, the data from 24 different sands are represented by open and

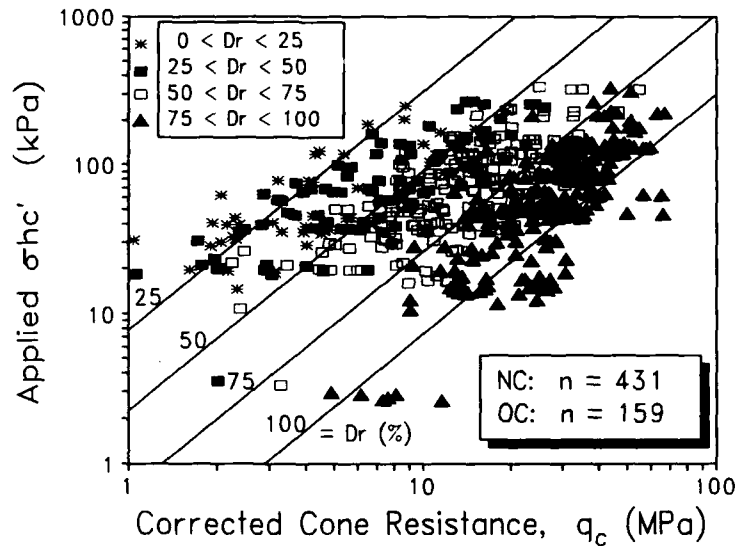


Figure 1. Generalized relationship between σ'_{vc} , q_c , and D_r from CPT calibration chamber database on unaged, uncemented, clean uniform sands.

closed symbols that have been grouped into four ranges of relative density and according to stress history (NC or OC). A preliminary evaluation of the data [11] indicated:

$$\sigma'_{vc} = (p_a/35)(q_c/p_a)^{1.25} e^{-D_r/20} \quad (1)$$

in which p_a = atmospheric pressure ($\approx 1 \text{ bar} \approx 1 \text{ tsf} \approx 1 \text{ kg/cm}^2 \approx 100 \text{ kPa}$) is introduced to provide dimensionless terms. Often, the profile of D_r for a sand deposit is not known nor is it directly measured. More commonly, the results of penetration tests are used to infer the in-situ D_r . A number of different correlations have been developed for evaluating D_r from SPT and CPT results. Based on the large number of tests contained in the current calibration chamber database, a recent relationship was formulated for the CPT by Kulhawy and Mayne [12]:

$$D_r = 100 \left[\frac{(q_c/p_a)/(\sigma'_{vc}/p_a)^{0.5}}{305 \text{ OCR}^{0.18}} \right] \quad (2)$$

which is analogous to the form used by Skempton [20] for relating D_r (in percent) to effective vertical stress (σ'_{vc}) and SPT-N value in sands. A more detailed and preliminary form of this equation has also been developed [12] which attempts to account for sand compressibility and aging effects. The simplified version given above is used herein due to the tentative nature of this development.

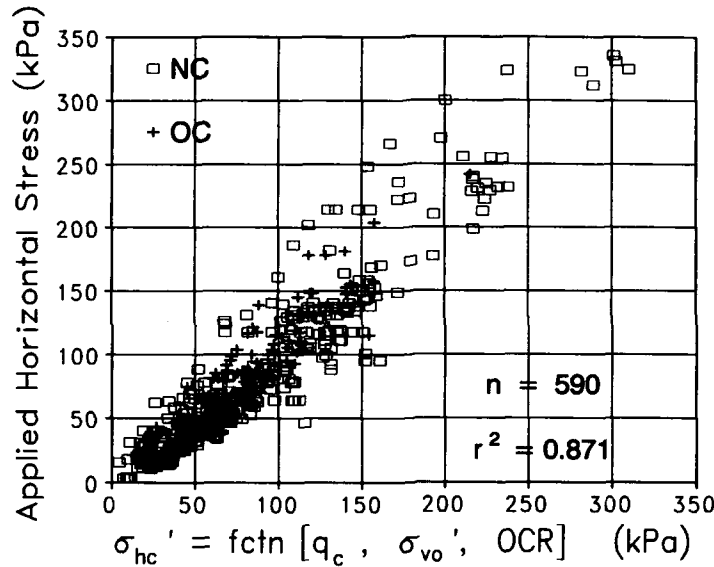


Figure 2. Statistical comparison of applied and predicted horizontal stresses for NC and OC sands using equation (4).

Eqn (2) is applicable only to the non-crushing region, corresponding to the limiting range of normalized cone tip resistances $(q_c/p_d)/(\sigma'_{vo}/p_d)^{0.5} < 400$. In this regard, calibration chamber tests by TeKamp [21] have not been included in the database since both the NC and OC tests were conducted at high relative densities beyond the particle crushing region. However, it is interesting to note that this separate series of data on Frigg Field sand independently confirms the power function term representing the effect of OCR. That is, the ratio of $q_c(OC)/q_c(NC)$ is approximately given by $OCR^{0.18}$. By combining Equations (1) and (2), the expression for effective horizontal stress becomes:

$$\sigma'_{hc}/p_d = \frac{(q_c/p_d)^{1.25}}{35 \exp\left\{\left[\frac{(q_c/p_d)/(\sigma'_{vo}/p_d)^{0.5}}{12.2 OCR^{0.18}}\right]^{0.5}\right\}} \quad (3)$$

A regression analysis between the applied σ'_{hc} versus predicted σ'_{hc} using Eqn (3) for $n = 590$ data points gives a best fit line through the origin ($b = 0$) with coefficient $m = 1.50$, coefficient of determination $r^2 = 0.729$, and standard error of the dependent variable, S.E. = 31.0. Therefore, by trial and error in optimizing the statistical fit, the equation was adjusted to give:

$$\sigma'_{hc}/p_d = \frac{(q_c/p_d)^{1.6}}{145 \exp\left\{\left[\frac{(q_c/p_d)/(\sigma'_{vo}/p_d)^{0.5}}{12.2 OCR^{0.18}}\right]^{0.5}\right\}} \quad (4)$$

which also better matches the exponent term determined by Parkin [19] and Houlsby and Hitchman [7]. A comparison of actual σ_{hc}' vs. predicted σ_{hc}' for NC and OC sands is presented in Figure 2. Regression statistics for this expression ($n = 590$) indicate a better fit with coefficient $m = 1.00$, $r^2 = 0.871$, and S.E. = 21.4. Possibly, including the effect of sand compressibility could further improve on this relationship.

A difficulty with the use of Eqn (4) for practical use is the fact that the OCR of natural sands is rarely known. However, if both sides of the equation are normalized with respect to the effective vertical stress, then:

$$K_o = \sigma_{hc}' / \sigma_{vo}' = \frac{(p_r / \sigma_{vo}') (q_c / p_d)^{1.6}}{145 \exp \left\{ \left[\frac{(q_c / p_d) / (\sigma_{vo}' / p_d)^{0.3}}{12.2 \text{ OCR}^{0.18}} \right]^{0.5} \right\}} \quad (5)$$

For sands which have experienced a simple load-unload history caused by mechanical overconsolidation, a compatible relationship should exist between K_o and OCR. As shown by Mayne and Kulhawy [16], the adopted form is taken as:

$$K_o = K_{oc} \text{OCR}^{1-K_{oc}} \quad (6)$$

in which K_{oc} corresponds to the NC horizontal stress coefficient of the sand. Tentatively, the author suggests the following form for practical use:

$$K_o = 0.35 \text{OCR}^{0.65} \quad (7)$$

unless better information is available for the particular sand under investigation. Eqn (7) can be rearranged in the form:

$$\text{OCR} = 5.04 K_o^{1.54} \quad (8)$$

The use of Eqns (8) and (5) require iteration until matching values of K_o are obtained. One side effect of this procedure is that an estimate of in-situ OCR is also made.

APPLICATIONS

The empirical relationship derived from the calibration chamber test database can be applied to three well-documented field sites that are underlain by relatively clean sand deposits.

Ukalerk, Canada

The site of the Ukalerk sand deposits lies within the Beaufort Shelf and has been reported by Jefferies [10]. The pre-Wisconsin deposit is offshore with a water depth of 26 m and the sand deposit of study (Unit C2) lies at depths of between 12 to 21 m below the mudline. Ukalerk sand is a subrounded sand with $D_{50} \approx 0.3$ mm, approximately 1 to 4 percent silt fraction, and occasional gravel. Figure 3 shows a estimated profile of σ_{hc}' developed from q_c data taken at the site. In the upper portions of the sand layer, the results compare favorably with interpreted SBP measurements made at the site using a Cambridge-type device. However, in the lower portions of the deposit, the CPT prediction is conservative by comparison. It is noted, however, that the procedure makes no attempt

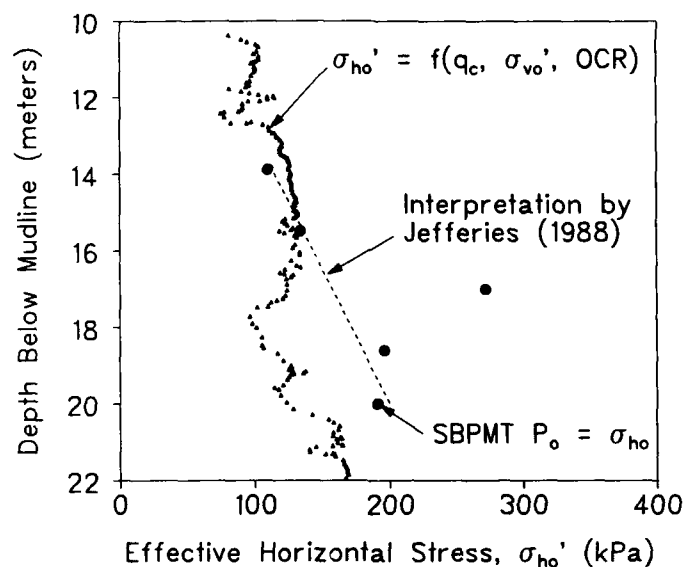


Figure 3. Estimated profile of σ'_{ho} with depth from in Ukalerk C2 sand.

to account for all factors affecting the in-situ value of K_o , such as aging, geochemistry, thermal effects, wave loading, etc.

Po River, Italy

The Holocene alluvial sands at Po River in Northern Italy have been extensively studied by in-situ and laboratory test methods [2, 3, 9, 13]. The subangular to subrounded sand has a $D_{50} \approx 0.2$ to 0.4 mm, 0 to 12 percent silty fines, with occasional fine gravels. Groundwater lies at a depth of 2 m and extensive laboratory testing on rare inclusions of clay lenses indicate the deposit to be slightly overconsolidated with $1.1 < OCR < 1.5$. The estimated K_o profile from CPT records is presented in Figure 4 with comparison values obtained from Camkometer SBP tests. Over the 25-m profile, the agreement between the two tests is rather good. In addition, the iterative procedure indicated an average $OCR \approx 1.20 \pm 0.12$ for the deposit.

Stockholm, Sweden

This site was initially occupied by 24 m of dry natural sand over bedrock, presumed to be normally consolidated. Excavation removed 16 m of the uppermost sand and a variety of in-situ tests were conducted on the remaining 8 m [5, 18]. Testing of the subangular sand ($D_{50} \approx 0.8$ to 1.0 mm; $C_u \approx 2.2$ to 3.0) included SPT, CPT, PMT, screw plate, weight soundings, Swedish ram soundings, density measurements, and triaxial tests. Figure 5 shows that the predicted profile of K_o with depth from the cone soundings compares well with that from the reconstructed stress history. Lift off stresses from standard PMTs in prebored holes at the site gave similar values. Figure 6 shows the CPT

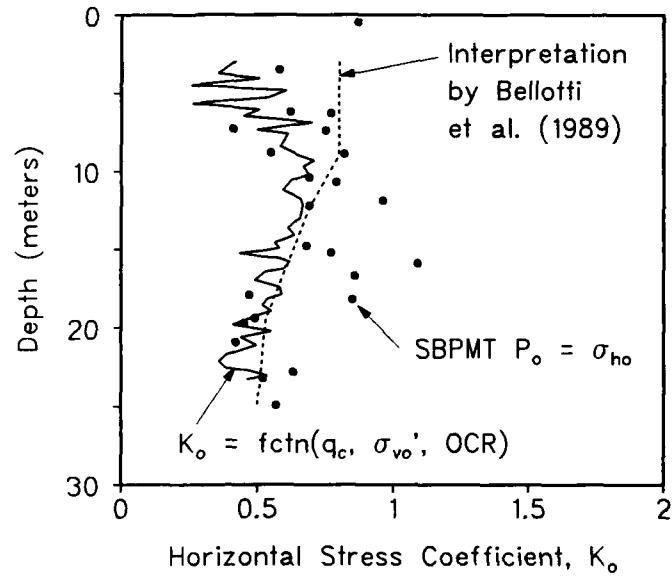


Figure 4. Estimated Profile of K_o in Po River sand.

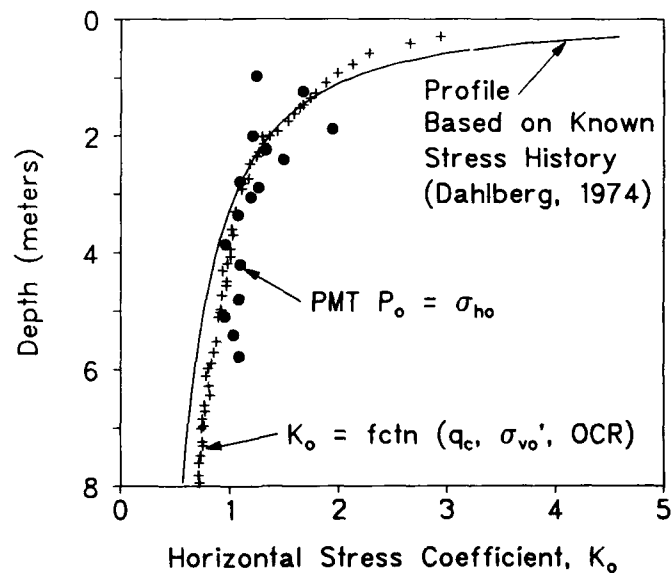


Figure 5. Estimated Profile of K_o in Stockholm sand.

estimated profile of OCR with depth from iterations in matching the K_0 profile. In addition to the OCRs calculated from known stress relief, yield stresses from screw plate tests substantiated the interpreted σ'_p profile at the site.

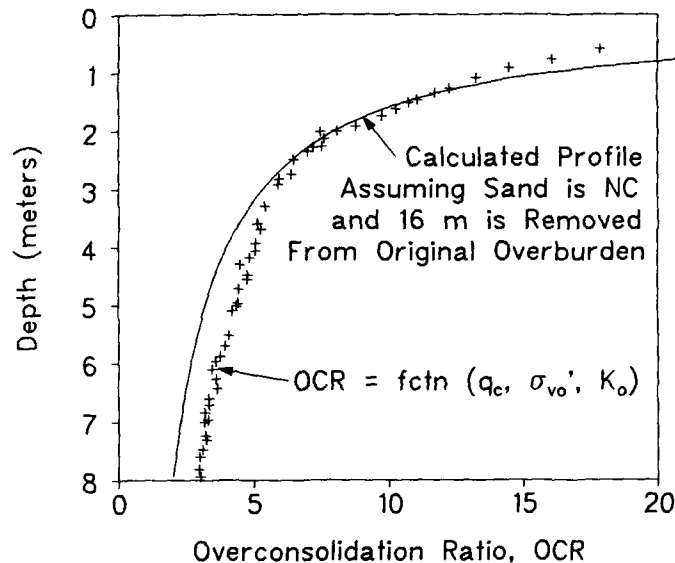


Figure 6. Profile of OCR with depth at Stockholm sand site.

CONCLUSIONS

A preliminary and tentative empirical procedure for estimating the in-situ K_0 of sands is presented based on CPT calibration chamber data from 24 sands. The method relates the effective horizontal stress (σ'_{ho}) to measured cone tip resistance (q_c) as a function of relative density (D_r). By including the effects of overconsolidation ratio (OCR) and effective vertical stress (σ'_{vo}), an iterative procedure is required to find the in-situ σ'_{ho} , assuming the sand has been loaded-unloaded mechanically and can be assigned a unique relationship between K_0 and OCR. The effects of aging, sand compressibility, particle crushing, fines content, cementation, geochemistry, and mineralogy are not considered herein but should be investigated in future studies.

REFERENCES

1. K. Been, B.E. Lingnau, J.H.A. Crooks, and B. Leach (1987), "Cone penetration test calibration for Erksak sand", Canadian Geot. J. 24 (4), 601-610.
2. R. Bellotti, V.N. Ghionna, M. Jamiolkowski, P.K. Robertson, and R.W. Peterson (1989), "Interpretation of moduli from SBPMT in sand", Geot. 39, No. 2, 269-292.
3. D. Bruzzi, V.N. Ghionna, M. Jamiolkowski, R. Lancellotta, and G. Manfredini (1986), "Self-boring pressuremeter in Po River sand", The Pressuremeter and Its Marine Application (STP 950), ASTM, Philadelphia, 57-74.

4. G.A. Chapman and I.B. Donald (1981), "Interpretation of static penetration tests in sand", Proc. 10th Intl. Conf. on Soil Mechanics and Foundation Engineering, Vol. 2, Stockholm, 455-458.
5. R. Dahlberg (1974), "Penetration, pressuremeter, and screw plate tests in a preloaded natural sand deposit", Proc. European Symposium on Penetration Testing, Vol. 2.2, Stockholm, 68-87.
6. J.C. Holden (1976), "The determination of deformation and shear strength parameters for sands using the electrical friction-cone penetrometer", Rept. 110, Norwegian Geot. Institute, Oslo, 55-60.
7. G.T. Houlsby and R. Hitchman (1988), "Calibration chamber tests of a cone penetrometer in sand", *Geotechnique* **38** (1), 39-44.
8. S.R. Huntsman, J.K. Mitchell, L.W. Klejbuk, and S.B. Shinde (1986), "Lateral stress measurement during cone penetration", *Use of In-Situ Tests in Geot. Engrg. (GSP 6)*, Ed. S.P. Clemence, ASCE, New York, 617-634.
9. M. Jamiolkowski, V.N. Ghionna, R. Lancellotta, and E. Pasqualini (1988), "New correlations of penetration tests for design practice", *Penetration Testing 1988*, Vol. 1, (ISOPT-1), Balkema, Rotterdam, 263-296.
10. M.G. Jefferies (1988), "Verification of q_c - Ψ function in sand strata", *Penetration Testing 1988*, Vol. 2, (ISOPT-1), Balkema, Rotterdam, 793-804.
11. F.H. Kulhawy, C.S. Jackson, and P.W. Mayne (1989), "First-order estimation of K_o in sands in clays", *Foundation Engineering: Current Principles and Practices (GSP 22)*, Vol. 1, ASCE, New York, 121-134.
12. F.H. Kulhawy and P.W. Mayne (1991), "Relative density, SPT, and CPT interrelationships", *Proceedings 1st International Conference on Calibration Chamber Testing*, Clarkson University, Potsdam, NY.
13. S. Marchetti (1985), "On the field determination of K_o in sand", Proc. 11th Intl. Conf. on Soil Mechanics and Foundation Engrg., Vol. 5, San Francisco, 2667-2672.
14. T. Masood, J.K. Mitchell, T. Lunne, and E.A. Hauge (1988), "In-situ testing at Hamilton Air Force Base and Bay Farm Island, CA", Joint Rept-Univ. of California, Berkeley and Norwegian Geot. Institute, Oslo, 56 p.
15. P.W. Mayne and F.H. Kulhawy (1991), "Calibration chamber database and boundary effects correction for CPT data", *Proceedings 1st International Conference on Calibration Chamber Testing*, Clarkson University, Potsdam, NY.
16. P.W. Mayne and F.H. Kulhawy (1982), " K_o -OCR relationships in soil", *Journal of the Geot. Engrg. Division (ASCE)*, **108** (GT6), 851-872.
17. J.K. Mitchell (1988), "New developments in penetration tests and equipment", *Penetration Testing 1988*, Vol. 1, (ISOPT-1), Balkema, Rotterdam, 245-261.
18. J.K. Mitchell and T. Lunne (1978), "Cone resistance as a measure of sand strength", *Journal of the Geot. Engrg. Division (ASCE)* **104** (GT7), 995-1012.
19. A.K. Parkin (1988), "The calibration of cone penetrometers", *Penetration Testing 1988*, Vol. 1, (ISOPT-1), Balkema, Rotterdam, 221-244.
20. A.W. Skempton (1986), "Standard penetration test procedures and effects in sands of overburden pressure, relative density, particle size, ageing, and overconsolidation", *Geotechnique* **36** (3), 425-447.
21. W.G.B. TeKamp (1982), "The influence of the rate of penetration on the cone resistance q_c in sand", Proc. European Symposium on Penetration Testing, Vol. 2, Amsterdam, 627-633.
22. A. Veismanis (1974), "Laboratory investigation of electrical friction-cone penetrometer in sand", Proc. European Symposium on Penetration Testing, Vol. 2.2, Stockholm, 407-419.
23. C.P. Wroth (1984), "The interpretation of in-situ soil tests" (24th Rankine Lecture), *Geot.* **34**, No. 4, 449-489.

CALIBRATION CHAMBER DATABASE AND BOUNDARY EFFECTS CORRECTION FOR CPT DATA

PAUL W. MAYNE* and FRED H. KULHAWY**

*School of Civil Engineering, Georgia Institute of Technology, Atlanta, GA 30332; **School of Civil and Environmental Engineering, Hollister Hall, Cornell University, Ithaca, NY 14853-3501

ABSTRACT

Calibration chamber tests were summarized from 24 sets of CPT data on sands to evaluate general cone relationships. However, the data can not be compared directly because of the influence of boundary effects on q_c . A simple general relationship was proposed to correct for these effects, and it includes the chamber diameter and the sand relative density. This relationship allows for a consistent comparison of equivalent "free field" data regardless of the data source.

INTRODUCTION

Many cone penetration test (CPT) correlations for sands have been developed from data obtained in laboratory calibration chambers that allow control of the sand uniformity, density, stress state, and stress history. Because of the finite size of calibration chambers, there is a boundary effect that will influence the measured cone tip resistance (q_c). In this paper, a database is developed for CPT calibration chamber tests that can be used to develop general cone relationships, as given elsewhere in this volume [16]. An assessment is made of the boundary effects on these data, and a simple relationship is proposed to correct the measured q_c data to represent equivalent "free field" data. The use of this relationship allows for direct comparison of all the CPT q_c data.

SOIL CHARACTERISTICS

Data were compiled from 24 sets of CPT calibration chamber tests on different sands. A listing of the sands, sources of data, and relevant index properties is given in Table I. The symbols column refers to that used on the correlation plots given elsewhere in this volume by Kulhawy and Mayne [16]. The entire database includes over 640 separate tests.

All of the calibration chamber tests were conducted on reconstituted sands that were unaged and uncemented. The majority were clean quartz sands. The percent fines ($\% < \text{No. 200 sieve}$) ranged from 0 to 6%, although most of the sands had less than 1% fines. The particle size at 50% finer (D_{50}) ranged from 0.16 to 1.0 mm, with an average of 0.38 mm. The particle size at 10% finer (D_{10}) ranged from 0.10 to 0.70 mm, with an average of 0.25 mm. All of the sands were uniformly graded, with a range of uniformity coefficient ($C_u = D_{60}/D_{10}$) from 1.10 to 2.60 and an average of 1.79. The specific gravity (G_s) of these sands ranged from 2.65 to 3.02, with an average of 2.68. The maximum void ratio ranged from 0.73 to 1.05, while the minimum void ratio ranged from 0.40 to 0.65.

For testing, the sands were prepared over a range of relative density (D_r) and overconsolidation ratio (OCR). Test values of D_r varied from 8 to 100%, with an overall mean value of $D_r = 65\%$ for all tests conducted. All 24 sands were tested in normally consolidated (NC) states of stress (OCR = 1), and seven of these also were tested at overconsolidated (OC) states of stress with $1 < \text{OCR} < 14.7$. The NC tests constitute approximately 75% of the entire database.

Copyright 1991 by Elsevier Science Publishing Company, Inc.
Calibration Chamber Testing
Editor: A.-B. Huang

TABLE I. Calibration chamber database for sands

No.	Symbol	Sand [Reference]	D ₅₀	D ₁₀	C _u	G _s	e _{max}	e _{min}
1	◇	Earlston [26]	0.33	0.16	2.60	2.65	0.727	0.404
2	◀◀	Edgar [10,26]	0.45	0.29	1.79	NA	0.919	0.543
3	⊕	Erksak [3]	0.35	0.18	2.20	2.65	0.963	0.525
4	△▲	Frankston [7]	0.31	0.18	2.05	NA	0.792	0.462
5	⊞	Hilton Mines [23]	0.20	0.15	2.00	3.02	1.050	0.620
6	○●	Hokksund [18, 20]	0.44	0.27	2.20	2.70	0.906	0.539
7	◇◆	Hokksund [1]	0.39	0.21	2.20	2.70	0.878	0.535
8	⊠	Hostun Fine [6]	0.35	0.18	2.22	NA	1.000	0.650
9	⊞	Lanchester 25/52 [25]	0.40	0.30	1.40	NA	0.818	0.563
10	◀	Leighton Buzzard [8]	0.37	0.26	1.50	NA	0.815	0.489
11	⊙	Leighton Buzzard [11]	0.85	0.70	1.30	NA	0.790	0.490
12	⊞	Lone Star 2 [27]	1.00	0.60	2.00	2.66	0.766	0.482
13	⊞	Lone Star 30 [27]	0.39	0.22	1.86	2.66	0.824	0.537
14	▷▷	Lone Star 60 [27]	0.30	0.18	1.48	2.66	0.908	0.566
15	⊞	Monterey 0 [12]	0.37	0.25	1.60	2.65	0.820	0.540
16	⊞	Monterey 0/30 [24]	0.45	0.35	1.37	2.65	0.803	0.563
17	◇	Oostershelde [9]	0.17	0.10	1.80	NA	0.887	0.562
18	▽	Ottawa [17]	0.28	0.26	1.10	NA	0.868	0.545
19	⊖	Ottawa 90 [23]	0.22	0.13	1.85	2.65	0.789	0.486
20	⊕	Reid-Bedford [23]	0.24	0.15	1.70	2.66	0.871	0.549
21	△	S. Oakleigh Fine [26]	0.17	0.12	1.60	2.65	0.932	0.570
22	▽▽	S. Oakleigh Medium [26]	0.32	0.17	2.20	NA	0.754	0.412
23	□■	Ticino [1,2,4,5]	0.50	0.41	1.58	2.67	0.915	0.568
24	◆	Toyoura [13]	0.16	0.13	1.46	2.64	0.977	0.605

Symbols: D₅₀ - particle size at 50% finer; D₁₀ - particle size at 10% finer
G_s - specific gravity of solids; C_u - uniformity coefficient
e_{max} - maximum void ratio; e_{min} - minimum void ratio

TABLE I. Calibration chamber database for sands (completed)

Angularity	Mineralogy	Chamber Diameter (mm)	Cone Diameter (mm)	D _r in Tests (%)	OCR in Tests
subrounded	quartz	760	50.0	20,45,65,73	1
subangular	quartz	1220	35.7	56,95	1 to 10
subrounded	quartz, 6% fines, trace chert	1400	35.7	69 to 99	1
subangular to rounded	quartz	1200	35.7	54 to 100	1 to 7.7
angular (S = 0.72, R = 0.23)	feldspar, quartz, mica, muscovite, iron, 3% fines	1220	35.7	30 to 84	1
angular	45% feldspar, 35% quartz, 10% mica	762,1220	25.2,35.7	8 to 100	1,8
subangular to angular	35% quartz, 10% mica	1200	20,25.4, 35.7	31,82,96	1,7.3, 14.5
subangular	quartz	180	11.3	15 to 95	1
subangular	95% quartz	254	9.5	0 to 100	1
subrounded	quartz	1200	35.7	40 to 97	1
subrounded	quartz	900	35.7	20 to 90	1
subrounded to subangular	quartz with feldspar	760	35.7	22 to 66	1
subrounded to subangular	quartz with feldspar	760	35.7	20 to 84	1
subrounded to subangular	quartz with feldspar	760	35.7	17 to 79	1,1.5, 3.6,5.9
subrounded (S = 0.80, R = 0.35)	quartz, trace feldspar	760	35.7	27 to 72	1
subrounded to subangular	quartz with feldspar	1500	23.2,35.7	24,64	1
rounded	quartz	1900	35.7	30 to 87	1
well-rounded	quartz	71.1	12.7	57	1,2,4
rounded	quartz, 0.2% fines	1220	35.7	20 to 83	1
subangular (S = 0.76, R = 0.29)	quartz, some feldspar, trace calcite	1220	35.7	24 to 81	1
subangular	quartz	760	35.7,50.0	28 to 86	1
subangular	quartz	760	35.7,50.0	44 to 89	1,2,4,8
subangular to angular (S = 0.79, R = 0.38)	30% quartz, 5% mica	1200	20,25.4, 35.7	16 to 98	1 to 14.7
subangular	high feldspar content	790	35.7	33 to 86	1

S - particle sphericity = $(6 \times \text{particle volume}/\pi)^{1/3}/\text{particle length}$

R - particle roundness (ratio of minimum radius of particle edges to inscribed radius of entire particle)

For the OC tests, the mean value of OCR was 3.01. In general, the sands were consolidated under K_0 conditions prior to testing. Exceptions include Leighton Buzzard sand [11], which was consolidated under general anisotropic conditions, Hostun sand [6], which was isotropically consolidated, and Monterey #0 sand [12], which had both K_0 and isotropically consolidated conditions. The mean value of K_0 for the NC specimens tested under K_0 and anisotropically consolidated conditions was 0.43. All of the OC specimens (except for one) were K_0 consolidated prior to cone penetration testing, and the mean value of K_0 was 0.91. The average value of applied effective vertical stress (σ_{vo}) for all tests was 152 kN/m².

The sands were placed in a dry state by air pluviation (raining), except for Erksak sand [3], which was tamped moist, and Lanchester sand [25], which was prepared by raining, tamping, and vibrating methods. In addition, the CPT tests were performed on dry sand, except for Erksak sand, which was back-pressure saturated, and Monterey #0 and Ticino sands, which were tested both dry and saturated. Furthermore, Jamiolkowski, et al. [14] state that Edgar, Ottawa, Reid-Bedford, and Hilton Mines sands were tested both "drained" and "submerged".

All tests used electric cones with a 60° cone angle. The cone diameters ranged from 9.5 to 50.0 mm, although 85% of the data were obtained with the standard 35.7 mm diameter cone. All cones were of the standard Fugro cylindrical shape, except for that of Villet and Mitchell [27], which had a reduced diameter behind the cone tip.

CALIBRATION CHAMBER BOUNDARY CONDITIONS

Most of the available data were obtained using flexible wall calibration chambers that allow yielding during cone penetration. This yielding gives measured cone tip resistance (q_c) values that are less than they would be in an infinite medium, and therefore the q_c values need to be corrected for these boundary effects. No generally accepted approach has been developed yet for making these corrections. However, recent research [e.g., 3, 19, 21] has shown that q_c increases with increasing ratio of chamber to cone diameter (B_c/B). In addition, the increase is more pronounced as the relative density increases. The correction factor used herein was derived from six available data sets from Table I where the B_c/B ratio was varied to allow evaluation of the boundary effects. These data are summarized in Figure 1. Based upon examination of these data and the trends noted above, the following correction factor was developed:

$$q_c(\text{corrected}) = q_c(\text{measured}) \left[\frac{(B_c/B) - 1}{70} \right]^{-D_r(\%) / 200} \quad (1)$$

Equation 1 assumes that there are no boundary effects when the diameter ratio (B_c/B) equals or exceeds 70. This value is somewhat of a compromise of the conclusions reached by Parkin and Lunne [21], who compared CPT results from both flexible and fixed wall chambers and concluded that a minimum diameter ratio of 50 was applicable for dense NC sands and a diameter ratio of at least 100 might be required for dense OC sands. However, recent work by Parkin [22] and Iwasaki, et al. [13] suggests that a maximum diameter ratio (B_c/B) of 70 is sufficient to achieve the "free field" condition. A plot of the correction from Eq. 1 is given in Figure 2, which shows increasing corrections needed for smaller B_c/B ratios and higher relative densities. The ratios of B_c/B for the 24 calibration chamber test series ranged from as low as 6 to as high as 65. Therefore, for some test series, a substantial correction was required to obtain the "free field" value of q_c .

Four different types of boundary conditions may be applied in flexible wall calibration chambers, as listed in Table II. Most of the tests summarized

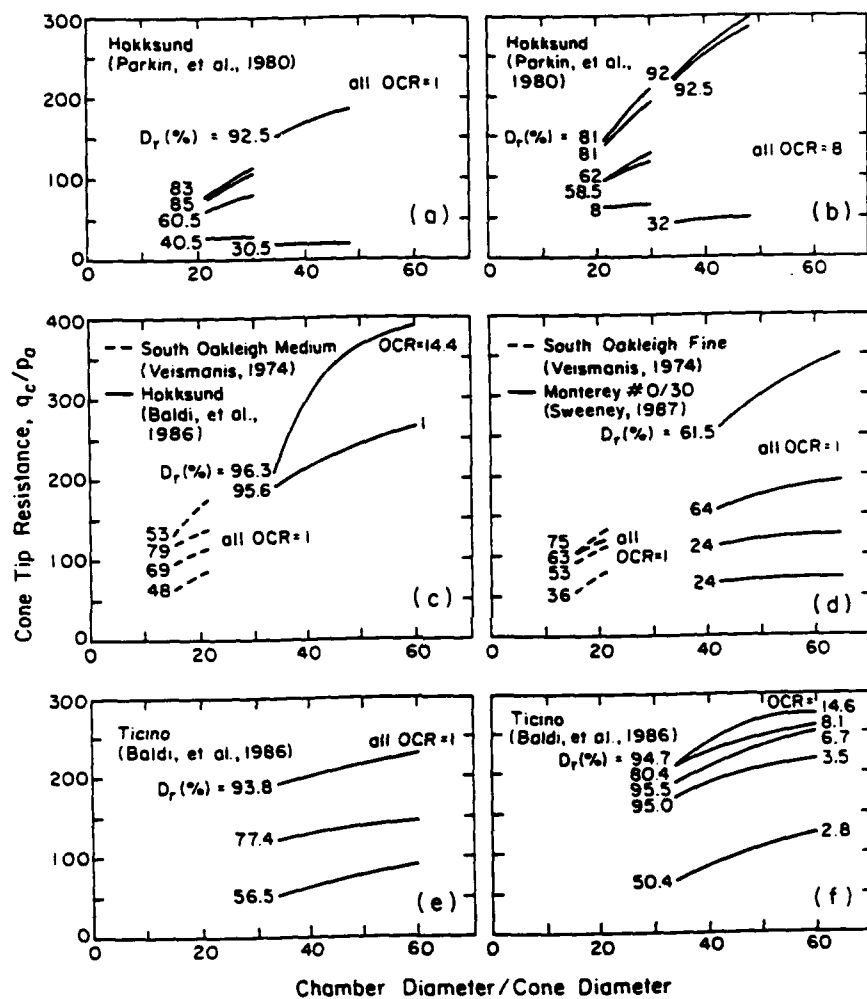


FIG. 1. Calibration chamber data for various sands

in Table I used Type A or C conditions, which more closely simulate field conditions. The proposed correction factor applies to these cases. It should be noted that the boundary conditions imposed in flexible wall calibration chambers represent only the average stresses and strains given by Table II. For Leighton Buzzard sand [8], which was tested under Type C conditions in a fixed-wall chamber, no correction was applied.

Only two of the sands used either Type B or D boundary conditions. The first was Toyoura sand, which was tested under Type B conditions. According to Iwasaki, et al. [13], no correction is required for this case. The second includes the three Lone Star sands [27], where the chamber used was of a different design than most and Type D conditions were imposed [3]. In addition, the cone employed in these tests had a reduced neck above the cone tip [19]. Therefore, for these sands, no correction factor was introduced because the

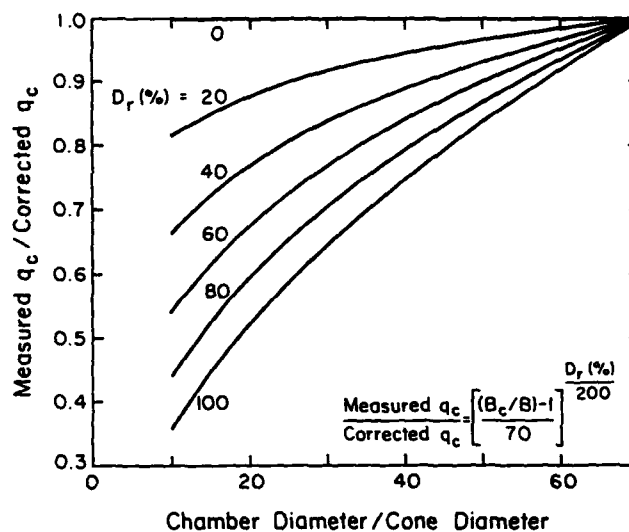


FIG. 2. CPT calibration chamber correction factor

TABLE II. Boundary conditions imposed in flexible wall calibration chambers

Type	Vertical	Horizontal
A	Stress constant	Stress constant
B	Change in strain is zero	Change in strain is zero
C	Stress constant	Change in strain is zero
D	Change in strain is zero	Stress constant

data are insufficient to develop this factor.

CONCLUSIONS

Data from 24 sets of CPT calibration tests on sands were summarized to develop general cone relationships. These data come from different chambers and can not be compared directly because of boundary effects. A simple relationship was proposed to correct for these effects. This relationship includes the chamber diameter and the sand relative density and therefore allows for a consistent comparison of CPT q_c data.

ACKNOWLEDGMENTS

This study was supported by the Electric Power Research Institute under RP-1493, and it has been previously reported in EPRI Report EL-6800 [15]. Vito J. Longo was the EPRI project manager. A. Avcişoy prepared the figures, and K. J. Stewart prepared the text.

REFERENCES

1. G. Baldi, R. Bellotti, V. Ghionna, M. Jamiolkowski, and E. Pasqualini, "Cone Resistance of a Dry Medium Sand", Proc. 10th Intl. Conf. Soil Mech. & Fndn. Eng. (2), Stockholm, 427-432 (1981).
2. G. Baldi, R. Bellotti, V. Ghionna, M. Jamiolkowski, and E. Pasqualini, "Interpretation of CPTs and CPTUs: Drained Penetration of Sands", Proc. 4th Intl. Geot. Sem. on Field Inst. & In-Situ Meas., Nanyang Tech. Inst., Singapore, 143-156 (1986).
3. K. Been, B.E. Lingnau, J.H.A. Crooks, and B. Leach, "Cone Penetration Test Calibration for Erksak Sand", Can. Geot. J., 24 (4), 601-610 (1987).
4. R. Bellotti, G. Bizzi, V. Ghionna, M. Jamiolkowski, S. Marchetti, and E. Pasqualini, "Preliminary Calibration Tests of Electrical Cone and Flat Dilatometer in Sand", Proc. 8th Eur. Conf. Soil Mech. & Fndn. Eng. (2), Brighton, 195-200 (1979).
5. R. Bellotti, G. Bizzi, and V. Ghionna, "Design, Construction, and Use of a Calibration Chamber", Proc. 2nd Eur. Symp. Pen. Test. (2), Amsterdam, 439-446 (1982).
6. J. Canou, M. El Hachem, A. Kattan, and I. Juran, "Mini Piezocone Investigation Related to Sand Liquefaction Analysis", Proc. 1st Intl. Symp. Pen. Test. (2), Orlando, 699-706 (1988).
7. G.A. Chapman and I.B. Donald, "Interpretation of Static Penetration Tests in Sand", Proc. 10th Intl. Conf. Soil Mech. & Fndn. Eng. (2), Stockholm, 455-458 (1981).
8. M.K. Chong, "Density Changes of Sand on Cone Penetration Resistances", Proc. 1st Intl. Symp. Pen. Test. (2), Orlando, 707-714 (1988).
9. G. Greeuw, F.P. Smits, and P. van Driel, "Cone Penetration Tests in Dry Oosterschelde Sand and the Relation with a Cavity Expansion Model", Proc. 1st Intl. Symp. Pen. Test. (2), Orlando, 771-776 (1988).
10. J.C. Holden, "Determination of Deformation and Shear Strength Parameters for Sands Using the Electrical Friction Cone Penetrometer", Rpt. 110, Norwegian Geot. Inst., Oslo, 55-60 (1976).
11. G.T. Houlsby and R. Hitchman, "Calibration Chamber Tests of a Cone Penetrometer in Sand", Geotechnique, 38 (1), 39-44 (1988).
12. S.R. Huntsman, J.K. Mitchell, L.W. Klejbuk, and S.B. Shinde, "Lateral Stress Measurement During Cone Penetration", Use of In-Situ Tests in Geot. Eng. (GSP 6), Ed. S.P. Clemence, ASCE, New York, 617-634 (1986).
13. K. Iwasaki, F. Tanizawa, S. Zhou, and F. Taksuoka, "Cone Resistance and Liquefaction Strength of Sand", Proc. 1st Intl. Symp. Pen. Test. (2), Orlando, 785-791 (1988).
14. M. Jamiolkowski, G. Baldi, R. Bellotti, V. Ghionna, and E. Pasqualini, "Penetration Resistance and Liquefaction of Sands", Proc. 11th Intl. Conf. Soil Mech. & Fndn. Eng. (4), San Francisco, 1891-1896 (1985).
15. F.H. Kulhawy and P.W. Mayne, "Manual on Estimating Soil Properties for Foundation Design", Rpt. EL-6800, Elec. Power Res. Inst., Palo Alto, 306 p. (1990).
16. F.H. Kulhawy and P.W. Mayne, "Relative Density, SPT, and CPT Interrelationships", This proc. vol. (1991).
17. J.R. Lambrechts and G.A. Leonards, "Effects of Stress History on Deformation of Sand", J. Geot. Eng. Div. (ASCE), 104 (GT11), 1371-1388 (1978).
18. T. Lunne and H.P. Christoffersen, "Interpretation of Cone Penetrometer Data for Offshore Sands", Rpt. 156, Norwegian Geot. Inst., Oslo, 1-11 (1985).
19. J.K. Mitchell and J.M. Keaveny, "Determining Sand Strength by Cone Penetrometer", Use of In-Situ Tests in Geot. Eng. (GSP 6), Ed. S.P. Clemence, ASCE, New York, 823-839 (1986).
20. A.K. Parkin, J. Holden, K. Aamot, N. Last, and T. Lunne, "Laboratory Investigation of CPTs in Sand", Rpt. 52108-9, Norwegian Geot. Inst., Oslo, 45 p. (1980).
21. A.K. Parkin and T. Lunne, "Boundary Effects in the Laboratory Calibration of a Cone Penetrometer for Sand", Proc. 2nd Eur. Symp. Pen. Test. (2),

- Amsterdam, 761-768 (1982).
22. A.K. Parkin, "Calibration of Cone Penetrometers", Proc. 1st Intl. Symp. Pen. Test. (1), Orlando, 221-244 (1988).
 23. J.H. Schmertmann, "Guidelines for Cone Penetration Test Performance and Design", Rpt. FHWA-TS-78-209, Fed. Highway Admin., Washington, 145 p. (1978).
 24. B.P. Sweeney, "Liquefaction Evaluation Using a Miniature Cone Penetrometer and Large Scale Calibration Chamber", PhD Thesis, Stanford Univ., 281 p. (1987).
 25. D. Thomas, "Deep Sounding Test Results and the Settlement of Spread Footings on Normally Consolidated Sands", Geotechnique, 20 (4), 472-488 (1968).
 26. A. Veismanis, "Laboratory Investigation of Electrical Friction Cone Penetrometers in Sand", Proc. Eur. Symp. Pen. Test. (2.2), Stockholm, 407-419 (1974).
 27. W.C.B. Villet and J.K. Mitchell, "Cone Resistance, Relative Density, and Friction Angle", Cone Pen. Test. & Experience, Ed. G.M. Norris and R.D. Holtz, ASCE, New York, 178-207 (1981).

Calibration Tests on the Cone Pressuremeter in Carbonate Sand

N.R.F. NUTT and G.T. HOULSBY

Department of Engineering Science, Oxford University,
Parks Road, Oxford, OX1 3PJ, U.K.

ABSTRACT

Tests on the cone pressuremeter in a quartz sand had previously been carried out in a large calibration chamber, and led to correlations being suggested from which the *in situ* horizontal stress and relative density could be inferred. In this Paper a new series of tests on a very crushable carbonate sand are presented and compared with the correlations established for silica sand. The significance of creep in tests in carbonate sand is identified, and its influence on the test results assessed.

INTRODUCTION

The cone pressuremeter is a more complicated instrument to analyse than the self-boring pressuremeter, because the penetration of the cone displaces soil outwards so that the test does not begin in nominally undisturbed soil. An analysis of the test in clay has been shown to agree well with observed tests, Houlsby and Withers (1988), but in sand the interpretation of the test must at present rely principally on the results of calibration tests.

A set of 21 calibration tests of the cone pressuremeter in silica sand has been carried out at Oxford University, and has resulted in a series of correlations from which cone pressuremeter tests could be used to infer the *in situ* values of horizontal stress and relative density. A major concern in the application of these correlations is whether they are only applicable to the silica sand used for the tests, or whether they have wider applicability. A similar set of tests on carbonate sand is reported in this paper in order that this applicability can be assessed. The carbonate sand was chosen because it differs enormously from the silica sand in the properties of the grains. The

silica sand consisted of very hard grains of size approximately 1.1 mm, which were not susceptible to crushing at the stress levels used; the carbonate sand consists of highly crushable soft grains of size approximately 0.24 mm. Further tests on other types of sand would also be desirable.

The principal aim of this paper is to demonstrate firstly that the measurements made with the cone pressuremeter depend on the same controlling parameters (horizontal stress and density) for carbonate sands as well as silica sands. Secondly a numerical comparison of the correlations obtained is made. A third objective, unrelated to the behaviour of silica sands, is the observation of creep behaviour of carbonate sand in the cone pressuremeter test.

TEST PROCEDURE

The cone pressuremeter tests reported in this Paper were carried out in a large calibration chamber 1.5 m in height and 1 m in diameter with flexible boundaries allowing control of both the vertical and lateral stresses. These stresses were applied by water-filled membranes which were attached to an air-water interface for precise pressure control. A driving rig fixed to the lid of the chamber enabled the cone pressuremeter to be inserted into the sample at a constant rate of 20 mm per second.

Carbonate sand from Dogs Bay on the west coast of Ireland was used for the tests. The sand contains a large proportion of skeletal mollusc fragments in the form of plates, hollow globules and tubes, and carbonate contents were found to range from 87% to 92%. Dogs Bay sand has a D_{50} of about 0.24 and a coefficient of uniformity of 2.75. Dry sand was used in all the tests and therefore the total and effective stresses were equal.

In each test the sample was prepared by raining the sand from a hopper with a sliding shutter plate at the base. Holes in the shutter plate of 20 mm diameter spaced on a triangular grid enabled the sand to be poured to a reasonably consistent density, and the relative density R_d of the samples for each test are listed in Table 1.

A 10 cm² cone pressuremeter was pushed into the sample and a continuous trace of cone resistance q_c was recorded during penetration. Insertion was stopped when the centre of the pressuremeter was at the midheight of the chamber, and the cone resistance as the cone tip passed the midheight is used in the analysis of results, and is listed in Table 1. A strain controlled pressuremeter test was then carried out. Silicon oil was used to inflate the pressuremeter and continuous measurements of the inflation pressure ψ were made by a pressure cell. Three strain-gauged arms spaced at 120° angular spacing at the centre of the pressuremeter recorded radial displacements of the membrane, and tests were taken to at least 40%

Test	σ_v (kPa)	σ_h (kPa)	K	R_d %	Voids ratio	q_c (MPa)	ψ_i (kPa)	$q_c - \sigma_h$ $\psi_i - \sigma_h$
DB0	48.6	48.3	0.99	6.7	1.77	2.23	339	7.5
DX1	59.2	28.7	0.48	22.4	1.64	0.74	232	3.5
DB2	148.8	72.7	0.49	16.5	1.69	3.48	582	6.7
DB3	58.2	27.1	0.47	28.4	1.59	2.92	379	8.2
DB4	23.0	46.2	2.01	23.0	1.63	2.43	354	7.8
DB5	38.6	37.8	0.98	23.9	1.63	1.29	266	5.5
DB6	98.6	97.8	0.99	22.1	1.64	3.99	631	7.3
DB7	23.2	47.2	2.03	25.7	1.61	2.24	323	8.0
DB8	60.8	118.9	1.96	28.1	1.59	4.78	748	7.4
DX9	148.9	147.8	0.99	31.0	1.57	5.16	922	6.5
DB11	58.2	27.9	0.48	27.5	1.60	1.49	223	7.5
DB12	149.6	74.6	0.50	28.4	1.59	3.58	598	6.7
DB13	39.4	38.2	0.97	32.7	1.55	2.07	307	7.6
DB14	148.9	74.8	0.50	29.0	1.58	3.81	572	7.5

Table 1. Results of cone pressuremeter tests on carbonate sand from Dogs Bay

logarithmic strain. If at this stage a clear limiting inflation pressure had not been reached, the limit pressure was taken as the pressure reached at 39% radial strain. Unload/reload loops to measure shear modulus were carried out during the pressuremeter test, usually at strains of 15%, 25% and 35%.

A summary of the pressuremeter results appears in Table 1. The pressures measured were corrected for membrane stiffness as measured by a calibration test in air, and the applied horizontal and vertical chamber stresses were corrected for the difference in height between the interface water-level and the level of the midheight of the chamber.

TEST RESULTS

Two independent tests can be obtained from the cone pressuremeter: a profile of cone resistance with depth and a plot of pressure with radial strain from the pressuremeter phase of the test. One of the main purposes of the latter is to use unload-reload loops to determine the shear modulus; this feature of the test is not discussed here, where the purpose is to concentrate principally on the measurements of cone resistance and limit pressure. The variables defining the soil condition which can be controlled for each test are density, horizontal stress and vertical stress, and these provide the basis for interpretation of parameters obtained from a cone pressuremeter (CPM) test.

Figure 1 shows the variation of cone resistance with depth of penetration for a typical test. The small maximum in resistance evident at about 70mm penetration is probably a result of manually flattening the sand surface by a straight edge after pouring the sample, creating an even surface onto which the chamber lid would be placed. The remainder of the curve, however, is clearly steady with depth and thus the cone resistance is easily determined.

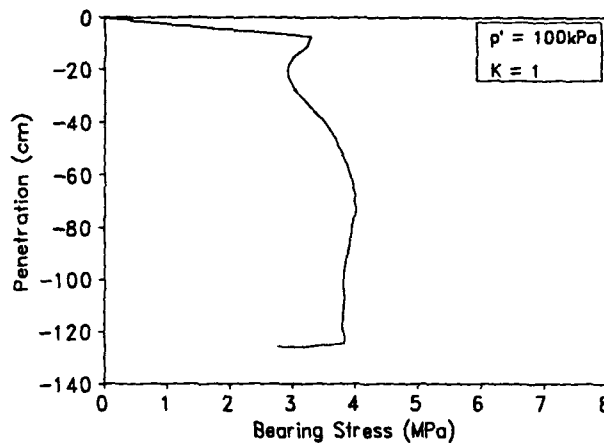


Figure 1. Test DB6, cone resistance against penetration

Because of the crushable nature of the carbonate sand, a zone of crushed sand forms at the tip of the cone pressuremeter during penetration and this is made evident by the presence of fine powdered sand adhering to the cone after extraction from the chamber.

Results from Housby & Hitchman (1988) and Schnaid (1991) in quartz sand showed that cone resistance is dependent upon horizontal stress rather than the vertical stress, and this is also found to be the trend for tests in carbonate sand. The q_c values for tests carried out at the same mean effective stress were found to increase with increasing stress ratio K (defined as the ratio σ'_h/σ'_v). Unlike tests on quartz samples, however, where overstressing a sample produces no significant effect on the results, overstressed carbonate sand samples resulted in somewhat higher values of cone resistance and limit pressure.

The pressuremeter curve shown in Figure 2 forms part of the same test as the cone profile in Figure 1. There exists a clear lift-off pressure in this test which is characteristic of tests performed at a K of 1.0 or 2.0 but significantly less in magnitude for tests at a K value of 0.5. However, unlike the self-boring pressuremeter, where the disturbance is kept to a minimum, it is not considered feasible in a CPM test to estimate the *in situ* horizontal stress from lift-off pressure. In the CPM test there is of course no reason to suppose that the lift-off pressure should be equal to the *in situ* horizontal stress. Nevertheless the initial part of the test appears to be influenced by the K value.

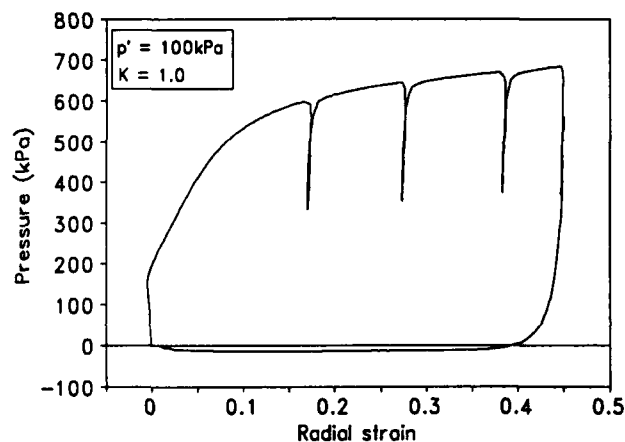


Figure 2. Test DB6, pressure against radial strain

During inflation of the pressuremeter, unload-reload loops were performed to obtain estimates of the elastic shear modulus, G of the soil. The increasing strain with the drop in pressure at the start of these loops signifies the susceptibility of the carbonate sand to creep. In order to assess the influence of creep, several of the basic test series were repeated with pressure-holding tests prior to the unloading portion of the loop. The pressure-holding tests resulted in marginally higher values of shear modulus and also provided a basis for interpreting the creep characteristics of the sand. This will be discussed in more detail in a later section of this Paper.

Upon unloading it can be seen that, after a correction for inflation in air, the pressuremeter experiences slightly negative pressure until the strain is almost zero. This is best explained by the expectation that fine particles become trapped in the crevices of the fully inflated Chinese lantern, thus providing a small resistance to the contraction of the lantern under decreasing pressure.

A number of tests with the cone pressuremeter were carried out by Schnaid (1991) in Leighton Buzzard sand, and reported by Schnaid and Houlsby (1990). It was found that a unique relationship exists between limit pressure and horizontal stress for each density tested. Similarly, results were obtained for the cone pressuremeter in carbonate sand. As shown in Figure 3, the carbonate sand results fall slightly below the loose silica sand results of Schnaid, but still follow a very similar trend. It would be expected that the limit pressures in the carbonate sand tests at higher horizontal stresses would decrease by comparison with those in silica sand tests as particle crushing begins to influence behaviour, although there does not appear to be a clear point at which such deviation occurs.

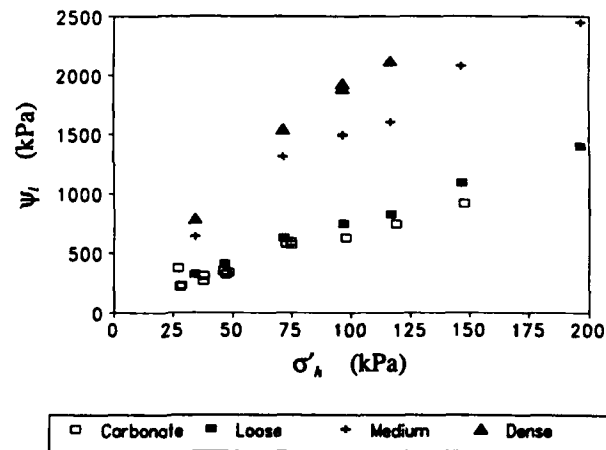


Figure 3. Limit pressure against horizontal stress (silica sand data from Schnaid, 1990)

In similar fashion the carbonate sand results have been superimposed on a plot of cone resistance against limit pressure in Figure 4. As with the silica sand results, a linear relationship links cone resistance to limit pressure for the particular density at which tests were carried out, but unlike the trend in Figure 3, the carbonate results fall between the loose and medium silica

sand results. This suggests that relative density is not the sole parameter for assessing sand behaviour, but that some additional feature which incorporates the differences in sand type should be accounted for.

One of the principal concerns in carrying out calibration chamber testing is the influence of the proximity of the chamber boundary. Schnaid and Houlsby (1991) present a review of the importance of the boundary, based on results from a variety of sands and testing chambers. Carbonate sand was not included in that study, but it may be deduced that at the relative densities tested the 1m diameter tank was sufficiently large for the effect of the proximity of the chamber boundary to be very small on measurements of both q_c and ψ_l . The ratio between these two measurements is even less influenced by the chamber boundary. These conclusions are based on experience principally for silica sand: the crushability of carbonate sand should further decrease the importance of the boundary.

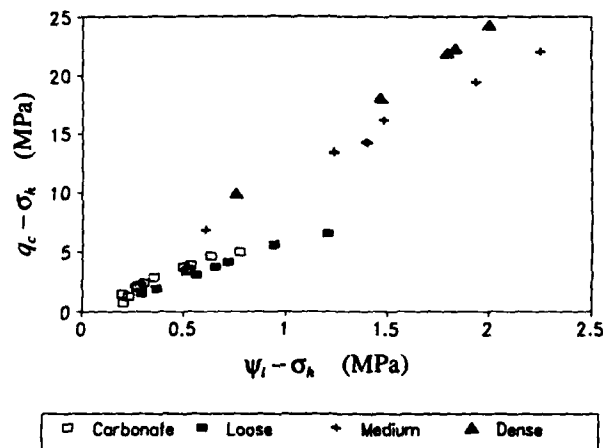


Figure 4. Cone resistance against limit pressure (silica sand data from Schnaid, 1990)

Data from silica sand had been used to establish the correlation (Schnaid and Houlsby, 1990):

$$R_d = \frac{1}{3} \frac{q_c - \sigma_h}{\sigma'_h} + 10$$

which is shown on Figure 5. Also shown on the Figure are the data from carbonate sand, showing that the same correlation would be appropriate. Semple (1988) suggested that a comparison between the behaviour of carbonate and silica sands is best made on a basis of voids ratio. These results indicate that in this context a comparison based on Relative Density is more satisfactory. Note that the horizontal stress is subtracted from the cone resistance for consistency with other analyses (Wroth, 1988). The correction is small in this case.

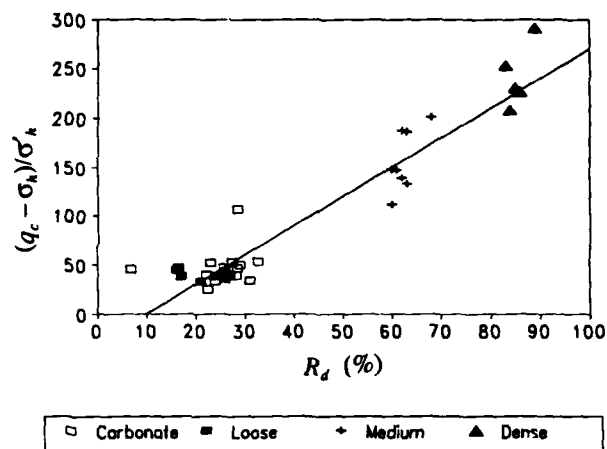


Figure 5. Cone resistance to horizontal stress ratio against relative density (silica sand data from Schnaid, 1990)

A correlation was also established between relative density and the cone resistance to limit pressure ratio (Schnaid and Houlsby, 1990):

$$R_d = 9 \frac{q_c - \sigma_h}{\psi_l - \sigma_h} - 30$$

which is shown in Figure 6. In this case the data for carbonate sand show that a slightly different correlation might be more appropriate, although the difference from the trend of the silica sand data is relatively small compared to the scatter. It is worth noting that the two outlying points from the carbonate sand data shown in Figures 5 and 6 correspond to the first two tests carried out. Later tests show more consistent behaviour as testing techniques became standardised.

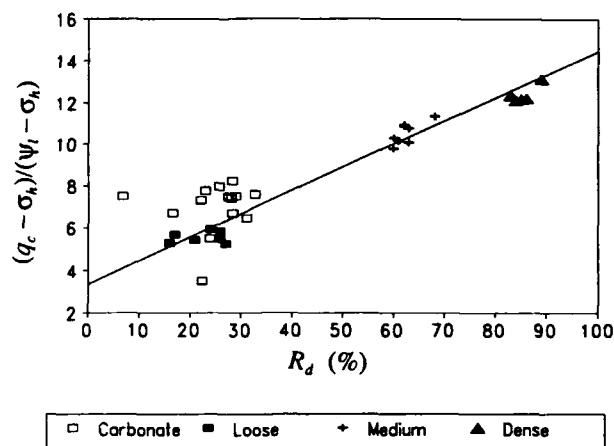


Figure 6. Cone resistance to limit pressure ratio against relative density (silica sand data from Schnaid, 1990)

It is extremely encouraging that the correlations established for silica sand should be apparently applicable also to carbonate sand with little modification. Caution should be exercised, however, as only limited data is at present available. A significant problem is that of establishing appropriate maximum and minimum density values for the carbonate sand and so defining the relative density.

CREEP TESTS

Of the basic tests carried out, a number of stress states were repeated with pressure-holding tests immediately prior to commencement of the unload-reload loops as shown in Figure 7. In each pressure-holding test the rate of strain was recorded and the test was continued until the strain rate became constant. Results of the pressure-holding stages from two such pressuremeter tests are shown in Figure 8. The increase in radial strain is plotted against time and while for all the tests the initial strain rate is constant, it is clear that creep of the soil is greatly dependent upon the stage of the pressuremeter test at which the pressure holding test is begun. At 12% strain most of the creep ceases after about 10 minutes. At higher strains, however, when the pressure-strain curve of Figure 7 becomes flatter, there appears to be continuing creep with time.

Creep in self-boring pressuremeter tests in carbonate sand has been observed by Fahey (1988) and in cone pressuremeter tests on two silica sands by Withers *et al.* (1989).

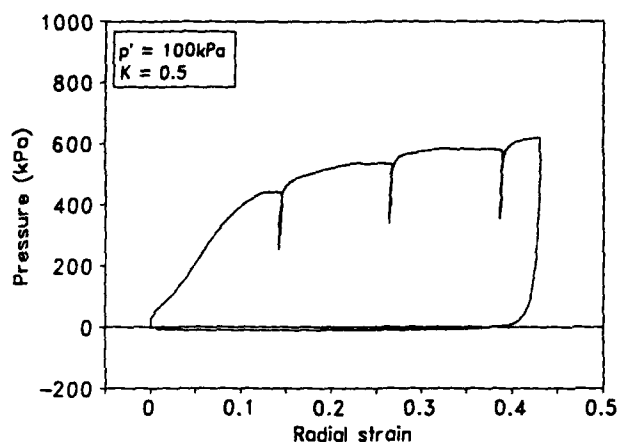


Figure 7. Test DB12, pressure against strain, incorporating three pressure-holding tests

To understand the link between creep and strain rate, additional tests were carried out where the rate of pressuremeter strain was manually controlled. Two rates of inflation were used, varying by an order of magnitude. The result of one such test is shown in Figure 9 where it is clear that the slower strain rate results in a reduced pressure, but on a seemingly parallel curve. This suggests that there exists a family of pressuremeter curves each corresponding to a particular rate of strain, with the curves essentially "parallel" to each other. Such curves can be used to interpret the creep behaviour during a pressure holding test. Upon holding pressure constant at a particular strain, the loading point travels horizontally across a succession of curves of decreasing strain rate. This model explains why it would be possible at high pressuremeter strains to observe continuing rather than stabilising creep, since the pressuremeter curves of the different strain rates are parallel and almost horizontal. Such behaviour is expected to be characteristic of carbonate sands, unlike silica sands where creep is much smaller since the response of the sand is less sensitive to variations in strain rate.

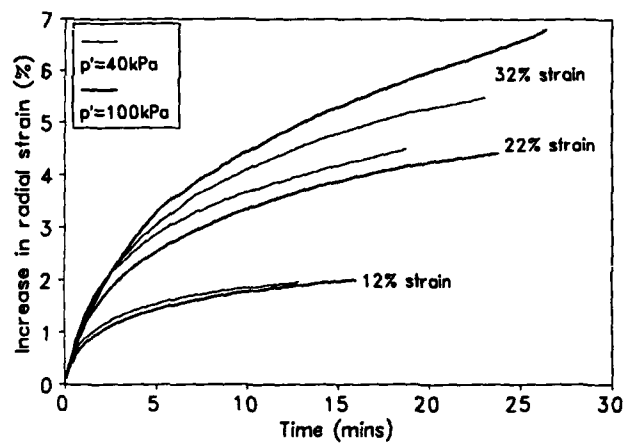


Figure 8. Test DB11 and DB12, strain increment against time for pressure-holding tests

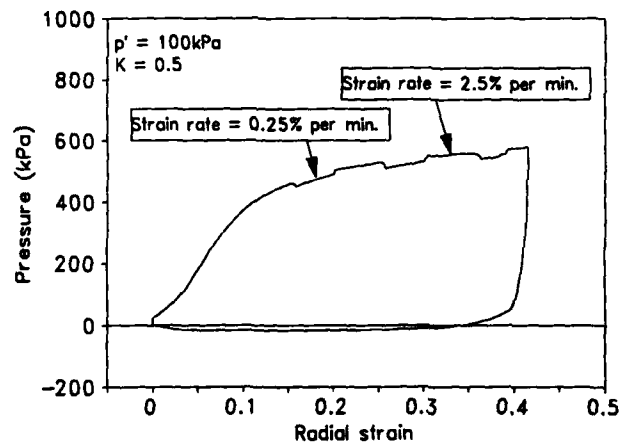


Figure 9. Test DB14, pressure against strain at different strain rates

CONCLUSIONS

Calibration tests on the cone pressuremeter in carbonate sand have established that similar patterns of behaviour are observed to those obtained from tests in silica sand. In particular both the cone resistance and the limit pressure are controlled principally by the horizontal stress and are relatively uninfluenced by the vertical stress.

Correlations established from silica sand data which could be used to establish relative density and horizontal stress from cone pressuremeter tests can be used with little modification in carbonate sand.

The pressures observed in tests on carbonate sand were found to be affected significantly by a tenfold change in the strain rate, indicating that the behaviour of the carbonate sand skeleton is rate dependent. This is linked to the fact that, if a constant pressure is held with the pressuremeter, creep strains are observed. This complication has a significant effect on the measurement of shear modulus, which is one of the principal purposes of the cone pressuremeter. Testing procedures need to be adapted so that the influence of creep strain can be eliminated from the measurement of shear modulus.

REFERENCES

- Fahey, M. (1988) "Self-boring Pressuremeter Testing in Calcareous Soil", Proc. Int. Conf. Calcareous Sediments, Perth, Vol. 1, 165-172
- Houlsby, G.T. and Hitchman, R.C. (1988) "Calibration Chamber Tests of a Cone Penetrometer in Sand", Géotechnique, Vol. 38, No. 1, 39-44
- Houlsby, G.T. and Withers (1988) "Analysis of the Cone Pressuremeter in Clay", Géotechnique, Vol. 38, No. 4, 575-587
- Schnaid, F. (1990) "A Study of the Cone Pressuremeter Test in Sand", D.Phil Thesis, Oxford University
- Schnaid, F. and Houlsby, G.T. (1990) "Calibration Chamber Tests of the Cone Pressuremeter in Sand", Proc. 3rd International Symposium on Pressuremeters, ISP3, Oxford, 2nd-6th April, 263-272
- Semple, R.M. (1988) "The Mechanical Properties of Carbonate Soils", Proc. Int. Conf. on Calcareous Sediments, Perth, 807-836
- Withers, N.J., Howie, J., Hughes, J.M.O. and Robertson, P.K. (1989) "Performance and Analysis of Cone Pressuremeter Tests in Sands", Géotechnique, Vol. 39, No. 3, 433-454
- Wroth, C.P. (1988) "Penetration Testing - A More Rigorous Approach to Interpretation", Proc. 1st Int. Symp. on Penetrometer Testing, ISOPT-1, Orlando, Vol. 1, 303-311

HOUSTON'S CALIBRATION CHAMBER: CASE HISTORIES

MICHAEL W. O'NEILL*

*University of Houston, Department of Civil and Environmental Engineering,
4800 Calhoun Road, Houston, TX 77204-4791

ABSTRACT

This paper describes a long, slender pressure chamber that was originally conceived for the testing of piles. Boundary conditions and scaling features are described, and two case histories of its past use are presented, indicating both the problems encountered in the use of the chamber and the results of the problems studied.

INTRODUCTION

The University of Houston (UH) has designed and constructed several calibration chambers, which this writer prefers to term "pressure chambers," since 1976. In each case, the motivation for construction of the chamber has been the study of the behavior impact-driven piles, piles installed by vibrators, or seismic response of piles. The subject of this paper is the largest of these chambers, which is a flexible-wall chamber capable of handling a saturated soil column approximately 0.8 m in diameter by 2.6 m high. This chamber, termed the Long Variable Lateral Pressure Sand Column (LVLPS), was constructed in 1985 for the specific purpose of studying the behavior of open-toed pipe piles in deep, offshore deposits of submerged sand (O'Neill and Raines, 1991). Subsequent applications have been made in this chamber to the calibration of electronic cone penetrometers in sands of varying relative density under controlled stress history (Mustafa and O'Neill, 1988), driveability of open-toed piles with varying values of internal wall friction (Raines et al., 1991), and vibratory driving of both closed-toe pipe piles and non-displacement piles (O'Neill et al., 1990; Vipulanandan et al., 1990). The design of the chamber is described briefly, followed by short discussions of the scaling rules used in this chamber, contrasts between the pressure chamber and the centrifuge for the purpose of the modelling of piling, and example results from two case studies illustrating how the chamber has been used.

DESIGN OF THE CHAMBER

The Houston LVLPS was first described by Vipulanandan et al. (1989). Essential features of that description are repeated here. The chamber and supporting gantry are shown in Fig. 1. The gantry is used to support pluvial compactors, as leads for large-scale model pile hammers and as reactions for loading tests. The gantry-chamber system is located in a high-bay room with a one-ton overhead crane, which is essential for the operation of the chamber. A cutaway elevation of the chamber itself is shown in Fig. 2. The soil column (usually sand) is contained within a series of four identical cylindrical steel cylinders, bolted together in series vertically. Each time the chamber is charged, the cylinders are disconnected and the soil placed first in the bottom cylinder and then in successively higher cylinders, and the cylinders are bolted back into place one by one. This operation is principally to allow for close control of the placement of soil and instruments in this rather tall chamber. In order to permit a depthwise variation of lateral stress steel flanges are placed completely around the interior of each cylinder every 12.5 in. (0.32 m) vertically. Molded rubber bladders ("air bags") are situated in the recesses formed by these flanges and the interior wall of the cylinders. In this manner, the pressure in each bladder can be controlled separately. A flat air bladder is also present under the steel plate on the top of the chamber and is controlled separately from the stresses in lateral boundary bladders. The top bladder and the top cap of the chamber have a 50-mm-diameter pass-through port centrally located to allow large model piles to enter the chamber and two much smaller pass-through holes diametrically opposite each other for drainage. The latter drains are screened to prevent pass-through of soil as water is expelled.

Under normal operating conditions granular soil is formed in the chamber by placing rolled teflon sheet forms inside the air membranes, supported laterally by the internal flanges to allow the sand to be placed by raining under approximate K_0 conditions. Slight air pressure is

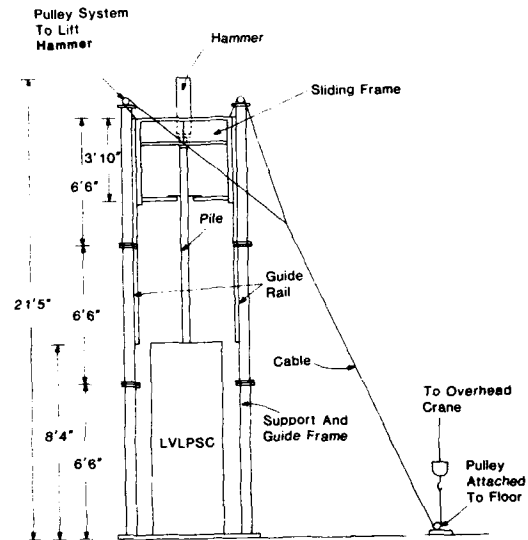


Figure 1. Testing System (1 in. = 25.4 mm; 1 ft = 0.305 m)

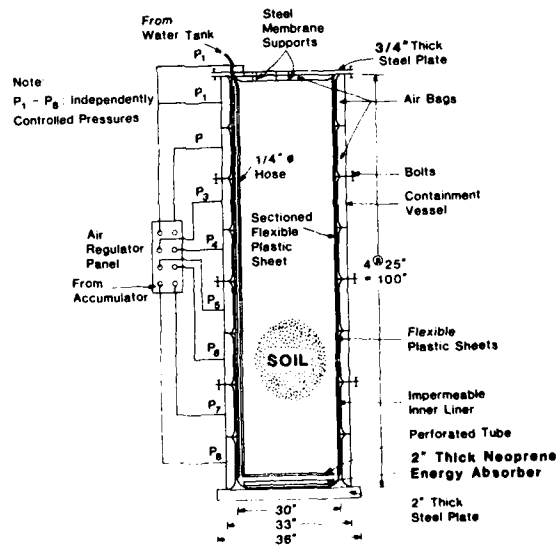


Figure 2. Schematic of LVLPS (1 in. = 25.4 mm)

applied to the lower membranes as the filling progresses in order to ensure that lateral deformation of the soil is kept to a minimum. If the soil is to be saturated, a continuous, thin-walled latex membrane is placed inside the teflon forms, and the soil placed directly against the membrane.

Saturation proceeds after filling of the chamber through a diffusion ring affixed to the base of the chamber. First, three to four pore volumes of carbon dioxide are forced upward from the ring through the pores to the drainage ports in the top of the chamber at low gradient. Replacement of air (primarily nitrogen) with carbon dioxide decreases the air entrapment during water saturation. This process normally requires 4 to 6 hours. Following gas purging, deaired water is introduced through the same diffusion ring under a head of about 10 ft (3.1 m), and the water saturates the pores from the base upward, driving air out. The saturation process takes from 4 hours to more than one day, depending upon the permeability of the soil in the column. As the water rises in the chamber, lateral membrane pressures are increased to balance the increased boundary pressures produced by the water and thus to maintain K_0 conditions in the soil column.

Boundary Conditions

Static Loading Effects. The chamber boundary conditions are summarized in Table 1. The thin-membrane-teflon-air bag sequence serves to reduce shear stresses at the boundary of the chamber to a minimum, and it is assumed that one boundary condition is that of zero vertical shear stress on the outer boundary of the soil column. The lateral and upper boundaries are flexible, so that a second boundary condition is constant lateral normal stress on the lateral surface of the soil column and approximately constant vertical stress on the upper horizontal surface. At the base of the chamber the only control is zero normal displacement. The chamber can be configured so that, when the soil column is saturated, drainage is allowed to occur only through the top ports and/or through a series of perforated vertical tubes distributed around the circumference of the sand column. Boundary stresses are then adjusted to the values required by the experiment.

Table 1. Boundary Conditions for UH Pressure Chamber

	Lateral Boundary	Top Boundary	Bottom Boundary
Stress/Displacement	Controlled normal stress; zero shear stress	Controlled normal stress	Zero normal displacement
Drainage	Radial drainage or undrained	Vertical drainage	Undrained

The lateral dimensions of the chamber were selected to be as small as possible, since the chamber is used primarily for parametric studies and must be filled, saturated, drained and emptied many times. The chamber as shown in Fig. 1 requires approximately 40 cu. ft. (1.14 m³) of soil. Parkin (1988), among others, has shown that ratios of chamber diameter to the diameter of solid penetrometers below about 60 produce boundary effects on the capacities of penetrometers. For overconsolidated sands ($K_0 > 1$) and for zero vertical strain and controlled lateral stress (similar to the conditions in the UH chamber), the effect is negligible down to a diameter ratio of 33. For the same conditions in normally consolidated sands, tip resistances reduced by about 15% at the diameter ratio of 33 compared to comparable results at a diameter ratio of 60. For diameter ratios down to about 14, Parkin indicates reductions in tip capacity of up to 70% in both normally consolidated and overconsolidated sand. The UH chamber has been used to calibrate standard-sized electrical cone penetrometers in normally consolidated sand at a diameter ratio of 23 under conditions of constant horizontal stress, constant vertical stress at the surface and zero vertical strain at the base of the chamber, for which Parkin's data would suggest that q_c values will be 20 - 25% below those that would exist at a diameter ratio of 60.

For testing of piles, conflicting size conditions exist. On the one hand, it is desirable to use as large a pile as possible in order to model diffusion processes during driving and to maintain a reasonable model to prototype ratio of pile diameter to soil particle diameter. On the other hand, as indicated above, it is desirable to have a chamber diameter ratio of about 60 to

essentially eliminate boundary effects. For most design applications, it is also sufficient to ensure that the results of the chamber tests are conservative. From this perspective, Wang (1985) analyzed the penetration of a solid, spherical-nosed penetrometer into non-dilating and non-contracting soil using a strain path procedure described by Baligh (1984) and concluded that the plastic zone around the penetrometer (pile) would be confined within a zone about 5 radii from the penetrometer. In slightly dilative soils, that zone would extend to 7.5 to 8 radii. A conservative assumption for using the chamber to develop relations between in-situ effective stresses and unit resistance values against the pile for design purposes is to ensure that the plastic zone is contained within the soil column and to allow the surrounding elastic soil to be simulated by a constant-normal-stress boundary. A better, although more involved, approach would be to replace the constant stress boundary with a boundary of constant stiffness; however, the UH chamber does not have this capability. Based on Wang's analysis, pipe piles as large as 4 in. (100 mm) in diameter (diameter ratio of 8.3) have been tested in the chamber. It has been general practice to terminate driving about 5 pile diameters above the base of the chamber based on experience with full-scale piles that soil properties below about 5 diameters beneath the pile toe have little effect on toe capacity.

Wave Reflection Effects. Modelling of pile driving also requires boundaries that absorb stress waves. A rubber waffle panel is provided at the base of the UH chamber for this purpose. The flexible lateral and top boundaries are less efficient at absorbing energy; however, overall radiation damping has been estimated to be on the order of 10% of critical in the UH chamber based on experimental logarithmic decrement studies of low-level impact of piles (Wong, 1985). Since this value is of the same order of magnitude as would occur in a pile embedded in an elastic half-space, the energy absorption characteristics of the chamber are considered adequate.

Scaling

Length Scaling Based on Geostatic Stresses: The Centrifuge. It should be noted that the centrifuge provides an ideal means of investigating pile behavior at great depth. One problem of interest to the author was to investigate pile behavior in a layer of saturated dense sand 30 to 38 m below the surface. The prototype pile was 48 in. (1.22 m) in diameter. According to centrifuge scaling rules, one could spin a one-plus-meter-deep deposit of saturated soil at 38 g's, drive a 32 mm-diameter (1220 mm / 38 g) pile in flight to a depth of one meter, and load test the pile in flight, using instruments in the bottom one-fourth of the pile to develop the necessary data. This procedure would require about a 70 ton-g centrifuge with a rather large bucket. With such a small pile, however, soil properties, or pore fluid viscosity, would have to be adjusted so that approximate similitude existed for the diffusion of pore water pressure between model and prototype. If such were not done, the changes in stresses in the immediate vicinity of the pile brought about by flow of pore water during driving, and therefore the static behavior of the pile, would be influenced. It is feasible to model these factors on a centrifuge, but it may not be cost effective compared to the use of a pressure chamber if many parameters are to be investigated.

Length Scaling Based on Geostatic Stresses: The Pressure Chamber. The same problem was modeled in the UH pressure chamber. The sand was heavily overconsolidated, and it was reasonable to assume that in-situ stress conditions were isotropic ($K_0 = 1$). The vertical effective stress at the top of the layer was applied to the top of the column of soil. In the pressure chamber, gravity stresses must be scaled by application of boundary stresses to simulate the effective stresses that occur at the depth to be simulated. If a finite depth interval is to be studied the depthwise increase in vertical effective stress cannot be simulated as is done in the centrifuge. Instead, however, depthwise variable lateral effective stress can be applied, as illustrated in Fig. 3, to replicate the approximate variation in the horizontal effective stress from the top to the bottom of the 8-m-thick layer. (The horizontal effective stress has a much more important effect on pile behavior than does the vertical effective stress.) The vertical gradient in lateral effective stress is higher than exists in-situ, however, which requires that the principal stress rotate and that shear stresses not present in the prototype soil develop in the chamber.

Finite element studies were conducted for several soils and boundary stress states to evaluate principal stress rotation and induced shearing stresses considering the effect of the driving port (Wang, 1985). Figure 3 shows computed contours of maximum shear stress in the chamber, modelling a 50-mm-radius driving port and the vertical variation of lateral stresses described above. Rotations of principal stresses were also computed. The soil was modelled using a simple Duncan-Chang (1970) model developed from CD triaxial compression test data

on sand at a relative density of 80%. The highest maximum shear stress induced by the gradient of lateral stress was about 5% of the peak shaft resistance later developed on the model pile, and the angle of rotation of the principal stresses was as high as 20° near the top of the chamber (pile port) but insignificant in the bottom 80% of the chamber. This set of boundary stresses was judged acceptable for modelling the problem, and modelling of vertical gradients of horizontal pressure appears justified if the depth of soil modelled is less than about four times the chamber height.

Modelling of the driving of piles in saturated soils requires that the pore pressure generation and dissipation rate effects simulate those that would be expected in the prototype. One method to accomplish this objective involves applying the familiar dimensionless groupings for diffusion with time-dependent loading. For a 1-g acceleration field,

$$\left(\frac{t_r c_v}{l^2}\right)_m = \left(\frac{t_r c_v}{l^2}\right)_p, \quad \text{and} \quad (1)$$

$$\left(\frac{t_d c_v}{l^2}\right)_m = \left(\frac{t_d c_v}{l^2}\right)_p, \quad (2)$$

in which c_v is the coefficient of consolidation, t_r is rise (loading) time, t_d is dissipation time and l is length. For model (m) and prototype (p) soils of equal compressibility, for pore fluids of identical viscosity in the model and the prototype, and using a 4 in. (100 mm) diameter model to simulate the behavior of a 48 in. (1.2 m) diameter prototype, Eq. 1 becomes

$$\left(\frac{t_{rm}}{t_{rp}}\right) = \left(\frac{k_p}{k_m}\right)\left(\frac{4}{48}\right)^2, \quad \text{and Eq. 2 becomes} \quad (3)$$

$$\left(\frac{t_{dm}}{t_{dp}}\right) = \left(\frac{k_p}{k_m}\right)\left(\frac{4}{48}\right)^2, \quad (4)$$

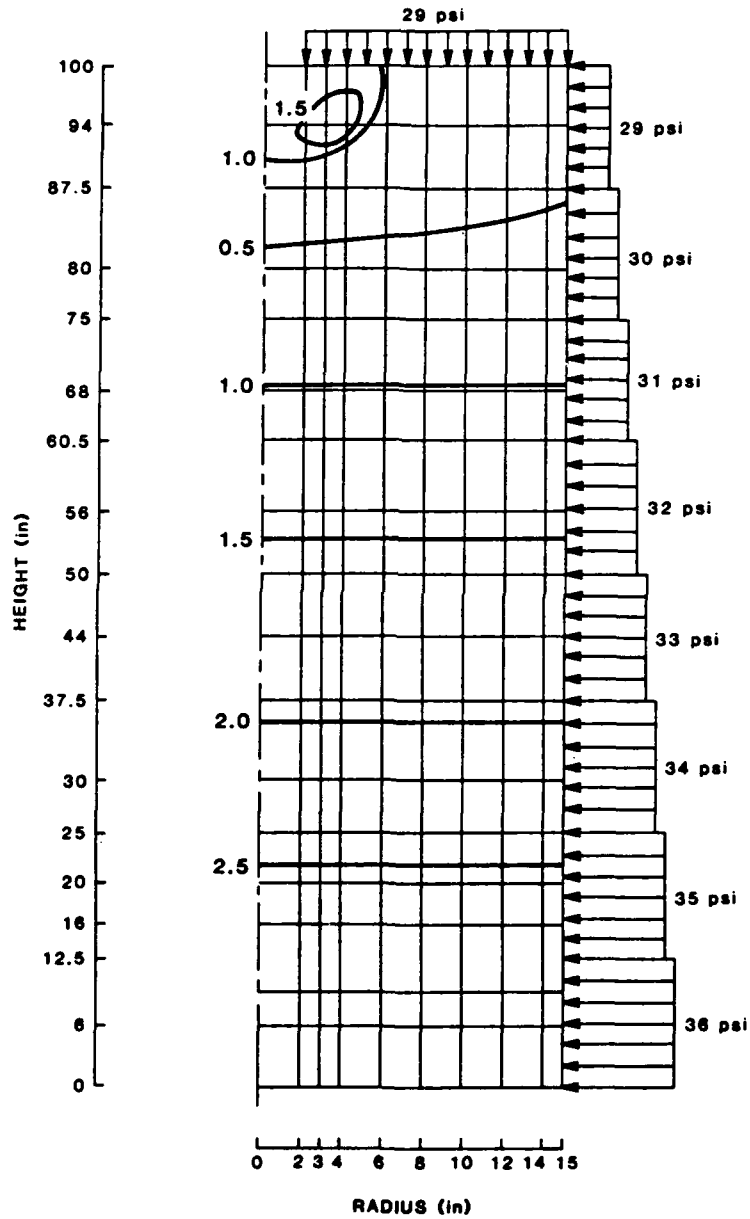
where k is the coefficient of Darcian permeability. Wave equation modelling of prototype driving systems can be made to determine the rise time of the compression wave at the pile head. For large-diameter piles of the type considered here, that time is on the order of 5 msec. Using a stiff hammer cushion, rise time in the model can be made to be on the order of 0.5 msec, requiring the k value of the model sand to be about one order of magnitude smaller than that of the prototype sand (Eq. 3). In the test described in Case Study No. 1, below, this was accomplished by modelling a clean medium prototype sand with $k = 0.15$ cm/sec with a clean fine sand with $k = 0.015$ sec. As suggested in Eq. 4, dissipation of excess pore pressure will occur much faster in the model than in the prototype with this permeability ratio. In order that the latent excess pore water pressures around the pile be modelled from blow to blow, it would be necessary to drive the model pile at about ten times the rate to be employed in the prototype (which is normally about 60 blows per minute). Slower driving will result in lower initial excess pore water pressures around the model pile than around the prototype at the beginning of the blow. The UH chamber and driving system accommodates the similitude required by Eq. 1 but at present does not contain a hammer capable of driving at such a rate as to satisfy Eq. 2. Equations 1 and 2 do not satisfy inertia similitude. Such can be accomplished in a 1-g pressure chamber only if $t_m = t_p$ (O'Neill and Ochoa, 1990), which in fact is the condition for the diffusion part of the driving cycle in the chamber ($t_{dm} = t_{dp}$) but not for the rise-time portion. Thus, scaling rules for diffusion and inertia are only partly satisfied as the chamber operates at present.

Modelling of inertia and diffusion has not been considered when the UH chamber has been used for calibration of penetrometers.

CASE STUDIES

Driveability of Non-Displacement Piles

A major study was conducted on the driveability and static behavior of open-ended steel pipe piles in saturated, dense sand using the UH pressure chamber (O'Neill and Raines, 1991;



NOTE : STRESSES ARE EFFECTIVE

Figure 3. Contours of Maximum Shear Stress (psi) (1 psi = 6.9 KPa; 1 in. = 25.4 mm)

Raines; O'Neill and Ugaz, 1992). One item of interest in the study was the effect of the angle of wall friction between the inside of the pile and the soil in the plug, both in terms of driveability and static capacity. The sand placed in the chamber was a clean, fine, poorly graded siliceous sand, locally called "San Jacinto River Sand." It was deposited in 150-mm-thick lifts by raining through a series of #10 sieves with a final drop height of about 1 m. The teflon forming jacket was "cinched" with rubber ties to prevent outward bulging of the sand during filling. After the chamber was filled, it was saturated with deaired water and the effective pressure distribution depicted in Fig. 3 was applied to model driving behavior in a layer of dense sand 30 - 38 m below the surface of a submerged sand deposit. Both gravimetric and nuclear density measurements indicated that the relative density in the chamber averaged 88% with this deposition procedure with a small coefficient of variation (less than 2%), and that the density was highly reproducible.

Pipe piles having similar characteristics were driven into the chamber. Each pipe was made of mild steel, was 100 mm in outside diameter (diameter ratio of 8.25), had a 4-mm-thick wall and was 2.54 m long. No special driving shoes were used in this portion of the study. The pile surfaces were sand blasted. For one pile the interior surface was then heavily oiled (Pile 1), for one lightly oiled (Pile 2) and for the third (Pile 3) no treatment was used. Coupons of the steel with the above surface treatment were subjected to sand-on-steel direct interface shear tests, with the sand deposited at the same relative density as the sand in the chamber, and it was determined that the resulting angles of wall friction, δ , were approximately 22°, 26° and 30°, respectively.

Pile 3 was driven into the chamber several times to assess repeatability. The driving system consisted of a single-acting hammer applying 1.0 ft-k (1.3 m-KN) of energy per blow at a rate of about 30 blows per minute (unscaled). During the early tests, no lateral drains were used around the sand column, and the sand tended to liquefy during driving. Once the lateral drain system was added, this effect was eliminated. Five tests on Pile 3 revealed repeatability of blow count and static capacity to within 10%. Piles 1 and 2 were then driven and load tested once each.

Each pile was driven to a depth of 21 diameters into the chamber, or to within 4 diameters of the base of the chamber. The piles did not act either as displacement piles or non-displacement piles during driving, as indicated in Fig. 4, which shows pile penetration vs. plug penetration. Pile 1 nearly cored, while in Piles 2 and 3, the plug penetrated with each blow of the hammer but not by as much as the pile penetrated. Thus, the effect of the closeness of the boundary is not as severe as had the pile been either solid or fully plugged during driving.

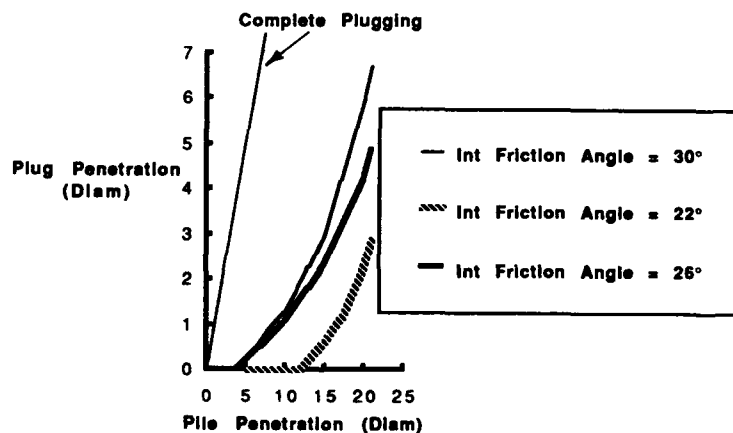


Figure 4. Pile Plug Penetration vs. Toe Penetration; Case History No. 1

Table 2 gives synoptic test results. Failure was determined in the static tests according to the Davisson criterion (Fellenius, 1975). It is clear that the lower the angle of internal wall friction the easier the pile drove; however, the static capacity was severely affected. Instruments in Pile 3 indicated that the toe resistance at failure was about 19 k (86 kN). While Piles 1 and 2 were uninstrumented except for instruments to measure force and acceleration at the pile heads, it is reasonable to assume that the external shaft resistance was approximately equal among the three.

Table 2. Comparison of Driving Rates and Static Capacities for Pile Driving Study

$\delta_{int.}$ (degrees)	Pen. Resistance Last 2 Diameters (Blows / in., 25 mm)	Final Plug Length (m)	Compressional Capacity (kN)
22	4	1.83	106
26	5	1.63	132
30	7	1.44	187

Thus, each pile probably carried about 23 k (102 kN) of shaft resistance. This suggests that Pile 1 continued to core during static loading (essentially zero internal shaft resistance), Pile 2 developed some internal shaft resistance but less than necessary for the plug to fail in end bearing, and Pile 3 was plugged solidly during static testing, allowing the pile to act as if it were closed-ended.

It is seen that the performance of the plugged pile is extremely sensitive to the angle of internal wall friction. The practical applications of the observations from the chamber tests are that if the primary objective of pile driving under the conditions modelled is penetration (e.g., to develop uplift resistance), artificial lubrication of the interior surface of the pile is useful, since it lowers considerably the number of hammer blows needed to drive the pile. On the other hand, if the objective is compression capacity, the pile should have an angle of internal wall friction well above 26 degrees, preferably 30 degrees. Such may not be possible in stratified deposits of sand and clay, even if the angle of wall friction is 30 degrees or higher prior to driving, due to the smearing action of the clay.

Simple Calibration of Electronic Cone Penetrometer

An investigator was interested in determining the relative density of submerged sand at very shallow depths using the electronic cone penetrometer (Fugro type). It was assumed that the shallow deposit of soil had been formed in modern geologic times by sedimentation under water under K_0 conditions but that later excavation had brought the value of K_0 to 1 (isotropic stress state). The UH chamber was used to calibrate the penetrometer under these stress history conditions, according to the following procedure (Mustafa and O'Neill, 1988).

Soil Column Preparation. After the forming jacket and watertight membrane were placed, sand was pluviated into the chamber, in different ways depending upon the relative density that was desired. The sand that was used was a large sample of the prototype sand, a fine siliceous sand Gulf of Mexico bay sand with small shell fragments. For the lowest relative density, saturation proceeded simultaneously with sand placement, keeping the free water level about 600 mm above the present soil surface. Dry sand was rained from a hopper using a spreading mechanism with two #10 sieves placed 150 mm apart. The soil was deposited in 150 mm thick lifts, the lift height being limited by the capacity of the hopper in the rainer. The lowest sieve was held just above the water surface. As the water/soil column rose, air pressures in the lateral bladders were increased in steps to balance the pressure of the deposited lifts of soil, to maintain K_0 conditions as the soil was added and the column of water rose. For this purpose it was assumed that $K_0 = 0.45$ and dry unit weight = 85 pcf. Since each lateral bladder has a height equal to the thickness of two lifts, it was not feasible to apply balancing pressures to every other present lift or to the lift below the present lift until the surface of deposited soil reached the top of the bladder. The average relative density obtained, through gravimetric measurements made on samples recovered from various points in the chamber after the test, was 14%. Table 3 provides results of the individual measurements to give some measure of variability. A separate check on average relative density in the chamber was made by dividing the total dry weight of

sand placed by the theoretical volume of the chamber without lateral deformation. The value so obtained was higher than that obtained from the samples, which suggested that some yielding of the lateral boundary had occurred during filling. That is, the actual volume was greater than the theoretical volume, most likely because the correcting pressures were applied to the lateral boundaries only after a lift was placed, allowing some expansion. In fact, the average increase in chamber diameter needed to accommodate the extra weight of dry soil would have been about 3.5%. It was concluded, however, that the soil was in a state close to the K_0 state since most of the lateral strain would have occurred in a lift of soil during the placement of that lift or the lift just above that lift, not after additional vertical stress had been added through placement of many subsequent lifts, and that the assessment of relative density of 14% was valid. Once the saturated sand column had been placed, the effective stress conditions were brought to $K = 1$ by increasing the lateral pressures simultaneously in the bladders. Finally, lead pads were placed on the top of the sand column to simulate the weight of the device that housed the cone, which was to sit on the soil surface. Lateral bladder pressures were then increased one last time to balance the calculated additional lateral effective soil pressure on the chamber boundaries due to the lead pads, which diminished with depth.

The deposition process is thus seen to be fairly complex, although straightforward using a pressure chamber. It would be possible to model these depositional and stress history conditions in a centrifuge, but, to the knowledge of the author, such has not been attempted.

Table 3. Dry Unit Weights and Relative Densities Measured After Testing for Low Relative Density (Gulf Bay Sand)

Position of Gravimetric Receptacle (m below sand surface / m from centerline - direction)	Dry Unit Weight (pcf)	Relative Density (%)
0.10 / 0.15 - NW	85.2	21
0.10 / 0.15 - NE	84.1	15
0.10 / 0.15 - SE	82.1	03
0.74 / 0.15 - NW	85.6	23
0.74 / 0.15 - NE	83.6	12
0.74 / 0.15 - SE	83.1	09
1.42 / 0.15 - NW	84.2	15
1.42 / 0.15 - NE	83.7	12
1.42 / 0.15 - SE	83.3	10
1.76 / 0.15 - NW	84.1	15
1.76 / 0.15 - NE	84.2	15
1.76 / 0.15 - SE	83.9	13

Observation of Table 3 indicates generally random variation of relative density within the chamber, except that along a line southeast of the centerline the relative density averaged only about 9%, while along a line northwest of the centerline the relative density averaged just over 18%. This effect may have been caused by a slight systematic tilting of the rainer during deposition.

Following electronic CPT testing at 14% relative density, other tests were also conducted, at average relative densities of 57% and 89%. The deposition procedures were changed from that described above. The sand was pluviated dry, and the chamber was completely filled with sand before the sand was saturated. The forming jacket was stiffened against internal pressure by using nylon bands outside of the jacket every 0.3 m vertically. Incremental increases were made in lateral chamber pressures assuming $K_0 = 0.38$ and 0.31, respectively ($K_0 = 0.95 - \sin \phi$), and dry unit weight = 90 and 95 pcf, respectively. During saturation, additional pressures were added continually as the water column rose in the chamber over several hours. The lateral pressures were then adjusted to the $K = 1$ condition, the lead

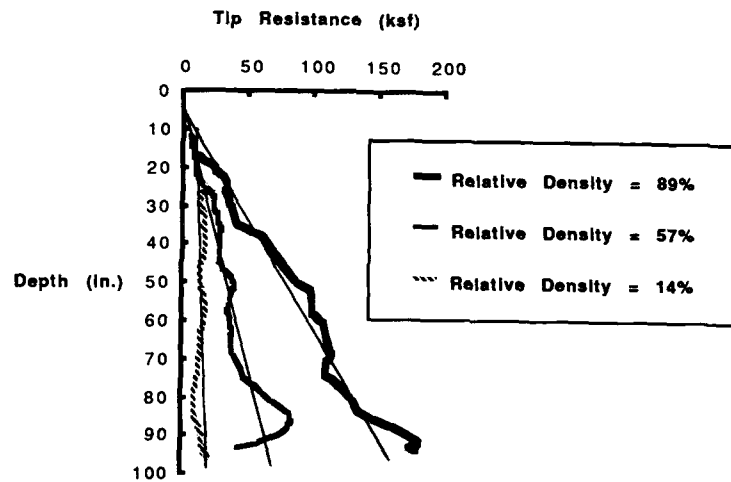


Figure 5. Toe Resistance (q_c) vs. Depth; Case History No. 2 (1 in. = 25.4 mm)

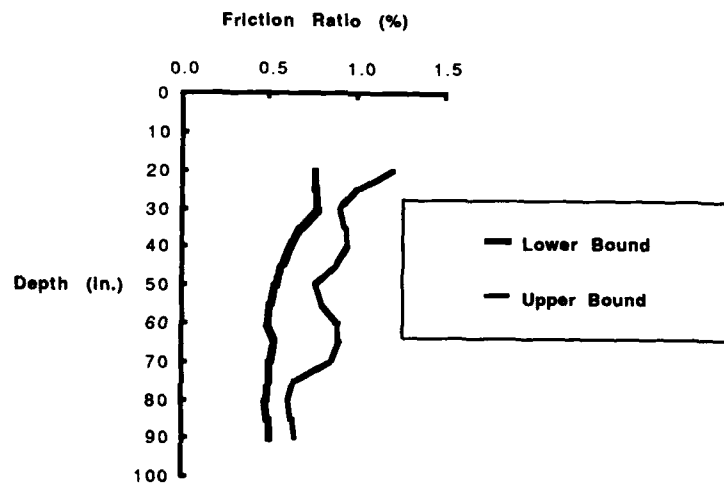


Figure 6. Friction Ratio vs. Depth; Case History No. 2 (1 in. = 25.4 mm)

pads placed, and the lateral pressures adjusted one final time. Much more uniformity was obtained in the sand using dry raining and at the higher relative densities. The coefficient of variation of relative density from gravimetric samples was 0.386, 0.063 and 0.019 for relative densities of 14%, 57% and 89%, respectively. Nearly identical results were obtained from bulk calculations of relative density as from the average of the samples in the latter two tests.

Test Results. For all CPT tests, the top of the chamber (Fig. 1) was removed, and the cone was pushed at a rate of 10 mm/sec into the center of the chamber. The diameter ratio for this study was 23. The results, in terms of tip resistance q_c vs depth and friction ratio vs depth, are shown in Figs. 5 and 6. The results appeared to be reliable down to a depth of 86 in. (2.18 m), or about 14 in. (0.36 m or 10 penetrometer diameters) above the base, based on the observations of the curve for 57% relative density. The thin lines on Fig. 6 are interpreted relations of q_c to relative density and depth for the soil deposited as described. For the highest relative density, the q_c values may represent a lower limit to the prototype values, since the boundary is flexible and the soil is dilative. Note that at the lowest relative density there is little dependence of q_c on depth, possibly because the structure of the soil is metastable (highly contractive). The friction ratios varied within small limits, and there was no consistent relation between relative density and friction ratio.

CONCLUSIONS

The LVLPS at the University of Houston has been used primarily for testing partial displacement piles, such as open-ended pipe piles, under impact and vibratory driving in both dry and saturated sands. The chamber is capable of applying a vertical gradient of lateral stress to simulate thick soil layers, which results in very small ambient shearing stresses as long as the layer thickness modelled is not more than about four times the height of the chamber. While the chamber is slender, it also has a flexible boundary, so that experimental results, in terms of developed pile resistance, are conservative with respect to the prototype and so should be appropriate for design applications. The chamber has also been used to model the stress history of shallow soil deposits subjected to cone penetration testing that would be very difficult to accomplish in present-generation centrifuges.

ACKNOWLEDGMENTS

The author wishes to acknowledge the following colleagues and organizations who assisted in the performance of the tests described in this paper, the design of the chamber, and in the definition of the problems and sponsorship of the studies: Dr. D. O. Wong, Dr. C. Vipulanandan, Dr. M. Ochoa, Mr. Muhammed Mustafa, Dr. O. G. Ugaz, Mr. R. Henson, Dr. J. Templeton, Dr. E. Clukey, Exxon Production Research Company, National Cooperative Highway Research Program, Fugro-McClelland Marine Geosciences, Inc., and the Department of Civil and Environmental Engineering of the University of Houston.

REFERENCES

- Baligh, M. M. (1984). "The Simple-Pile Approach to Pile Installation in Clays," in *Analysis and Design of Pile Foundations*, Ed. by J. R. Meyer, ASCE, October, pp. 310 - 330.
- Duncan, J. M., and Chang, C-Y (1970). "Nonlinear Analysis of Stress and Strain in Soils," *JSMFD*, ASCE, Vol. 95, No. SM5, September, pp. 1629 - 1653.
- Fellenius, B. H. (1975). "Test Loading of Piles and New Proof Testing," *JGED*, ASCE, Vol. 101, No. GT9, September, pp. 855 - 869.
- Mustafa, M., and O'Neill, M. W. (1988). "Static Resistance of Full-Sized Cone Penetrometer in University of Houston LVLPS in Submerged Sand at Varying Relative Density for $K = 1$ Conditions," *Report No. UHCE 88-15*, Dept. of Civil Engineering, Univ. of Houston, May.

- O'Neill, M. W., and Ochoa, M. (1990). "Response of Tension Piles to Simulated Seismic Motion in Saturated Fine Sand," *Report No. UHCEE 90-9*, Department of Civil and Environ. Engineering, Univ. of Houston, December.
- O'Neill, M. W., and Raines, R. D. (1991). "Load Transfer for Pipe Piles in Highly Pressured Dense Sand," *JGE*, ASCE, Vol. 117, No. 8, August.
- O'Neill, M. W., Vipulanandan, C., and Wong, D., "Laboratory Modeling of Vibro-Driven Piles," *JGE*, ASCE, Vol. 116, No. 8, August, pp. 1190 - 1209.
- Parkin, A. K. (1988). "The Calibration of Cone Penetrometers," in *Penetration Testing 1988*, Vol. 1, Ed. by J. de Ruiter, Balkema, Rotterdam, pp. 221 - 243.
- Raines, R. D., Ugaz, O. G., and O'Neill, M. W. (1992). "Driving Characteristics of Open-Toe Piles in Dense Sand," *JGE*, ASCE, Vol. 118, in press.
- Vipulanandan, C., Wong, D., and O'Neill, M. W. (1990). "Behavior of Vibro-Driven Piles in Sand," *JGE*, Vol. 116, No. 8, August, pp. 1211 - 1230.
- Vipulanandan, C., Wong, D., Ochoa, M., and O'Neill, M. W. (1989). "Modeling of Displacement Piles in Sand Using a Pressure Chamber," in *Foundation Engineering: Current Principles and Practices*, Vol. 1, Ed. by F. H. Kulhawy, ASCE, June, pp. 526 - 541.
- Wong, D. O. (1985). "Design and Analysis of an Apparatus to Simulate Density Stresses in Deep Deposits of Granular Soils," thesis presented in partial fulfillment of the requirements for the degree of Master of Science in Civil Engineering, University of Houston, June, 1985.

Chamber Testing of Piles in Calcareous Sand and Silt

Alan K. Parkin

Abstract: The double-wall type calibration chamber is a versatile rig for the study of in-situ test instruments in sand. This paper describes adaptations made to the Monash chamber in order to study pile performance and installation techniques in a selection of saturated calcareous sands and silts, for application to structures in Bass Strait, S.E. Australia. Raining techniques were found to be generally inappropriate for forming samples of silty materials. For driven pipe piles, plugging was found to be insignificant, so that pile capacity could not be related simply to CPT records.

1. INTRODUCTION

Calcareous (or carbonate) sands are found in many warmer or temperate seas around the world, including Bass Strait, off south-eastern Australia, which is an area of significant hydrocarbon development. Conventional driven piles have been found to provide poor support in such materials (10 to 15 kPa) evidently as a result of particle crushing (Angemeer et al., 1973), leading to the widespread adoption of grouted insert piles (Hyden et al., 1988). Whilst these have performed well, giving adhesions of better than 400 kPa, their installation has been slow and expensive, and hopes for a more economic solution were therefore directed to the development of the driven grouted pile (DGP).

Following initial developments in France (Nauroy et al., 1988), a programme of development was undertaken by Esso Australia Ltd., at a variety of scales for application on projected production platforms in Bass Strait. One component of this investigation was undertaken jointly by CSIRO Division of Geomechanics and Monash University, based on the use of the Monash Calibration Chamber, and under the supervision of Exxon Production Research Co. This investigation required that the existing chamber be modified to accommodate samples of a range of calcareous materials, with provision for the driving, grouting and cyclic load testing of model piles in these samples.

2. THE MONASH CALIBRATION CHAMBER

The Monash Calibration Chamber evolved from the design of a small chamber described by Holden (1971), and is one of a family of similar chambers, whose evolution is traced by Parkin (1988). These chambers were designed specifically for the study of cone penetrometers in samples of clean dry sand and have not been extensively applied to other test devices (mostly dilatometer) or other materials.

In essence, the equipment consists of a large triaxial sample, 1.2 m diameter by 1.8 m high, enclosed in rubber membranes and compressed by a lateral water jacket and a base piston (Fig. 1). The exterior cell wall is of cavity construction to facilitate the imposition of K_0 lateral constraint, and a water cushion on the base piston is used to measure the vertical stress and to assure its uniformity. An overhead hinged reaction frame provides restraint to hold the cell together (against the force of the base piston), whilst also mounting an electro-mechanical drive system for a standard cone penetrometer on the sample axis. Further details are given by Chapman (1980), Bellotti et al., (1982) and others.

In normal use with clean sands, sample formation is by raining from a stationary sand spreader that is lifted over the top of the calibration chamber (during which the reaction frame must, of course, be tilted to one side). The Monash equipment is similar to that described by Bellotti et al. (1982), both of which originate in a design from the Norwegian Geotechnical Institute. Such equipment allows very homogenous samples to be prepared at a range of relative density (at least in the range $D_r = 50$ to 100%) by varying the rate of sand deposition through the insertion of screen plates with different hole sizes. The equipment is less successful in producing samples of low relative density because of the high rates of flow required and the resulting air currents within the chamber.

3. PILE TEST SPECIFICATIONS

A test arrangement was required to allow model piles of 100 and 150 mm diameter to be driven to an embedded depth of 1 m, with provision for cyclic axial loading after grouting of the pile/sand interface. It was also necessary to be able to run a CPT test, at least for control on sample quality, and desirably to obtain a measure of material properties. The test brief allowed more than one test to be performed in any sample, provided each pile should have a clearance of not less than 2 diameters from any other pile or the sample boundary. However, the validity of this criterion, for the purpose of adequately isolating each pile test, could not be established at the outset.

Because the original CRB test chamber of Veismanis (1974) (taking a sample 0.9 m dia. by 1.2 m high) was also available at Monash, these requirements could be met in either of two test configurations. Based on the CRB chamber, a single pile, driven centrally, could be tested in each sample, requiring perhaps 20 such samples, with additional samples for CPT testing. Alternatively, using the large Monash Chamber, up to three piles could be tested in each sample, using the configuration of Fig. 2 in which the piles are distributed on either side of the overhead reaction beam. This latter arrangement also allowed a CPT test to be conducted on the sample axis, if it can be presumed not to interfere with the pile clearance requirements (which appears to have been a reasonable presumption).

In the outcome, the second of these alternatives was preferred on the basis that it required fewer samples and allowed CPT testing alongside the test piles. It did, however mean that the test samples would contain a significant dead volume below the pile tips, in addition to which jack mountings were required to be provided on the sides of the reaction beam, imposing a substantial torsional loading. A vital factor in making this arrangement possible was the rather narrow profile of the reaction beam, as compared with other installations of this type.

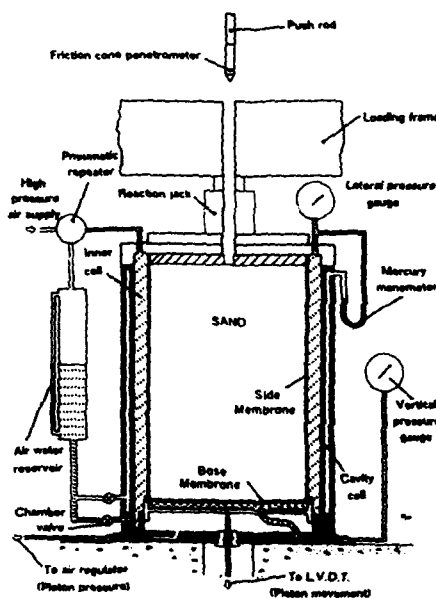


Fig. 1

The Monash calibration chamber

4. EQUIPMENT MODIFICATIONS FOR PILE LOAD TESTING

4.1 Calibration Chamber

For the proposed pile disposition of Fig. 2, it was necessary to bore holes through the 140 mm thick chamber lid and the underlying 40 mm plywood sample platen on each of the three pile locations. Because the sealing of the lateral membrane depended (particularly in the critical stages) on the development of vacuum between the platen and the chamber lid, it was necessary to maintain a seal around these three pile access ports (and the CPT hole) by means of O-rings in the platen and soft rubber gaskets matching the thickness of the lateral membrane. However, because of the loss of area, the overall suction force available for this purpose was clearly much reduced, making the membrane sealing operation significantly less sure.

Each of the access ports was provided with a split collar to guide the test piles during driving (removed during testing), and each was filled with a wooden plug and sealed with a bolted cover plate when not in use. Two additional holes were also required for leads to electrical piezometers, sealed on the top side with glands.

The complexity of these arrangements obviously required close indexing of the platen and the chamber lid, from machining through to sample formation, and the platen had to be seated on each sample whilst secured to the chamber lid (which in turn was indexed to the chamber wall)

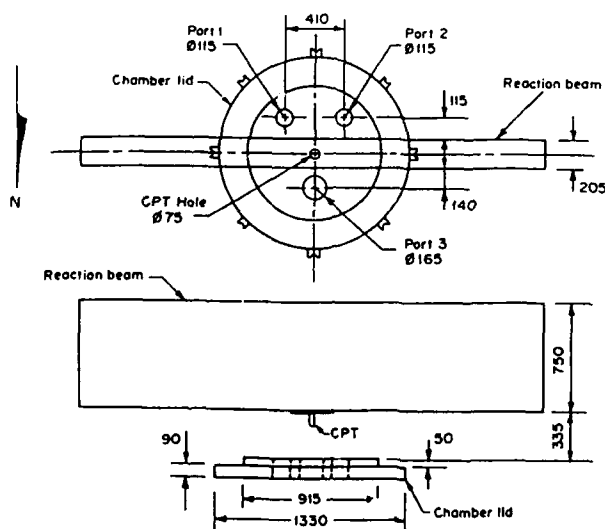


Fig. 2 Test pile layout and lid modifications

4.2 Reaction Beam

The reaction beam has a deep narrow profile, 200 mm wide, fabricated from 25 mm plate. This narrow profile was necessary in order to gain access over each of the pile locations for the mounting of a 25 tonne Instron servo-controlled jack.

Jack mountings were therefore welded on both sides of the reaction beam, with the Instron jack being rotated around the three positions as required (by mobile crane, being beyond the reach of the laboratory overhead crane). The jack mounting plates were required to provide a vertical clearance of about 750 mm over the chamber lid, to provide for pile head fittings, two load cells and the jack shaft, all of which required positive coupling to allow for 2-way cyclic loading. Because of the eccentric loading to the reaction beam, a system of lateral bracing to a nearly stiff column was installed during testing.

In the case of the 150 mm pile location, the reaction beam already mounted the electro-mechanical drive unit for the CPT, so that this had to be re-located on a hinged table that could be swung aside during activities through this port.

Initially, the jack mountings supported the pile driving equipment during installation of the test piles.

4.3 Sand Spreader

Because the calcareous materials to be used in this project were particularly dusty, the existing sand spreader was modified to provide a complete dust seal. In anticipation that it might also be necessary to rain *in vacuo*, these modifications included additional strengthening and sealing for this purpose.

These modifications included the sealing of the slideway for the shutter assembly, conversion of the perspex under-barrel to steel, stiffening of the sand hopper and full welding of all seams. A lid was also made, but was not straightforward because of the insufficient lifting height of the overhead crane.

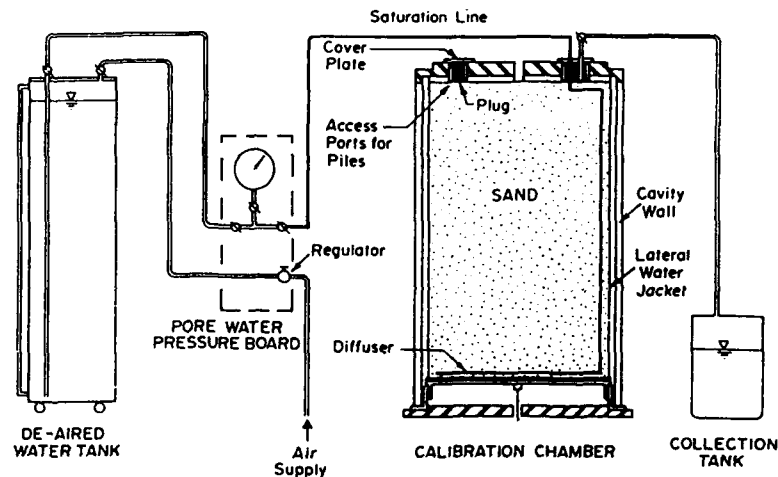


Fig. 3 Saturation arrangements

4.4 Saturation Arrangements

Whilst the sand spreader must necessarily operate with very dry material, substantially saturated samples were required for the pile investigation. Unlike the quasi-static cone

test, it was necessary to be able to model the dynamic driving and cyclic loading conditions in a submerged state as well as providing a realistic environment for grouting operations.

In the system adopted (Fig. 3), water was expelled from a saturation water reservoir of 0.5 m³ capacity via a pore-pressure control board to the sample, under a pressure of 30 to 50 kPa. There it entered the sample through one of the pile ports and was fed to a spiral diffuser on the base of the sample via 20 mm polythene pipe. Excess water drained from the top of the sample, via the same pile port, to a collection tank so that the volume of water retained in the sample could be calculated. Flushing in this manner was continued until the effluent water was judged to be fairly free of entrained air. At the conclusion of testing, the sample could be partly de-watered by applying vacuum to the diffuser (protected by a cover of filter cloth) so that the sample was self-supporting during excavation. Calculated saturations were in the range of 80 to 100%.

5. MATERIALS

The investigation used three different materials (designated A, B and C), all highly calcareous and ranging from a medium sand through to a sandy silt (Fig. 4). Soil A was obtained by dredging adjacent to the Kingfish B Platform in Bass Strait and consisted largely of coral and shell fragments. Soil C was obtained from a Tertiary deposit of calcarenite at an on-shore test site in South Australia. Neither soil has any significant cementation. Both these soils were air dried (in the main) before being screened through a 4.75 mm (B.S No. 4) sieve, but Soil C was found to contain a proportion of cohesive lumps that needed to be broken down by hand.

Soil B, by contrast was manufactured as an analogue of a much finer (and cemented) sediment at another Bass Strait site, from where an adequate volume of material was not available. This soil was produced by processing some 1.5 m³ of Soil A through a variable gap disc mill to form a product within specified grading limits. However, whilst modelling grading, this procedure failed to preserve the porous nature of the particles, as reflected in the density limits (Table 1) and other effects reported later. (For Soil B, as with other fine-grained cohesionless soils, the standard procedure for determining maximum dry density was found to be unsuitable, due to the pumping of fines. Instead, soil was compacted at a range of moisture contents, from which a maximum dry density could be determined).

Table I - Physical Properties of Soils

Soil	G _s	ρ_{\min} (t/m ³)	ρ_{\max} (t/m ³)
A	2.71	1.07	1.34
B	2.71	1.45	1.74
C	2.68	1.03	1.34

6. SAMPLE FORMATION

6.1 Soil Placement

Whilst void ratios were specified for the various samples, no precedent was available to predict how these silty materials would perform during sample formation. It was also clear that they would have to be relatively dense, as the base piston had a very limited stroke (67 mm or 3.7%), providing only limited capacity to accommodate the volume changes expected during saturation, consolidation and the driving of three piles. Trials were therefore run using small charges of A soil in the sand rainer, which indicated that the 10 mm screen would be most appropriate.

However, when using a larger charge of sand during the formation of the first sample (CH1), flow was found to be reluctant, and even ceased altogether unless the screen plate was agitated with a concrete vibrator. The resulting void ratio of 1.38 ($D_r = 28\%$) was, not surprisingly, appreciably over the target of 1.20, but there was no scope to improve on this, as the sand was even less likely to flow through a finer screen plate. In forming a repeat sample of this material (CH4), only the top 1.2 m was rained into place because of insufficient time to prepare an adequate quantity of dry sand. The lower part was, in this case, placed wet and stamped into place to a void ratio of 1.0, with the remainder placed dry to a void ratio of 1.34 ($D_r = 36\%$).

Although Soil C was rather finer than Soil A, it was decided in the first instance that this should also be rained dry from the sand spreader (CH 2A). This required considerable assistance from vibration, but produced a sample of such low density that the volume change during saturation and consolidation was enough to cause the confining membranes to be torn from the base piston. Several weeks were lost before this sample could be reformed (CH 2B), in this case by placing wet soil and stamping into place at a void ratio of 1.33 (because of the impracticality of drying, or processing through the sand spreader).

For Soil B, being much finer again, it was quite clear that new methods would have to be found. Saturation of a dry-formed sample was expected to be difficult, and the volume change on consolidation likely to be beyond the capacity of the base piston. At the specified void ratio of 0.95, the saturated water content was computed as 35%, but soil mixed to this value proved to be quite sloppy and altogether unsuitable for sample formation: this indicated that the analogue soil was not reproducing the in-situ soil because of the degradation of porous particles during grinding.

It was decided that this soil should be pre-mixed to an appropriate water content and compacted in place, with that water content being just sufficient to give workability and to enable the soil to be brought to saturation, as evidenced by the formation of a laitance on the surface. Any excess water would contribute to excess volume change. A series of trial placements were made in small and large oedometers at moisture contents from 17 to 35%, before a figure of 18% was adopted as being feasible for a sample (CH 3). (This is also the optimum moisture content determined from compaction tests).

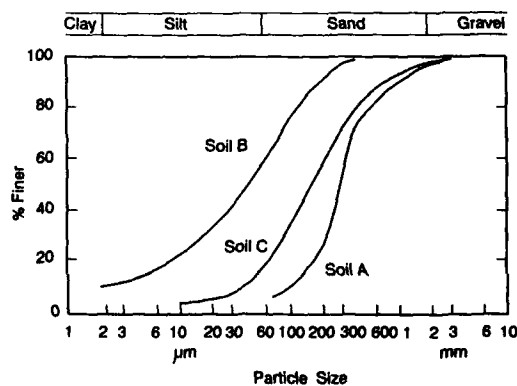


Fig. 4 Particle size distributions

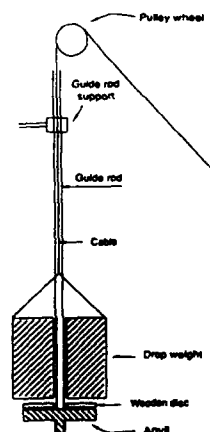


Fig. 5 Pile driving equipment (basic unit)

Because there was insufficient Soil B to form a full sample (due to the considerable time required for grinding), the bottom 0.7 m was formed from Soil A, allowing piles to be tested in the Soil B above with the specified clearance of 2 diameters from the pile tips to the interface. For the bottom portion, Soil A was mixed to 35% water content in a paddle mixer, transferred to the sample and stamped into place at a void ratio of 1.0. When this layer reached the required height, it was flushed with water and covered with a layer of filter cloth. For the remainder of the sample, Soil B was mixed with 18% water in the same paddle mixer (adding dry soil to water) and compacted in place by stamping. Gyrotory floating proved to be an effective way of finishing each layer, which was kept covered with wet cloth between mixes (or submerged overnight). Throughout sample formation, the water level in the lateral water jacket was raised at the same rate to provide lateral support and to avoid bursting the sample former. The final void ratio achieved in Soil B was determined to be 0.52, indicating the extent of particle alteration caused by grinding.

Because this sample was fully saturated, the lateral water jacket could not be expected to provide support to the sample during the removal of the sample former and the placement of the top platen. Therefore suction was applied to the base diffuser and maintained for 5 days until a suction of 40 kPa was reached on a pore-pressure transducer embedded near the Soil A/Soil B interface. During this time, a substantial volume of water was discharged to the water trap of the vacuum pump and the sample settled about 15 mm (which was made up by additional dry soil placed on top).

6.2 Chamber Sealing and Consolidation

After sample formation (and filling the water jacket), the plywood top platen was set in place, and the former lifted out. The lateral membrane was then secured to the platen with a python clip, and folded over the top and secured with ducting tape. A bead of silicone sealant was applied over the top before fitting the chamber lid and applying vacuum to the lid cavity. This vacuum (> 23 mm mercury) was maintained throughout the sealant curing period and for the duration of the chamber test (up to 4 weeks).

Whilst it is normal practice to consolidate samples under K_0 conditions, this was not done in this case, partly because the volume changes were too great for the available piston travel, and partly because the test pressures required at the end of consolidation were otherwise specified. The lateral pressure was first raised in 50 kPa steps to about 60% of the required value before raising the vertical pressure, and finally completing consolidation under isotropic stress ($K = 1$). This ensured that the major part of the volume change was radial, economizing as far as possible on piston travel (for which some reserve had to be maintained for later pile-driving). After consolidation, a standard CPT test was conducted under a K_0 boundary condition, which was then maintained for the pile installations. The CPT was not withdrawn until the conclusion of pile testing.

7. THE PILE TESTING PROGRAMME

7.1 Model Piles and Pile Driving System

Test piles were fabricated from mild steel tube of 100 and 150 mm OD and 5 mm wall thickness, with a 26° external level on the leading edge. All piles were 1.3 m long, allowing for 0.9 m of embedment, and were provided with a steel cap with a central screwed hole.

Bonded resistance strain gauges were mounted externally as diametrically opposed pairs (forming a half-bridge) at each of 6 levels (24 in all). After earlier difficulties, gauges were mounted in a recess milled into the pile wall, where they were secured with epoxy cement and coated with a waterproofing agent. The cavity was then filled flush, and the leads

brought up the pile interior to termination. Piles were also equipped with grout injection ports at 3 levels.

The pile driving system consisted of an anvil and attached guide rod, which screwed onto the pile cap, and a 20 kg donut hammer, operated manually by a rope and pulley system (Fig. 5). A plywood pad on the anvil eliminated rebound. For the 150 mm piles, however, this arrangement was felt to be too light and labour intensive, so that an alternative system was devised, based on a guide tube (attached to the jack reaction plate) and an automatic release mechanism.

7.2 Pile Installation and Testing

When the excess pore-pressures from consolidation and the CPT test had dissipated (as registered on embedded piezometers at 0.55 and 1.00 m depth), the selected pile port was opened and a split driving collar bolted in place to locate the pile during driving. The pile was then located in the port, with the driving gear attached and driven to the prescribed depth under a K_0 condition. For this operation, one of the uppermost strain gauges was connected to a high speed logger in order to measure pile stress at the instant of hammer impact.

During driving in Soils A and C the lateral pressure fell steadily (from the initial value of 280 kPa) to about 200 kPa after some 0.55 m penetration, evidently as a result of particle crushing and consolidation associated with the dissipation of dynamic pore pressures. As this was felt to be the minimum pressure that could be tolerated, driving was stopped whenever it was reached, and the lateral pressure raised to 225 kPa before continuing. Pile driving records were obtained as in Fig. 6. (Pressure loss during driving in Soil B was much less, presumably because of the greater density and less compressible particles).

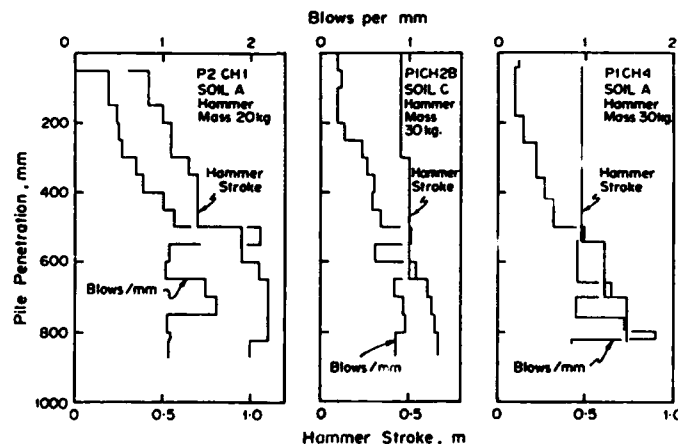


Fig. 6 Pile driving records

On reaching the prescribed depth, the driving system was removed and the height of the internal soil plug was determined by probing through the pile cap. A 25 t servo-controlled loading jack was bolted to the reaction plate and attached to the pile head via 2 load cells and a 2-way coupling able to accommodate some misalignment (Fig. 7).

The initial stage of pile testing (after the dissipation of excess pore pressures) consisted of a static pull test, in which the pile was loaded in tension at a displacement rate of 1 mm/min up to peak capacity, and then relaxed to zero by unloading at the same rate. At a later stage, after grout injection through the pile wall, a sequence of reversing cyclic load was applied.

7.3 Test Results

CPT tests were performed in all samples, but showed significant differences because of the differences in character of each of the samples. For the pluviated samples (CH1 and CH4), the record of tip resistance clearly reflects density variations (not characteristic of clean sands) during the 3-stage formation (Fig. 8), whilst for the pre-mixed and compacted Soil C (CH2B) tip resistance is varying in concert with measured water contents (Fig. 9) (which variations came about because this sample had to be salvaged from the failed CH2A test and had to be mixed up from wet material). In the case of Soil B (CH3), which was mixed from dry material, the degree of control is clearly much better (Fig. 10), the CPT reaching a reasonable plateau at 12.7 MPa before coming under the influence of the filter cloth interface. Numerical results in the significant regions are listed in Table II, showing a somewhat greater friction ratio in the more silty materials and significantly greater strength in the dense B sample.

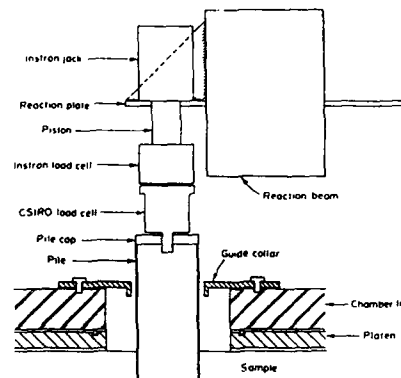


Fig. 7 Pile test arrangement

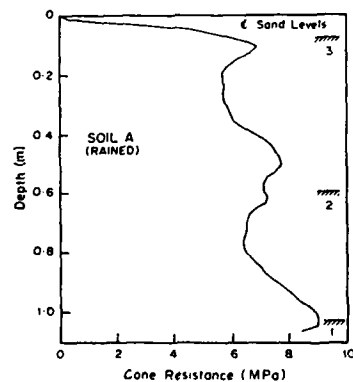


Fig. 8 Penetrometer test, Chamber 1

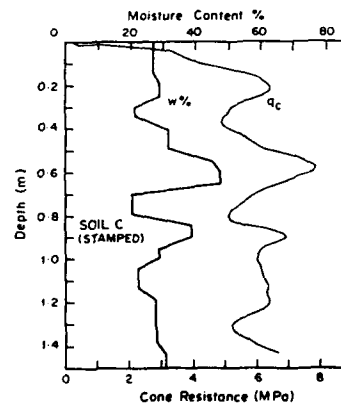


Fig. 9 Penetrometer test and moisture content, Chamber 2B

Table II - CPT Results

Test	Soil	σ_3 (kPa)	q_c (MPa)	f_t (kPa)	F.R.
CH1	A	275	7.8	69	0.88
CH4	A	267	7.55	66	0.88
CH2B	C/A	272	6.35	63	0.99
CH3	B/A	280	12.7	126	0.99

During pile driving, a nominal average side resistance could be determined from the dynamic force at the pile head and the embedded area, and this can be seen to drop rapidly with initial penetration (as observed also by Poulos, 1988), evidently as a result of particle crushing on the interface (Fig. 11 being typical). In this phase, there seemed to be little plugging of the pile tip, the soil plug occupying 70% or more of the embedded pile volume in the case of the sandy materials, or 110% in the case of the silty Soil B (reflecting its greater initial density). From the size of the soil plug, it can be concluded that base resistance during driving is not great and that remoulding of the external soil is negligible. Therefore, there is every reason to believe that the specified clearance between test piles is sufficient to ensure their independent action.

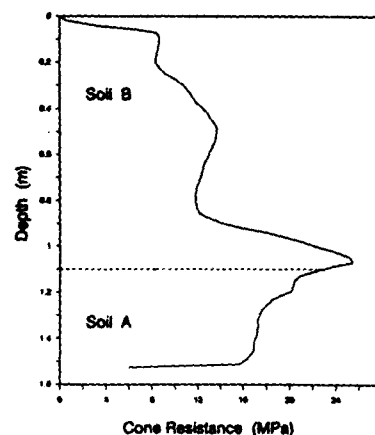


Fig. 10 Penetrometer test, Chamber 3

During pull testing, load-displacement curves were obtained from the output of the jack load cell, as in Fig. 12. This shows the larger 150 mm pile to have significantly larger capacity, as would be expected, whilst otherwise capacity appears to decrease for finer materials.

From the output of the strain gauges at maximum load, a pile load - depth relationship was derived and plotted against a normalised depth (Z/L). Of the resulting plots (Figs. 13 and 14), only the curve for test P2 CH1 is clearly of the form expected. A similar curve is plotted for test P1 CH4 which shows a total capacity that has increased with pile diameter, but with a base load in tension of a magnitude that cannot be explained. The remaining tests show a scatter which makes interpretation somewhat ambiguous. A parabolic curve fitted by regression, for example, has a curvature opposite to P2 CH1, and indicates a significant base load as well as a shear stress increasing in magnitude up the pile shaft. If, however, a straight line is fitted to each of these curves, then the slope yields an average skin friction, included with principal results in Table III. On this basis (and noting P2 CH1 is inflated by some 30% higher cell pressure) skin friction would appear to decrease with fineness, regardless of other factors such as density, but such interpretation is hampered by the uncertainty of the result for P1 CH4.

From the regressed curves for tests P2 CH1 and P1 CH4 and hand fitted curves of similar character for the other two tests, plots of shear stress v. depth were prepared (Figs. 13 and 14), although again the result for test P1 CH4 must be regarded as uncertain because of the apparent base load. These results show a shear stress decreasing by > 50% over about six diameters in depth for all materials. (The use of a regressed curve for P1 CH2B indicates a stress *increasing* up the shaft, which, although possible in terms of elastic theory (Randolph, 1988), has not yet been reported in practice in calcareous soils).

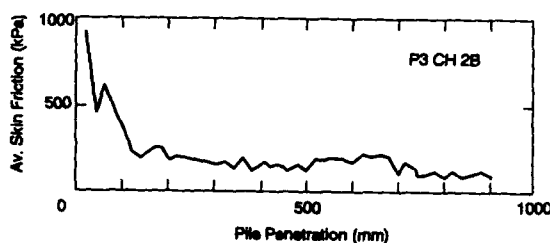


Fig. 11 Nominal av. skin friction during driving

Ultimately, the need is to be able to predict these developed shear stresses from a CPT test, requiring a full displacement device to be compared with one of near zero displacement in highly crushable soils. If a very variable shear stress can be validly averaged, then τ_v/f_v varies from about 2 (CH1) to 0.4 (CH3). A high value for CH1 (whilst reflecting some influence of a higher cell pressure) was thought to be due to this pile not being driven under K_0 conditions, which makes it more likely that a high contact stress was maintained in spite of particle crushing. The low value for CH3, on the other hand, may reflect very tight conditions around the CPT tip in this much denser and stiffer material, together with a greater relaxation in contact stress along the pile shaft resulting also from the same stiffness and enhanced arching capacity.

8. CONCLUSIONS

In this project, a large calibration chamber has been modified to allow cyclic load testing of 100 and 150 mm diameter piles, driven through the chamber lid into samples of three different calcareous sands. These modifications taxed the capabilities of the chamber in almost every conceivable way, from reduced vacuum for sealing and the number of ports required, the vastly extended duration of test, the salt water environment, the loading on the sample former and the measures required to deal with compressible samples.

Sample formation by raining was used in the case of Soil A, but was found to be barely satisfactory and clearly inappropriate for the two finer soils. Soils B and C were therefore pre-mixed with water and compacted in place, causing severe loading on the former and problems of sample support during former removal. Soil B, produced by grinding as an analogue of an in-situ soil, clearly had deficiencies, such that its void ratio (0.52) failed to reproduce the in-situ value (0.95).

Table III Summary, Pile Pull Tests

Pile No. Nom. O.D. (mm)	Driven Length (mm)	Soil Type	Init. Void Ratio	Lateral Pressure (kPa)	Peak Load (kN)	Av. Skin Friction (kPa)	Displ. at Peak Load (mm)
P2 CH1 (100)	770	A	1.38	300	35	135	14.6
P1 CH 2B (100)	870	C	1.33	225	25.5	70	7.8
P1 CH 4 (150)	830	A	1.34	225	47	75	10.0
P1 CH 3 (100)	905	B	0.51	220	22	55	10.0

During pile driving, there was little evidence of plugging, implying little densification around the tips or interference with other piles (at least for calcareous sands). Measurements of total load during driving and shear stress during pull testing both point to a diminishing contact stress up the pile shaft due to particle crushing (although some results are rather indeterminate). This considerable variation in contact stress makes it difficult to establish an appropriate value of shear stress to compare with CPT results.

Such comparisons are also hindered by variations in soil density and bonding, and the degree of plugging (whether the pile is a zero or full-displacement device). The pile in Soil B, for example, indicated an average shear stress of half f_c from the CPT, probably reflecting the absence of soil compaction around the tip and a soil that is more self-supporting and stiffer than the other two. For the pile tests in Soils A and C, there is generally agreement with the CPT, except for test P2 CH1. This test is not entirely satisfactory because of the apparent base load, but its high capacity is believed to be due to its being installed not under K_0 conditions, leading to the maintenance of a higher contact stress on the shaft.

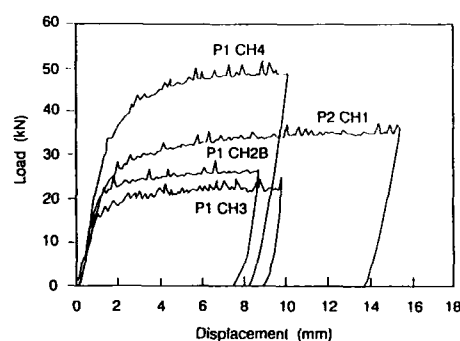


Fig. 12 Load-displacement curves, pull tests

ACKNOWLEDGEMENT

Results reported herein are drawn from a research study undertaken jointly by CSIRO Division of Geomechanics and Monash University (both Melbourne, Australia) under contract to Exxon Production Research Company (Houston), acting on behalf of Esso Australia Ltd. and BHP Petroleum Ltd. The permission of each of these bodies to publish in this instance is gratefully acknowledged. Particular recognition is made of the contribution of Dr. T.W. Dunnivant, who conceived and supervised the project on behalf of EPR, and Mr. D. R. Willoughby and Dr. C. Tan of CSIRO who were responsible for all matters relating to pile driving and testing. Substantial contributions were made by Mr. Y. W. Yee, graduate student, and Mr. C. Powell (both Monash) in sample preparation and technical services. Mr. J. M. Hulett (EPR), Mr. A. M. Hyden (EAL) and Mr. S. Anderson (Wolohan Grill and Partners) also participated in project supervision.

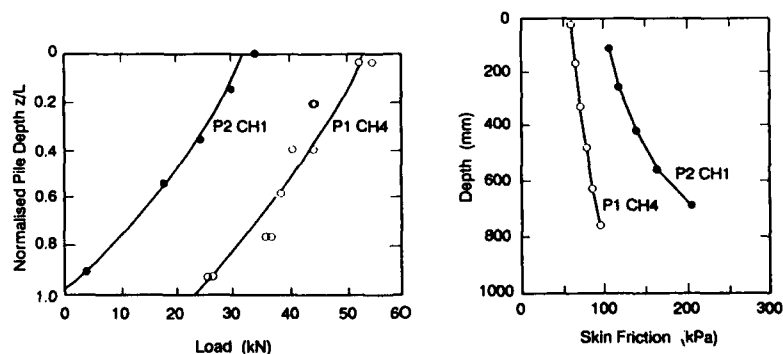


Fig. 13 Distributions of load and skin friction at peak, Soil A

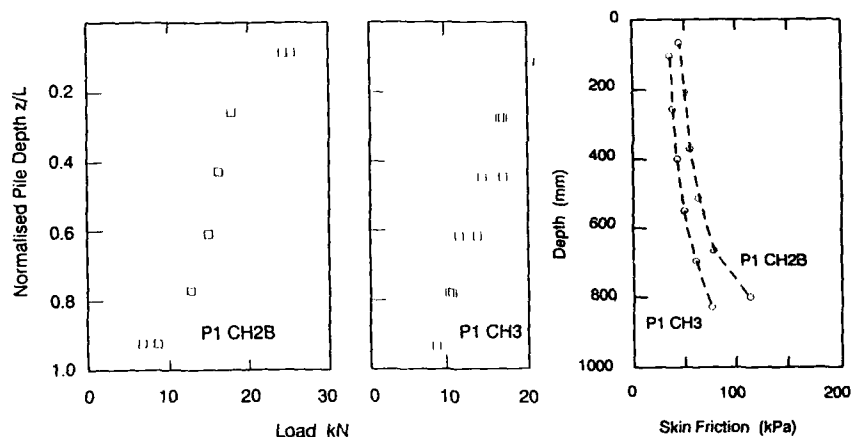


Fig. 14 Distributions of load and skin friction at peak, Soils B and C

REFERENCES

- Angemeer, J., Carlson, E.D. and Klick, J.H. (1973) Techniques and results of offshore pile load testing in calcareous soils. Proceedings, 5th Annual Offshore Technology Conference, Paper OTC 1894 (Houston), Vol. 2, pp 677-692.
- Bellotti, R., Bizzi, G. and Ghionna, V. (1982). Design, construction and use of a calibration chamber. Proceedings, 2nd European Symp. on Penetration Testing (ESOPT II) Amsterdam V. 2, pp 439-446.
- Chapman, G.A. (1980). Interpretation of friction cone penetrometer tests in sand. Ph.D. Thesis, Monash University, Australia.
- Holden, J.C. (1971). Laboratory research on static cone penetrometers. Report No. CE-SM-71-1, Dept. Civil Eng., Univ. of Florida. See also: Veismanis, A. (1974). Laboratory investigation of electrical friction cone penetrometers in sands. Proceedings, European Symp. on Penetration Testing (ESOPT), Stockholm, Vol. 2.2, pp 407-419.
- Hyden, A.M., Hulett, J. M., Murff, J.D. and Abbs, A.F. (1988). Design practice for grouted piles in Bass Strait calcareous soils, Proceedings, Int. Conf. on Calcareous Sediments (Perth, W. Aust.), Vol. 1, pp 297-304.
- Nauroy, J.F., Brucy, F. and Le Tirant, P. (1988). Skin friction of piles in calcareous sands. Proceedings Int. Conf. on Calcareous Sediments, Perth, Vol. 1, pp. 239-244.
- Parkin, A. K., Yee, Y.W., Tan, C.P. and Willoughby, D.R. (1990). Driven model piles tested in calcareous sand in a large calibration chamber. Proceedings, 22nd Annual Offshore Technology Conference, Paper OTC 6242 (Houston), Vol. 1, pp 389-397.
- Parkin, A.K. (1988). The calibration of cone penetrometers (Special Lecture), Proceedings, 1st Int. Symp. on Penetration Testing (ISOPT 1), Orlando, Florida, 1 : 221-243.

Poulos, H.G. (1988). The mechanics of calcareous sediments. Jaeger Memorial Lecture to 5th Australia-New Zealand Conf. on Geomechanics. (Sydney) Australian Geomechanics (August 1988), pp 8-41.

Randolph, M.F. (1988). Evaluation of grouted insert pile performance. Proceedings, Int. Conf. on Calcareous Sediments (Perth), Vol. 2, pp. 617-626.

Tan, C. P., Parkin, A.K. and Yee, Y.W. (1990). Monotonic testing of a model pile driven in a calcareous sandy silt. Proceedings, 22nd Off-shore Technology Conference, Paper OTC 6242 (Houston), Vol. 1, pp 399-404.

Yee, Y.W. (1989). Cone penetrometer and model pile tests in calcareous soils. Master of Engineering Science Thesis, Monash University, Australia.

MODEL PRESSUREMETER TESTING IN AN AUTOMATED FLEXIBLE WALL CALIBRATION CHAMBER

D. PENUMADU¹, Student Member, ASCE, A. SKANDARAJAH¹, Student Member, ASCE, and J. L. CHAMEAU², Member, ASCE

¹ Graduate Research Assistant, Purdue University, W. Lafayette, IN 47907;

² Professor of Civil Eng., Purdue University, W. Lafayette, IN 47907

ABSTRACT

An automated control and data logging system has been developed to perform model pressuremeter tests in clays using a flexible wall calibration chamber. The tremendous potential of self-boring pressuremeter has not been realized in practice due to drawbacks associated with strain rate effects, stress relief, relaxation and soil disturbance. Several of these important questions related to cavity expansion and pressuremeter testing in clays are being investigated using the newly developed calibration chamber test set up. Methods for slurry preparation and consolidation under K_0 conditions are presented. Special considerations have been given to prepare high quality specimens and perform pore pressure measurements. Electro-pneumatic control, double wall calibration chamber, slurry mixing and vacuuming tank, slurry consolidometer, piezometer and model pressuremeter are described. Preliminary test results indicate successful performance of the system.

INTRODUCTION

A series of one eighth scale model pressuremeter tests are being conducted to evaluate the effects of strain rate and stress disturbance in cavity expansion of cohesive soils. The initial phase of the research involved the development of an automated control and data logging system to perform model pressuremeter tests in a double wall calibration chamber. The calibration chamber built for a previous research study (Huang [5]) was modified to work with the new set up.

The test set up includes a double wall calibration chamber, a slurry consolidometer, differential piston pump, model pressuremeter, piezometer, electro-pneumatic control, data acquisition system and control panels. The paper describes the flexible wall calibration chamber system and the procedure involved in preparing uniform specimens obtained by consolidating a slurry of kaolin or kaolin-silica mix. The performance of newly designed piezometers is also discussed. Using the same soils, tests were performed in a cuboidal shear device to simulate pressuremeter stress paths, with strain rates varying from 0.01% per minute to 5.0% per minute. The experimental data indicated an increase in undrained strength of 15% for each tenfold increase in strain rate Skandarajah et al. [7]. One of the main objectives of this research is to confirm the strain rate effects measured in the true triaxial simulation. Calibration chamber test results will also be used to calibrate the anisotropic model developed for the study.

STRAIN CONTROLLED PRESSUREMETER TESTS IN A CALIBRATION CHAMBER

Most of the scaled in situ tests using a calibration chamber has been performed in granular soils. In the past, pressuremeter tests in calibration

chamber were performed in granular soils by Jewell et al. [6] and in cohesive soils by Huang et al. [4]. A calibration chamber provides a controlled environment to perform this type of testing with the unique capability of subjecting soil samples to known stress history and boundary conditions. It also makes it possible to work with uniform and reproducible samples. The calibration chamber approach for pressuremeter testing in cohesive soils has been used by Huang [6] prior to this research. Other studies concentrated field pressuremeter tests and comparison with conventional laboratory tests on samples from the same site. It is believed that calibration chamber technique for cohesive soils is a desirable alternative.

The two types of calibration chambers used in practice are the rigid-wall and flexible wall chambers. A rigid-wall chamber has a rigid wall that ensures no lateral strain. The main disadvantage in a rigid-wall chamber is that, to avoid boundary effects, the size of the chamber must be much larger than the in-situ device that is being calibrated. This makes the testing expensive and time consuming. In a flexible wall chamber, it is possible to have independent control on vertical and lateral stresses, which makes the simulation of field tests possible with relatively small samples. The flexible wall chamber used in the current research has two walls, the inner wall being slightly thinner than the outer one so that if the cell pressure at some stage exceeds its yield value, it would burst inward ensuring the safety of the working environment. The two types of boundary conditions used are BC1: Constant vertical stress and zero lateral strain, and BC2: Constant vertical stress and constant lateral stress. It can accommodate a specimen of size 200 mm in diameter and 367 mm in height. The design allows for K_0 consolidation as well as pressuremeter testing on that specimen at the end of consolidation. In the flexible wall chamber, the sample is hydraulically confined around a soft membrane which makes it possible to have independent control on lateral and vertical stresses. In order to make the consolidation and testing time manageable, the specimen dimensions were scaled down to the above mentioned values. The following sections give a detailed account of the salient features of the test set up, techniques of sample preparation, chamber consolidation, and strain controlled model pressuremeter testing.

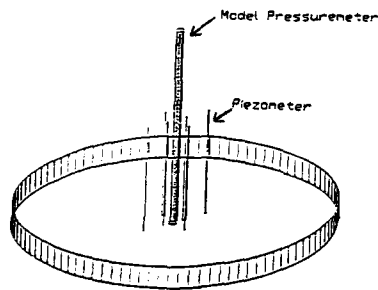
1) Chamber Top Platen

The chamber top platen is shown in Fig. 1. It is a 28 mm thick aluminum platen and 200 mm in diameter. The model pressuremeter is attached to it at its center through 1/4" NPT. Piezometers are also attached to this platen. They are arranged diagonally opposite at 20 mm, 27 mm, and 44 mm respectively. It is thus possible to obtain two porepressure readings at the same distance from the center of the probe. The tips of the piezometers extend approximately to the center of the probe. The chamber platen provides connectors for back pressuring and also for initial flushing. The pore and probe pressures are measured using high sensitivity Model AB type pressure transducers (Data Instruments, Inc.) and the chamber top platen has all the mounting adapters attached to it. Prior to using the platen in the slurry consolidometer, all the piezometers and model pressuremeter are filled with deaired distilled water and thoroughly flushed to remove any entrapped air bubbles. The model pressuremeter has a custom made 9.5 mm ID, 0.8 mm thick latex membrane. Since light has detrimental effect on latex, when not in use, the platen is stored in a dark place.

2) Piezometers

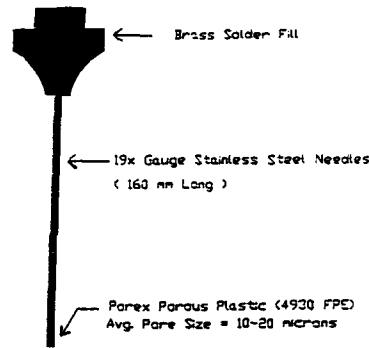
Evaluating pore pressures is an important and integral part of calibration chamber test and is essential to the success of undrained testing. It is important to saturate the piezometers completely so that negative pore pressures resulting from cavitation are avoided. However, excess positive pore

pressure should also be avoided. The piezometer shown in Fig. 2 was designed based on these considerations. The piezometer is typically made of 19 gauge stainless steel hypodermic needle. The needle is attached to the 1/8" pipe union through brass solder. The total length is 160 mm and the tip is plugged with fine polyethylene porous plastic having a mean pore size of 10 to 20 microns. At the end of each test, porous plastic plugs are removed using 0.56 mm plain steel acoustic string. The small diameter of the pressure sensitive area makes it ideal for instantaneous response. Initial test results indicate their acceptable performance and authors are considering to improve their performance by using silicone oil instead of water for initial saturation of the piezometers.



Chamber Top Platen

Fig. 1



Piezometer Cross-Section

Fig. 2

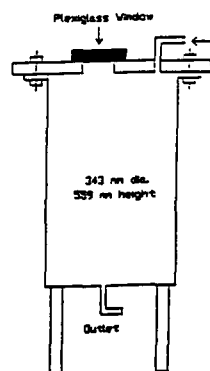
3) Slurry Tank

The slurry preparation procedure must be systematically followed to obtain uniform and reproducible specimens. The slurry preparation involves three phases: slurry mixing, slurry vacuuming, and transfer to consolidometer. A tank shown in Fig. 3 has been designed to perform these tasks. It is 343 mm in diameter and 559 mm in height. Known amounts of water and kaolin-silica mix are added to the tank and are thoroughly mixed using conventional heavy duty mixer with 1/3 H.P. motor and type 316 stainless steel blades, at 1725 rpm, until a uniform mix is obtained. Subsequently, the mix is subjected to full vacuum for a period of six hours by which time the air entrapped during mixing is removed. A pressure of 5 psi is applied to the surface of the mix to transfer the slurry slowly into the consolidometer through 25.4 mm tygon flexible tubing. The mix is placed gradually from bottom to top in the consolidometer and the chances of air entrapment are minimized. Since very viscous mixing is involved, it is important to properly select the suitable motor and blades for obtaining a uniform slurry.

4) Slurry Consolidometer

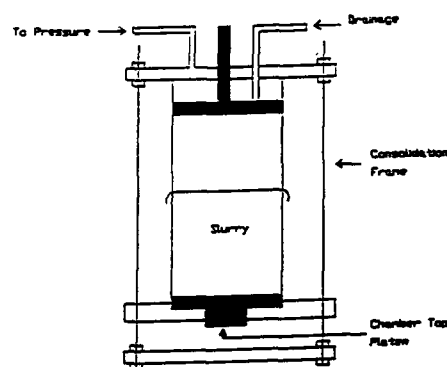
The soils used for testing to date are Georgia kaolin and crushed Ottawa silica. Deionized-deaired water is added to the soil and uniform slurry mix is obtained using the technique mentioned above. The water content corresponds to twice the liquid limit of the soil. The slurry is then transferred to the slurry consolidometer shown in Fig. 4. The device is used to consolidate the slurry from an initial height of 800 mm to a final height of approximately 350 mm. The slurry consolidometer has 2 steel pipe compartments having an inside

diameter of 200 mm. The chamber top platen becomes the bottom platen for this device, with all the piezometers and model pressuremeter attached to it. A porous stone is attached to the piston and the slurry is consolidated by 207 kPa air pressure applied to the piston. Double drainage is allowed for the slurry to consolidate under K_0 conditions. It takes approximately 12 days for the completion of primary consolidation. The lower compartment has same height as the soil sample. It is split longitudinally in two halves and bolted together. The interior is lined with sandpaper which is required to prevent slippage of the membrane caused by adhesion between clay and the membrane during the process of consolidation. The additional space for the slurry during the initial phase of the consolidation is provided by the upper compartment which is bolted to the lower one. The 0.64 mm thick custom made latex membrane for the specimen extends out of the lower compartment and provides a seal between the two cylinders (Fig. 4). This completes the first phase of the consolidation process. The sample confined in the lower compartment and encased in the latex membrane is then transferred to the calibration chamber with the split mold. Since the sample is transported without touching it, and no mechanical extrusion is involved, disturbance is essentially eliminated.



Slurry Tank

Fig. 3



Slurry Consolidometer

Fig. 4

5) Differential Piston Pump

A differential piston pump is used to expand the probe at a constant rate of strain (Fig. 5). It has two pistons of diameters 12.738 mm and 9.525 mm, respectively. They are attached to stepper motor and a DCDT. Through the stepper motor control box, four different speeds are preset with a switch box. By controlling the rate of movement of the stepper motor and with the input valve closed, the volume of water injected to the probe can be regulated at a constant rate. Thus, with the preset switch box, it is possible to obtain four constant strain rates for the probe expansion. A device of this accuracy is necessary because a radial strain of 12% for the model pressuremeter corresponds to a differential piston movement of only 37 mm.

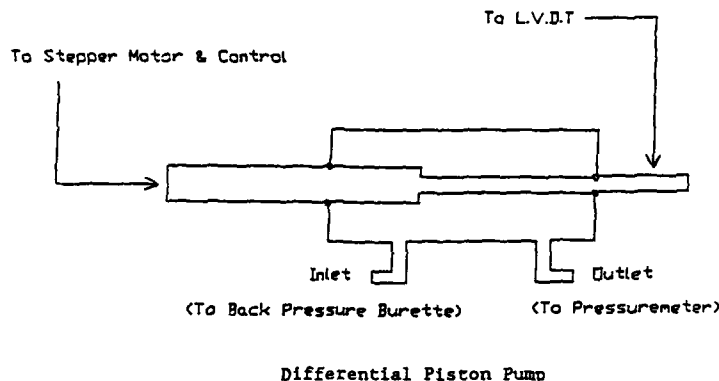


Fig. 5

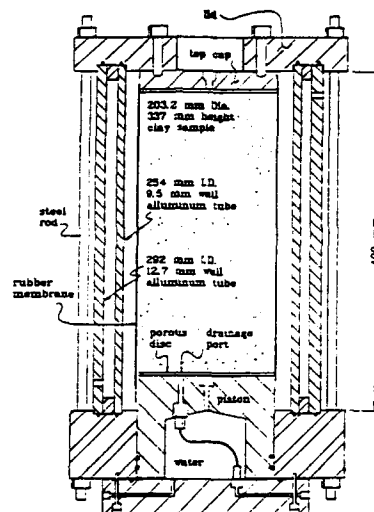
6) Electro-pneumatic Control

During the second phase of consolidation inside the calibration chamber it is essential to create a rigid system with no lateral deformation in the horizontal plane. To ensure this, the cell and wall pressures are balanced throughout the consolidation process. A differential pressure transducer monitors the pressure difference between cell and wall, sends the resulting voltage signal to an electro-pneumatic transducer which converts the input voltage to an appropriate output pressure which is applied to the annular space between the internal and external walls. This electro-pneumatic control assures a zero lateral deformation condition, which is essential for successful K_0 consolidation.

7) Flexible Wall Calibration Chamber

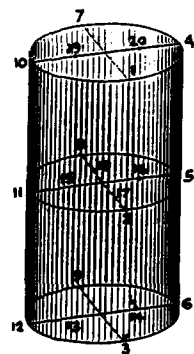
The schematic of the flexible wall calibration chamber is shown in Fig. 6 (after Huang [5]). Upon completion of the slurry consolidation in the consolidometer, the sample confined in the lower compartment (bolted split mold) is transferred to the chamber and placed upside down. During the transfer operations it is critical to center the sample on the piston of the calibration chamber before placing it. Once it is supported on the piston platen, it is very difficult to re-align it without disturbing the sample. The piston providing the vertical stress inside the chamber has the same diameter as that of the sample and has a maximum vertical travel of 62 mm. Since the sample is encased in a membrane and is attached to top and bottom platens with two 158 mm o-rings, both ends of the sample are isolated from the cell water. Hence the stresses in horizontal direction through cell pressure, and vertical direction through piston pressure, can be independently controlled. By balancing the pressure between cell and wall, and by maintaining constant piston pressure and preventing volume change in the cell-water system, conditions simulating K_0 consolidation are obtained. The sample at the end of the first phase of the consolidation process in the slurry consolidometer does not have uniform water contents along the vertical direction due to friction between clay and rigid wall. By subjecting this sample to a second phase of K_0 consolidation and avoiding rigid boundary, a very uniform sample is obtained. Fig. 7 shows the three dimensional profile of the variation of water contents

for a typical kaolin-silica mix specimen. Porous discs are placed at both ends of the sample to permit double drainage. During K_0 consolidation, loss of sample volume is replaced by the piston movement, therefore allowing displacements in the vertical direction only. K_0 consolidation under an effective vertical stress of 276 kPa was performed using a single load increment method proposed by Campanella and Vaid [1].



Double Wall Calibration Chamber

Fig. 6



Location	Water Content (%)
1	28.53
2	28.32
3	27.04
4	28.52
5	28.10
6	27.14
7	28.63
8	28.52
9	27.06
10	28.79
11	27.93
12	27.65
13	28.33
14	28.47
15	28.58
16	28.57
17	28.47
18	28.65
19	28.74
20	28.90

Moisture Content Variation

Fig. 7

In summary, the five step procedure that accomplishes chamber K_0 consolidation is made of the following steps:

- 1) Close the pore water drainage lines.
- 2) Increase cell and axial pressures to back pressure + effective consolidation pressure (690 kPa + 276 kPa) simultaneously.
- 3) Maintain a constant cell-water system.
- 4) Open the drainage lines and permit drainage against high back pressures.
- 5) Monitor axial deformation and cell pressure changes, and electro-pneumatically control the wall pressure.

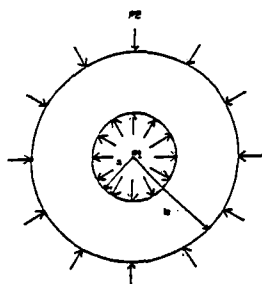
Because of the limited vertical movement of the piston, very soft samples could not be tested using the present calibration chamber.

8) Boundary Effects

The sample is eighteen times larger than the diameter of the pressuremeter probe. In order to evaluate the radial distance at which stress increase diminishes to zero a simple elasticity based approach can be used. The equation of equilibrium for a cylindrical cavity is (tension being positive):

$$\frac{d\sigma_r}{dr} - \left(\frac{\sigma_\theta - \sigma_r}{r} \right) = 0$$

Introducing compatibility and plane strain conditions, the variation of radial and circumferential stresses (Fig. 8) are:



$$\sigma_r = -p_1 - \frac{(p_1 - p_2)}{\left(\frac{a^2}{b^2} - 1\right)} + \frac{(p_1 - p_2)}{\left(\frac{1}{b^2} - \frac{1}{a^2}\right)} \left(\frac{1}{r^2}\right)$$

$$\sigma_\theta = -p_1 - \frac{(p_1 - p_2)}{\left(\frac{a^2}{b^2} - 1\right)} - \frac{(p_1 - p_2)}{\left(\frac{1}{b^2} - \frac{1}{a^2}\right)} \left(\frac{1}{r^2}\right)$$

Stress-State of Sample

Fig. 8

For a maximum probe pressure of 1173 kPa ($\epsilon_r = 12\%$) and a cell pressure of 830 kPa, elasticity based analyses indicate that the stress increase is essentially negligible at a radial distance equivalent to 9 times the probe radius (Fig. 9). Numerical analysis by Carter et al. [2] have shown that in a soil mass which extends laterally to infinity, the stress increase diminishes to essentially zero at approximately 20 times the cavity radius as radial strain reaches about 25%. In the chamber pressuremeter tests, maximum radial strain was limited to 12%. Elasticity based arguments coupled with the numerical analysis by Carter et al. [2] thus indicate that the size of the probe to soil specimen ratio is satisfactory within the strain range of interest.

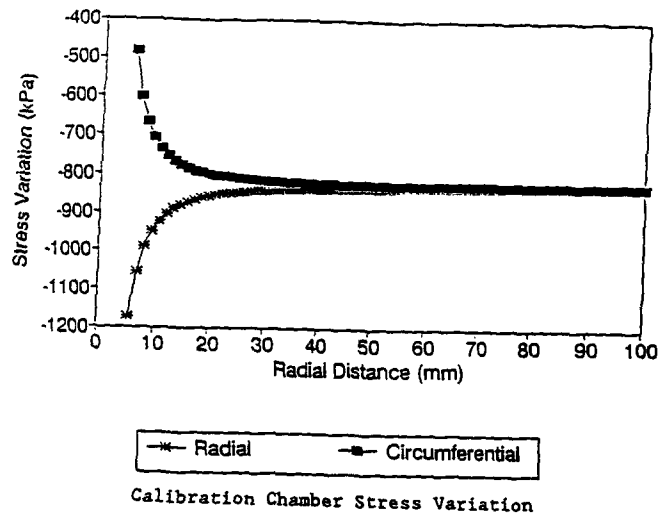


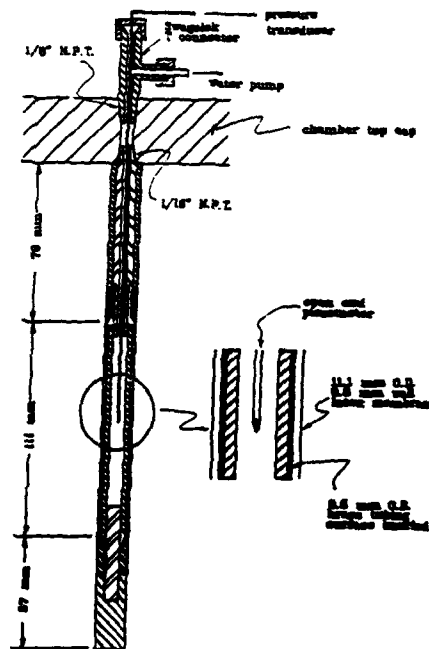
Fig. 9

9) The Model Pressuremeters

Based on the design concept of a single cell lateral load tester made by Oyo Corporation, Tokyo, Japan (Suyama et al. [8]), one eighth scaled water inflated model pressuremeters were built as a part of an earlier research program. The probe has a diameter of 11.1 mm and is 112 mm long. Custom made 9.5 mm ID, 0.8 mm thick latex membranes are used as the probe membrane. The fluid pressure is measured at the center of probe, accounting for the head loss. Strain controlled pressuremeter tests are performed by injecting constant amount of fluid, using the differential piston pump. Details of the model pressuremeter are shown in Fig. 10 (after Huang [5]).

10) Strain-Controlled Testing

The complete control system involved in the strain-controlled probe expansion is shown in Fig. 11. Initial calibration chamber tests using the model pressuremeter have been performed in a 50/50 blend of kaolin and very fine crushed silica. The slurry was K_0 consolidated under a pressure of 207 kPa around the model pressuremeter and six

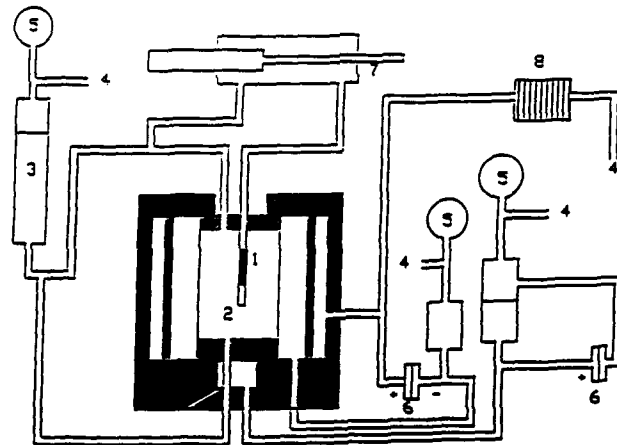


Model Pressuremeter Cross-Section

Fig. 10

piezometer needles, and then transferred to the calibration chamber. The performance of the piezometers was evaluated during the β parameter check. After saturation, the specimen was subjected to a second phase K_0 consolidation in the chamber under an effective vertical stress of 276 kPa against a back pressure of 690 kPa. A strain controlled pressuremeter test was performed at the end of chamber consolidation. All the control and acquisition during the testing was performed by a Keithly series 500 data acquisition system. The probe expansion curve obtained at the end of the test represents the combined effect of system compliance, membrane stiffness and the soil resistance. The raw data is shown in Fig. 12. The system compliance was measured by inserting the model pressuremeter in a tight-fitting thick walled brass tube. The membrane stiffness was evaluated by performing the pressuremeter test in an empty chamber with cell pressure equal to horizontal stress obtained at the end of chamber consolidation. The net pressuremeter curve is obtained from probe expansion curve by subtracting the system compliance and the membrane stiffness.

The results of initial testing indicate that small radial strains occurred before exceeding the true soil lateral stress which is the chamber cell pressure at the end of K_0 consolidation. Hence with reasonable accuracy, true "lift-off" point can be evaluated using the model pressuremeter under controlled conditions. Essentially elastic behavior was observed for the unload-reload cycle.



- | | |
|--------------------------|-------------------------------------|
| 1) Model Pressuremeter | 5) Pressure Gage |
| 2) Soil Sample | 6) Differential Pressure Transducer |
| 3) Back Pressure Burette | 7) Differential Piston Pump |
| 4) Air Pressure | 8) Electro-Pneumatic Control |

Calibration Chamber Control System

Fig. 11

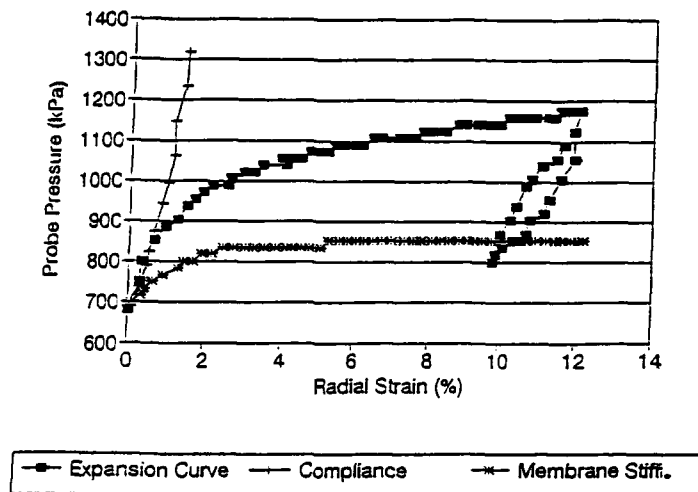


Fig. 12

Using the same soil, series of true triaxial testing have also been performed. The pressuremeter stress path was simulated on 100 mm cube samples that were strained at different rates. The results indicate an increase in undrained strength of 15% for each tenfold increase in strain rate. This will be confirmed using the results obtained from the calibration chamber. The effects of interpolation technique of probe-expansion curve on strength parameters will also be studied. The test results will also be used for calibrating an anisotropic model developed for the study. With this model one can predict the behavior of clay type material under any desired stress path from the results obtained under a particular stress path, such as the pressuremeter stress path.

CONCLUDING REMARKS

An automated calibration chamber system which includes a double wall chamber, slurry consolidometer, piezometers, electro-pneumatic control, model pressuremeter, data acquisition and control system has been developed. From the initial testing, the following are concluded:

- a) By employing standard slurry preparation techniques and two phase consolidation process, a very uniform sample can be obtained.
 - b) True lateral stress predictions can be made using pressuremeter.
- This also reflects the disturbance free state obtained at the end of chamber consolidation.

ACKNOWLEDGEMENTS

The work reported herein, performed at Purdue University, was part of a research program sponsored by the US Air Force Office of Scientific Research. This support is gratefully acknowledged. The help provided by Prof. A.B. Huang of Clarkson University is greatly appreciated.

REFERENCE

1. Campanella, R.G., and Vaid, V.P., "A Simple K_0 Triaxial Cell", Canadian Geotechnical Journal, Vol. 9, pp. 249 (1972).
2. Carter, J.P., Randolph, M.F., and Wroth, C.P., "Stress and Pore Pressure Changes in Clay During and After the Expansion of a Cylindrical Cavity", International Journal for Numerical and Analytical Methods in Geomechanics, Vol. 3, pp. 305-322 (1979).
3. Chapman, G., "A Calibration Chamber for Field Testing Equipment", Proceedings of the European Symposium on Penetration Testing, Stockholm, pp. 59-65 (1974).
4. Huang, A.B., Holtz, R.D., and Chameau, J.L., "A Calibration Chamber for Cohesive Soils", Geotechnical Testing Journal, GTJODJ, Vol. 11, No. 1, pp. 30-35 (1988).
5. Huang, A.B., "Laboratory Pressuremeter Experiments in Clay Soils", Ph.D. thesis, Purdue University, West Lafayette, Indiana (1986).
6. Jewell, R.J., Fahey, M., and Wroth, C.P., "Laboratory Study of the Pressuremeter Test in Sand", Geotechnique, Vol. 30, pp. 507-531 (1980).
7. Skandarajah, A., Penumadu, D., and Chameau, J.L., "Strain Rate Effects on Pressuremeter Testing", Eighth ASCE Engineering Mechanics Specialty Conference, Columbus, OH (1991).
8. Suyama, K., Imai, T., and Ohya, S., "Lateral Load Tester (LLT). Its Method and Accuracy", Symposium on the Pressuremeter and Its Marine Applications, Paris (1982).

PENETRATION RESISTANCE OF FINE COHESIONLESS MATERIALS

RICHARD W. PETERSON

U.S. Army Engineer Waterways Experiment Station, Vicksburg, MS 39180

ABSTRACT

Guided by the principles of dimensional analysis and similitude, a laboratory investigation was conducted to assess the penetration resistance of fine cohesionless materials. Variables which were investigated included the effects of specimen density, particle size, penetration rate, and induced pore water pressure. A small-scale penetration apparatus and scaled penetrometers were constructed. Four uniform gradations of glass beads were tested; particle sizes ranged from medium sand to silt. Specimens were molded to a range of densities and tested at an inundated or an air-dry state. For inundated specimens, pore pressure transducers were placed in the stress chamber as each specimen was molded. The penetration rate for the study reported herein ranged from 3.1 to 0.02 in./sec (8.0 to 0.04 cm/sec).

Based upon an analysis which was consistent with the cavity expansion theory, it was determined that penetration resistance was dependent upon the density of the specimens and the effective stress conditions. For the study reported herein, the effects of particle size and penetration rate were negligible. An effective stress model was proposed for predicting the penetration resistance of drained or partially drained cohesionless materials.

INTRODUCTION

Certain soils, such as silty or sandy soils, do not lend themselves to undisturbed sampling by conventional methods for geotechnical engineering investigations. Because of the difficulty of obtaining quality samples of cohesionless soils, in situ tests, such as the Standard Penetration Test (SPT) and the Cone Penetration Test (CPT), have received increasing interest for geotechnical site investigations. However, analyses of in situ test data are generally based upon empirical correlations. In an effort to overcome this uncertainty, the laboratory calibration chamber or stress chamber has been used to gain insight on the use and interpretation of in situ tests [1-6]. Although specific technological advances for interpretation of penetration tests on clean medium to coarse sands have been reported, few studies have been conducted, and little information is known about the penetration resistance of fine sands and silty sands. Analyses of in situ test data obtained in these materials have generally consisted of empirical adjustment factors applied to the correlations developed for coarser sands. Examples include adjusted SPT blowcounts [7-9] or adjusted cone penetration resistances [10].

Because of the uncertainty of interpretation of penetration data for silty sands, a laboratory investigation was conducted to develop an interpretative methodology for the penetration resistance of fine cohesionless materials. Following the principles of dimensional analysis and similitude, a small-scale penetration apparatus was designed and fabricated. An artificial material, glass beads, was selected for the investigation because the effects of plasticity of the fines and a variation of the shape and hardness of the particles for different

gradations of material were eliminated. Variables which were isolated and studied during the investigation included the effects of specimen density, particle size, penetration rate, and induced pore pressure on penetration resistance. This manuscript summarizes the laboratory investigation and conclusions which were obtained as a result of the study.

EQUIPMENT

A small stress chamber system was designed and fabricated to conduct the laboratory penetration tests. The stress chamber consisted of a rigid metal cylinder, 15-in. (38 cm) diameter by 12 in. (30 cm) high, which was used to confine the test specimen. Vertical stress was applied to the specimen by three pneumatic cylinders which acted on a rigid platen. A 0.35-in. (0.89 cm) diameter cone penetrometer was pushed into the test specimen by an actuator which was controlled by a closed-loop hydraulic system. Three holes were placed in the wall of the rigid cylinder on arcs of 120 degrees at distances of 3-, 6-, and 9-in. (7.6, 15.2, and 22.9 cm) from the top of the chamber; these holes permitted the electrical wires for instrumentation, such as pore pressure transducers, which was placed in the test specimens to be connected to data acquisition and recording equipment.

Supplemental laboratory tests, including triaxial compression tests, were conducted to obtain strength and deformation data required for analysis of penetration tests according to the cavity expansion theory. These tests were conducted in conventional laboratory testing equipment; a description of the testing equipment is not presented herein.

MATERIAL

Four uniform gradations of glass beads were selected for assessing the penetration resistance of fine cohesionless material. The gradations were identified according to U.S. Standard sieves sizes as 40 to 50 (0.425 to 0.300 mm), 70 to 100 (0.212 to 0.150 mm), 140 to 200 (0.106 to 0.075 mm), or 270 to 400 (0.053 to 0.038 mm) [11]; hereinafter, these gradations are identified as 40-50, 70-100, 140-200, or 270-400 materials, respectively. According to the manufacturer's literature, the spheres were described as "containing not more than 15 percent irregularly shaped particles" and "reasonably free of sharp angular particles, particles showing milkiness or surface scoring, and foreign matter" [12]. It was also reported that the hardness of glass beads was equivalent to the hardness of feldspar minerals on Moh's scale, the crushing strength was approximately 40,000 psi (275 MPa), and the modulus of elasticity of solid glass, rather than of beads in bulk, was 9,660,000 psi (67 GPa). The specific gravity, representative grain size distribution curve, and the maximum and minimum densities for each material were determined according to procedures which were described elsewhere [11,13,14]. Test results are summarized in FIG. 1.

SPECIMEN PREPARATION PROCEDURES

Pluvial deposition was used to mold most of the specimens. The technique consisted of slowly pulling a wire mesh through material which had been placed in the stress chamber; it was judged this operation was similar to the pluvial deposition technique described by other researchers [1,3,5,6,15] except the free fall distance of the soil was approximately zero. To saturate a specimen, hereinafter referred to as a "wet" specimen or test, a vacuum of approximately 14 psi (100 kPa) was applied to the specimen and allowed to remain overnight. On the following morning, deaired distilled water was permitted to

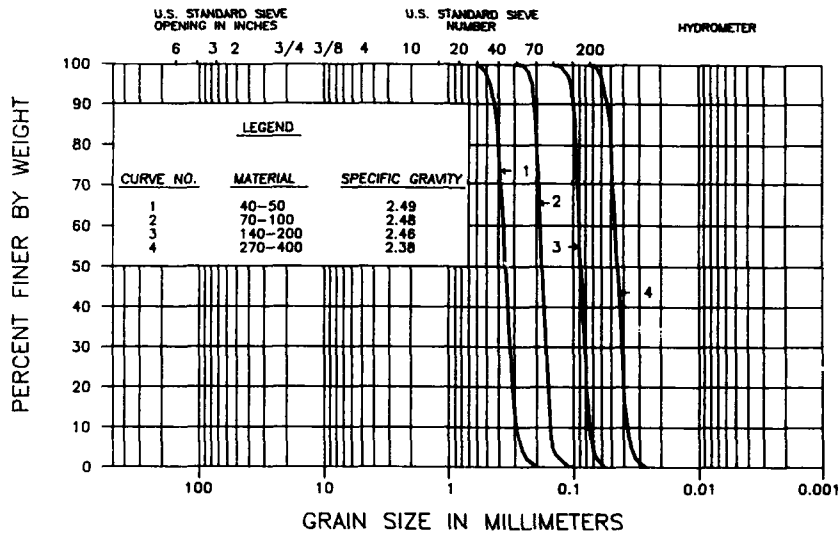


FIG. 1. Physical properties of four gradations of glass beads used for his investigation.

seep into the specimen. After a volume of water which was about 50 percent greater than the volume of voids in the test specimen had flowed through the specimen, the vacuum was slowly reduced to atmospheric pressure. Each specimen was consolidated by a vertical stress of 28 psi (190 kPa) prior to conducting the penetration test. It is noteworthy that, although the degree of saturation for the penetration test specimens was not checked, similar procedures have been used extensively for saturating undisturbed and remolded triaxial specimens [16,17]; typically, values of Skempton's pore pressure parameter, B , were 0.95 or greater at atmospheric pressure for most triaxial specimens molded of cohesionless soil.

DISCUSSION OF TEST RESULTS

The results of penetration tests conducted on wet and dry specimens molded of the 40-50, 70-100, 140-200, or 270-400 material are presented as void ratio versus penetration resistance in FIG. 2 and are summarized in Tables I-IV, respectively. Examination of the data for dry specimens indicated that penetration resistance increased as the void ratio of the specimens was decreased. The data also documented that penetration resistance was not affected significantly by particle size or for rates of penetration from 0.02 to 3.1 in./sec (0.04 to 8.0 cm/sec) provided the comparison was based upon specimens molded to comparable void ratios. For wet specimens, penetration resistance generally increased as the void ratio of the specimens was decreased. However, for void ratios greater than approximately 0.66, the penetration resistances of wet specimens were somewhat less than the penetration resistances of dry specimens, regardless of the gradation of material; for these specimens, induced pore pressures increased as the void ratio of the specimens was increased. For specimens which were molded to void ratios less than 0.66, the penetration resistances of wet specimens were equivalent to the penetration resistances of comparable dry specimens; for these specimens, induced pore pressures were small or negligible.

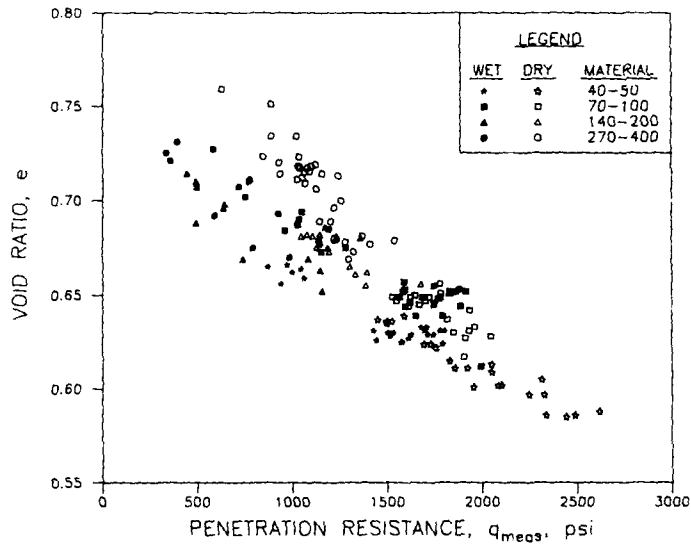


FIG. 2. Void ratio versus measured penetration resistance for wet and dry specimens molded of 40-50, 70-100, 140-200, or 270-400 material.

Although these observations inferred that induced pore pressure influenced the penetration resistance of wet specimens, Schmertmann [6] and Last [15] reported the penetration resistance of certain soils was affected by inundation of the specimens, regardless of the magnitude of the induced pore pressure. Examination of the test data obtained for specimens molded of 40-50 or 70-100 materials indicated the penetration resistances of wet or dry specimens were comparable provided that specimens were molded to similar void ratios; for these specimens, induced pore pressures were small or negligible. This observation documented that penetration resistance was not affected significantly by saturation of the specimens provided that induced pore pressures were negligible.

To assess the penetration resistance of fine cohesionless materials, the penetration resistance for each specimen was calculated according to the cavity expansion theory, as given by Equation 1 [18]:

$$q_{calc} = c N_c^c + \sigma_o N_q^c \quad (1)$$

where:

- q_{calc} = calculated cone penetration resistance
- c = shear strength intercept or cohesion
- N_c^c = cone bearing capacity factor for cohesion
- σ_o = in situ mean normal stress
- N_q^c = cone bearing capacity factor for frictional soils

For the study reported herein, the in situ stress, σ_o , was not measured and cohesion was assumed to be zero. Consequently, the vertical consolidation stress, σ_v , was substituted for σ_o in Equation 1 and rewritten as Equation 2:

$$q_{calc} = \sigma_v N_q^c \quad (2)$$

Al-Awkati [18] defined the cone bearing capacity factor for frictional soils as:

$$N_q^c = [1 + \sin \phi'] [I_r \sec \phi']^{(\sin \phi')/(1 + \sin \phi')} \quad (3)$$

where:

ϕ' = effective angle of internal friction

I_r = reduced rigidity index

He defined the reduced rigidity index, I_r , as the term which was used to account for the effects of compressibility of geologic materials on bearing capacity and penetration resistance. However, Al-Awkati reported that N_q^c had to be empirically adjusted to account for the shape of the expanding cavity which was neither spherical nor cylindrical. Guided by the results of cone penetration tests which were conducted in the Duke stress chamber on Edgar and Chattahoochee sands, he recommended a modified cone bearing capacity factor, N_q^* , for predicting penetration resistance:

$$N_q^* = [1 + \sin \phi']^{1.9} [I_r \sec \phi']^{(1.9 \sin \phi')/(1 + \sin \phi')} \quad (4)$$

Thus, Equation 2 was rewritten as:

$$q_{calc} = \sigma_v N_q^* \quad (5)$$

The penetration resistance of each specimen was calculated according to Equations 4 and 5. Values are summarized in TABLES I-IV. Results are presented in FIG. 3 as measured penetration resistance versus calculated penetration resistance for the 40-50, 70-100, 140-200, and 270-400 materials. As can be seen from these data, the cavity expansion theory modeled the measured penetration resistances of dry specimens of 40-50, 70-100, or 140-200 materials well; the scatter of data was of the order of 100 to 200 psi (7 to 14 tsf or 0.7 to 1.4 MPa). For wet specimens molded of these materials, the calculated penetration resistances generally modeled the measured penetration resistances provided that penetration resistances were greater than approximately 1000 to 1200 psi (70 to 85 tsf or 6.9 to 8.3 MPa); for these tests, induced pore pressures were extremely small or zero. For tests in which the measured penetration resistances were less than approximately 1000 to 1200 psi (70 to 85 tsf or 6.9 to 8.3 MPa), the calculated penetration resistances were slightly larger than the measured penetration resistances; for these tests, induced pore pressures were recorded. For tests on dry specimens of 270-400 material, the calculated penetration resistances were approximately 200 psi (14 tsf or 1.4 MPa) less than the measured penetration resistances. For tests conducted on wet specimens of 270-400 material, the calculated penetration resistances were approximately 200 psi (14 tsf or 1.4 MPa) greater than the measured penetration resistances; for these tests, recorded values of induced pore pressures were relatively large. From these data, it was concluded the cavity expansion theory could be used to predict the penetration resistance of dry specimens or wet specimens provided that induced pore pressures were small or negligible. However, it was also noted that the method did work well when induced pore pressures were fairly large.

From the preceding observations, it was concluded that the penetration resistance must be expressed in terms of effective stresses. Equations 4 and 5 were reexamined. Effective stress parameters were used for calculating the cone bearing capacity factor, given as Equation 4. Equation 5 indicated that penetration resistance was a function of the applied stress and the cone bearing capacity factor. Based upon the results of penetration tests on dry

Table II. Summary of Penetration Tests on 70-100 Material

Set No	Fluid	Diameter in ³	Core Velocity cm/sec	Penetration Test Data			Core Pressure			Bearing Capacity Factor D ₁	Relative Density D _r	Void Ratio e	Calculated Penetration Resistance		Normalized Penetration Resistance q _{net} /q _{netc}	Calculated Pore Pressure	Estimated Pore Pressure	Effective Penetration Resistance
				In	Depth	Resistance	Top	Mid	Bot				RAI	RAI				
1	water	70	4	0	0	1031	0.10	0.14	0	42	47	0.67	198	0.860	1.51	0.05	1046	
2	water	70	4	0	0	1036	0.06	0.12	0	42	47	0.67	198	0.860	1.51	0.05	1046	
3	water	70	4	0	0	1110	0.06	0.04	0	42	47	0.67	198	0.860	1.51	0.05	1046	
4	water	70	4	0	0	1110	0.06	0.04	0	42	47	0.67	198	0.860	1.51	0.05	1046	
5	water	70	4	0	0	1110	0.06	0.04	0	42	47	0.67	198	0.860	1.51	0.05	1046	
6	water	70	4	0	0	1110	0.06	0.04	0	42	47	0.67	198	0.860	1.51	0.05	1046	
7	water	70	4	0	0	1110	0.06	0.04	0	42	47	0.67	198	0.860	1.51	0.05	1046	
8	water	70	4	0	0	1110	0.06	0.04	0	42	47	0.67	198	0.860	1.51	0.05	1046	
9	water	70	4	0	0	1110	0.06	0.04	0	42	47	0.67	198	0.860	1.51	0.05	1046	
10	water	70	4	0	0	1110	0.06	0.04	0	42	47	0.67	198	0.860	1.51	0.05	1046	
11	water	70	4	0	0	1110	0.06	0.04	0	42	47	0.67	198	0.860	1.51	0.05	1046	
12	water	70	4	0	0	1110	0.06	0.04	0	42	47	0.67	198	0.860	1.51	0.05	1046	
13	water	70	4	0	0	1110	0.06	0.04	0	42	47	0.67	198	0.860	1.51	0.05	1046	
14	water	70	4	0	0	1110	0.06	0.04	0	42	47	0.67	198	0.860	1.51	0.05	1046	
15	water	70	4	0	0	1110	0.06	0.04	0	42	47	0.67	198	0.860	1.51	0.05	1046	
16	water	70	4	0	0	1110	0.06	0.04	0	42	47	0.67	198	0.860	1.51	0.05	1046	
17	water	70	4	0	0	1110	0.06	0.04	0	42	47	0.67	198	0.860	1.51	0.05	1046	
18	water	70	4	0	0	1110	0.06	0.04	0	42	47	0.67	198	0.860	1.51	0.05	1046	
19	water	70	4	0	0	1110	0.06	0.04	0	42	47	0.67	198	0.860	1.51	0.05	1046	
20	water	70	4	0	0	1110	0.06	0.04	0	42	47	0.67	198	0.860	1.51	0.05	1046	
21	water	70	4	0	0	1110	0.06	0.04	0	42	47	0.67	198	0.860	1.51	0.05	1046	
22	water	70	4	0	0	1110	0.06	0.04	0	42	47	0.67	198	0.860	1.51	0.05	1046	
23	water	70	4	0	0	1110	0.06	0.04	0	42	47	0.67	198	0.860	1.51	0.05	1046	
24	water	70	4	0	0	1110	0.06	0.04	0	42	47	0.67	198	0.860	1.51	0.05	1046	
25	water	70	4	0	0	1110	0.06	0.04	0	42	47	0.67	198	0.860	1.51	0.05	1046	
26	water	70	4	0	0	1110	0.06	0.04	0	42	47	0.67	198	0.860	1.51	0.05	1046	
27	water	70	4	0	0	1110	0.06	0.04	0	42	47	0.67	198	0.860	1.51	0.05	1046	
28	water	70	4	0	0	1110	0.06	0.04	0	42	47	0.67	198	0.860	1.51	0.05	1046	
29	water	70	4	0	0	1110	0.06	0.04	0	42	47	0.67	198	0.860	1.51	0.05	1046	
30	water	70	4	0	0	1110	0.06	0.04	0	42	47	0.67	198	0.860	1.51	0.05	1046	
31	water	70	4	0	0	1110	0.06	0.04	0	42	47	0.67	198	0.860	1.51	0.05	1046	
32	water	70	4	0	0	1110	0.06	0.04	0	42	47	0.67	198	0.860	1.51	0.05	1046	
33	water	70	4	0	0	1110	0.06	0.04	0	42	47	0.67	198	0.860	1.51	0.05	1046	
34	water	70	4	0	0	1110	0.06	0.04	0	42	47	0.67	198	0.860	1.51	0.05	1046	
35	water	70	4	0	0	1110	0.06	0.04	0	42	47	0.67	198	0.860	1.51	0.05	1046	
36	water	70	4	0	0	1110	0.06	0.04	0	42	47	0.67	198	0.860	1.51	0.05	1046	
37	water	70	4	0	0	1110	0.06	0.04	0	42	47	0.67	198	0.860	1.51	0.05	1046	
38	water	70	4	0	0	1110	0.06	0.04	0	42	47	0.67	198	0.860	1.51	0.05	1046	
39	water	70	4	0	0	1110	0.06	0.04	0	42	47	0.67	198	0.860	1.51	0.05	1046	
40	water	70	4	0	0	1110	0.06	0.04	0	42	47	0.67	198	0.860	1.51	0.05	1046	
41	water	70	4	0	0	1110	0.06	0.04	0	42	47	0.67	198	0.860	1.51	0.05	1046	
42	water	70	4	0	0	1110	0.06	0.04	0	42	47	0.67	198	0.860	1.51	0.05	1046	
43	water	70	4	0	0	1110	0.06	0.04	0	42	47	0.67	198	0.860	1.51	0.05	1046	
44	water	70	4	0	0	1110	0.06	0.04	0	42	47	0.67	198	0.860	1.51	0.05	1046	
45	water	70	4	0	0	1110	0.06	0.04	0	42	47	0.67	198	0.860	1.51	0.05	1046	
46	water	70	4	0	0	1110	0.06	0.04	0	42	47	0.67	198	0.860	1.51	0.05	1046	
47	water	70	4	0	0	1110	0.06	0.04	0	42	47	0.67	198	0.860	1.51	0.05	1046	
48	water	70	4	0	0	1110	0.06	0.04	0	42	47	0.67	198	0.860	1.51	0.05	1046	
49	water	70	4	0	0	1110	0.06	0.04	0	42	47	0.67	198	0.860	1.51	0.05	1046	
50	water	70	4	0	0	1110	0.06	0.04	0	42	47	0.67	198	0.860	1.51	0.05	1046	
51	water	70	4	0	0	1110	0.06	0.04	0	42	47	0.67	198	0.860	1.51	0.05	1046	
52	water	70	4	0	0	1110	0.06	0.04	0	42	47	0.67	198	0.860	1.51	0.05	1046	
53	water	70	4	0	0	1110	0.06	0.04	0	42	47	0.67	198	0.860	1.51	0.05	1046	
54	water	70	4	0	0	1110	0.06	0.04	0	42	47	0.67	198	0.860	1.51	0.05	1046	
55	water	70	4	0	0	1110	0.06	0.04	0	42	47	0.67	198	0.860	1.51	0.05	1046	
56	water	70	4	0	0	1110	0.06	0.04	0	42	47	0.67	198	0.860	1.51	0.05	1046	
57	water	70	4	0	0	1110	0.06	0.04	0	42	47	0.67	198	0.860	1.51	0.05	1046	
58	water	70	4	0	0	1110	0.06	0.04	0	42	47	0.67	198	0.860	1.51	0.05	1046	
59	water	70	4	0	0	1110	0.06	0.04	0	42	47	0.67	198	0.860	1.51	0.05	1046	
60	water	70	4	0	0	1110	0.06	0.04	0	42	47	0.67	198	0.860	1.51	0.05	1046	
61	water	70	4	0	0	1110	0.06	0.04	0	42	47	0.67	198	0.860	1.51	0.05	1046	
62	water	70	4	0	0	1110	0.06	0.04	0	42	47	0.67	198	0.860	1.51	0.05	1046	
63	water	70	4	0	0	1110	0.06	0.04	0	42	47	0.67	198	0.860	1.51	0.05	1046	
64	water	70	4	0	0	1110	0.06	0.04	0	42	47	0.67	198	0.860	1.51	0.05	1046	
65	water	70	4	0	0	1110	0.06	0.04	0	42	47	0.67	198	0.860	1.51	0.05	1046	
66	water	70	4	0	0	1110	0.06	0.04	0	42	47	0.67	198	0.860	1.51	0.05	1046	
67	water	70	4	0	0	1110	0.06	0.04	0	42	47	0.67	198	0.860	1.51	0.05	1046	
68	water	70	4	0	0	1110	0.06	0.04	0	42	47	0.67	198	0.860	1.51	0.05	1046	
69	water	70	4	0	0	1110	0.06	0.04	0	42	47	0.67	198	0.860	1.51	0.05	1046	
70	water	70	4	0	0	1110	0.06	0.04	0	42	47	0.67	198	0.860	1.51	0.05	1046	
71	water	70	4	0	0	1110	0.06	0.04	0	42	47	0.67	198	0.860	1.51	0.05	1046	
72	water	70	4	0	0	1110	0.06	0.04	0	42	47	0.67	198	0.860	1.51	0.05	1046	
73	water	70	4	0	0	1110	0.06	0.04	0	42	47	0.67	198	0.860	1.51	0.05	1046	
74	water	70	4	0	0	1110	0.06	0.04	0	42	47	0.67	198	0.860	1.51	0.05	1046	
75	water	70	4	0	0	1110	0.06	0.04	0	42	47	0.67	198	0.860	1.51	0.05	1046	
76	water	70	4	0	0	1110	0.06	0.04	0	42	47	0.67	198	0.860	1.51	0.05	1046	
77	water	70	4	0	0	1110	0.06	0.04	0	42	47	0.67	198	0.860	1.51	0.05	1046	
78	water	70	4	0	0	1110	0.06	0.04	0	42	47	0.67	198	0.860	1.51	0.05	1046	
79	water	70	4	0	0	1110	0.06	0.04	0	42	47	0.67	198	0.860	1.51	0.05	1046	
80	water	70	4	0	0	1110	0.06	0.04	0	42	47	0.67	198	0.860	1.51	0.05	1046	
81	water	70	4	0	0	1110	0.06	0.04	0	42	47	0.67	198	0.860	1.51	0.05	1046	
82	water	70	4	0	0	1110	0.06	0.04	0	42	47	0.67	198	0.860	1.51	0.05	1046	
83	water	70	4	0	0	1110	0.06	0.04	0	42	47	0.67	198	0.860	1.51	0.05	1046	
84	water	70	4	0	0	1110	0.06	0.04	0	42	47	0.67	198	0.860	1.51	0.05	1046	
85	water	70	4	0	0	1110	0.06	0.04	0	42	47	0.67	198</					

$1.0 \text{ in} = 2.54 \text{ cm}$
 $1.0 \text{ cm/sec} = 0.4 \text{ in/sec}$
 $1.0 \text{ psi} = 0.07 \text{ tsi} = 6.9 \text{ kPa}$
 $(\sigma_v - u) = 28.0 \text{ psi}; u = 0 \text{ psi}$

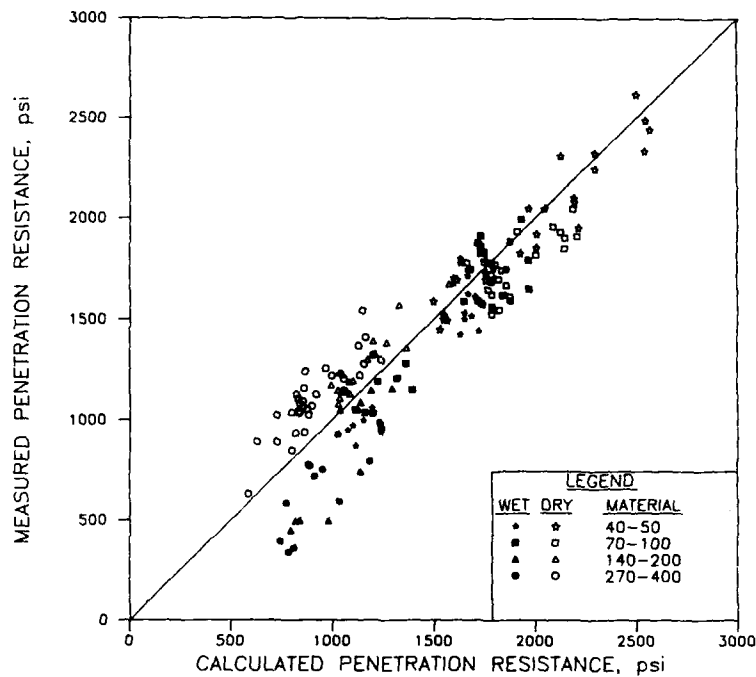


FIG. 3. Measured penetration resistance versus calculated penetration resistance for wet and dry specimens molded of 40-50, 70-100, 140-200, or 270-400 material.

specimen molded of each of the materials and wet specimens of 40-50 or 70-100 materials, it was concluded the cone bearing capacity factor could be calculated with a high degree of confidence, regardless of whether the specimens were wet or dry. From the results of tests on wet specimens of 140-200 or 270-400 materials, it was noted that penetration resistance was related to the induced pore pressure; as the induced pore pressure increased, the penetration resistance decreased. These observations inferred that the vertical stress, σ_v , must be treated as an effective stress, $(\sigma_v - u)$. Hence, Equation 5 was rewritten as:

$$q_{calc} = (\sigma_v - u) N_q \quad (6)$$

where:

u = induced pore pressure

To evaluate this hypothesis, the measured and calculated penetration resistances and the measured and calculated pore pressures were compared, as given by Equation 7:

$$q_{meas}/q_{calc} = [(\sigma_v - u_{me}) N_q^* / (\sigma_v - u) N_q] \quad (7)$$

where:

q_{meas} = measured penetration resistance

- q_{calc} = penetration resistance calculated according to Equation 6
 u_{du} = pore pressure induced in a zone in the immediate proximity of the penetrometer
 u = pore pressure used for calculation of penetration resistance according to Equation 6; the value was assumed to be zero

Since it had been determined that N_q^* was independent of the induced pore pressure and the value of u was assumed to be zero, Equation 7 was rearranged and rewritten as:

$$u_{du} = \sigma_v (1 - q_{meas}/q_{calc}) \quad (8)$$

From Equation 8, it can be seen that penetration resistance was dependent upon the initial in situ consolidation stress and the pore pressure which was induced during penetration; this observation is consistent with Schmertmann's [19] conclusion that penetration resistance was dependent upon the initial in situ effective radial stress as well as induced pore pressure.

Based upon Equation 8, a comparison of measured pore pressures and calculated pore pressures was made. Unfortunately, the data indicated that a poor quantitative relationship existed; calculated values of induced pore pressure were typically 10 to 100 times larger than measured values. However, an explanation for the apparent discrepancy was available. The induced pore pressures were measured by transducers located at a radial distance of approximately 1-1/2 in. (4 cm) from the center of the penetrometer at depths of 3-, 6-, or 9-in. (8, 15, or 23 cm) from the top of the chamber. From the theory of consolidation, it can be shown that induced pore pressures tended to dissipate before the measurements were made, although the percent of dissipation was unknown.

To permit a meaningful comparison of calculated and measured pore pressures, an estimate of the percent of dissipation of induced pore pressure was made by a finite element computation. The results indicated the induced pore pressure at a distance of five to six cone diameters should be about two to three percent of the pore pressure measured on the face of the cone. This value agreed with data reported by Levadoux and Baligh [20]; using a more sophisticated model, their study indicated approximately 95 percent of the induced pore pressure dissipated within six cone diameters. Guided by these findings, the measured pore pressure for each specimen was compared with two percent of the value of the induced pore pressure which was calculated according to Equation 8. Good agreement of measured and calculated pore pressures resulted.

The results of measured penetration resistances were compared with the penetration resistances which were calculated according to Equations 4 and 6 using effective stress parameters and effective stresses. For these computations, the measured values of induced pore pressure were multiplied by 50 to obtain the values of induced pore pressure required in Equation 6. From the data which are presented in FIG. 4, one may observe that a good agreement of the measured and calculated penetration resistances existed. For the data which were presented in this figure, increased penetration resistances were due to increased density of the test specimens, increased effective stresses caused by a decrease of the induced pore pressure, or both.

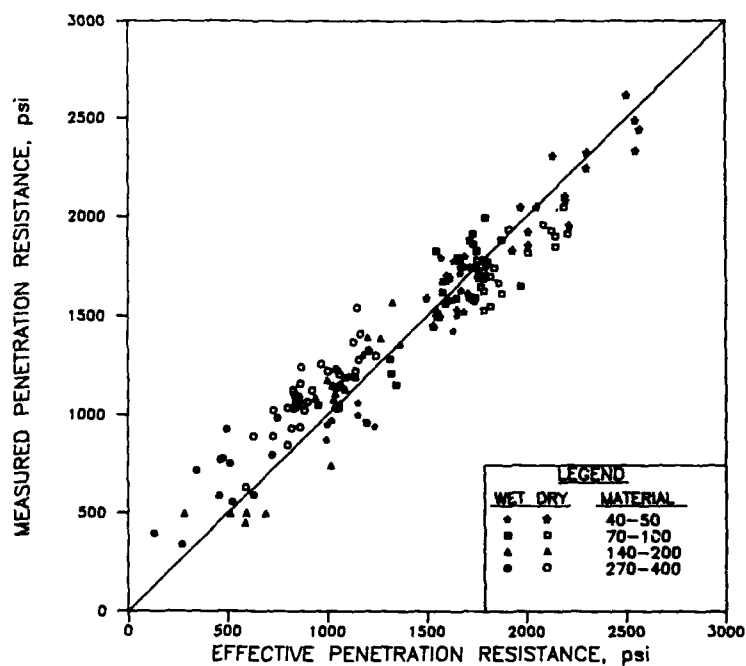


FIG. 4. Measured penetration resistance versus penetration resistance calculated from effective stress parameters for specimens molded of 40-50, 70-100, 140-200, or 270-400 material.

SUMMARY

For the study reported herein, several observations and/or conclusions were obtained:

- (a) For dry specimens, penetration resistance increased as the density of the specimens was increased.
- (b) For dry specimens, the effect of particle size was negligible provided the density of specimens was comparable.
- (c) For dry specimens, varying the rate of penetration from 0.02 to 3.1 in./sec (0.04 to 8.0 cm/sec) did not affect penetration resistance provided the density of specimens was comparable.
- (d) The penetration resistance of wet specimens was affected by pore pressure which was induced by the penetrating cone.
- (e) Provided that effective stresses were used in the computations, the cavity expansion theory modeled the measured penetration resistance extremely well.

ACKNOWLEDGMENTS

The study described and the resulting data presented herein were obtained from research conducted at the U.S. Army Engineer Waterways Experiment Station, Vicksburg, Mississippi, under the auspices of the Office, Chief of Engineers Civil Works Research and Development-Soils Program. Valuable suggestions and assistance were provided by the staff of the Geotechnical Laboratory. Permission was granted by the Chief of Engineers to publish this information.

REFERENCES

1. R. Bellotti, G. Bizzi, and V. Ghionna, "Design, Construction and Use of a Calibration Chamber," Proceedings, Second European Symposium on Penetration Testing, 2, pp. 439-446 (1982).
2. G.A. Chapman, "A Calibration Chamber for Field Test Equipment," Proceedings, European Symposium on Penetration Testing, 2:2, pp. 59-65 (1974).
3. W.F. Marcuson and W.A. Bieganousky, "Laboratory Standard Penetration Tests on Fine Sands," Journal of the Geotechnical Engineering Division, ASCE, 103, GT6, pp. 565-588 (1977).
4. A.K. Parkin, "The Calibration of Cone Penetrometers," Penetration Testing 1988, 1, pp. 221-244 (1988).
5. A.K. Parkin and T. Lunne, "Boundary Effects in the Laboratory Calibration of a Cone Penetrometer in Sand," Proceedings, Second European Symposium on Penetration Testing, 2, pp. 761-768 (1982).
6. J.H. Schmertmann, "Study of Feasibility of Using Wissa-Type Piezometer Probe to Identify Liquefaction Potential of Saturated Fine Sand," U.S. Army Engineer Waterways Experiment Station, Vicksburg, MS (1978).
7. H.B. Seed, R.B. Seed, L.F. Harder, and H. Jong, "Re-evaluation of the Slide in the Lower San Fernando Dam in the Earthquake of Feb. 9, 1971," University of California, Berkeley, CA (1988).
8. K. Terzaghi and R.B. Peck, Soil Mechanics in Engineering Practice, John Wiley and Sons, Inc., pp. 425-426 (1948).
9. J.R. Wagner, "Liquefaction Potential Evaluation for Arcadia Dam," Proceedings, International Conference on Case Histories in Geotechnical Engineering, 1, pp. 425-432 (1984).
10. S.G. Zhou, "Influence of Fines on Evaluating Liquefaction of Sand by CPT," Proceedings, International Conference on Recent Advances in Geotechnical Earthquake Engineering and Soil Dynamics, 1, pp. 167-172 (1981).
11. American Society for Testing and Materials, 1989 Annual Book of ASTM Standards, Volume 04.02, Concrete and Aggregates.
12. Ferro Corporation, "Technical Data on the Chemical and Physical Properties of Standard Microbeads," Jackson, MS (1982).
13. Department of the Army, Office of the Chief of Engineers, "Laboratory Soils Testing," Washington, DC (1970).
14. American Society for Testing and Materials, 1989 Annual Book of ASTM Standards, Volume 04.08, Soil and Rock, Building Stones, Geotextiles.
15. N. Last, "The Introduction of Cone Penetration Tests on Saturated Samples of Hokksund Sand in the NGI Calibration Chamber," Norwegian Geotechnical Institute, Oslo, Norway (1979).

16. R.T. Donaghe, P.A. Gilbert, and W.F. Marcuson, III, Discussion of "New Procedure for Saturating Sand Specimens" by N.S. Rad and G.W. Clough, Journal of Geotechnical Engineering, ASCE, 112, 1, pp. 103-105 (1986).
17. V.H. Torrey, III, J.B. Dunbar, and R.W. Peterson, "Retrogressive Failures in Sand Deposits of the Mississippi River," U.S. Army Engineer Waterways Experiment Station, Vicksburg, MS (1988).
18. Z.A. Al-Awkati, "On Problems of Soil Bearing Capacity at Depth," Duke University, Durham, NC (1975).
19. J.H. Schmertmann, "Penetration Pore Pressure Effects on Quasi-Static Cone Bearing, q_c ," Proceedings, European Symposium on Penetration Testing, 2:2, pp. 345-351 (1974).
20. J. Levadoux and M.M. Baligh, "Consolidation after Undrained Piezocone Penetration. I: Prediction," Journal of Geotechnical Engineering, ASCE, 112, 7, pp. 707-726 (1986).

OVERVIEW OF A LARGE STRESS CHAMBER SYSTEM

RICHARD W. PETERSON* and KANDIAH ARULMOLI**

*U.S. Army Engineer Waterways Experiment Station, Vicksburg, MS 39180

**The Earth Technology Corporation, Long Beach, CA 90802

ABSTRACT

As a result of the uncertainties related to in situ testing, geotechnical site investigations, or soil-structure interaction problems, it was recommended that the U.S. Army Engineer Waterways Experiment Station obtain a large calibration chamber, hereinafter referred to as a stress chamber, to study these problems. A survey was conducted to obtain current literature describing stress chambers, capabilities and limitations of each chamber, and current or planned research using the respective chambers. Guided by the findings of the survey, a modular stress chamber system was designed and is being fabricated. Because of unique features of the device, it is believed this apparatus can be used to resolve problems, such as scale effects and boundary conditions, which have been identified as a result of investigations conducted in smaller chambers.

INTRODUCTION

Under the auspices of the Office, Chief of Engineers, U.S. Army, the Geotechnical Laboratory (GL) at the U.S. Army Engineer Waterways Experiment Station (WES) was charged with establishing a comprehensive long-range plan for research in geotechnical engineering. Professor Lymon Reese of the University of Texas, Austin, Texas, was hired as a consultant to advise the GL. In his report, Reese [1] stated "the general problem of site characterization... ..is one of the most severe problems currently faced by civil engineers." Reese recommended that GL construct a large calibration chamber, hereinafter referred to as a stress chamber, to investigate uncertainties related to in situ testing, geotechnical site investigation, and soil-structure interaction. Reese warned GL that the full potential of the facility could not be realized unless the apparatus was constructed after existing designs were studied and necessary improvements were made. He concluded "the facility would be expensive to construct, and expensive to operate, but could provide high quality data of a sort that would be difficult if not impossible to obtain in the field."

Based upon Reese's guidance, the literature was perused, technical liaison was established with researchers knowledgeable on the use of large chambers, a concept for a state-of-the-art stress chamber system was developed, and the apparatus was designed and is currently being fabricated. An overview of the study is presented herein.

EXISTING APPARATUS

Stress chambers have evolved from little more than steel drums [2] and large rigid-walled cylinders [3-7] to apparatus capable of testing large triaxial-shaped specimens [8-11]. Although rigid-walled chambers were used successfully to advance technology, these devices have become obsolete because rigid walls limited the capability for simulating in situ

stresses. Furthermore, the size of specimens required for minimizing boundary effects, such as side wall friction and arching [4], have demonstrated that smaller and more cost effective flexible boundary chambers can be used. For example, Holden [12] suggested that a ratio of chamber diameter to penetrometer diameter of 200:1 was necessary to minimize boundary effects in dense sand specimens molded in a rigid wall chamber. For comparison, Parkin and Lunne [10] presented test data which indicated that boundary effects were negligible for dense specimens of sand confined by flexible boundaries provided the diameter ratio was greater than approximately 60:1. Because of the undesirable effects caused by boundary conditions and the difficulties associated with molding, testing, and analysis of data obtained from cubical or rectangular specimens, i.e., stress concentrations at the corners of the specimen, etc., the cylindrical specimen was judged to be a more desirable shape than the cubical specimen. Only triaxial-type devices designed for testing cylindrical specimens are discussed herein.

One of the first stress chambers was constructed by the Road Construction Authority (RCA), Victoria, Australia [9,13]. The device was designed and built for the purpose of calibrating the RCA cone penetrometer under controlled laboratory conditions. The soil specimen was 2.5-ft (0.76 m) diameter by 3.0-ft (0.91 m) high. Vertical stress was transferred to the soil specimen through a rigid top platen and a "cushion" base platen; the cushion platen consisted of a pressurized membrane located between the soil specimen and a rigid platen. A large reaction frame, attached to a hardened floor, restrained the chamber lid and provided a reaction for the penetrometer. Vertical displacement of the specimen was measured by an LVDT (linear variable differential transformer). Lateral confinement was provided by pressurized water in the annular space between the membrane surrounding the soil specimen and the chamber barrel. A double-wall chamber was designed for determining lateral displacement or volume change. By maintaining equal pressures in the annulus formed by the wall of the inner chamber and the soil specimen and in the annulus formed by the inner and outer chamber barrels, sufficient rigidity was obtained for monitoring lateral displacements of the specimen; lateral displacements were related to the change of volume of the cavity between the specimen and the inner chamber barrel. Boundary conditions included combinations of zero average strain or constant pressure. Specimens were molded by raining sand from a motorized hopper which was moved forward and backward above the chamber.

Several chambers were constructed during the 1970's. In general, the design and/or operation of each chamber was improved based upon experience gained from the use of chamber(s) which had been constructed previously. Only significant improvements of each device are noted herein. The chamber at the University of Florida (UF), Gainesville, Florida, was designed for testing back-pressure saturated soil specimens. Nominal dimensions of the specimens were 4-ft (1.2 m) diameter by 4-ft (1.2 m) high [9,14]. A larger chamber was built at Monash University (MU), Clayton, Australia, to permit friction sleeve measurements to plateau during stage testing of a cone penetrometer. The dimensions of the specimens were 4-ft (1.2 m) diameter by 6-ft (1.8 m) high [9]. The Norwegian Geotechnical Institute (NGI), Oslo, Norway, constructed a stress chamber which could test a specimen 3.9-ft (1.2 m) diameter by 4.9-ft (1.5 m) high [15,16]. The principal improvement to the NGI facility was the implementation of a stationary sand spreader. The stress chamber which was constructed at the ENEL-CRIS Laboratory, Milan, Italy [8,17], was designed for testing back-pressure saturated specimens 3.9-ft (1.2 m) diameter by 4.9-ft (1.5 m) high under a vertical stress of 220 psi (1.5 MPa) and a horizontal stress of 150 psi (1.0 MPa); the working pressure of the other chambers was of the order of 100 psi (0.7 MPa). Other improvements to the ENEL-CRIS chamber included a self-reacting chamber design which did not require a hardened floor for structural integrity of the system.

Since the 1970's, several other stress chambers have been designed and constructed. In general, the design of these devices was similar to the devices described in the preceding paragraphs. Sizes of the specimens ranged from approximately 2.5- to 5.0-ft (0.76 to 1.52 m) diameter by 2.5- to 5.0-ft (0.76 to 1.52 m) high. For most of the devices, the soil specimen was sandwiched between a rigid top platen and a cushion base platen. Vertical consolidation stresses were usually applied by a piston which was located below the base platen. To eliminate the possibility of inadvertently omitting one or more of these apparatus, a comprehensive listing of these devices is not presented herein. Only unique features of selected devices are discussed. The chamber which is located at Virginia Polytechnic Institute and State University, Blacksburg, Virginia, was constructed with a single wall. Lateral deformations were measured by LVDT's [18]. The chamber at the University of California, Berkeley, California, consisted of a cylindrical pressure vessel with a hemispherical cap affixed to its bottom and a flat plate attached to its top. Load transfer rods which were attached to the flat plate at the top of the chamber were used to apply vertical stress to the specimen [19]. Fouse [20] described an apparatus located at the University of Texas, Austin, Texas. Vertical stresses were transferred to the soil specimen by concentric bladders which are located at the top of the chamber. The concentric bladders surround a central cylinder that served as a guide for a model test pile. The chamber at North Carolina State University, Raleigh, North Carolina, was constructed of a fiber reinforced concrete top and base, a fiberglass piston, and a fiberglass chamber [21]. These materials were selected for the apparatus because they did not interfere with the electromagnetic field around the inductance coils which were used to measure the deformation of the soil specimen. A small chamber, which served as a model for a larger chamber, was constructed at the University of Grenoble, France [22]. Vertical and horizontal stresses were applied to the soil specimen across flexible membranes. A unique feature of the apparatus which is located at the University of Houston, Houston, Texas, was the use of toroidal bladders to apply radial stress to the test specimen. The stress which could be applied by each bladder was independent of the stress in the other bladders [32].

USES OF STRESS CHAMBERS

Investigations to evaluate or calibrate in situ test devices such as cone penetrometers, pressuremeters, and dilatometers as well as studies involving pile behavior have provided the impetus for developing most of the large stress chambers. However, a well conceived design for a chamber would allow a much broader spectrum of civil engineering problems to be investigated without requiring major modifications to the device. Uses include soil-structure interaction studies involving in situ test devices and soil sampling apparatus, pile behavior studies, research on the strength and deformation characteristics of earth-rock mixtures, hydrogeologic investigations, far field weapons effects studies, investigations of the thermal behavior of soil as related to construction in cold regions, and the assessment of waste disposal techniques in landfills.

LIMITATIONS OF STRESS CHAMBERS

Three limitations of the use of the stress chamber for investigating geotechnical engineering problems which include the effects of aging on soil behavior, the influence of boundary conditions on test results, and the lack of a methodology for molding uniform, replicate specimens of a variety of soil types and gradations to a range of densities have been identified. A discussion of these limitations follows.

Aging Effects

Aging effects have been acknowledged as influencing soil behavior, although few comprehensive studies to assess the effects of aging on geotechnical engineering parameters have been conducted. Seed [24] reported that the cyclic strengths of compacted specimens of sand increased more than 25 percent after aging 100 days as compared with specimens which were not aged prior to testing. Anderson and Stokoe [25] reported that low amplitude dynamic shear moduli for compacted specimens of silts and clays increased 6 to 13 percent per logarithmic cycle of time. Kavazanjian and Mitchell [26] reported the coefficient of lateral earth pressure at rest K_0 increased from 0.5 to 0.6 in 1 week following primary consolidation of specimens of San Francisco Bay Mud. Brown [27] reported that measured values of K_0 decreased approximately 30 percent for a plastic kaolinite and 40 percent for a nonplastic rock flour as compared with the initial values in only 14 days after primary consolidation. Lukas [28] used pressuremeter tests to evaluate the effectiveness of dynamic compaction. As compared with the precompaction conditions, the pressuremeter modulus decreased more than 50 percent immediately after dynamic compaction; after 50 days, the pressuremeter modulus was slightly larger than the precompaction modulus; after 70 days, the pressuremeter modulus had increased by more than 100 percent as compared with the precompaction modulus.

These studies indicated that soil behavior may change with time. Although the quantitative behavior of "virgin soil" in the stress chamber may be somewhat different than the behavior of "aged soil" in the field, tests conducted in a large stress chamber can be used to develop a qualitative assessment, and in some situations, a quantitative assessment of the soil-structure interaction phenomenon to a degree which is not possible using conventional geotechnical investigation techniques.

Boundary Effects

For some time, the profession has known that boundary conditions, such as system compliance, the physical size or shape of the specimen, etc., affected values obtained from conventional geotechnical tests. For example, Balla [29] demonstrated that triaxial test data were dependent upon the ratio of the height to diameter of the specimen. He suggested that a ratio of 2.0 should be used. Marachi, et al., [30] presented data which indicated the angle of internal friction obtained by a triaxial test was less than the angle of friction obtained by a plane strain test. Martin, et al., [31] reported that membrane compliance for triaxial tests could introduce an error of considerable magnitude for which quantitative calculations or corrections could not be easily made. However, the effects of boundary conditions in the stress chamber were not documented until Parkin and Lunne [10] reported that the penetration resistance of dense sand specimens was affected by the applied boundary conditions, i.e., controlled stress or controlled strain, for ratios of chamber diameter to cone diameter less than approximately 60. Robertson and Campanella [32] studied the results of numerous CPT tests conducted in large chambers and in natural deposits of layered soils and concluded that the cone could "feel" hard or soft strata of geologic materials at a distance of 10 to 20 cone diameters in front of the penetrometer.

From these studies, it is evident that boundary conditions may affect the geotechnical engineering parameters which are obtained from laboratory tests. Unfortunately, little is known regarding the qualitative or quantitative effects of boundary conditions on engineering parameters. Additional research is needed to gain insight on this problem.

Specimen Uniformity

In general, stress chamber specimens are molded by pluvial deposition in air. Initially, specimens were formed by a motorized sand spreader which travelled forward and backward over the stress chamber [33]. Because of the difficulty of achieving uniform specimens due to air currents caused by the movement of the sand spreader, the traveling spreader was replaced by a static sand rainer [34]. Although more uniform specimens were constructed using the static sand rainer, Bellotti, et al., [35] reported difficulty of molding uniform specimens at medium densities, i.e., relative densities of 35 to 65 percent. Because of these difficulties, research to develop methods to constitute laboratory specimens, especially of geologic materials other than uniform sands, has continued. Rad and Tumay [36] reported a study of factors which affected sand specimen preparation by pluvial deposition in air. They concluded that deposition intensity had the greatest effect on the relative density of specimens. Rad and Tumay suggested that specimens could be constituted to different densities by changing the shutter porosity (deposition intensity) while keeping the height of fall, the diffuser sieve opening, and the distance between diffuser sieves constant. Jamiolkowski [37] reported limited success in pluviating silty sand in air provided the soil was sufficiently moist for the fines to adhere to the sand grains but dry enough to prevent the fines from adhering to the diffuser sieves on the static sand rainer. Parkin [38] reported difficulty of molding silty sand specimens by pluvial deposition in a vacuum. He reported that the material tended to arch across the openings of the diffuser sieves in the sand rainer.

PROPOSED STRESS CHAMBER

A review of the literature has identified several features which are desirable for a new stress chamber. The system should include the capability of applying combinations of constant stress, zero average strain, or feedback control to simulate in situ conditions in the stress chamber environment. To accomplish this, all boundaries should be flexible or the specimen should be of sufficient size to minimize the influence of rigid boundaries. Based upon the studies reported by Parkin and Lunne [10] and Robertson and Campanella [32], the height and diameter of the specimen should be at least 5- to 6-ft (1.5 to 1.8 m) to minimize the effects of boundary conditions when testing the 10-cm² cone penetrometer. Obviously, a larger chamber would be needed for larger test devices. Toroidal bladders should be used to apply lateral stress to the specimen. This feature would allow application of a various lateral stresses as a function of the height of a specimen for testing layered soils. The chamber should be designed as a self-reacting pressure vessel to withstand an internal working pressure of approximately 290 psi (2.0 MPa); these features were selected to match the mechanical pressure system of the GL and to alleviate the requirement for a hardened floor for structural integrity of the system. A computer controlled closed-loop hydraulic system could be used to control stress and/or deformation in the test specimen and to activate the test apparatus, such as a model pile or a cone penetrometer.

To fulfill the requirements for a multi-purpose test apparatus, a modular stress chamber system was designed. The modular chamber concept consisted of cylinder modules which could be assembled to test specimens of selected sizes. An isometric drawing of an open-ended cylinder module is presented in FIG. 1. A cross section of the assembled stress chamber, which can be formed by stacking several cylinder modules, is presented in FIG. 2. The nominal diameters of the cylinder modules which were selected were 2-1/2, 5-, and 10-ft (0.8, 1.5, and 3.0 m). The heights of the modules were 1- and 2-ft (0.3 and 0.6 m). As can be envisioned from the sketches which were presented in Figs. 1 and 2, the size of the specimen can be easily changed to meet the testing requirements. A qualitative

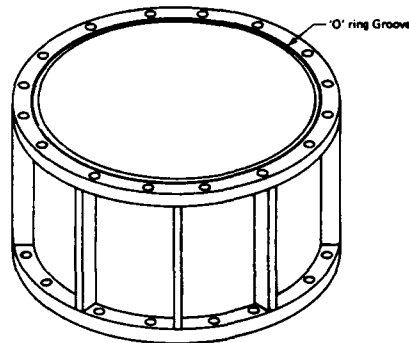


FIG. 1. Isometric of a typical cylinder module.

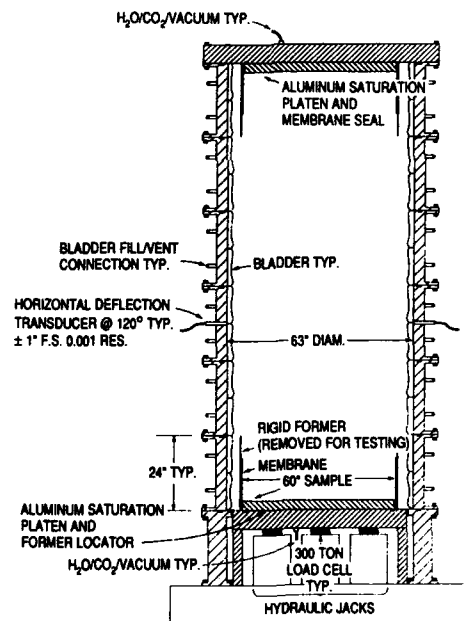


FIG. 2. Section of the modular stress.

assessment of the modular stress chamber concept indicated the method was a cost effective technique for studying complex geotechnical engineering phenomena; smaller specimens could be used for testing relatively small devices or for conducting qualitative assessments of specific engineering parameters, whereas larger specimens could be used for testing larger devices, conducting quantitative assessments of specific engineering parameters, or investigating scale effects.

The system was designed to test specimens molded to selected heights and diameters by merely interchanging the top and base platens, cylinder modules, and chamber top. Axial load will be applied to the specimen by an actuator controlled by a closed-loop hydraulic system. Axial deformation will be measured by one or more LVDT's located below the base platen. Lateral pressure will be applied to the soil specimen across 1-ft (0.3 m) high toroidal bladders affixed to the inside of the respective cylinder modules. Lateral deformation will be measured by LVDT's affixed to the cylinder modules. Ports for electrical wires for instrumentation which can be placed in the soil specimen will be located on selected cylinder modules. A top-mounted ram assembly will provide a reaction for the in situ device or model pile. The 5-ft (1.5 m) diameter stress chamber, which is currently being fabricated, was designed for testing back-pressure saturated specimens; the nominal working pressures are 225-psi (1.5 MPa) vertical stress and 150-psi (1.0 MPa) horizontal stress.

SUMMARY

The modular stress chamber system which was described herein has been designed with unique features which are generally not available in private, university, or government laboratories. When fabrication and assembly of the system are completed, specimens ranging from 2-1/2- to 10-ft (0.8 to 3.0 m) diameter can be tested; the height of the specimens can be varied by merely stacking the cylinder modules. Toroidal bladders will be used to apply lateral stress. This feature will permit a variation of lateral stress with depth for testing layered soils. Instrumentation can be placed in a specimen as it is molded which will permit an assessment of the response of the soil to the loading conditions as well as the response of the in situ test apparatus to known conditions.

ACKNOWLEDGMENTS

A study of the concepts and technical feasibility of a modular stress chamber system was conducted under the auspices of the Office, Chief of Engineers. Technical liaison was established with researchers knowledgeable on use of large stress chambers. Based upon the valuable suggestions and assistance provided by these researchers as well as the staffs of the Geotechnical Laboratory, U.S. Army Engineer Waterways Experiment Station, Vicksburg, Mississippi, and The Earth Technology Corporation, Long Beach, California, a large stress chamber system has been designed and is being fabricated. Permission was granted by the Chief of Engineers to publish this information.

REFERENCES

1. L.C. Reese, "Plan for Long-Range Research in Soil Mechanics at Waterways Experiment Station," University of Texas at Austin, Austin, TX (1985).
2. U.S. Army Engineer Waterways Experiment Station, "Density Changes of Sand Caused by Sampling and Testing," Vicksburg, MS (1952).
3. S.S. Cooper, "Laboratory Investigation of Undisturbed Sampling of Cohesionless Material Below the Water Table," U.S. Army Engineer Waterways Experiment Station, Vicksburg, MS (1976).
4. P.F. Hadala, "Sidewall Friction Reduction in Static and Dynamic Small Blast Load Generator Tests," U.S. Army Engineer Waterways Experiment Station, Vicksburg, MS (1968).

5. M.J. Hvorslev, "Use of WES Large Triaxial Device or a Stacked-Ring Test Bin in the Four-Foot Blast Load Generator," U.S. Army Engineer Waterways Experiment Station, Vicksburg, MS (1963).
6. N. Last, "Cone Penetration Tests on Samples of Dry Hokksund Sand in a Rigid Walled Chamber," Norwegian Geotechnical Institute, Oslo, Norway (1979).
7. F.P. Smits, "Cone Penetration Tests in Dry Sand," Proceedings, Second European Symposium on Penetration Testing, 2, pp. 877-881 (1982).
8. R. Bellotti, G. Bizzi, and V. Ghionna, "Design, Construction and Use of a Calibration Chamber," Proceedings, Second European Symposium on Penetration Testing, 2, pp. 439-446 (1982).
9. G.A. Chapman, "A Calibration Chamber for Field Test Equipment," Proceedings, European Symposium on Penetration Testing, 2:2, pp. 59-65 (1974).
10. A.K. Parkin and T. Lunne, "Boundary Effects in the Laboratory Calibration of a Cone Penetrometer in Sand," Proceedings, Second European Symposium on Penetration Testing, 2, pp. 761-768 (1982).
11. J.H. Schmertmann, "Study of Feasibility of Using Wissa-Type Piezometer Probe to Identify Liquefaction Potential of Saturated Fine Sands," U.S. Army Engineer Waterways Experiment Station, Vicksburg, MS (1978).
12. J.C. Holden, "Stresses and Strains in a Sand Mass Subjected to a Uniform Circular Load," University of Melbourne, Melbourne, Australia (1967).
13. J.C. Holden, Personal Communications, Road Construction Authority, Victoria, Australia (1985).
14. J.L. Davidson, "A Study to Establish Correlations Between Piezometer Probe Test Results and In Situ Permeability," University of Florida, Gainesville, FL (1980).
15. N. Last, "The Introduction of Cone Penetration Tests on Saturated Samples of Hokksund Sand in the NGI Calibration Chamber," Norwegian Geotechnical Institute, Oslo, Norway (1979).
16. A.K. Parkin, "The Friction Cone Penetrometer: Laboratory Calibration for the Prediction of Sand Properties," Norwegian Geotechnical Institute, Oslo, Norway (1977).
17. A. Parkin, "Visit to ENEL Laboratories, Milano, Italy," Norwegian Geotechnical Institute, Oslo, Norway (1982).
18. G.W. Clough, Personal Communications, Virginia Polytechnic Institute and State University, Blacksburg, VA (1985).
19. W.C.B. Villet and J.K. Mitchell, "Cone Resistance, Relative Density, and Friction Angle," Proceedings, Cone Penetration Testing and Experience, ASCE, pp. 178-208 (1981).
20. J.L. Fouse, "Group Behavior of Auxiliary Loaded Piles in Sand," University of Texas at Austin, Austin, TX (1984).
21. R.H. Borden, Personal Communications, North Carolina State University, Raleigh, NC (1986).
22. M. Boulon, Personal Communications, Institut de Mecanique de Grenoble, Grenoble, France (1986).
23. M.W. O'Neill, Personal Communications, University of Houston, Houston, TX (1986).
24. H.B. Seed, "Soil Liquefaction and Cyclic Mobility Evaluation for Level Ground During Earthquakes," Journal of the Geotechnical Engineering Division, ASCE, 105, GT2, pp. 201-255 (1979).
25. D.G. Anderson and K.H. Stokoe, II., "Shear Modulus, A Time Dependent Soil Property," Dynamic Geotechnical Testing, ASTM, pp. 66-90 (1978).
26. E. Kavazanjian, Jr. and J.K. Mitchell, "Time Dependence of Lateral Earth Pressure," Journal of Geotechnical Engineering, ASCE, 110, 4, pp. 530-533 (1984).

27. R.W. Brown, "Ko Behavior of Normally Consolidated Fine-Grained Soils During One-Dimensional Secondary Compression Aging and the Quantitative Prediction of the Quasi-Preconsolidation Effect," University of Florida, Gainesville, FL (1985).
28. R.G. Lukas, "Densification of Loose Deposits by Pounding," Journal of the Geotechnical Engineering Division, ASCE, 106, GT4, pp. 435-446 (1980).
29. A. Balla, "Stress Conditions in Triaxial Compression," Journal of the Soil Mechanics and Foundations Division, ASCE, 81, SM6, pp. 57-84 (1960).
30. N.D. Marachi, J.M. Duncan, C.K. Chan, and H.B. Seed, "Plane-Strain Testing of Sand," Laboratory Shear Strength of Soil, ASTM, pp. 294-302 (1980).
31. G.R. Martin, W.D.L. Finn, and H.B. Seed, "Effects of System Compliance on Liquefaction Tests," Journal of the Geotechnical Engineering Division, ASCE, 104, GT4, pp. 463-479 (1978).
32. P.K. Robertson and R.G. Campanella, "Guidelines for Use and Interpretation of the Electronic Cone Penetration Test," Hogentogler and Company, Inc., Gaithersburg, MD (1984).
33. A. Veismanis, "Laboratory Investigation of Electrical Friction-Cone Penetrometers in Sand," Proceedings, European Symposium on Penetration Testing, 2:2, pp. 407-419 (1974).
34. J.C. Holden, "The Calibration of Electrical Penetrometers in Sand," Norwegian Geotechnical Institute, Oslo, Norway (1977).
35. R. Bellotti, V. Crippa, S. Pedroni, G. Baldi, C. Fretti, D. Ostricati, V. Ghionna, M. Jamiolkowski, and E. Pasqualini, "Laboratory Validation of In Situ Tests," Draft of the Paper to be Included in Italian Geotechnical Society Jubilee Volume for the Eleventh International Conference on Soil Mechanics and Foundation Engineering, San Francisco, CA (1985).
36. N.S. Rad and M.T. Tumay, "Factors Affecting Sand Specimen Preparation by Raining," Geotechnical Testing Journal, ASTM, 10, 1, pp. 31-37 (1987).
37. M. Jamiolkowski, Personal Communications, Politecnico di Torino, Torino, Italy (1985).
38. A.K. Parkin, Personal Communications, Monash University, Clayton, Victoria, Australia (1986).

MINIATURE CPT TESTS IN DENSE MONTEREY NO.0/30 SAND IN A FLEXIBLE DOUBLE-WALLED CALIBRATION CHAMBER

A. J. PUPPALA,¹ Y. B. ACAR,² AND M. T. TUMAY.³

^{1,2} Graduate Research Assistant and Associate Professor, respectively, Civil Engineering Department, Louisiana State University, Baton Rouge, LA 70803.

³ Professor, Civil Engineering Department, Louisiana State University, Baton Rouge, LA 70803;
Director (Currently) , Geomechanics Program, National Science Foundation, Washington, DC. 20550.

ABSTRACT

Preliminary miniature cone penetration test results in dense monterey No.0/30 sand are presented. The tests are conducted in a flexible double-walled calibration chamber. The chamber size is 0.64 m (70 in.) in diameter and 1.78 m (70 in.) in height. Specimens are prepared by dry pluvial deposition. A miniature friction cone (1.27 cm diameter) is used to minimize the chamber size effects. These preliminary results are compared with previous studies reported on the same sand. The results show reasonable agreement between the tests conducted in the different calibration chambers. The influence of chamber size and testing location on the test results are discussed. The crushability of this sand around the cone is also investigated and reported.

INTRODUCTION

The difficulty in obtaining undisturbed specimens in cohesionless deposits prompts the need to use in-situ testing techniques like CPT. In-situ testing instruments are calibrated by laboratory tests conducted in homogenous and reproducible soil specimens, under accurately controlled states of stress and deformation. Such calibration is indispensable in development of these tests and in interpretation of the parameters obtained from the testing [1, 2, 3]

Most laboratory studies using CPT or PCPT are conducted either in large triaxial tests [4] or in calibration chambers with rigid or flexible walls [5, 6]. Generally, there are two approaches for interpreting CPT results; correlations of soil parameters directly with measured quantities or comparison of predictions of theoretical models with the experimental model results obtained in large calibration chambers. The latter approach has been extensively used by different investigators [7, 8, 9, 10, 11].

Chambers of varying designs and dimensions have been developed in the last two decades [10, 11]. The fundamental thrust in different designs has often been to reduce the chamber size, boundary effects and also the uncertainties associated with specimen preparation. A flexible, double walled chamber of 63.5 cm in diameter and 177.8 cm in height is recently constructed, equipped and installed in Louisiana State university [12]. This chamber is used with a miniature cone of 1.27 cm diameter in calibration testing. The use of smaller cone reduces the chamber size effects on the results. This type of cone is often used in classification and determination of engineering properties of highway embankment and pavements [12].

Published 1991 by Elsevier Science Publishing Company, Inc.
Calibration Chamber Testing
Editor: A.-B. Huang

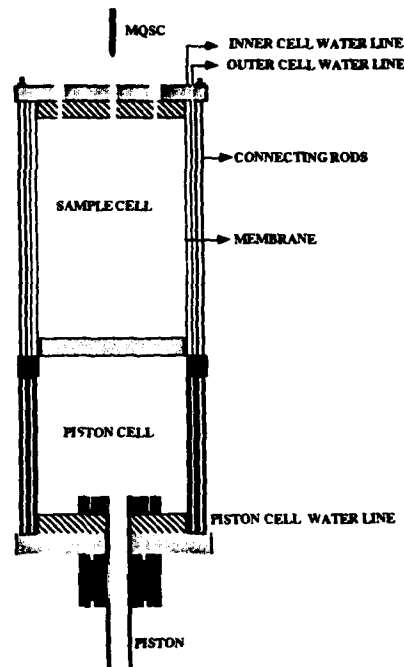


Figure 1: Schematic of the Chamber

This paper presents the results of preliminary tests conducted in the flexible wall calibration chamber using the miniature cone. These tests are a part of an ongoing study investigating the effect of cementation on penetration. Monterey No. 0/30 sand is used in specimen preparation. The preliminary results are compared with previous studies reported on the same sand. Reasonable agreement is displayed between the tests conducted in the different calibration chambers. The influence of chamber size and test location on penetration resistance and sleeve friction are discussed. The crushability of this sand around the cone is also investigated.

THE CALIBRATION CHAMBER AND THE MQSC

The schematic of the chamber installed in LSU is shown in the Figure 1. The chamber is 1.78 m (70 in.) high and 0.64 m (25 in.) in diameter. This chamber is primarily constructed for calibrating cone penetrometers under controlled boundary conditions. It permits K_p and isotropic consolidation of specimens and allows testing under the traditional four boundary conditions.

The soil specimen is of 0.53 m in diameter and 0.79 m in height. A data acquisition

and monitoring system controls and automates the testing. Consolidation and testing can be done either manually or through the computer with the data acquisition system. Electro-pneumatic transducers are used to allow DA conversion for automation. Two pneumatic transducers apply the vertical stresses through the piston cell and the other two provide the pressure compensation between the sample inner and outer cells during K_0 consolidation and penetration phase.

The Miniature Quasi-Static cone penetrometer (MQSC) is a 1.27 cm^2 cross-sectional area subtraction type Fugro-McClelland cone penetrometer with a friction sleeve of 6.3 cm long (25 cm^2) and an apex angle of 60 degrees. The diameter ratio defined as the ratio of chamber diameter to that of the cone is around 42 for the present investigation.

SPECIMEN PREPARATION AND TESTING PROCEDURE

Monterey sand No. 0/30 is used for the present study. This sand is mainly of quartz type with rounded to subrounded particles and is classified as SP on Unified Soil Classification. The maximum and minimum dry density of this sand are 14.04 and 16.65 kN/m^3 . The specific gravity of this sand is 2.67. This sand has been extensively used and characterized in several laboratory studies in USA for the last three decades. It is specifically selected since there exists well documented calibration chamber test results [10, 13].

Pluviation technique is used in specimen preparation. A pluviator is designed and constructed. Figure 2 presents a schematic diagram of this pluviator. The major factors that affect the relative density of the specimens are the shutter porosity, the sieve opening and the height of fall [14, 15]. Two different shutters with porosities 6.0 and 8.3 percent and three different sieves (ASTM No:6, 1/2 and 1/4) are selected. The height of fall is varied between 5 cm to a maximum of 15 cm. Specially constructed neoprene membrane is placed in the specimen chamber (see Figure 2) which is then brought underneath the pluviation setup. The aluminum shutters are rotated so as to line up the holes and the sand is pluviated in the chamber lined with the membrane.

After pluviation, the specimen is weighed and the relative density is calculated. The specimens above 80 percent relative density are prepared by using the No. 1/4 sieve and shutter with a porosity of 6 percent. A suction pressure of 80 kPa is applied to the specimen for about 30 minutes and then the specimen is transferred to the testing chamber. This suction is necessary to hold the specimen intact when the setup molds are removed. The inner and outer chambers along with the top plate are placed over the specimen and the top plate is fixed to the bottom piston assembly with 12 uniformly spaced rods. The space between the inner and the outer chambers and also the space between the membrane and the specimen are filled with deaired water. Subsequently, the specimen is consolidated under K_0 conditions (zero lateral strain). Penetration tests are conducted on the specimen (under BC3) at two different locations shown in Figure 3. The influence of boundary effects on the results is investigated by conducting a test at location B, close to the perimeter of the chamber. The cone is penetrated in two stages of 25 cm push length. This push length is found necessary to prevent buckling.

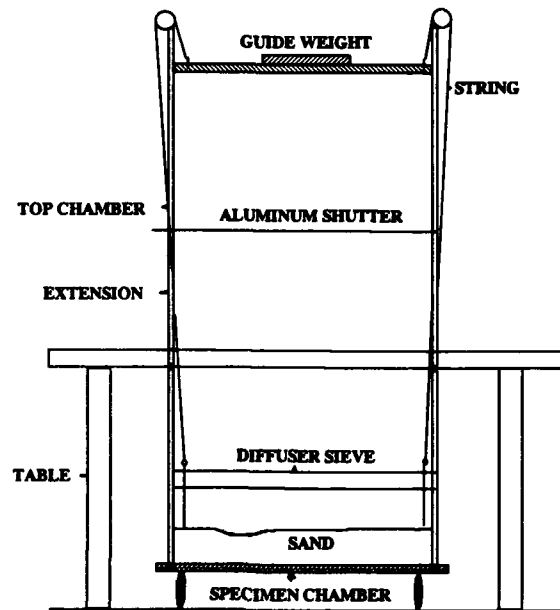


Figure 2: Schematic of the Pluviation Setup

CHAMBER TOP PLATE

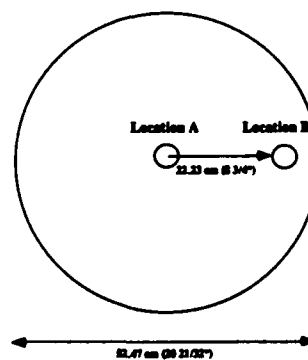


Figure 3: Position and Location of Tests

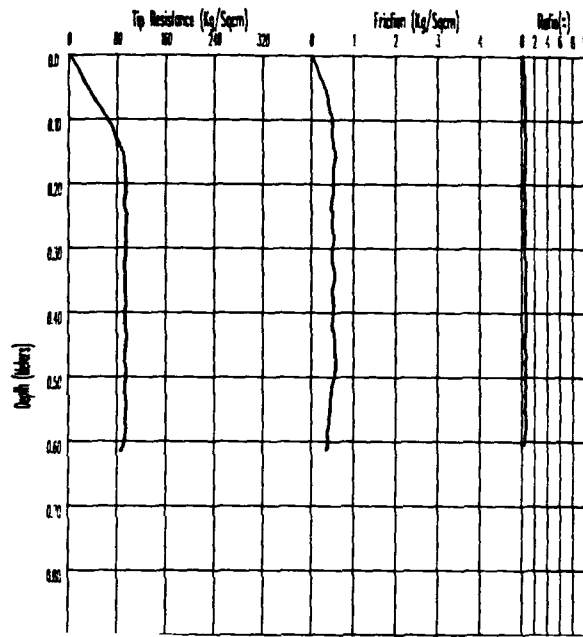


Figure 4: Penetration Test Results on a Monterey Sand Specimen of Relative Density 86 percent

ANALYSIS OF RESULTS

The penetration test results on a specimen of 86 percent relative density are shown in Figure 4. The confining stresses recorded during penetration are shown in the Figure 5. The vertical and horizontal stresses at the end of consolidation are 100 and 37 kPa rendering a K_0 value of 0.37. It is noted that there is not a considerable change in the horizontal stress during penetration. This observation implies that penetration does not lead to high volumetric strains at the boundaries and is an important implication of the minimized boundary effects. As previously reported by Parkin [16], the diameter ratio of 42 is significant enough to reduce the chamber size effects on the results.

In performance assessment of the tests conducted in this calibration chamber using the MQSC, repeatability and accuracy of the results are to be considered.

Repeatability

In an attempt to evaluate repeatability and precision, tests on specimens with similar relative density are compared. The tip and friction resistance profiles for both specimens are presented in the Figure 6. There is little difference in the tip resistances recorded in the two tests; however, there is slight variation (40 kPa to 68 kPa) in friction resistance. Slight changes in density along the depth may result in such differences in sleeve friction recorded along the relatively small sleeve area (25 cm²).

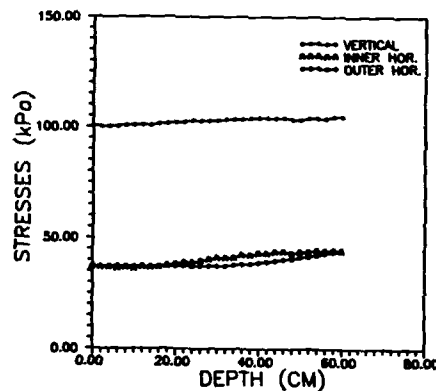


Figure 5: Stresses During Cone Penetration

Accuracy

Accuracy requires testing a material with known tip resistance and sleeve friction value in the present test setup. There is not yet such defined material in calibration chamber testing. Furthermore, a round robin testing of a specific sand in different chambers and under selected boundary conditions is not yet available. The authors selected Monterey No.0/30 sand for qualitative comparison purposes.

In an attempt to compare the test results in the present chamber with that of Villet and Mitchell [10] and Schmertmann [13], two more specimens of similar relative density are prepared and consolidated to 200 kPa and 300 kPa respectively. Figure 7 shows the tip resistance profiles of the tests conducted at these vertical stresses along with the test conducted at 100 kPa. The tip and friction resistance increase with the increase in the vertical stress. The profile for 200 kPa shows that the tip resistance reached a peak value of 22 MPa at a penetration depth of around 40 cm. This test is stopped at this stage because the cone rod is observed to buckle. This test needs to be repeated; however, for the present analysis, the peak tip resistance of 22 MPa is selected for the specimen tested under consolidation stress of 200 kPa.

Villet and Mitchell's tests are conducted in a pressure chamber of 80 cm (32 in.) in height and 76 cm (30 in.) in diameter. A cone penetrometer of 10 cm² tip area (3.56 cm diameter) and a base apex angle of 60 degrees is used. Their diameter ratio is around 20. Schmertmann's results are stated to be valid for the Fugro cone in normally consolidated saturated, recent, uncemented fine SP sands. The sand used by Schmertmann [13] is well defined to be subrounded to angular. The diameter ratio in this study is around 34. Dry pluviation is adopted for specimen preparation in both studies.

The tip resistance versus effective vertical stresses are plotted along with the results

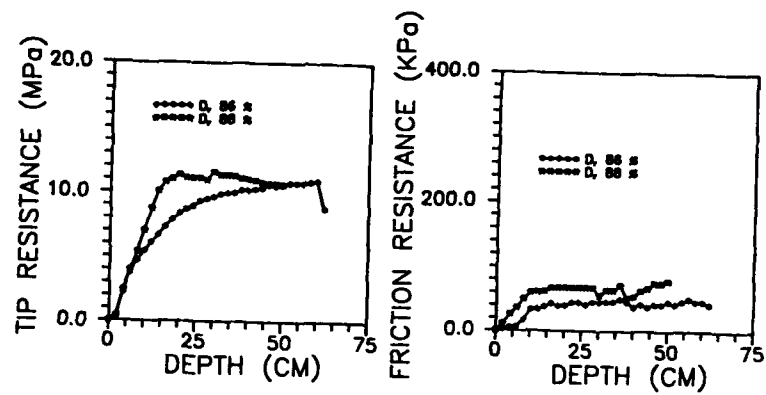


Figure 6: Comparison of Tip and Friction resistances on two specimens of similar relative densities

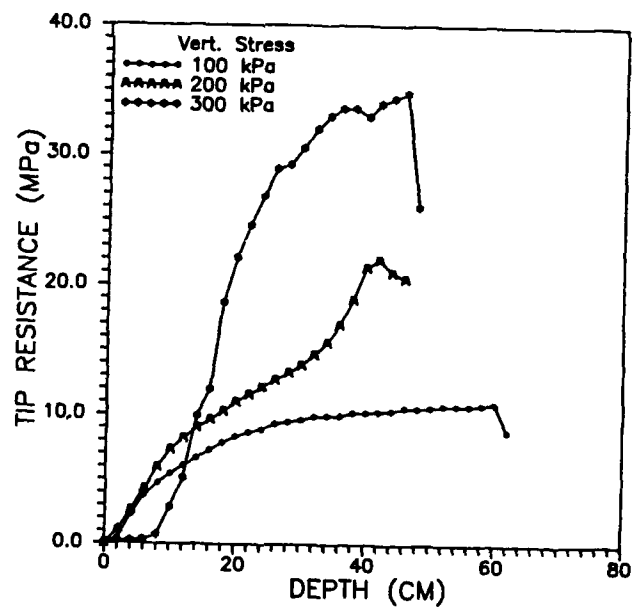


Figure 7: Tip Resistance versus Vertical Consolidation Stress for the Dense Specimens ($82\% < D_r < 86\%$)

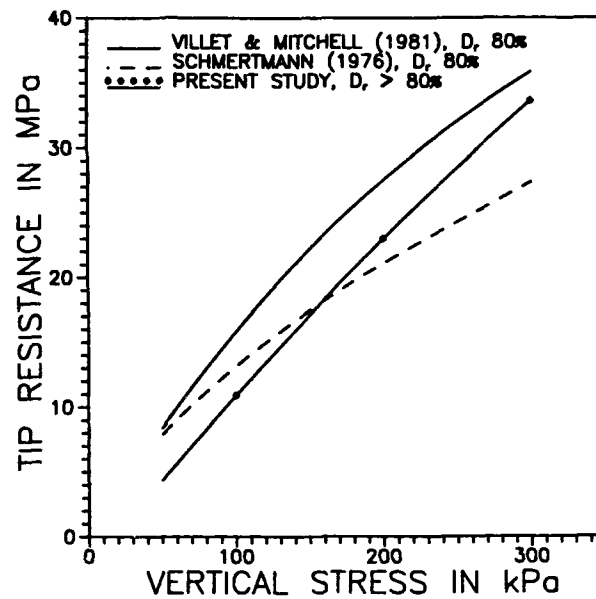


Figure 8: Comparison with Villet and Mitchell[10] and Schmertmann[13] Results

of Villet and Mitchell (1981) [10] and Schmertmann [13] in Figure 8. The miniature cone of 1.27 cm^2 predicted lower tip resistance than the 10 cm^2 cone used in the test results of Villet and Mitchell [10]. There are two possible reasons for this difference:

1. Tests by Villet and Mitchell[10] are conducted under constant stress boundary conditions. The K_0 values used by Villet and Mitchell [10] were around 0.5, substantially larger than the K_0 values obtained in this study (0.32 - 0.42).
2. The diameter ratio in Villet and Mitchell [10] is 20, significantly smaller than the diameter ratio of 42 used in this study. In dense sands, q_c increases substantially with the decrease in diameter ratio [16]. Therefore, there may have been influence of boundaries in test results reported by Villet and Mitchell.

However, there seems to be a reasonable agreement between the results obtained in this study and that reported by Villet and Mitchell [10]. It is noted that the results reported by Schmertmann [13] are significantly different at higher confining stresses (greater than 150 kPa). The influence of boundaries, the physical characteristics of the sand used, crushability and the type of boundary conditions may well be the reasons for this difference.

It is envisioned that the size of the penetrometer will not have a significant effect on penetration resistance in this sand. Specifically, the size will influence the strain rates and the radius of influence. Therefore the results obtained with the MQSC in this sand is expected to be in reasonable agreement with tests obtained with larger cones.

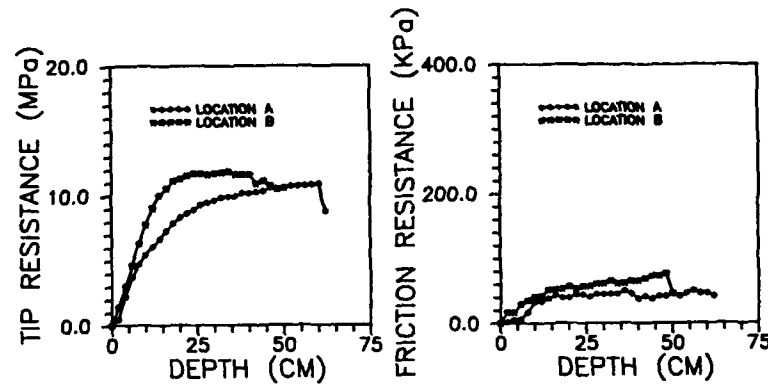


Figure 9: Influence of Location on the Test Results ($84 \% < D_r < 86 \%$)

Location of Testing

The influence of the location of testing on penetration resistance is presented in Figure 9. The first test is conducted at location A which is the center of the specimen. The second test is conducted at location B which is closer to the edge. It is interesting to note that location has minor influence on the tip resistance. However, there is a difference in friction resistance ($0.45 - 0.65 \text{ kg/cm}^2$). This difference is possibly due to the effects of inhomogeneities in specimen preparation. The soil pluviating near the edge of the sieve may result in a different density than in the middle. Boundary effects may have also lead to this difference in sleeve friction. The reasons for differences in sleeve friction need to be further investigated.

Crushability of the Sand During the Penetration

In an attempt to evaluate crushability of the sand around the cone, the sand within 3.5 cm of the cone is collected and a grain size distribution analysis is conducted. The grain size distributions of tested and untested sand are presented in the Figure 10. The sand tested under 200 kPa and 300 kPa shows some variation in gradation with the untested sand. The results also demonstrate that there is significant crushing of the material retained on ASTM sieves No. 30, 40 and 50.

The investigators also observed crushed sand powder all along the penetration profile. The sand collected from under the cone is passed through ASTM sieve No.200 [17]. A coefficient named as *Crushability under Cone* is used to measure the crushability. CUC is defined as the ratio of the weight of sand passed through No.200 sieve of a penetration tested sand per 1000 gms to that of a untested sand. CUC depends upon the influence

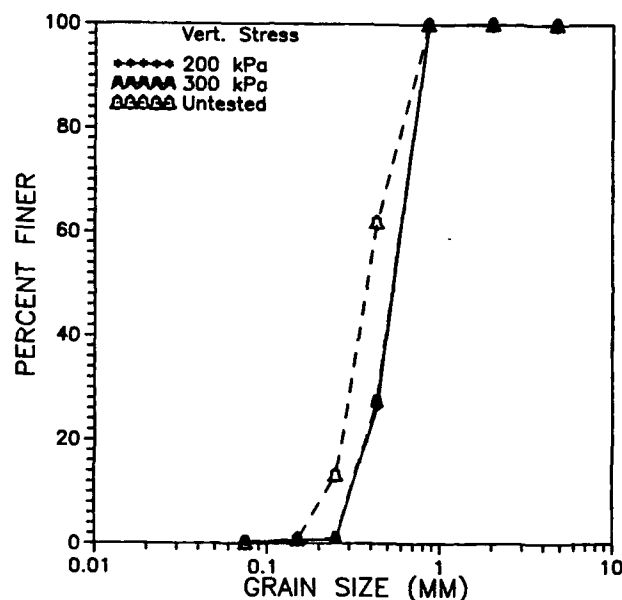


Figure 10: Grain Size Distribution Curves

zone from which the penetrated sand is collected. In the present study, sand is collected from a zone of three times the penetrometer diameter around the tested location. There was not any observable crushing beyond this region. The CUC values from the sand collected from specimens tested under vertical consolidation stress of 200 and 300 kPa are 2.8 and 3.8 respectively.

CONCLUSIONS

Preliminary tests conducted in flexible, double-walled calibration chamber using the miniature cone (MQSC) demonstrate that the chamber size effects are minimized. The test location has some influence on the friction resistance, while the tip resistance is not affected. Tip resistances at relative density of 84-88 % are compared with test results reported by Villet and Mitchell [10] and Schmertmann [13]. Sieve analyses shows that there is some crushing of this sand during penetration. This crushing is not observed beyond a distance of 3 times the diameter of the cone.

While the MQSC gives comparable results with those of previous studies, the results of this study further demonstrate that significantly different calibration charts may be obtained due to differences in characteristics of the sand used, boundary conditions and testing procedures.

ACKNOWLEDGEMENTS

The study investigating cone penetration in cemented sands is supported by the Na-

tional Science Foundation under Grant No. MSS-9020368 and the Civil Engineering Department of Louisiana State University. The funds provided by these institutions are gratefully acknowledged. Dr. Dario De Lima, designed and fabricated the calibration chamber. Messrs. Semih Arslan and Chris Gascon assisted in the laboratory study. Their assistance is appreciated. Any opinions, findings, conclusions and recommendations expressed in this material are those of the writers and do not necessarily reflect the views of the sponsors.

REFERENCES

1. Bellotti, R., Crippa, V., Pedroni, V. and Ghionna, V.N., "Saturation of Sand Specimen for Calibration Chamber Tests," Proc. of the First International Symp. on Penetration Testing, Vol. 2, ISOPT-1, Orlando, Florida, pp.661-672, March 1988.
2. Acar, Y.B. and Tumay, M.T., "Strain Field Around Cones in Steady Penetration," Journal of Geotechnical Engineering, ASCE, Vol.112, No.2, pp 207-213, February, 1986.
3. Tumay, M.T., Boggess, R.L. and Acar, Y., "Subsurface Investigations with Piezocone Penetrometer", in 'Cone Penetration Testing and Experience' edited by G.M. Norris and R.D. Holtz, Proc. Session sponsored by Geotechnical Engineering Division at ASCE, National Convention, St. Louis (Missouri), Oct. 1981
4. Canou, J., Hachem, M.El., Kattan, A. and Juran, I., "Mini Piezocone (M-CPTU) Investigation Related to Sand Liquefaction Analysis," Proceedings of the First International Symp. on Penetration Testing, Vol. 2, ISOPT-1, Orlando, Florida, pp.699-706, March 1988.
5. Parkin, A.K., "The Calibration of Cone Penetrometers", Proc. of the First International Symp. on Penetration Testing, Vol. 2, ISOPT-1, Orlando, Florida, pp.661-672, March 1988.
6. Been, K., Jefferies, J.H., Crooks, A. Rothenburg, L., "The Cone penetration tests in sands: part ii. General Inference of State," Geotechnique 37, pp. 285-299, 1987.
7. Viesmanis, A., "Laboratory Investigation of Electrical Friction Cone Penetrometers in Sands", Proc. European Symposium on Penetration Testing, Stockholm, Vol. 2.2, pp. 407-419, 1974
8. Chapman, G.A., "A Calibration Chamber for Field Test equipment," Proc. European Symposium on Penetration Testing, Stockholm, Vol. 2.2, pp.59-65, 1974
9. Holden, J.C., "The Calibration of Electrical Penetrometers in Sand," Norwegian Geotechnical Institute, Int. Rep. 52108-2, 1977
10. Villet, W.C.B. and Mitchell, J.K., "Cone Resistance, Relative Density and Friction Angle: Cone Penetration Testing and Experience", Proc. ASCE National Convention, St. Louis, MO, pp 178-208, 1981.
11. Bellotti, R., Bizzi, G. and Ghionna, V.N., "Design, Construction and Use of a Calibration Chamber," Proceedings, 2nd European Symp. Penetration Testing, Amsterdam, 2, pp.439-446, 1982.

12. Dario De Lima, "Development, Fabrication and Verification of the LSU In-situ Testing Calibration Chamber (LSU/CALCHAS) ," Ph.D. Thesis, Louisiana State University, 1990.
13. Schmertmann, J.H., " An Updated Correlation Between Relative density, D_r , and Fugro Type Electric Cone Bearing, q_c ," Contract Report DACW 39-76-M6646, Waterways Experiment Station, 1976.
14. Rad, N.S., "Effect of Cementation on Penetration Resistance of Sand" , Final report submitted to Fugro International, Department of Civil Engineering, Report No. GE-84/01, Louisiana State University, June 1984, 222 pages
15. Rad, N.S. and Tumay, M.T., "Factors Affecting Sand Specimen Preparation by Raining," Technical Note, Geotechnical Testing Journal, American Society of Testing and Materials, Vol.10, No.I, March 1987, pp.31-37.
16. Parkin, A.K., " The Friction Cone Penetrometer: Laboratory Calibration for the Prediction of Sand Properties," Norwegian Geotechnical Institute, Int. Rep. 52108-5, 1986.
17. Bellotti, R., Ghionna, V.N. and Pedroni, S., "Compressibility and Crushability of Sands at Higher Stresses," (this symposium).

Correlation of Initial Tangent Modulus and Cone Penetration Resistance

Glenn J. Rix¹ and Kenneth H. Stokoe, II²

¹ Assistant Professor, School of Civil Engineering, Georgia Institute of Technology, Atlanta, Georgia 30332

² Brunswick-Abernathy Regents Professor, Department of Civil Engineering, University of Texas at Austin, Austin, Texas 78712

ABSTRACT

Calibration chamber measurements of the cone tip resistance, q_c , and resonant column measurements of the initial tangent shear modulus, G_{max} , for washed mortar sand show that both quantities depend on the vertical and horizontal effective stresses and soil density. However, G_{max} and q_c depend on the state of stress and density to different degrees, making a unique correlation between them impossible. Data from this study are compared to the correlation between G_{max} and q_c proposed by Baldi et al. (1989). All data show a trend of decreasing G_{max} to q_c ratio with increasing normalized cone tip resistance (or relative density), but values of this ratio differ for different sands. This suggests that there are factors that affect G_{max} and/or q_c that these correlations do not include. A modified correlation is presented that indicates the uncertainty in using G_{max} - q_c correlations for different uncemented, quartz sands.

INTRODUCTION

Geotechnical engineers often use penetration resistance from standard penetration tests (SPT) or cone penetration tests (CPT) to estimate the initial tangent shear modulus, G_{max} . Ohta and Goto [1] and Imai and Tonouchi [2] have developed correlations between SPT blow count and G_{max} . Correlations between CPT tip resistance, q_c , and G_{max} have been developed by Sykora and Stokoe [3], Robertson and Campanella [4], Rix [5], Baldi et al. [6], Bellotti et al. [7], Lo Presti and Lai [8], and Baldi et al. [9]. These correlations were created using field observations, laboratory measurements, calibration chamber measurements, and empirical estimates of G_{max} and q_c .

This paper describes calibration chamber measurements of cone penetration resistance in washed mortar sand at low values of vertical effective stress encountered in near-surface cohesionless soils (depths less than 13 m). Cone tip resistances and resonant column measurements of the initial tangent shear modulus are used to study the relationship between G_{max} and q_c . A case study is also presented of a site in the Imperial Valley of Southern California that liquefied during a magnitude 6.6 earthquake in 1979. Independent, in situ measurements of G_{max} and q_c in three different sand deposits provided an opportunity to evaluate the accuracy of correlations between cone penetration resistance and initial tangent shear modulus.

TEST EQUIPMENT AND PROCEDURE

Washed mortar sand has been used extensively for dynamic soil property investigations at the University of Texas [10]. It was used in the calibration chamber so that cone tip resistances could be compared with previously measured initial tangent shear moduli for the same material. A grain size distribution curve for washed mortar sand is shown in Fig. 1 and index properties are summarized in Table 1. The grain size distribution was checked periodically during the study to assure that no segregation occurred due to pluviation.

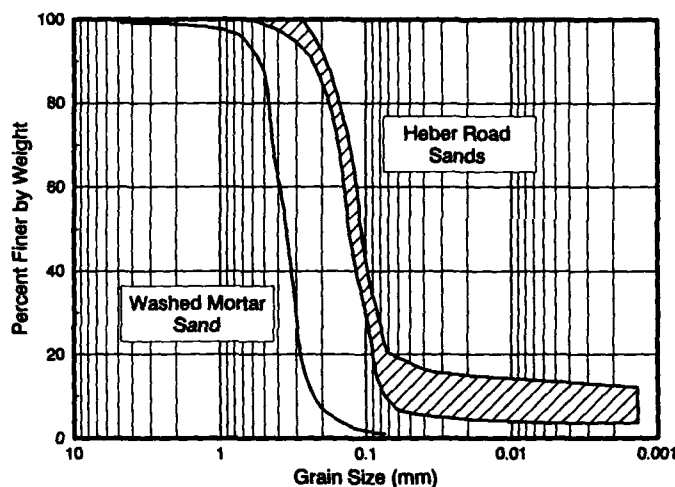


Figure 1 Grain Size Distributions for Washed Mortar Sand and Heber Road Sands

Specimens were prepared in a calibration chamber with an inside height of 107 cm and an inside diameter of 86 cm. Loose specimens were constructed using a piece of hardware cloth with 1/4-in. (0.64-cm) openings stretched across a 76-cm diameter frame. This frame was placed on the bottom of the calibration chamber and about 15 cm of sand was loosely poured on top of it. Using an overhead crane, the frame was slowly lifted through the layer of sand. The gentle lifting and redeposition of the sand resulted in a uniform, loose layer. The entire specimen was constructed by repeating the process of placing the sand in layers and lifting the frame slowly upward through the layer. This method of constructing loose specimens yielded consistent values of density. The average dry density of the five specimens constructed in this manner was 14.5 kN/m, which corresponds to an average relative density, D_r , of 12.6 percent. The standard deviation of the dry density was 0.11 kN/m³.

Medium dense specimens were constructed by pluviating air-dried sand into the calibration chamber. An 86-cm diameter stationary rainer with uniformly spaced, 0.95-cm diameter holes in the bottom was used to control the intensity of flow of the sand. The flow of

Table 1 Index Properties of Washed Mortar Sand and Heber Road Sands

Index Property	Washed Mortar Sand	Heber Road Sands
Unified Classification	SP	SM
Median Grain Diameter	0.35 mm	~0.12 mm
Percent Fines	< 1	10 to 22
Specific Gravity	2.67	-
Minimum Void Ratio	0.563	-
Maximum Void Ratio	0.839	-
Grain Shape	Subangular to Subrounded	Subrounded to Rounded

sand could be interrupted as needed by a rotating shutter plate. The gap between the rainer and the top of the chamber was enclosed with a polyethylene curtain to control dust. During pluviation, a minimum height of fall of 76 cm was always maintained. Since the capacity of the rainer was insufficient to fill the entire chamber at once, the specimen was constructed in 15-cm lifts. The average dry density of the medium dense specimens was 16.0 kN/m^3 with a standard deviation of 0.20 kN/m^3 . The average relative density was 73.3 percent.

Pluviation was also used to construct dense specimens. To increase the density further, the specimen was vibrated during and after raining by a pneumatic vibrator attached to the wall of the calibration chamber. The combination of pluviation and vibration yielded an average dry density of 16.7 kN/m^3 with a standard deviation of 0.13 kN/m^3 . The average relative density of these specimens was 97.2 percent.

Stress-controlled boundaries were used for all tests in this study. The vertical and horizontal effective stresses were selected to yield one of three values of the effective coefficient of lateral earth pressure ($K = 0.5, 1.0, \text{ and } 2.0$). Values of vertical effective stress ranged from 17.2 kPa to 103.4 kPa. This range of vertical effective stress was chosen to simulate values encountered in near-surface deposits that may be susceptible to liquefaction. All confining pressures are referenced to the mid-height of the specimen.

Stress paths used to apply the confining pressures in this study differ from those often used in other calibration chamber studies (e.g., [11]). In this study, vertical and horizontal stresses were applied to yield a selected value of K directly. In many other investigations, the sample is first normally consolidated and then the desired overconsolidation ratio is obtained by reducing the vertical stress to simulate mechanical overconsolidation. The residual horizontal stress is used to calculate the coefficient of lateral earth pressure. We do not believe that the different stress paths used in this study adversely affected the values of cone tip resistance since the tip resistance is primarily a function of the current state of stress and not of stress history [6, 7, 9, 12, 13, 14].

The cone penetrometer was a standard Fugro-type electrical cone. An MTS system was used to push the cone at a rate of 2 cm/s. Since the hydraulic cylinder had a maximum stroke of 61 cm, each penetration test was performed in two stages. During the first stage the cone was pushed about 46 cm. Penetration was stopped while an extension rod was inserted, and the cone was pushed another 46 cm.

Because specimen construction was time consuming, the first and second penetration stages were often conducted at different confining pressures to maximize the number of penetration tests. Several tests were also performed with the same confining pressures during both stages. Comparisons between these single-stage tests and the two-stage tests showed that the two-stage approach was valid [5].

Specimen densities were calculated using the total weight and volume of the specimen. The uniformity of pluviated specimens was periodically verified using six small containers placed at various radial and vertical locations during pluviation. As an example, for Test No. 2 the six densities ranged from 15.5 kN/m^3 to 16.0 kN/m^3 . The average value of these measurements was 15.75 kN/m^3 , which agrees with the value obtained by weighing the entire chamber (15.83 kN/m^3). Following penetration, sand near the cone was removed and discarded to avoid reusing crushed particles.

RELATIONSHIP BETWEEN G_{MAX} AND q_c

Cone penetration tests performed in calibration chambers are influenced by the boundaries of the chamber [15]. The effect of the boundaries depends on the ratio of the

diameters of the calibration chamber and the cone penetrometer and the relative density of the sand. Mayne and Kulhawy [16] have summarized data concerning these boundary effects and have developed the following expression:

$$\frac{q_c \text{ (corrected)}}{q_c \text{ (measured)}} = \left[\frac{\frac{B_c}{B} - 1}{70} \right]^{-0.005 D_r} \quad (1)$$

where B_c is the diameter of the chamber, B is the cone diameter, and D_r is the relative density of the sand. Equation 1 was used to correct the cone tip resistance. The ratio of the diameters of the chamber and cone used in this study was 24. A summary of the test conditions and measured and corrected cone tip resistances is presented in the Appendix.

An expression commonly used for the relationship between cone tip resistance, relative density, and effective stress is [6, 17]:

$$q_c = C_0 p_a \left(\frac{\sigma'_{v0}}{p_a} \right)^{C_1} \left(\frac{\sigma'_{h0}}{p_a} \right)^{C_2} \exp(C_3 D_r) \quad (2)$$

where σ'_{v0} is the vertical effective stress, σ'_{h0} is the horizontal effective stress, D_r is the relative density expressed as a decimal, and p_a is atmospheric pressure in the same units as σ . C_0 , C_1 , C_2 and C_3 are regression constants. A multiple regression analysis yielded $C_0 = 33.5$, $C_1 = 0.22$, $C_2 = 0.64$, $C_3 = 2.49$, and a coefficient of determination (r^2) equal to 0.91.

Resonant column tests were used to measure the initial tangent shear moduli of washed mortar sand [10]. Isotropic, biaxial, and triaxial confinement of solid and hollow cylindrical specimens were used to evaluate the effect of state of stress on the initial tangent shear modulus. The tests confirmed earlier research showing that the initial tangent shear modulus is a function of the individual principal stresses instead of the mean effective stress [18, 19]. An equation similar in form to that originally proposed by Hardin [20] but modified to include the individual principal stresses was used to express the results:

$$G_{max} = \frac{A}{0.3 + 0.7e^2} \left(\frac{\sigma'_a}{p_a} \right)^{na} \left(\frac{\sigma'_b}{p_a} \right)^{nb} p_a \quad (3)$$

where G_{max} is the initial tangent shear modulus, e is the void ratio, σ'_a is the effective stress in the direction of wave propagation, σ'_b is the effective stress in the direction of particle motion, and p_a is the atmospheric pressure in the same units as G_{max} , σ'_a , and σ'_b . Regression analyses yielded $A = 685$ and $na = nb = 0.22$ for washed mortar sand. Equation 3 was used to calculate values of G_{max} for each combination of density and state of stress in the 42 cone penetration tests. The values of σ'_a and σ'_b were assumed to be the vertical and horizontal stresses, respectively. Values of G_{max} are included in the Appendix.

Equations 2 and 3 show that q_c and G_{max} are dependent on the vertical and horizontal stresses and the density. Since both depend on the same parameters, it is reasonable to expect q_c and G_{max} to be correlated. However, it is important to note that q_c and G_{max} depend on the state of stress and density to different degrees. The sum of the exponents C_1 and C_2 in Eq. 2 differs from the sum of the exponents na and nb in Eq. 3. Furthermore, q_c and G_{max} depend on the relative density (or void ratio) differently. This means that a unique correlation between q_c

and G_{\max} should not be expected. Conversely, correlations must include either the density or state of stress explicitly or these parameters must be included implicitly through appropriate normalizations of the quantities involved [4, 5].

A correlation that includes the vertical effective stress or relative density explicitly is shown in Fig. 2. This figure was prepared using an assumed value of the coefficient of lateral earth pressure ($K = 0.5$) to remove the horizontal effective stress as an independent variable. Figure 2 contains two families of curves for different values of the vertical effective stress and relative density. Solid lines in the figure are for different values of vertical effective stress ranging from 20 kPa to 100 kPa; dashed lines are for different relative densities. We have chosen to present the correlation in this manner to emphasize that the relationship between cone tip resistance and initial tangent shear modulus depends on the state of stress and density of the soil.

A more convenient correlation for uncemented, predominantly quartz sands is shown in Fig. 3 [9]. In this correlation the effective stress and density of the soil are included by normalizing the cone tip resistance with respect to the square root of the vertical effective stress. Lancellota [21] has shown that normalized cone tip resistance correlates well with relative density. Thus, the ratio of G_{\max} to q_c decreases with increasing density. This relationship is also apparent in Fig. 2. The influence of the horizontal effective stress on G_{\max} and q_c is shown in Fig. 3 by the lines bounding the cross-hatched area. These lines, for

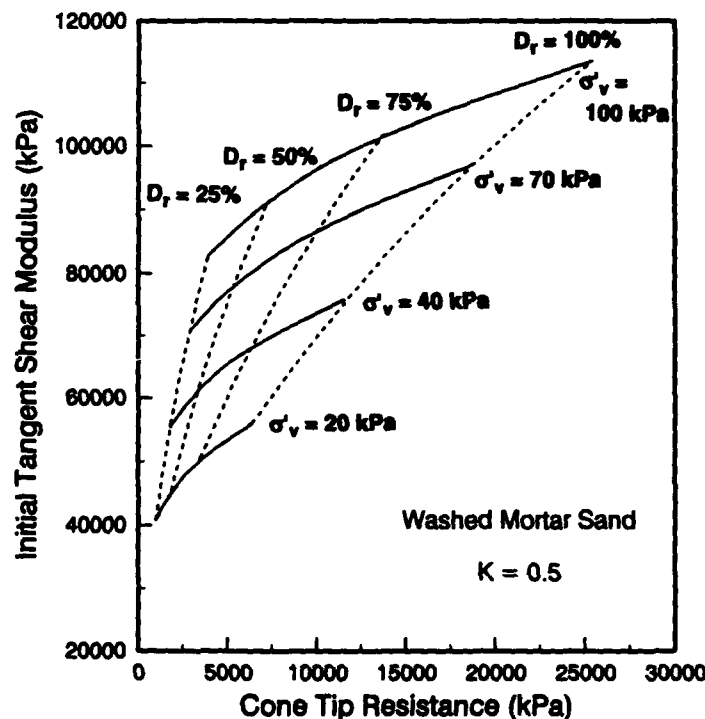


Figure 2 Correlation Between Initial Tangent Shear Modulus and Cone Tip Resistance for Washed Mortar Sand

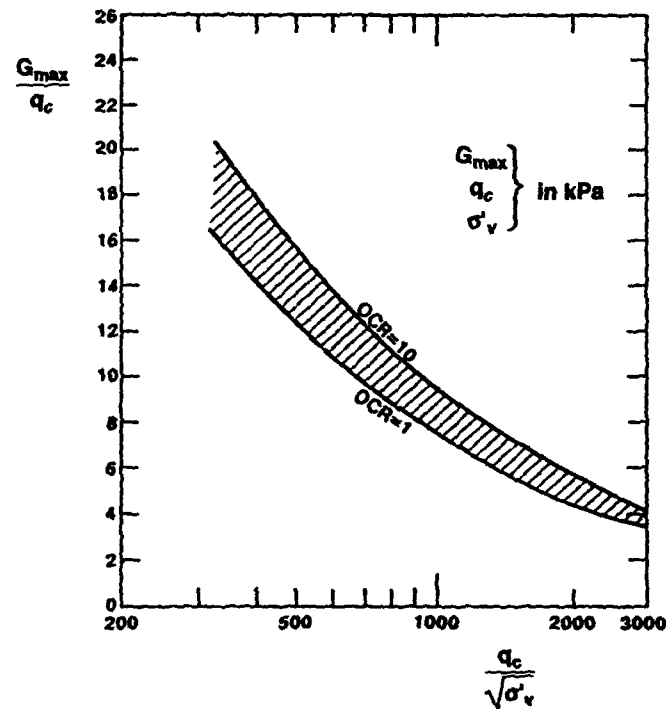


Figure 3 Correlation Between G_{max} and q_c Proposed by Baldi et al. [9]

overconsolidation ratios of 1 and 10, account for the residual horizontal stresses due to overconsolidation.

Jamiolkowski and Robertson [22] have plotted data from three cohesionless soil deposits in this normalized form. These deposits were slightly silty to silty sands and gravelly sands. All were normally to lightly overconsolidated ($OCR < 2$), uncemented, and less than 3000 years old (Late Holocene)[8]. The data from these three sites plot within the cross-hatched area shown in Fig. 3 except for several points from the gravelly sand site that may have been affected by the presence of gravel.

The data from this study are plotted in normalized form in Fig. 4. Also shown in the figure is the cross-hatched area from Fig. 3. The washed mortar sand data have the same trend of decreasing ratio of G_{max} to q_c for increasing relative density. For normalized penetration resistances less than 1000, the washed mortar sand data plot above the range suggested by Baldi et al. [9]. This means that for sands with low relative densities the correlation underpredicts G_{max} by 30 to 40 percent, depending on the value of the normalized tip resistance.

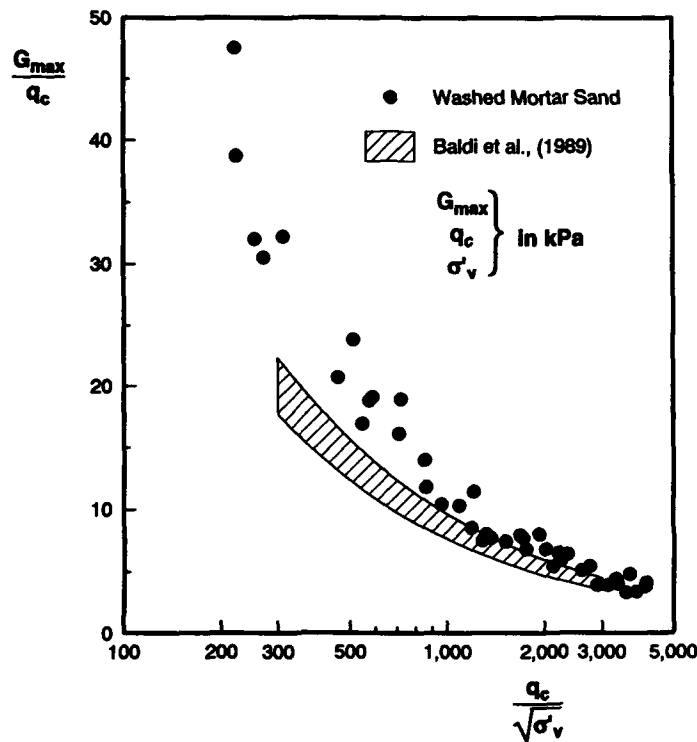


Figure 4 Comparison of Washed Mortar Sand Data with Correlation Proposed by Baldi et al. [9]

HEBER ROAD CASE STUDY

On October 15, 1979 an earthquake ($M = 6.6$) occurred along the Imperial Fault in Southern California that resulted in extensive liquefaction of near-surface sands. The sands that liquefied were confined to a remnant stream channel passing through the area [23]. In January, 1981, University of Texas and US Geological Survey personnel performed crosshole tests and cone penetration tests to evaluate the characteristics of sands that did and did not liquefy. Because initial tangent moduli and cone tip resistances were independently measured, this case study provides an opportunity to evaluate the accuracy of laboratory-based correlations between G_{max} and q_c when applied to field situations.

Three sands with different depositional histories are present in the area of the remnant stream channel. A cross section of the site is shown in Fig. 5. The point bar (Unit A_1), channel fill (Unit A_2), and levee (Unit A_3) deposits are Late Holocene in age. The different depositional histories have resulted in different densities. The point bar deposit is the densest of the three, followed by the levee deposit and the channel fill. Sand boils and a lateral spread occurred in the channel fill following the 1979 earthquake. No surficial evidence of

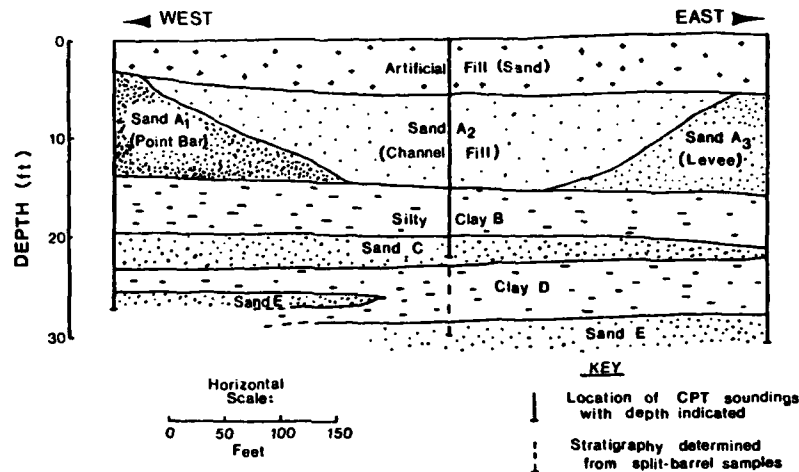


Figure 5 Cross Section of Heber Road Site Showing Point Bar, Channel Fill, and Levee Deposits [24]

liquefaction was observed in the point bar and levee deposits. The range of grain size distributions and index properties of the three sands are given in Fig. 1 and Table 1, respectively. The three sands are similar except for the fines content that ranged from 22 percent (channel fill) to 10 percent (point bar). No evidence of cementation was observed in any of the three sands.

Measured values of initial tangent shear modulus and cone tip resistance were used to calculate the ratio of G_{max} to q_c and the normalized tip resistance. Vertical effective stresses were calculated using assumed total unit weights of 15.7 kN/m^3 above the water table and 17.3 kN/m^3 below. The depth of the observed water level was 1.8 m. Data for the three Heber Road sands are plotted in Fig. 6 with the correlation suggested by Baldi et al. [9]. Here the data plot below the correlation. This may be the result of the additional fines in these sands. If the correlation were used to estimate the initial tangent shear modulus at the Heber Road site, the values would be overpredicted by 30 to 40 percent.

CONCLUSIONS

Calibration chamber studies of cone tip resistance and resonant column tests on washed mortar sand show that both G_{max} and q_c depend on the current state of effective stress and the density of the soil. On this basis, it seems reasonable to expect a correlation between the two quantities. It is important to note, however, that G_{max} and q_c depend differently on the effective stresses and density. This means that a unique correlation between G_{max} and q_c is not possible. Correlations must either include the effective stresses or density explicitly or account for their effect by appropriate normalizations of G_{max} or q_c .

When data from this study on washed mortar sand are plotted in the form suggested by Baldi et al. [9], the observed ratios of G_{max} to q_c are higher than the predicted ratios for

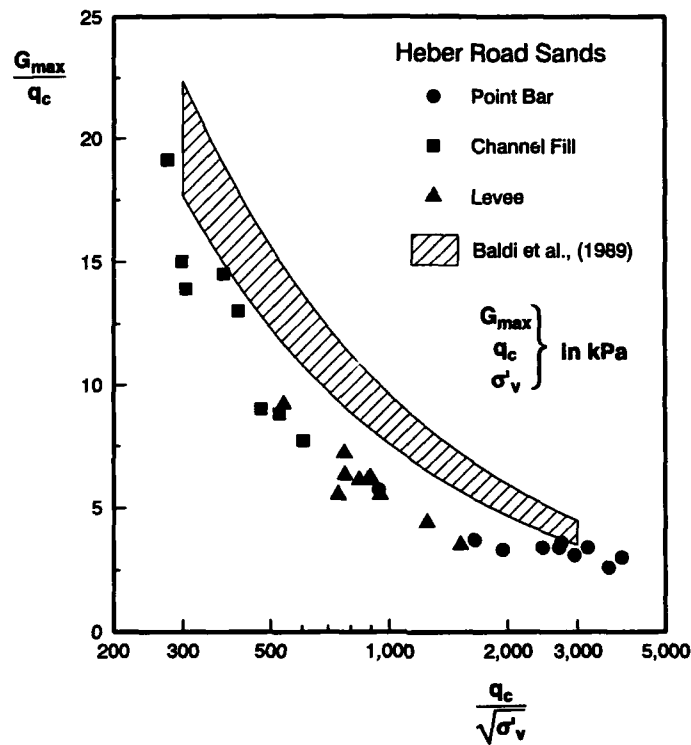


Figure 6 Comparison of Heber Road Data with Correlation Proposed by Baldi et al. [9]

normalized cone tip resistances less than 1000. In situ seismic measurements and cone penetration tests at the Heber Road site provided another opportunity to evaluate the accuracy of the suggested correlation. For this site, the observed ratios of G_{max} to q_c are lower than the predicted ratios. It appears that for an individual sand, the ratio of G_{max} to q_c as a function of the normalized cone tip resistance is well defined, but the values of this ratio differ from sand to sand. This suggests that there may be factors such as fines content, particle angularity, and particle mineralogy that influence G_{max} and/or q_c that are not included in these correlations between G_{max}/q_c and the normalized tip resistance. Until these factors can be identified, it may be more appropriate to use a correlation between G_{max} and q_c that indicates the uncertainty in using the correlation for different sands.

Figure 7 shows a proposed correlation similar to that of Baldi et al. [9] that includes data from this study on washed mortar sand and the Heber Road sands. The average value is given by:

$$\frac{G_{max}}{q_c} = 1634 \left[\frac{q_c}{\sqrt{\sigma'_v}} \right]^{0.75} \quad (4)$$

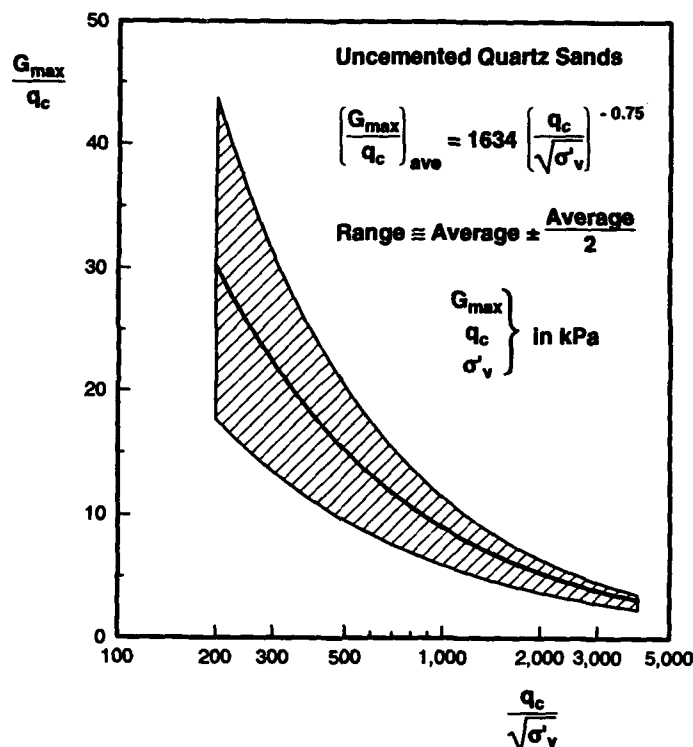


Figure 7 Proposed Modified Correlation Between G_{\max} and q_c for Uncemented, Quartz Sands Showing Average and Range in Values

where G_{\max} , q_c , and σ'_v are in kPa. The range in the ratio of G_{\max} to q_c for a given value of the normalized penetration resistance is about ± 50 percent.

REFERENCES

1. Ohta, Y., and Goto, N., (1978), "Empirical shear wave velocity equations in terms of characteristic indexes," *Earthquake Engineering and Structural Dynamics*, Vol. 6, pp. 167-187.
2. Imai, T., and Tonouchi, K., (1982), "Correlation of N-values with S-wave velocity," *Proceedings, Second European Symposium on Penetration Testing*, Amsterdam, Vol. 2, pp. 67-72.
3. Sykora, D.W., and Stokoe, K.H., II, (1983), "Correlations of in situ measurements in sands with shear wave velocity," *Geotechnical Engineering Report GR83-33*, University of Texas at Austin, Austin, Texas.
4. Robertson, P.K., and Campanella, R.G., (1983), Interpretation of cone penetration tests - Part I: Sands," *Canadian Geotechnical Journal*, Vol. 20, No. 4, pp. 718-733.

5. Rix, G.J., (1984), "Correlation of elastic moduli and cone penetration resistance," Thesis submitted to the University of Texas at Austin in partial fulfillment of the requirements for the degree of Master of Science.
6. Baldi, G., Bellotti, R., Ghionna, V., Jamiolkowski, M., and Pasqualini, E., (1986), "Interpretation of CPTs and CPTUs - Part II: Drained penetration in sands," *Proceedings, Fourth International Geotechnical Seminar on Field Instrumentation and In Situ Measurements*, Singapore.
7. Bellotti, R., Ghionna, V., Jamiolkowski, M., Lancellota, R., and Manfredini, G., (1986), "Deformation characteristics of cohesionless soils from in situ tests," *Use of In Situ Tests in Geotechnical Engineering*, Geotechnical Special Publication No. 6, S.P. Clemence, Ed., ASCE, pp. 47-73.
8. Lo Presti, D.C.F., and Lai, C., (1989), "Shear wave velocity from penetration tests," *Atti del Dipartimento di Ingegneria Strutturale* No. 21, Politecnico di Torino, Torino, Italy.
9. Baldi, G., Bellotti, R., Ghionna, V., Jamiolkowski, M., and Lo Presti, D.C.F., (1989), "Modulus of sands from CPTs and DMTs," *Proceedings, XII ICSMFE, Rio de Janeiro*, Vol. 1, pp. 165-170.
10. Ni, S.-H., (1987), "Dynamic properties of sand under true triaxial stress states from resonant column/torsional shear tests," dissertation submitted to the University of Texas at Austin in partial fulfillment of the requirements for the degree of Doctor of Philosophy.
11. Bellotti, R., Bizzi, G., and Ghionna, V.N., (1982), "Design, construction, and use of a calibration chamber," *Proceedings, Second European Symposium on Penetration Testing*, Amsterdam.
12. Lambrechts, J.R., and Leonard, G.A., (1978), "Effects of stress history on deformation of sand," *Journal of the Geotechnical Engineering Division*, ASCE, Vol. 104, No. 11, pp. 1371-1387.
13. Clayton, C.R.I., Hababa, M.B., and Simons, N.E., (1985), "Dynamic penetration resistance and the prediction of the compressibility of a fine sand - a laboratory study," *Geotechnique*, Vol. 24, No. 1, pp. 19-31.
14. Jamiolkowski, M., Ghionna, V., Lancellota, R., and Pasqualini, E., (1988), "New correlations of penetration tests for design practice," *Penetration Testing 1988*, J. de Ruiter, Ed., Balkema, Rotterdam.
15. Parkin, A.K., and Lunne, T., (1982), "Boundary effects in the laboratory calibration of a cone penetrometer for sand," *Proceedings, Second European Symposium on Penetration Testing*, Amsterdam.
16. Mayne, P.W., and Kulhawy, F.H., (1991), "Calibration chamber database and boundary effects correction for CPT data," *Proceedings, First International Symposium on Calibration Chamber Testing*, Potsdam, New York.
17. Schmertmann, J.H., (1976), "An updated correlation between relative density, D_r , and Fugro-type electric cone bearing, q_c ," US Army Waterways Experiment Station Report DACW 39-76-M6646.
18. Roessler, S.K., (1979), "Anisotropic shear modulus due to stress anisotropy," *Journal of the Geotechnical Engineering Division*, ASCE, Vol. 105, No. 7, pp. 871-880.
19. Stokoe, K.H., II, Lee, S.H.H., and Knox, D.P., (1985), "Shear moduli measurements under true triaxial stresses," *Advances in the Art of Testing Soils under Cyclic Conditions*, ASCE, pp. 166-185.
20. Hardin, B.O., (1978), "The nature of stress-strain behavior for soils," *Earthquake Engineering and Soil Dynamics*, ASCE, Vol. 1, pp. 3-90.
21. Lancellota, R., (1983), "Analisi di affidabilità in ingegneria geotecnica," *Atti del Istituto Scienza Costruzioni* No. 625, Politecnico di Torino, Torino, Italy.

22. Jamiolkowski, M., and Robertson, P.K., (1988), "Future trends for penetration testing," *Proceedings, Penetration Testing in the UK, Birmingham*, pp. 321-342.
23. Youd, T.L., and Bennett, M.J., (1983), "Liquefaction sites, Imperial Valley, California," *Journal of the Geotechnical Engineering Division, ASCE*, Vol. 109, No. 3.
24. Sykora, D.W., and Stokoe, K.H., II, (1982), "Seismic investigation of three Heber Road sites after October 15, 1979 Imperial Valley earthquake," *Geotechnical Engineering Report GR82-24, University of Texas at Austin, Austin, Texas*.

APPENDIX - SUMMARY OF TESTS

Test No.	Vertical Effective Stress (kPa)	Horizontal Effective Stress (kPa)	Coeff. of Lateral Earth Pressure	Void Ratio	Relative Density (%)	Uncorrected Cone Tip Resistance (kPa)	Corrected Cone Tip Resistance (kPa)	Initial Tangent Shear Modulus (kPa)
1	75.8	68.9	0.9	0.748	33.0	6953	8353	86497
2	24.1	17.2	0.7	0.642	71.4	2805	4172	58246
3	34.5	34.5	1.0	0.612	82.2	6335	10012	76816
4	17.2	17.2	1.0	0.612	82.2	1893	2991	56624
5	68.9	34.5	0.5	0.652	67.8	4893	7135	84171
6	68.9	34.5	0.5	0.631	75.4	7414	11276	86914
7	34.5	17.2	0.5	0.640	72.1	2255	3369	63193
8	68.9	68.9	1.0	0.582	93.1	11062	18572	109074
9	103.4	51.7	0.5	0.637	73.2	8022	12055	102942
10	34.5	17.2	0.5	0.596	88.0	7629	12453	67578
11	68.9	34.5	0.5	0.547	105.8	16396	29542	98732
12	17.2	17.2	1.0	0.548	105.4	5413	9734	62391
13	34.5	34.5	1.0	0.548	105.4	10807	19432	84640
14	34.5	17.2	0.5	0.562	100.4	10493	18342	71152
15	103.4	51.7	0.5	0.562	100.4	16838	29434	115378
16	17.2	17.2	1.0	0.610	83.0	5246	8325	56797
17	34.5	34.5	1.0	0.610	83.0	9610	15250	77051
18	34.5	17.2	0.5	0.786	19.2	1177	1309	50620
19	68.9	34.5	0.5	0.786	19.2	2020	2248	68671
20	17.2	17.2	1.0	0.788	18.5	824	913	43330
21	34.5	34.5	1.0	0.788	18.5	1647	1826	58782
22	34.5	68.9	2.0	0.814	9.1	3285	3455	65851
23	68.9	68.9	1.0	0.814	9.1	4305	4528	76699
24	103.4	51.7	0.5	0.780	21.4	2295	2585	82827
25	103.4	103.4	1.0	0.780	21.4	4138	4661	96471
26	17.2	34.5	2.0	0.787	18.8	1912	2124	50544
27	51.7	103.4	2.0	0.787	18.8	4589	5097	81960
28	17.2	34.5	2.0	0.634	74.3	5266	7962	63775
29	34.5	68.9	2.0	0.634	74.3	10669	16131	86517
30	68.9	34.5	0.5	0.687	55.1	7796	10592	79791
31	68.9	68.9	1.0	0.687	55.1	9218	12524	92935
32	17.2	34.5	2.0	0.553	103.6	8522	15170	72124
33	34.5	68.9	2.0	0.553	103.6	13543	24107	97844
34	17.2	17.2	1.0	0.607	84.1	3138	5010	57057
35	34.5	34.5	1.0	0.607	84.1	6158	9832	77404
36	34.5	17.2	0.5	0.613	81.9	4050	6388	65851
37	103.4	51.7	0.5	0.613	81.9	8483	13379	106782
38	51.7	103.4	2.0	0.636	73.6	10493	15800	103100
39	103.4	103.4	1.0	0.636	73.6	11768	17720	120084
40	68.9	68.9	1.0	0.566	98.9	16053	27837	111749
41	103.4	103.4	1.0	0.566	98.9	22437	38907	133575
42	51.7	103.4	2.0	0.578	94.6	17416	29479	112618

CHARACTERIZATION OF SOIL IN CALIBRATION CHAMBERS WITH SEISMIC WAVES

KENNETH H. STOKOE, II,¹ JAMES NGAR-KOK LEE,²
AND SHANNON HSIEN-HENG LEE³

¹Brunswick-Abernathy Regents Prof., Univ. of Texas, Dept. of Civil Engrg., Austin, TX 78712-1076

²Graduate Research Asst., Univ. of Texas, Dept. of Civil Engrg., Austin, Texas 78712-1076

³Associate Prof., Natl. Taiwan Inst. of Technology, Dept. of Construction Engrg., Taipei 10772, Taiwan, ROC

ABSTRACT

Seismic measurements can be performed in soil confined in calibration chambers to evaluate the small-strain shear and constrained moduli of the soil and the variation of moduli with direction. Geophones placed in the soil during sample construction can be used as seismic sources and receivers. Typical measurements in dry sand confined in a 2.1-m cubical chamber are used to illustrate this approach. Inherent and stress-induced anisotropy in the sand are clearly identified with these measurements. A cross-anisotropic model is used to represent the sand under both isotropic loading and biaxial loading with equal principal horizontal stresses. In both loading cases, the horizontal plane is a plane of isotropy. The seismic measurements required to evaluate the five independent elastic constants in a cross-anisotropic model are discussed.

INTRODUCTION

Many calibration chambers (CC) are in use today. The chambers are generally used to load carefully constructed samples of soil with known boundary conditions. Models or prototype systems are then inserted into the soil to evaluate their performance in a known geotechnical environment. Evaluation of the performance of in situ devices are typical uses of calibration chambers, with the most well known results in the U.S. probably the Gibbs and Holtz (1957) SPT relationships and the Schmertmann (1976) CPT relationships.

Most calibrations chambers have the shape of a right circular cylinder and thus can be used to load soil isotropically ($\bar{\sigma}_1 = \bar{\sigma}_2 = \bar{\sigma}_3$) or biaxially ($\bar{\sigma}_1 > \bar{\sigma}_2 = \bar{\sigma}_3$ or $\bar{\sigma}_1 = \bar{\sigma}_2 > \bar{\sigma}_3$). There are a few cubical calibration chambers in use. Cubical chambers have the advantage of being able to load soil under true triaxial ($\bar{\sigma}_1 > \bar{\sigma}_2 > \bar{\sigma}_3$) states of stress as well as isotropically and biaxially. Generally, stress controlled boundaries are used, although a few devices also have strain controlled boundaries (Baldi et al, 1981; and Parkin and Lunne, 1982). The soil most often used in CC testing is a uniform sand which is placed by dry pluviation.

The characteristics of soil in calibration chambers are generally not evaluated in place at any time during testing. An approach based on seismic measurements of body waves, compression and shear waves, is presented herein. The seismic measurements can be performed in the soil at any time during CC testing. The measurements are used to determine the initial tangent shear and constrained moduli of the soil and the variation of moduli with direction in the soil specimen. These measurements permit one to know the small-strain stiffness of the soil and to characterize the anisotropic nature of the soil. It is possible to identify two types of anisotropy with body waves. The first is inherent (or structural) anisotropy which refers to a physical characteristic of the material that is independent of the applied stress. If the material is isotropic and under an isotropic stress condition, then the stiffness should be independent of direction. If the material is anisotropic and under an isotropic stress condition, then the stiffness should depend on direction. Inherent anisotropy is normally associated with the depositional process and grain characteristics (Arthur and Menzies, 1972; and Oda, 1972). The other type of anisotropy is due to the applied stress state and is called stress-induced anisotropy. A biaxial ($\bar{\sigma}_1 = \bar{\sigma}_2 > \bar{\sigma}_3$, or $\bar{\sigma}_1 > \bar{\sigma}_2 = \bar{\sigma}_3$) or true triaxial ($\bar{\sigma}_1 > \bar{\sigma}_2 > \bar{\sigma}_3$) stress condition is associated with stress-induced anisotropy.

The purposes of this paper are: 1. to introduce seismic testing with body waves to evaluate the small-strain stiffness and the anisotropic character of sand, and 2. to introduce a

cross-anisotropic model to simulate the behavior of sand under isotropic and biaxial stress conditions in calibration chambers. A cross-anisotropic (also called transversely isotropic) model is the simplest anisotropic model for this purpose. With this model, it is assumed that one plane, typically the horizontal plane in a CC, is the plane of isotropy. The model requires five independent elastic constants, hence five independent seismic wave measurements. Testing done in the cubical calibration chamber at The University of Texas is used to illustrate the necessary measurements and the applicability of the cross-anisotropic model.

SEISMIC TESTING WITH BODY WAVES

Calibration Chamber

A large cubical calibration chamber was constructed at the University of Texas in 1979 with funding from the United States Air Force Office of Scientific Research (Kopperman et al, 1982; and Knox et al, 1982). The chamber was constructed so that basic studies in seismic wave propagation under three-dimensional states of stress ($\bar{\sigma}_1 > \bar{\sigma}_2 > \bar{\sigma}_3$) could be conducted. Therefore, the chamber was constructed as a cubical chamber, rather than the cylindrical shape of most chambers. With this chamber, 7-ft (2.15-m) cubes of dry sand can be loaded under various states of isotropic, biaxial and true triaxial stresses, with principal effective stresses ranging from 4 psi (27 kPa) to about 45 psi (310 kPa).

The cubical calibration chamber is referred to as the large-scale triaxial chamber (LSTC). The chamber is simply a free-standing, heavily reinforced steel box. Equipment associated with the LSTC is shown in Fig. 1. Each wall of the triaxial chamber is designed to represent a principal plane so that axes perpendicular to the walls of the device represent principal directions. To permit independent control of the pressure in each of the three principal directions, confining pressures are applied to the soil mass using six membranes placed on the inside of each wall; one on both the top and bottom and one on each of the four sides. Each membrane has two ports located at diagonal corners so that water can be allowed to fill up or drain from the membrane. When the membranes are full of water, air pressure is used to pressurize them. Plastic sheets with grease between the sheets are placed between the soil and membranes to minimize any shearing stresses which might tend to develop on any of the membranes. Therefore, this chamber is designed to operate only with stress controlled boundaries.

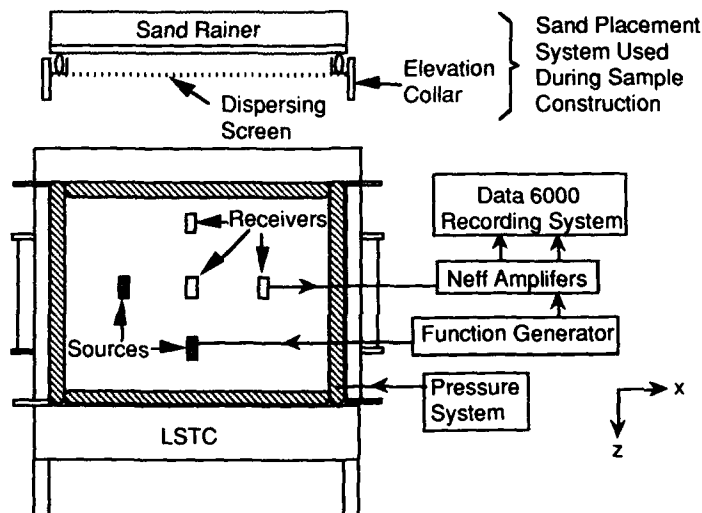


Fig. 1. Diagrammatic Sketch of Experimental Set-Up for Seismic Wave Testing in the Large Scale Triaxial Chamber (LSTC).

Sources, Receivers and Recording Equipment

Seismic instruments (geophones) are placed in the LSTC during construction of the soil specimen. The instruments are placed in such a manner that body waves, either compression (P) or shear (S) waves, can be generated and monitored. This arrangement is illustrated in Fig. 2 for measurements along one line in a horizontal plane. To generate compression waves (i.e. body waves whose direction of wave propagation and particle motion are the same), the source and receivers are placed so that the axis of motion of each instrument is aligned with the direction of wave propagation as illustrated in Fig. 2a. To generate shear waves, (i.e. body waves whose direction of particle motion is perpendicular to the direction of wave propagation), the source and receivers are placed so that the axis of motion of each instrument is perpendicular to the direction of wave propagation. However, two types of shear waves, namely SH- and SV-waves, can be generated and monitored in a horizontal plane. For SH-waves, wave propagation and particle motion are both contained in the horizontal plane. Therefore, geophones are placed as illustrated in Fig. 2b. For SV-waves, wave propagation is in the horizontal plane while particle motion is in the vertical plane. Therefore, geophones are placed in the horizontal plane but oriented vertically as shown in Fig. 2c.

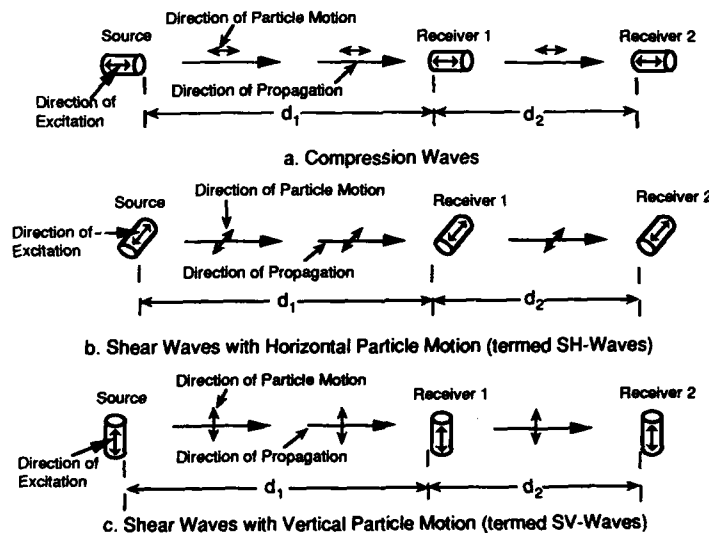


Fig. 2. Illustration of Geophone Arrangement Used for Generation and Measurement of Body Waves Propagating in a Horizontal Direction.

In this work, geophones (also called velocity transducers) were used as both sources and receivers for the first time. Geophones with natural frequencies in the range of 40 to 100 Hz were found to work well. For a geophone to operate as a source, a waveform of a given frequency, amplitude and number of cycles is sent to the geophone using a function generator and amplifier as shown in Fig. 1. The generated waves in the soil are monitored with similar geophones at known distances from the source. Input and output waveforms are recorded and interpreted with various electronic devices. A Data 6000 digital oscilloscope was used to capture the waveforms and store them on floppy disks for later analysis.

To excite the geophone source, a sine wave with a frequency ranging from 1000 to 4000 Hz was used. Generally two to four cycles of excitation at a peak voltage from 10 to 25 V was sent to the source. For the soil (dry sand) tested, this input created wavelengths ranging from approximately 0.3 to 1 ft (0.09 to 0.31 m), which resulted in the shortest wavelength being more than about four times the least dimension of the receiver. To minimize ambient noise and

enhance the recorded waveform, averaging was employed with the digital recorder. Normally, ten averages were used for each time record. A final record is shown in Fig. 3. It is worth noting that all data were collected before any interference with reflected waves occurred.

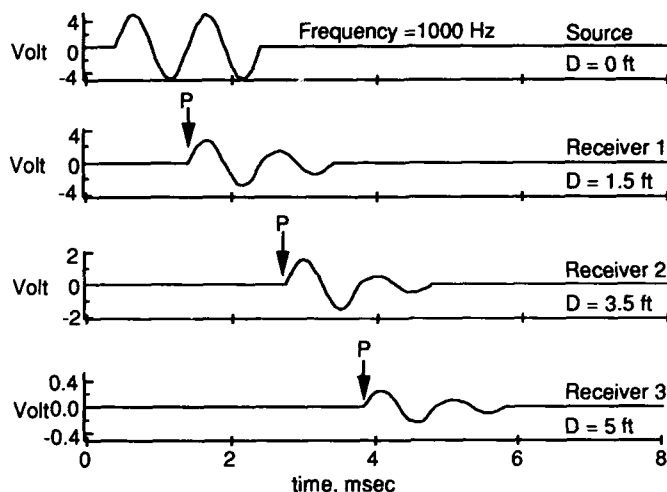


Fig. 3. Typical Time Records for P-Wave Measurements in a Horizontal Plane (Truncated after Two Cycles of Motion).

Wave Velocity Measurements

Once a wave record is obtained, propagation velocity is calculated simply by dividing travel distance by travel time. It should be noted that for all velocity calculations, measurements should be performed in the far field, as shown by Sanchez-Salinero et al (1986). Otherwise, the velocity may be adversely affected by the near-field effect. The near-field effect attenuates to an insignificant level in about two wavelengths from the source. Therefore, to eliminate this effect, the first receiver should be placed at least two wavelengths from the source.

Velocity measurements can be obtained by two methods. The first is called a direct measurement. In this case, velocity is determined by the time measured from the source to a receiver, illustrated by measurement over distance d_1 in Fig. 2. Problems with timing errors, arrival identifications, and system compliances can adversely affect this measurement (Hoar, 1982), and care must be taken in applying this method. The second method is called an interval measurement. In this case, velocity is measured between two receivers along the propagation direction as illustrated by the measurement over distance d_2 in Fig. 2. By using the interval method, the wave arrival time is easier to interpret, and problems associated with the direct measurement are minimized. In this study, only interval measurements were used.

Soil Tested

The soil used in these tests was a medium dense, washed mortar sand which classifies as SP in the Unified Soil Classification System. The sand has a specific gravity of 2.67 and a mean grain diameter of about 0.46 mm. This sand was chosen for several reasons. First, the static and dynamic properties of the sand are independent of loading time. Second, it is easy to handle and place, and when placed by the raining technique, uniform medium dense samples can be duplicated from one sample to the next. Finally, the dynamic properties of dry sand are insensitive to frequency, number of loading cycles, and stress history in the range tested.

The soil sample was prepared by raining the sand through air (pluviation). Raining sand through air has been shown to yield uniform, medium dense samples when the height of fall is 2.5 ft (0.76 m) or greater (Bieganousky and Marcuson, 1976). Therefore, a 7-ft (2.15-m) wide rainer was constructed. The rainer travelled in the east-west direction on a collar which elevated it 3 ft (0.91 m) above the top of the triaxial chamber. With this rainer, uniform sand samples were constructed. The density of the sample used in this study was 101.3 pcf (13.1 kN/m³), with a standard deviation of 2.0 pcf (0.26 kN/m³) (Lee, 1991).

Testing Series

Body wave propagation measurements were performed under various state of stress. The first step was to perform tests with isotropic confinement ($\bar{\sigma}_1 = \bar{\sigma}_2 = \bar{\sigma}_3$). The aim of these tests was to evaluate structural anisotropy. After the effect of isotropic confinement was studied, a biaxial stress state ($\bar{\sigma}_1 > \bar{\sigma}_2 = \bar{\sigma}_3$ or $\bar{\sigma}_1 = \bar{\sigma}_2 > \bar{\sigma}_3$) was then applied. In this stress series, the horizontal stresses were kept constant at 12 psi (83 kPa), and the vertical stress was varied from 6 psi (41 kPa) to 21 psi (145 kPa). The aim of this series was to evaluate stress-induced anisotropy. Additional testing was performed with other series of biaxial stresses and then with a series of true triaxial stresses. However, only a portion of the results are presented herein to illustrate how wave velocities can be used to characterize the stiffness and anisotropic nature of the sand under isotropic and biaxial stress states.

RESULTS OF BODY WAVES PROPAGATING AND POLARIZED ALONG PRINCIPAL STRESS DIRECTIONS

Effect of Isotropic Confinement

The variation in P- and S-wave velocities with isotropic confinement has been studied by Knox et al (1982), Kopperman et al (1982), Chu et al (1984) and Lee and Stokoe (1986) in the past. In these studies, the seismic waves were propagated and polarized along principal stress directions. The authors will not elaborate on these findings again. But for completeness, a summary of results under isotropic (and biaxial) confinement is presented and updated with results from Lee (1991). These studies concluded that the relationship between wave velocity and effective stress can be represented by a power law as :

$$V_p = C_1 \bar{\sigma}_0^m \quad (1)$$

and

$$V_s = C_2 \bar{\sigma}_0^n \quad (2)$$

where V_p = P-wave velocity,
 V_s = S-wave velocity,
 $\bar{\sigma}_0$ = effective isotropic confining pressure,
 C_1 = material constant in compression,
 C_2 = material constant in shear,
 m = slope of $\log V_p - \log \bar{\sigma}_0$ relationship, and
 n = slope of $\log V_s - \log \bar{\sigma}_0$ relationship.

The results from one series of tests in this study (Lee, 1991) are shown in Fig. 4. These results are in agreement with the earlier studies. From the figure, structural anisotropy is most easily shown with the P-wave velocities, i.e. velocities of the two horizontally propagating P-waves (V_{xx} and V_{yy}) are about equal and are higher than the velocity of the vertically propagating P-wave (V_{zz}). Hence, the horizontal plane can be modelled as the plane of isotropy as discussed in the section on cross-anisotropy. The shear wave velocities also show this result but with slightly more scatter. The SH-wave that is confined to the horizontal plane exhibits a higher velocity (V_{xy}) than the other shear waves which involved deformations in the vertical plane (V_{yz} and V_{zx}) and which have velocities that are more nearly equal.

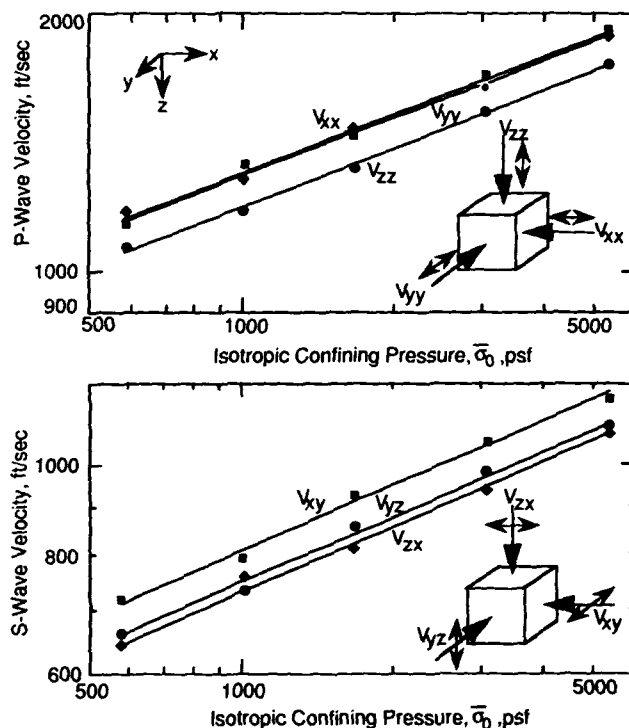


Fig. 4. Variation in P- and S-Wave Velocities Along the Three Principal Stress Directions Under Isotropic Loading.

Effect of Biaxial Confinement

One set of results from the biaxial confinement series (Lee, 1991) is shown in Fig. 5. In this series, the principal stresses in X- and Y-directions were held constant at 12 psi (83 kPa), while the principal stress in the Z-direction was varied from 6 psi (41 kPa) to 21 psi (145 kPa). The results in the figure show that P-wave velocities in the horizontal plane, V_{xx} and V_{yy} , were essentially unchanged. However, the P-wave velocity in the vertical direction, V_{zz} , varied with stress in the same manner as under isotropic confinement. These results suggest that P-wave velocity is only related to the effective principal stress in direction of wave propagation as:

$$V_p = C_1 \bar{\sigma}_a^{ma} \quad (3)$$

where $\bar{\sigma}_a$ = effective principal stress in the direction of wave propagation,
 C_1 = material constant in compression, and
 ma = slope of the $\log V_p - \log \bar{\sigma}_a$ relationship.

Shear wave velocities under biaxial confinement are more complex than P-wave velocities. The S-wave contained in the horizontal plane exhibited a velocity (V_{xy}) which remained essentially constant, since the confining pressures in the direction of wave propagation and particle motion (X- and Y-axes) were both held constant. The second group of S-waves exhibited velocities (V_{yz} and V_{zx}) which varied with stress in the Z-direction. This may be explained by the fact that only one stress in either the direction of wave propagation or particle

motion varied under this state of biaxial loading. These results lead to the following simplified equation [patterned after Roesler (1979)]:

$$V_s = C_2 \bar{\sigma}_a^{na} \bar{\sigma}_b^{nb} \quad (4)$$

where $\bar{\sigma}_a$ = effective principal stress in the direction of wave propagation,
 $\bar{\sigma}_b$ = effective principal stress in the direction of particle motion,
 na = slope of the $\log V_s - \log \bar{\sigma}_a$ relationship, and
 nb = slope of the $\log V_s - \log \bar{\sigma}_b$ relationship.

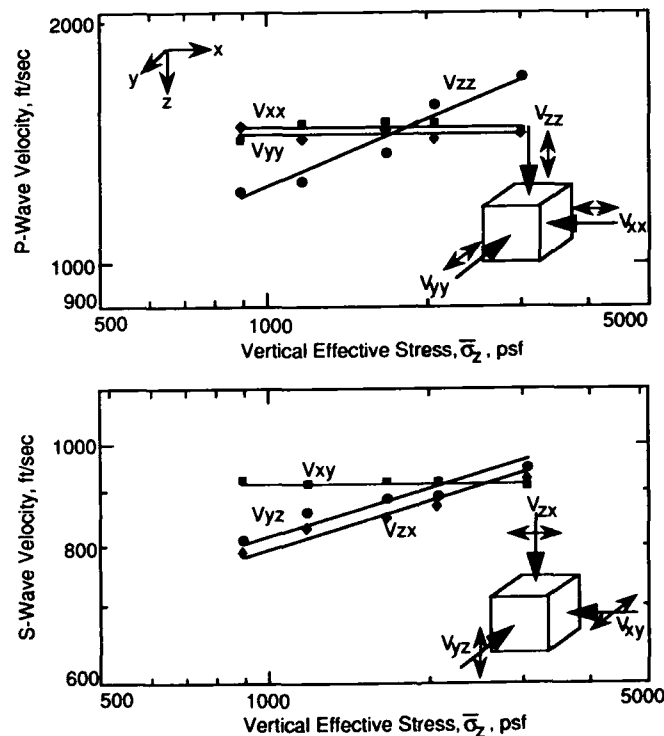


Fig. 5. Variation in P- and S-Wave Velocities Along the Three Principal Stress Directions Under Biaxial Loading with Only the Vertical Effective Stress Changing.

RESULTS OF COMPRESSION WAVES PROPAGATING AND POLARIZED ALONG OBLIQUE DIRECTIONS TO THE PRINCIPAL STRESSES

The results of compression wave tests in this study (Lee, 1991) are the most complete to date. The completeness is due to the fact that waves were not only propagated and polarized along principal stress directions but also along five oblique directions to the principal stresses. Two cases are considered herein. The first case is for isotropic loading under a confining pressure of 12 psi (83 kPa). The second case is for biaxial loading with the horizontal stresses equal to 12 psi (83 kPa) and a vertical stress of 7 psi (48 kPa). In both cases, only the results from P-wave testing are shown because the thrust of this was directed towards compression wave measurements.

Isotropic Confinement

In the experimental set-up, it was possible to determine the velocities of P-waves propagating in seven different directions in both the horizontal plane and the vertical plane. These measurements allowed one to create a wave surface, a diagram showing how ray velocity varies with direction of propagation. Ray velocities are those velocities determined directly from the velocity measurements, distance divided time. In the horizontal plane, ray velocities in all seven directions are essentially equal (within the scatter expected in the measurements) as shown in Fig. 6a. Hence, the wave surface in this plane can be represented by a circle drawn through the data as shown in the figure. These results show that the horizontal plane is a plane of isotropy. Similarly, a wave surface can be defined by the ray velocities in the vertical plane as shown in Fig. 6b. In this plane, the data form an elliptical wave surface. The same circle representing the uniform velocities in the horizontal plane is drawn for comparison. The measurements show that compression wave velocity in the vertical direction is smaller than compression wave velocity in the horizontal direction, even though the specimen is under an isotropic confining stress. The ratio between the horizontal and vertical compression wave

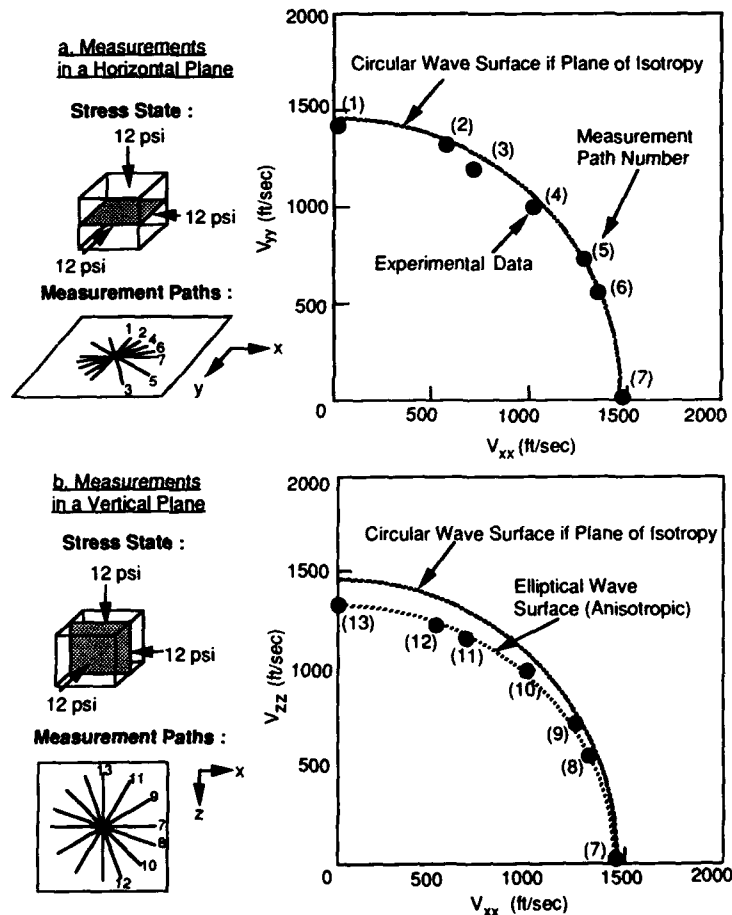


Fig. 6. Variation in P-Wave Velocities with Propagation Direction for Measurements in the Horizontal and Vertical Planes Under Isotropic Loading.

velocities is 1.10. The figure also shows that as the angle from vertical increases, the compression wave velocity increases. This change occurs because of structural anisotropy which is clearly determined by the seismic tests.

Biaxial Confinement

Wave surfaces for P-waves propagating in the horizontal and vertical planes were also developed under biaxial loading. For this case, the horizontal effective stresses were maintained constant at 12 psi (83 kPa). The wave surface in the horizontal plane, shown by the circle in Fig. 7a, remained essentially identical to the wave surface determined under an isotropic confinement of 12 psi (83 kPa). This result supports the point that compression wave velocity depends only on the principal stress in the direction of wave propagation. The shape of the wave surface in the vertical plane is shown by the data points in Fig. 7b. The shape is still elliptical as it was under isotropic loading. However, the velocities of the vertically propagating and obliquely propagating P-waves are smaller than when the isotropic stress condition was applied, showing the effect of stress-induced anisotropy. The ratio between the horizontal and vertical P-wave velocities has increased to 1.18.

The wave surfaces shown in Fig. 7 also support the previous discussion that, for P-waves propagating along principal stress directions, P-wave velocity is dependent only on the principal stress in the direction of wave propagation. However, the elliptical wave surface in Fig. 7b (and also in Fig. 6b) shows that measurement of P-waves propagating at oblique directions to the principal stresses do not relate as simply to the elastic moduli of the material as P-waves measured along principal stress directions. This point is addressed in the next section dealing with a cross-anisotropic model.

CROSS-ANISOTROPIC MODEL

Based on the preceding results showing the shapes of the wave surfaces in the horizontal and vertical planes, the horizontal plane is demonstrated to be a plane of isotropy (i.e. constrained and shear moduli are independent of direction in this plane under isotropic and biaxial loadings). However, the vertical plane is a plane in which stiffness varies with directions, hence it is anisotropic. For such a system, the simplest anisotropic model one can use was suggested by Love (1892) which is a cross-anisotropic model, also called a transversely isotropic model. This model requires five independent elastic constants to describe the material. The stress-strain relationship can be expressed as follows:

$$\begin{Bmatrix} \sigma_x \\ \sigma_y \\ \sigma_z \\ \tau_{xy} \\ \tau_{yz} \\ \tau_{zx} \end{Bmatrix} = \begin{bmatrix} C_{11} & C_{12} & C_{13} & 0 & 0 & 0 \\ C_{12} & C_{11} & C_{13} & 0 & 0 & 0 \\ C_{13} & C_{13} & C_{33} & 0 & 0 & 0 \\ 0 & 0 & 0 & C_{44} & 0 & 0 \\ 0 & 0 & 0 & 0 & C_{66} & 0 \\ 0 & 0 & 0 & 0 & 0 & C_{66} \end{bmatrix} \begin{Bmatrix} \epsilon_x \\ \epsilon_y \\ \epsilon_z \\ \gamma_{xy} \\ \gamma_{yz} \\ \gamma_{zx} \end{Bmatrix} \quad (5)$$

where C_{11} = constrained modulus in the isotropic (horizontal) plane, M_H ,
 C_{33} = constrained modulus in the anisotropic (vertical) plane, M_V ,
 C_{44} = shear modulus in the isotropic (horizontal) plane, G_{HH} ,
 C_{66} = shear modulus in the anisotropic (vertical) plane, G_{HV} , and
 C_{13} = fifth independent elastic constant determined by propagating a body wave at an oblique direction or measuring a modulus at an oblique direction.

The dependent variable C_{12} can be determined from the following relationship:

$$C_{12} = C_{11} - 2C_{44} \quad (6)$$

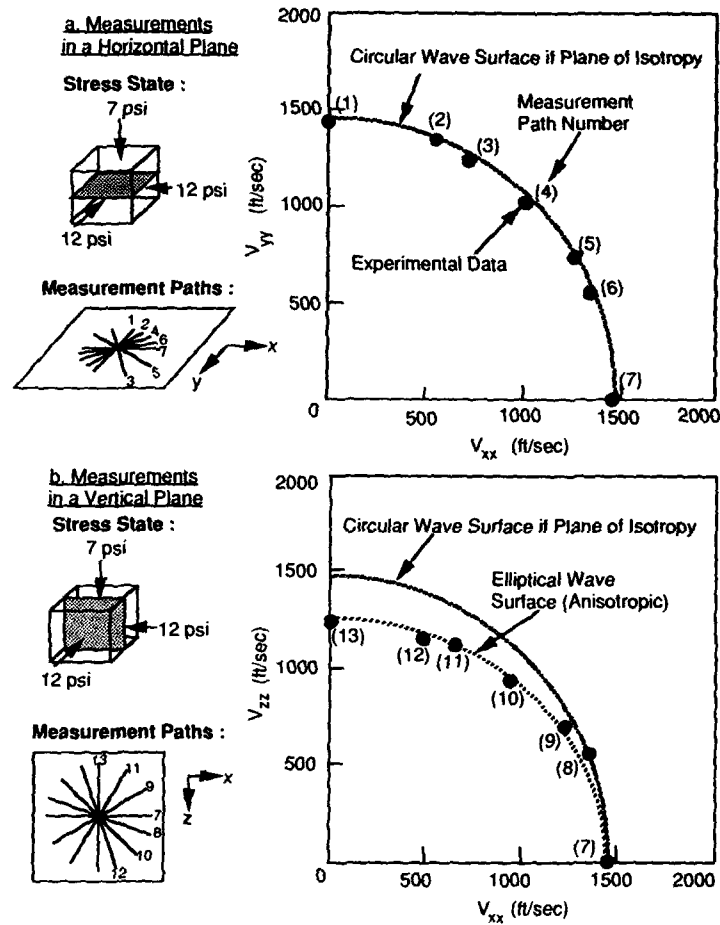


Fig. 7. Variation in P-Wave Velocities with Propagation Direction for Measurements in the Horizontal and Vertical Planes Under Biaxial Loading.

Four of the five elastic constants in a cross-anisotropic model can be determined from seismic body wave velocities along principal stress directions as follows:

$$M_v = \rho V_{zz}^2 \quad (7)$$

$$M_H = \rho V_{xx}^2 = \rho V_{yy}^2 \quad (8)$$

$$G_{HH} = \rho V_{xy}^2 = \rho V_{yx}^2 \quad (9)$$

$$G_{HV} = \rho V_{xz}^2 = \rho V_{yz}^2 = \rho V_{zx}^2 = \rho V_{zy}^2 \quad (10)$$

where ρ = mass density of soil = γ/g (where γ is the total unit weight and g is gravitational acceleration).

M_v = constrained modulus in the vertical plane (in the anisotropic plane),

M_H = constrained modulus in the horizontal plane (in the isotropic plane),

G_{vH} = shear modulus in the vertical plane.

- G_{HH} = shear modulus in the horizontal plane,
 V_{zz} = compressional wave velocity in the vertical direction,
 V_{xx} or V_{yy} = compressional wave velocity in either horizontal direction,
 V_{xz} or V_{yz} = shear wave velocity in the vertical plane for either horizontally propagating wave,
 V_{zx} or V_{zy} = shear wave velocity in the vertical plane for either vertically propagating wave, and
 V_{yx} or V_{xy} = shear wave velocity for either wave contained in the horizontal plane.

It must be noted that: 1. all velocities listed above are for stress waves propagating and polarized along principal stress directions, 2. the principal stress directions are horizontal and vertical, and 3. the horizontal plane is the plane of isotropy. The associated seismic measurements in a calibration chamber are illustrated as direct measurements in Fig. 8.

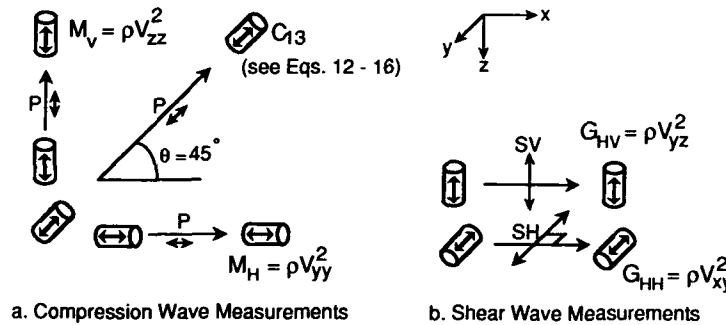


Fig. 8. Body Wave Measurements Required to Determine the Five Elastic Constants of a Cross-Anisotropic Material When the Horizontal Plane is the Plane of Isotropy.

To obtain the fifth elastic constant, one needs to understand a particular property in anisotropic wave theory. Consider a point source generating a seismic wave in an isotropic full space. After a unit time, a wave surface is generated as shown in Fig. 9a. If the material is isotropic, the wave surface is a circle as shown, and the phase velocity equals the wave velocity (also called ray velocity). The phase velocity is the velocity of the wave normal to the wave surface. But in an anisotropic medium, the wave surface is no longer circular as shown in Fig. 9b. The velocity which we obtained experimentally is the ray velocity. However, the phase velocity is the velocity required to calculate the elastic constants. Therefore, it is necessary to convert the ray velocity to phase velocity by the following relationship:

$$\text{Phase velocity} = \text{Ray velocity} \cdot \cos \psi \quad (11)$$

Once we obtained the phase velocity and the angle from the vertical of the ray path, θ , the fifth elastic constant can be obtained from the following expression:

$$V_p(\theta) = \sqrt{(p + q)/2\rho} \quad (12)$$

$$p = C_{11} \sin^2 \theta + C_{33} \cos^2 \theta + C_{66} \quad (13)$$

$$\text{and } q = \sqrt{[(C_{11} - C_{66}) \sin^2 \theta - (C_{33} - C_{66}) \cos^2 \theta]^2 + (C_{13} - C_{66})^2 \sin^2 \theta \cos^2 \theta} \quad (14)$$

If θ is 45° , as shown in Fig. 8, the equation can be simplified to:

$$p = \frac{C_{11} + C_{33}}{2} + C_{66} \quad (15)$$

$$q = \sqrt{0.5 (C_{11} - C_{33})^2 + (C_{13} - C_{66})^2} \quad (16)$$

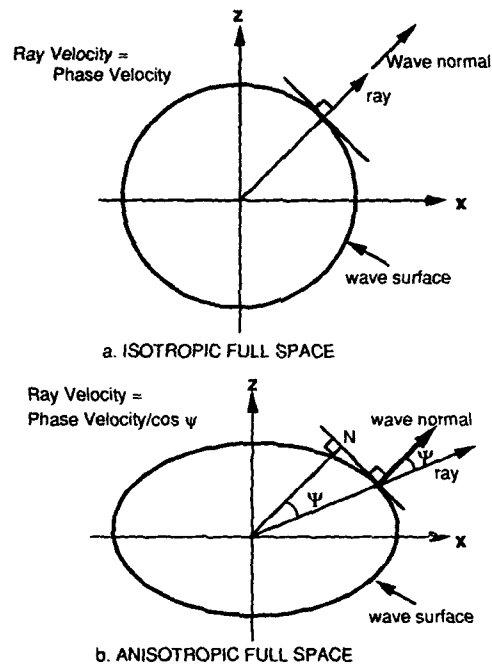


Fig. 9. Directions of Ray and Wave Normal on the Wave Surface from a Point Source in Isotropic and anisotropic Full Spaces.

Numerical Example

To illustrate how to obtain the elastic constants for a cross-anisotropic model, the results from the two examples described previously in isotropic and biaxial loading are shown in Table 1. It should be noted that ray and phase velocities in the principal stress directions are equal. This is not true for P-waves propagating in oblique directions as indicated in Table 1. The fifth elastic constant is determined by the phase velocity. To complete all elastic constants needed to model a cross-anisotropic material, the dependent variable C_{12} is also included in the table.

Table 1. Elastic Constants for a Cross-Anisotropic Model from Seismic Wave Velocities

Elastic Constant to be Determined	Isotropic Loading $\bar{\sigma}_1 = \bar{\sigma}_2 = \bar{\sigma}_3 = 12 \text{ psi}$			Biaxial Loading $\bar{\sigma}_1 = \bar{\sigma}_2 = 12 \text{ psi}; \bar{\sigma}_3 = 7 \text{ psi}$		
	Ray Velocity (fps)	Phase Velocity (fps)	Value of Elastic Constant (psf x 10^6)	Ray Velocity (fps)	Phase Velocity (fps)	Value of Elastic Constant (psf x 10^6)
$C_{11} = M_V$	1317	1317	5.45	1230	1230	4.76
$C_{33} = M_H$	1451	1451	6.62	1451	1451	6.62
$C_{44} = G_{HH}$	914	914	2.63	923	923	2.68
$C_{66} = G_{VV}$	825	825	2.14	834	834	2.19
C_{13}	1403	1378	10.09	1330	1306	9.05
C_{12}	-	-	0.19	-	-	0.38

CONCLUSIONS

Compression and shear wave velocities can be measured at selected times during calibration chamber testing by placing geophones in the soil during sample construction. The geophones are used as both seismic sources and receivers. Small-strain shear and constrained moduli of the soil sample and the variation of moduli with direction are determined. With these measurements, both structural and stress-induced anisotropy can be identified.

For seismic testing under isotropic ($\bar{\sigma}_1 = \bar{\sigma}_2 = \bar{\sigma}_3$) or biaxial ($\bar{\sigma}_1 > \bar{\sigma}_2 = \bar{\sigma}_3$ or $\bar{\sigma}_1 = \bar{\sigma}_2 > \bar{\sigma}_3$) stress states, the sand in the large-scale triaxial chamber could be modelled as a cross-anisotropic material. In both of these loading cases, the horizontal plane was the plane of isotropy. This result was clearly shown by compression wave measurements in the horizontal and vertical planes. A minimum of five independent seismic measurements, three involving P-waves and two involving S-waves, is required to characterize the sand as a cross-anisotropic material.

ACKNOWLEDGEMENTS

The authors would like to thank the United States Air Force Office of Scientific Research at Bolling Air Force Base for supporting this research. Major John J. Allen was the initial project manager after which Lt. Col. Dale Hokanson assumed the project management. The support, encouragement and guidance of the project managers is greatly appreciated. Dr. Jose M. Roesset actively and continuously contributed to the work. His insight and suggestions were significant and much appreciated. Finally, the help of the many graduate students who participate in this work is sincerely appreciated!

REFERENCES

1. Arthur, J. R. F. and Menzies, B. K. (1972), "Inherent Anisotropy in a Sand," *Geotechnique* 22 No. 1, pp. 115-128.
2. Baldi, G., Bellotti R., Ghionna, V., Jamiolkowski, M. and Pasqualini, E. (1981), "Cone Resistance of a Dry Medium Sand," X ICSEFE, Stockholm.
3. Bieganousky, W.A. and Marcuson, W.F., III (1976), "Uniform Placement of Sand," *J. of Geotechnical Engineering Division, American Society of Civil Engineers*, Vol. 102, No. GT3, March, pp. 229-233.
4. Chu, H. Y. F., Lee, S. H. H., and Stokoe, K. H., II (1984), "Effects of Structural and Stress Anisotropy on Velocity of Low-Amplitude Compression Wave Propagating Along Principal Stress Directions in Dry Sand," *Geotechnical Engineering Report GR84-6*, Department of Civil Engineering, The University of Texas at Austin.
5. Gibbs, H. J. and Holtz, W. G. (1957), "Research on Determining the Density of Sands by Spoon Penetration Testing," *Proc. 4th International Conference Soil Mechanics and Foundation Engineering*, London, 1 pp. 35-39.
6. Hoar, R. J. (1982), "Field Measurement of Seismic Wave Velocity and Attenuation for Dynamic Analyses," Ph.D. Dissertation, Department of Civil Engineering, The University of Texas at Austin.
7. Knox, D. P., Stokoe, K. H., II, and Kopperman, S. E. (1982), "Effect of State of Stress on Velocity of Low-Amplitude Shear Waves Propagating Along Principal Stress Directions in Dry Sand," *Geotechnical Engineering Report GR82-23*, Department of Civil Engineering, The University of Texas at Austin.
8. Kopperman, S. E., Stokoe, K. H., II, and Knox, D. P. (1982), "Effect of State of Stress on Velocity of Low-Amplitude Compression Waves Propagating Along Principal Stress Directions in Dry Sand," *Geotechnical Engineering Report GR82-22*, Department of Civil Engineering, The University of Texas at Austin.
9. Lee, N.J. (1991), "Inherent and Stress-Induced Anisotropy of Sand Determined by Body Wave Velocities," Ph.D. Dissertation, Department of Civil Engineering, The University of Texas at Austin (in progress).

10. Lee, S. H. H., and Stokoe, K. H., II (1986), "Investigation of Low-Amplitude Shear Wave Velocity in Anisotropic Material," Geotechnical Engineering Report GR 86-6, Department of Civil Engineering, The University of Texas at Austin.
11. Love, A. (1892), "A Treatise on the Mathematical Theory of Elasticity," Chapter 6, pp. 149-165.
12. Oda, M. (1972), "Initial Fabrics and Their Relations to Mechanical Properties of Granular Material," Soils and Foundations, 12(2), pp. 1-28.
13. Parkin, A.K., and Lunne, T. (1982), Boundary Effects in the Laboratory Calibration of a Cone Penetrometer for Sand," Proceedings, Second European Symposium on Penetration Testing, Amsterdam.
14. Roesler, S. (1979), "Anisotropic Shear Modulus Due to Stress Anisotropy," Journal of Geotechnical Engineering Division, American Society of Civil Engineers, Vol. 105, GT7, pp. 871-880.
15. Sanchez-Salinero, I., Roesset, J.M. and Stokoe, K.H., II (1986), "Analytical Studies of Body Wave Propagation and Attenuation," Geotechnical Engineering Report GR86-15, Department of Civil Engineering, The University of Texas at Austin.
16. Schmertmann, J. H. (1978), "An Updated Correlation Between Relative Density, D_r , and Fugro-Type Electric Cone Bearing, q_c ," U.S. Waterways Experiment Station, Contract Report DACW 29-76-M6646.

MINIATURE PIEZOCONE PENETRATION TESTS ON SOFT SOILS IN A CALIBRATION CHAMBER SYSTEM

GEORGE Z. VOYIADJIS¹, MEHMET T. TUMAY², AND PRADEEP U. KURUP³
Department of Civil Engineering, Louisiana State University, Baton Rouge, LA 70803

ABSTRACT

This paper describes miniature piezocone penetration tests in cohesive samples of known stress history in a calibration chamber system. The design features of the slurry consolidometer is described as is the technique to prepare large cohesive samples instrumented to monitor spatial pore pressure distribution. Additionally, the characteristics of the LSU calibration chamber system and its capabilities are briefly summarized. The penetration profiles and the dissipation test results are presented.

INTRODUCTION

The use of the electronic cone penetrometer test (CPT) with pore pressure monitoring capability to enhance assessment of engineering parameters of soils is still at an early stage of development. Measurements of pore water pressures generated while advancing a probe into the ground, and their subsequent dissipation were first made in Sweden in the early 1970's by Wissa et al. [1] and Torstensson [2]. No simultaneous measurements of cone resistance, sleeve friction and pore pressures were feasible at that time. During 1969-73, the Norwegian Institute of Technology used a piezometric probe which could measure only pore pressures. It was necessary to carry out separate CPT's in order to combine measurements of pore pressure and cone resistance [3]. Subsequent development in transducer technology during the late 1970's involved the incorporation of piezometric elements into the standard electric cone penetrometers which made simultaneous measurements of pore pressures, cone resistance and sleeve friction possible [4-7].

Calibration chamber tests for calibrating cone penetrometers, pressuremeters and dilatometers in cohesionless samples have been carried out in the past by a number of investigators. However, their application to cohesive samples has been limited [8,9]. Piezocone penetration tests (PCPT) in cohesive soils have been primarily in-situ tests and reference test parameters obtained from conventional laboratory tests on undisturbed samples were used for calibration purpose. In spite of the care taken, samples obtained from the field are subject to disturbances during the sampling and handling process prior to laboratory testing. This paper describes miniature piezocone penetration tests in cohesive samples of known stress history in a calibration chamber system. The design features of the slurry consolidometer is described as is the technique to prepare large cohesive samples instrumented to monitor spatial pore pressure distribution. Additionally, the characteristics of the LSU calibration chamber system and its capabilities are briefly summarized.

¹Professor of Civil Engineering

²Professor of Civil Engineering and currently Director of Geomechanics Program, National Science Foundation, Washington, D.C.

³Doctoral Candidate

TESTING EQUIPMENT

Slurry Consolidometer

The slurry consolidation technique has been used in the past by Krizek and Sheeran [10], Huang [8] and Bunting [9]. The LSU slurry consolidometer designed by the authors is similar to that designed by Bunting [9]. There are, however, significant differences specifically related to the loading system. The slurry consolidometer (Figure 1) consists of two PVC tubes having an inside diameter of 525 mm and height 812.8 mm. The base plate is made of aluminum, 25 mm thick and 525 mm in diameter. Eight pore pressure access ducts connected to pressure transducers extend through the base plate into the soil. The lower tube is split longitudinally into two halves which are held together by a metal frame. The upper tube is bolted to the lower one using six steel rods connecting an aluminum top lid to the bottom base frame. This assembly acts as a reaction frame for the loading system.

The loading system consists of a reaction frame with a hydraulic jack bolted to the top lid. The jack is powered by an air-hydraulic pump. The pump has an automatic pressure make-up feature. With the air pressure continuously applied to the air motor controlled through a regulator, the pump will cycle automatically whenever circuit pressure drops below the pump stall pressure. This feature enables the stress to be maintained

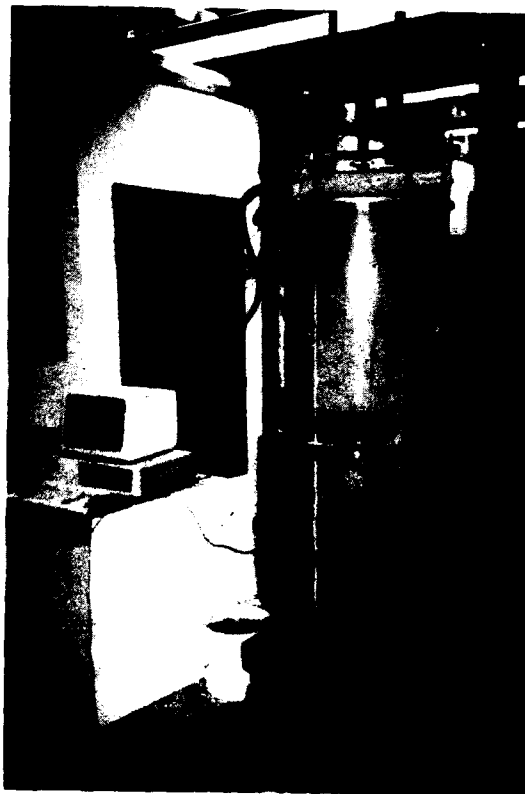


Figure 1. Slurry consolidometer.

constant at the desired level as the soil consolidates. Load from the jack is transferred to the soil through a steel rod and an aluminum piston plate. The piston plate and the aluminum base plate have porous plastic discs attached to one end. There are connections on the plate to permit two-way drainage. An LVDT connected to the piston rod measures the vertical deformation of the sample during the consolidation phase. The data acquisition software developed in Pascal, acquires and appends data (pore pressures and deformation) into a file and also displays the data on a computer screen in a graphic form (plotted against log time in seconds) during the slurry consolidation process.

The loading system designed by Bunting [9] uses inflatable inner truck tubes pressing against a rigid plate. The measured internal pressure of the tubes as obtained by Bunting [9] does not necessarily provide the normal contact stress applied by the rigid plate on the soil.

Calibration Chamber System

The Louisiana State University Calibration Chamber System (Figure 2) (LSU/CALCHAS) designed by de Lima [11] and Tumay and de Lima [12] consists of a calibration chamber, a panel of controls, a data acquisition system, a hydraulics and chucking system, a penetration depth measurement system and the cone penetrometers. The LSU/CALCHAS was initially designed to test compacted samples and was able to simulate K_0 consolidation and the four traditional boundary conditions commonly referred in literature as:

- BC1: Constant vertical stress and constant lateral stress
- BC2: Zero vertical strain and zero lateral strain
- BC3: Constant vertical stress and zero lateral strain
- BC4: Zero vertical strain and constant lateral stress

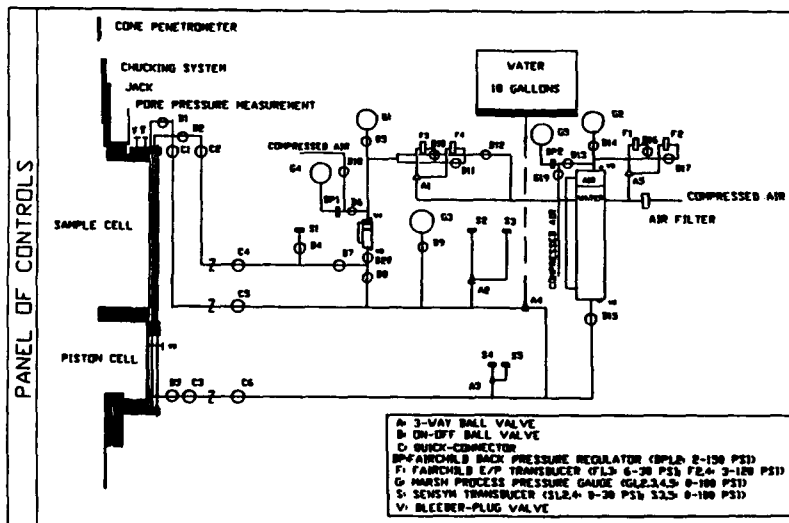


Figure 2. Schematic layout of LSU/CALCHAS.

Modifications and additions were made by the authors to the CALCHAS to adapt it for the testing of soft cohesive soils. Additions were made to the panel of controls which included a back pressure system to saturate soft cohesive samples. The data acquisition software was written to permit piezocone penetration testing in samples instrumented to monitor spatial pore pressure distribution. With the above enhancements it was possible to conduct consolidation and test at a variety of stresses.

The calibration chamber (Figure 3) is a double walled flexible chamber that can house samples 525 mm in diameter and 810 mm in height. Its walls are made out of 6.35 mm thick stainless steel 304 plates rolled into cylindrical shells, 910 mm high. The internal diameter of the inner and outer walls are 558 mm and 584 mm, respectively. The sample top and bottom plates are made of 6061T-6 aluminum and is 525 mm in diameter and 38 mm thick. The sample bottom plate rests on a piston cell ring made of 6061T-6 aluminum. The sample top plate is bolted to the chamber top plate 635 mm in diameter and 38 mm thick. The chamber top plate, sample cell inner and outer walls, and the piston cell ring are connected together using twelve stainless steel rods.

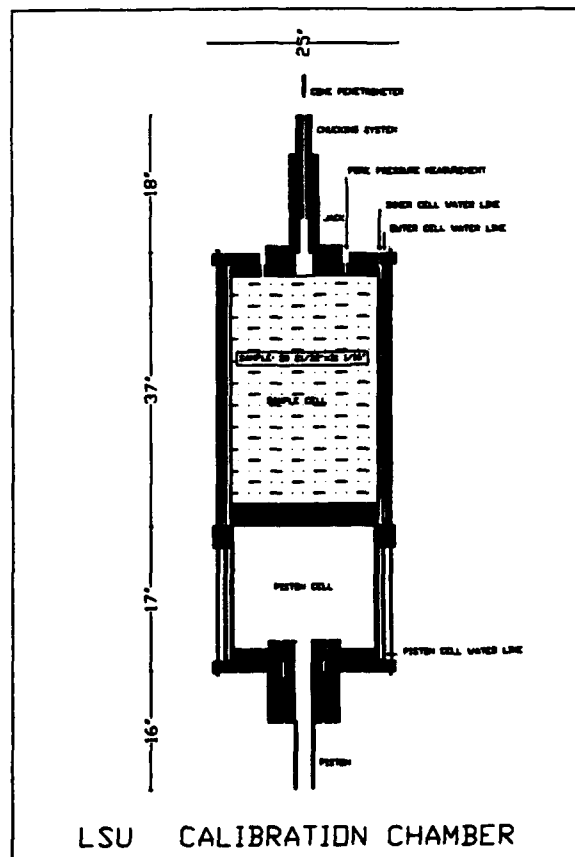


Figure 3. Cross-section of the calibration chamber.

The original hydraulic system was modified and made as collapsible push jack 2,140 mm in height in its extended state. It is mounted on top of the top lid of the chamber. It allows for penetrating the sample in a single stroke of 640 mm. Such a single stroke continuous penetration is desirable especially in saturated cohesive samples where stress relaxation and pore pressure dissipation can occur during a pause in between strokes. The penetration depth during the penetration phase is measured using an electronic analog to digital converter, depth decoding system.

The panel of controls is designed to allow servo control of the testing process. It consists of four Fairchild model T-5700 electro-pneumatic transducers for independent control of the vertical and horizontal stresses by D/A signals sent from an IBM personal computer through a data translation board DT-2801A. The panel also has five SenSym ST2000 pressure transducers and three Marsh process gauges to measure the vertical and horizontal stresses in the sample. There are two back pressure regulators, on-off valves, air water systems to pressurize the piston and sample cells and to saturate samples under back pressure. More details on the design and operation of the chamber can be found in the dissertation of de Lima [11].

CONE PENETROMETERS

Miniature Piezocone Penetrometer

The miniature piezocone penetrometer used for this test was designed by Fugro-McClelland Engineers B.V., The Netherlands. It has a projected cone area of 100 mm² and a cone apex angle of 60°. The maximum normal load capacity is 5 kN. The penetrometer has two alternatives for the filter location. The choice is available for the filter located in the lowest 1/4 of the cone at the very tip or starting 0.5 mm above the base of the cone and 2 mm vertical height. The filter is made of sintered stainless steel and has a pore size of 30 µm. The pressure transducer has a stainless steel sensing diaphragm and has a measuring range of 3.5 MPa. There is no friction sleeve in the penetrometer. In order to measure sleeve friction, a miniature quasi-static cone penetrometer (MQSC) was used.

MQSC Penetrometer

The Miniature Quasi Static Cone (MQSC) penetrometer is a 127 mm² cross-sectional area subtraction type Fugro-McClelland cone penetrometer, with a friction sleeve 63 mm long and an apex angle of 60°. It measures cone resistance and the combined cone and local side friction resistances. The MQSC push rod has a reduced diameter of 9.53 mm compared to the cone which is 12.72 mm in diameter. This is in contrast to the piezocone penetrometer which has a push rod of the same diameter as the cone.

TEST PROCEDURE

Soil Description

Two different soil mixtures were used to prepare the test specimens. A mixture of 50% kaolinite and 50% Edgar fine sand by weight was used to prepare the K-50 specimen. The K-33 specimen was prepared from a mixture of 33% kaolinite and 64% fine sand. The Atterberg limits of the two soil mixtures are shown in Table 1.

Table 1. Atterberg limits of the soil mixtures.

Soil	Liquid Limit (%)	Plastic Limit (%)	Plasticity Index (%)
K-50	30	16	14
K-33	20	14	6

Slurry Consolidation

The clay specimen was prepared in two stages: (1) Slurry consolidation in a consolidometer from a high water content slurry, and (2) chamber consolidation to higher stresses in a calibration chamber which is free from the rigid boundary effects of a slurry consolidometer. This two stage technique is known to provide high quality cohesive samples [16]. Soil slurry was prepared by mixing kaolinite and fine sand with deionized water at a water content of twice the liquid limit. The mixing was done in two large 40 gallon polyethylene tanks using a heavy duty chemical mixer.

Eight pressure transducers with pore pressure access ducts (made of stainless steel tubes 1.65 mm OD and 0.23 mm wall thickness), were connected to the bottom plate prior to slurry placement. This enabled pore pressure measurements at four different radial distances and at two different heights (390 mm and 570 mm from the top of the sample). The ducts and the transducer ports were saturated by flushing them with deaired water using a closed system CPV 1000 pump. The pressure transducers were assembled keeping it submerged in a tray of deaired water. To ensure complete saturation, the open end of the duct was plugged with saturated porous plastic filter and immersed in deaired water and subjected to vacuum. This method removed traces of microbubbles if any in the system. Slurry was poured into the slurry consolidometer very carefully so as not to entrap any air in it. The aluminum piston plate with the steel rod was placed on top of the slurry in the upper tube of the consolidometer.

Consolidation stress was applied to the soil slurry by loading the top end of the piston rod using a 12 ton hydraulic jack. The sample was normally consolidated to 138 kPa in a period of six weeks. The specimen enclosed in the rubber membrane was then transferred into the calibration chamber where it was consolidated at an isotropic stress of 208 kPa. The consolidation in the chamber was performed against a back pressure of 138 kPa. Cone penetration tests were conducted at the end of the consolidation phase. Table 2 shows the summary of the cone penetration tests.

Reference soil parameters (Table 3) were obtained from tests (consolidated undrained triaxial tests and standard one dimensional consolidation tests) conducted on undisturbed samples obtained from the large specimen.

TEST RESULTS

K-50 Specimen

The piezocone penetration profile for PCPT1 with the filter located at 0.5 mm above the base of the cone is shown in Figure 4. The specimen has an 80 mm thick layer of fine sand at the top which was made loose prior to the cone penetration. The cone resistance and pore

Table 2. Summary of cone penetration tests.

Test	Specimen		Filter Location		Test Location in the Specimen		
	K-50	K-33	0.5 mm above the base	Tip	Center	150 mm from Center	75 mm from Center
PCPT1	X		X			X	
PCPT2	X			X	X		
QCPT	X						X
PCPT3		X	X		X		
PCPT4		X		X		X	

Table 3. Reference soil parameters.

Specimen	Undrained Shear Strength s_u (kPa)	A_f	Rigidity Index I_r	Horizontal Coefficient of Consolidation ($c_h \times 10^{-3} \text{ cm}^2/\text{s}$)
K-50	60*	1.10*	267*	13.3 to 14.9
K-33	80	0.49	100	27 to 29.5

*Data obtained from Dr. Huang, Clarkson University, Potsdam, New York.

pressures during piezocone penetration in the top layer is not shown since they do not reflect the true properties of the layer. However, the cone resistance and sleeve friction in the sand layer were measured using the MQSC penetrometer. It was observed that the penetration induced pore pressures reached a stable value after 90 mm penetration into the clay layer.

The dissipation result D1 for PCPT1 is shown in Figure 5. The excess pore pressure has been normalized as $\Delta u/\Delta u_i$ and plotted against time on a logarithmic scale. Δu is the excess pore pressure at time t and Δu_i is the initial excess pore pressure which is taken as the pore pressure immediately at the end of penetration. It can be observed that the final Δu is greater than zero even after a long time has elapsed because of the impermeable boundaries.

The penetration profile for PCPT2 with the filter located at the tip is shown in Figure 6. This penetration was performed in two strokes. A dissipation test was performed at a depth of 390 mm and subsequently the penetration was continued to a depth of 570 mm where a second dissipation test was conducted. There was an initial increase in the cone resistance when the penetration was resumed following the dissipation test. This is probably due to an increase in the stiffness of the soil due to the consolidation around the cone.

The dissipation result D2 for PCPT2 at a depth of 570 mm is shown in Figure 7. It can be seen that the normalized excess pore pressure at the beginning of the dissipation test

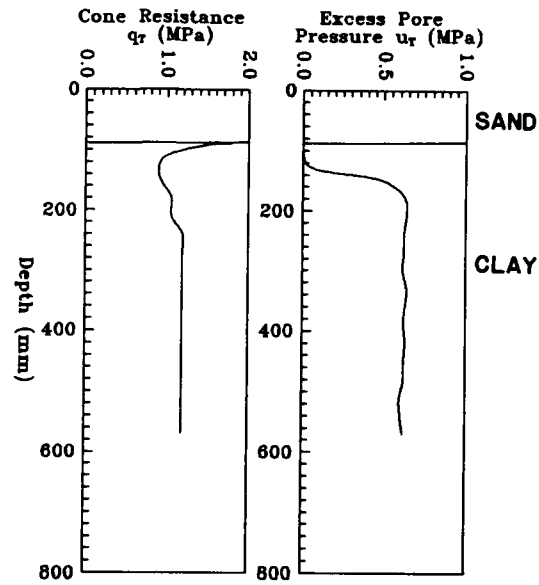


Figure 4. Penetration Profile for PCPT1.

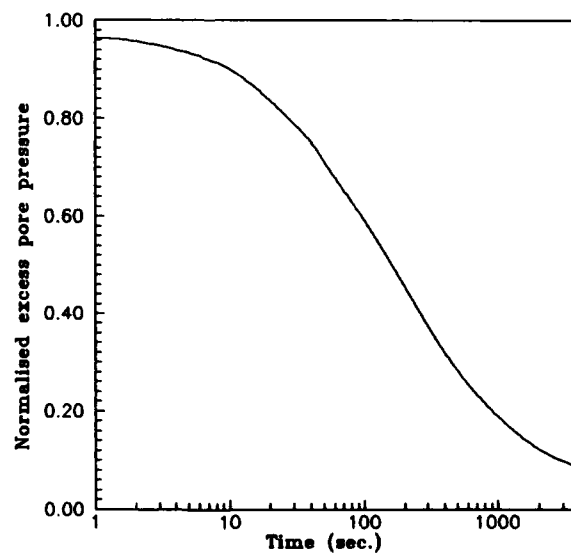


Figure 5. Dissipation result for PCPT1.

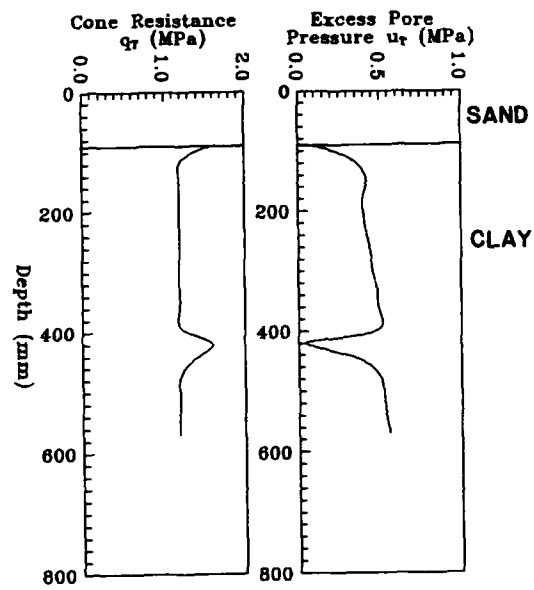


Figure 6. Penetration Profile for PCPT2.

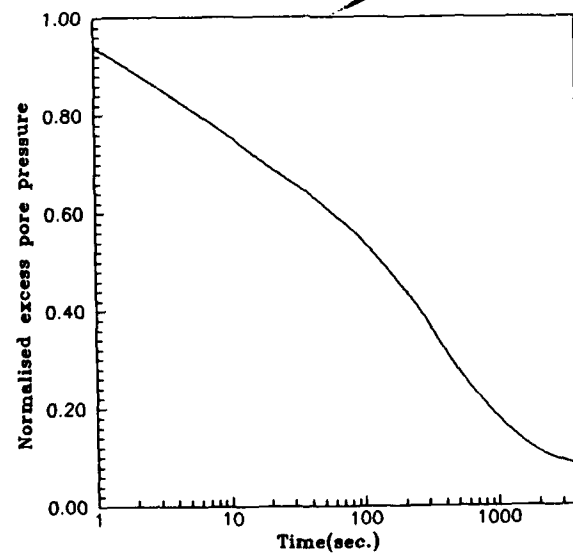


Figure 7. Dissipation result for PCPT2.

D2 is lower than that of test D1. This can be attributed to the normal stress reduction at the tip of the cone when penetration ceases.

The penetration profile for QCPT using the MQSC penetrometer is shown in Figure 8. The cone resistance and the sleeve friction are high while penetrating the sand layer, with subsequently the two values dropping down while penetrating into the clay layer. Both reach a stable value at approximately 100 mm penetration into the clay layer. The interface between the two layers is characterized by a sharp increase in the friction ratio which is the ratio between the sleeve friction and the cone resistance expressed as a percentage. This test was performed in a single stroke up to a depth of 480 mm.

K-33 Specimen

The piezocone penetration profile for PCPT3 is shown in Figure 9. This specimen had no sand layer on top. The measured cone resistance was slightly (6 percent) higher for this specimen as compared to the K-50 specimen. Both the cone resistance and the penetration induced pore pressures reached a stable value at about 90 mm depth of penetration. A slight drop in the cone resistance and excess pore pressure was observed after 480 mm of penetration. The dissipation test D3 (Figure 10) performed at a depth of 570 mm showed a trend similar to that of test D1 for the K-50 specimen.

The penetration profile PCPT4 (Figure 11) confirmed the fact that the penetration induced pore pressures measured at the tip reaches a stable value only at a very large penetration depth (greater than 500 mm). The possible reasons for this are low permeability of the filter element, and/or soil smearing of the filter. The dissipation curve D4 (Figure 12)

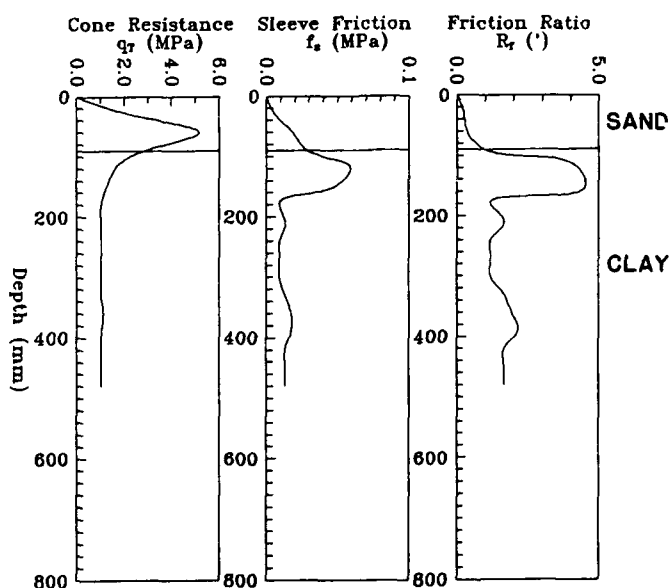


Figure 8. Penetration profile for QCPT.

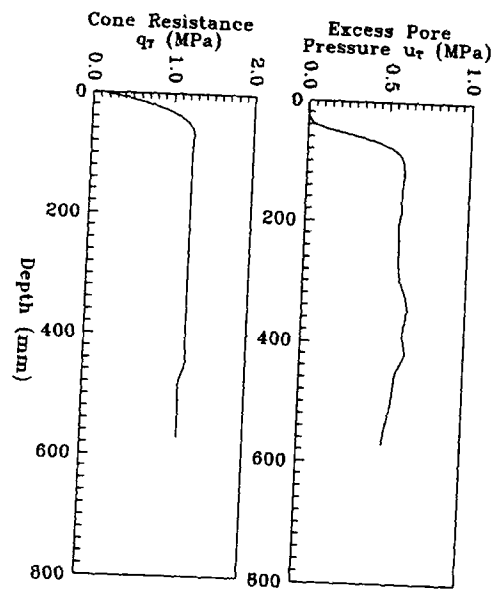


Figure 9. Penetration Profile for PCPT3.

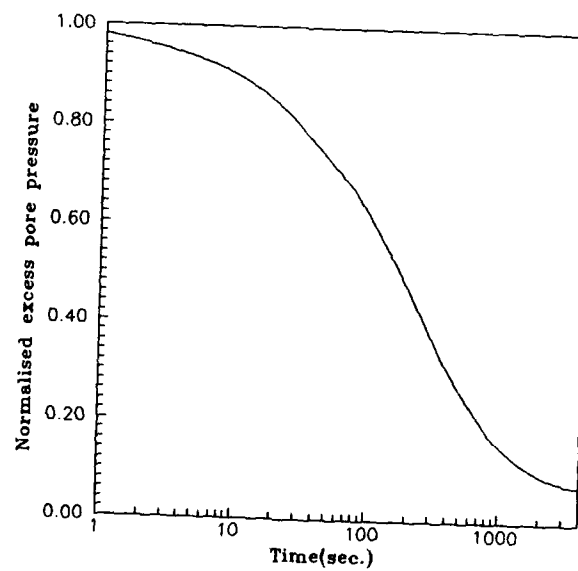


Figure 10. Dissipation result for PCPT3.

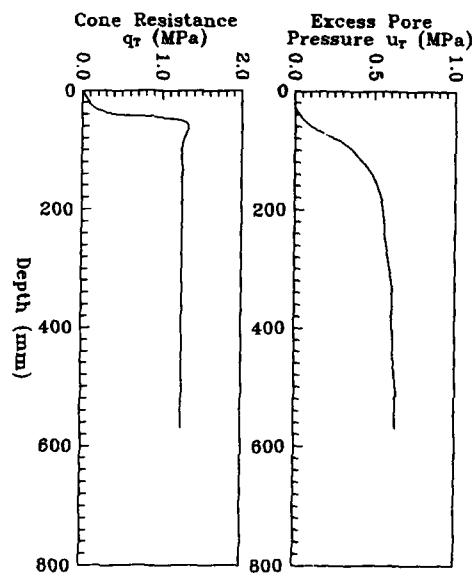


Figure 11. Penetration Profile for PCPT4.

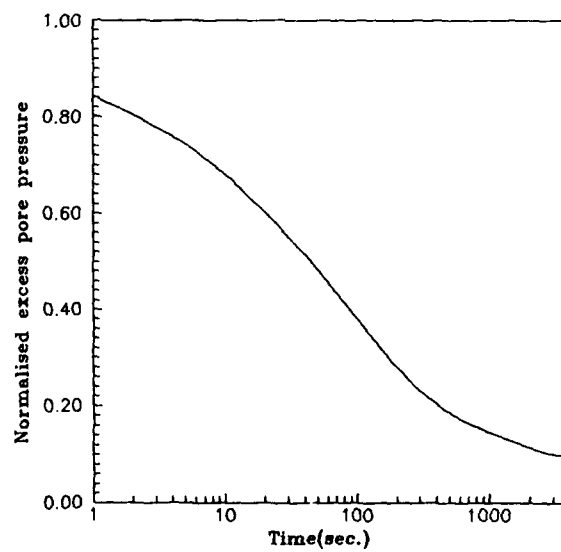


Figure 12. Dissipation result for PCPT4.

was similar in trend to the dissipation test D2 on the K-50 specimen. However, the dissipation rate in D4 was faster compared to that in D2 because of the higher percentage of sand in the K-33 specimen.

INTERPRETATION OF THE TEST RESULTS

Interpretation of PCPT data is often complex as it is influenced by many variables. A number of factors such as stress history, rigidity index (stiffness), sensitivity, soil anisotropy, soil fabric (macrofabric), and strain rate influence the PCPT data. The design of the penetrometer especially the thickness, location and pore size of the filter element along with the possibility of its clogging and smearing has a significant effect on the magnitude of the pore pressure generated and its subsequent dissipation. A detailed interpretation of the above test results is beyond the scope of this paper.

Undrained Shear Strength

The behavior of the soil around an advancing cone is very complex in nature. A number of methods have been developed to estimate the undrained shear strength s_u from PCPT data. The undrained shear strength may be estimated using the following equation suggested by Lunne et al. [13].

$$s_u = \frac{q_T - \sigma_{vo}}{N_{kT}}$$

where q_T = corrected cone resistance, σ_{vo} = total overburden pressure, and N_{kT} = cone factor.

Based on the reference s_u obtained from consolidated undrained triaxial tests on undisturbed soil samples yielded an N_{kT} of 16 for the K-50 specimen and 13 for the K-33 specimen. The above values of N_{kT} are higher compared to the theoretical values derived from analytical models. However, N_{kT} values have been reported to vary between 4 and 30 in actual practice with $N_{kT} = 10$ to 15 in normally consolidated clays. One main reason for the high N_{kT} values observed is due to the fact that the penetration tests were performed on isotropically consolidated specimens which yielded a higher cone resistance value. The effect of the horizontal in-situ stress has not been taken into account. Analysis based on the strain path method along with large strain finite element analysis [14] has confirmed the importance of horizontal stress and rigidity index on the cone factor. The type of test to obtain the reference s_u can also affect the N_{kT} values because of the different stress path followed.

Semi-empirical relations based on cavity expansion theories using penetration induced pore pressures may also be used to estimate s_u . The following expression is used to obtain the correlation factor $N_{\Delta u}$ which varies between 2 and 20.

$$s_u = \frac{\Delta u}{N_{\Delta u}}$$

In Table 4, the value of $N_{\Delta u}$ computed using the reference s_u is shown. In PCPT2, the penetration pore pressure did not reach a maximum stable value resulting in a low value of $N_{\Delta u}$.

Table 4. $N_{\Delta u}$ from piezocone tests.

Specimen	$N_{\Delta u}$	
	Experimental from Reference S_u	
	for Δu Measured Behind Tip	for Δu Measured on Cone Face
K-50	10.40	9.36
K-33	9.80	10.50

Coefficient of Consolidation

The dissipation test result obtained from a piezocone penetration test can be used to predict the coefficient of consolidation in the horizontal direction. It is widely accepted that the soil consolidation around the cone penetrometer takes place in the recompression mode and c_h is usually evaluated at 50% dissipation level.

Torstensson [2] proposed the following expression based on cavity expansion theory to evaluate the horizontal coefficient of consolidation:

$$c_h = \frac{T_{50} r_o^2}{t_{50}}$$

where T_{50} = time factor at 50% dissipation (T is given for both cylindrical and spherical solution), t_{50} = time for 50% dissipation, and r_o = equivalent penetrometer radius.

Houlsby and Teh [14] used a modified time factor T^* taking into account the importance of the rigidity index I_r on the size of the plastified zone. The model is based on the strain path method and the following expression was suggested:

$$c_h = \frac{T^*_{50}}{t_{50}} R^2 \sqrt{I_r}$$

where T^*_{50} = modified time factor at 50% dissipation (given for various location of the filter element), and R = radius of the penetrometer.

The coefficient of consolidation estimated using the above models is compared with the reference c_h (obtained from laboratory tests) in Table 5.

CONCLUSIONS

Interpretation of PCPT data is often complex as it is influenced by a number of factors such as stress history, rigidity index, sensitivity, soil anisotropy, soil fabric and strain rate. Values of the cone factor N_{kT} and the correlation factor $N_{\Delta u}$ obtained from PCPT were higher compared to the theoretical values indicating the importance of horizontal stress and rigidity index. The pore pressures recorded by the filter element at the tip reached a stable value only for a relatively large depth of penetration as compared to that of the filter located 0.5 mm above the base of the cone. The dissipation result from the piezocone test gave a reasonable estimation of the coefficient of consolidation c_h .

Table 5. Estimated and reference c_h values.

Sample	Test	Estimated $c_h \times 10^{-3} \text{ cm}^2/\text{sec}$		Reference $c_h \times 10^{-3} \text{ cm}^2/\text{sec}$
		Torstensson	Houlsby and Teh	
K-50	PCPT1	4.5	7.2	13.8 to 14.9
	PCPT2	3.1	2.2	
K-33	PCPT3	2.8	4.3	27 to 29.5
	PCPT4	3.9	2.9	

ACKNOWLEDGMENT

This work was sponsored by the National Science Foundation under grants MSM-9046426 and MSS-9018249.

REFERENCES

1. A.E.Z. Wissa, R.T. Martin and J.E. Galanger, "The Piezometer Probe," Proceedings ASCE Specialty Conference on In-Situ Measurement of Soil Properties, Raleigh, North Carolina, 1 536-545 (1975).
2. B.A. Torstensson, "Pore Pressure Sounding Instrument," Proceedings, ASCE Specialty Conference on In-Situ Measurement of Soil Properties, Raleigh, North Carolina, 2 48-54 (1975).
3. N. Janbu and K. Senneset, "Effective Stress Interpretation of In-situ Static Penetration Tests," Proceedings of the European Symposium on Penetration Testing, ESOPT I, Stockholm, Sweden, 22, 181-193 (1974).
4. M.T. Tumay, R.L. Boggess and Y. Acar, "Subsurface Investigation with Piezo-cone Penetrometer," ASCE Specialty Publication, 325-342 (1981).
5. M.M. Baligh, A.S. Azzouz, Z.A.E. Wissa, R.T. Martin and J.J. Morrison, "The Piezocone Penetrometer," ASCE, Geotechnical Division, Symposium on Cone Penetration Testing and Experience, St. Louis, 247-263 (1981).
6. R.G. Campanella and P.K. Robertson, "Applied Cone Research," Symposium on Cone Penetration Testing and Experience, "Geotechnical Engineering Div., ASCE, 343-362 (1981).
7. H.M. Zuidberg, L.H.J. Schaap and F. Beringen, "A Penetrometer for Simultaneous Measurement of Cone Resistance, Sleeve Friction and Dynamic Pore Pressure," ESOPT II, Amsterdam, Proceedings, 2, 963-970 (1982).
8. A.B. Huang, R. D. Holtz and J.L. Chameau, "A Calibration Chamber for Cohesive Soils," Geotechnical Testing Journal, GTJODJ, 11, 1, 30-35 (1988).
9. R.D. Bunting, "An Experimental Study of Flat-Plate Penetration Tests in Saturated Clay," Master Thesis, Clarkson University, New York (1990).
10. R.J. Krizek and D.E. Sheeran, "Slurry Preparation and Characteristics of Samples Consolidated in the Slurry Consolidometer," Technical Report No. 2, Contract No. DACW39-70-C-0053, U.S. Army Corps of Engineers, Waterways Experiment Station, Vicksburg, Mississippi, 1-5 (1970).

11. D.C. de Lima, "Development, Fabrication and Verification of the LSU In Situ Testing Calibration Chamber," Ph.D. Dissertation, Louisiana State University, Baton Rouge (1990).
12. M.T. Tumay and D.C. de Lima, "Calibration Chamber Testing," Technical Report, Louisiana State University, Baton Rouge, Louisiana (1990).
13. L. Lunne, H.P. Christoffersen and T.I. Tjelta, "Engineering Use of Piezocone Data in North Sea Clays," Proceedings XI ICSMFE, San Francisco (1985).
14. G. Houlsby and C.I. Teh, "Analysis of the Piezocone in Clay," ISOPT I, Orlando, Florida, Proceedings, 2, 777-783 (1988).

PRINCIPLES AND EXAMPLES OF CENTRIFUGE MODELING

Dobroslav Znidarčić
University of Colorado, Boulder

INTRODUCTION

As a technique for studying physical models of earth structures and foundations centrifuge modeling has received much attention in the last two decades. During that time the technique has developed and matured to represent an essential part of the overall geotechnical engineering research effort. Centrifuge modeling can be viewed as an alternative and a complement to widely used numerical techniques. Like other physical modeling techniques it has many advantages; the most important of which is its ability to study phenomena for which well-defined theories do not exist. In addition to its use as a research or design tool, centrifuge modeling has found its place in geotechnical engineering education as well (Craig, 1989).

In his "Summary of the State-of-the-art in Centrifuge Model Testing", Ko (1988) reviewed the history of the technique, the basic principles, and available facilities around the world. Though the initial concept of centrifuge modeling is more than one-hundred years old, its application to geotechnical problems began in the early 1930s. Real development started in the 1960s and 1970s, when rapid development of electronically based instrumentation facilitated acquisition of more quantitative data from the experiments.

The intent of this paper is to provide a short review of the fundamental principles of centrifuge model testing and with several examples of recent projects demonstrate the potential of this relatively new technique.

BASIC PRINCIPLES

The main reason for physical modeling of earth structures in an increased gravity environment is the pressure sensitivity of the earth material and the fact that, in many geotechnical problems, the self weight of the material is the dominant loading force that leads to deformations and ultimately to failures. Deformation and strength characteristics of soils are governed by the stress level, which is controlled in turn by the self-weight forces of the soil itself. While small physical models of a prototype can duplicate its geometry, the requirement that the stress level be the same at the homologous points between the model and the prototype can be satisfied only if the unit weight of the soil is increased by the same factor by which the dimensions in the model are reduced. This is easily accomplished by spinning the model in a centrifuge to a gravity level that is N times higher than the Earth's gravity. The principles of centrifuge modeling are best illustrated by the example of modeling slope stability problem shown in Figure 1. The stability of a slope in a cohesive material can be expressed in terms of a dimensionless "Stability Number" (Taylor, 1937). If a model slope is to represent conditions equivalent to the prototype it must have the same stability number. Since the height of the slope is reduced in the model by a factor N , for the stability number to remain the same, the unit weight of the material must be increased by the same factor. Keeping the same soil density by

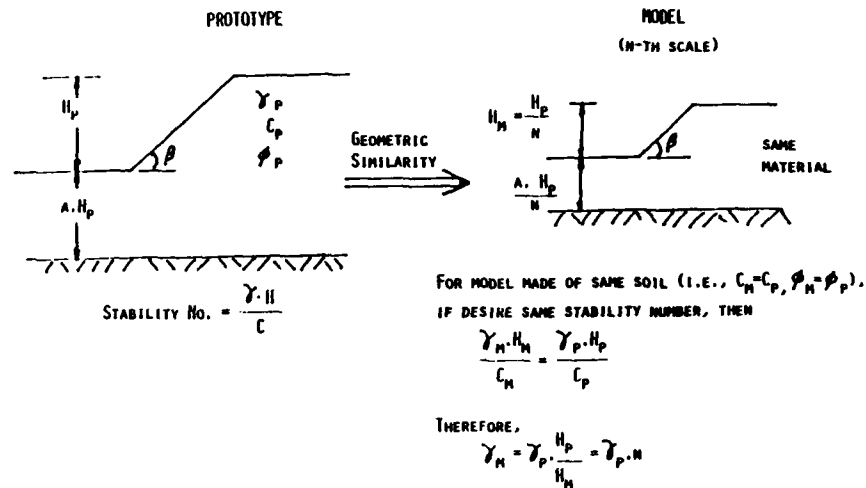


Figure 1. Scaling Relations for Slope Stability

using the prototype soil for constructing the model and increasing the gravity, the desired effect of increased weight is achieved. There are other methods for increasing body forces in the soil, such as generating seepage forces, but increasing the gravity field by centrifugation is still the most convenient technique.

It is evident that the same stability factors in the model and prototype can be attained by decreasing the shear strength of soil and keeping its unit weight the same, that is, performing the experiment in the Earth's gravity field. By reducing the compaction effort or compression load during the model preparation phase, the shear strength of soil can be reduced to the desired value. The unit weight of softer material will not be much different from the prototype condition and any variation could be taken into account when determining the shear strength so that the model stability number corresponds to that of the prototype. Thus, by changing the soil characteristics in the model, it is possible to satisfy the scaling relationship while testing scaled models in the normal gravity field. However, the situation is more complicated when dealing with the material in which both cohesion and friction contribute to the strength, or when the problems studied are dependent on the deformation characteristics of soil as well. In these cases, applying the concept of modeling material characteristics to satisfy the scaling relations is not feasible. The only practical approach is to use the prototype material to construct the model and test it in the increased gravity field for which the scaling requirements are automatically satisfied.

It is interesting that in hydraulic modeling studies it is customary to model the prototype material so that the scaling relations are satisfied without the requirement of testing in the increased gravity field. While this approach may be convenient for modeling coarse-grained materials, for which the grain and pore sizes determine water flow and sediment transport characteristics, a similar approach would not work when dealing with fine-grained soils. For geotechnical physical modeling, the only feasible solution is to use the prototype material in order

to have same constitutive characteristics and satisfy the scaling requirements by increasing the gravity.

Prior to studying any problem by testing physical models, a proper set of scaling relations relevant to the problem should be developed. Several approaches have been used to derive these relations, including dimensional analysis, derivation from governing equations, and from the principals of mechanical similarity between a model and a prototype. Croce et al. (1984) used the principle of mechanical similarity that originated from Newton (1686); it requires that all forces acting on similar systems be proportional. Starting from the basic requirement that stresses in a model must be equal to those in the prototype (in order to have the same soil behavior) scale factors for various forces and time, for time dependent-problems, are derived. These factors are summarized in Table I for forces normally encountered in geotechnical problems. In the table, N is the factor by which the size of the prototype is reduced in the model as well as the factor by which the gravity level is increased to satisfy the similarity requirement.

TABLE I. Scale factors for forces related to scale factors for time (from Croce et al., 1984)

Time	Weight Force	External Force	Viscous Force	Inertia Force	Seepage Force
1	N^2	N^2	N^2	N^4	N^4
N	N^2	N^2	N	N^2	N^3
N^2	N^2	N^2	1	1	N^2

Since the weight forces in the centrifuge are always scaled by N^2 , and they are present in any geotechnical problem, all other forces relevant to the problem must be scaled by the same factor. While the external forces are readily scaled by the same factor, independent of the time scale, the scaling of other forces depends on the scale for time. If a process in which viscous forces are dominant is to be modeled in the centrifuge, the mechanical similarity between the model and the prototype will be satisfied only if the time is scaled by 1, because only then is the scaling factor for viscous forces also N^2 . This means that there is no time benefit in studying creep phenomena in the centrifuge. On the other hand, when modeling dynamic problems, similarity is achieved when the time is shortened by factor N. For seepage problems including consolidation, time is scaled by the factor N^2 which provides a convenient reduction in testing time. It is noted that the presented analysis clearly demonstrates the conflict in scaling relations if several of the time-dependent processes are to be modeled in the centrifuge simultaneously. However, for practical purposes, if one group of forces dominates the process, while the others have only secondary influence, the similarity between the model and prototype will be satisfied. One example in which the conflict of the scaling requirements can affect the results is centrifuge modeling of earthquake-induced liquefaction. In this case, pore pressure is generated by the dynamic action at the prototype rate, scaled by factor N; while the same pore pressure is simultaneously dissipated due to consolidation at a rate, scaled by the factor N^2 from the prototype value. Thus, special steps must be taken to reconcile this conflict. One possibility is to change the pore fluid, reduce the soil permeability, and slow the consolidation process by the factor N.

The derived scaling relations must be verified experimentally before observations and measurements made on physical models in the centrifuge could be accepted as representative of the prototype behavior. Verifications are needed to confirm that processes to be modeled are well understood and that all the forces relevant to the problems are accounted for in the derivation of the scaling relations. The ideal verification would be to compare the centrifuge test results to the behavior of the corresponding prototype. However, such an approach defeats the main reason for centrifuge modeling because it requires construction of a full-scale structure under well controlled conditions. Obviously, this task is nearly impossible or prohibitively expensive. The main issue in experimental verification of the scaling relations is the dependence of the physical process on the gravity level which can be explored, by performing experiments at a minimum of two different gravities, neither of which must be equal to the Earth's gravity. In other words, there is nothing inviolable about Earth's gravity of 9.81 m/s^2 . The concept of comparing results of two physical experiments at different gravity levels to verify the scaling relations is called "modeling of models" and is illustrated in Figure 2 (Ko, 1988); logarithmic scales are used for convenience of presentation over a wide range of sizes. The figure illustrates how a prototype with a characteristic length of 10 meters at "normal" gravity of 1 g (A1) can be modeled by a series of models with various sizes at corresponding gravity levels. In particular, such a prototype could be simulated by a 1 m model at 10g or by a 0.1 m model at 100g levels. On the other hand, the 1 m - 10 g model (A2) can be viewed as a prototype of the 100 g model (A3). By comparing the performance of these experiments, the scaling relations can be verified and the results extrapolated to the "real" prototype at 1 g. Gravity ratios need not be 10 but any convenient number as long as the two gravity levels are not too close to prevent reasonable discrimination. A factor of 2 to 5 is usually reasonable between the two models. Large ratios are undesirable because of the size limitations of common centrifuges, and because of the problems associated with extreme miniaturization of complex structures. It is noted that if a structure on the Moon is to be modeled, a 1 g experiment will represent a reduced prototype size-increased gravity model and an additional centrifuge experiment will complete the "modeling of models" loop.

PHILOSOPHY AND ADVANTAGES OF CENTRIFUGE MODELING

There are several ways to solve geotechnical engineering problems with centrifuge modeling. Ko (1988) lists four philosophies that can be adopted to view the role of centrifuge modeling:

- (a) prototype modeling,
- (b) investigation of new phenomena,
- (c) parametric studies,
- (d) validation of numerical models.

Prototype modeling is an obvious and direct application of the centrifuge modeling technique to the solution of actual engineering problems; however, this approach is also the most difficult and possibly most controversial. It is difficult, if not impossible, to duplicate the field situation that normally results from complex geological processes. Often, field conditions must be idealized and only the most important features are duplicated properly in the model. As will be discussed later,

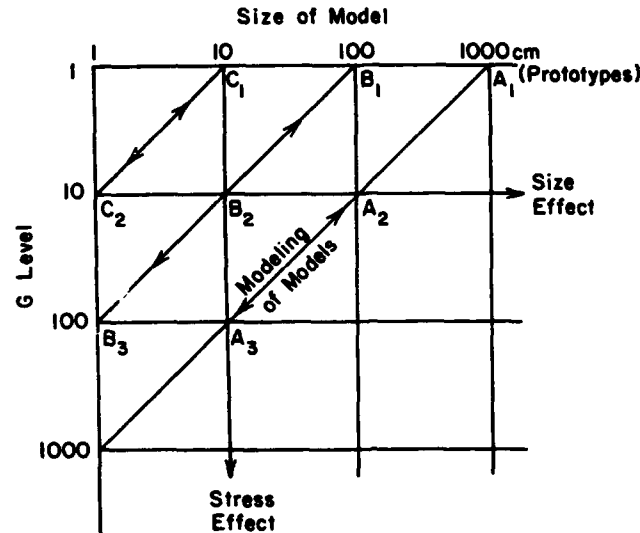


Figure 2. Principle of Modeling of Models (from Ko, 1988)

the idealization required for centrifuge modeling is generally less restrictive than assumptions routinely accepted for other methods of the analysis.

Centrifuge modeling has been successfully applied to the study of phenomena that are not well understood. Examples include plate tectonics, crater formation by explosives, and various earthquake-induced phenomena. Observations of earthquake-induced events in the field is difficult and costly due to uncertainty in the time and place of earthquake occurrence. A centrifuge with the shake table is an attractive alternative in which the desired event can be triggered at will under controlled conditions and with adequate similarity to the field situation. Problems for which alternative methods of the analysis do not exist may also be placed in this category; such as the holding capacity of ship anchors. Because of their complex geometry and the large deformations in the soil that surrounds the anchors, current analysis techniques cannot be successfully applied. The problem is usually solved by empirically developed design charts with very few data points from actual field tests. Again, the centrifuge offers an attractive alternative in which the models of actual anchors are tested under controlled conditions and the results scaled and extrapolated to the field conditions. Other examples include reinforced earth structures, soil nailing, and similar problems for which even load transfer mechanisms are not yet well understood.

Parametric studies in the geotechnical centrifuge is an example where efforts for performing physical model experiments are best rewarded. Normally a major effort is required to organize and build the first model of a structure, while the actual testing and small variations in the model are easily performed. By changing some model parameters (geometry, load application conditions or seepage characteristics) the sensitivity of the results to these changes can be evaluated and the most critical factors identified. This leads directly to the

possibility of design charts development using a geotechnical centrifuge. Examples of this application will be discussed later.

The most powerful potential application of centrifuge modeling is in the validation process of various numerical or other methods of analyses. In these, centrifuge modeling results obtained under well controlled conditions are re-created by the analysis and a good comparison verifies the implemented numerical model and the solution algorithm.

To evaluate advantages of physical modeling of geotechnical problems in the centrifuge, a comparison with numerical modeling techniques is made. Any modeling technique, physical or numerical, requires acceptance of some simplifying assumptions in the analysis process. It is customary to simplify the problem geometry to facilitate the analysis. This may include transferring a three-dimensional problem to a two-dimensional model, simplifying a complex stratification with few well-defined zones of homogeneous materials, and accepting well defined boundaries beyond which the material response has no consequence on the performance of the structure. Both numerical and physical modeling techniques adopt similar approaches to geometrical simplification, with one exception: While, in many cases the numerical techniques are still limited to two-dimensional problems, centrifuge modeling does not impose this restriction. On the contrary, it is easier to perform centrifuge modeling of a three-dimensional problem in which there is no need to deal with the boundary friction, such as in the case of plane strain problems.

The next step in numerical modeling is representation of constitutive properties of the materials. It is safe to say that this is the most challenging step to solving any geotechnical problem. In the past 20 to 30 years much effort has been invested in developing various constitutive models and implementing them in numerical schemes. While many models, with varying degree of success, have been developed, none is capable of simulating all the intricacies of soil behavior, especially in the zones of large deformations and when the material is close to failure. As stated earlier, in centrifuge modeling, prototype soils are used and there is no need for simplification of soil response to different loadings. If stress levels are properly modeled, the soil response in the centrifuge will be the same as in the prototype. This is the single most important advantage of centrifuge modeling techniques. Anyone who has faced the tedious process of measuring and choosing model parameters will appreciate this advantage.

Often, when analyzing a geotechnical problem, it is necessary to know or to assume *a priori* the deformation pattern and the form of the failure zones. Centrifuge modeling of the same problem does not require this step. Once the model is constructed and the load applied, deformation and failure will take place in a form similar to the corresponding prototype. No prior knowledge of this pattern is needed.

Finally, once all previous simplifications are made, further approximations in the solution algorithm are necessary to make the analysis tractable. These simplifications may be in the form of the assumed stress distribution along the failure zone in the slope stability analysis or in the choice of the discretization pattern for a finite element analysis. A numerical solution scheme must be chosen, as well. These steps are avoided when a physical modeling technique is chosen as the analysis method. It is seen that despite the large effort usually required to construct a physical model, the centrifuge testing technique has

many advantages that make it an attractive and powerful tool for studying geotechnical problems.

EXAMPLES OF CENTRIFUGE MODELING

Nearly all conceivable geotechnical problems have been modeled in geotechnical centrifuges. Examples range from seepage to consolidation problems and flow of pollutants through soils; from dynamic soil structure interaction to earthquake induced liquefaction; and from shallow and deep foundations to slope stability and retaining walls, either conventional or with soil reinforcement and nailing. With current concerns about natural and man-made hazards, particular attention is given to studying earthquake-induced phenomena and transport mechanisms for hazardous materials. There are a number of centrifuges around the world equipped with shaking tables that can, in flight, simulate the acceleration record of an actual earthquake. With recent advances in electronic measuring techniques and data acquisition systems, the available possibilities in modeling and observing actual structures in the geotechnical centrifuges are limitless. Several examples of some recent projects are described here to demonstrate the potential of centrifuge modeling.

Slope stabilization with horizontal drains

Resnick (1989) and Resnick and Znidarčić (1990) studied the influence of horizontal drains using the geotechnical centrifuge. The goal was to demonstrate the use of the centrifuge modeling technique for the design chart development. The gravity level was the same in all tests and was equal to 100 times Earth's gravity. The model container assembly, in which the model slopes were constructed and tested, is illustrated in Fig. 3. Bonny silt was used as the model material in all experiments. Water was supplied to the reservoir behind the slope from a toroidal container mounted on the centrifuge arm. The water level in the reservoir was monitored by a pressure transducer connected to a PC-based data acquisition system. Pore water pressures within the model slopes were measured by means of a number of miniature pore pressure transducers connected to the data acquisition system. Up to nine pore pressure transducers were embedded in the model slopes during the model preparation phase of the experiments. An example of how the pore pressure transducers were positioned within the model slopes is shown in Fig. 3. Three linear variable differential transformers were located on the crest of the model slope (Fig. 3) and were connected to a strip chart recorder so that continuous measurements of crest deformation could be obtained. In particular, the moment of slope failure could be detected by the sudden displacement of the LVDTs. A closed circuit video camera was mounted on the centrifuge arm so that the slope surface and the moment of failure could be observed during testing. Sintered bronze porous tubes were used to construct the drains. The outside of the porous tubes were wrapped with filter paper.

The experiments started by spinning the centrifuge to the desired gravity level. After the appropriate velocity was reached, the upstream water level was increased to a desired height and maintained at that level until steady-state seepage conditions were achieved. Typically, each level was maintained for about three hours of model time (3.4 years at prototype scale), at which time the water level was increased to the next height. When steady-state seepage conditions had been reached for

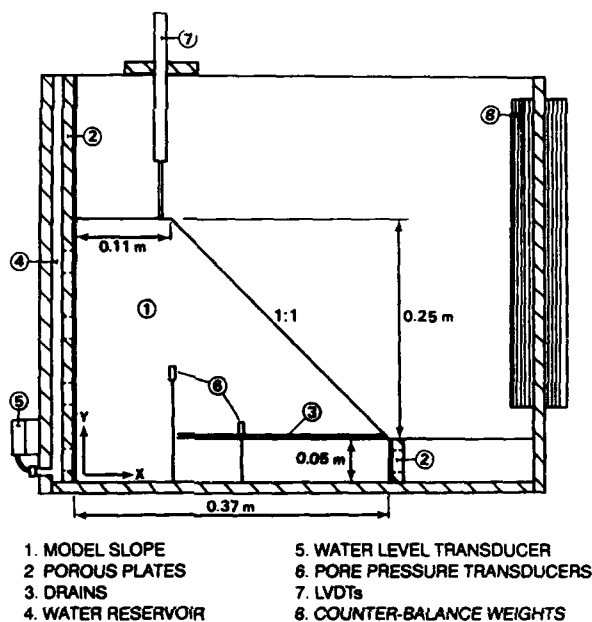


Figure 3. Model Container

the last targeted reservoir level, the model slope was induced to fail by seepage forces, by increasing the upstream water level to a critical height. Normally, after about five to ten minutes of seepage, the slope would fail under transient flow conditions. The transient, rather than steady state, flow conditions were required to avoid the problem of surface erosion as observed in preliminary tests, in which the steady state phreatic surface for the water level at the critical height exited at the slope face causing a significant amount of erosion before a general slope failure was recorded.

Five experiments were performed without horizontal drains installed in the model slopes. These experiments had the global objective of providing data for reference conditions, which were compared to experiments with drains. A total of four experiments were performed with horizontal drains installed in the model slopes. Each of the four model slopes had a drain, or drains, of the same size (i.e., diameter and length) installed, only the number and spacing of drains changed from test to test.

The experiments with drains had either one, two or four drains installed, creating a prototype spacing between drains of "infinity", 10.2 and 5.1 m, respectively. Placing drains in the slopes and changing the spacing produced a definite effect on experimental piezometric levels and observed failure surfaces, especially for those tests in which two or four drains were installed. Installing horizontal drains in the model slopes changed the seepage pattern from a two-dimensional problem to a three-dimensional problem.

Slope stability calculations were performed using the slip surface that was observed in one of the reference tests and the piezometric profiles for the various steady state piezometric

profiles of the slopes with horizontal drains. The results of these calculations are presented in Fig. 4, which is a diagram that indicates how the percent increase in factor of safety is related to the drain spacing index (S/H) and the relative height of the upstream water level (H_w/H). A drain blanket would have a drain spacing index of zero. The relative height of the upstream water level is defined as the pressure head measured at the upstream boundary from an elevation corresponding to the top of the toe (H_u) divided by the slope height ($H=25.4$ m). The upper and lower points for each water level and drain spacing represent the range of increase in factor of safety for the different X-Y planes (e.g., drain and midway planes). The solid lines represent the average values for the increase in factor of safety. As can be seen in Fig. 4, as the drain spacing index decreases, or as

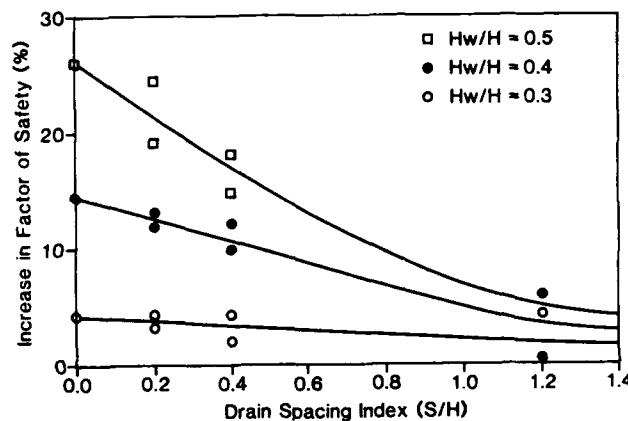


Figure 4. Stability Diagram for Drains

the relative height of the upstream water level increases, the percent increase in factor of safety increases. Thus, for smaller drain spacings and higher initial water levels, larger increases in stability will be obtained. The values that are shown in Fig. 4 are valid for the presented position of the drains. This position of the drains might not have been the optimal position, and larger increases in stability might have been seen if the drains were installed in different positions.

The limited capacity of the centrifuge used in this research imposed restrictions on the slope geometry, which had two detrimental effects. First, the factor of safety for the slope with no seepage present was 1.22, which imposed an upper limit on the stabilizing effect that the installed drains may have produced. Second, the slope failures were always induced under transient flow conditions in order to avoid erosion problems, preventing reliable evaluation of the pore pressure distribution within the slope at the moment of failure. Using a larger centrifuge with a bigger model container and higher acceleration capacity will enable testing of flatter slopes for which the maximum factor of safety will be much higher, allowing more discrimination in evaluating the beneficial effect of the installed drains. For such a slope the phreatic surface will not exit on the slope face and there will be no erosion problems. Thus, it will be possible to induce slope failure under well controlled steady-state seepage conditions.

Shallow foundation

Shallow footings on sand were tested under vertical central and eccentric loads, and under inclined loads in the geotechnical centrifuge. Details of the testing program and results are reported by Saad (1991) and by Saad and Znidarčić (1991). In order to ensure plane strain conditions, three adjacent footings were made along one line, shown in Figure 5. Footings were loaded

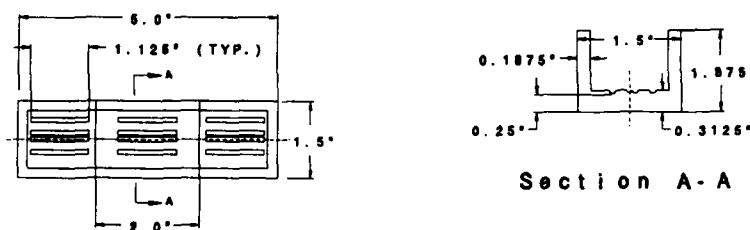


Figure 5. Details of the Footing for the Plane Strain Conditions

with a rigid mechanism so that they penetrate into the soil uniformly; therefore, the one in the middle was in a plane strain condition. The load on each footing was measured separately using a load cell. Each footing had a U-shaped section with longitudinal grooves in the base at different locations from the centerline for different eccentricities. The footings were made of aluminum; sand was glued to the bottom to simulate rough base conditions. The footing deformation was measured using several linear variable differential transformers (LVDTs) at various locations so that footing rotation and settlement could be calculated. The results of this experimental program are summarized in Figure 6 a, b and c. They clearly indicate that the conventional methods of accounting for load inclination are conservative for small angles, while they are on the unsafe side for load eccentricity. A good agreement between experiments and theoretical predictions is noted for a centrally loaded footing. However, the predicted values are sensitive to the proper choice of the angle of internal friction, which is always a problem in practical applications.

Contaminant flow in soils

To verify the applicability of the centrifuge modeling technique to studying the flow of nonaqueous phase liquid (NAPL) in an aquifer, Illangasekare et al. (1991) performed a simple set of experiments in which one-dimensional infiltration of NAPL into sand, under controlled conditions in the laboratory (1 g), was compared to the centrifuge experiment at 20 g. A good agreement between the prototype performance with the scaled centrifuge results shown in Figure 7 clearly verifies the theoretical scaling relations. Besides being able to study the problem on a much smaller model in the centrifuge, the time required to perform the experiment is also shorter; an important consideration when studying flow processes in fine-grained soils. The same process that would require a prohibitively long time in the laboratory under 1 g, can be conveniently completed in the

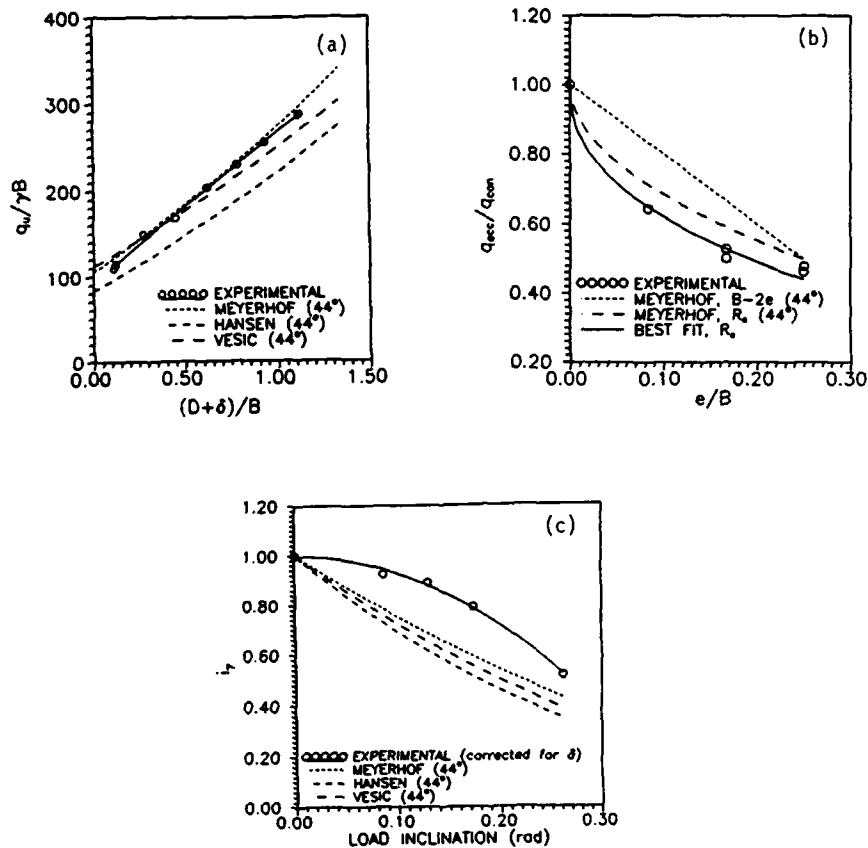


Figure 6. Test Results: (a) Vertical Central Loading, (b) Eccentricity Reduction Factor, (c) Inclination Reduction Factor

centrifuge within a day. It is particularly noted that capillary effects are properly scaled in the centrifuge, which is essential when dealing with any type of multiphase flow that includes unsaturated conditions.

CONCLUSIONS

The presented discussion and examples demonstrate the applicability of the centrifuge modeling technique to the analysis of many geotechnical problems. The prototype stress conditions are properly duplicated in this type of physical modeling, which is essential for pressure-sensitive material like soil. Recent advances in the electronic methods of measurement facilitate acquisition of high quality data from the experiments, making them a quantitative rather than strictly qualitative tool. The increased number of geotechnical centrifuges around the world, makes this technique a widely available and convenient method to address challenging geotechnical problems.

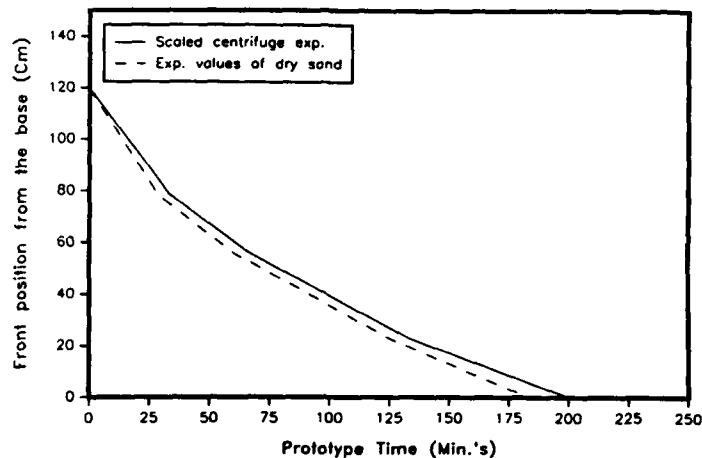


Figure 7. Comparison of Prototype and Scaled Centrifuge Results

REFERENCES

- Aiban, A. S. (1991) *Shallow Foundations on Sands*, Ph.D. Dissertation, University of Colorado, Boulder.
- Aiban, A. S. and Znidarčić, D. (1991) *Shallow footings on sand under vertical central, eccentric and inclined loads*, Proceedings of the International Conference Centrifuge 91, Ko, H. Y. and McLean, F. G., ed., A.A.Balkema, Rotterdam.
- Craig, W. H. (1989) *The Use of a Centrifuge in Geotechnical Engineering Education*, Geotechnical Testing Journal, GTJODJ, Vol. 12, No. 4, pp. 288-291.
- Croce, P., Pane, V., Znidarčić, D., Ko, H. Y., Olsen, H. W., and Schiffman, R. L. (1984) *Evaluation of Consolidation Theories by Centrifuge Modelling*, Proceedings of the International Conference on Applications of Centrifuge Modelling to Geotechnical Design, Manchester University, United Kingdom, pp. 380-401.
- Illangasekare, T. H., Znidarčić, D., Al-Sheridda, M. and Reible, D. D. (1991) *Multiphase flow in porous media*, Proceedings of the International Conference Centrifuge 91, Ko, H. Y. and McLean, F. G., ed., A.A.Balkema, Rotterdam.
- Ko, H. Y. (1988) *Summary of the state-of-the-art in centrifuge model testing*, in *Centrifuges in Soil Mechanics*, Craig, W. H., James, R.G. and Schofield, A. N., ed., A.A.Balkema, Rotterdam.
- Newton, I. (1686) *Philosophiae Naturalis Principia Mathematica* (Propositio XXXIII), English Translation by A. Motte (1729), Revised by F. Cajori (1934), University of California Press, Berkeley and Los Angeles, California.
- Resnick, G. S. (1988) *Centrifugal modeling of seepage, slope stability and the influence of horizontal drains*, thesis presented to the University of Colorado, at Boulder, Colorado, in partial fulfillment of the requirements for the degree of Master of Science.
- Resnick, G. S., and Znidarčić, D. (1990) *Centrifugal Modeling of Drains for Slope Stabilization*, Journal of Geotechnical Engineering, ASCE, Vol. 116, No. 11, pp. 1607-1624.
- Taylor, D. W. (1937) *Stability of Earth Slopes*, Journal of Boston Society of Civil Engineers, Vol. 24, No. 3.

LIST OF AUTHORS

- | | |
|------------------------------|-----------------------------|
| Acar, Y.B. 339 | Lee, S.H.-H. 363 |
| Almeida, M.S.S. 41 | LoPresti, D. 213 |
| Anderson, W.F. 55 | Lunne, T. 225 |
| Arulmori, K. 329 | Ma, M.Y. 175 |
| Been, K. 67 | Manassero, M. 237 |
| Bellotti, R. 79, 91 | Mayne, P.W. 197, 249, 257 |
| Borden, R.H. 101 | O'Neill, D.A. 213 |
| Brandon, T.L. 119 | O'Neill, M.W. 277 |
| Bunting, R.D. 161 | Nutt, N.R.F. 265 |
| Carney, T.C. 161 | Parkin, A. 289 |
| Chameau, J.-L. 303 | Pedroni, S. 79, 91 |
| Clough, G.W. 119 | Penumadu, D. 303 |
| Fioravante, V. 135 | Peterson, R.W. 41, 315, 329 |
| Foray, P. 147 | Puppala, A.J. 339 |
| Fretti, C. 79 | Pyrah, I.C. 55 |
| Ghionna, V.N. 13, 79 | Rix, G.J. 351 |
| Holden, J.C. 1 | Schmertmann, J.H. 1 |
| Houlsby, G.T. 265 | Skandarajah, A. 303 |
| Huang, A.-B. 161, 175 | Stokoe, K.H. 351, 363 |
| Jamiolkowski, M. 13, 41, 135 | Tanizawa, F. 135 |
| Kosar, K.M. 67 | Tatsuoka, F. 135 |
| Kulhawy, F.H. 185, 197, 257 | Turnay, M.T. 339, 377 |
| Kurup, P.U. 377 | Voyiadjis, G. 377 |
| Lee, J.N.-K. 363 | Znidarcic, D. 393 |
| Lee, J.S. 175 | |